

Handbook of Antennas for EMC

Second Edition

Thereza M. Macnamara



with contributions from John McAuley

Handbook of Antennas for EMC

Second Edition

For a listing of recent titles in the
Artech House *Antenna and Electromagnetics Analysis Series*,
turn to the back of this book.

Handbook of Antennas for EMC

Second Edition

Thereza M. Macnamara
with
John McAuley



**ARTECH
HOUSE**

BOSTON | LONDON
artechhouse.com

Library of Congress Cataloging-in-Publication Data

A catalog record for this book is available from the U.S. Library of Congress

British Library Cataloguing in Publication Data

A catalog record for this book is available from the British Library.

ISBN 13: 978-1-63081-424-3

Cover design by John Gomes

© 2018 Artech House

685 Canton Street

Norwood, MA

All rights reserved. Printed and bound in the United States of America. No part of this book may be reproduced or utilized in any form or by any means, electronic or mechanical, including photocopying, recording, or by any information storage and retrieval system, without permission in writing from the publisher.

All terms mentioned in this book that are known to be trademarks or service marks have been appropriately capitalized. Artech House cannot attest to the accuracy of this information. Use of a term in this book should not be regarded as affecting the validity of any trademark or service mark.

10 9 8 7 6 5 4 3 2 1

*To my three granddaughters, Shanti Jasmine (aka Cheeky),
Sophia Jane (aka Softie), and Teya Mared (aka Twinks)
who will hopefully read this when they are older*

—T.M.M.

Contents

Preface	xiii
CHAPTER 1	
Introduction to Antennas	1
1.1 Requirements of an Antenna for EMC	1
1.1.1 Types of Antennas	2
1.2 Main Characteristics of an Antenna	3
1.2.1 Radiation Resistance	4
1.2.2 Radiation Pattern	5
1.2.3 Main Lobe	8
1.2.4 Sidelobe	12
1.2.5 Front-to-Back Ratio	13
1.2.6 Bandwidth	13
1.2.7 Aperture Size	15
1.2.8 Antenna Correction Factors	15
1.2.9 Polarization	16
1.2.10 Relationships Between the Key Parameters	20
References	26
CHAPTER 2	
Basic Math for EMC Engineers	27
2.1 Angles	27
2.1.1 Convention for Angles	27
2.2 Basic Trigonometry	28
2.2.1 Reciprocal Trigonometric Functions	28
2.2.2 Inverse Trigonometric Functions	32
2.3 Powers, Indices, and Logarithms	33
2.3.1 Multiplication of Numbers	34
2.3.2 Relationship Between dBm and dBmV	36
2.4 Real and Complex Numbers	36
2.4.1 Addition of Complex Numbers	40
2.4.2 Complex Conjugate	42
2.5 Scalars and Vectors	42
2.5.1 Position Vector	42
2.5.2 Vector Addition and Subtraction	42
2.5.3 Vector Multiplication	44
2.5.4 Phasors	46

2.6	Fourier Analysis and Transforms	48
2.6.1	Fourier Analysis	48
2.6.2	Fourier Transforms	48
2.7	Parameters	50
2.7.1	Mathematical Definition of Parameters	50
2.7.2	Parameters Used by Engineers	52
2.8	Fundamental Units and Dimensions	52
2.8.1	Checking Formulas by Dimensions	55

CHAPTER 3

Antenna Theory	57	
3.1	Unit Vectors	57
3.2	Scalar and Vector Fields	59
3.2.1	Spatial Rates of Change of Scalar and Vector Fields	59
3.2.2	Gradient of a Scalar Field	59
3.2.3	Divergence of a Vector Field	61
3.2.4	Curl of a Vector	62
3.3	Maxwell's Equations	64
3.3.1	Maxwell's First Equation	65
3.3.2	Maxwell's Second Equation	67
3.3.3	Maxwell's Third Equation	68
3.3.4	Maxwell's Fourth Equation	69
3.4	Boundary Conditions	70
3.4.1	Tangential Component of the Electric Field	70
3.4.2	Tangential Component of the Magnetic Field	71
3.4.3	Normal Component of the Electric Field	72
3.4.4	Normal Component of the Magnetic Field	73
3.5	Fields Due to a Radiating Dipole	73
3.5.1	Field Due to a Current Element	74
3.5.2	Fields at Large Distances from Wire Antennas	75
3.6	Power Flux Density for a Plane Wave	75
3.7	Wave Impedance for a Plane Wave	78
3.8	Radiation Resistance	78
3.9	Far Field of Antennas	79
3.9.1	Far Field for Wire Antennas	79
3.9.2	Far Field for Aperture Antennas	79
References	81	

CHAPTER 4

Antennas for Frequencies Below 1 MHz	83	
4.1	Mechanism of Radiation	83
4.2	Near and Far Fields of Antennas	84
4.3	Wave Impedance	85
4.4	Difference Between Receiving and Transmitting Antennas	86
4.5	Small Antennas	88
4.6	Baluns	88

4.7	Radiation Power Factor	89
4.7.1	Operating Efficiency	92
4.8	Matching Antennas	92
4.9	Effective Length and Effective Height	93
4.9.1	Effective Length	93
4.9.2	Effective Height	94
4.10	E-Field Antennas	95
4.10.1	Small Dipole	96
4.10.2	Short Monopoles	97
4.10.3	Ground Plane Dependence	98
4.10.4	Top-Loaded Monopoles	98
4.10.5	Parallel Element E-Field Generator	101
4.11	H-Field Antennas	102
4.11.1	Helmholtz Coils	102
4.11.2	Small Magnetic Loops	104
4.11.3	Single-Turn Shielded Loops	106
4.11.4	Simple Multiturn Loop Probe	108
	References	109

CHAPTER 5

	Antennas for Frequencies Between 1 MHz and 1 GHz	111
5.1	Resonant Monopoles	111
5.2	Discone Antenna	112
5.3	Cavitenna	114
5.4	Resonant and Large Dipoles	114
5.5	Folded Dipoles	115
5.6	Triangular Dipoles	118
5.7	Biconical Antennas	119
5.8	Yagi-Uda Antenna	122
5.9	Frequency-Independent Antennas	124
5.10	Log Periodic Antenna	124
5.11	BiLog [®]	130
5.12	Helical Antennas	132
5.13	Large and Resonant Loops	135
5.14	Double-Ridged Horn	137
	References	137
	Selected Bibliography	137

CHAPTER 6

	Antennas for Frequencies Above 1 GHz	139
6.1	Frequency-Independent Antennas	139
6.2	Band Theory	139
6.3	Log Spiral	141
6.3.1	Modes of Radiation	145
6.3.2	Rotation of Radiation Pattern with Frequency	146
6.3.3	Planar Log Spiral	146

6.3.4	Slot Planar Log Spiral	147
6.3.5	Cavity-Backed Spiral	153
6.3.6	Conical Log Spiral	153
6.4	Archimedes Spiral	163
6.4.1	Cavity-Backed Archimedean Spiral	163
6.5	Microstrip Planar Spiral	165
6.6	Discone Antenna	166
6.7	Double-Ridged Horns	168
6.7.1	Waveguide Theory	168
6.7.2	Modes in Square and Rectangular Waveguides	171
6.7.3	Double-Ridged Waveguides	175
6.7.4	Double-Ridged Waveguide Horns	177
	References	183
	Selected Bibliography	184

CHAPTER 7

	Calibration of Antennas	185
7.1	Gain	185
7.1.1	Measurement of Gain	186
7.1.2	Purcell's Method	191
7.1.3	Two-Antenna Method	195
7.1.4	Three-Antenna Method	195
7.2	Calculation of Gain	196
7.2.1	<i>E</i> -Plane Sectoral Horn	197
7.2.2	<i>H</i> -Plane Sectoral Horn	202
7.2.3	Gain of a Pyramidal Horn	207
7.3	Example	209
7.3.1	Accurate Method	210
7.3.2	Semi-Accurate Method	211
7.3.3	Approximate Method	211
7.4	Antenna Correction Factor	211
	References	217

CHAPTER 8

	Introduction to Electromagnetic Compatibility Measurements	219
8.1	Radiated Emissions	220
8.1.1	Differential and Common Mode Radiation	221
8.1.2	Measurement of Radiated Emissions	221
8.1.3	Classes of Computer Equipment	222
8.1.4	Measuring Radiated EMI	223
8.2	Radiated Susceptibility and Immunity	228
8.2.1	Immunity to Radiated Electric Field Strength	229
8.2.2	Immunity to Conducted Radiated Interference	229
8.2.3	Magnetic Field Immunity	231
8.2.4	Immunity to Electrical Fast Transients	231
8.2.5	Immunity to Electrostatic Discharges	233

8.3	Conducted Emissions and Immunity	234
8.3.1	Immunity to Conducted Common- and Differential-Mode Voltages	235
8.4	Shielding Effectiveness of Solid Materials	236
8.4.1	Reflection Loss	238
8.4.2	Absorption Loss	252
8.4.3	Multiple Reflection Loss	257
8.4.4	Total Shielding Effectiveness	258
8.5	Measuring Shielding Effectiveness	262
8.5.1	Magnetic or <i>H</i> -Mode SE Measurements	262
8.5.2	Electric or <i>E</i> -Mode SE Measurements	263
8.5.3	Plane Wave SE Measurements	263
8.5.4	Ventilation Holes	266
8.6	Electrostatic Discharge	266
8.6.1	ESD Spectrum	267
8.6.2	Direct and Indirect ESD	269
8.6.3	ESD Models	269
8.6.4	Testing for ESD Susceptibility	269
8.7	Instrumentation	270
8.7.1	Measuring Receivers	270
8.7.2	Spectrum Analyzers	271
	References	271
	Selected Bibliography	272

CHAPTER 9

	Theory and Applications of Measurement Sites and Enclosures	273
9.1	TEM Waves	273
9.1.1	Power Flux Density	274
9.1.2	Wave Impedance	275
9.1.3	TEM Transmission Lines	276
9.2	TEM Cells	283
9.2.1	Parallel Stripline Cells	283
9.2.2	Circular Coaxial TEM Cells	285
9.2.3	Rectangular and Square TEM Cells	288
9.3	Modes in Circular Waveguides	299
9.3.1	Cut-Off Waveguide Ventilation Panels	300
9.4	Resonant Cavities	305
9.4.1	Degeneracy	306
9.4.2	Mode Stirrers	306
9.5	Shielded Rooms	307
9.5.1	Unlined Shielded or Screened Rooms	307
9.5.2	Absorber-Lined Chambers	309
9.5.3	Anechoic Chambers	314
9.6	Open Area Test Sites	318
9.6.1	Free-Space OATS	322
9.7	Reverberation Chamber	323

9.7.1	Reverberation Chamber Requirements of EN 61000-4-21	326
9.7.2	Validation Procedure	327
9.7.3	Testing an EUT	329
9.7.4	Immunity Testing	331
9.8	Radiated Emissions	331
9.8.1	Free-Space Field	332
	References	333
Appendix A: List of Acronyms and Abbreviations		335
Appendix B: Preferred Scientific Prefixes		349
Appendix C: List of Scientific Constants		351
Appendix D: Conductivities of Common Metals		353
Appendix E: Dielectric Constants and Loss Tangents of Common Materials		355
Appendix F: Conversion Table for $\text{dB}\mu\text{V}$ to μV , dBV , dBW , dBm , and Watts		357
Appendix G: The Electromagnetic Spectrum		363
Appendix H: Frequency Band Designations		365
Appendix I: Conversion Between Gain in dB and Gain as a Linear Ratio Gain in dBi to Linear Gain		367
Appendix J: The Periodic Table Listed Alphabetically by Chemical Symbol		369
Appendix K: Magnetic Permeabilities of Common Metals		373
Appendix L: Polarization Matching Matrix		375
Appendix M: Resistivities of Common Materials		377
Appendix N: Radio Frequency Protection Guides for Nonionizing Radiation		379
Appendix O: List of Symbols		381
About the Authors		391
Index		393

Preface

This handbook is intended as a background and reference book primarily for electromagnetic compatibility (EMC) engineers, but others seeking specific or general information on antennas, as well as circuit design engineers and quality assurance managers, will also find it very useful. The treatment is essentially practical, but it aims to be authoritative and reliable. Postgraduate students studying electromagnetic theory, antennas and propagation, and EMC topics will also find this book invaluable in understanding the concepts of EM radiation.

This handbook explains the principles of antenna theory, without going into great mathematical detail. The reader is expected to have attained an academic level of Higher National Diploma (HND) or have had some practical experience as a test engineer in the EMC field.

The required characteristics of an antenna depend on the application. In general, for EMC applications, the larger the bandwidth, the fewer the number of antennas required to cover the total frequency range.

For emission testing and radio monitoring site surveys, the antenna should be omnidirectional and capable of receiving electric and magnetic fields of any polarization. Other practical considerations, such as using receivers that cover the same frequency ranges as the antennas, may also influence the antenna selection. Portability, weight, and size are obviously also very important considerations for site surveys.

For immunity and susceptibility testing, the antenna should also be broadband, but it has to be capable of handling high power, since it has to produce high electric or magnetic fields.

For shielding or screening effectiveness measurements, the transmitting antenna should be capable of handling high power, so that the required dynamic range can be produced. Both receiver and transmitter antennas should also be highly directional, so that only the field through the material under test is measured. However, at the low end of the frequency range, single element antennas cannot produce directional beams.

This book is written in such a way that each section in a chapter can be referred to independently, and, for instance, the reader does not have to read a chapter from the beginning in order to find the definition of a particular symbol. The details of each symbol are given after each equation. Although this may seem repetitious to the reader reading the book from the beginning, this approach is invaluable to the reader seeking to refer to a particular topic, not wishing to spend time looking up the meaning of symbols used in equations and formulas. Each chapter is also written so as to be fairly self-contained, although this was not always possible.

Reference to textbooks is given with the particular page or section number. This enables the reader to quickly access the particular topic, and the author considers this a welcome departure from references made to entire books, with the reader required to find the relevant section.

This book uses SI units throughout, and lists all the abbreviations and acronyms commonly used. The SI units avoid the use of the solidus (forward slash or division sign), and instead the use of negative indices is recommended. However, the solidus is commonly used in some cases, and has been retained in these cases.

Chapter 1 explains the main properties of an antenna in a qualitative manner, and is useful for the engineer not familiar with antennas or the jargon used. Chapters 2 and 3 assist engineers in the revision of the mathematics required for the theoretical side of engineering. These were requested by colleagues who felt that math textbooks were too complicated, and gave too much irrelevant detail that were not applicable to EM theory. These chapters are written in such a way that they can be omitted by those familiar with mathematics or by those who do not wish to study the theoretical aspects of antennas.

Chapters 4, 5, and 6 describe antennas that are classified according to frequency. They give the theoretical basis for the antennas, and also describe the practical aspects, so that engineers can deduce the electrical properties of an antenna by examination of the physical characteristics of the antenna. These chapters are followed by Chapter 7 on standard horns. These are used to calibrate antennas used for measurements. Chapters 8 and 9 provide an introduction to EMC measurements and the theory and applications of measurement sites and enclosures.

Finally, the appendices contain lists of acronyms, preferred scientific prefixes, scientific constants, conductivities, dielectric constants, conversions between decibels relative to one millivolt (dBmV) and volts or watts, symbols, the periodic table in alphabetic order, and frequency wavebands.

Every care has been taken in the preparation of the manuscript. However the author would appreciate any comments on the topics covered, or errors in the text, be they typographical or factual.

Introduction to Antennas

This chapter deals with antennas, without considering the theoretical aspects in any great depth. This enables EMC engineers to understand the main characteristics of an antenna in a qualitative manner, without recourse to the intricacies of Maxwell's equations. It also gives approximate formulas to enable engineers to obtain some key parameters, if other parameters are known. The main features required of an antenna for EMC and radio monitoring applications are also discussed.

An antenna is a device for radiating or receiving an electromagnetic radio signal. It transfers energy between a transmission line and free space, that is, it transforms a guided wave to a free space wave.

The term antenna is used as a generic term for both wire antennas such as dipoles, and for aperture antennas such as horns, reflectors, and so forth. However, its use is sometimes restricted to aperture antennas in the upper RF and microwave regions, that is, above about 300 MHz, whereas the term aerial is sometimes used at the lower frequencies.

1.1 Requirements of an Antenna for EMC

The important features required of an antenna depend on the application. For emission testing and radio monitoring site surveys, the antenna should ideally be omnidirectional, broadband, and capable of receiving electric and magnetic fields of any polarization. Other practical considerations, such as using receivers which cover the same frequency ranges as the antennas, may also influence the antenna selection. Portability, weight, and size are obviously also very important considerations for site surveys.

For immunity and susceptibility testing, the antenna should also be broadband, but it has to be capable of handling high power, since it has to produce high electric or magnetic fields.

For shielding or screening effectiveness measurements, the transmitting antenna should be capable of handling high power, and have high gain, so that the required dynamic range can be produced. Both receiving and transmitting antennas should also have narrow beamwidths, so that only the field through the material under test is measured.

In general, for EMC applications, the larger the bandwidth, the fewer the number of antennas required to cover the total frequency range.

1.1.1 Types of Antennas

Antennas can be broadly classified by the directions in which they radiate or receive electromagnetic radiation. They can be isotropic, omnidirectional, or highly directional.

An isotropic antenna is a hypothetical antenna which radiates uniformly in all directions, so that the electric field at any point on a sphere (with the antenna at its center) has the same magnitude. Figure 1.1 depicts the radiation obtained from an isotropic antenna. This cannot be realized in practice, since in order to radiate uniformly in all directions an isotropic antenna would have to be a point source. The nearest approximation to an isotropic antenna is a Hertzian dipole, which is a dipole that is very small in terms of wavelength. The length of a Hertzian dipole is about one hundredths of the wavelength at its operating frequency, and its pattern is still not isotropic.

An omnidirectional antenna is one that radiates uniformly in one plane. Examples of omnidirectional antennas are monopoles, dipoles, and biconicals. Figure 1.2 shows the radiation from a vertical dipole. The radiation is uniform in the horizontal plane, and in the vertical plane the cross section of the radiation is in the form of two circles.

A directional antenna is one that radiates most of its power in one particular direction. Examples of directional antennas are horns, reflector systems, log-periodics, and Yagis. Figure 1.3 shows the radiation from a reflector antenna. For a circularly symmetrical reflector, the radiation pattern is the same in all planes.

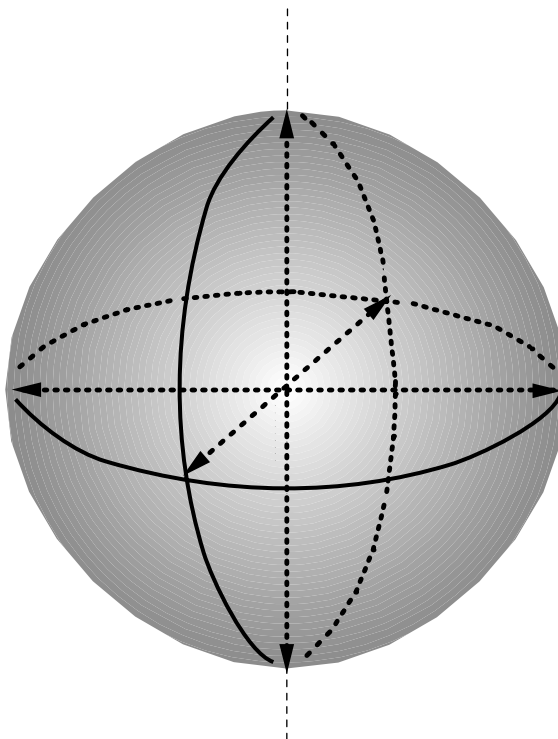


Figure 1.1 An isotropic antenna radiating uniformly in all directions.

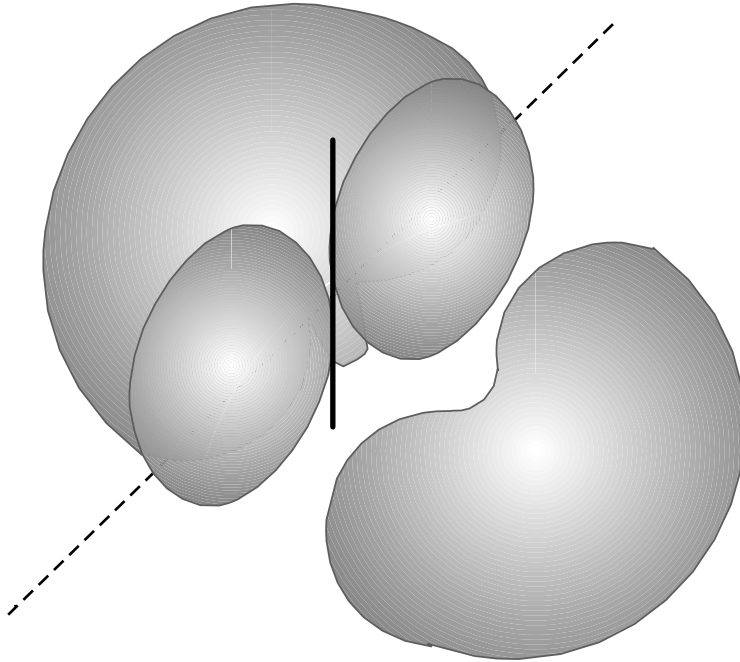


Figure 1.2 An omnidirectional dipole antenna.

1.2 Main Characteristics of an Antenna

An antenna is chosen for its use in a particular application, by consideration of its main physical, as well as its electrical, characteristics. We also need to ensure that the antenna performs in the desired manner in the particular measurement system.

An antenna can be characterized by the following factors, not all of which are meaningful to all antenna types:

- Its radiation resistance;
- Its radiation pattern;
- The beamwidth and gain of its main lobe;
- The position and magnitude of its sidelobes;

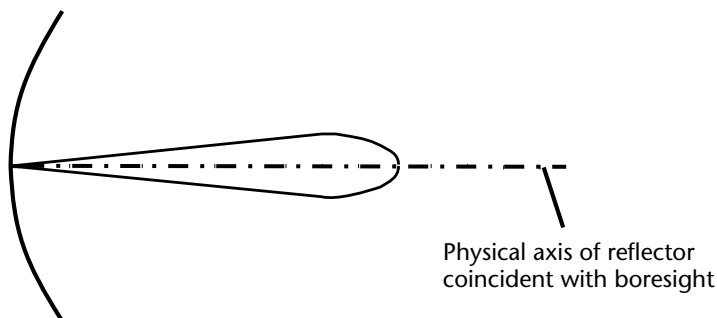


Figure 1.3 A directional reflector antenna.

- The magnitude of its backlobe;
- Its bandwidth;
- Its aperture;
- Its antenna correction factor (ACF);
- The polarization of the electric field that it transmits or receives;
- The power that it can handle.

There are two principal planes in which the antenna characteristics are measured. These are known as the azimuth and elevation planes, and can be considered as the horizontal and vertical planes, respectively, for land based antennas. The angles in the azimuth plane are conventionally denoted by the Greek letter phi (ϕ), and in the elevation plane they are denoted by the Greek letter theta (θ). In some cases however, the azimuth angles are denoted by θ and elevation angles by ϕ .

Some characteristics such as beamwidth and sidelobes are the same in both planes for symmetrical antennas, such as circular waveguide horns and reflectors. Other characteristics such as the gain on boresight (i.e., where the azimuth and elevation planes intersect) can only have a single value. In general, for unsymmetrical antennas the characteristics are different in the two principal planes, with a gradual transition in the intervening region between these two planes.

1.2.1 Radiation Resistance

We can consider an antenna as a load terminating the transmission line that feeds it. In the ideal case, this load will have an impedance that is purely resistive, that is, the load will not have any reactive component, such as an inductance or capacitance. In practice, the impedance of an antenna is made up of a self-impedance and a mutual impedance [1, p. 29]. The self-impedance is the impedance that would be measured at the terminals of the antenna when it is in free space, given no other antennas or reflecting objects in the vicinity. When the antenna is sufficiently isolated from other objects, this mutual impedance tends to zero. On the other hand, in some antennas such as the Yagi array, the operation depends on the mutual coupling between the driven element and the other parasitic passive elements. The self-impedance (Z_a) consists of a real part which is the resistance (R_a), and an imaginary part which is the self-reactance (X_a). In antennas such as the loop or dipole, the resistance and the reactance are in series. The self-impedance is given by

$$Z_a = R_a + jX_a \quad (1.1)$$

The antenna resistance, R_a , accounts for the power absorbed by the antenna and appearing at its terminals. This power is mainly reradiated by the antenna, but a small amount is dissipated by it in the form of ohmic losses in the antenna structure. The resistance of the antenna can thus be visualized as a sum of radiation resistance R_a and an ohmic loss resistor R_o , which dissipates a power of P_o . This ohmic power loss contributes to the loss of efficiency of the antenna and is of the order of fractions of a decibel [2, p. 39]. The rest of the power is radiated and is associated with a radiation resistance R_r . Thus the actual power P_r radiated by the antenna is given by

$$P_r = I^2 R_r \quad (1.2)$$

where I is the current.

At RF and lower frequencies, this concept of radiation resistance can be used because it is possible to define a unique driving point at which the antenna can be dissociated from the feed network and represented as a separate network. The magnitude of the impedances depends on the position of the driving point. In cases where the driving point is arbitrary, the equivalent circuit of the antenna can be either a series or parallel inductance-capacitance-resistance (LCR) network. In this case the radiation and ohmic resistances appear in parallel [2, p. 39]. Radiation resistances vary from 73Ω for a resonant dipole to 0.01Ω for a high-frequency (HF) notch antenna [1, p. 29].

1.2.1.1 Tuning Circuits

When the antenna has the same impedance as the transmission line that feeds it, the antenna is said to be matched to the line. When this occurs maximum power is transferred from the transmission line to the antenna. In general however, the impedance of the antenna is not the same as that of the transmission line. When the transmission line has a purely resistive impedance and the antenna has an impedance that contains a different resistive value, as well as a reactive part, the optimum transfer of power can be achieved by the use of tuning circuits between the transmission line and the antenna. In principle, these circuits consist of an LCR circuit in which the capacitance of the capacitor is altered in order to provide the maximum transfer of power.

1.2.2 Radiation Pattern

The antenna is a reciprocal device, that is, it radiates or receives electromagnetic energy in the same way. Thus, although the radiation pattern is identified with an antenna that is transmitting power, the same properties would apply to the antenna if it was receiving power. Any difference between the received or radiated powers can be attributed to the difference between the feed networks and the equipment associated with the receiver and transmitter. The antenna radiates the greatest amount of power along its boresight, and it also receives power most efficiently in this direction.

The radiation pattern is a very important characteristic of an antenna. It enables us to get a clearer idea of the key features of an antenna which cannot be obtained from the textual technical description of the antenna. For instance, when the sidelobe level of an antenna is quoted, this level pertains to the near-in lobes, and the average level of the two lobes is quoted, thus any asymmetry in the radiation pattern cannot be deduced. In textual technical descriptions, the level, position and number of other sidelobes are rarely quoted. In EMC measurements these other lobes and the positions of nulls can be very important, and knowledge of their details can enable the engineer to determine if a low level of received signal is attributable to a null, or if there is genuinely a low level in a particular direction.

The radiation pattern of an antenna is peculiar to the type of antenna and its electrical characteristics, as well as its physical dimensions. It is measured at

a constant distance in the far field of the antenna. The radiation pattern of an antenna is usually plotted in terms of relative power. The power at boresight, that is, at the position of maximum radiated power, is usually plotted at 0 dB, and thus the power at all other positions appear as negative values. In other words the radiated power is normalized to the power at boresight. If the power had been plotted in linear units, the normalized power would be one at boresight. The main reason for using decibels instead of linear power is because the power at the nulls is often of the order of 10,000 times less than the power on boresight and thus the scale would have to be very large to cover the whole range of power values.

The radiation pattern is usually measured in the two principal planes, the azimuth and the elevation planes. The radiated power is plotted against the angle made with the boresight direction.

If the antenna is not physically symmetrical about each of its principal planes, then we would also expect its radiation pattern in these planes to be unsymmetrical.

The radiation pattern can be plotted using rectangular/Cartesian or polar coordinates. The rectangular plots can be read more accurately (since the angular scale can be expanded), but the polar plots give a more pictorial representation and are thus easier to visualize; rather like an analogue clock, or plan position indicator (PPI) used in many radar sets.

1.2.2.1 Rectangular/Cartesian Plots

These are standard x - y plots where the axes are plotted at right angles to each other. The vertical, or y -axis, is used for the dependant variable, and the x -axis is used for the independent variable. The y -coordinate is called the ordinate, and the x -coordinate is called the abscissa. In a radiation plot, the angle with respect to boresight is varied and the magnitude of the radiated power is measured; thus the angle is the independent variable, and the power radiated is the dependent variable. The magnitudes of the powers are the ordinates and the angles are the abscissae. It is important to remember that the power radiated is measured in the far field. The graph paper used to plot radiation patterns is not standard in the mathematical sense. The x - and y -axes are not numbered in ascending order from the origin of coordinates, as in the case of standard graph paper. All values, whether negative or positive, are shown without a sign. A typical rectangular plot of an antenna radiation pattern is shown in Figure 1.4. The y -axis can show two sets of scales, one graduated from 0 to 4 dB, and another scale from 0 to 8 dB. Scales of 40 dB and 80 dB are obtained by multiplying the scales by 10. It should be noted that the zero is at the top, and thus the numbers below should really be shown as negative values of -4 dB and -8 dB. Similarly the x -axis can show three sets of angular scales of 5 degrees, 30 degrees, and 180 degrees on either side of the zero. These show the angles measured clockwise and counterclockwise from the boresight position, and in standard mathematical convention, these would be denoted by positive and negative signs, but on radiation graph paper the signs are omitted. Thus the radiation pattern can be plotted over 10 degrees, 60 degrees, or the whole 360 degrees. The engineer or technician who performs the measurements usually encircles or marks the scale used by ticking the relevant boxes in the key for each of the axes.

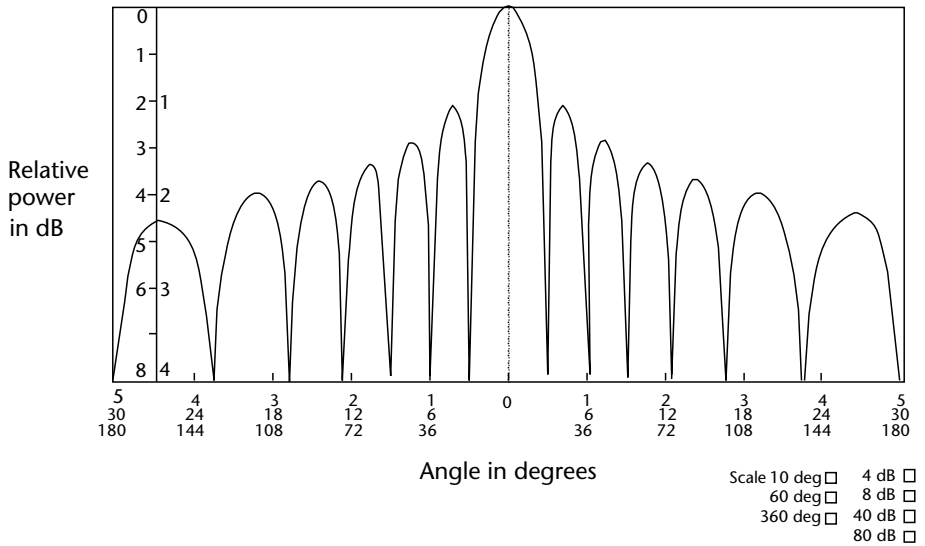


Figure 1.4 Rectangular plot of an antenna radiation pattern.

1.2.2.2 Polar Plots

In a polar plot the angles are plotted radially from boresight, and the intensity or power is plotted along the radius, as shown in Figure 1.5. This gives a pictorial representation of the radiation pattern of the antenna, and is easier to visualize than the rectangular plots. However, since the scale of the angular positions cannot be increased (i.e., they can only be plotted to scale from zero to 360 degrees),

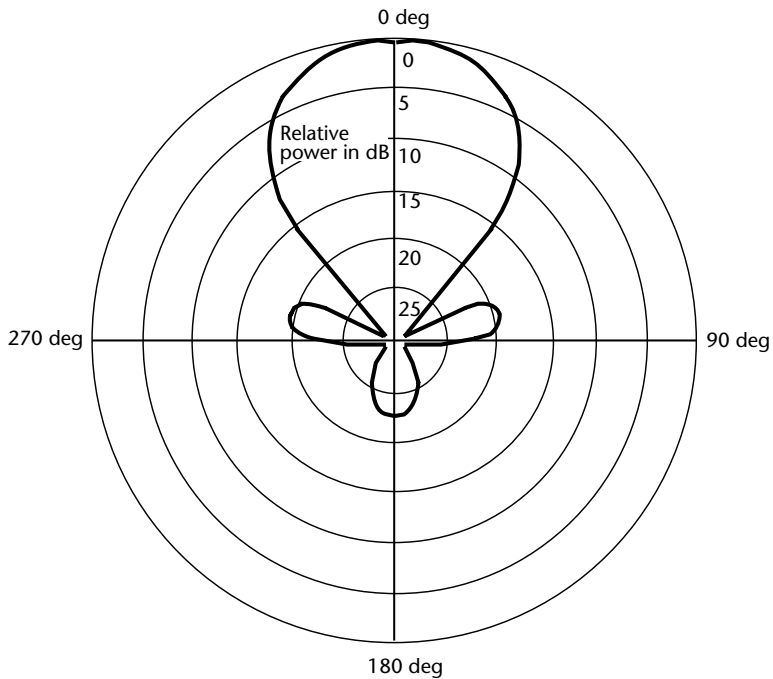


Figure 1.5 Polar plot of an antenna radiation pattern.

the accuracy cannot be increased as in the case of rectangular plots. The scale of the intensity or power however can be varied as in the case of rectangular plots. On polar plots, each circle represents a contour plot where the power has the same magnitude and is shown relative to the power at boresight. Since the power is, in general, a maximum value at boresight, these levels will always be less than the power at boresight and should thus be shown as negative values. However they are usually written without a sign, and should be assumed to be negative, contrary to standard arithmetic convention. Figure 1.5 shows levels from 0 dB to 25 dB in 5 dB steps. Some polar plots start at +10 dB as the maximum, go through the zero dB, and then down to -30 dB. In almost all cases the signs are omitted.

1.2.3 Main Lobe

The main lobe of an antenna is in the direction of maximum radiation. This is not necessarily on the physical main axis of the antenna, but this is generally the case for most antennas used for EMC applications. The characteristics of an antenna, such as the beamwidth and gain, are related to the main lobe alone. The peak of the main lobe is called the boresight of the antenna, and the radiation pattern is often positioned so that its boresight is coincident with the zero angular position of the graph, even when the antenna is not physically symmetrical. Figure 1.6 shows the radiation pattern of a symmetrical antenna.

1.2.3.1 Beamwidth—Half Power and 10 dB

The beamwidth only pertains to the main beam of the antenna and not the side lobes. The beamwidth of an antenna is, in general, inversely proportional to its physical size; so that the larger the antenna, the smaller its beamwidth for the same

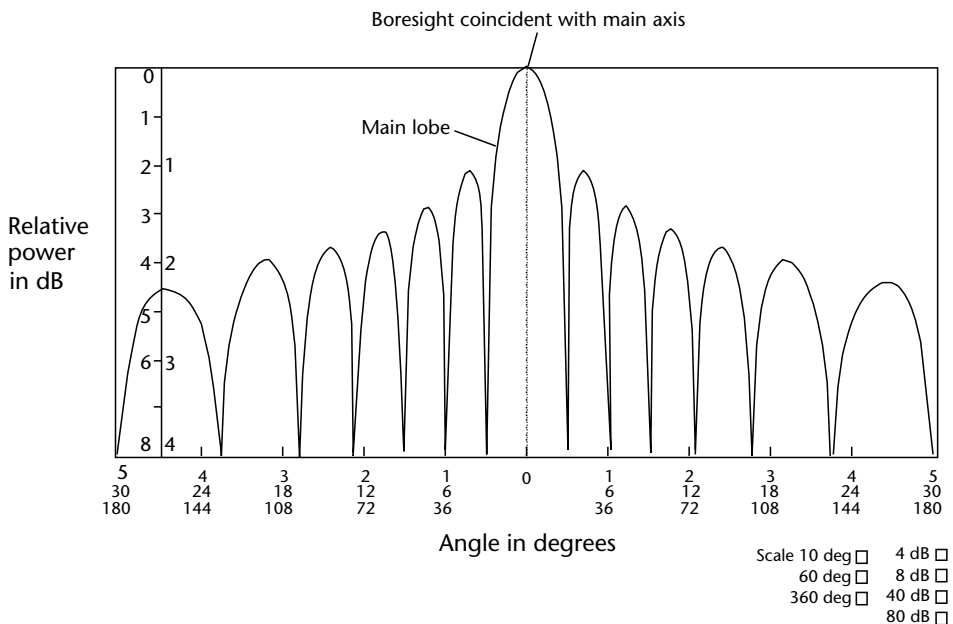


Figure 1.6 Rectangular plot of the radiation pattern of a symmetrical antenna.

frequency. If the antenna does not have the same dimensions in all planes, the plane containing the largest dimension will have the narrowest beamwidth. Thus, for a rectangular horn, as shown in Figure 1.7, the beamwidth in the horizontal, or azimuth plane AA' , is narrower than that in the vertical or elevation plane, BB' . The planes AA' and BB' are also known as the H (magnetic) and E (electric) planes respectively, for this type of antenna.

Definition of Beamwidth

The beamwidth of an antenna is commonly defined in two ways. The most well known definition is the 3-dB beamwidth, or half-power beamwidth (HPBW), but the 10-dB beamwidth is also used, especially for antennas with very narrow beams.

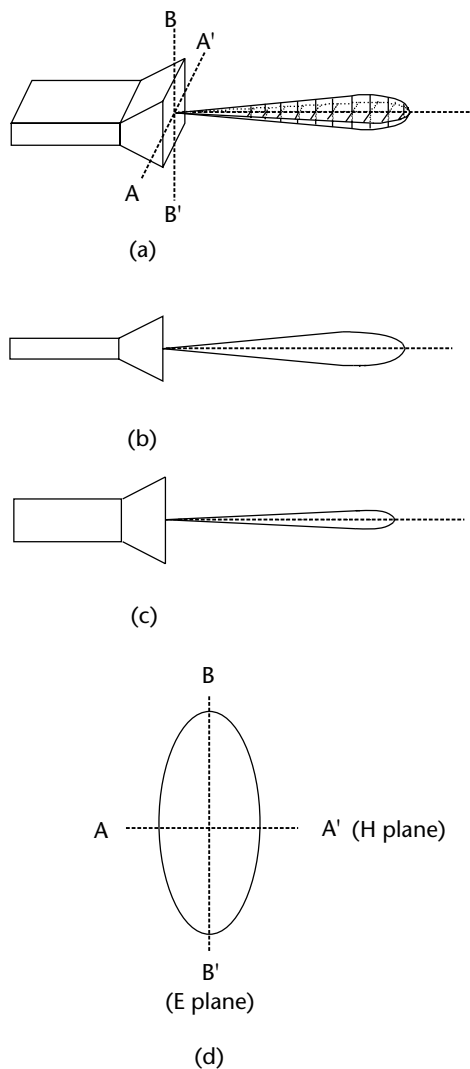


Figure 1.7 Main lobe of a rectangular pyramidal horn showing the beams in the principal planes. (a) Main lobe of a rectangular pyramidal horn; (b) side view showing the vertical or E plane beamwidth; (c) plan view showing the horizontal or H plane beamwidth; (d) Front view of the beams.

The 3-dB beamwidth (or half-power beamwidth) of an antenna is taken as the width in degrees (or sometimes in radians) at the points on either side of main beam where the radiated power is half the maximum value.

In Figure 1.8, the 3-dB level where the power is half that of the power at boresight occurs at points K and L on the radiation pattern. The difference in degrees can be read off the x -axis as 25 degrees, and this is the HPBW. The 10-dB beamwidth is the width in degrees (or sometimes in radians) at the points on either side of main beam where the radiated power is 10 dB, that is, one tenth of the maximum value.

The points on the radiation pattern of Figure 1.8 where the power is 10 dB (i.e., one tenth) below the power on boresight are at points M and N. The difference in degrees between these points is 44 degrees. Thus we say that the 10-dB beamwidth is 44 degrees.

1.2.3.2 Boresight Directivity/Gain

The terms directivity (or directive gain) and gain are often used synonymously but in fact they are not the same. The gain allows for the efficiency of the antenna, whereas the directivity does not. For instance, if we say that the linear directivity is 100 and the efficiency is 95%, then the gain of the antenna would be 95. In other words, the gain of the antenna is the product of the directivity and the efficiency. In general, the gain of the antenna is that quoted in the specification, and so we shall refer to this characteristic instead of the directivity.

The term gain is not the same as that of, for instance, an amplifier. An antenna is not usually an active device. We can think of an antenna as concentrating the electromagnetic energy in one particular direction, similar to the way in which the reflector of a torch concentrates the light from a lightbulb into a narrow, bright beam. The total light output is the same whether or not the reflector is present; but

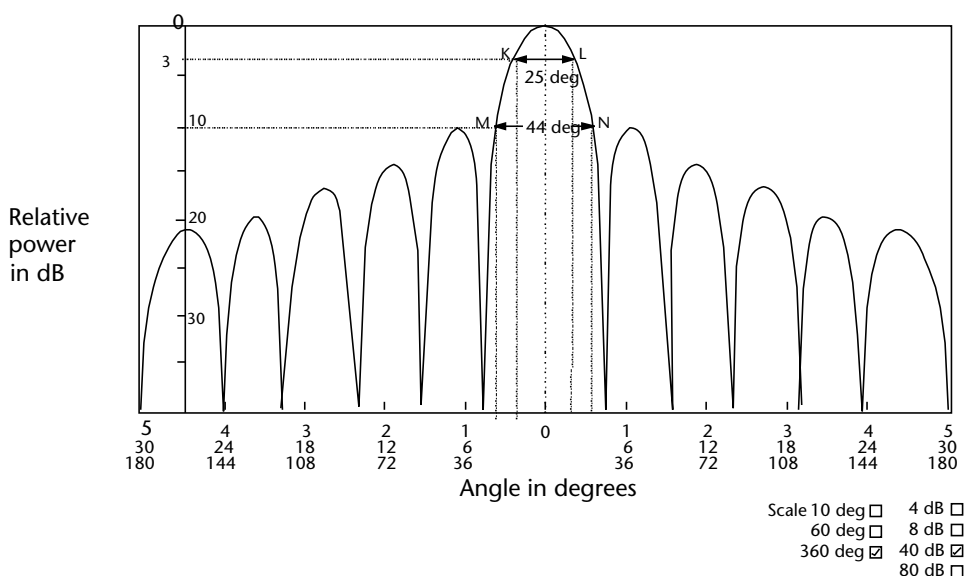


Figure 1.8 A radiation pattern showing the 3- and 10-dB beamwidths.

with the reflector the light is concentrated in just one direction, depending on the type and position of the reflector.

The IEEE distinguishes between the directivity of an antenna and the directivity in free space. They are explained in a qualitative manner in this chapter.

Directive Gain of an Antenna

This is defined as 4π times the ratio of the radiation intensity in a given direction to the total power radiated by the antenna. The factor of 4π relates to the total number of angles (in solid angles or steradians) at a point in three dimensions, just as 2π gives us the total number of angles (in radians) at a point in one plane. This can be considered as a measure of the ability of the antenna to concentrate the energy (that would normally be radiated over 4π solid angles or steradians) into a smaller number of angles.

Directive Gain in Physical Media

This definition of the gain of an antenna relates the power radiated by the antenna to that radiated by an isotropic antenna (that radiates equally in all directions) and is quoted as a linear ratio, or in dBi (for isotropic). When we say that the gain of an antenna is, for instance, 20 dBi (100 in linear terms), we mean that an isotropic antenna would have to radiate 100 times more power to give the same intensity at the same distance as that directional antenna.

The gain G as a linear ratio is defined as:

$$G = \frac{\{\text{power radiated on boresight}\}}{\{\text{power radiated by an isotropic antenna}\}}$$

The gain G_{dB} expressed in decibels is defined as

$$G_{\text{dB}} = 10\log_{10}(G) \quad (1.3)$$

To convert the gain in dB to the gain G as a linear ratio, the following formula is used:

$$G = 10^{(G_{\text{dB}}/10)} \quad (1.4)$$

The gains of antennas vary between about 2 dBi for a dipole to around 70 dBi for a ground station satellite antenna. These represent linear gain ratios of 1.58 and 10,000,000 respectively, compared to an isotropic antenna.

Relative and Absolute Gain

The radiation pattern of an antenna shows the power on boresight as 0 dB and the power in other directions as negative values. The gain in all directions is plotted relative to the gain on boresight. In order to find the absolute gain in any particular direction the gain on boresight must be known. If this gain is in decibels then this value can just be added to the gain at any point to give the absolute gain. However,

if the boresight gain is given as a linear ratio then this has to be converted to dB using the formula:

$$G_{\text{dB}} = 10\log_{10} \{\text{the gain as a linear ratio}\} \quad (1.5)$$

The absolute gain on boresight is measured by comparison with a standard gain antenna. A standard gain antenna is a reference one that has its gain calculated or measured to a high degree of accuracy.

1.2.4 Sidelobe

The sidelobes are, strictly speaking, any of the maxima marked A, B, C, D, and so forth in Figure 1.9. However, in practice only the near-in lobes marked A are referred to as sidelobes. Sometimes, the irregularities in the main beam of the radiation pattern mean that there are small peaks, such as those marked F in Figure 1.9, that could be mistaken for sidelobes. For this reason, the sidelobes are sometimes defined as the peaks where the difference between the peak and an adjacent trough is at least 3 dB. The sidelobes are characterized by their level below the boresight gain and their angular position relative to boresight.

1.2.4.1 Sidelobe Level

The sidelobe level is usually quoted as the level below the boresight gain. Since the radiation pattern is plotted with the boresight gain at 0 dB, the sidelobe level should be quoted in negative dB. However the sidelobe level is usually quoted as a positive quantity. Where the sidelobe levels are different, the average level is taken. The absolute level of the sidelobe can only be calculated if the absolute boresight gain is known.

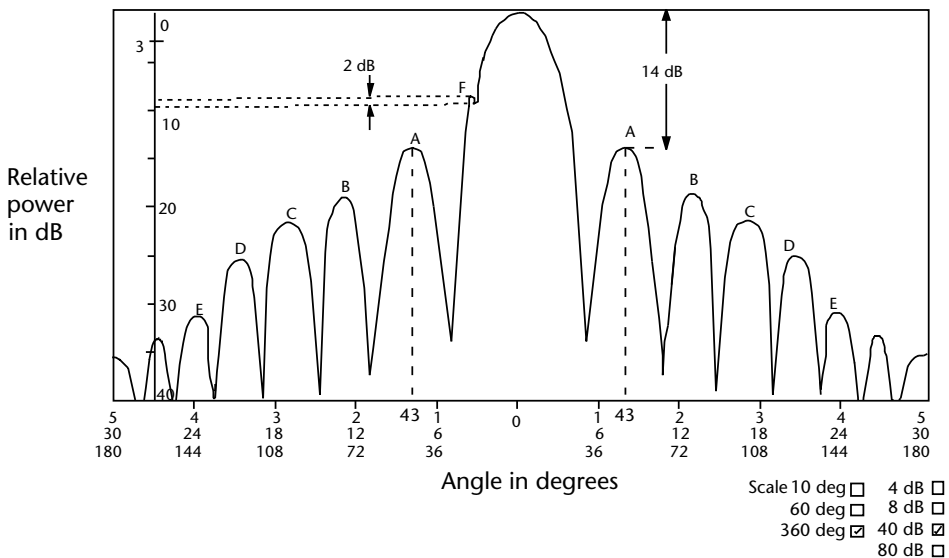


Figure 1.9 A radiation pattern showing the sidelobe levels and positions.

An aperture antenna such as a reflector can be illuminated by its feed in several ways. If we say that it is uniformly illuminated, we mean that the magnitude of electric field across its aperture has a constant value and the phase at each point is the same. This type of illumination will produce a radiation pattern with the narrowest beamwidth, but this is accompanied by the highest level of sidelobe. Adjustment of the phase and/or magnitude of the illumination can result in reduction of the sidelobe level but this usually also broadens the beamwidth.

For an antenna that is symmetrical about its main physical axis, the radiation pattern is, in general, also symmetrical. Thus the level of the sidelobes on opposite sides of the main beam would be the same. If the antenna is not physically symmetrical about its principal axis, then we would also expect its radiation pattern to be unsymmetrical. The level of the sidelobes on either side of the main beam would also be different if the antenna was unsymmetrical. The radiation pattern shown in Figure 1.9 is that of a symmetrical antenna, and thus both the main sidelobe levels are the same at a level of -14 dB.

1.2.4.2 Sidelobe Position

The angular position of the sidelobes relative to the position of the main beam is usually quoted in degrees rather than radians. For a physically symmetrical antenna, where the radiation pattern is not symmetrical, the average of the two angular positions is taken as the sidelobe angular position. Figure 1.9 shows the radiation pattern of an antenna that is symmetrical about its physical axis. The sidelobes are at equal angles of 43 degrees off boresight.

1.2.5 Front-to-Back Ratio

The front-to-back ratio is a measure of the ability of a directional antenna to concentrate the beam in the required forward direction. In linear terms, it is defined as the ratio of the maximum power in the main beam (boresight) to that in the backlobe. It is usually expressed in decibels as the difference between the levels on boresight and at 180 degrees off boresight. In Figure 1.10, the backlobe is shown at the 180 degree position as being 35 dB below the level at boresight. In linear terms, this means that the level of the backlobe is 3,162 times less than the level on boresight. In decibels, the front-to-back ratio is a difference of +35 dB, in this case, but the sign is usually omitted.

1.2.6 Bandwidth

The bandwidth of an antenna is a measure of its ability to radiate or receive different frequencies. The bandwidth is the range of frequencies that the antenna can receive (or radiate) with a power efficiency of 50% (0.5) or more, or a voltage efficiency of 70.7% (that is, $\sqrt{0.5}$). A wide bandwidth is achieved at the expense of gain. In other words, if the antenna had the same size but a narrower bandwidth, its gain would be higher. The operating frequency range is specified by quoting the upper and lower frequency, but bandwidth is often quoted as a relative value.

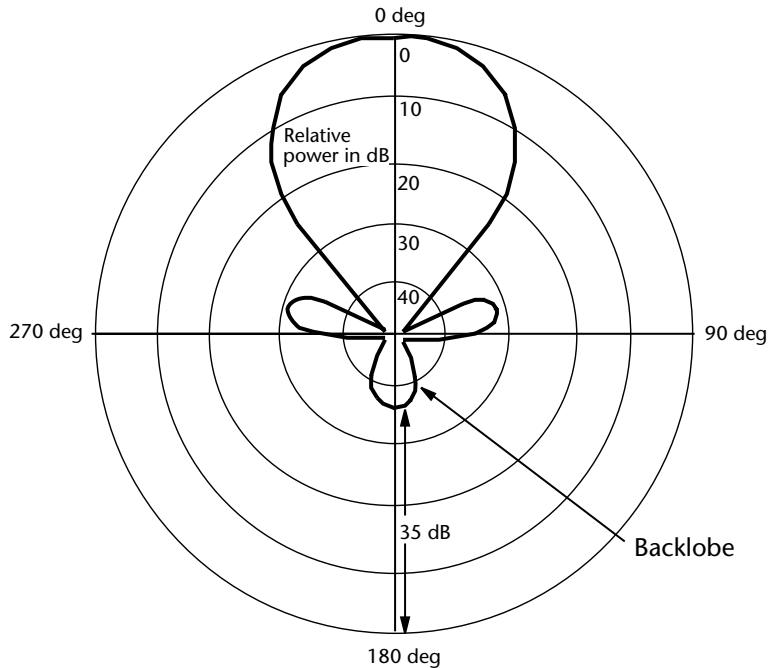


Figure 1.10 An antenna radiation pattern showing the backlobe.

The bandwidth is commonly expressed in one of two ways; either as a percentage or as a fraction or multiple of an octave. (An octave is a band of frequencies, between one frequency and the frequency that is double or half the first frequency: for instance, we have an octave between 10 MHz and 20 MHz.) When it is expressed as a percentage bandwidth, its center frequency should be quoted, and the percentage expressed relative to this center frequency. When it is expressed in octaves, its lower and upper frequencies should also be quoted.

1.2.6.1 Percentage Bandwidth

When the bandwidth is expressed in terms of a percentage, it is defined by the following relation

$$B_w = \left(\frac{\Delta f}{f} \right) \times 100 \quad (1.6)$$

where f is the frequency at the center of the band and Δf is the difference between the lowest and highest frequency of operation.

Example: An antenna can be used over the frequency range from 1 to 2 GHz. Express this as a percentage bandwidth.

Solution: First we take the difference between its upper and lower frequencies, which is 1 GHz. The center frequency in this case is the average of 1 and 2 GHz, that is, 1.5 GHz. Thus Δf is 1 GHz and f is 1.5 GHz. Using (1.6), we get $B_w = 66.7\%$.

The bandwidth of the antenna can be described as 66.7% at 1.5 GHz, or 1.5 GHz \pm 33.35%, or 1.5 GHz \pm 0.5 GHz.

1.2.6.2 Bandwidth as a Fraction or Multiple of an Octave

When the bandwidth is expressed in terms of a fraction or multiple of an octave, it is defined by the following relation

$$B_w = \log_2 \left(\frac{f_{\text{high}}}{f_{\text{low}}} \right) \quad (1.7)$$

where f_{high} is the highest frequency of operation and f_{low} is the lowest frequency of operation.

Many calculators do not have logs to the base 2. In these cases we can still obtain logs to this base by using the following formula

$$\log_2 \left\{ \frac{f_{\text{high}}}{f_{\text{low}}} \right\} = \frac{\log_{10} \left\{ \frac{f_{\text{high}}}{f_{\text{low}}} \right\}}{\log_{10} 2} \quad (1.8)$$

Example: An antenna is quoted as having an operating frequency range from 500 MHz to 9 GHz. What is its frequency bandwidth in octaves?

Solution: The ratio of the upper frequency to its lower frequency is 18. If we do not have a calculator that can give us logs to a base of 2, and we want to find the $\log_2 18$, we must divide $\log_{10} 18$ by the $\log_{10} 2$. The result is 4.17 octaves to two decimal places.

1.2.7 Aperture Size

The aperture of an antenna governs the size of its beamwidth. In general, the larger the aperture, the narrower the beamwidth, and the higher the gain at a given frequency. The aperture size can be defined in two ways; either in terms of the actual physical size, in meters or feet, or in terms of wavelength. For instance, if we say that an antenna has an aperture of two wavelengths, then its actual physical size depends on its operating frequency. At a frequency of 1 GHz, the physical aperture is 60 cm, whereas at 10 GHz, its physical aperture is only 6 cm. It is more meaningful to refer to an antenna size in terms of its operating wavelength when the antenna is a narrowband or single frequency one, because its beamwidth and gain are directly related to the aperture in terms of its operating wavelength. In this case we have to calculate its wavelength to find its physical dimensions. However, in the case of broadband antennas, its physical size is more appropriate because there is a range of operating wavelengths.

1.2.8 Antenna Correction Factors

When an EMC engineer performs a site survey, for instance, they want to measure the maximum electric field strength or intensity at a particular location. However,

the receiver reading is displayed in terms of voltage or decibels relative to one volt (dBV). The engineer has to convert this value to the electric field intensity that is actually present at the position at which the antenna has been placed. In order to obtain this value, the engineer has recourse to a set of tables or graphs showing the relationship between the receiver reading and the electric field intensity for that particular antenna, covering its operating frequency range. This correction factor is sometimes just called the antenna factor.

The IEEE dictionary defines the antenna correction factor as a term or factor which is applied to the reading of the receiver to enable the reading to be converted to the field strength in either volts per meter (electric field strength) or amperes per meter (magnetic field strength). This factor takes into account:

- The effective height/length of the antenna;
- The loss in the balun matching network between the antenna and the balun;
- The loss due to the mismatch between the balun matching network and the transmission line connecting the balun to the receiver;
- The loss due to the total length of the transmission line cables between the antenna and the receiver.

To be more accurate, the antenna factor should also take into account the proximity of the antenna to ground and the frequency of measurement. The unit of antenna factor is m^{-1} in linear terms and it is the ratio of the electric field strength at the antenna and the voltage reading of the receiver. Thus, the antenna factor A_f is given by

$$A_f = \frac{E}{V} \quad (1.9)$$

However, we are usually given the antenna factor in dB, and the gain of the antenna is also given in dB. We must add the antenna factor to the gain of the antenna. Then, we must convert this value A_f in dB to a linear value using the following formula;

$$A_f = 10^{(A_f/20)} \quad (1.10)$$

This linear value, A_f is the number by which we must multiply the receiver reading to obtain the true electric field at the antenna location.

1.2.9 Polarization

Although this could apply equally to the magnetic or electric polarization, it is used almost exclusively to describe the shape and orientation of the locus of the extremity of the electric field vector as it varies with time at a fixed point in space. This locus could be a straight line, an ellipse, or a circle.

1.2.9.1 Linear Polarization

In the case of linear polarization, the electric field varies sinusoidally in one plane, as depicted in Figure 1.11. This shows the variation with time at a fixed point in space. It is important to realize that a similar variation with distance also exists. Figure 1.11 shows the case for vertical polarization. Note that the extremity of the electric field vector at any fixed point in space is a straight line with a maximum value that is equal to twice the amplitude of the sine curve that depicts the variation of the electric field with time.

Horizontal polarization is shown in Figure 1.12. The electric field can also be polarized at any other angle between 0 and 90 degrees to the horizontal. However, in general the only other angle commonly used is 45 degrees. This is known as slant polarization.

The polarization of a receiving antenna must match that of the incident radiation to detect the maximum field. If the angles are not the same, only the component that is parallel to the plane of incident polarization will be detected. If we have a vertically polarized antenna, and the incident radiation is slant polarized, the magnitude of its component in the vertical plane will be reduced by a factor of $\cos(45 \text{ degrees})$. Thus only $1/\sqrt{2}$ or 0.707 of the electric field will be received. Since the radiated power is proportional to the square of the electric field, the power received will only be half (0.707^2) of the incident power.

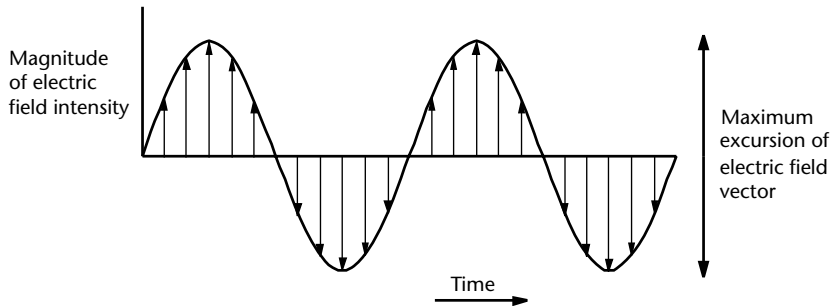


Figure 1.11 Variation of an electric field with time at a fixed point in space for vertical polarization.

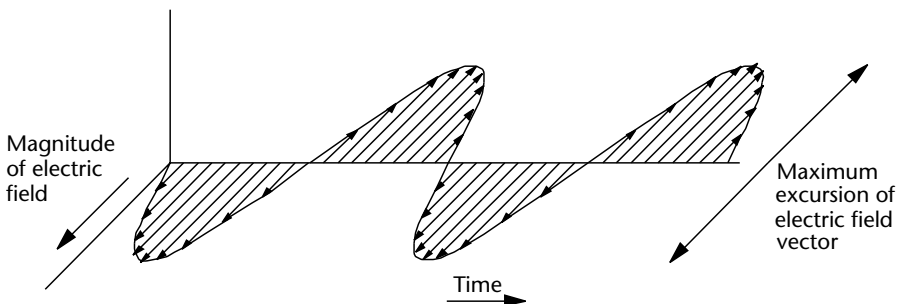


Figure 1.12 Variation of an electric field with time at a fixed point in space for horizontal polarization.

1.2.9.2 Elliptical or Circular Polarization

Circular polarization is a special case of elliptical polarization, and thus elliptical and circular polarizations are considered together in this section.

The axial ratio is the ratio of the major to minor axis. When this ratio is equal to one that is, the major and minor axes are equal, we have circular polarization. Whereas when it is infinite it means that the minor axis is zero, in essence, we have linear polarization.

It should be noted that the axial ratio, ξ , is not the same as the mathematical definition of the ellipticity of an ellipse. The ellipticity E_1 varies between 0 and 1. The ellipticity E_1 and axial ratio are related by the following equation:

$$E_1 = 1 - \frac{1}{\xi} \quad (1.11)$$

Circular polarization is a difficult concept to visualize. The electric field vector at each point in space sweeps out a circle, through each period in time. Circular polarization can be generated by two electric vectors of equal magnitude that are orthogonal (at right angles) and are also in-phase quadrature, that is, in the time domain they are 90 degrees out of phase with each other. Consider the two electric vectors depicted in Figure 1.13(a), showing the variation of the electric field in two directions, y and x , that are perpendicular to each other. At a time denoted by point A, the electric field is at a maximum, say of value one in the x -direction, and zero in the y -direction. Thus, the resultant is one in the x -direction, as shown in Figure 1.13(c). One eighth of a period later, the electric fields in both the x - and y -directions are 0.707, as depicted in Figure 1.13(b). The resultant is (using Pythagoras' theorem) $\sqrt{(0.707)^2 + (0.707)^2}$, which is equal to one, but note that this is at an angle of 45 degrees to the resultant at A. This is at 45 degrees to both the y - and x -directions. At intermediate positions between A and B the resultant is still one, but at angles between 0 degrees and 45 degrees to the resultant at A. At C, a further one eighth of a period later, the electric field is zero in the x -direction, but it has the maximum magnitude of one in the y -direction. Thus, the resultant is now one in the y -direction, which is at right angles to the resultant vector at A. If we look at successive times, we can see that the resultant vector retains a value of one, but presents successively increasing angles with the initial resultant vector at A, until a whole period later at H when the resultant vector has a value and angle coincident with the resultant at A. Thus, we can see that in the time interval representing one period in time, the electric field has maintained its magnitude of one, but has rotated through 360 degrees, or one revolution.

In the case of elliptical polarization, the electric field vectors may also be orthogonal (perpendicular to each other) and in-phase quadrature, but they may not have the same magnitude. Elliptical polarization may also result if the orthogonal electric fields have the same magnitudes, but they have a phase relationship that is not 90 or 270 degrees. Other cases of elliptical polarization could be the result of orthogonal electric fields that are of unequal magnitudes and not in-phase quadrature. Figure 1.14 shows two examples of elliptical polarization. In Figure 1.14(a), the major

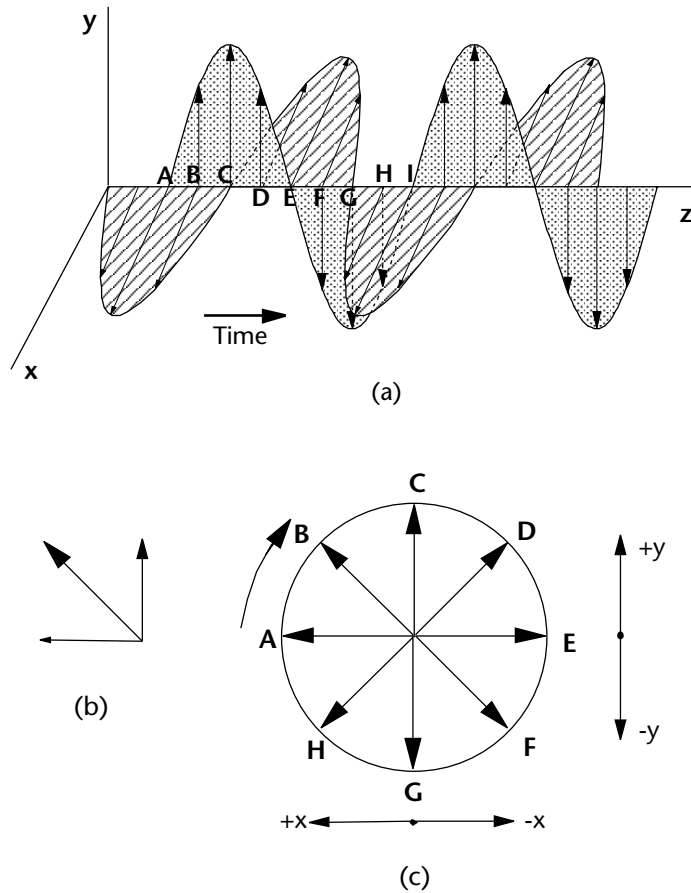


Figure 1.13 Circular polarization produced by two-plane polarized orthogonal waves in-phase quadrature. (a) Two plane polarized waves at right angles and in-phase quadrature, (b) summation of vectors at time B, (c) resultants of the two electric vectors over one period.

axis is vertical, whereas in Figure 1.14(b) the major axis is horizontal. If the ratio of the major to minor axis in either of these cases is infinity, this would mean that the minor axis has a magnitude of zero, and we would have linear polarization of vertical or horizontal orientation.

Sense of Polarization

In the example shown in Figure 1.13, the electric field vector rotates in a clockwise direction. We call this clockwise rotation of the electric field vector right-hand circular polarization (RHCP). If the resultant vector were to move in a counterclockwise direction, the wave would be a left-handed circular polarized (LHCP) wave. An LHCP wave would have resulted if either of the component electric field vectors had started half a period later. For instance if the vertical electric field had commenced with the field shown at E, the vertical electric field an eighth of a period later would have been 0.707 in the negative y-direction, that is, downwards. This would give a resultant of magnitude one at 45 degrees between the positive x- and the negative y-directions. The resultant electric field has rotated in the counterclockwise direction.

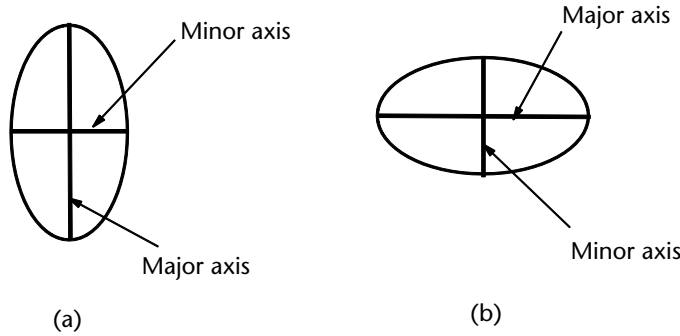


Figure 1.14 Two cases of elliptical polarization (a) Major axis vertical (b) Major axis horizontal

1.2.10 Relationships Between the Key Parameters

The characteristics of an antenna are not always quoted by the manufacturers. In general though, we can usually deduce the unknown parameters if sufficient information is given. These formulas do not take into consideration losses in the receiving system, and apply only to ideal conditions. The formulas also assume that the aperture of the antenna is very large in terms of the wavelength at the operating frequency.

1.2.10.1 Gain from Beamwidth

The gain of an antenna depends on the individual gains in the elevation and azimuth planes. The gains in these planes are inversely proportional to the half-power beamwidths. The narrower the beamwidth, the higher the gain.

The rectangular aperture could be a horn or any other aperture. The formulas for both are given here, for completeness, although the EMC engineer will most probably only encounter horns in the general course of measurements.

Rectangular Aperture with Uniform Illumination

For a uniformly illuminated aperture, the sidelobe level is 13 dB below the main beam. The linear gain for this type of rectangular aperture, assuming 100 % efficiency, is given by [3, p. 14]

$$G = \frac{41,300}{(\theta_1 \theta_2)} \quad (1.12)$$

where θ_1 and θ_2 are the half-power beamwidths (in degrees) in the two orthogonal planes.

Conical Log Spiral

The linear or numeric directivity, with respect to a circularly polarized isotropic source of a conical log spiral with a small cone angle, can be calculated from the HPBW's in the orthogonal planes from the formula [4, p. 493]

$$D = \frac{32,000}{(\theta_1 \phi_1)} \quad (1.13)$$

where θ_1 and ϕ_1 are the HPBW's in the two orthogonal planes in degrees and D is the linear directivity.

Rectangular Horn

In the case of a rectangular horn, the illumination across the aperture is not uniform, and the efficiency is of the order of 60%. In the H plane, which is along the larger dimension a , the electric field has a half-sinusoidal variation, as shown in Figure 1.15, and the sidelobe level is 26 dB below the main beam. The sidelobe level in the E plane, or along the narrow dimension b , is 13 dB. The linear gain of the horn on boresight, is given by

$$G = \frac{31,000}{(\theta_1 \theta_2)} \quad (1.14)$$

where θ_1 and θ_2 are the HPBW's in degrees in the E and H planes (i.e., along the a and b dimensions).

Circular Aperture with uniform illumination

For an antenna with a circular aperture and uniform illumination, the beamwidths are the same in all the planes, and the sidelobe level is 18 dB below boresight. The linear gain G of a circular aperture antenna, assuming 100% efficiency, is given by

$$G = \frac{52,000}{(\theta^2)} \quad (1.15)$$

where θ is the beamwidth in degrees in each of the planes.

Circular Aperture with Nonuniform Illumination

If the circular aperture has nonuniform illumination, such that there is a 10-dB taper across the aperture (i.e., the variation between the center and edge is 10 dB)

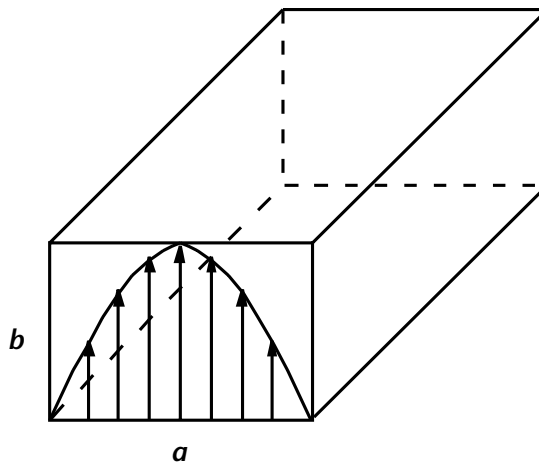


Figure 1.15 Electric field variations across a rectangular waveguide supporting the fundamental mode.

then the sidelobe level is reduced to 26 dB below that of the main beam. In this case, the efficiency of the antenna is also reduced to about 50 %, and the linear gain is given by

$$G = \frac{26,000}{(\theta^2)} \quad (1.16)$$

1.2.10.2 Beamwidth from Aperture Size and Shape

The beamwidth of an antenna is different in each plane, except for antennas with circular symmetry about boresight. Even in the case of circular symmetrical reflectors, the beamwidths are not necessarily the same in all planes. The larger the dimension in a particular plane, the narrower the beamwidth is in that plane.

Beamwidth of a Rectangular Horn

For a rectangular horn, the broad dimension is known as the H plane, the electric field in this plane is not uniform, and has a variation as is shown in Figure 1.15. This variation produces a sidelobe level of 26 dB below that of the main beam. Because this dimension is larger than the E plane, or narrow dimension, the beamwidth in this plane is smaller. The HPBW [5, p.9] in degrees is given by

$$\theta_B = \frac{67\lambda}{a} \quad (1.17)$$

where λ is the wavelength, and a is the dimension of the broadside of the waveguide. The wavelength and the broadside dimension can be measured in meters, centimeters, or inches, as long as the units used for λ and the dimension a are the same.

In most cases, we are quoted the frequency rather than the wavelength. It is therefore more convenient to use a formula involving the frequency, such as

$$\theta_B = \frac{20,100}{aF} \quad (1.18)$$

where F is the frequency in MHz and, in this case, the dimension a must be in meters.

For the E plane (the narrow dimension b of the waveguide), the sidelobes are only 13 dB below that of the main beam, and the beamwidth is wider than that in the H plane. The equivalent formulas for the beamwidth are

$$\theta_E = \frac{56\lambda}{b} \quad (1.19)$$

where λ is the wavelength, and b is the narrow dimension of the waveguide. The wavelength and the broadside dimension can be measured in meters, centimeters, or inches, as long as the units used for λ and the dimension b are the same.

In most cases, we are quoted the frequency rather than the wavelength. It is therefore more convenient to use a formula involving the frequency, such as

$$\theta_E = \frac{16,800}{bF} \quad (1.20)$$

where F is the frequency in MHz and b is in meters.

Example: A standard-gain rectangular waveguide horn operating at 10 GHz has an aperture of 36 cm \times 20 cm. Calculate the beamwidths in each of its principal planes.

Solution: The principal planes referred to in this case are the E and H planes. The dimensions a and b will be 0.36m and 0.2m, and the frequency is 10,000 MHz. Using (1.18) we get the H plane beamwidth as

$$\theta_B = \frac{20,100}{0.36 \times 10,000}$$

This gives a beamwidth of 5.6 degrees in the H plane.

Similarly, using (1.20) gives an E plane beamwidth of 8.4 degrees. Note that these values are for ideal antennas and do not allow for efficiencies of less than 60%. In practice, the efficiency would be less than 60%, and the measurement would introduce further errors, so that the actual beamwidth obtained could be about 1.5 times the calculated value.

1.2.10.3 Gain from Aperture Size and Shape

The gain of an antenna depends on the shape and size of the aperture, as well as the electric field distribution across the radiating aperture. The electric field distribution is commonly referred to as aperture illumination.

Rectangular Horn

The maximum linear gain is on boresight, and is thus where the E and H planes intersect. For a rectangular horn, the illumination across the aperture is not uniform. This reduces the efficiency of the horn to about 60%, but this nonuniform illumination produces lower sidelobe levels, typically of the order of 26 dB below the main beam. In addition, it should be noted that the broadband ridged waveguide horns, in common usage, will not have a gain as high as a normal smooth-walled rectangular pyramid horn. The ridged waveguide horn sacrifices the higher gain for its wider bandwidth characteristic.

For a horn of dimensions a and b , the linear gain G is given by

$$G = \frac{8ab}{\lambda^2} \quad (1.21)$$

where λ is the wavelength.

Note that the units used for the dimensions a and b , can be expressed in any form, that is, metric or imperial, as long as the same units are also used for the wavelength.

In most cases, we are quoted the frequency rather than the wavelength. It is therefore more convenient to use a formula involving the frequency. Moreover,

instead of calculating the linear gain, it could be calculated in decibels referred to isotropic (dBi) as

$$G_{\text{dB}} = 10 \log_{10} \left\{ \frac{abF^2}{11,250} \right\} \quad (1.22)$$

where a and b are the dimensions of the aperture of the waveguide in meters, and F is the frequency in MHz.

If the dimensions of the waveguide are given in centimeters, and the frequency in MHz, the gain in dBi can be calculated from the following formula

$$G_{\text{dB}} = 10 \log_{10} \left\{ \frac{abF^2}{1.125} \right\} \quad (1.23)$$

Rectangular Aperture with Uniform Illumination

For a uniformly illuminated aperture, the efficiency can approach 100%, but the sidelobe level is also high; typically of the order of 13 dB below the level of the main beam.

The linear gain G for a uniformly illuminated aperture, with 100% efficiency, and dimensions a and b , is given by

$$G = \frac{16ab}{\lambda^2} \quad (1.24)$$

Note that the units used for the dimensions a and b can be expressed in any form, as long as the same units are also used for the wavelength.

In most cases, we are quoted the frequency rather than the wavelength. It is therefore more convenient to use a formula involving the frequency. We could also calculate the gain in dBi, instead of the linear gain

$$G_{\text{dB}} = 10 \log_{10} \left\{ \frac{16abF^2}{90,000} \right\} \quad (1.25)$$

where a and b are the dimensions of the aperture of the waveguide in meters and F is the frequency in MHz.

If the dimensions of the waveguide are given in centimeters, and the frequency in MHz, the gain in dBi can be calculated from the following formula

$$G_{\text{dB}} = 10 \log_{10} \left\{ \frac{16abF^2}{9} \right\} \quad (1.26)$$

Circular Aperture

The circular aperture could be a parabola or any other aperture, such as a circular horn. The formulas for both are given here for completeness, although the

EMC engineer will most likely only encounter parabolas in the general course of measurements.

Circular Aperture with Uniform Illumination

For an aperture with uniform illumination, such as a parabola, the efficiency may be as high as 100%, but the sidelobe level is of the order of 13 dB below the level of the main beam.

The linear gain G for a uniformly illuminated aperture, with 100% efficiency, and diameter a , is given by

$$G = \frac{10ab}{\lambda^2} \quad (1.27)$$

Note that the units used for the dimension a can be expressed in any form, metric or imperial, as long as the same units are also used for the wavelength.

In most cases, we are quoted the frequency rather than the wavelength. It is therefore more convenient to use a formula involving the frequency. We could also calculate the gain in dBi, instead of the linear gain.

$$G_{\text{dB}} = 10 \log_{10} \left\{ \frac{(aF)^2}{9,000} \right\} \quad (1.28)$$

where a is the diameter of the aperture of the parabola in meters and F is the frequency in MHz.

If the diameter of the parabola is given in centimeters and the frequency in MHz, the gain in dBi can be calculated from the following formula

$$G_{\text{dB}} = 10 \log_{10} \left\{ 10 \frac{(aF)^2}{9} \right\} \quad (1.29)$$

Circular Aperture with Nonuniform Illumination

A circular aperture having an illumination taper can be used to give a reduced sidelobe level. In this case, the illumination at the center is higher than that at the edges. For instance, if we say that the taper is 10 dB, we mean that the power at the edges of the parabola is 10 dB (or 10 times) lower than that at the center. The sidelobe level is reduced to 26 dB below that of the main beam, but the efficiency is also reduced to the order of 50%.

The linear gain G for a uniformly illuminated aperture, with 100% efficiency, and diameter a , is given by

$$G = \frac{5a^2}{\lambda^2} \quad (1.30)$$

Note that the units used for the dimension a can be expressed in any form, metric or imperial, as long as the same units are also used for the wavelength.

In most cases, we are quoted the frequency rather than the wavelength. It is therefore more convenient to use a formula involving the frequency. We could also calculate the gain in dBi, instead of the linear gain.

$$G_{\text{dB}} = 10 \log_{10} \left\{ \frac{(aF)^2}{18,000} \right\} \quad (1.31)$$

where a is the diameter of the aperture of the parabola in meters and F is the frequency in MHz.

If the diameter of the parabola is given in centimeters, and the frequency in MHz, the gain in dBi can be calculated from the following formula

$$G_{\text{dB}} = 10 \log_{10} \left\{ \frac{(aF)^2}{1.8} \right\} \quad (1.32)$$

References

- [1] Rudge, A. W., K. Milne, A. D. Olver, and P. Knight (eds.), *The Handbook of Antenna Design, Volume 1*, London, UK: Peter Peregrinus Ltd., 1982.
- [2] Silver, S. (ed.), *Microwave Antenna Theory and Design*, MIT Radiation Lab Series, New York: McGraw-Hill, 1949
- [3] BS 6657:1991 British Standard *Guide to Prevention of Inadvertent Initiation of Electroexplosive Devices by Radio Frequency Radiation*, November 29, 1991.
- [4] Dyson, J. D., "The Characteristics and Design of the Conical Log Spiral," *IEEE Trans. on Antennas and Propagation*, Vol. AP-13, July 1965, pp. 488–499.
- [5] Hill, J. E., *Gain of Directional Antennas*, Watkins-Johnson Company Tech Notes, Vol. 3, No. 4, Palo Alto, CA, July/August 1976.

Basic Math for EMC Engineers

This chapter gives an overview of the mathematics required by engineers in the EMC field. It is not intended as a replacement for mathematics textbooks, but as a revision course, with emphasis being on the application of mathematical principles to the theoretical aspects of the book. The topics are also explained in a qualitative manner, so that the concepts may be understood without recourse to rigorous mathematical treatments. If the reader intends to pursue EM theory, it is strongly recommended that this chapter is studied before proceeding with Chapter 3.

2.1 Angles

The angle between two lines is defined as the amount that one line must be rotated in order to be superimposed onto the other line. Angles can be measured in degrees or radians. In navigation and geography, angles are measured exclusively in degrees, whereas in mathematics, science, and engineering, both degrees and radians are used.

$$2\pi \text{ radians} = 360^\circ$$

$$1 \text{ radian} = 180/\pi \text{ degrees}$$

Since π is approximately equal to 3.142

$$1 \text{ radian} = 57.3^\circ$$

2.1.1 Convention for Angles

There are two main conventions used for angles; namely the ones used in (a) navigation, and (b) mathematics. It is important to appreciate the difference between the two conventions, since the mathematical convention is used for radiation patterns, but the EMC engineer may encounter the navigational convention in the military field when dealing with emissions or susceptibility. To convert from mathematical angles D_m to navigational angles D_n , we use

$$D_n = 90^\circ - D_m \quad \text{for } 0^\circ < D_m < 90^\circ \quad (2.1)$$

for mathematical angles between 0° and 90°

$$D_n = 450^\circ - D_m \quad \text{for } 90^\circ < D_m < 360^\circ \quad (2.2)$$

for angles between 90° and 360° .

2.1.1.1 Convention for Navigation

In navigation, the angles are called bearings, and they are referenced to the geographic north. The bearings are measured as positive angles (using three digits) in a clockwise direction from the geographic north, and they vary from 0° to 360° . Thus north is 000° or 360° , east is 090° , south is 180° , and west is 270° , as shown in Figure 2.1(a).

2.1.1.2 Convention for Mathematics

In mathematics, the angles are referenced to the positive x -axis, so that when the angle A , shown in Figure 2.1(b), is 0° or 360° , the direction is parallel to the x -axis; angle $A = 90^\circ$ is along the y -axis, $A = 180^\circ$ is along the negative x -axis, and $A = 270^\circ$ is along the negative y -axis. Mathematicians also use angles greater than 360° , so that $A = 450^\circ$ is the same as 90° , (along the y -axis) and so on.

The angles are divided into four sectors called quadrants. The first quadrant contains angles between 0° and 90° , the second quadrant contains angles between 90° and 180° , the third quadrant contains angles between 180° and 270° , and the fourth quadrant contains angles between 270° and 360° . These are shown in Figure 2.1(b).

2.2 Basic Trigonometry

The basic trigonometric functions are defined by the projections of lines onto the x - and y -axes, as shown in Figure 2.2(a). They can also be represented by the sides of a right-angled triangle, like the triangle depicted in Figure 2.2(b).

The variations of the trigonometric functions are plotted in Figure 2.3. We can see that $\sin A$ is positive in the first and second quadrants, $\cos A$ is positive in the first and last quadrant, and $\tan A$ is positive in the first and third quadrant. Summarising, we can say that all the functions are positive in the first quadrant, $\sin A$ is positive in the second quadrant, $\tan A$ is positive in the third quadrant, and $\cos A$ is positive in the last quadrant, as shown in Figure 2.3(d). The positive values of the trigonometric functions can be remembered by the mnemonic “all silly tomcats” reading counterclockwise from zero in the direction of increasing angles, or by the acronym ACTS reading clockwise from the first quadrant.

2.2.1 Reciprocal Trigonometric Functions

The reciprocal trigonometric functions are secant (sec), cosecant (cosec) and cotangent (cot), and are respectively defined as

$$\sec A = \frac{1}{\cos A} \quad (2.3)$$

$$\operatorname{cosec} A = \frac{1}{\sin A} \quad (2.4)$$

$$\cot A = \frac{1}{\tan A} \quad (2.5)$$

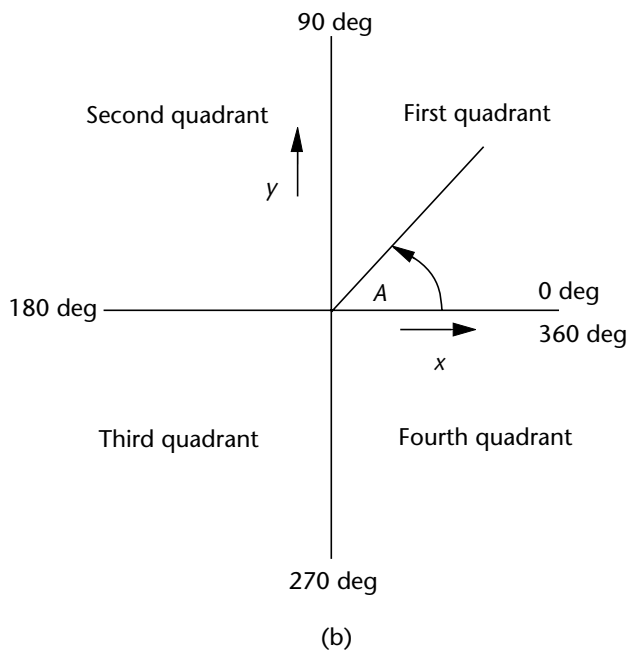
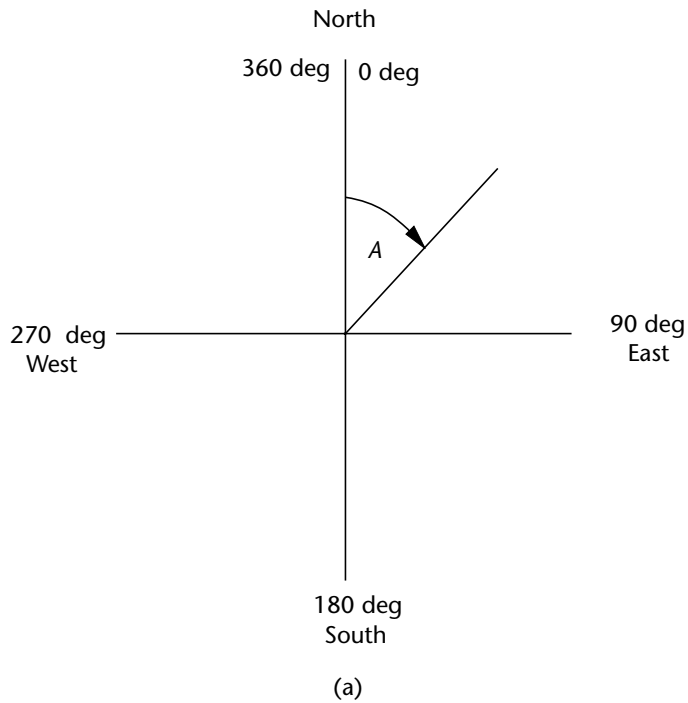
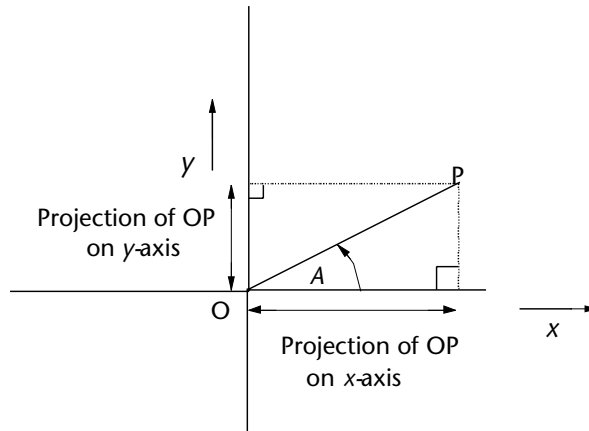


Figure 2.1 Convention for angles used in navigation and mathematics. (a) Bearings used for navigation, and (b) convention used in mathematics.

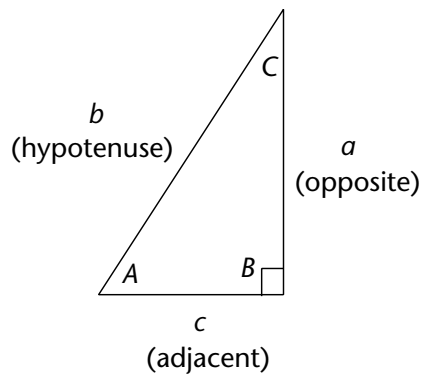


$$\sin A = \frac{\text{projection of OP on } y\text{-axis}}{\text{length of OP}}$$

$$\cos A = \frac{\text{projection of OP on } x\text{-axis}}{\text{length of OP}}$$

$$\tan A = \frac{\text{projection of OP on } y\text{-axis}}{\text{projection of OP on } x\text{-axis}}$$

(a)



$$\sin A = \frac{a}{b}$$

$$\cos A = \frac{c}{b}$$

$$\tan A = \frac{a}{c}$$

(b)

Figure 2.2 Basic trigonometric functions of an angle. (a) Trigonometric functions as projections, and (b) trigonometric functions in a right-angled triangle.

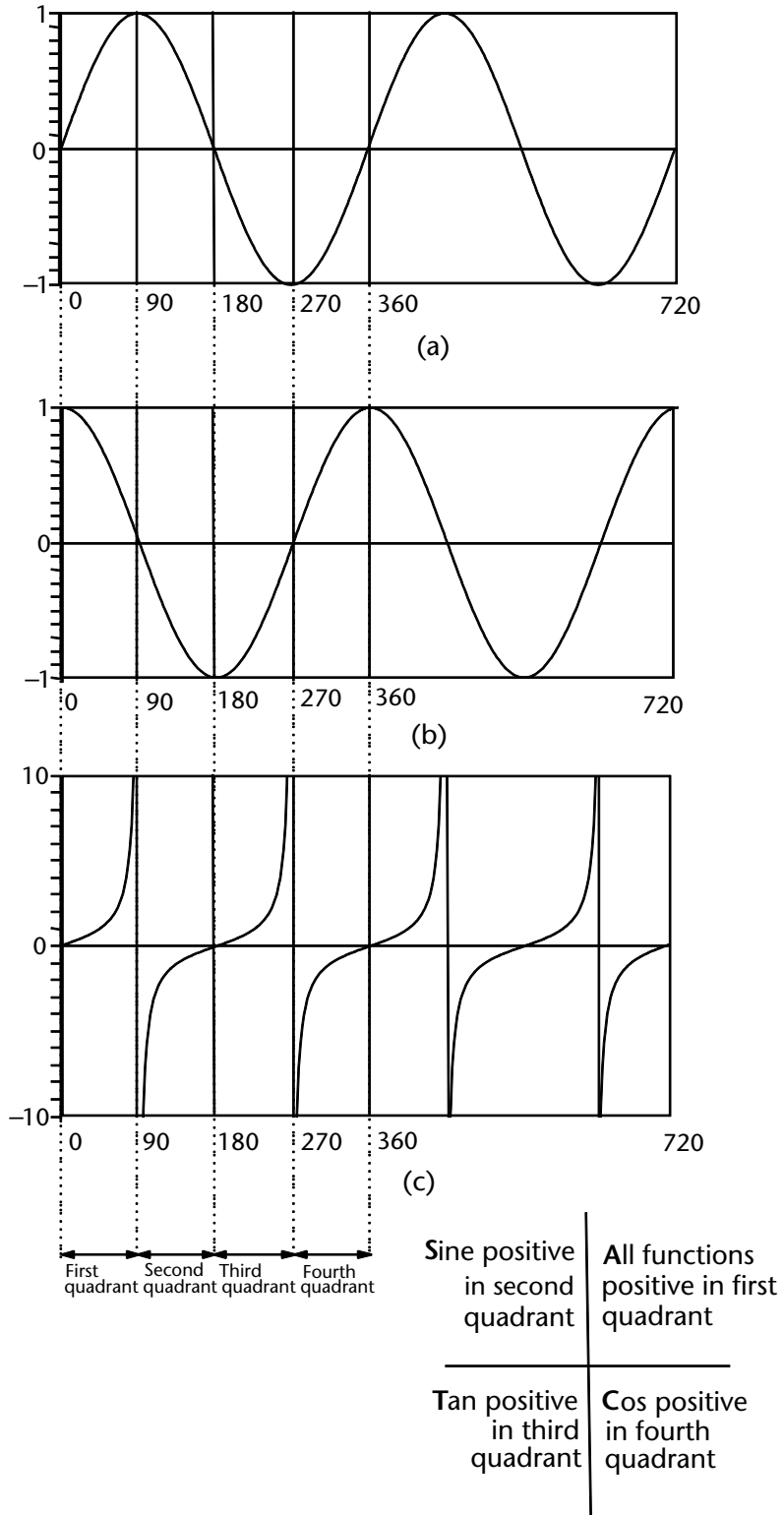


Figure 2.3 Variation of trigonometric functions with angle. (a) Variation of sine with angle, (b) variation of cosine with angle, and (c) variation of tangent with angle.

2.2.2 Inverse Trigonometric Functions

These are not the same as the reciprocal trigonometric functions, and refer to the angles whose trigonometric functions are the stated values. On calculators and in program code, they are often denoted by \sin^{-1} , asin , or arcsin in the case of sine functions, with similar annotation for the other functions. For example, if we know that the sine of an angle ($\sin A$) is 0.5, and we want to calculate the angle, we would key in the number 0.5 on the calculator and then press the \sin^{-1} or the asin key to get the result of 30° (assuming that the calculator is in degree mode).

2.2.2.1 Common Trigonometric Identities

$$\sin^2 A + \cos^2 A = 1 \quad (2.6)$$

$$\sec^2 A = 1 + \tan^2 A \quad (2.7)$$

$$\text{cosec}^2 A = 1 + \cot^2 A \quad (2.8)$$

Note that the powers of trigonometric functions are written as $\cos^2 A$, $\cos^3 A$, and so forth, and not $(\cos A)^2$ or $(\cos A)^3$.

2.2.2.2 The Cosine Formula

The cosine formula is useful for calculating the angle in the case of any acute-angled triangle as shown in Figure 2.4(a), if the sides are known. Alternatively the side opposite a known angle can be calculated if the other two sides are known. The cosine formula is given by

$$a^2 = b^2 + c^2 - 2bc(\cos A) \quad (2.9)$$

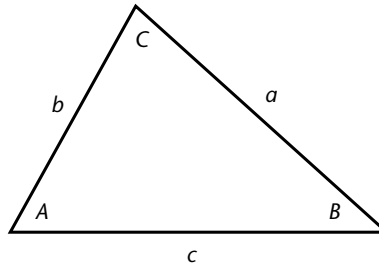
Similar formulas for calculating b or c can be used, as shown in Figure 2.4. The sides c and b may be inclined at an angle A , which is greater than 90° (in the case of an obtuse-angled triangle, as shown in Figure 2.4(b)); but the formula of (2.9) still applies. In the case of angles between 90° and 180° , the cosine is negative, so that the last term in (2.9) becomes positive.

The cosine formula is useful for calculating the magnitude of vectors that are inclined at an angle of A . The lengths of the sides b and c are chosen to be the relative lengths of two vectors inclined at an angle A , and the resultant is represented by the length of the third side a .

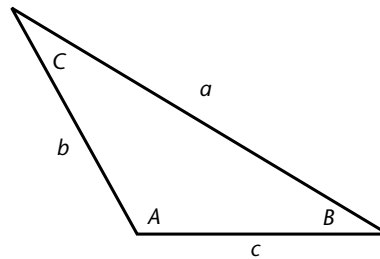
2.2.2.3 The Sine Formula

The sine formula is given by

$$\frac{a}{\sin A} = \frac{b}{\sin B} = \frac{c}{\sin C} \quad (2.10)$$



(a)



(b)

Sine formula

$$\frac{a}{\sin A} = \frac{b}{\sin B} = \frac{c}{\sin C}$$

Cosine formula

$$a^2 = b^2 + c^2 - 2bc \cos A$$

$$b^2 = a^2 + c^2 - 2ac \cos B$$

$$c^2 = a^2 + b^2 - 2ab \cos C$$

Figure 2.4 Sine and cosine formulas for acute and obtuse angled triangles. (a) Acute-angled triangle, and (b) obtuse-angled triangle.

The sides a , b and c are the sides opposite angles A , B , and C , as shown in Figure 2.4 This formula is useful for calculating the magnitudes and/or angles between vectors that are represented by the sides of any triangle.

2.3 Powers, Indices, and Logarithms

Powers, indices, and logarithms are all ways of expressing the same concept. When we have a number $A = x^3$, we say that x is raised to the power of 3. We could also say the index of the base x is 3, or that the logarithm of A to the base x is 3, which is written as $\log_x A = 3$. We use the standard convention of omitting the positive sign if the power is positive. If the power is negative, then the number is equal to the reciprocal of the positive power, that is, if $A = x^{-3}$, then we can say that it is also equal to $1/x^3$. We can take the logarithm of a number to any base. If we take it to a base of 10, it is called a common logarithm, or log, and when no base has been stated it is usually assumed to be a base of 10. It is also convenient to use logarithms to a

base of e (where $e = 2.718$) and these are called natural, or Napierian, logarithms and written as \ln . Logarithms are used because of the ease with which numbers can be multiplied and divided once they are converted into logarithms. The rules that apply to operations of multiplying, dividing, and squaring of indices are described in the following sections.

2.3.1 Multiplication of Numbers

Consider two numbers, $A = x^2$ and $B = x^3$. If we rewrite them in their full form ($A = x$ multiplied by itself twice and $B = x$ multiplied by itself three times) and then take their product, we get x multiplied by itself five times, that is, x^5 . Note that we could get this result by adding the indices 2 and 3. The general rule for the multiplication of two or more numbers (that can be expressed as powers to the same base) is to sum their indices or powers, as is shown by

$$x^2 \times x^3 \times x^4 = x^{(2+3+4)} = x^9 \quad (2.11)$$

In the case of logs, when we multiply numbers, we add the logarithms.

$$\log_x(AB) = \log_x A + \log_x B \quad (2.12)$$

The rule for multiplication applies whether the indices are positive or negative integers, or fractions, as the following example illustrates.

$$x^2 \times x^{-3.5} \times x^4 = x^{(2-3.5+4)} = x^{2.5} \quad (2.13)$$

Note that since negative indices can be written as the reciprocals of positive indices, (2.13) can also be written in the following way

$$x^2 \times \frac{1}{x^{3.5}} \times x^4 = x^{(2-3.5+4)} = x^{2.5} \quad (2.14)$$

Note that the index of the denominator is subtracted from the indices of the numerator.

In the case of logs, the following rule applies:

$$\log_x\left(\frac{A}{B}\right) = \log_x A - \log_x B \quad (2.15)$$

When we raise numbers to a power, we multiply the indices. This is demonstrated by the following rule:

$$(x^3)^4 = x^{3 \times 4} = x^{12} \quad (2.16)$$

In the case of logarithms, we can say that the following rule applies:

$$\log_x (A^2) = 2\log_x A \quad (2.17)$$

Logs were used to multiply and divide large numbers in the days before the availability of handheld electronic calculators. Tables of logs and antilogs to the base ten (and base e) were available. Let us consider two numbers, 30 and 50. If we want to find their product we can multiply them in the normal way, but alternatively, we could put them in logarithmic form, add the logs together, and then find the antilog of their sum. The log of 30 is 1.477, and the log of 50 is 1.699, giving the sum of 3.176. Taking the antilog of 3.176 we get the result 1500. However, in engineering we use the decibel (abbreviated to dB) to express the relative magnitudes of two quantities such as transmitted and received powers. The ratios could be several orders of magnitude (10^6 or more), and decibels are a convenient form of writing these large ratios. The decibel is defined as ten times the log of a number. Thus, 30 expressed in decibels is 14.77. Note that since $10 = 10^1$, the log of 10 is one but 10 expressed in decibels is 10. If we have a power P_1 that is 10 times larger than another power P_2 , then the ratio of P_1 to P_2 is ten, and in decibels we say that the ratio of P_1 to P_2 is +10 dB. However, if we consider the ratio of P_2 to P_1 , we get 0.1 or 10^{-1} , which is -10 dB. Summarizing, we can state the following

$$10\log\left(\frac{p_1}{p_2}\right) = -10\log\left(\frac{p_2}{p_1}\right) \quad (2.18)$$

It is common practice to relate a power to 1 mW. In this case the power P_1 is divided by 1 mW, and then expressed in decibels, called decibels referred to one milliwatt (dBmW). For instance, if P_1 is 10W, the ratio of P_1 to 1 mW is 10000 or 10^4 , and expressed in decibels it would give us +40. However, if we were to be told that a power of +40 dB existed, we would not be able to state the absolute value of P_1 , since all we could deduce would be that the relative power was 10,000 times greater than another power level. To ascertain the actual value of P_1 we would have to specify that it has a value of +40 dBmW (which is usually shortened to dBm); this tells us that it is 10^4 greater than 1 mW (i.e., that it is 10W).

If we had a level of -40 dBm, we know that this power is 10^{-4} or 10^4 less than 1 mW, and is therefore 0.1 μ W. We will always get a negative number of decibels when we take the log of a number less than one. Of course, decibels are not just multiples of ten, they could be any number. It is useful to remember that the number in decibels is ten times the power to which 10 is raised. Thus, +3 dBm is $10^{+0.3}$ mW, which is 1.9995 times greater than 1 mW (i.e., 2 mW approximately). Thus, for every +3 dB, the power doubles. Similarly, for every -3dB, the power is halved. Approximate conversions between decibels referred to one milliwatt and milliwatts are shown in Table 2.1. Accurate conversion tables are given in Appendix F.

Table 2.1 Approximate Relationship Between dBm and mW

dBm	-15	-12	-10	-9	-6	-3	0	+3	+6	+9	+10
mW	0.03	0.06	0.1	0.13	0.25	0.5	1	2	4	8	10

2.3.2 Relationship Between dBm and dBmV

There is often confusion between decibels expressed as a power ratio (e.g., dBm) and decibels expressed as a voltage ratio (e.g., dBmV). The decibel was first introduced as 10 times the log of a power ratio, so that when it is used for voltages, we must remember that the power P is proportional to the square of the voltage V ($P = V^2/R$) Thus, the following relationship applies:

$$10\log\left(\frac{p_1}{p_2}\right) = -10\log\left(\frac{V_1}{V_2}\right)^2 \tag{2.19}$$

Using the rule of (2.16), we can see that raising the ratio of voltages to a power of 2 results in the index being twice that of the ratio of the powers. Thus the value in decibels will be 20 times the index of 10 for the voltage ratios, but only 10 times the index of 10 for power ratios. In the case of voltage ratios, we can therefore say that for every +20 dB the voltage ratio increases by a factor of 10, and for every +6 dB the voltage ratio doubles. The level of voltages encountered in EMC is relatively low, so the voltages are usually related to 1 mV. Thus, in decibels, they are expressed in decibels referred to one millivolt (dBmV). Table 2.2 gives an approximate conversion between dBmV and mV. Accurate conversion tables are given in Appendix F.

The conversion between dBμV and mV is given in Appendix F. The larger dBμV levels are used for many military and susceptibility measurements, whereas dBmV are levels more commonly used in commercial applications

2.4 Real and Complex Numbers

Consider a quadratic (an equation with a squared term or a product of two variables such as x^2 or xy) of the form

$$y = x^2 - 4 \tag{2.20}$$

We can plot it and obtain the curve of Figure 2.5(a). The solution(s) occurs when the curve crosses the x -axis (i.e., when $y = 0$). We can see that we have the two solutions, or roots, at $x = +2$ and -2 .

We could also solve it analytically, by factorisation when $y = 0$.

$$\begin{aligned} x^2 - 4 &= 0 \\ (x - 2)(x + 2) &= 0 \\ x &= +2 \text{ or } -2 \end{aligned}$$

Table 2.2 Approximate Relationship Between dBmV and mV

dBmV	-30	-24	-20	-18	-12	-6	0	+6	+12	+18	+20
mV	0.03	0.06	0.1	0.13	0.25	0.5	1	2	4	8	10

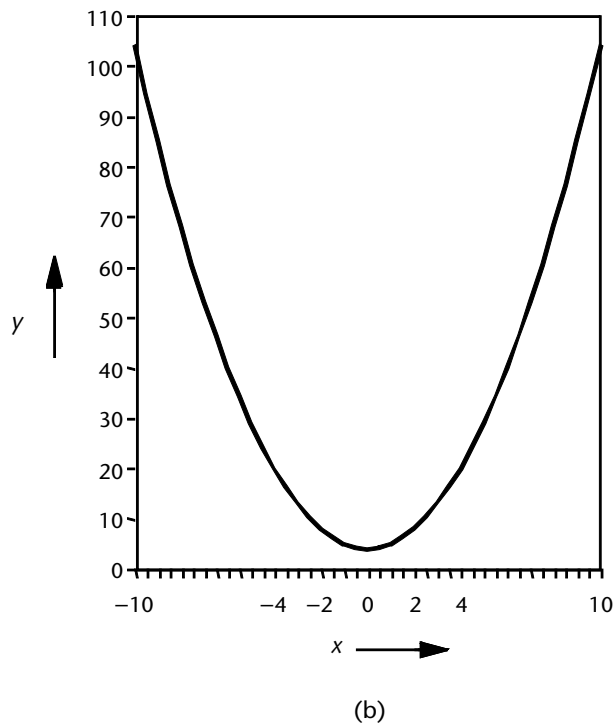
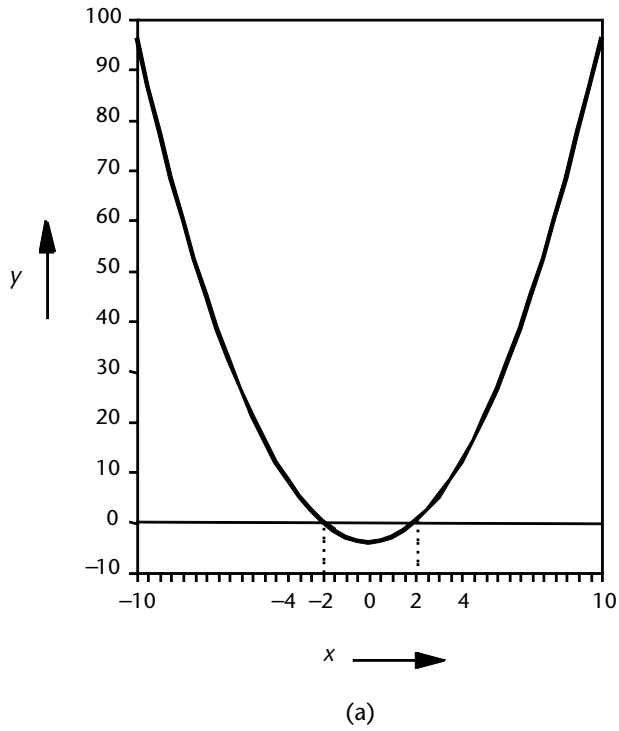


Figure 2.5 Graphs of quadratic functions. (a) $y = x^2 - 4$ showing real roots, and (b) $y = x^2 + 4$ showing no real roots.

In either solution, we get real roots.

Now let us consider the quadratic

$$y = x^2 + 4 \quad (2.21)$$

When we plot the quadratic, we can see from Figure 2.5 (b), that it does not cross the x -axis. Thus it does not have any real roots. We cannot factorize it, but we can solve it algebraically by using the formula for obtaining the roots of a quadratic expressed in the form $ax^2 + bx + c$. The roots of such an equation are given by

$$x = \frac{-b \pm \sqrt{b^2 - 4ac}}{2a} \quad (2.22)$$

where

a is coefficient of the x^2 term,

b is coefficient of the x term,

and c is coefficient of the constant (number).

In (2.21), a is equal to 1, b is equal to zero, and c is equal to 4. Inserting these values into the formula of (2.22) we get

$$x = \frac{-0 \pm \sqrt{0^2 - 16}}{2} = \frac{\pm\sqrt{-16}}{2} \quad (2.23)$$

We cannot take the square root of a negative quantity (since the product of two negative or positive numbers would always be positive), however if we write -16 as the product of -1 and $+16$, then the solution can be written as

$$x = \frac{\pm 4\sqrt{-1}}{2} = \pm 2\sqrt{-1}$$

The square root of -1 is denoted by the letter i or j . In general, mathematicians tend to use i , and physicists and engineers tend to use j (j is also called an operator sometimes). Thus, the roots of (2.21) are $+2j$ and $-2j$ and these are imaginary numbers. In order to depict these roots we define a complex plane which represents the real numbers on the x -axis and the imaginary numbers on the y -axis. This type of diagram is sometimes called an Argand diagram (after J. R. Argand) and is shown in Figure 2.6. In the quadratic equation (2.21), the roots do not have any real parts, and thus they appear on the y -axis (or imaginary axis) of Figure 2.6 where x (the magnitude of the real part) is zero.

In general, the solution of quadratics results in roots that are real or complex. The complex roots have both real and imaginary parts, of the form $x + jy$. For example if we consider the equation below

$$y = x^2 + 4x + 5 \quad (2.24)$$

The roots occur when $y = 0$, and using the formula of (2.22) we get the following values for x

$$x = \frac{-4 \pm \sqrt{16 - 20}}{2}$$

$$x = -2 + j \text{ or } -2 - j$$

These are shown in the Argand diagram (Figure 2.6) by encircled crosses.

In the case of higher order equations (such as cubics of the form $y = ax^3 + bx^2 + x + c$), the roots could be a mixture of real and complex roots.

We can also represent complex numbers in polar form, by a position vector (see Section 2.5 on scalars and vectors) of length R , which makes an angle ϕ with the positive direction of the x -axis, as depicted in Figure 2.7. The vector is uniquely described by the quantity $R e^{j\phi}$. The x -coordinate (or abscissa) is given by $R \cos \phi$, and the y -coordinate (or ordinate) on the imaginary axis is given by $jR \sin \phi$. The length of R represents the magnitude of the vector and is also called the modulus, or absolute value. The modulus value is conventionally denoted by vertical lines on either side of R , as $|R|$. The modulus can be calculated by applying Pythagoras' theorem to give us

$$|R| = \sqrt{(x^2 + y^2)} \quad (2.25)$$

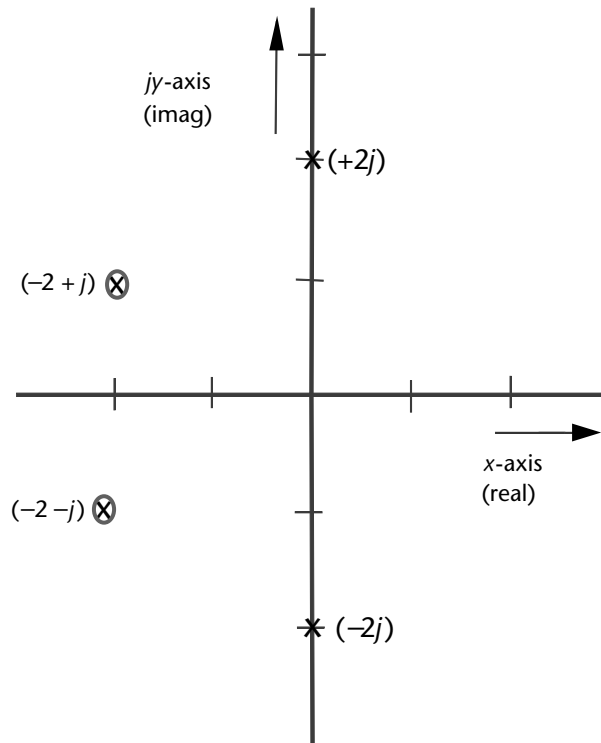


Figure 2.6 Argand diagram.

The angle ϕ , which the vector \mathbf{R} makes with the x -axis, is called the argument, and can be calculated by simple trigonometry since

$$\tan \phi = \frac{y}{x} \quad (2.26)$$

so that ϕ is given by

$$\phi = \tan^{-1}\left(\frac{y}{x}\right) \quad (2.27)$$

Note that when $\phi = \pi/2$, or 90° , there is no real part, only an imaginary part, and \mathbf{R} is vertical or parallel to the y -axis. We can see this algebraically as well, since according to the identity of L. Euler (1707–1783),

$$e^{\pm j\theta} = \cos \theta \pm j \sin \theta \quad (2.28)$$

$$\mathbf{R}e^{\pm j\theta} = \mathbf{R} \cos \frac{\pi}{2} + j\mathbf{R} \sin \frac{\pi}{2} \quad (2.29)$$

and $\cos \pi/2 = 0$, whereas $\sin \pi/2 = 1$; so that

$$\mathbf{R}e^{\pm \pi/2} = j\mathbf{R}$$

Similarly when $\phi = 0^\circ$, $e^{j0} = 1$, so that $\mathbf{R}e^{j0} = \mathbf{R}$. The evaluation of the position vector for other angles ϕ , can be undertaken in a similar manner by calculating the trigonometric functions in the respective quadrants.

2.4.1 Addition of Complex Numbers

When we add complex numbers, we must add the real parts together and the imaginary parts to each other. We cannot add real parts to the imaginary parts. Thus if we have two complex numbers, P and Q , such that $P = 3 + 5j$ and $Q = 6 + 8j$, $P + Q = 9 + 13j$. This property of complex numbers is utilized in what is known as stub matching of components to transmission lines.

If we have a load which has susceptance (1/reactance) of $+jB$ in parallel with its conductance of $G_1 = 0.2S$ (siemens), and we want to connect it to a line whose characteristic impedance is 50Ω (i.e., a characteristic admittance of $0.02S$), we would get a standing wave since the load does not have the same impedance as the transmission line. This would result in a loss of power transfer, and in some cases could lead to voltage breakdown in high-power systems. In order to match the load to the line, we would connect a stub, which is a short-circuited line, in parallel with the transmission line, as near to the load as possible. The conductance of the load can be varied by adjusting the position of the stub so that the conductance presented to the line equals $0.2S$. The susceptance of the stub can be varied by adjusting its

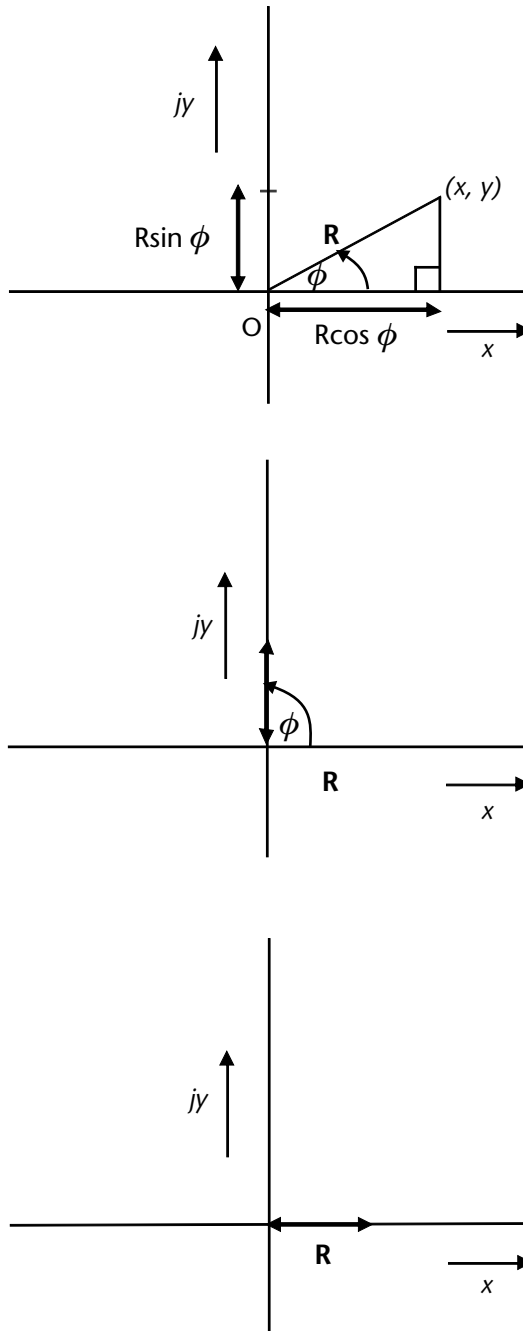


Figure 2.7 Polar representations of complex numbers. (a) In general, R has real and imaginary parts. (b) When $\phi = 90^\circ$, R is imaginary. (c) When $\phi = 0^\circ$, R is real.

length so that its susceptance is equal and opposite to that of the load (i.e. it is $-jB$). Thus, the resultant susceptance is zero, and the conductance is $0.2S$. The load now presents an impedance that is the same as that of the transmission line, so that it is matched, and maximum power transfer can be effected.

2.4.2 Complex Conjugate

The complex conjugate of a number has the same real part as the number, but its imaginary part has a sign opposite to that of the number. For instance, if we have a complex number $S = (a + jb)$, its complex conjugate is $(a - jb)$ and is denoted by using an asterisk as a superscript after the letter (S^*). Conjugate matching is used to match two components that do not have purely resistive impedances.

2.5 Scalars and Vectors

A scalar quantity is one that has magnitude but no direction. Examples of scalars are mass, resistance, time, and power. A vector quantity has magnitude and direction. Examples of vectors are weight, force, current, magnetic field, and electric field.

2.5.1 Position Vector

A vector may be used to indicate the position of a point in space or in a plane, relative to another point (usually the origin of co-ordinates). The vector \mathbf{R} in Figure 2.8(a) denotes the position of the point (x,y) .

2.5.2 Vector Addition and Subtraction

Vectors can be added by using a parallelogram or triangle rule. The vectors are represented by scaled lines, whose lengths are proportional to the relative magnitudes and whose directions represent the directions in which the vectors act. Usually one vector is considered to be the reference vector and the second vector is drawn at an angle representing the relative angles between the two vectors. When more than two vectors are to be added, two are first chosen to add together and then the resultant is added to the third, and so on.

2.5.2.1 Parallelogram Rule

Consider two vectors, \mathbf{A} and \mathbf{B} , representing the adjacent sides of a parallelogram shown in Figure 2.8(b); the lengths of the sides correspond to the relative magnitudes of the vectors, and the angle between them is the angle between the directions of the vectors. Note that their directions are both away from their common point of intersection. A parallelogram is constructed by drawing a line through the end of vector \mathbf{A} parallel to vector \mathbf{B} , and a line through the end of vector \mathbf{B} parallel to vector \mathbf{A} . The resultant is a vector \mathbf{R} represented by the diagonal (through the point O) of the parallelogram, and is denoted by the double arrow.

2.5.2.2 Triangle Rule

In this case, the vectors to be added represent two sides of the triangle, shown in Figure 2.8(c), but note that their directions are cyclic, so that the direction of vector \mathbf{A} is towards their common point, whereas the direction of vector \mathbf{B} is away

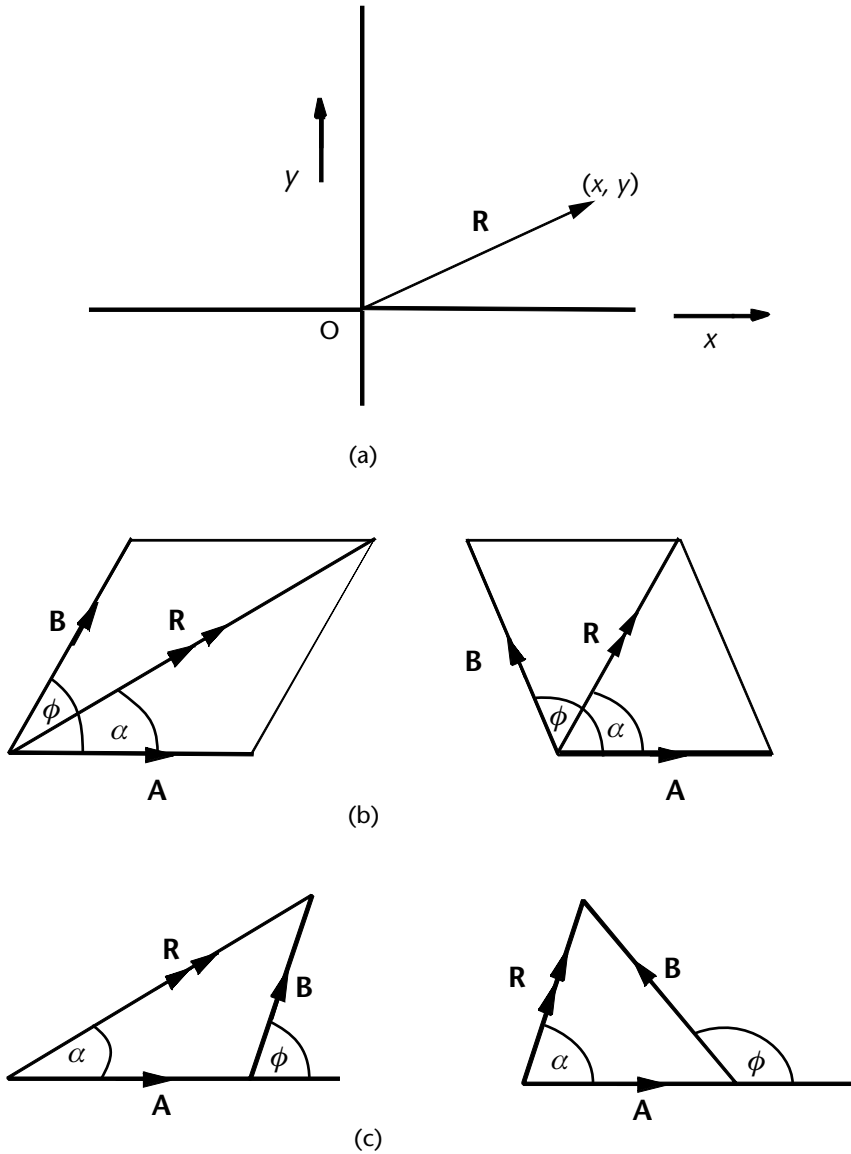


Figure 2.8 Rules for the addition of vectors. (a) \mathbf{R} is the position vector for the point (x, y) . (b) Parallelogram rule for vector addition. (c) Triangle rule for vector addition.

from their common point. The resultant \mathbf{R} of the two vectors is represented by the third side of the triangle, and its direction is anticlockwise to the direction of the two component vectors. The length of the resultant is measured and the appropriate scale applied to calculate its magnitude. The angle which the resultant makes with either of the component vectors can be measured with a protractor.

A more accurate method of finding the magnitude and direction of the resultant is by calculation, using the cosine formula of (2.9) to calculate the length of the resultant, and then the sine formula of (2.10) to calculate its direction.

2.5.3 Vector Multiplication

Vectors can be multiplied in two different ways. We can take their

1. Scalar or dot product,
2. Vector or cross product.

2.5.3.1 Scalar or Dot Product

The dot product of two vectors **A** and **B** is written with a dot between them, and is defined as

$$\mathbf{A} \cdot \mathbf{B} = \mathbf{B} \cdot \mathbf{A} = AB \cos \theta = BA \cos \theta \quad (2.30)$$

where

- A** and **B** (in bold characters) are vector quantities,
- A and B (with normal attributes) are scalars,
- and θ is the angle between the vectors **A** and **B**.

Note that the dot product of the two vectors is a scalar, and is the product of the magnitude of one vector and the resolute of the other one (the component of the other one resolved in the direction parallel to the first), as shown in Figure 2.9(a). It follows that when θ is zero, the two vectors are parallel and the dot product is equal to the product of the magnitudes of the two vectors. We can see that this is the case algebraically, since $\cos \theta$ is equal to 1, when θ is zero. When θ is 90° , the two vectors are perpendicular and the resolute of one in the direction parallel to the other is zero; and this results in the product also being zero. In physics, we encounter many cases of the dot product of vectors. For instance, we may have an object such as a train, which is constrained to travel in a straight line subjected to a force F is applied at an angle θ , as shown in Figure 2.9(b), the resolute of the force in the direction of motion of the train is $F \cos \theta$. When $\theta = 0^\circ$, $\cos \theta = 1$, and the resolute has its maximum value of F ; whereas when $\theta = 90^\circ$, $\cos \theta = 0$, and the resolute has its minimum value of zero, that is, the force F does not contribute to the tractive force of the locomotive.

2.5.3.2 Vector or Cross Product

The vector product of two vectors **A** and **B** is written with a cross (or multiplication sign) between them, and is defined as

$$\mathbf{A} \times \mathbf{B} = \mathbf{k}AB \sin \theta = -\mathbf{k}BA \sin \theta \quad (2.31)$$

The cross product is the product of one vector and the resolute of the other in the direction perpendicular to the first and in the plane containing the two vectors, and \mathbf{k} is the unit vector (see Section 3.1). The resolute of **A** perpendicular to **B** is $A \sin \theta$, if θ is the angle between the vectors. The product is a vector whose direction is perpendicular to the plane containing the two vectors, and governed by the

right-hand rule. The vector product $\mathbf{A} \times \mathbf{B}$ is in the opposite direction to the vector product $\mathbf{B} \times \mathbf{A}$. In Figure 2.9(c) we can see that if we take the vector product of $\mathbf{A} \times \mathbf{B}$ we move in a counterclockwise direction from \mathbf{A} to \mathbf{B} , and thus the resultant is in the upward direction; whereas if we take the vector product of $\mathbf{B} \times \mathbf{A}$ we move in a clockwise direction from \mathbf{B} to \mathbf{A} , and thus the resultant is in the downward direction. If we say that $\mathbf{A} \times \mathbf{B}$ is positive, then $\mathbf{B} \times \mathbf{A}$ is negative. The unit vector \mathbf{k} is used to show that the resultant vector is in the direction of the z -axis, whereas $-\mathbf{k}$ denotes a vector in the negative z -direction.

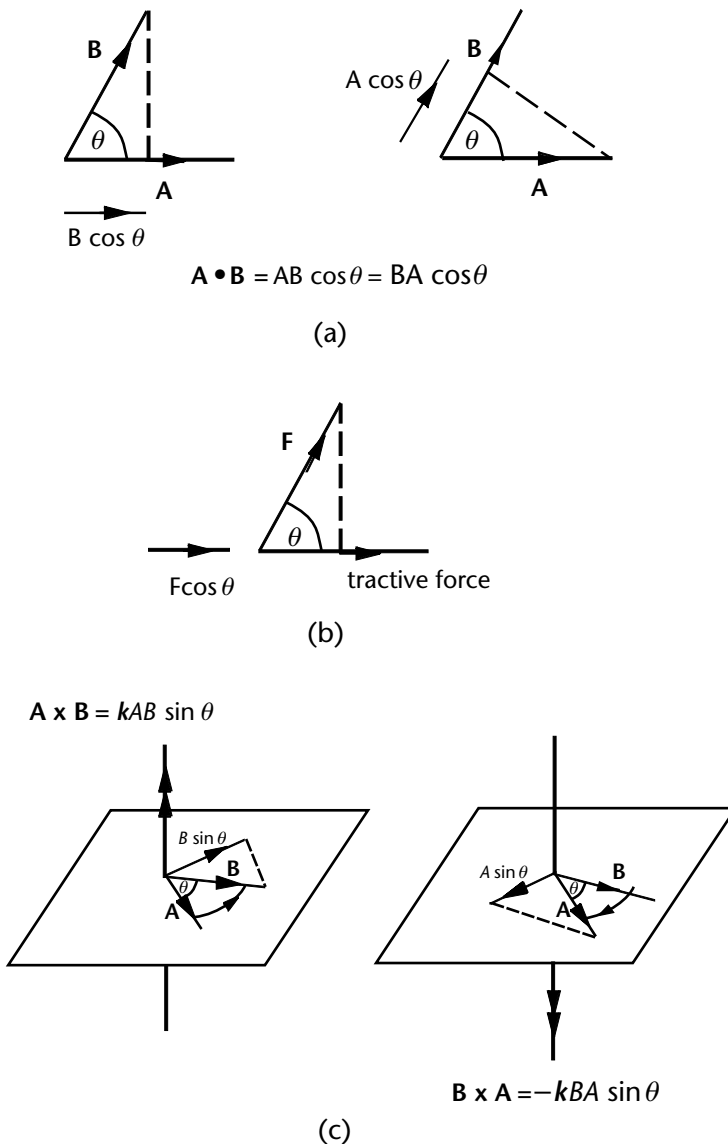


Figure 2.9 Scalar and vector product of vectors. (a) Scalar or dot product. (b) Effect of the force depends on the angle θ . (c) Vector or cross product of vectors.

We encounter the vector product in the Poynting's power flux vector, which is the product of the electric field intensity \mathbf{E} , and the magnetic field intensity \mathbf{H} . Poynting's power flux vector gives us the power density (power per unit area) at a particular location and is given by

$$\mathbf{P} = \mathbf{E} \times \mathbf{H} \quad (2.32)$$

where \mathbf{P} is in watts per square meters (W m^{-2}), \mathbf{E} is in volts per meter (V m^{-1}), and \mathbf{H} is in amperes per meter, (A m^{-1}). \mathbf{E} and \mathbf{H} are often written in V/m and A/m .

2.5.4 Phasors

A phasor is a rotating vector representing a quantity which rotates in time rather than in space, at an angular velocity equal to the phase velocity of the quantity. In engineering, we use phasors to represent sinusoidal variations such as voltages, and the length of the phasor is proportional to the amplitude of the variation. If the voltage is mains AC power at 50 Hz, one cycle takes $1/50$ of a thousandth of a second (or 0.02 sec) and thus the phasor would take 0.02 sec to complete one revolution, or 2π radians. In one second it would sweep out 50 revolutions, or 100π radians, so we can say that the angular velocity ω is 100π radians per second (since $\omega = 2\pi f$). At any time t , the vector sweeps out an angle ωt . If we have more than one voltage at the same angular velocity, but with relative phase differences, then we can depict both the phasors on the same diagram. Since both the vectors are rotating at the same velocity, the relative phase difference will be the same whether they are stationary or rotating; so we shall keep them stationary. If we have a sinusoidal variation, as shown in Figure 2.10(b), then the length of the vector shows the amplitude or maximum value in each cycle. Consider the circuit of Figure 2.10(a), which shows an inductor in series with a resistor connected to a sinusoidally varying voltage source. We want to calculate the total voltage V_t across the inductor and resistor. The voltage waveforms across the inductor and resistor respectively are shown in Figure 2.10(b, c) with amplitudes of V_1 and V_2 . In the case of a pure inductor, the voltage V_2 would lead the voltage V_1 by exactly 90° , but in the general case we shall consider V_2 leading V_1 by a phase of ϕ . These voltages can be represented on a phasor diagram by two straight lines scaled to represent the relative amplitudes of V_1 and V_2 ; separated by an angle ϕ . The vector V_1 is taken as the reference phasor, and since V_2 leads V_1 by a phase of ϕ degrees, V_2 is drawn at an angle of $+\phi$. The resultant is found by using the laws of vector addition. The use of vectors as phasors is a very useful tool for analysing the voltages and currents which are subjected to sinusoidal variations. We would normally find the resultant of two sinusoidal variations by adding the sine waves on a point-by-point basis. If we have $V_1 = V_2 = 1$ (each representing one unit) and ϕ equal to 60° , we would get the waveform of Figure 2.10(d), which has an amplitude of 1.732, and a phase of 30° compared with the voltage across the resistor. In order to find the resultant using phasors, we can draw a scaled drawing, as shown in Figure 2.10(e), and by using the parallelogram or triangular rule, we can directly measure the angle (30°) and length of the resultant (1.732 units). Alternatively, we could draw a sketch of

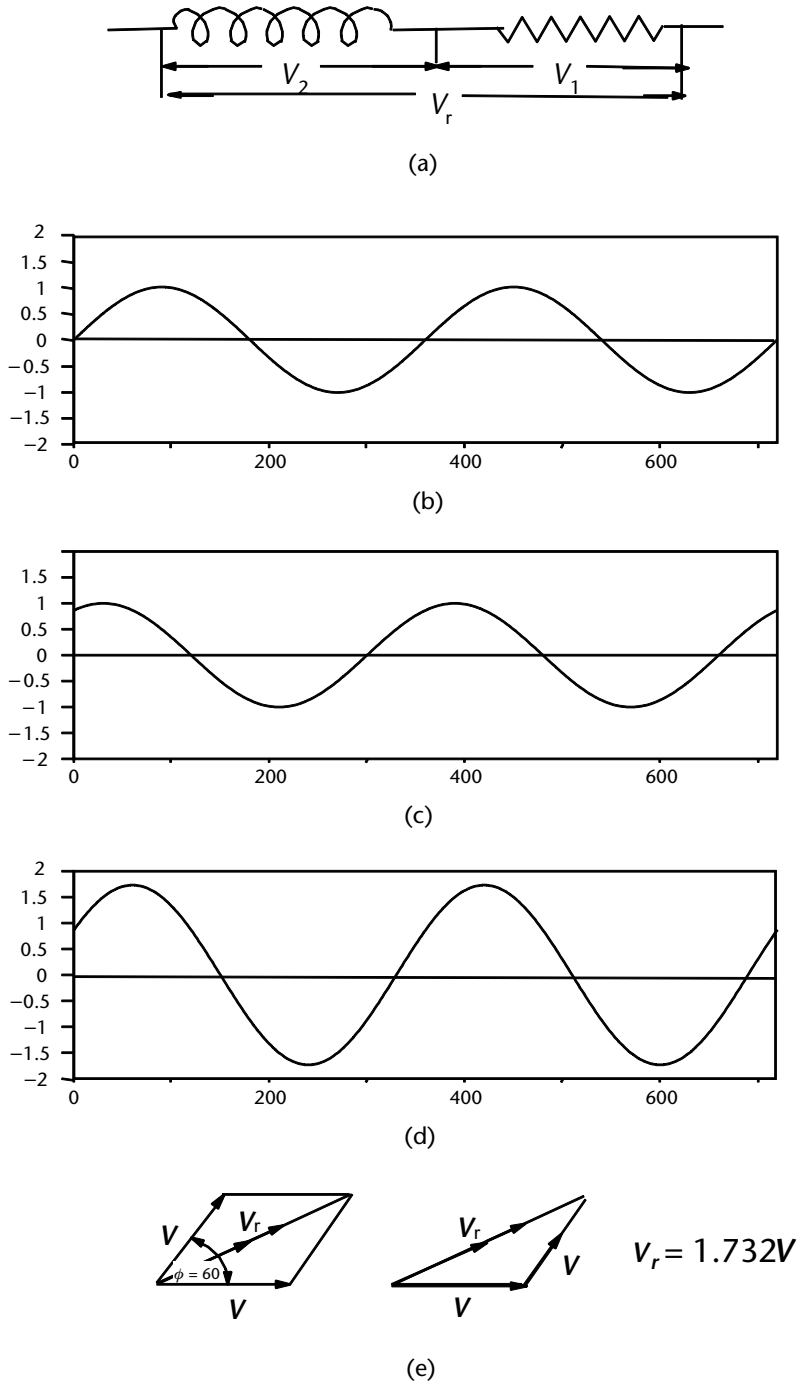


Figure 2.10 Addition of waveforms using algebraic addition and phasors. (a) Circuit of an inductor in series with a resistor, (b) $V \sin \omega t$, (c) $V \sin (\omega t + \phi)$, (d) $V \sin \omega t + V \sin (\omega t + \phi)$, and (e) addition of waveforms using vectors as phasors.

the three vectors, then use the cosine rule to calculate the length of the resultant, and the sine rule to calculate the angle of the resultant.

2.6 Fourier Analysis and Transforms

Fourier analysis was first suggested by J. B. J. Fourier (1768–1830). He showed that a square wave could be decomposed into a sum of sine waves. Fourier transforms are used to transform a function from one domain to another, such as from the time to the frequency domains.

2.6.1 Fourier Analysis

Consider a square wave of frequency f ($= \omega/2\pi$) as shown in Figure 2.11(a). This wave has a period T equal to $2\pi/\omega$. If we add together a sine wave of the same frequency and a sine wave of three times the frequency but one third of the amplitude ($\sin 3\omega t/3$, as shown in Figures 2.11(b, c), we would get the resultant wave of Figure 2.11(d). This looks similar to the square wave, but is not a very good approximation. If we add another sine wave of five times the frequency and one fifth of the amplitude ($\sin 5\omega t/5$, we would get the plot of Figure 2.11(e). As we add more terms, we get nearer to the shape of a square wave. To get an exact square wave function $f(\omega t)$ we have to add an infinite number of terms of the series, given by the following summation

$$f(\omega t) = \frac{4}{\pi} \sum_{n=1}^{\infty} \frac{\sin(2n-1)\omega t}{(2n-1)\omega t} \quad (2.33)$$

where ω is the angular frequency in radians per second.

Note that each term is an odd multiple of the frequency of the first term $\sin \omega t$, and the amplitudes are reciprocals of the odd numbers. The first term is called the fundamental, and the other terms are known as higher-order harmonics. The second term has three times the frequency of the fundamental, and is therefore known as the third harmonic. If we add together the first eight terms of the above series we get a fairly good approximation to the square wave. The resultant is shown in Figure 2.11(f) and is given by the following sum:

$$f(\omega t) = \frac{4}{\pi} \left(\sin \omega t + \frac{1}{3} \sin 3\omega t + \frac{1}{5} \sin 5\omega t + \dots + \frac{1}{15} \sin 15\omega t \right) \quad (2.34)$$

Most periodic and many other nonperiodic waveforms can be decomposed into a summation of periodic sine and cosine waves.

2.6.2 Fourier Transforms

We have seen how the square wave can be decomposed into a summation of sine waves. The waves of Figure 2.11 show us the variation of the intensity or displacement

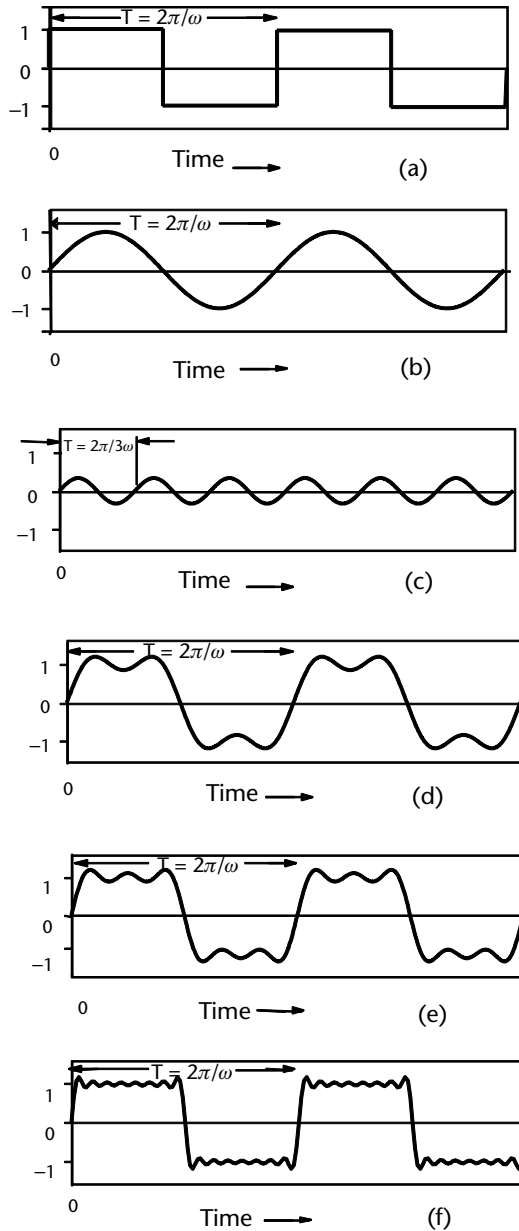


Figure 2.11 Fourier analysis of a square wave. (a) Square wave of frequency $f = \omega/2\pi$ and amplitude 1, (b) sine wave of frequency $f = \omega/2\pi$ and amplitude 1, (c) sine wave of frequency $f = 3\omega/2\pi$ and amplitude $1/3$, (d) summation of the first two terms $\sin \omega t + (\sin 3\omega t)/3$, (e) summation of the first three terms $\sin \omega t + (\sin 3\omega t)/3 + (\sin 5\omega t)/5$, (f) summation of the first eight terms.

with time (i.e., the pattern in the time domain). If we were to look at the variation of the intensity with frequency for a sine wave, we would get a single line at a frequency $f (= \omega/2\pi)$ and the length of the line would be equal to the amplitude (the maximum value of the intensity). This type of plot, which shows us the variation in the frequency domain, is called the frequency spectrum and is shown in Figure

2.12(a). The Fourier transform has transformed a time domain plot into the frequency domain. In the case of the square wave, if we were to look at its spectrum we would get a series of lines with the slope of the amplitudes equal to -6 dB per octave (the amplitude is halved each time the frequency is doubled). The time and frequency domain plots are shown in Figure 2.12(b). For a square pulse, we would get the time and frequency domain plots of Figure 2.12(c). In antenna technology, we use the Fourier transform to transform the illumination across an antenna to the electric field variation in the far field. For example, if we have a uniform illumination (constant electric field and no phase variation) across an antenna, this is the same as the square pulse shown in Figure 2.12(c), and its Fourier transform is given by

$$f(\theta) = \frac{\sin u}{u} \quad (2.35)$$

where

$$u = (\pi a \sin \theta) / \lambda,$$

a is the width of the aperture of the antenna,

and θ is the angle measured from the normal to the aperture.

The radiation pattern, which is the variation of power (proportional to the square of the electric field) with angle θ , is given by

$$F(\theta) = \frac{\sin^2 u}{u^2} \quad (2.36)$$

The exact number, height, and position of the sidelobes depend on the size of the electrical aperture, a/λ , that is, the size in terms of the wavelength. In Figure 2.12(d), we have the radiation pattern for an antenna that is 10 wavelengths long. Note that the y -scale shows the power in decibels, and is therefore a logarithmic scale.

Other uses for Fourier transforms are in measuring the frequency content of transients and pulses so that their effect on equipment can be estimated.

2.7 Parameters

We must distinguish between the strict definition of parameters used by mathematicians and the parameters used by engineers.

2.7.1 Mathematical Definition of Parameters

A parameter is defined by mathematicians as a third variable on which the other two variables depend. For instance, instead of writing the equation of a circle as

$$x^2 + y^2 = a^2 \quad (2.37)$$

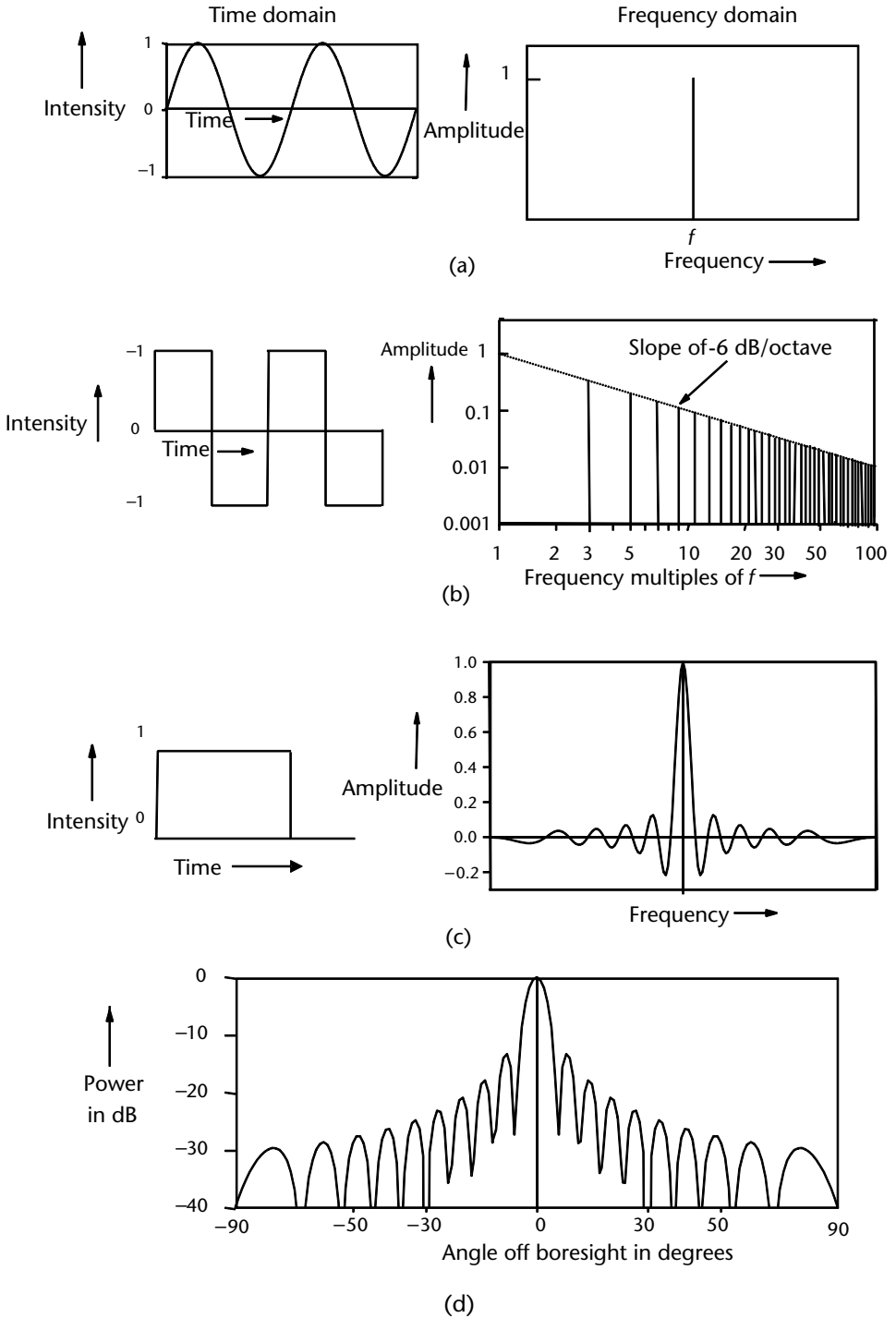


Figure 2.12 Fourier transforms. (a) Fourier transform of a sine wave, (b) Fourier transform of a square wave, (c) Fourier transform of a square pulse, (d) far-field radiation pattern for uniform illumination, (f) far-field radiation pattern for uniform illumination.

or

$$y = \sqrt{a^2 - x^2} \quad (2.38)$$

each of the variables can be written in terms of another variable θ .

$$x = a \cos \theta \quad (2.39)$$

$$y = a \sin \theta \quad (2.40)$$

Equations (2.39) and (2.40) are known as parametric equations, and θ is known as the parameter. These are depicted in Figure 2.13(a).

We can see that if we were to square (2.39) and (2.40) and add them together, we would get the following

$$x^2 + y^2 = a^2 \cos^2 \theta + a^2 \sin^2 \theta \quad (2.41)$$

This is the same as the equation of the circle given by (2.37), since

$$\cos^2 \theta + \sin^2 \theta = 1 \quad (2.42)$$

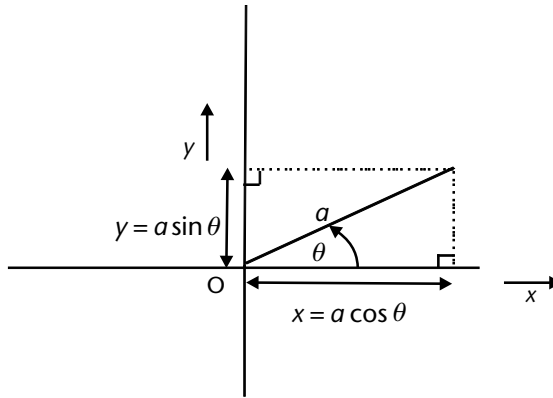
2.7.2 Parameters Used by Engineers

Engineers tend to use the term parameter in a different way. If we consider the equation of a circle, (2.37), the value of a determines the radius of the circle, and it can take on any constant magnitude for each series of x and y values. If we give it a number of fixed values, we would get a series of concentric circles, which have the origin of coordinates as their center, as shown in Figure 2.13(b). We can now say that we are plotting y against (or vs. for versus) x with a as a parameter. If we were to increase a in infinitesimally small steps from an initial value of zero, we would get a solid disc since the circles of increasing radii would be touching.

In EMC engineering, we encounter many cases of variables that are dependent on two or more other variables. For instance, we have the shielding effectiveness (SE) of a material dependent on the frequency as well as on the conductivity. We could choose the conductivity as the independent variable (x -axis) and plot the SE against conductivity for a number of fixed frequencies to get different plots on the same graph. We would then say that frequency is the parameter.

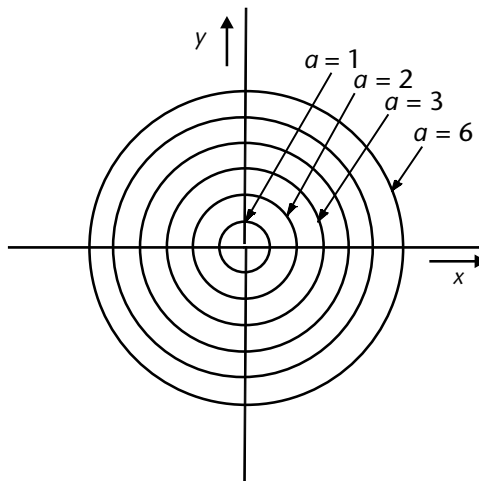
2.8 Fundamental Units and Dimensions

All physical quantities can be expressed as a combination of the fundamental or basic units, also called SI (Système International) base units. The relationship between a physical quantity and the fundamental units is called its dimension. These fundamental units are shown in Table 2.3.



Parametric equations are $x = a \cos \theta$ and $y = a \sin \theta$ where θ is the parameter

(a)



Plots of $y = \sqrt{a^2 - x^2}$ with a as a parameter

(b)

Figure 2.13 Parameters used by mathematicians and engineers. (a) Parametric equations are $x = a \cos \theta$, and $y = a \sin \theta$, where θ is the parameter. (b) Plots of $y = \sqrt{a^2 - x^2}$ with a as a parameter.

Table 2.3 Fundamental or SI Base Units

<i>Physical Quantity</i>	<i>Name of Base Unit</i>	<i>Unit</i>	<i>Symbol</i>	<i>Dimension</i>
Mass	kilogram	kg	<i>m</i>	M
Length	meter	m	<i>l</i>	L
Time	second	s	<i>t</i>	T
Current	amperes	A	<i>I</i>	I
Thermodynamic temperature	degrees kelvin	K	<i>T</i>	K

Table 2.4 Dimensions of Commonly Used Physical Quantities

<i>Physical Quantity</i>	<i>Name of Unit</i>	<i>Unit</i>	<i>Symbol</i>	<i>Fundamental Units</i>
Acceleration	meters per second squared	m s ⁻²	α	LT ⁻²
Angular frequency	radians/s	radians/s	ω	T ⁻¹
Capacitance	farad	F	C	M ⁻¹ L ⁻² T ⁴ I ¹
Charge	coulomb	C	Q	IT
Conductance/susceptance	siemen	S	G	M ⁻¹ L ⁻² T ³ I ² (same as admittance)
Conductivity	siemen-meter	S-m	σ	M ⁻¹ L ⁻³ T ³ I ²
Current	ampere	A	I	I
Current density	amperes per square meter	A m ⁻²	J	IL ⁻²
Dielectric constant	no units	no units	ϵ_r	ϵ/ϵ_o (same as relative permittivity)
Distance or length	meter	m	d	L
Electric field intensity	volts per meter	V m ⁻¹	E	MLT ⁻³ I ⁻¹
Energy	joule	J	E or W_e	ML ² T ⁻²
Force	newton	N	F	MLT ⁻²
Frequency	hertz	Hz	f	T ⁻¹
Impedance	ohm	Ω	R	ML ² T ⁻³ I ⁻² (same as resistance)
Inductance	henry	H	L	ML ² T ⁻² I ⁻²
Length	meter	m	l	L
Mass	kilogram	kg	m	M
Magnetic field intensity	amperes per meter	A m ⁻¹	H	IL ⁻¹
Magnetic flux density	tesla	T	B	MT ⁻² I ⁻¹
Permeability	henries per meter	H m ⁻¹	μ	MLT ⁻² I ⁻²
Permittivity	farads per meter	F m ⁻¹	ϵ	M ⁻¹ L ⁻³ T ⁴ I ²
Power	watts	W	P	ML ² T ⁻³
Power density	watts per meter	W m ⁻²	P_d	MT ⁻³
Relative permeability	no units	no units	μ_r	μ/μ_o
Relative permittivity	no units	no units	ϵ_r	$\epsilon\epsilon_o$ (same as dielectric constant)
Resistance/reactance	ohm	Ω	R	ML ² T ⁻³ I ⁻² (same as impedance)
Resistivity	ohm-meter	Ω -m	ρ	ML ³ T ⁻³ I ⁻²
Skin depth	meter	m	δ	L
Time	second	s	t	T
Velocity	meters per second	m s ⁻¹	v	LT ⁻¹
Voltage	volt	V	V	ML ² T ⁻³ I ⁻¹
Wavelength	meter	m	λ	L

Consider the units of energy, for instance. Energy can be defined as the product of force and distance. Force, in its turn, can be defined by Newton's law as the product of mass and acceleration. Since acceleration is the rate of change of velocity, its dimensions are LT^{-2} (i.e., its SI base units are $m\ s^{-1}$), and thus we get energy = ML^2T^{-2} for the dimension of energy. Since the energy is in joules, this gives us the fundamental units of the joule. Note that joule is written with a lower case initial letter, although it is a proper name; whereas the unit J is denoted by an uppercase letter.

The dimensions for power in watts can be derived from the units for energy, since power is the number of joules per second. The dimensions of power are therefore ML^2T^{-3} . The dimensions for voltage in volts can be derived from the units for power, since power is the product of volts and amps. The dimensions of volts are therefore $ML^2T^{-3}I^{-1}$. The dimensions of inductance in henries can be derived in a similar manner, since, according to Lenz's law, the inductance is induced electromotive force (EMF) divided by the rate of change of current. Thus the dimensions of henries are $ML^2T^{-2}I^{-2}$.

The dimensions of SI units most commonly used in EMC engineering are listed in Table 2.4.

2.8.1 Checking Formulas by Dimensions

Reducing a physical quantity to fundamental units is useful in verifying the correctness of formulas or in resolving ambiguities. For instance, formulas often contain the symbols μ and ϵ for relative permeability and permittivity, respectively, when these should have the subscript r (i.e., μ_r and ϵ_r).

We can also understand the physical meaning of formulas if we can derive their dimensions. For instance, if we consider the product of the electric and magnetic field intensities we know from Table 2.4 that electric field has the dimensions of $MLT^{-3}I^{-1}$, and magnetic field has the dimensions of IL^{-1} ; thus the product has dimensions given by

$$\mathbf{E} \times \mathbf{H} = MLT^{-3}I^{-1}IL^{-1}$$

which gives us the following

$$\mathbf{E} \times \mathbf{H} = MT^{-3}$$

Referring to Table 2.4, we can see that these are the same as the units for power density and $\mathbf{E} \times \mathbf{H}$ is known as Poynting's power flux vector. It is left to the reader to verify that the dimensions for $\sqrt{\mu\epsilon}$ are the same as those for resistance.

Antenna Theory

This chapter deals with more advanced vector algebra, which is required to understand Maxwell's equations and the theoretical aspects of antennas. It is strongly recommended that Chapter 2 be studied by engineers who are not conversant with mathematics or would like to revise the application of their knowledge to the theoretical understanding of antennas. This chapter is written in such a way as to be self-contained, and it can be entirely omitted by the reader who does not wish to study antenna theory. Although Maxwell's equations are quoted, they are explained qualitatively with greater emphasis being placed on the boundary conditions applicable to conducting surfaces. The concepts of a vector power density and radiation resistance of wire antennas are introduced. The derivation of the far-field distance for wire and aperture antennas is also included. Vectors are denoted by bold letters and scalars are denoted by normal characters.

3.1 Unit Vectors

We have seen, in Chapter 2, how we can draw vectors to scale and then construct parallelograms or triangles in order to calculate the sum of two vectors. Instead of saying that we have a vector \mathbf{A} in a particular direction, we can say that we have a scalar F in the direction of a unit vector \mathbf{r} . The vector \mathbf{A} can then be considered to be the dot product of the scalar F and the unit vector \mathbf{r} .

In rectangular coordinates, unit vectors are represented by \mathbf{i} , \mathbf{j} , and \mathbf{k} along the x -, y -, and z -axes, respectively. Unit vectors are sometimes denoted with a circumflex above (e.g., $\hat{\mathbf{i}}$, $\hat{\mathbf{j}}$, and $\hat{\mathbf{k}}$).

In cylindrical polar coordinates, unit vectors are represented by \mathbf{a}_r , \mathbf{a}_θ , and \mathbf{a}_z along the radial direction, the direction of angular rotation θ , and along the z -axis normal to the plane containing \mathbf{a}_r and \mathbf{a}_θ , respectively. In spherical polar coordinates \mathbf{a}_ϕ is used instead of \mathbf{a}_z , where ϕ is the angle of rotation in the x - y plane. The unit vectors in rectangular and polar coordinates are depicted in Figure 3.1.

Unit vectors are used to express any vector in terms of three unit vectors. If we want to multiply vectors, we first write them in terms of three unit vectors and then multiply them together. For example if we want to calculate their cross product, we write them in the following manner

$$\begin{aligned} \mathbf{A} \times \mathbf{B} &= (\mathbf{i}A_x + \mathbf{j}A_y + \mathbf{k}A_z) \times (\mathbf{i}B_x + \mathbf{j}B_y + \mathbf{k}B_z) \\ \mathbf{A} \times \mathbf{B} &= \mathbf{i}A_x \times \mathbf{i}B_x + \mathbf{i}A_x \times \mathbf{j}B_y + \mathbf{i}A_x \times \mathbf{k}B_z + \mathbf{j}A_y \times \mathbf{i}B_x + \mathbf{j}A_y \\ &\quad \times \mathbf{j}B_y + \mathbf{j}A_y \times \mathbf{k}B_z + \mathbf{k}A_z \times \mathbf{i}B_x + \mathbf{k}A_z \times \mathbf{j}B_y + \mathbf{k}A_z \times \mathbf{k}B_z \end{aligned} \quad (3.1)$$

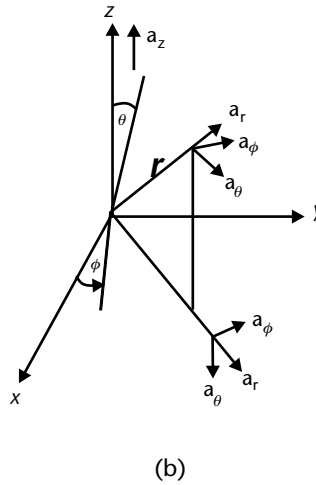
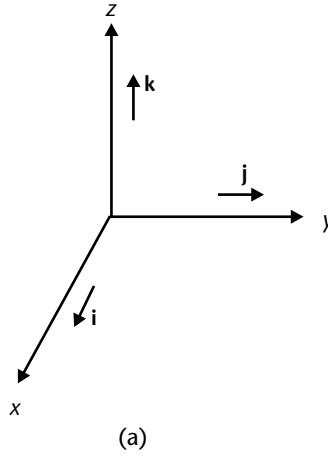


Figure 3.1 Unit vectors in (a) right-handed rectangular coordinates, and (b) polar coordinates.

Since we have $\mathbf{i}A_x$ and $\mathbf{i}B_x$ in the same direction, that is, the angle between them is zero, their cross product is zero. The same holds true for the cross product of $\mathbf{j}A_y$ and $\mathbf{j}B_y$, and the cross product of $\mathbf{k}A_z$ and $\mathbf{k}B_z$.

We also know that the cross product of $\mathbf{i}A_x$ and $\mathbf{j}B_y$ gives us a vector $\mathbf{k}A_xB_y$ along the z -axis. On the other hand, the cross product of $\mathbf{k}A_z$ and $\mathbf{j}B_y$ gives us a vector $\mathbf{i}A_zB_y$ along the negative x -axis; that is, it is equal to $-\mathbf{i}A_zB_y$.

The same applies to the other cross products. Thus the following relationships apply:

$$\begin{array}{lll}
 \mathbf{i}A_x \times \mathbf{i}B_x = 0 & \mathbf{j}A_y \times \mathbf{j}B_y = 0 & \mathbf{k}A_z \times \mathbf{k}B_z = 0 \\
 \mathbf{i}A_x \times \mathbf{j}B_y = \mathbf{k}A_xB_y & \mathbf{i}A_x \times \mathbf{k}B_z = -\mathbf{j}A_xB_z & \mathbf{j}A_y \times \mathbf{i}B_x = -\mathbf{k}A_yB_x \\
 \mathbf{j}A_y \times \mathbf{k}B_z = \mathbf{i}A_yB_z & \mathbf{k}A_z \times \mathbf{i}B_x = \mathbf{j}A_zB_x & \mathbf{k}A_z \times \mathbf{j}B_y = -\mathbf{i}A_zB_y
 \end{array} \quad (3.2)$$

Thus the cross product of \mathbf{A} and \mathbf{B} can be written as the sum of the following three vectors:

$$\mathbf{A} \times \mathbf{B} = \mathbf{i}(A_y B_z - A_z B_y) - \mathbf{j}(A_x B_z - A_z B_x) + \mathbf{k}(A_x B_y - A_y B_x) \quad (3.3)$$

This cross product can also be written in the form of a matrix as

$$\mathbf{A} \times \mathbf{B} = \begin{vmatrix} \mathbf{i} & \mathbf{j} & \mathbf{k} \\ A_x & A_y & A_z \\ B_x & B_y & B_z \end{vmatrix} \quad (3.4)$$

3.2 Scalar and Vector Fields

In Chapter 2, we have encountered scalars and vectors which have fixed magnitudes and directions. We now consider scalar and vector fields. In this case, we have scalars and vectors which are functions of position (i.e., they are point functions). Their magnitudes and/or directions depend on position. Scalar point functions define scalar fields, and vector point functions define vector fields.

3.2.1 Spatial Rates of Change of Scalar and Vector Fields

There are three types of rates of change:

1. Gradient, or grad;
2. Divergence, or div;
3. Curl or rot.

These rates of change can be expressed in terms of a vector operator called del or nabla, which is represented by the symbol ∇ . The operator is defined by the following relationship

$$\nabla = \mathbf{i} \frac{\partial}{\partial x} + \mathbf{j} \frac{\partial}{\partial y} + \mathbf{k} \frac{\partial}{\partial z} \quad (3.5)$$

It should be noted that del is not a vector but an operator, and operates on a scalar or vector.

The gradient, divergence, and curl of scalar and vector fields are invariant, that is, they are independent of the coordinate system.

3.2.2 Gradient of a Scalar Field

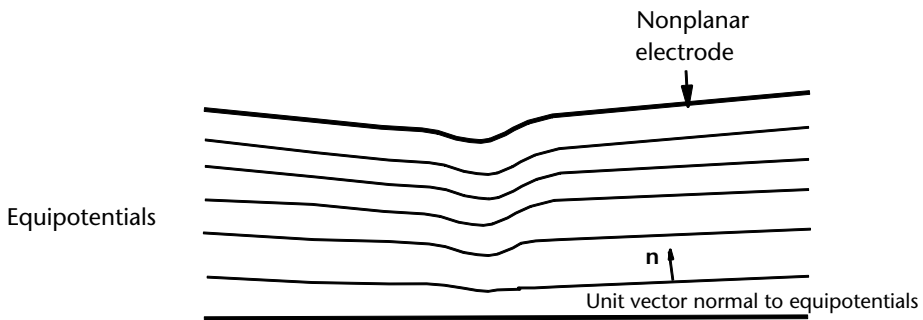
If we have a scalar point function ϕ , then at a point P surrounded by a surface S and enclosing a volume V , we can define the gradient of ϕ as a vector showing the direction and magnitude of the maximum space variation at any point in space. In

rectangular coordinates, the gradient of the function is the sum of the individual gradients along each of the three mutually perpendicular axes and is given by

$$\text{grad } \phi = i \frac{\partial \phi}{\partial x} + j \frac{\partial \phi}{\partial y} + k \frac{\partial \phi}{\partial z} \quad (3.6)$$

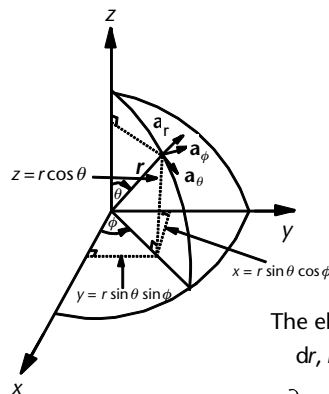
We can also write the gradient in terms of the operator del as $\nabla \phi$.

For example, if we have a series of equipotentials (between two electrodes), the equipotentials will be parallel but not necessarily planar if the electrodes are not planar, as shown in Figure 3.2. The voltage potential is a scalar quantity, but the rate of change with distance, of the voltage potential is the electric field and this is a vector. The gradient is defined as the maximum rate of increase in the direction normal to the equipotentials.



$$\text{Grad } V = i \frac{\partial V}{\partial x} + j \frac{\partial V}{\partial y} + k \frac{\partial V}{\partial z}$$

(a)



The elements of length are
 $dr, r d\theta, r \sin \theta d\phi$

$$\text{grad } V = \mathbf{a}_r \frac{\partial V}{\partial r} + \mathbf{a}_\theta \frac{1}{r} \frac{\partial V}{\partial \theta} + \mathbf{a}_\phi \frac{1}{r \sin \theta} \frac{\partial V}{\partial \phi}$$

(b)

Figure 3.2 The gradient of a scalar field in (a) rectangular coordinates, and (b) spherical polar coordinates.

In the general case for rectangular coordinates, the voltage gradient will have components along each of the x -, y -, and z -axes, and is given by

$$\text{grad}V = i \frac{\partial V}{\partial x} + j \frac{\partial V}{\partial y} + k \frac{\partial V}{\partial z} \quad (3.7)$$

This can also be written in terms of the operator del as ∇V .

In polar coordinates, the elements of length are dr , $r d\theta$, and $r \sin\theta d\phi$, and $\text{grad}V$ is given by

$$\text{grad}V = a_r \frac{\partial V}{\partial r} + a_\theta \frac{1}{r} \frac{\partial V}{\partial \theta} + a_\phi \frac{1}{r \sin\theta} \frac{\partial V}{\partial \phi} \quad (3.8)$$

3.2.3 Divergence of a Vector Field

In the field of electromagnetism, we encounter magnetic fluxes which diverge from magnetic poles. The divergence of the magnetic flux would be defined, in this case, as the total flux coming out of (or diverging from) unit volume as the volume shrinks to zero. The divergence is given as

$$\text{div } A = \lim_{\text{vol} \rightarrow 0} \lim \frac{\int_{\text{flux}}}{\int_v dV_u} \quad (3.9)$$

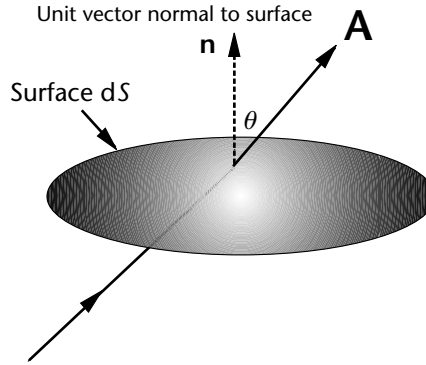
In general, the divergence can be defined as the normal surface integral over a surface as the volume tends to zero.

$$\text{div } \phi = c \frac{\oint_s A \cdot dS}{\int_v dV_u} \quad (3.10)$$

The vector $d\mathbf{S}$ is the product of the scalar area dS and the unit vector \mathbf{n} normal to the surface element dS . The element dS must be small enough so that it can be considered as a plane area and so that \mathbf{A} varies negligibly over it. The dot product of \mathbf{A} and $d\mathbf{S}$ is then taken in the usual manner by multiplying $d\mathbf{S}$ and $A \cos\theta$ if the angle between the vector \mathbf{A} , and the normal to the elemental surface is θ , as shown in Figure 3.3.

The integral of this dot product is sometimes called the normal surface integral of \mathbf{A} over dS , and is the numerator of (3.10). Note that the divergence of a vector field is a scalar. This bears a resemblance to the dot product of vectors, which is a scalar.

The integral in the numerator of (3.10) is sometimes written as a double integral. This is because we can consider the vector \mathbf{A} to be integrated over the element of area dS , multiplied by the vector $d\mathbf{S}$ and then the dot product is integrated over the total surface S [1, p. 725]. The divergence is often written in terms of the operator del or nabla, as $\nabla \cdot V$.



$$\text{div } \mathbf{A} \text{ in rectangular coordinates} = \frac{\partial A_x}{\partial x} + \frac{\partial A_y}{\partial y} + \frac{\partial A_z}{\partial z}$$

div \mathbf{A} in spherical polar coordinates is given by

$$\text{div } \mathbf{A} = \frac{1}{r^2} \frac{\partial}{\partial r} (r^2 A_r) + \frac{1}{r \sin \theta} \frac{\partial}{\partial \theta} (\sin \theta A_\theta) + \frac{1}{r \sin \theta} \frac{\partial A_\phi}{\partial \phi}$$

Figure 3.3 The divergence of a vector field: div \mathbf{V} in rectangular coordinates

$$\begin{aligned} &= \frac{\partial A_x}{\partial x} + \frac{\partial A_y}{\partial y} + \frac{\partial A_z}{\partial z}; \text{ div } \mathbf{A} \text{ in spherical polar coordinates} \\ &= \frac{1}{r^2} \frac{\partial}{\partial r} (r^2 A_r) + \frac{1}{r \sin \theta} \frac{\partial}{\partial \theta} (\sin \theta A_\theta) + \frac{1}{r \sin \theta} \frac{\partial A_\phi}{\partial \phi} \end{aligned}$$

In rectangular coordinates, we can also write the divergence of a vector in differential form as

$$\text{div } \mathbf{A} = \lim_{\text{vol} \rightarrow 0} \left(\frac{\partial A_x}{\partial x} + \frac{\partial A_y}{\partial y} + \frac{\partial A_z}{\partial z} \right) \quad (3.11)$$

In polar coordinates div \mathbf{A} is given by

$$\text{div } \mathbf{A} = \frac{1}{r^2} \frac{\partial}{\partial r} (r^2 A_r) + \frac{1}{r \sin \theta} \frac{\partial}{\partial \theta} (\sin \theta A_\theta) + \frac{1}{r \sin \theta} \frac{\partial A_\phi}{\partial \phi} \quad (3.12)$$

3.2.4 Curl of a Vector

The curl was a term first used by James Clerk Maxwell [2], who took an idea that William Thomson (better known as Lord Kelvin) had of calculating a vector from another vector. The curl of a physical field defines its rotation or vorticity. This is one of the most difficult concepts to interpret physically. It is best explained in terms of a physical phenomenon we can observe in everyday life [3, pp. 2–4]. Consider an object floating downstream on the surface in the y -direction, as shown in Figure 3.4(a). If the stream is flowing in the y -direction with no eddies and has uniform velocity across its width (in the x -direction) the object would move in the y -direction alone. However, in the general case there are eddies caused by the variation in the velocities of the stream in the x - and z -directions. These variations cause

the object to turn. For simplicity, let us consider variations in the velocities in the x - and y -directions only for an object floating on the surface. The components of the velocities at corner P in the x - and y -directions (along PS and PQ) are v_x and v_y , respectively. The velocity gradients of these components in the y - and x -directions are $\partial v_x/\partial y$ and $\partial v_y/\partial x$, and assuming these gradients are positive, the velocities along QR and SR will be $v_x + (\partial v_x/\partial y)dy$ and $v_y + (\partial v_y/\partial x)dx$. The differences in the velocities along the opposite sides of the object cause the object to turn. The direction of rotation will depend on which velocity gradient is the larger. If $\partial v_y/\partial x$ is the larger gradient, the object will turn in a counterclockwise direction looking down on the x - y plane.

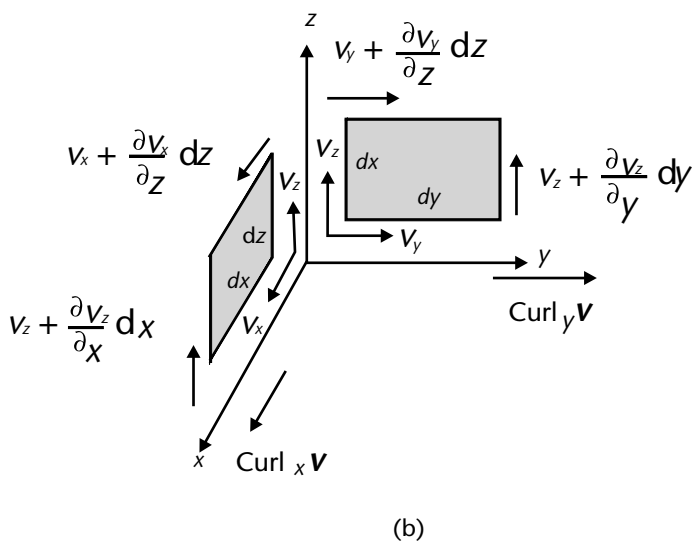
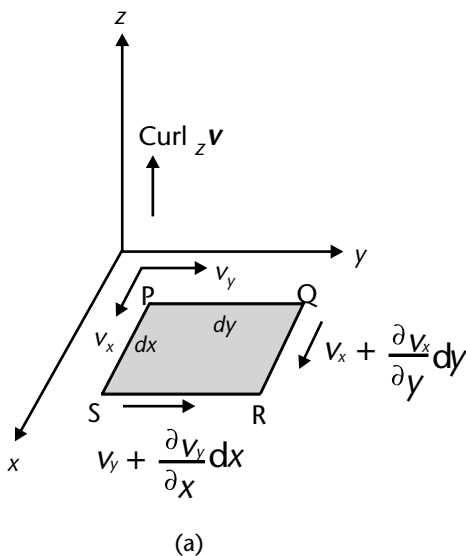


Figure 3.4 The curl of a vector field: (a) $\text{Curl}_z \mathbf{v}$ component of $\text{Curl } \mathbf{v}$ and (b) $\text{Curl}_x \mathbf{v}$ and $\text{Curl}_y \mathbf{v}$ component of $\text{Curl } \mathbf{v}$.

The $\text{curl}_z \mathbf{v}$ is defined [3] as the vector in the positive z -direction that is the result of this counterclockwise rotation in the x - y plane. We can see that this is the same direction that is defined by the right-hand screw rule, that is, if we turn a screw in an counterclockwise direction looking down on the x - y plane, it would move in the positive z -direction. The $\text{curl}_z \mathbf{v}$ is given by

$$\text{curl}_z \mathbf{v} = \mathbf{k} \left(\frac{\partial v_y}{\partial x} - \frac{\partial v_x}{\partial y} \right) \quad (3.13)$$

where \mathbf{k} is the unit vector in the positive z -direction. We can similarly define $\text{curl}_x \mathbf{v}$ and $\text{curl}_y \mathbf{v}$ along the positive x - and y -axes, as shown in Figure 3.4(b). The total curl of the vector is the sum of these three individual curls, and is given by

$$\text{curl } \mathbf{v} = i \left(\frac{\partial v_z}{\partial y} - \frac{\partial v_y}{\partial z} \right) - j \left(\frac{\partial v_z}{\partial x} - \frac{\partial v_x}{\partial z} \right) + k \left(\frac{\partial v_y}{\partial x} - \frac{\partial v_x}{\partial y} \right) \quad (3.14)$$

Note the similarity between this vector and the cross product of two vectors that we encountered in Chapter 2 and Section 3.1. The curl can also be written in terms of the del operator as the cross product of del and the velocity vector \mathbf{v} , and the right-hand side of (3.14) can be written as a matrix; thus we have the curl given by

$$\nabla \times \mathbf{v} = \begin{vmatrix} i & j & k \\ \frac{\partial}{\partial x} & \frac{\partial}{\partial y} & \frac{\partial}{\partial z} \\ v_x & v_y & v_z \end{vmatrix} \quad (3.15)$$

In the spherical polar coordinate system, the curl in each direction is given by

$$\text{curl}_r \mathbf{A} = \frac{a_r}{r \sin \theta} \left[\frac{\partial}{\partial \theta} (\sin \theta A_\theta) - \frac{\partial A_\phi}{\partial \phi} \right] \quad (3.16)$$

$$\text{curl}_\theta \mathbf{A} = \frac{a_r}{r \sin \theta} \left[\frac{\partial}{\partial \theta} (\sin \theta A_\theta) - \frac{\partial A_\phi}{\partial \phi} \right] \quad (3.17)$$

$$\text{curl}_\phi \mathbf{A} = \frac{a_\phi}{r} \left[\frac{\partial}{\partial r} (r A_\phi) - \frac{\partial A_r}{\partial \theta} \right] \quad (3.18)$$

3.3 Maxwell's Equations

Maxwell's equations are based on the previous work of Gauss, Faraday, Biot, and Savart. He expressed their laws in concise terms, and also introduced the idea of a displacement current. This explains the magnetic field caused by the buildup of electric charges, (as in the case of the plates of a capacitor) in a similar way to the

magnetic field caused by the flow of electrons in a conductor. Until Maxwell's time, it was assumed that a magnetic field could only be produced by a conduction current (i.e., electrons flowing in a conductor). This ruled out a magnetic field being produced in a region of zero conductivity. Maxwell assumed that any change in an electrostatic field produced an attendant magnetic field and vice versa. This magnetic field is related to the electrostatic field change in the same way as the magnetic field is related to the change of conduction current. Thus, if we have a static charge on an insulator, such as an ebonite disk, and if we rotate the disk we will have what is known as displacement current, and a magnetic field will be produced. It was not until 1889 (after Maxwell's death in 1879) that Rowland showed that displacement current was the result of electrostatic buildup of charge on the electrodes of a capacitor. The electrostatic lines of force precede the charges and the attendant magnetic field.

Maxwell's equations are sometimes called the EM field equations, because only the first two are attributable to Maxwell. However, all four are normally called Maxwell's equations and are denoted as such in this book.

In the EMC field we are mainly concerned with the electric and magnetic fields in free space, that is, in source-free media.

3.3.1 Maxwell's First Equation

This equation is based on Ampere's law, which states that the line integral of the magnetic field intensity is equal to the total current enclosed (i.e. the sum of the conduction and displacement currents), and is given by

$$\oint \mathbf{H} \cdot d\mathbf{l} = I_{\text{conduction}} + I_{\text{displacement}} \quad (3.19)$$

where \mathbf{H} is the magnetic field intensity in amperes per meter (A m^{-1}), and $d\mathbf{l}$ is an elementary length in meters (m).

The conduction and displacement currents can be written in terms of the conduction and displacement current densities \mathbf{J}_c and \mathbf{J}_d , respectively, and the area. Thus, (3.19) can be written as

$$\oint \mathbf{H} \cdot d\mathbf{l} = \int_S (\mathbf{J}_c + \mathbf{J}_d) \cdot d\mathbf{S} \quad (3.20)$$

where \mathbf{J}_c is the conduction current density in A m^{-2} , \mathbf{J}_d is the displacement current density in A m^{-2} , and $d\mathbf{S}$ is the element of area perpendicular to the current flow in square meters (m^2).

The conduction current density \mathbf{J}_c is in turn related to the electric field intensity by the following relation $\mathbf{J}_c = \sigma \mathbf{E}$, where \mathbf{J}_c is the conduction current density in A m^{-2} , σ is conductivity in S m^{-1} and \mathbf{E} is the electric field intensity in V m^{-1} .

The displacement current density \mathbf{J}_d is equal to the rate of change (with time) of the electric flux (or displacement) density \mathbf{D} . Thus we can say that \mathbf{J}_d is given by

$$\mathbf{J}_d = \frac{\partial \mathbf{D}}{\partial t} \quad (3.21)$$

where J_d is the displacement current density in amperes per square meter ($A\ m^{-2}$), and D is the electric flux density in coulombs per square meter ($C\ m^{-2}$).

The electric flux density can be written in terms of the electric field as

$$\mathbf{D} = \epsilon\mathbf{E} \quad (3.22)$$

where ϵ is the permittivity in farads per meter ($F\ m^{-1}$) and \mathbf{E} is the electric field in volts per meter ($V\ m^{-1}$).

We can write (3.20) as

$$\oint \mathbf{H} \cdot d\mathbf{l} = \int \left(\sigma\mathbf{E} + \frac{\partial}{\partial t}(\epsilon\mathbf{E})J_d \right) dS \quad (3.23)$$

Stokes' theorem states that the curl of a vector is the maximum value of the line integral around an elementary surface as the surface shrinks to zero. Thus the curl is given by

$$\text{curl } \mathbf{A} = \lim_{S \rightarrow 0} \frac{\oint \mathbf{A} \cdot d\mathbf{l}}{\delta S} \quad (3.24)$$

Applying Stokes' theorem to (3.23) we get

$$\int_S \text{curl } \mathbf{H} \cdot d\mathbf{S} = \int_S \left(\sigma\mathbf{E} + \frac{\partial}{\partial t}(\epsilon\mathbf{E}) \right) dS \quad (3.25)$$

If we assume that the surface becomes very small, $dS \rightarrow \Delta S$, $\text{curl } \mathbf{H}$ and \mathbf{E} can be considered to be approximately uniform over this area and almost independent of the area. Equation (3.25) can be written as

$$\text{curl } \mathbf{H} = \sigma\mathbf{E} + \epsilon \frac{\partial \mathbf{E}}{\partial t} \quad (3.26)$$

This is Maxwell's first equation in differential vector form.

We can also write this equation in scalar differential form for each component of the magnetic field intensity \mathbf{H} , using the definition of the component of a curl given by (3.13).

$$\begin{aligned} \frac{\partial H_z}{\partial y} - \frac{\partial H_y}{\partial z} &= \epsilon \frac{\partial E_x}{\partial t} + \sigma E_x \\ \frac{\partial H_x}{\partial z} - \frac{\partial H_z}{\partial x} &= \epsilon \frac{\partial E_y}{\partial t} + \sigma E_y \\ \frac{\partial H_y}{\partial x} - \frac{\partial H_x}{\partial y} &= \epsilon \frac{\partial E_z}{\partial t} + \sigma E_z \end{aligned} \quad (3.27)$$

In integral form, the first equation is given by (3.23) and it can be stated as: The magnetomotive force around a closed path is equal to the conduction current plus the time derivative of the electric flux density through any surface bounded by the path [3, p. 204].

3.3.2 Maxwell's Second Equation

This equation is based on Faraday's law, which states that a magnetic flux of Φ induces an electromotive force (EMF) in a conductor. This induced EMF has a magnitude $|V|$ that is proportional to the rate of change of the flux Φ , and this is given by

$$V = -\frac{d\phi}{dt} \quad (3.28)$$

The negative sign indicates that the voltage opposes the flux causing it.

This voltage V is also equal to the line integral of the electric field \mathbf{E} over the length of the conductor. This integral is found by taking the dot product of \mathbf{E} and $d\mathbf{l}$, and then integrating over the whole length of the conductor. Thus we have

$$|V| = \int \mathbf{E} \cdot d\mathbf{l} \quad (3.29)$$

where \mathbf{E} is the electric field in volts per meter (V m^{-1}) and $d\mathbf{l}$ is the elemental length of the total loop. Thus we can say that

$$\oint \mathbf{E} \cdot d\mathbf{l} = -\frac{d\phi}{dt} \quad (3.30)$$

where ϕ is the magnetic flux in webers. The flux is related to the flux density by the following relation

$$\phi = \int \mathbf{B} \cdot d\mathbf{S} \quad (3.31)$$

where \mathbf{B} is the magnetic flux density in tesla (webers per square meter) and $d\mathbf{S}$ is the vector area, that is, the area normal to the flux density \mathbf{B} .

Combining the above two equations, we get

$$\oint_{\text{perimeter}} \mathbf{E} \cdot d\mathbf{l} = - \int_{\text{surface}} \frac{d}{dt} (\mathbf{B} \cdot d\mathbf{S}) \quad (3.32)$$

which is sometimes quoted as Maxwell's second equation in integral form, and it can be stated that the EMF around a closed path is equal to the time derivative of the magnetic displacement through any surface bounded by the path [3, p. 106]. By analogy with electric current, we can call the time derivative of the magnetic flux

the magnetic current. Thus, we can state Maxwell's second equation as: The electric voltage around a closed path is equal to the magnetic current through the path.

To derive Maxwell's equation in differential form, we use Stokes' theorem which states that the curl of a vector is the maximum value of the line integral around an elementary surface as the surface shrinks to zero. Thus the curl is given by

$$\text{curl } \mathbf{A} = \lim_{S \rightarrow 0} \frac{\oint \mathbf{A} \cdot d\mathbf{l}}{\delta S} \quad (3.33)$$

Using Stokes' theorem for a vector \mathbf{E} we can therefore write the right-hand side of (3.32) in the following form

$$\oint_{\text{perimeter}} \mathbf{E} \cdot d\mathbf{l} = - \int_{\text{surface}} \text{curl } \mathbf{E} \cdot d\mathbf{S} \quad (3.34)$$

Combining (3.32) and (3.34) we get

$$\int_s \text{curl } \mathbf{E} \cdot d\mathbf{S} = - \frac{\partial}{\partial t} \int_s \mathbf{B} \cdot d\mathbf{S} \quad (3.35)$$

If we assume that the surface becomes very small, that is $d\mathbf{S} \rightarrow \Delta S$, the curls \mathbf{E} and \mathbf{B} are approximately constant over this area. Equation (3.35) thus reduces to

$$\text{curl } \mathbf{E} \cdot \Delta S = \frac{\partial}{\partial t} (\mathbf{B} \cdot \Delta S) \quad (3.36)$$

Since ΔS is independent of time, we can rewrite (3.36) in the following form

$$\text{curl } \mathbf{E} \cdot \Delta S = \Delta S \frac{\partial}{\partial t} (\mathbf{B})$$

This gives us Maxwell's second equation in differential form as

$$\text{curl } \mathbf{E} = - \frac{\partial \mathbf{B}}{\partial t} \quad (3.37)$$

where \mathbf{E} is the electric field in volts per meter (V m^{-1}) and \mathbf{B} is the magnetic flux density in tesla (Wb m^{-2}).

3.3.3 Maxwell's Third Equation

Maxwell's third equation is based on Gauss' theorem, which states that the total outward flux is proportional to the total charge enclosed. From the definition of divergence, given by (3.9), we have

$$\operatorname{div} \mathbf{A} = \lim_{\text{vol} \rightarrow 0} \frac{\int \text{flux}}{\int_{V_u} dV_u}$$

In the case of Gauss' theorem, we have to consider the divergence of the electric flux density \mathbf{D} . Writing the total outward flux in terms of this divergence we have

$$\text{total flux} = \operatorname{div} \mathbf{D} \int_{V_u} dV_u = \int_{V_u} \rho dV_u \quad (3.38)$$

If we consider a volume that has an infinitesimal size of ΔV_u , we can assume that the charge distribution ρ is constant over it, and (3.38) can be written as

$$\operatorname{div} \mathbf{D} \int_{\Delta V_u} dV_u = \int_{\Delta V_u} \rho dV_u$$

which reduces to Maxwell's third equation, namely

$$\operatorname{div} \mathbf{D} = \rho \quad (3.39)$$

where \mathbf{D} is the electric flux density or charge per unit area ($= \epsilon \mathbf{E}$) in coulombs per square meter (C m^{-2}), ϵ is the permittivity in farads per meter (F m^{-1}), \mathbf{E} is the electric field intensity in volts per meter (V m^{-1}) and ρ is the charge distribution per unit volume in coulombs per meter (C m^{-3}).

In integral form this equation can be written as

$$\int_S \mathbf{D} \cdot d\mathbf{S} = \int_{V_u} \rho dV_u \quad (3.40)$$

where S is a closed surface. It can be stated that the total electric displacement through the surface enclosing a volume is equal to the total charge within the volume [3, p. 104].

3.3.4 Maxwell's Fourth Equation

Maxwell's fourth equation is the magnetic flux equivalent of the electric flux defined by the third equation. The divergence of the magnetic flux density \mathbf{B} is equal to the distribution of the magnetic poles enclosed. Maxwell's fourth equation states that the divergence of \mathbf{B} is zero. We would expect this to be the case since there are no free north or south magnetic poles. A north pole would travel to the south pole of a magnet and a south pole would travel to the north pole. Thus the poles would always appear in pairs and the resultant magnetic pole strength would be zero. Maxwell's fourth equation can be written in differential vector form as

$$\operatorname{div} \mathbf{B} = 0 \quad (3.41)$$

where \mathbf{B} is the magnetic flux density in tesla (Wb m^{-2})

In integral form this equation can be written as

$$\int_S \mathbf{B} \cdot d\mathbf{S} = 0 \quad (3.42)$$

where S is a closed surface. It can be stated that the net magnetic flux emerging through any closed surface is zero [3, p. 104].

3.4 Boundary Conditions

We must consider what happens to the fields at the interfaces between two media. The conditions that govern these fields are known as boundary conditions. In general, the media are dielectrics, but in the EMC field the media are usually free space and a conductor. Let us first define a conductor. A conducting medium is defined as one in which an electric field or voltage potential is always accompanied by a movement of electric charges carried by free electrons. There can be no static charge in a perfect conductor, since any electric field causes the electric charges to redistribute themselves until the electric field is zero [3, p. 2]. However all conductors have a finite conductivity, and at high frequencies the electric field penetrates the conductor to a depth that is inversely proportional to the conductivity. The electric field decays exponentially and asymptotically approaches zero as it penetrates the conductor. As the conductivity approaches infinity (i.e., that of a perfect conductor) the depth of penetration gets smaller and the current forms a thinner skin on the surface of the conductor. The skin depth is the distance from the surface of the conductor at which the electric field is equal to $1/e$ ($1/2.718$) of its magnitude at the surface.

We shall consider the tangential and normal components of the \mathbf{E} and \mathbf{H} fields in each medium on either side of the interface, as shown in Figure 3.5.

3.4.1 Tangential Component of the Electric Field

The tangential component of the electric field is continuous if both the media are dielectrics, as shown in Figure 3.5. This means that the tangential component of the \mathbf{E} field is the same inside each media near the interface, that is, we can say that

$$\mathbf{E}_{t1} = \mathbf{E}_{t2} \quad (3.43)$$

where \mathbf{E}_{t1} is the tangential electric field in medium 1 in voltage per meter (V m^{-1}) and \mathbf{E}_{t2} is the tangential electric field in medium 2 in voltage per meter (V m^{-1}).

3.4.1.1 Tangential Component of the Electric Field for Conductors

If the second medium is a perfect conductor, the tangential component of the electric field \mathbf{E}_{t2} is zero. We know that this must be the case since the electric field is the voltage per unit length, and the voltage applied across a perfect conductor will immediately fall to zero. This is to be expected from Ohm's law ($V = IR$), since the

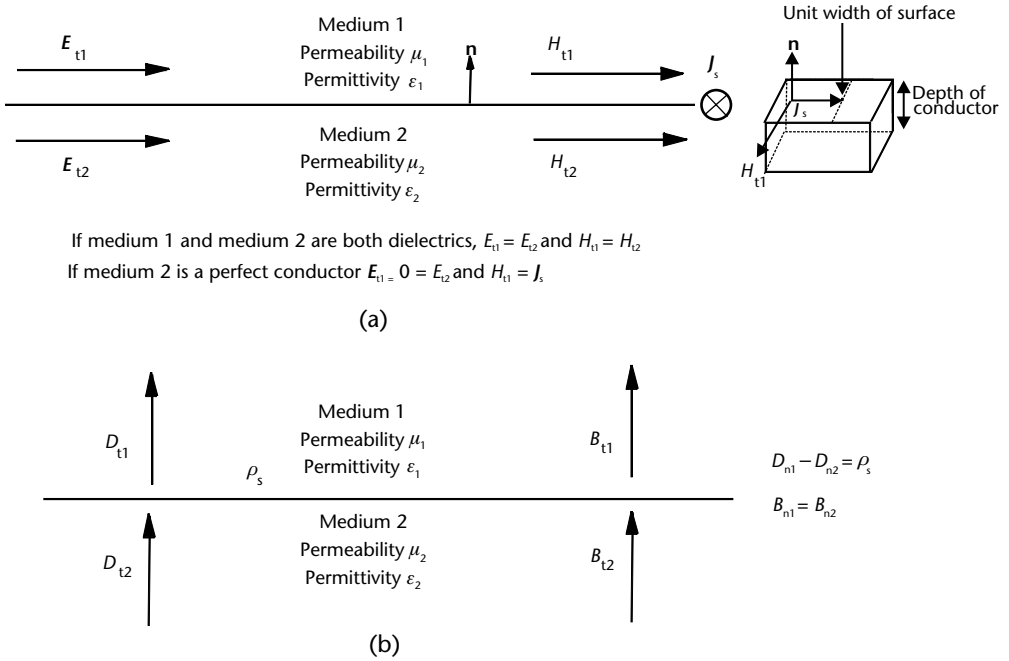


Figure 3.5 Boundary conditions at the interface of two media: (a) for the tangential \mathbf{E} and \mathbf{H} fields, and (b) for the normal \mathbf{D} and \mathbf{B} fields.

resistance is zero for a perfect conductor and thus the voltage will also be zero. Since the tangential electric field is zero just inside the conductor, it must also be zero just outside the conductor in order to satisfy (3.43).

For conductors with finite conductivity, the electric field falls to zero at a distance inside the conductor which depends on the frequency, permeability, and conductivity of the conductor.

3.4.2 Tangential Component of the Magnetic Field

The tangential component of the magnetic field \mathbf{H} is continuous if both the media are dielectrics, and so long as the current density and the electric flux density are finite. This means that the tangential component of the \mathbf{H} field is the same inside each media near the interface, that is, we can say that

$$\mathbf{H}_{t1} = \mathbf{H}_{t2} \tag{3.44}$$

where \mathbf{H}_{t1} is the tangential magnetic field in medium 1 in amperes per meter (A m^{-1}) and \mathbf{H}_{t2} is the tangential magnetic field in medium 2 in amperes per meter (A m^{-1}).

3.4.2.1 Tangential Component of the Magnetic Field at the Interface with a Conductor

If the second medium is a perfect conductor, the tangential magnetic field is zero just inside the conductor surface, but it is not zero just outside the interface in the first medium. This would appear to violate the condition of (3.44), but this is not

the case since the equation is only true for finite values of the current density. In the case of a perfect conductor, the finite current flows on the surface as a sheet of zero thickness. This makes the current density (which is the current per unit area) infinite, since the area we are considering is the product of the depth into the conductor and the distance on the surface perpendicular to the direction of flow of the current. We can define the surface current density \mathbf{J}_s as the current per unit width of the conducting surface. The tangential component of the magnetic field just outside the surface of the conductor is equal to this surface current density. This relationship is given by

$$\mathbf{J}_s = \mathbf{n} \times \mathbf{H}_{t1} \quad (3.45)$$

where \mathbf{J}_s is the surface current density in amperes per meter (A m^{-1}), \mathbf{H}_{t1} is the tangential magnetic field in medium 1, in amperes per meter (A m^{-1}), and \mathbf{n} is the unit vector normal to the surface. The surface current density is induced on the surface of the conductor by the EM field.

In general, the tangential magnetic field at the interface between a dielectric and a conductor can be stated to be discontinuous by an amount equal to the surface current density (or current per unit width) of the conductor surface, that is, we can say that

$$\mathbf{J}_s = \mathbf{H}_{t1} - \mathbf{H}_{t2} \quad (3.46)$$

3.4.3 Normal Component of the Electric Field

Let us consider the normal component of the electric flux density \mathbf{D} . The difference between the normal components of the electric flux density \mathbf{D} is equal to the surface charge density; that is, we can say that the normal component of the electric flux density is discontinuous by an amount equal to the surface charge density. This is given by the following relation

$$\mathbf{D}_{n1} - \mathbf{D}_{n2} = \rho_s \quad (3.47)$$

where \mathbf{D}_{n1} and \mathbf{D}_{n2} are the normal electric flux densities in mediums 1 and 2, in coulombs per square meter (C m^{-2}) in medium 2, and ρ_s is the surface charge density in coulombs per square meter (C m^{-2}).

Since $\mathbf{D} = \epsilon\mathbf{E}$, we can write (3.47) as

$$\epsilon_1 \mathbf{E}_{n1} - \epsilon_2 \mathbf{E}_{n2} = \rho_s \quad (3.48)$$

where ϵ_1 and ϵ_2 are the permittivities in medium 1 and 2, respectively, in farads per meter (F m^{-1}) and \mathbf{E}_{n1} and \mathbf{E}_{n2} are the electric field intensities in medium 1 and 2, respectively, in volts per meter (V m^{-1}).

3.4.3.1 Normal Component of the Electric Field for a Charge-Free Boundary

In a charge-free boundary, the surface charge density ρ_σ is zero, so the electric flux density is continuous, and (3.47) can be written as

$$\mathbf{D}_{n1} = \mathbf{D}_{n2}$$

and (3.48) reduces to

$$\mathbf{E}_{n1} = \mathbf{E}_{n2}$$

where ϵ_1 and ϵ_2 are the permittivities in medium 1 and 2, respectively, in farads per meter (F m^{-1}), and \mathbf{E}_{n1} and \mathbf{E}_{n2} are the electric field intensities in medium 1 and 2, respectively, in volts per meter (V m^{-1}).

3.4.3.2 Normal Component of the Electric Field at the Interface with a Conductor

If the second medium is a perfect conductor, \mathbf{D}_{n2} is zero, so that $\mathbf{D}_{n1} = \rho_s$, where \mathbf{D}_{n1} is the electric flux density in coulombs per square meter (C m^{-2}) in medium 2, and ρ_s is the surface charge density, also in coulombs per square meter (C m^{-2}).

The surface charge density is induced on the surface of the conductor by the EM field. Since the tangential component of the electric field in medium 2 is zero, it follows that at the interface of a dielectric and a perfect conductor, the resultant electric field in the dielectric is normal to the interface.

3.4.4 Normal Component of the Magnetic Field

The normal component of the magnetic flux density is continuous at the boundary of two dielectric media. This means that $\mathbf{B}_{n1} = \mathbf{B}_{n2}$, where \mathbf{B}_{n1} and \mathbf{B}_{n2} are the magnetic flux densities (in tesla) in mediums 1 and 2, respectively. Since the magnetic flux density is equal to the product of the magnetic field and the magnetic permeability, we can say that

$$\mu_1 \mathbf{H}_{n1} = \mu_2 \mathbf{H}_{n2} \quad (3.49)$$

where \mathbf{H}_{n1} and \mathbf{H}_{n2} are the magnetic fields in amperes per meter (A m^{-1}) in medium 1 and 2, respectively, and μ_1 and μ_2 are the magnetic permeabilities in henries per meter (H m^{-1}) in mediums 1 and 2, respectively.

3.4.4.1 Normal Component of the Magnetic Field for Conductors

In the case of the boundary between a conductor and a dielectric, the magnetic permeability of the conductor is much larger than that of a dielectric, so the normal component of the magnetic field inside the conductor will be much smaller than that in the dielectric. This means that $\mu_2 \gg \mu_1$. Thus, it follows from (3.49) that the normal component of the magnetic field inside the conductor (\mathbf{H}_{n2}) is much smaller than that in the dielectric (\mathbf{H}_{n1}).

3.5 Fields Due to a Radiating Dipole

In order to derive the EM fields of a radiating dipole, we can imagine it to be made up of elementary dipoles attached end to end. Each elementary dipole can be considered

to be fed by a current which radiates and results in electric and magnetic fields in the free space surrounding it.

3.5.1 Field Due to a Current Element

Let us consider a current element, as shown in Figure 3.6, that is short enough for the current I to be uniform across it. The element is also assumed to a thin wire, so that the current flows longitudinally through it and there are no components of the current in its transverse cross section, that is, there are no radial or azimuthal currents. We usually want to calculate the fields at a radial distance from the element so it is better to use spherical polar coordinates rather than rectangular coordinates. If the current through the element is alternating, then the current has a magnitude of $I \cos \omega t$. There is a finite time for the EM wave to travel from the element to a point P at a distance r . If the velocity of the EM wave is v meters per second, the time for the wave to reach P will be r/v seconds. This means that there will be a phase delay of $\omega r/v$ radians, if the angular frequency is ω radians per seconds.

The only component of the magnetic field is that given by the right-hand screw rule. This is the component in the ϕ -direction in the plane transverse to the current element.

In the case of the electric field, we would not expect to have a component of the electric field in the transverse plane perpendicular to the vertical element (since this would be at right angles to the electric polarization vector). Thus the components of the E field would be in the θ - and the radial r -directions only.

The instantaneous values of the component fields can be derived by applying Maxwell's equations [3, p. 304], and are given by the following expressions

$$\mathbf{H}_\phi = \frac{Idl \sin \theta}{4\pi} \left[-\frac{\omega \sin \omega \left(t - \frac{r}{v} \right)}{rv} + \frac{\cos \omega \left(t - \frac{r}{v} \right)}{r^2} \right] \quad (3.50)$$

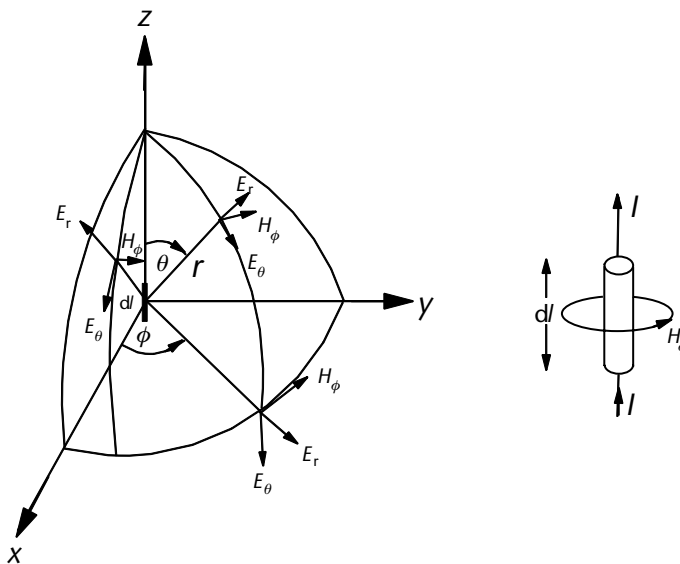


Figure 3.6 Fields due to a radiating current element.

$$\mathbf{E}_\theta = \frac{Idl \sin \theta}{4\pi\epsilon} \left[-\frac{\omega \sin \omega \left(t - \frac{r}{v} \right)}{rv^2} + \frac{\cos \omega \left(t - \frac{r}{v} \right)}{r^2 v} + \frac{\sin \omega \left(t - \frac{r}{v} \right)}{\omega r^3} \right] \quad (3.51)$$

$$\mathbf{E}_r = \frac{2Idl \cos \theta}{4\pi\epsilon} \left[-\frac{\cos \omega \left(t - \frac{r}{v} \right)}{r^2 v} + \frac{\sin \omega \left(t - \frac{r}{v} \right)}{\omega r^3} \right] \quad (3.52)$$

In (3.50), the first term on the right-hand side is the radiation field or distant field term, and the second term is the induction field term. The radiation field term is not present for steady (DC) currents, and takes account of the finite time of propagation of a EM wave, which does not apply in the DC case. It contributes to the flow of energy away from the element, whereas the induction field term contributes to energy which is stored in the field during one quarter of the cycle and returned during the next quarter. We can see that the radiated field term is inversely proportional to the distance r , whereas the induction field term is inversely proportional to the square of the distance. This means that the induction field decays rapidly as the distance increases and becomes negligible compared with the radiation field at large values of r .

In the electrostatic case, $\omega \rightarrow 0$, and thus the $1/r$ and $1/r^3$ terms in (3.51) as well as the $1/r^3$ term in (3.52) will be zero (since $\sin \omega(t - r/v) = 0$). This leaves us with the $1/r^2$ terms only for \mathbf{E}_θ and \mathbf{E}_r .

3.5.2 Fields at Large Distances from Wire Antennas

At large distances, the terms that are inversely proportional to the square and cube of the distance will be reduced to very small magnitudes, and thus they can be ignored. This means that the radial component of the electric field \mathbf{E}_r can be ignored. The second and third terms of \mathbf{E}_θ and the second term of \mathbf{H}_ϕ can also be ignored. We can therefore write the electric and magnetic fields at large distances from the dipole in terms of the \mathbf{E}_θ and \mathbf{H}_ϕ , which are given by

$$\mathbf{E}_\theta = \frac{Idl \sin \theta}{4\pi\epsilon} \left[\frac{\omega \sin \omega \left(t - \frac{r}{v} \right)}{rv^2} \right] \quad (3.53)$$

$$\mathbf{H}_\phi = \frac{Idl \sin \theta}{4\pi} \left[-\frac{\omega \sin \omega \left(t - \frac{r}{v} \right)}{rv} \right] \quad (3.54)$$

3.6 Power Flux Density for a Plane Wave

The power flux density is a vector known as Poynting's power flux vector, and its direction is in the direction of propagation of the EM wave. In the case of a plane

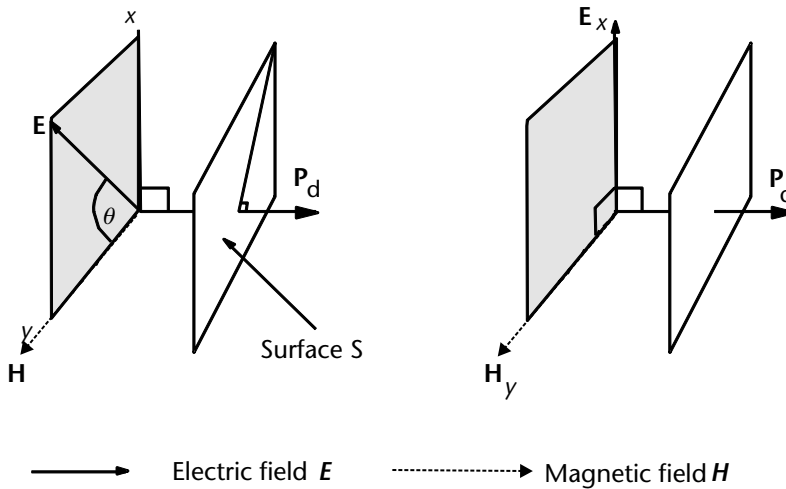
wave, the electric and magnetic fields are perpendicular to each other, and the plane containing these vectors is perpendicular to the direction of propagation of the wave, as shown in Figure 3.7(a).

The power density, \mathbf{P}_d , is defined as the vector or cross product of the electric and magnetic field intensities, and is given by

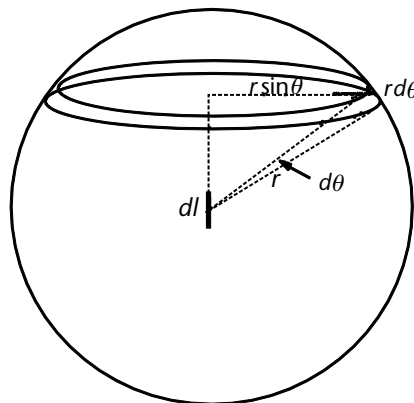
$$\mathbf{P}_d = \mathbf{E} \times \mathbf{H}$$

The magnitude of the power flux density is given by the real part of this product, since this is the only part that contributes to the power. The magnitude is given by

$$P_d = \text{Re}(\mathbf{E} \times \mathbf{H}) \quad (3.55)$$



(a)



(b)

Figure 3.7 Power flux density: (a) Poynting's power flux vector \mathbf{P}_d , and (b) calculation of total power radiated over a sphere.

where Re stands for the real part of the expression in the brackets, \mathbf{E} is the amplitude of electric field in volts per meter (V m^{-1}) and \mathbf{H} is the amplitude of magnetic field in amperes per meter (A m^{-1}).

For sinusoidally alternating fields, the magnitude of the average (in time) Poynting's power flux vector is half the magnitude of that given by (3.55). This is because the root mean square (RMS) of the electric and magnetic fields is $1/\sqrt{2}$ of their amplitudes, or peak values. The average power density $\mathbf{P}_{d(\text{ave})}$ is given by

$$\mathbf{P}_{d(\text{ave})} = \frac{1}{2} \text{Re}(\mathbf{E} \times \mathbf{H}^*)$$

where $\mathbf{P}_{d(\text{ave})}$ is the average power density in watts per square meter (W m^{-2}), \mathbf{E} is the amplitude of electric field in volts per meter (V m^{-1}), and \mathbf{H} is the amplitude of the magnetic field in amperes per meter (A m^{-1}). To calculate the total average power radiated in the far field, we take the average power density (i.e., the product of the expressions for \mathbf{H}_ϕ and \mathbf{E}_θ given by (3.53) and (3.54)) and integrate it over a sphere. In order to perform this integration, we consider an elemental thin annular shell on a sphere, as shown in Figure 3.7. Its width is $r d\theta$ and its circumference is $2\pi r \sin \theta$, and thus its area is $2\pi r^2 \sin \theta d\theta$. The total average power radiated is found by integrating this annular shell with respect to θ , from 0 to π in order to get the area over the whole sphere. Note that we only need to consider the amplitudes of \mathbf{H}_ϕ and \mathbf{E}_θ and thus the total average power \mathbf{P}_{ave} is given by

$$\begin{aligned} \mathbf{P}_{\text{ave}} &= \frac{1}{2} \int_0^\pi \left(\frac{\omega^2 l^2 d l^2 \sin^2 \theta}{16\pi^2 r^2 v^3 \epsilon} \right) 2\pi r^2 \sin \theta d\theta \\ &= \frac{\omega^2 l^2 d l^2}{16\pi^2 v^3 \epsilon} \int_0^\pi (\sin^3 \theta d\theta) \end{aligned} \quad (3.56)$$

since $\sin^3 \theta$ can be written as $\sin \theta (1 - \cos^2 \theta)$, we can integrate this expression more readily to give

$$\mathbf{P}_{\text{ave}} = \frac{\omega^2 l^2 d l^2}{16\pi^2 v^3 \epsilon} \left[-\cos \theta + \frac{\cos^3 \theta}{3} \right]_0^\pi$$

Evaluation of the expression in square brackets yields $4/3$, and thus the average power is given by

$$\mathbf{P}_{\text{ave}} = \frac{l^2 d l^2 \omega^2}{12\pi v^3 \epsilon} \quad (3.57)$$

For free-space propagation, the velocity v is equal to the speed of light c , which is in turn equal to $1/\sqrt{(\mu_0 \epsilon_0)}$. Additionally, $\epsilon = \epsilon_0$, $\omega = 2\pi f$, and $c = f/\lambda$. Thus the total average power is given by

$$\mathbf{P}_{\text{ave}} = \frac{\pi l^2 d l^2}{3\lambda^2} \sqrt{\frac{\mu_0}{\epsilon_0}} \quad (3.58)$$

This is the total average power radiated by a current element carrying a uniform current along its length. This current element is called a doublet, or a Hertzian dipole. In practice, a Hertzian dipole cannot be realized; although a very short dipole of $<\lambda/10$ is a fairly good approximation. The current along the length of a radiating wire and a triangular distribution of current is a better approximation for a short dipole. This would give an average current equal to half the maximum, and thus $I^2/4$ should be substituted for I^2 in (3.58), giving the total average power as

$$P_{\text{ave}} = \frac{\pi l^2 dl^2}{12\lambda^2} \sqrt{\frac{\mu_0}{\epsilon_0}} \quad (3.59)$$

3.7 Wave Impedance for a Plane Wave

We can think of an EM wave having an impedance in the same way as a transmission line has a characteristic impedance. The wave impedance ξ , is usually called the intrinsic impedance and is defined as the ratio of the electric and magnetic field intensities. We can see that dimensionally this would be the case, since the units of the electric and magnetic fields are volts per meter (V/m^{-1}) and amperes per meter (A/m^{-1}), so the units of their ratio gives us impedance. The electric and magnetic fields are very complex near the antenna, but in the far field the fields are given by the expressions of (3.53) and (3.54).

$$\xi = \frac{E_\theta}{H_\phi} = \frac{1}{\epsilon v} \quad (3.60)$$

For free space, $\epsilon = \epsilon_0$ and $v = c = 1/\sqrt{\mu_0\epsilon_0}$.

Thus the free-space wave impedance ξ_0 , given by (3.60), can be written as

$$\xi_0 = \sqrt{\frac{\mu_0}{\epsilon_0}} \quad (3.61)$$

3.8 Radiation Resistance

The total average power given by (3.58) is equivalent to the familiar expression of $I^2R/2$ for average power in the case of a sinusoidally alternating current. In this case, since the element is radiating, we call its resistance the radiation resistance. Thus, we get an expression for the radiation resistance of the current element given by

$$R = \frac{2\pi}{3} \sqrt{\frac{\mu_0}{\epsilon_0}} \left(\frac{dl}{\lambda}\right)^2 \quad (3.62)$$

Inserting the values of $4\pi \times 10^{-7}$ and $1/(36\pi \times 10^9)$ for μ_0 and ϵ_0 , respectively, in (3.62), we get the following expression $R = 80\pi^2 \sqrt{(dl/\lambda)^2}$ for the radiation resistance of a current element dl , through which a constant current I flows.

If we assume that the current distribution is triangular as a more realistic situation, we get the expression for the power density given by (3.59), and hence the radiation resistance is given by

$$R = 20\pi^2 \sqrt{\left(\frac{l}{\lambda}\right)^2} \quad (3.63)$$

This is a fairly good approximation for dipoles of less than $\lambda/4$. The corresponding expression for short monopoles of length $<\lambda/8$ is given by

$$R = 10\pi^2 \sqrt{\left(\frac{l}{\lambda}\right)^2} \quad (3.64)$$

Note that in this case the length l is twice the physical length of the monopole, since if we have a monopole on an infinite ground plane it has an image, and therefore its length appears to be doubled.

3.9 Far Field of Antennas

The distance from an antenna at which a plane wave can be assumed to exist depends on the whether we have a wire or an aperture antenna.

3.9.1 Far Field for Wire Antennas

We can define the far-field distance as the distance from the dipole at which the magnitude of the induction field is equal to the radiated field. Comparing the amplitudes of these two terms given by (3.50) we get

$$\frac{\omega}{rv} = \frac{1}{r^2} \quad (3.65)$$

where the velocity v is the speed of light c , and ω is the angular velocity in radians per second and is therefore equal to $2\pi f$. Also, since $f = c/\lambda$, (3.65) reduces to $r = \lambda/2\pi$ which is the distance from wire antennas at which the intrinsic impedance of the wave has a purely resistive value of 120π . This is the impedance of a plane wave; and thus, this is also the distance at which a plane wave can be assumed to exist. In practice, the far-field distance is taken as double this value, that is, λ/π is usually taken as the far-field distance.

3.9.2 Far Field for Aperture Antennas

Aperture antennas, such as horns and reflectors, tend to operate at higher frequencies, mainly in the microwave region above 300 MHz. In this region, the approach is similar to that used in optics, and the far field is known as the Fraunhofer region. Let us consider a point along the axis as the center of a family of spheres, with radii

that increase in steps of $\lambda/2$ from R , to $R + n\lambda/2$, where n is an integer. The spheres divide the aperture into a series of annular regions, three of which are shown in Figure 3.8(a, b). In the perspective view, for reasons of clarity, the plane of the aperture is shown transparent and the outer spherical sections are shown in outline.

We can see that as we move away from the aperture, the size of the Fresnel zones increase, and the number of the zones decrease. The limit of the Fresnel region is taken as the distance at which the whole aperture (of diameter D) is just one Fresnel

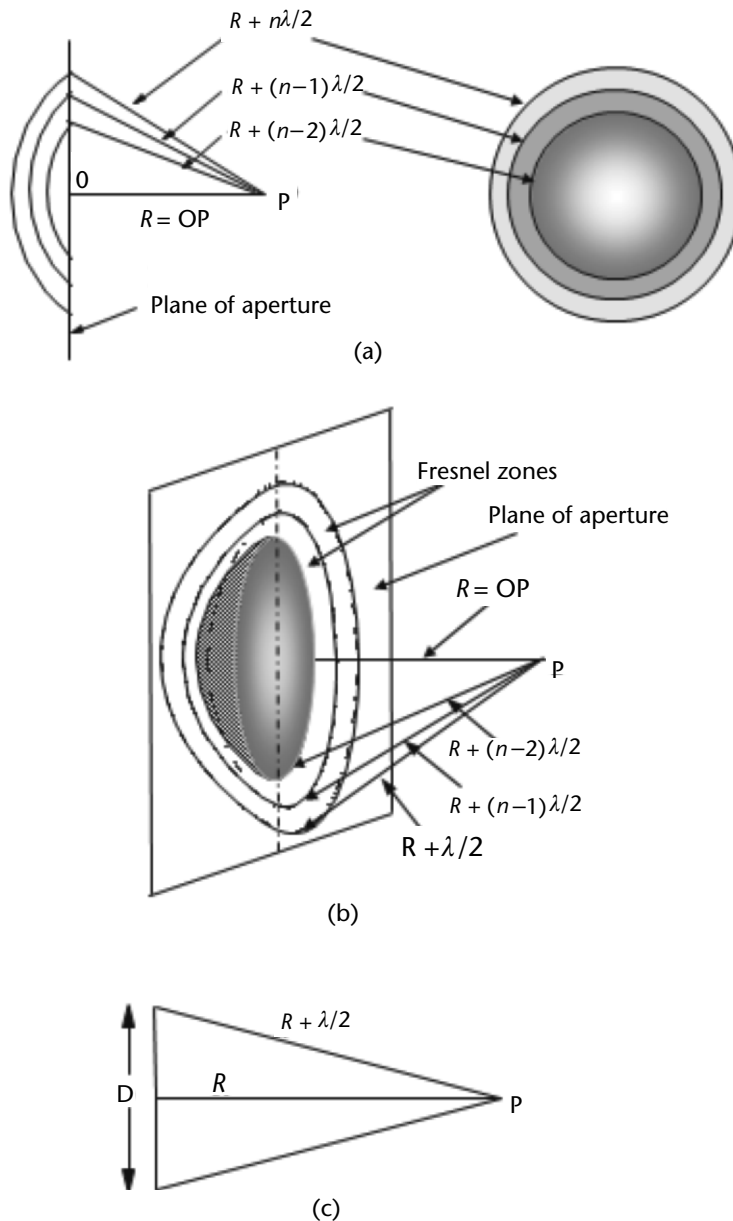


Figure 3.8 Fresnel zones and Fraunhofer region: (a) Cross sectional and front views of spheres with center P , (b) perspective view of Fresnel zones, and (c) calculation of the Fraunhofer distance.

zone. This means that if the distance P along the axis is R , the distance from P to the edge of the aperture is $(R + \lambda/2)$. Using Pythagoras' theorem, we get

$$\begin{aligned}\left(R + \frac{\lambda}{2}\right)^2 &= \left(\frac{D}{2}\right)^2 + R^2 \\ R^2 + \lambda R + \frac{\lambda^2}{4} &= \frac{D^2}{4} + R^2 \\ \lambda R &= \frac{D^2}{4} - \frac{\lambda^2}{4}\end{aligned}$$

For $D > \lambda$, λ^2 is negligible compared with D^2 , and hence we can say that

$$R = \frac{D^2}{4\lambda} \quad (3.66)$$

Distances less than $D^2/4\lambda$ are considered to be in the Fresnel region; however $D^2/4\lambda$ is not the point at which the Fraunhofer region starts, since the path difference between the center and the edge of the aperture is $\lambda/2$. The Fraunhofer, or far field, is considered to be the point at which the path differences between points on the aperture are negligible. The Fraunhofer region is usually taken as $2D^2/\lambda$ or $4D^2/\lambda$. If we compare the ratio of the gain at each of these two distances with that at infinity G_0 [4, p. 188] we get

- at $2D^2/\lambda$, the ratio of G to G_0 is 0.94;
- at $4D^2/\lambda$, the ratio of G to G_0 is 0.99.

Thus, the distance $4D^2/\lambda$ more accurately represents the far-field distance for an aperture antenna, although the $2D^2/\lambda$ is often the distance used for EMC measurements.

References

- [1] Fewkes, J. H., and J. Yarwood, *Electricity, Magnetism, and Atomic Physics Volume 1 (Electricity and Magnetism)*, University Tutorial Press Ltd., 2nd Edition, 1962.
- [2] Mahin, P. J., "Maxwell's Grand Unification," *IEEE Spectrum*, March 1992, p. 46.
- [3] Jordan, E. C., *Electromagnetic Waves and Radiating Systems*, Constable and Co. Ltd., 1953.
- [4] Silver, S., *Microwave Antenna Theory and Design First Edition*, McGraw-Hill Book Co. Inc.: New York, 1949.

Antennas for Frequencies Below 1 MHz

This chapter describes the antennas used at frequencies from 50 Hz to 1 MHz. The mechanism of radiation is explained qualitatively, and effective height and length is defined. Electric and magnetic wave impedances are introduced, and the difference between receiving and transmitting antennas is explained by considering the dipole as an example. At frequencies below 1 MHz the wavelength is greater than 300m, and thus the antennas used have to be small fractions of a wavelength in order to have antennas of manageable proportions. The physical distances involved (between the antenna and the DUT) are also a few meters, which mean that the electrical distances (distances in terms of wavelength) are small fractions. This leads to measurements being performed in the near field of antennas. Under these conditions, the radiation pattern (which is the radiated power in the far field) is not relevant. The antennas used at these frequencies tend to be simple wire antennas such as dipoles, monopoles, and loops. The dipoles are generally used for receiving, whereas monopoles and loops are used for receiving as well as transmitting. The antennas also tend to have preamplifiers that are used to overcome the loss experienced between the antenna and the receiver or transmitter. This loss is a result of connecting a balanced antenna to an unbalanced line (such as a coaxial line), as well as a result of the impedance mismatch between the antenna and the transmission line to which it is connected. This chapter also explains the concept of radiation power factors and describes the circuits used to balance and match the antenna to the transmission line.

4.1 Mechanism of Radiation

When an electron is suddenly accelerated or decelerated, the effect of its field takes a finite time to reach a distant point. This time depends on the distance and the velocity of the light. If the electron is subjected to a sinusoidally alternating acceleration the field also changes in a similar manner. Since the magnitude of the field depends on the acceleration experienced by the electron, it depends on the frequency f of the alternating current [1]. At higher frequencies (i.e., in the kHz range and above) the charge distribution on the antenna reverses sign more rapidly than the collapsing field lines near the antenna. This reversing field repels the collapsing field and pushes it away, so that the latter forms closed loops that expand as they travel away from the antenna at the speed of light. In the induction field near a vertical dipole, the electric field lines are in the vertical plane, as shown in Figure 4.1(a),

and the magnetic field is in the horizontal plane. Beyond this region the radiated field is shown in Figure 4.1(b–e) at every quarter of a cycle [2].

4.2 Near and Far Fields of Antennas

Near the antenna where interference effects predominate, the resultant wave is of a complex nature, and the power density (the power per unit area) does not decrease monotonically (i.e., it does not decrease consistently) as the distance from the antenna increases, but follows an oscillatory pattern. This is detailed in Chapter 7. Because of this dependence of the field on distance, standards specify the distance at which measurements have to be performed. This also explains why the measurements of

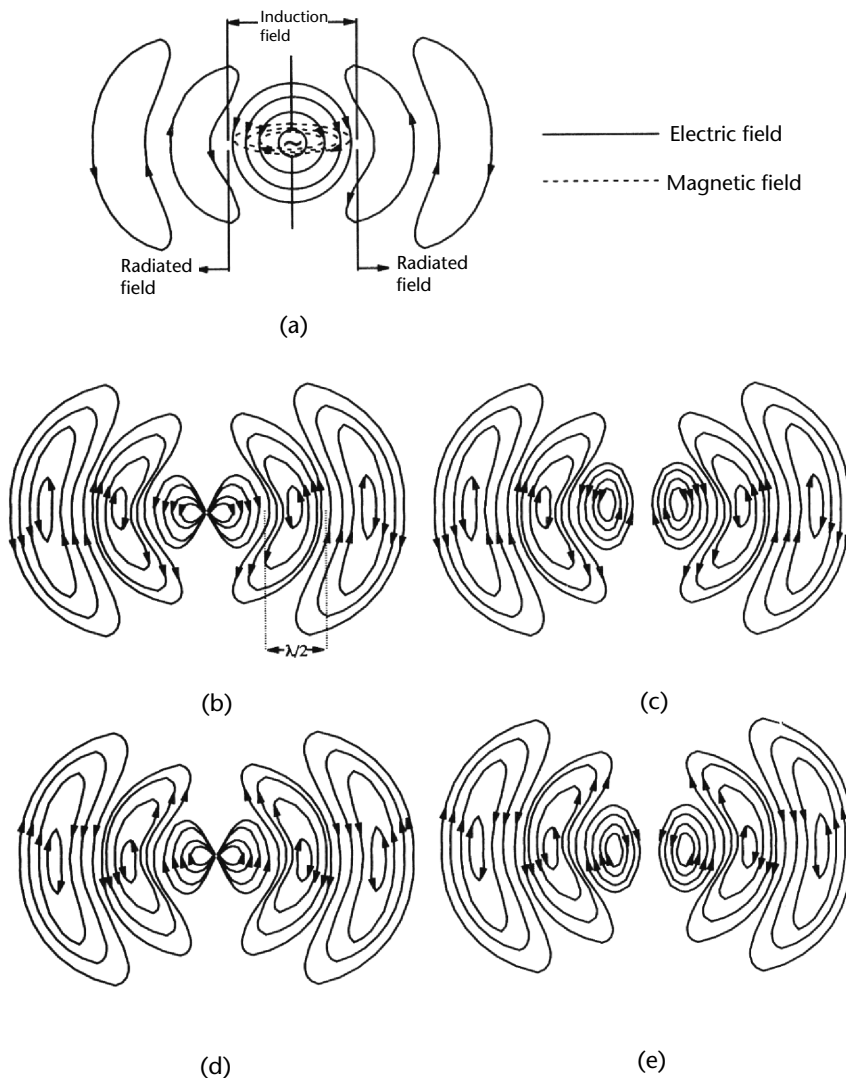


Figure 4.1 Mechanism of radiation: (a) induction field near a radiating dipole, (b) radiated field at $\omega t = 0$, (c) radiated field at $\omega t = \pi/2$, (d) radiated field at $\omega t = \pi$, (e) radiated field at $\omega t = 3\pi/2$.

power at 3m and 10m do not follow the inverse square law. The near field is reactive, as explained in Chapter 3, and the space is occupied mainly by stored energy in the electric and magnetic fields. In the far field where a plane wave exists, the electric and magnetic fields are perpendicular to each other and to the direction of propagation of the wave. Figure 4.2 shows a plane wave propagating in the z -direction with the electric field in the y -direction. It shows the spatial distribution (the variation with distance) of the electric and magnetic fields at a fixed instant in time. It is important to remember that these fields also vary with time in a similar sinusoidal way, which results in the propagation of the wave, as in the case of shallow water waves in a ripple tank. The electric and magnetic fields are in time phase with each other, unlike the situation in circuits containing inductors and capacitors where the phase between the fields is 90° .

4.3 Wave Impedance

In the near field of an antenna, the intrinsic impedance of the wave is larger or smaller than it is beyond the Fresnel region, in the far field. The intrinsic wave impedance in the far field is that of a plane wave, that is, 120π or 377Ω . However, in the near field (distances $< \lambda/2\pi$ for wire antennas), the intrinsic wave impedance ξ depends on the type of radiator. In the near field of magnetic sources such as loops, the wave impedance ξ_H at a distance r is approximately equal to $240\pi^2 r/\lambda$, whereas in the near field of electric sources such as monopoles and dipoles, the wave impedance ξ_E is approximately equal to $60\lambda/r$. We can see that at $r = \lambda/2\pi$ the wave impedance for both fields is equal to 120π . The intrinsic wave impedances for electric and magnetic sources are shown in Figure 4.3 for distances in terms $\lambda/2\pi$. Thus, 1 on the x -axis represents a distance of $\lambda/2\pi$. The solid curves show the theoretical values of the electric and magnetic wave impedances ξ_E and ξ_H , whereas the dotted

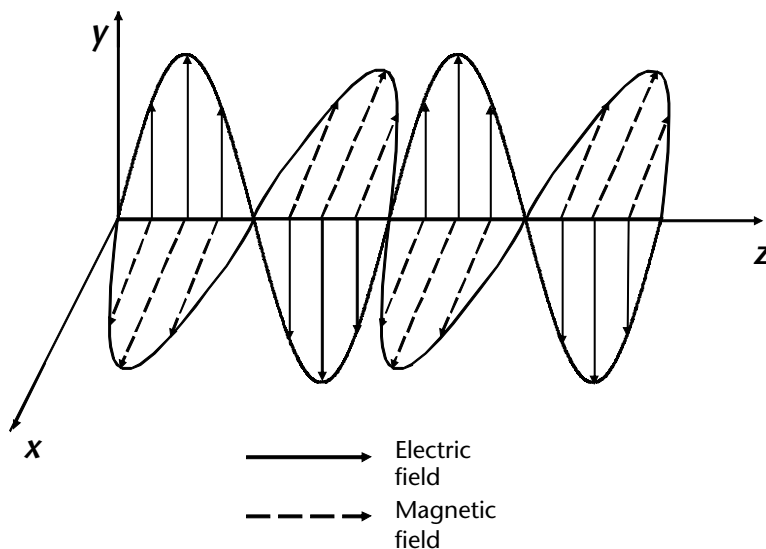


Figure 4.2 Plane wave in free space.

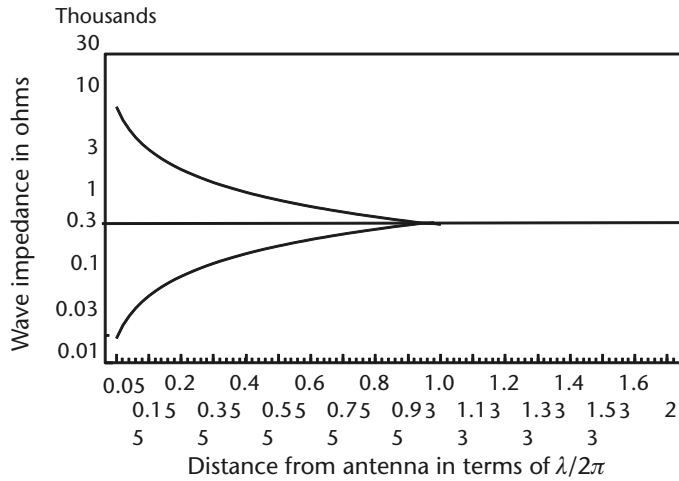


Figure 4.3 Wave impedance variations with distance from source.

curves show the actual impedances. It can be seen that, in the case of the dotted curves, the impedances asymptotically approach 377Ω at a point beyond the value of 1, at a value approaching 2, that is, a physical distance of λ/π . It will also be seen that in the near field of magnetic sources the wave has a low impedance, whereas the near field of electric sources the wave has a high impedance. Low wave impedances induce high currents, whereas high wave impedances induce low currents. EMC standards specify the type of field required at different frequencies. Further details are given in Chapter 9.

4.4 Difference Between Receiving and Transmitting Antennas

The reciprocity theorem states that an antenna has the same characteristics whether it is radiating or receiving. These characteristics are the impedance, radiation pattern, and so forth. However one of the main differences between a radiating and receiving antenna is the orientation of the antenna's radiation pattern for optimum transmission and reception [3, p. 546]. The optimum pattern is used in transmission to direct the signal in a given direction(s). If there is noise in a particular direction, then increasing the directivity of the antenna in that direction will increase the signal-to-noise ratio in that direction. However, in reception, the optimum condition is not the maximum received power but the highest signal-to-noise ratio. If the noise is coming from the same direction as the signal, then increasing the directivity in that particular direction will not increase the signal-to-noise ratio, since both the signal and the noise will be increased.

Another important difference between a transmitting and receiving antenna is the distribution of current along the length. In the case of a thin transmitting dipole that is fed centrally, the current distribution is approximately sinusoidal, as shown in Figure 4.4(a). The thinner the antenna, the closer the approximation to a sinusoidal distribution is. The instantaneous currents I_1 and I_2 in the upper and lower arms of the dipole respectively, are given by

$$I_1 = I_{\max 1} \sin \beta(H - z) \quad (4.1)$$

$$I_2 = I_{\max 2} \sin \beta(H + z) \quad (4.2)$$

where $I_{\max 1}$ and $I_{\max 2}$ are the maximum values or amplitudes of the currents in the upper and lower arms of the dipole, H is the half length of the dipole and β is the phase constant or wave number $2\pi/\lambda$.

The input impedance Z_a of the dipole is approximately given by

$$Z_a = -jZ_0 \cot(\beta H) \quad (4.3)$$

where Z_0 is the characteristic impedance given by

$$Z_0 = 120 \left[\log_e \left(\frac{2H}{a} \right) - 1 \right] \quad (4.4)$$

where a is the radius of the conductor of the dipole.

In the case of a receiving dipole, the current distribution is a function of the length, the direction of the arrival of the incident wave, and the impedance of the load connected to the dipole. In most cases the load is the receiver. The current does not approximate a sinusoidal current distribution, except in the case of resonant half-wave dipoles. We can think of the receive dipole as an unsymmetrically-fed dipole. Consider the dipole of Figure 4.4(b), which is fed at a point at a distance h from the center. If we ignore the radiation resistance and assume that the total input impedance is made up of the sum of the impedances of the two sections of lengths $(H - h)$ and $(H + h)$, then the total impedance is given by

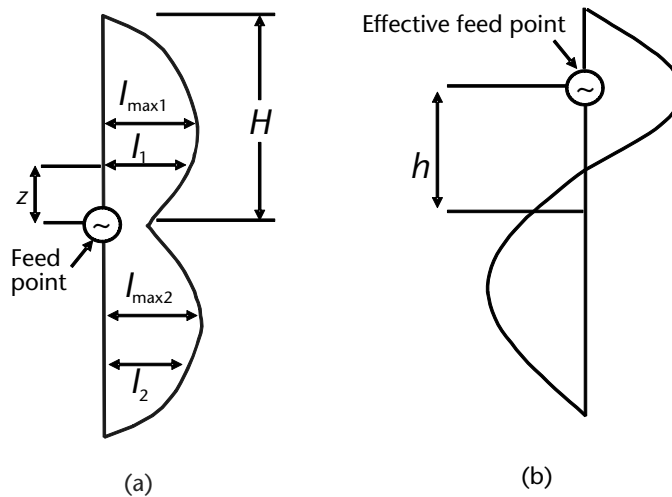


Figure 4.4 Current distribution on (a) transmit and (b) receive antennas.

$$Z_{\text{total}} = Z_{(H+b)} + Z_{(H-b)} \quad (4.5)$$

where

$$Z_{(H-b)} = \frac{1}{2} jZ_{01} \cot \beta(H - b) \quad (4.6)$$

and

$$Z_{(H+b)} = \frac{1}{2} jZ_{01} \cot \beta(H + b) \quad (4.7)$$

where Z_{01} and Z_{02} are the characteristic impedances of the two sections. As Z_{01} gets larger, Z_{02} gets smaller. If we assume that these characteristic impedances are approximately equal, they will each be equal to Z_0 given by (4.4).

4.5 Small Antennas

At frequencies below 1 MHz, where the wavelength is greater than 300m, antennas have electrical sizes (the size in terms of wavelength) that are fractions, that is, magnitudes that are $\ll 1$. These fractions are usually taken as $< \lambda/8$ for monopoles and $< \lambda/4$ for dipoles. The antennas are called small antennas, although their physical size may be several meters. Another definition of a small antenna by Weiner, [8, p. 6–1] is one that occupies a small fraction of a radiansphere. A radiansphere is defined as a sphere of radius $\lambda/2\pi$. It will noted that this is the far field distance for wire antennas we encountered in Chapter 3, where the magnitude of the induction and radiation fields are equal. Within this sphere the stored field predominates, whereas outside this sphere the radiation field predominates.

4.6 Baluns

The transmission line connecting an antenna to the receiver or transmitter is usually a coaxial line. When a dipole is connected to a coaxial line, one arm is connected to the inner conductor and the other arm is connected to the outer conductor. Since the arms are not coupled to the line in the same way, an imbalance occurs. If the dipole is fed by a two-wire line, there would be no imbalance, since the two-wire parallel line is connected to each arm of the dipole in the same way. However, the loss experienced by two-wire lines makes them unsuitable, except at very low frequencies. Let us consider a coaxial line feeding a dipole, as shown in Figure 4.5(a). The currents I_1 and I_2 that flow along the inner and outer conductors are equal and opposite. At a fixed point in time, I_1 is flowing down the inner conductor (and the right arm of the dipole) and I_2 is flowing up the inside of the cylindrical outer conductor [3, p. 539]. The current I_2 flows to the top of the outer conductor, and at point A it divides into two, with I_3 flowing down the outside of the conductor, and

I_2 and I_3 flowing along the left arm of the dipole. The equivalent circuit is shown in Figure 4.5(b). The magnitude of the current I_3 depends on the impedance to ground, Z_g , provided by this path along the outer conductor. In order to make I_3 as small as possible, we use a balun, which ideally balances the line by canceling this outside current [5, p. 365]. In practice, I_3 is made as small as possible by making Z_g as large as practicable. Balun is an abbreviation of balanced-unbalanced. The balun can consist of a quarter-wave line in the form of a skirt of effective length equal to a quarter of a wavelength, as shown in Figure 4.5(c). The skirt is a concentric cylinder whose lower end is connected to the outer conductor at point C. The impedance between points A and B depends on the Q of the shorted quarter-wave section. In theory, if the section is exactly an effective quarter wave, this impedance would be infinite; in practice, it can be set to a very high value for a band of frequencies. This type of balun is sometimes called a Bazooka balun [5, p. 366].

In another arrangement for a balun, shown in Figure 4.5(d), the outer conductor feeds the left arm of the dipole, and the inner conductor is connected to the right arm of the dipole. A transmission line of approximately a quarter of a wavelength is attached between the right arm and the outer conductor at C. These baluns are relatively narrow band. Ferrite devices can be used to increase the bandwidth, as in the case of the combined balun-transformer described in Section 4.8.

4.7 Radiation Power Factor

A term called the radiation power factor was introduced by Weiner [4] in 1947. It is defined as the reciprocal of the Q factor of the combination of the reactance of the antenna X_a and its effective radiation resistance R_e . The radiation power factor PF_{rad} of the antenna is the ratio of R_e to X_a and is given by

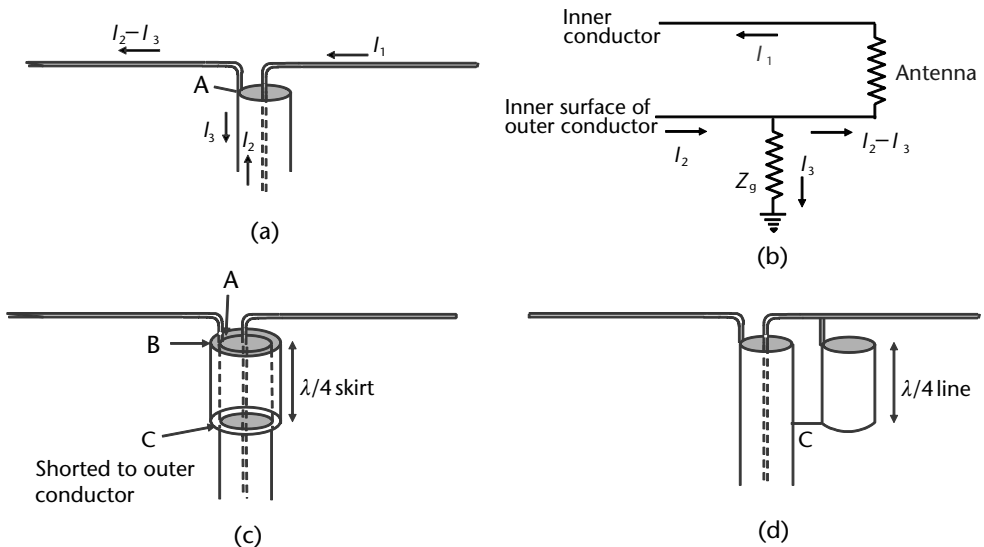


Figure 4.5 Baluns between coaxial lines and dipoles: (a) Coaxial line feeding a dipole without a balun, (b) equivalent circuit of the dipole and coaxial line without a balun, (c) a bazooka balun consisting of an outer concentric skirt, (d) a coaxial balun.

$$PF_{\text{rad}} = \frac{R_e}{X_a} \quad (4.8)$$

This radiation power factor is $\ll 1$, and is proportional to the size of the antenna. It limits the operating efficiency of the antenna. The radiation efficiency of a transmitting antenna represents the percentage of available power from a transmitter that is radiated into free space. In the case of receiving antennas, it is the percentage of power from free space that is delivered to the receiver, and is a measure of the ability of the received signal to overcome the noise level in the circuitry. A small dipole behaves like a capacitor, whereas a small loop behaves like an inductor. The equivalent circuits of a small dipole and a small loop are shown in Figure 4.6.

In the case of a small dipole, the antenna has a capacitive reactance $1/\omega C$, and the power it radiates can be assumed to be coming from a small inductance L_a in parallel with a much larger resistance R_a . The inductance L_a has a reactance that is

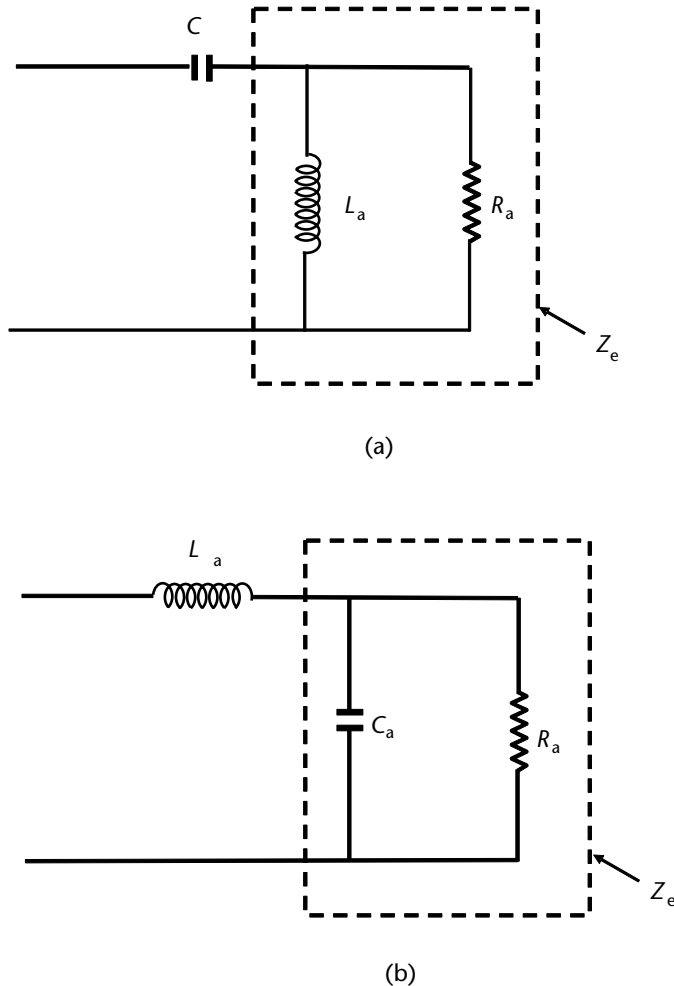


Figure 4.6 Equivalent circuits for (a) small dipole, and (b) a loop.

$\ll 1/\omega C$. The combination of the resistance R_a and the inductance L_a is an impedance Z_e which is given by

$$\begin{aligned}\frac{1}{Z_a} &= \frac{1}{j\omega L_a} + \frac{1}{R_a} \\ Z_a &= \frac{j\omega L_a R_a}{R_a + j\omega L_a} \\ Z_a &= \frac{j\omega L_a}{1 + j\omega L_a / R_a}\end{aligned}\quad (4.9)$$

Since $j\omega L_a$ is much smaller than the resistance R_a , using the binomial expansion $(1 + x)^{-1} \simeq (1 - x)$, we get

$$Z_a = j\omega L_a \left(1 - \frac{j\omega L_a}{R_a} \right) \quad (4.10)$$

$$Z_a = j\omega L_a - \frac{j^2 \omega^2 L_a^2}{R_a} \quad (4.11)$$

Since $j^2 = -1$, (4.11) can be written as

$$Z_a = j\omega L_a + \frac{\omega^2 L_a^2}{R_a}$$

The total antenna impedance Z_a is this impedance Z_e in series with the capacitance C , and is given by

$$Z_a = \frac{1}{j\omega C} + j\omega L_a + \frac{\omega^2 L_a^2}{R_a}$$

since $j\omega L \ll 1/j\omega C$, it can be ignored. The total antenna impedance Z_a is therefore given by

$$Z_a = \frac{1}{\omega C} + \frac{\omega^2 L_a^2}{R_a} \quad (4.12)$$

The first term on the left-hand side of (4.12) is the effective reactance X_e and the second term is the effective resistance R_e . The radiation power factor PF_{rad} is the ratio of the resistive to the reactive parts, and is given by

$$PF_{\text{rad}} = \frac{\omega^3 L_a^2 C}{R_a} \quad (4.13)$$

Thus we can see that the radiation power factor is proportional to the cube of the frequency.

4.7.1 Operating Efficiency

The operating efficiency is defined as the ratio of the radiation power factor and the combination of the radiation and loss power factors. The operating efficiency η_{op} is given by

$$\eta_{\text{op}} = \frac{PF_{\text{rad}}}{PF_{\text{rad}} + PF_{\text{loss}}} \quad (4.14)$$

Using the binomial expansion, (4.14) can be rewritten as

$$\eta_{\text{op}} = 1 - \frac{PF_{\text{loss}}}{PF_{\text{rad}}} + \left[\frac{PF_{\text{loss}}}{PF_{\text{rad}}} \right]^2 \quad (4.15)$$

To a first approximation, the third term of (4.15) can be ignored. Thus we can see that the smaller the ratio of PF_{loss} and PF_{rad} , the greater is the operating efficiency. Small antennas have high loss and low radiation power factors, and hence their operating efficiency is small.

As the size of antennas increase, their operating efficiencies also increase. Tuning units with reactances opposite to the reactance of the antenna are used, so that the tuning units used for dipoles and loops consist mainly of inductors and capacitors, respectively.

For passive antennas operating over narrow frequency bands, adjustable tuning units (step or continuous) are used and the relative bandwidth is less than the radiation power factor PF_{rad} . The efficiency is limited by the PF_{loss} which is the dissipative loss in the antenna and the tuning circuit. In broadband operation, fixed tuning units are used. The relative bandwidth is much greater than PF_{rad} and the efficiency is limited by the ability of the passive network to match the antenna to the receiver or transmitter.

4.8 Matching Antennas

The antenna can be regarded as a transformer that matches the impedance of a transmission line (usually 50Ω for a coaxial line) to 377Ω for a plane wave in free space. The antenna must be matched to (have the same impedance as) the characteristic impedance of the transmission line feeding it or connecting it to the receiver. If the antenna is not matched, maximum power transfer will not take place. The antenna can be matched to the transmission line by inserting a transformer or tuning circuit between them. In the case of an electric dipole, which has a capacitive impedance, a transformer with double-inductive tuning is a common device used for tuning a dipole [4, Figure 6-1] as shown in Figure 4.7(a). A combined balun transformer incorporating a ferrite core, such as that shown in Figure 4.7(b), can

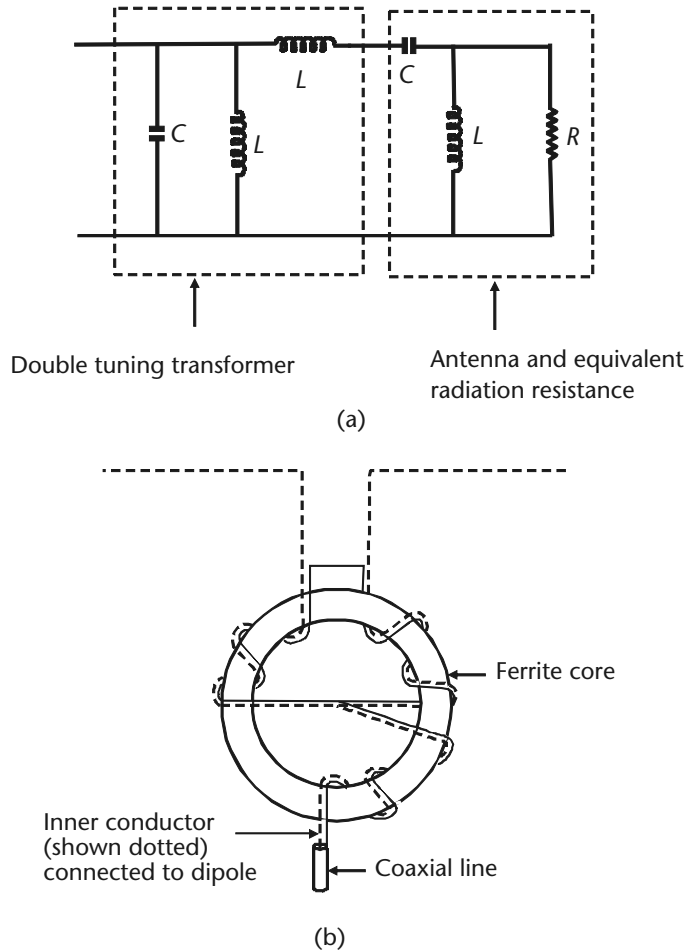


Figure 4.7 (a) Double-inductive transformer, and (b) combined balun/transformer for a dipole.

be used to obtain bandwidths of 8:1. The ferrite core maintains a high impedance over a large bandwidth [5, p. 368].

4.9 Effective Length and Effective Height

There are many definitions of effective length and effective height depending upon the application. There are the general definitions used in electric engineering and specific ones used in EMC engineering.

4.9.1 Effective Length

The IEEE dictionary [6] defines effective length in two ways, depending on whether the antenna is radiating or receiving.

1. For an antenna radiating linearly-polarized waves, the effective length is defined as the length of a straight conductor oriented perpendicularly to the

direction of maximum radiation, having a uniform current equal to that at the antenna terminals and producing the same far-field strength as the antenna. Thus, if an antenna has a triangular current distribution, its effective length would be the length it would have to be if its maximum current I_{\max} (usually at the feed point) were to be distributed uniformly across its entire length.

2. In the case of the same antenna receiving linearly-polarized waves from the same direction, the effective length is defined as the ratio of the open-circuit voltage developed at the terminals of the antenna to the component of the electric field strength in the direction of antenna polarization.

4.9.2 Effective Height

The IEEE dictionary [6] defines the term effective height in two ways.

1. The unqualified definition is the height of the center of radiation above the effective ground level.
2. For low-frequency applications, the term is applied to loaded or unloaded vertical antennas, and defined as the moment of the current distribution in the vertical section, divided by the input current.

In EMC low-frequency applications, the term effective height is generally used in two ways.

1. Firstly it is defined in one of the ways that the IEEE dictionary defines the effective height, that is, as the moment of the current distribution in the vertical section, divided by the input current. The moment of current distribution is the current at a particular point multiplied by its distance from the position of maximum current. The position of maximum current occurs at the input terminals in the case of radiating antennas.

For a short thick monopole of length $< 0.1\lambda$ the effective height h_{eff} is given by

$$h_{\text{eff}} = \frac{\int_0^l I(z) dz}{I_{\max}} \quad (4.16)$$

where

h_{eff} is the effective height in meters (m),

l is the physical length of the monopole in meters (m), and

$I(z)$ is the current at a distance z along the monopole in amperes (A).

The current $I(z)$ is given by

$$I(z) = \frac{I_{\max}}{l} z \quad (4.17)$$

Thus, (4.16) can be written as

$$h_{\text{eff}} = \int_0^l \frac{I_{\text{max}}}{l} \frac{z dz}{I_{\text{max}}} \quad (4.18)$$

Integrating with respect to z gives us

$$h_{\text{eff}} = \left[\frac{I_{\text{max}}}{l} \frac{z^2}{2} \right] \frac{z dz}{I_{\text{max}}} \quad (4.19)$$

which reduces to

$$h_{\text{eff}} = \frac{l}{2} \quad (4.20)$$

Thus, we can see that the effective height is only equal to half its physical height/length.

2. The other way in which the effective height is defined is similar to the IEEE definition of the effective length for a receive antenna, but is broadened to cover magnetic as well as electric fields. It is defined as the ratio of the antenna open-circuit voltage to the strength of the field component being measured. The effective height [7] of a magnetic radiator such as a loop antenna can be considered as the number of volts measured per tesla (T) of incident magnetic flux density, whereas in the case of an electric radiator, such as a dipole, it is the number of volts measured per meter (V m^{-1}) of incident electric field. In other words, it acts as a conversion between teslas (T) (or V m^{-1}) and volts.

$$h_{\text{eff}} = \frac{V}{\mathbf{B}} \text{ or } \frac{V}{\mathbf{E}} \quad (4.21)$$

where V is the voltage in volts at the output terminals of the antenna, B is the incident magnetic flux density in teslas, and E is electric field in volts per meter.

4.10 E-Field Antennas

Electric field wire antennas are, in general, linear wires carrying current with the electric field in the space surrounding the antenna, having the same polarization as the direction of the current in the wire. At low frequencies below 1 MHz, E-field antennas are mainly dipoles and monopoles. The parallel element is another antenna used to provide an electric field for susceptibility measurements. Dipoles are usually used as receiving probes and monopoles are used for transmitting as well as receiving.

4.10.1 Small Dipole

At low frequencies the dipole is usually used as a receiving probe to give relative values of electric field strengths, rather than absolute values. For example, it may be used to check the integrity of a shielded room or equipment casing by identifying leakage from rogue seams and apertures. It can be used for absolute measurements if it has been calibrated or if it is used in a calibrated test site. A small radiating dipole behaves like a current element and it is sometimes called a Hertzian dipole or a doublet. We have seen (in Chapter 3) that the instantaneous values of the component fields shown in Figure 4.8(a) can be derived by applying Maxwell’s equations [3, p. 304] and are given by the following expressions

$$H_{\phi} = \frac{Idl \sin \theta}{4\pi} \left[\frac{\omega \sin \omega(t - r/v)}{rv} + \frac{\cos \omega(t - r/v)}{r^3} \right] \quad (4.22)$$

$$E_{\theta} = \frac{Idl \sin \theta}{4\pi} \left[-\frac{\omega \sin \omega(t - r/v)}{rv^2} + \frac{\cos \omega(t - r/v)}{r^2 v} + \frac{\sin \omega(t - r/v)}{\omega r^3} \right] \quad (4.23)$$

$$E_r = \frac{2Idl \cos \theta}{4\pi} \left[\frac{\cos \omega(t - r/v)}{r^2 v} + \frac{\sin \omega(t - r/v)}{\omega r^3} \right] \quad (4.24)$$

where I is the current in amperes, dl is the length of the element in meters, ω is the angular frequency in radians per meter, r is the radial distance from the element in meters, ϵ is the permittivity of the medium in farads per meter, v is the velocity of the wave in the medium in meters per second.

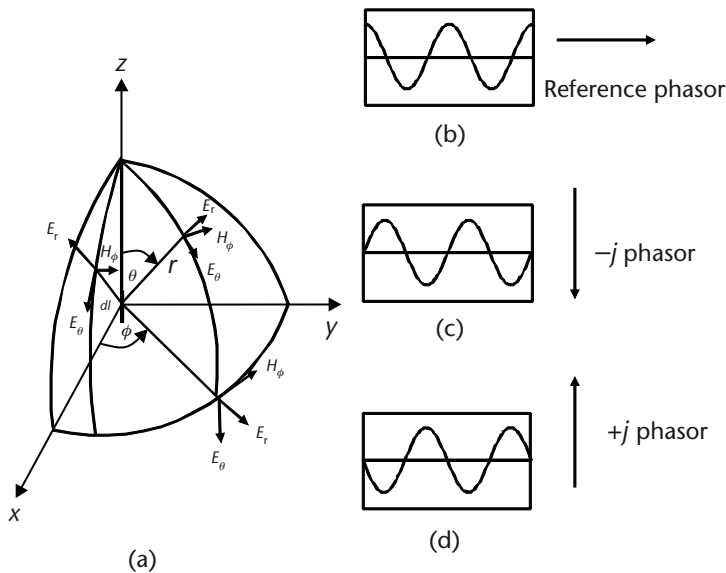


Figure 4.8 Electric and magnetic fields due to a small radiating dipole. (a) Orientation of the electric and magnetic field vectors from a radiating dipole, (b) cosine term, (c) positive sine term, and (d) negative sine term.

If we consider the RMS values of a time-varying field of the form $e^{-j\omega t}$ and we use the cosine term as the reference phasor, as shown in Figure 4.8(b), then the sine term lags behind the cosine phasor and can be represented by a phasor of $-j$, as shown in Figure 4.8(c). Similarly the negative sine term can be represented by a phasor of $+j$ as shown in Figure 4.8(d). The phase constant β can be used to replace the ratio ω/v . Equations (4.22) to (4.24) can therefore be rewritten in the following forms

$$\mathbf{H}_\phi = \frac{j\beta^2 Idl}{4\pi} \left[\frac{1}{\beta r} - \frac{1}{(\beta r)^2} \right] \sin\theta e^{-j\beta r} \quad (4.25)$$

$$\mathbf{E}_\theta = 30\beta^2 Idl \left[\frac{1}{\beta r} - \frac{j}{(\beta r)^2} - \frac{1}{(\beta r)^3} \right] \sin\theta e^{-j\beta r} \quad (4.26)$$

$$\mathbf{E}_r = 60\beta^2 Idl \left[\frac{1}{(\beta r)^2} - \frac{j}{(\beta r)^3} \right] \cos\theta e^{-j\beta r} \quad (4.27)$$

Near the antenna, that is, at distances $< 0.01\lambda$, the $1/r$ and $1/r^2$ terms can be ignored in comparison with the $1/r^3$ term. Thus, only the last terms in \mathbf{E}_r and \mathbf{E}_θ need to be considered. The \mathbf{H}_ϕ component can be ignored, since it does not have a $1/r^3$ term. The \mathbf{E}_r and \mathbf{E}_θ are given by

$$\mathbf{E}_r = \frac{j60Idl}{r^3} \cos\theta e^{-j\beta r} \quad (4.28)$$

$$\mathbf{E}_\theta = \frac{j30Idl}{r^3} \sin\theta e^{-j\beta r} \quad (4.29)$$

It can be seen that the \mathbf{E}_r vector has twice the magnitude of the \mathbf{E}_θ vector, and the phase between the two vectors is 90° . The ratio of the \mathbf{E}_r to \mathbf{E}_θ in the near field is given by

$$\frac{\mathbf{E}_r}{\mathbf{E}_\theta} = 2 \cot\theta \quad (4.30)$$

4.10.2 Short Monopoles

Monopoles are used at low frequencies for transmitting as well as receiving. Monopoles can be made more broadband by making the diameter of the conductor larger. Length-to-diameter ratios (l/d) of 10 to 10^4 are common (Weiner [8]). A linear dipole with an l/d ratio of 5,000 and a bandwidth of 3% can have its bandwidth extended to 30% by keeping its length constant, but having its l/d ratio decreased to 260 [5, p. 333]. The monopole could be fed by a coaxial line, with the center conductor being connected to the conductor of the monopole, and the outer conductor connected to the ground plane.

For monopoles of height $H < 0.2\lambda$ the approximate reactance X_a is given by

$$X_a = Z'_a \cot\left(\frac{2\pi H}{\lambda}\right) \quad (4.31)$$

where the value of Z'_a [3, p. 512] has been found empirically (by comparison with experimental results) to be given by

$$Z'_a = 60 \left[\log_e \left(\frac{H}{a} \right) - 1 \right] \quad (4.32)$$

where a is the radius of the conductor of the monopole.

For very thin monopoles, that is, where the radius is much smaller than the length, the current distribution is approximately sinusoidal and independent of the size of the ground plane [8]. However, for thick monopoles or rods, the current distribution is no longer sinusoidal and the current distribution on the monopole, as well on the ground plane, is a function of the radius of the ground plane.

4.10.3 Ground Plane Dependence

In cases where the ground plane is small in terms of wavelengths, the outer edge of the ground plane diffracts the incident radiation in all directions. The currents on the top and bottom surfaces of the ground plane are equal in magnitude, but they must be opposite in direction since the net current at the edge is zero. This outer edge diffraction becomes more significant as the size of the ground plane gets smaller, since the currents are larger near the monopole. Edge diffraction can alter the input impedance by more than 100% and the gain by more than 6 dB compared with a monopole on an infinite ground plane.

For monopoles with infinite and zero ground planes, the peak directivity occurs at the horizon (i.e., at $\theta = 90^\circ$) as shown in Figure 4.9(a, c). However, in general, it can be said that as the size of the infinite ground plane is decreased, the peak directivity occurs at smaller angles ($\theta < 90^\circ$), although this variation is not monotonic. The directivity at $\theta = 90^\circ$ for a short monopole with no ground plane is 1.76 dBi, whereas with a large but finite ground plane the directivity at $\theta = 90^\circ$ is -1.249 dBi, and with an infinite ground plane the directivity is 4.77 dBi [8]. The magnitude of the peak directivity for a short monopole with no ground plane is also smaller 1.76 dBi as compared with 4.77 dBi for a large or infinite ground plane. The radiation resistance R_{rad} of a monopole with no ground plane is $20\pi^2(h/\lambda)^2$ whereas with a large or infinite ground plane the radiation resistance is $40\pi^2(h/\lambda)^2$.

At frequencies up to 1 MHz where the wavelength is greater than 300m it is possible to have a ground plane consisting of wires instead of a solid one. A ground plane of eight or more radial wires is often used, as shown in Figure 4.9(d).

4.10.4 Top-Loaded Monopoles

A monopole can be loaded by attaching a disk at the top, or by bending it into the shape of an L or T, as shown in Figure 4.10. Top loading can increase the effective

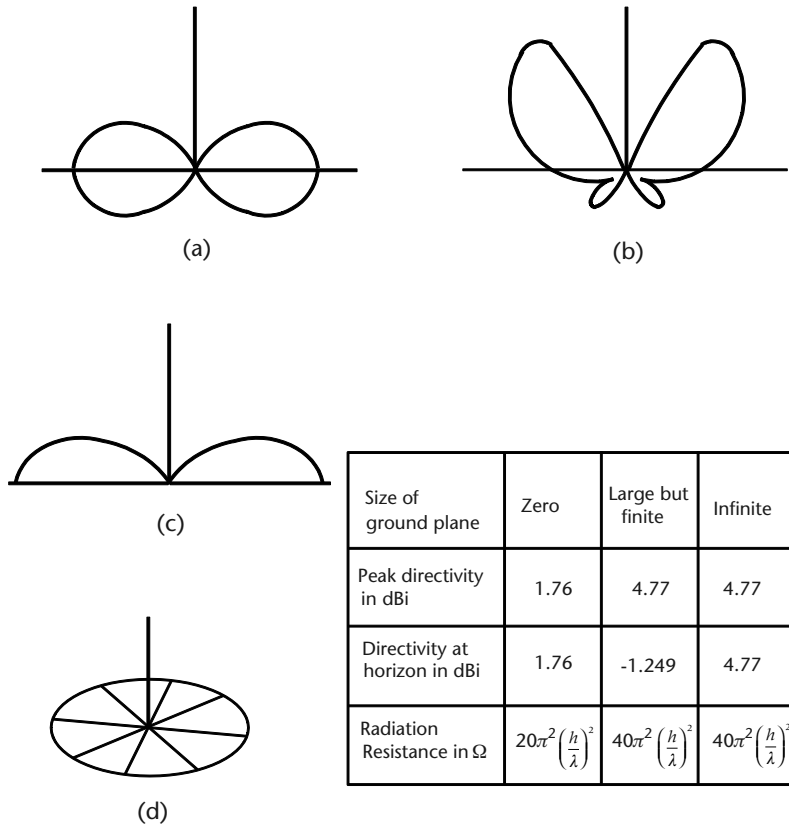


Figure 4.9 Variation of the radiation pattern for a monopole with the size of ground plane: (a) Zero ground plane, (b) finite ground plane of diameter $10\lambda/\pi$, (c) infinite ground plane, (d) monopole with radial wire ground plane.

length by a factor of two; this increases the gain of the antenna. Top loading can also decrease the capacitive reactance of a short antenna [3]. In the case of a receiving antenna, a large shunt capacitance requires a high inductive tuning circuit; this lowers the efficiency of the total circuit and hence the signal received.

In the case of transmitting antennas, the current I depends on the voltage V and the capacitive reactance X_a of the antenna (i.e., $I = V/X_a$). The power radiated is given by

$$P_{\text{rad}} = I^2 R_{\text{rad}} \tag{4.33}$$

where R_{rad} is the radiation resistance of the antenna.

Since the current $I = V/X_a$, the power radiated can be written as

$$P_{\text{rad}} = \frac{V^2 R_{\text{rad}}}{X_a^2} \tag{4.34}$$

If X_a is large, the voltage has to be increased to very large values to radiate even reasonable amounts of power. Thus by reducing the magnitude of X_a , we can

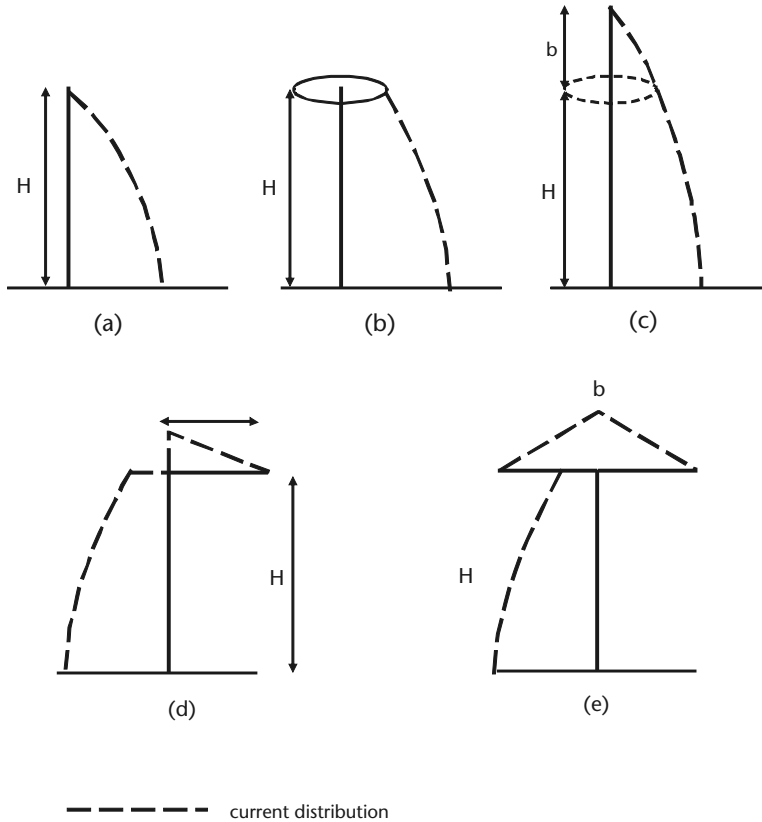


Figure 4.10 Top-loaded monopoles: (a) Unloaded monopole, (b) top hat monopole, (c) current distribution on a monopole of length $H + b$, (d) L-shaped antenna, and (e) T-shaped antenna. (After [11])

increase the power radiated. Top loading by use of a top hat changes the current distribution of the unloaded monopole as shown in Figure 4.10(a) to that shown in Figure 4.10(c). This shows the current distribution that would be present if the monopole was extended by a length b equivalent to the effective increased length of the top loaded monopole. In the case of the L- or T-shaped antennas shown in Figure 4.10(d, e), the bent sections draw the same amount of current that would be drawn by an additional length b connected to the antenna. This additional length b is approximately equal to the physical length of the horizontal portion of the L- and T-shaped antennas. Without top loading, the radiation resistance would be $40\pi^2(b/\lambda)^2$. However for a loaded monopole of total effective length $(H + b) < 0.1\lambda$ the radiation resistance R_{rad} is given by

$$R_{\text{rad}} = 160\pi^2 \left(\frac{H}{\lambda}\right)^2 \left[1 + \frac{H}{H+b} + \frac{1}{4} \left(\frac{H}{H+b}\right)^2 \right] \quad (4.35)$$

We have seen from (4.20) that the effective height of a short thick monopole is half its physical length. By top loading, the effective height can be increased to 0.8 of its physical length in the frequency range 10 kHz to 40 MHz. In the lower frequency range, 20 Hz to 150 kHz, an effective height of around 0.63 of the physical

length can be obtained. A preamplifier can be used to provide a match between the high impedance of the rod antenna and the low impedance of the receiver, so that no signal loss occurs between them. Most 41-inch active rod antennas have an ACF of around 6 to 8 dB/m. In the absence of a preamplifier, the loss could be substantially higher than 12 dB, especially at the lower operating frequency of the rod antenna.

4.10.5 Parallel Element E-Field Generator

The parallel element E-field generator provides an electric field for susceptibility testing to military standards such as MIL-STD 462. It consists of two parallel horizontal wires about 2m long that are fed by a voltage of the order of 50 to 75V [9]. The operating bandwidth is from 10 kHz to 30 MHz in two bands, and the electric field produced between the elements is approximately 200 V m^{-1} . At 1m from the antenna and along the center line the electric field strength is approximately 20 V m^{-1} . In a typical arrangement, the parallel wires are connected across the secondary of an impedance matching transformer. The primary of the transformer forms the load of a transmission line as shown in Figure 4.11(c).

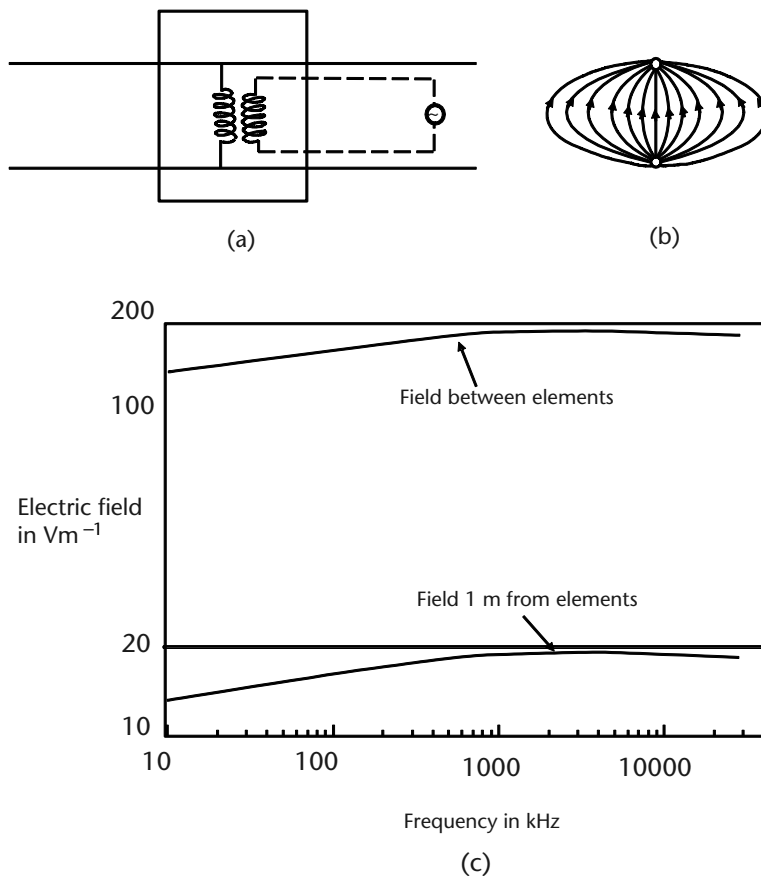


Figure 4.11 Parallel element E-field generator: (a) Typical feed arrangement for the parallel element, (b) side view showing electric field lines, (c) variation of the electric field with frequency.

4.11 H-Field Antennas

For magnetic field measurements, loops or coils of wire are used for receiving as well as transmitting. At frequencies below 1 MHz, the loops are small in terms of wavelength. The loops can consist of a single turn of wire or multiturn coils. At very low frequencies (e.g., at general AC electric power frequencies) a pair of coils, known as Helmholtz coils, are used to provide a uniform magnetic field.

4.11.1 Helmholtz Coils

Helmholtz coils are used to provide uniform magnetic fields for immunity and susceptibility measurements. They consist of a pair of coils of equal diameter, wound as flat rings, as shown in Figure 4.12. The coils are placed in a parallel configuration and at a distance apart that is equal to the radius of either coil. The coils are wound in the same sense, that is, both are clockwise or counterclockwise, and the

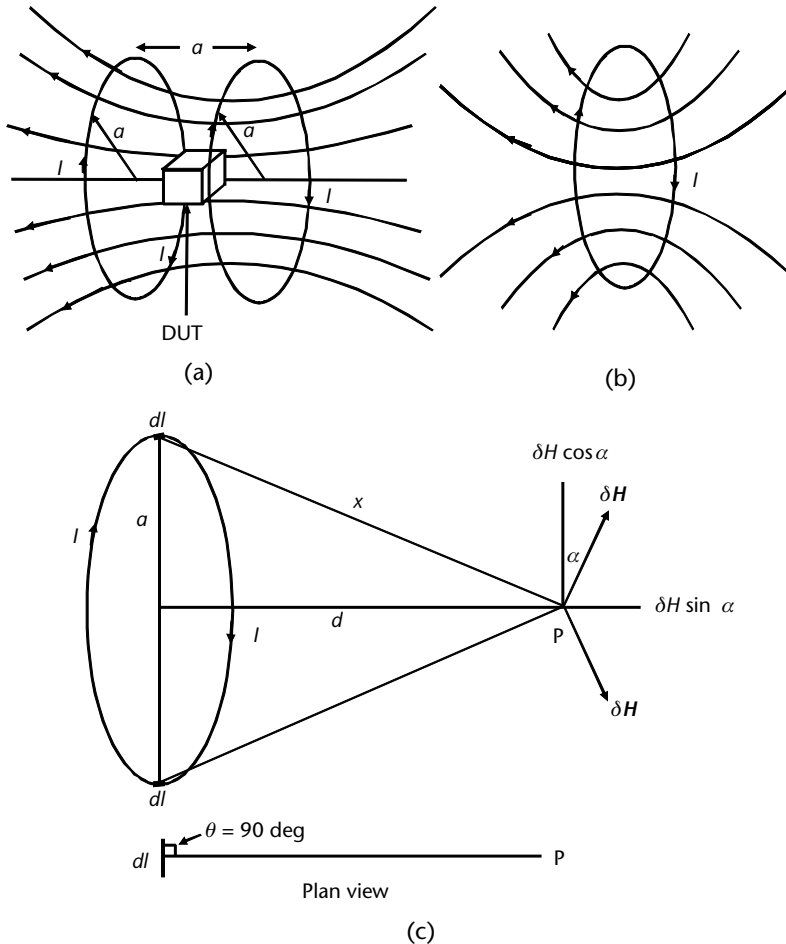


Figure 4.12 Magnetic fields due to Helmholtz coils for a uniform magnetic field: (a) Helmholtz arrangement of coils, (b) magnetic field lines of force for a single coil, (c) magnetic fields due to a current element on a coil.

same current flows in the both coils. This arrangement produces a uniform magnetic field in the area between the coils. The device under test (DUT) should be placed midway between the pair of coils and also near to the common axis of the pair.

If a single coil had been used, the magnetic lines of force would have been like that shown in Figure 4.12(b).

Consider an element δl at a point A on a coil with radius a , as shown in Figure 4.12. The magnetic field $\delta \mathbf{H}$ at point P on the axis due to the element δl carrying a current I is given by

$$\delta \mathbf{H} = \frac{I \delta l \sin \theta}{4\pi x^2} \quad (4.36)$$

where x is the distance between P and the element and θ is the angle between the element δl and the line joining it to P.

The direction of the magnetic field vector $\delta \mathbf{H}$ is at an angle α to the plane containing the coil. This is the same as the magnitude of the vector \mathbf{H}_ϕ in the near field, given by (4.25), since the first term can be ignored for very small electrical distances. This vector can be resolved into vertical and horizontal components of $\delta \mathbf{H} \cos \alpha$ and $\delta \mathbf{H} \sin \alpha$. If we consider another element diametrically opposite at point B, the magnetic field at P due to it will have a vertical component of $\delta \mathbf{H} \cos \alpha$ that is in the opposite direction (vertically downwards) to that due to the element at A, and will therefore cancel out the vertical component of the field due to A. This is true for all diametrically opposite points, so that for a circular coil, there will be no resultant vertical magnetic field. Thus, there will only be a horizontal magnetic field (parallel to the axis of the coil) which is found by taking the line integral of $\delta \mathbf{H} \sin \alpha$ around the circumference ($2\pi a$) of the coil. The resultant magnetic field is given by

$$\mathbf{H}_r = \oint_0^{2\pi a} \delta \mathbf{H} \sin \alpha \quad (4.37)$$

The magnitude of $\delta \mathbf{H}$ is given by (4.36), but in this case the angle θ between the element and the line joining it to P is 90° , and thus $\sin \theta$ is equal to 1. The resultant \mathbf{H}_r can therefore be written as

$$\mathbf{H}_r = \oint_0^{2\pi a} \frac{I \delta l \sin \alpha}{4\pi x^2} \quad (4.38)$$

$$\mathbf{H}_r = \frac{I a \sin \theta}{2x^2} \quad (4.39)$$

If d is the distance along the axis, then by using Pythagoras' theorem, we can see that $\sin \alpha$ can be written as

$$\sin \alpha = \frac{a}{\sqrt{a^2 + d^2}} \quad (4.40)$$

And since $x^2 = a^2 + d^2$, (4.39) can be rewritten in the following form

$$\mathbf{H}_r = \frac{Ia^2}{2(a^2 + d^2)^{3/2}} \quad (4.41)$$

In the case of a pair of coils, each having N turns and radius a and separated by a distance a , the resultant magnetic field \mathbf{H}_r along the common axis and midway between the coils (at $d = a/2$) is given by

$$\mathbf{H}_r = \frac{2NIa^2}{2(a^2 + a^2/4)^{3/2}} \quad (4.42)$$

This reduces to

$$\mathbf{H}_r = \frac{8NI}{5a\sqrt{5}} \quad (4.43)$$

It can be seen that the resultant magnetic field is proportional to the current I and the number of turns on the coils. The diameter of the conductor used to wind the coils determines the current handling capacity. Maximum currents of 20A are common. The magnetic field is also inversely proportional to the radius (a) of the coils, but the smaller radius will also restrict the size of the DUT. The diameters of commercially available Helmholtz coils vary between 0.5 and 3m.

Sets of two (biaxial) or three (triaxial) coils are used to provide uniform magnetic fields along two or three mutually perpendicular axes. It is important to remember that the field is only uniform near the common axis of each pair of coils; thus the larger the DUT, the larger the coil diameter required.

4.11.2 Small Magnetic Loops

Single-turn loops are used to receive magnetic fields, whereas multiturn loops are used for receiving as well as transmitting. The loop is sometimes called a magnetic dipole. The small loop has similar fields to that from a small dipole, but with the \mathbf{E} and \mathbf{H} fields interchanged. The polarization of the electric field in the horizontal plane is tangential to the loop, as shown in Figure 4.13, unlike the situation of the dipole where the electric field is in the same direction as the axis of the dipole. The electric and magnetic fields radiated by a small single-turn loop are given by

$$\mathbf{E}_\phi = 30\beta^3 IdA \left[\frac{1}{\beta r} - \frac{1}{(\beta r)^2} \right] \sin\theta e^{-j\beta r} \quad (4.44)$$

$$\mathbf{H}_\theta = \frac{\beta^3 IdA}{4\pi} \left[\frac{1}{\beta r} - \frac{j}{(\beta r)^2} - \frac{1}{(\beta r)^3} \right] \sin\theta e^{-j\beta r} \quad (4.45)$$

$$\mathbf{H}_r = \frac{j\beta^3 IdA}{2\pi} \left[\frac{1}{(\beta r)^2} - \frac{j}{(\beta r)^3} \right] \cos\theta e^{-j\beta r} \quad (4.46)$$

where I is the current in the loop in amperes, dA is the area of the loop in meters squared, and β is the phase constant and equals $2\pi/\lambda$ in meters. If the loop has N turns, each of the expressions in (4.44)–(4.46) must be multiplied by N .

Near the antenna, that is, at distances $< 0.01\lambda$, the $1/r$ and $1/r^2$ terms can be ignored in comparison with the $1/r^3$ term. Thus, only the last terms in \mathbf{H}_r and \mathbf{H}_θ need to be considered. The \mathbf{E}_ϕ component can be ignored since it does not have a $1/r^3$ term. The \mathbf{H}_r and \mathbf{H}_θ terms in the near field are given by

$$\mathbf{H}_r = \frac{IdA}{2\pi r^3} \cos\theta e^{j\beta r} \quad (4.47)$$

$$\mathbf{H}_\theta = -\frac{IdA}{4\pi r^3} \sin\theta e^{j\beta r} \quad (4.48)$$

It can be seen that the \mathbf{H}_r vector has twice the magnitude of the \mathbf{H}_θ vector, and the phase between the two vectors is 90° . The ratio of the \mathbf{H}_r to \mathbf{H}_θ in the near field is given by

$$\frac{\mathbf{H}_r}{\mathbf{H}_\theta} = -2 \cot\theta \quad (4.49)$$

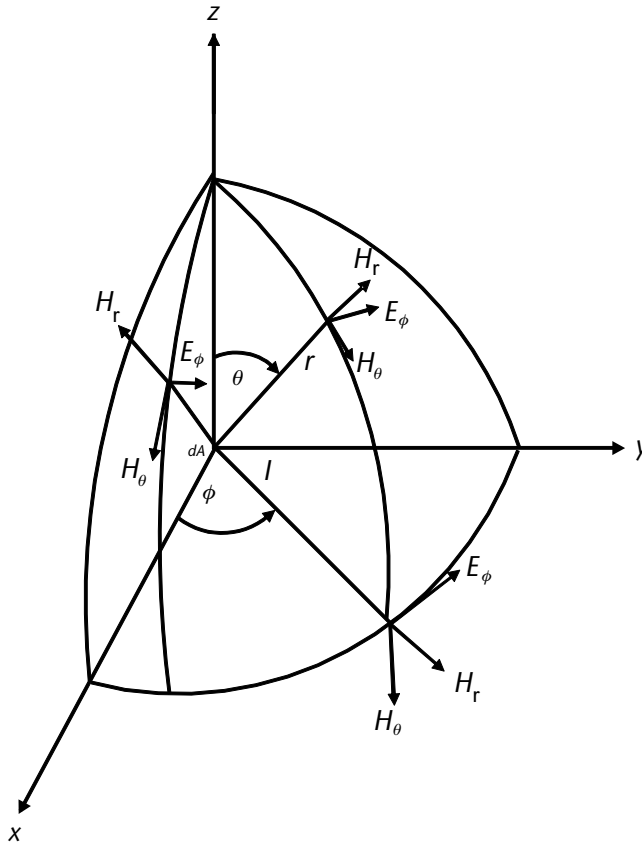


Figure 4.13 Fields due to a small radiating loop.

4.11.3 Single-Turn Shielded Loops

Shielded loops reject the electric field and sample the magnetic field over a small area. Only a short length of the loop conductor is exposed to the incident magnetic field. The shield is sometimes called a Faraday shield. There are two types of shielded loops, the balanced and unbalanced type. The shield is made of metal whose thickness is several skin depths to prevent any direct interaction between the currents on the internal and external surfaces of the shield. The effective terminals CD are at the small gap formed between the two halves of the loop,

The loop can be assumed to consist of a series combination of an internal impedance Z_{int} , an external inductance Z_{ext} , and a radiation resistance R_{rad} . In practice, there is also a distributed capacitance (between the sides of the turn) in parallel with these impedances, but this is often omitted since it can be compensated by having a larger variable capacitance in parallel. The internal impedance Z_{int} consists of an inductance L_{int} in series with a resistance R_{int} . Thevenin's equivalent circuit for a receiving loop is shown in Figure 4.14(a). The voltage V_l , developed at the load, is given by

$$V_l = \frac{V_{\text{OC}} Z_l}{(Z + Z_l)} \quad (4.50)$$

where Z_l is the load impedance in ohms (Ω), Z is the input impedance of the loop in ohms and V_{OC} is the open-circuit voltage in volts.

In the case of the unbalanced loop, the coaxial line is bent into a semicircle and the inner conductor is extended beyond the outer conductor and connected to the solid semicircle, as shown in Figure 4.14(b). The semicircular loop of length πb and the transmission line of length b , connect the terminals CD to the load, which has an impedance Z_l .

The incident magnetic flux density produces a voltage of V_{OC} at the gap CD that is given by

$$V_{\text{OC}} = j\omega AB \quad (4.51)$$

where V_{OC} is the open-circuit voltage in volts, ω is the angular frequency in radians per second, A is the area of the loop in meters squared, and B is the flux density in teslas. It is assumed that the magnetic flux density is uniform over the area of the loop. This would be the case for a small loop.

It should be noted that only the component of the magnetic field density that is perpendicular to the plane of the loop is instrumental in inducing the voltage produced. In the general case, the relative orientation between the loop and the incident wave is shown in Figure 4.14(c), and the induced voltage is given by

$$V_{\text{OC}} = j\omega AB \cos\theta \sin\phi \quad (4.52)$$

where V_{OC} is the open-circuit voltage in volts, ω is the angular frequency in radians per second, A is the area of the loop in meters squared, B is the flux density in teslas, and ϕ and θ are the angles following the normal polar notation.

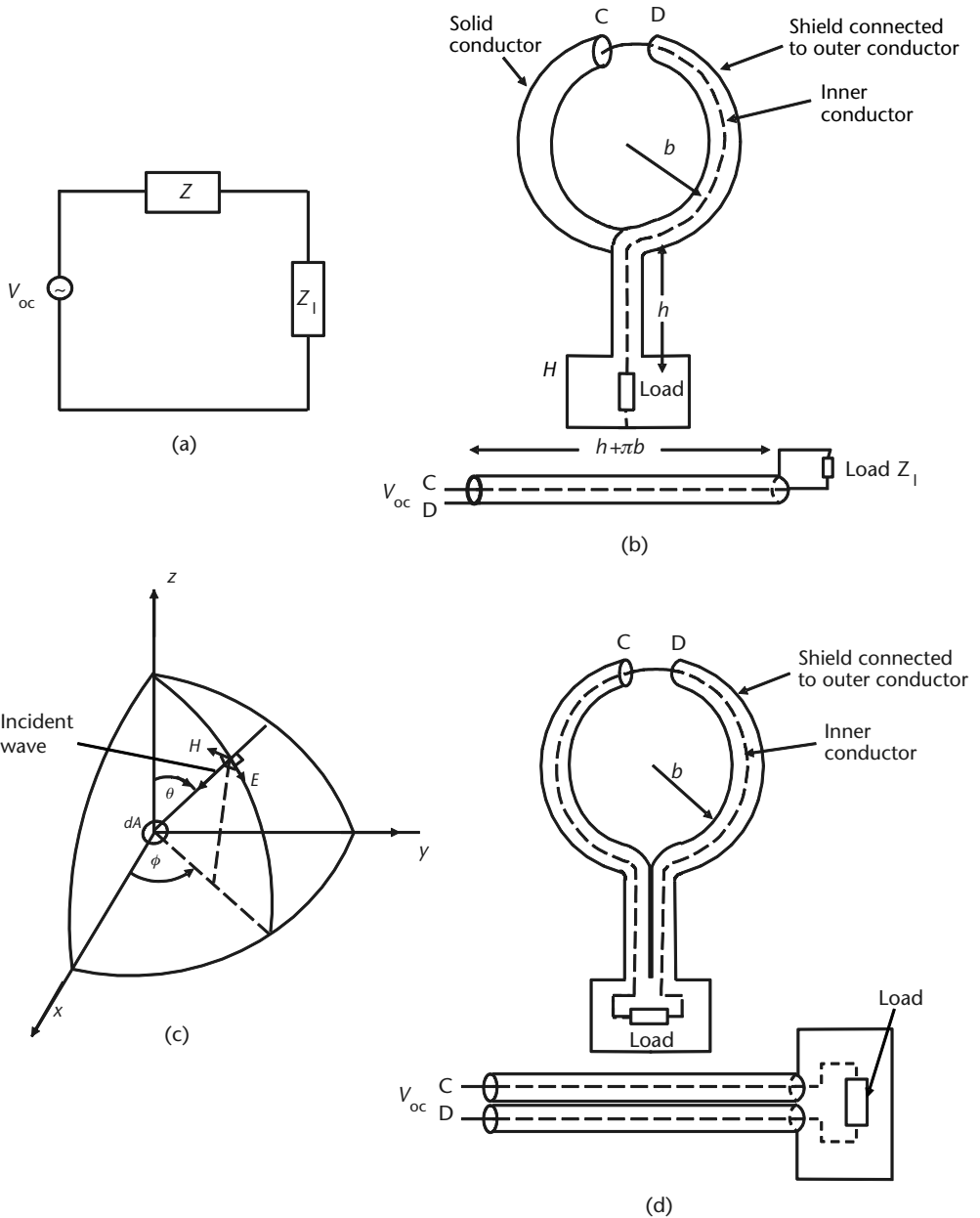


Figure 4.14 Shielded single-turn loops: (a) Equivalent circuit for a receiving loop, (b) shielded unbalanced single-turn loop, (c) plane wave incident on a loop, (d) shielded balanced single-turn loop.

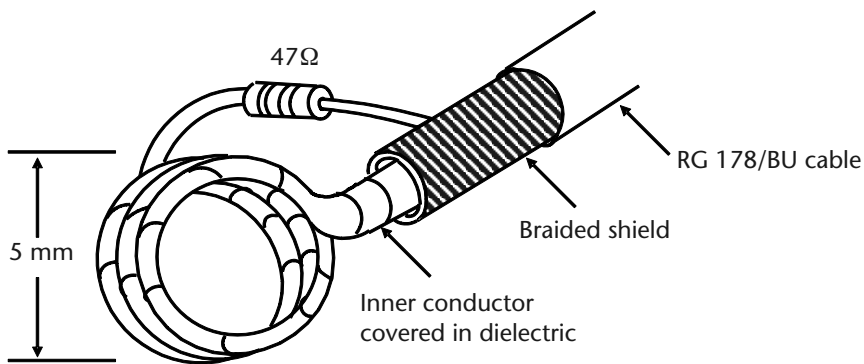
In the case of the balanced shielded loop, the coaxial line is bent into a circle, and the inner conductor is exposed by the removal of the outer conductor and dielectric as shown in Figure 4.14(d). The equivalent circuit is the same as that of the unbalanced loop. The problem with this design is that some sort of balun is required to connect it to an unbalanced coax.

4.11.4 Simple Multiturn Loop Probe

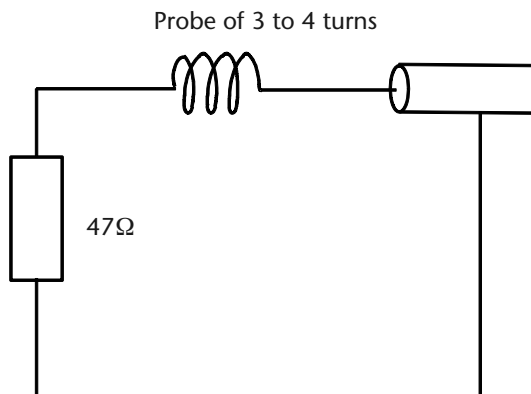
A simple probe can be constructed by forming the inner conductor of a coaxial cable into a 3 or 4 turn coil, as shown in Figure 4.15(a). The coil is then connected to the outer conductor via a 47Ω resistor [10]. The equivalent circuit is shown in Figure 4.15(b).

The signal generator reading is in volts, although the magnetic flux density (in tesla) is being measured. The effective height of a loop antenna as defined in Section 4.9 is the number of volts measured per tesla (T) of incident magnetic flux density. The area of the loop is usually given in centimeters, and incident magnetic flux density is of the order of picotesla (pT). Thus, the effective height can be defined in volts per picotesla, as in MIL-STD 461A [7] and is given by the following relation

$$\frac{V}{B} = 2\pi N A f \times 10^{-16} \quad (4.53)$$



(a)



(b)

Figure 4.15 A small multiturn loop probe: (a) A simple multiturn probe made from coaxial cable, (b) equivalent circuit of a simple probe.

where \mathbf{B} is the magnetic flux density in picoteslas (10^{-12} tesla), N is the number of turns, A is the area of the loop in centimeters squared, and f is the frequency in hertz.

References

- [1] Lucas, J. G., "Antenna Systems," *Student Quarterly Journal*, June 1967, pp. 186–195.
- [2] Connor, F. R., *Introductory Topics in Electronics and Telecommunications—Antennas Second Edition*, London: Edward Arnold, 1992.
- [3] Jordan, E. C., *Electromagnetic Waves and Radiating Systems*, Constable and Co. Ltd., 1953.
- [4] Johnson, R. C., and H. Jasik, *Antenna Engineering Handbook*, McGraw-Hill Book Company, 1984.
- [5] Balanis, C. A., *Antenna Theory—Analysis and Design*, Harper and Row, 1982.
- [6] Jay, F. (ed.), *IEEE Standard Dictionary of Electrical and Electronics Terms Fourth Edition*, 1988.
- [7] MIL-STD 461A *Electromagnetic Emission Interference Characteristics Requirements for Equipment*, Washington D.C.: U.S. Government Printing Office, August 1968.
- [8] Weiner, M. M., "Monopole Element at the Center of a Circular Ground Plane Whose Radius is Small or Comparable to a Wavelength," *IEEE Trans. on Antennas and Propagation*, Vol. 35, May 1987, pp. 488–495.
- [9] Shepherd, D., "A Five-Decade System for Testing RFI Susceptibility," *RF Design*, September 1988, pp. 20–23.
- [10] Torselli, J. V., "Electromagnetic Compatibility in Pocketable Equipment," *IEEE Trans. on EMC*, Vol. 16, November 1974, pp. 337–344.
- [11] Fewkes, J. H., and J. Yarwood, *Electricity, Magnetism and Atomic Physics Second Edition*, Volume 1, University Tutorial Press Ltd., 1962.

Antennas for Frequencies Between 1 MHz and 1 GHz

At frequencies between 1 MHz and 1 GHz, wire (as well as aperture) antennas are used. The wire antennas can be realized as free-standing wires or as printed circuits on a dielectric support. Since the wavelength at 1 GHz is 30 cm, resonant dipoles and monopoles are both manageable sizes. This chapter describes monopoles, dipoles, and loop antennas. It also discusses folded and triangular dipoles, and the biconical which can all be considered to be variants of the dipole. Other antennas described are the log periodic and Yagi antenna, which are really arrays of dipoles, and the discone antenna, which is a variant of the monopole. The helical antenna can be considered to be a type of loop. The bilog antenna is a combination of the triangular (bowtie) antenna and the log periodic. The broadband antennas such as the biconical, log spiral (which is described in Chapter 6), and log periodic can be considered to be variants of frequency independent (FI) antennas, although only the log spiral is a truly FI antenna. Double-ridged horns are also used at these frequencies, but these are described in Chapter 6.

5.1 Resonant Monopoles

A monopole is connected to the inner conductor of the coaxial line, and the ground plane is connected to the outer conductor, as shown in Figure 5.1(a). At frequencies in the MHz range, monopoles can be an appreciable fraction of, or larger than, a wavelength and these monopoles can therefore be considered to be large monopoles. When a monopole is approximately a quarter of a wavelength long, it is resonant and it radiates the maximum power at this frequency. It has a purely resistive impedance of 36.8Ω at resonance. This resistance varies slightly with the gap between the inner and outer conductor of the coaxial line feeding the antenna. The ratio of the radii of the outer and inner diameters (b/d) should be 1.868 for a line of characteristic impedance of 37Ω [1, p. 605]. Experimental data shows that the resonant length of a monopole occurs when the length is 0.236λ and the ratio of the diameter to length (l/d) of the conductor is 0.00318λ . At 100 MHz, the monopole would have a diameter of 9.5 mm and its length would be 0.708m. When the monopole is $> \lambda/4$ long, it exhibits an inductive impedance. The radiation pattern varies with the size of ground plane [2], as in the case of the short monopoles described in Chapter 4. Figure 5.1(b–g) shows the variation of the radiation pattern of the resonant monopole with the electrical diameter (the diameter in terms of wavelength) of the ground

plane. As the ground plane diameter is increased from zero to $6.5\lambda/\pi$, the main lobe (position of peak directivity) moves from the horizon ($\theta = 90^\circ$) to smaller angles and then increases again, but the variation is not monotonic (it does not increase or decrease consistently). The peak directivity varies from 1.88 dBi for zero ground plane to 5.16 dBi in the case of an infinite ground plane. The radiation resistance varies between 19.43Ω and 36.54Ω , as shown in the table given in Figure 5.1.

5.2 Discone Antenna

The discone antenna, which is sometimes called a Kandoian antenna (after its inventor), consists of a disk mounted on a truncated cone. The disk and cone could be solid or made of wires. The discone antenna can be considered to be a stub antenna (a thick monopole) that has been top-loaded by connecting a disk to its free end, and in which the ground plane has been modified to form a cone [3, p. 723]. Alternatively, it can be considered as a variant of the biconical antenna, where one of the cones has been flattened to a disk. The antenna is simple to construct and also easy to feed. The center conductor of the coaxial cable feeding the antenna is connected to the disk, and the outer conductor of the coaxial cable is connected to the top (or narrow) end of the cone, as shown in Figure 5.2(a). The azimuth radiation pattern of the discone is omnidirectional, as in the case of a vertical dipole, and the radiated electric field vector is vertically polarized. The diameter of the narrow end of

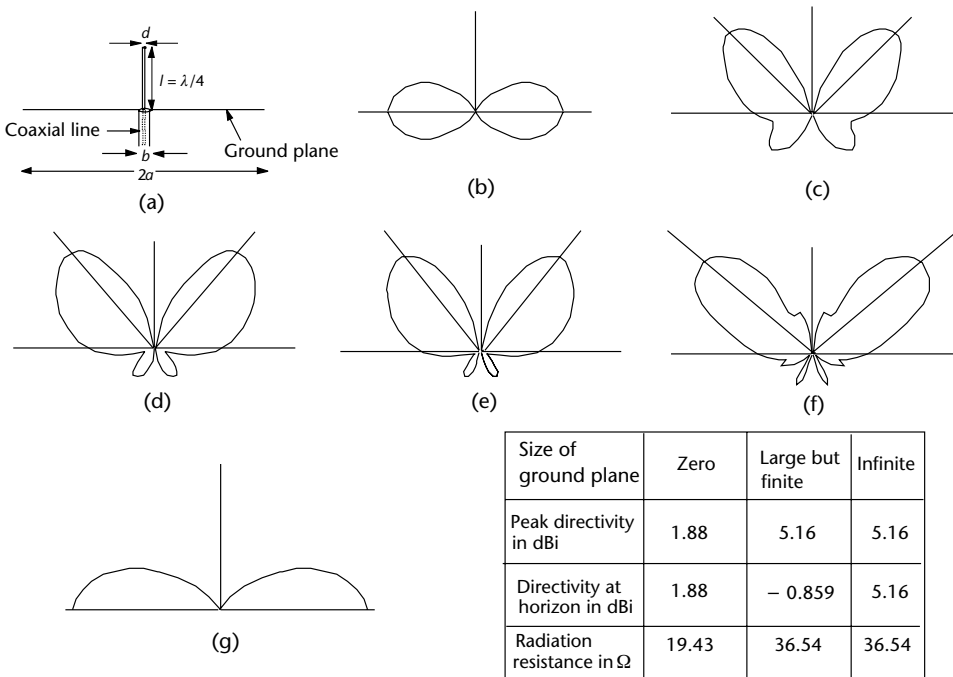


Figure 5.1 Variation of the radiation pattern of a resonant monopole with the size of the ground plane. (a) Monopole fed by coaxial line, (b) zero ground plane, (c) ground plane diameter = $3\lambda/\pi$, (d) ground plane diameter = $4\lambda/\pi$, (e) ground plane diameter = $5\lambda/\pi$, (f) ground plane diameter = $6.5\lambda/\pi$, (g) infinite ground plane.

the cone, C_{\min} , is inversely proportional to the bandwidth of the antenna and the slant height L is a function of the frequency [4]. The slant height must be greater than a quarter of a wavelength at the lowest operating frequency (i.e., $L > \lambda_c/4$).

Nail [4] has found that the disk-to-cone spacing affects the impedance match, and the optimum impedance match to a 50Ω transmission line is independent of the cone flare angle ϕ for angles between 25 and 90 degrees. The optimum impedance match is obtained when the disk-to-cone spacing is $0.3 C_{\min}$ (the diameter of the top of the cone) and the disk diameter D is $0.7 C_{\max}$ (the diameter of the base of the cone). This applies when C_{\min} is electrically small ($< \lambda/75$) at the high-frequency end and the diameter w of the feed pin is not taken into account. It is also assumed that the disk-to-cone spacing s is much less than the diameter of the disk D . At large angles, the discone acts like a high-pass filter, in that once the cone length L exceeds $\lambda/4$, the match to a 50Ω line remains good over an extremely large frequency range. The radiation pattern of the discone antenna is omnidirectional

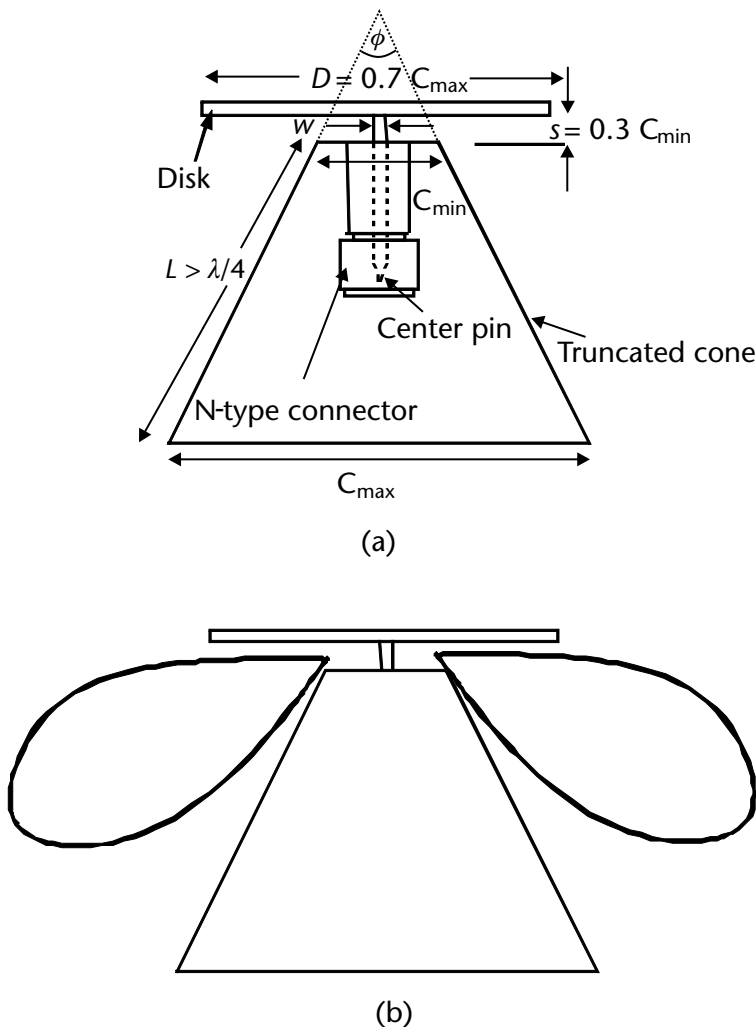


Figure 5.2 The discone, or Kandoian, antenna. (a) Physical characteristics of a discone antenna, and (b) radiation pattern of a discone in the elevation plane.

in the azimuth plane, as in the case of a monopole, and in the elevation plane the pattern is tilted downwards, as shown in Figure 5.2(b).

5.3 Cavitenna

The Cavitenna is used in the frequency range of 20 MHz to 300 MHz. It is a top-loaded monopole which is mounted by the use of magnetic clamps to the side or ceiling of a shielded room. The wall (or ceiling) forms the ground plane for the monopole and the room is excited like a cavity. These resonances account for the spurious readings obtained when measurements are made at certain positions and for some frequencies. They also account for the lack of repeatable measurements.

5.4 Resonant and Large Dipoles

When the length of a dipole approaches half a wavelength, the dipole resonates and maximum power is radiated. The radiation resistance is found to be about 73Ω , and the condition for zero reactance occurs when the dipole length is about 0.5λ for thin wires, but the dipole length is less than 0.5λ for thicker wires, which are used for wider bandwidths [5, p. 547]. The peak linear directivity at the resonant frequency is 1.64, which is 2.15 dBi. The radiation pattern in the azimuth plane (assuming sinusoidal current distribution) is omnidirectional, as shown in Figure 5.3(a). In the elevation plane we have the familiar figure of eight for a vertical center-driven dipole, as shown in Figure 5.3(b), with the main lobes on the horizon at $\theta = 90^\circ$ and -90° . As the length of the dipole increases above half a wavelength, the pattern in the elevation plane gets narrower and the peak directivity increases, as shown in Figure 5.3(c, d); and when the length is 1.25λ , minor lobes appear, as shown in Figure 5.3(e). As the length is increased further, the lobes at the horizon become narrower and the sidelobes get larger. For longer electrical lengths the main lobes are no longer on the horizon. The pattern breaks up so that there are four main lobes, as shown in Figure 5.3 (f–j).

The effective height h of a half-wave dipole [6, p. 4–24] depends on the angle θ between the axis of the dipole and the point of observation and is given by

$$h = \frac{\lambda}{\pi} \frac{\cos\left(\frac{\pi}{2} \cos\theta\right)}{\sin\theta} \quad (5.1)$$

We can see that on the axis where angle θ is 90° the effective height is λ/π .

The impedance Z_d of a half-wave resonant dipole is given by

$$Z_d = R(kl) - j \left[120 \left(\log_e \frac{1}{a} - 1 \right) \cot(kl) - X(kl) \right] \quad (5.2)$$

where k is the phase constant $2\pi/\lambda$, a is the radius of the conductor, and $R(kl)$ and $X(kl)$ are functions shown in Figure 5.4.

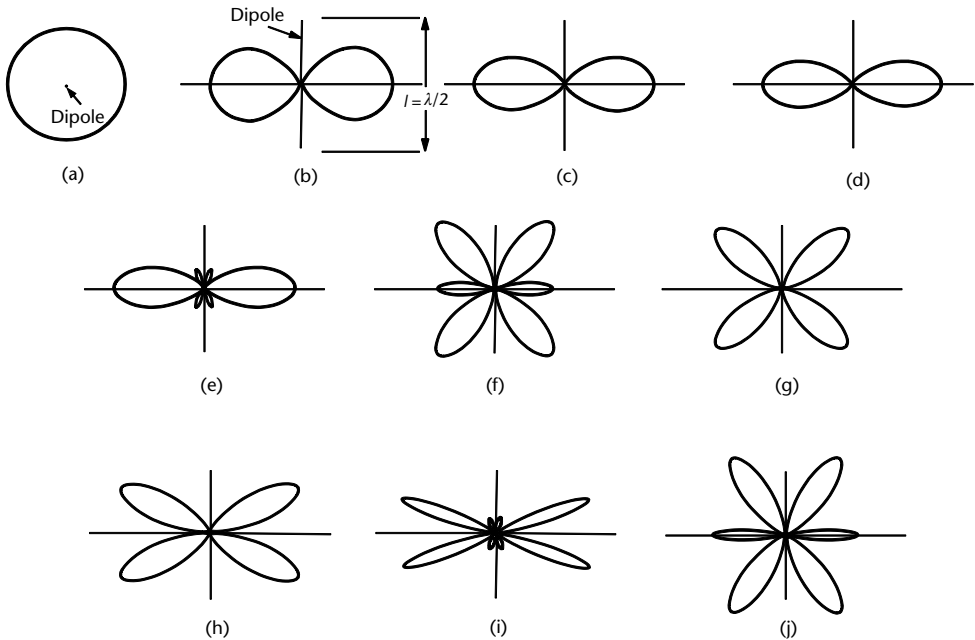


Figure 5.3 Radiation patterns for large and resonant dipoles: (a) Azimuth plane pattern, (b) elevation pattern for $\lambda/2$ dipole, (c) elevation pattern for $3\lambda/4$ dipole, (d) elevation pattern for λ dipole, (e) elevation pattern for 1.25λ dipole, (f) elevation pattern for 1.5λ dipole, (g) elevation pattern for 1.75λ dipole, (h) elevation pattern for 2λ dipole, (i) elevation pattern for 2.5λ dipole, and (j) elevation pattern for 2.75λ dipole.

5.5 Folded Dipoles

The folded dipole is a very popular antenna because of its ease of construction and its impedance. The dipole is formed by joining two cylindrical dipole elements of equal length $2l$ at their ends and driving one of the elements at its center, as shown in Figure 5.5(a). The dipole connected to the signal source is known as the driven element, and the dipole connected to the driven element is known as the parasitic

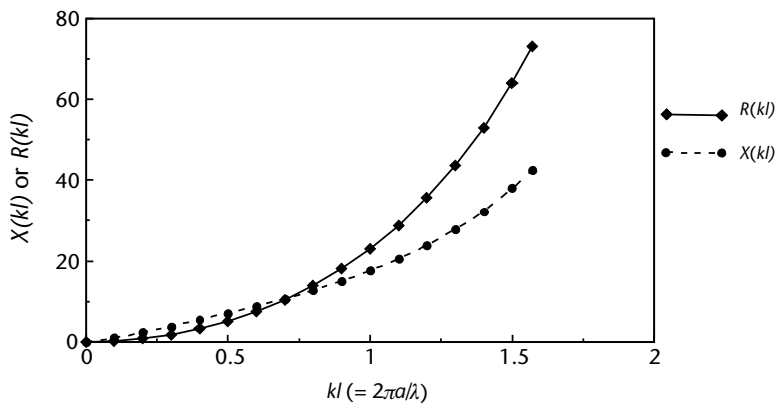


Figure 5.4 Functions $R(kl)$ and $X(kl)$.

element. The dipoles can be identical or of different radii r_1 and r_2 . The folded dipole is often constructed from commercially available twin wire transmission lines [7, p. 10]. The solid dielectric will reduce the phase velocity of the EM wave so that its wavelength is no longer equal to the free-space wavelength, but is reduced to a value of $\lambda\sqrt{\epsilon_r}$, where ϵ_r is the dielectric constant of the material. The wavelength of the transmission line currents is reduced by a proportionate amount. However, the dielectric material has a negligible effect on the antenna currents, and thus the resonant length remains unchanged. One method of construction that satisfies both requirements is to use shorting elements so that the distance between the shorted portions is as shown in Figure 5.5(b); this ensures that the lengths of the radiating elements are correct for air, but the transmission line modes are satisfied in the dielectric.

The excitation of the folded dipole can be considered as the superposition of common and differential modes, as shown in Figure 5.5(c). In the case of the common mode, the driving voltages in the two elements are both V and they have the

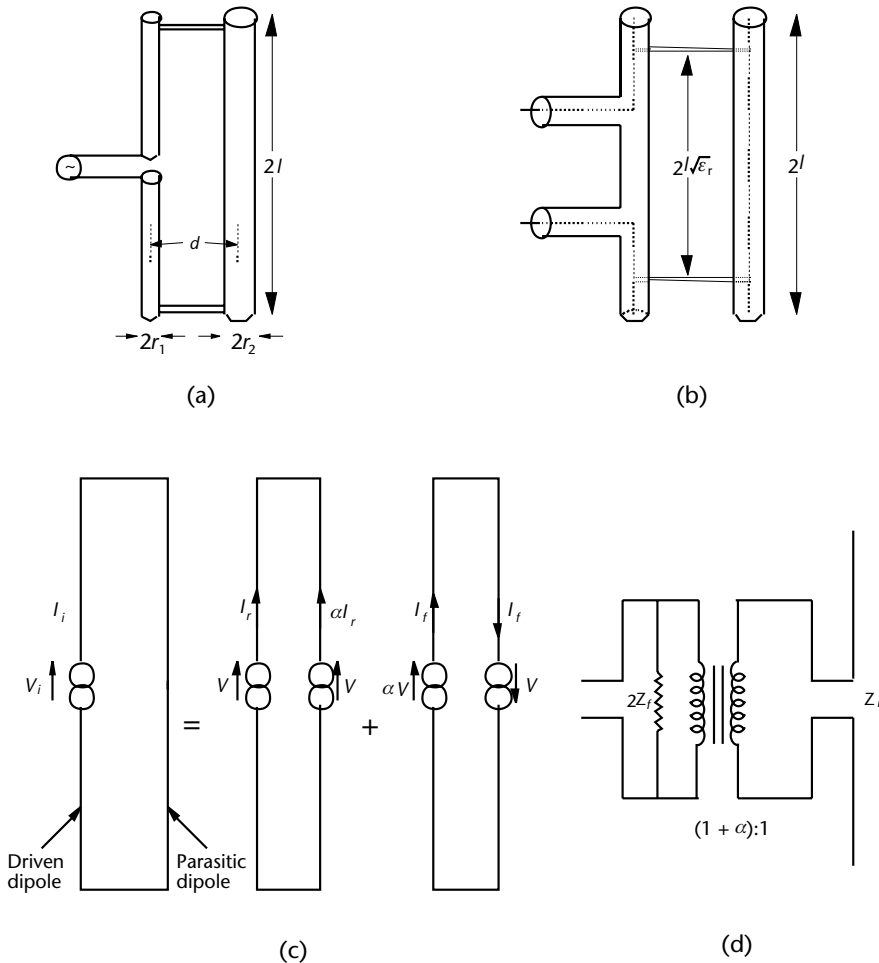


Figure 5.5 The folded dipole antenna. (a) Physical characteristics, (b) the folded dipole made from coaxial cable, (c) decomposition of a folded dipole into common and differential modes, and (d) equivalent circuit of a folded dipole.

same polarity. The currents in the driven and parasitic arms are I_r and αI_r , respectively, where α is the current division factor and is given by

$$a = \frac{\cosh^{-1}[(x^2 - u^2 + 1)/2v]}{\cosh^{-1}[(x^2 + u^2 - 1)/2uv]} \quad (5.3)$$

where $v (= d/r_1)$ is the ratio of the dipole spacing to the radius of the driven dipole, and $u (= r_2/r_1)$ is the ratio of the radii of the parasitic and driven elements.

The differential mode driving voltages in the two elements are V and αV , and they have opposite polarity. The currents in the driven and parasitic arms are both I_f .

For a half-wave folded dipole whose elements are of equal length $2l$, the input impedance is close to that of a 300Ω twin-wire transmission line.

The input impedance of a folded dipole of total length $2l$, greater than or equal to λ , is given by

$$Z_{in} = \frac{2(1 + \alpha)^2 Z_r Z_f}{2Z_f + (1 + \alpha)^2 Z_r} \quad (5.4)$$

where α is the current division factor given by (5.3), and Z_r is impedance of the common mode and is given by

$$Z_r = \frac{V}{(1 + \alpha)^2 I_r} \quad (5.5)$$

and Z_f is impedance of the differential mode and is given by

$$Z_f = \frac{(1 + \alpha)V}{2I_f} \quad (5.6)$$

These equations assume that the element spacing d and the radii r_2 and r_1 are all much smaller than the length $2l$ of the elements.

When the element length $2l$ is equal to $\lambda/2$, the impedance Z_f is much larger than $Z_r(1 + \alpha)^2$ so the denominator of (5.4) can be taken as $2Z_f$, and (5.4) reduces to

$$Z_{\lambda/4} = Z_r(1 + \alpha)^2 \quad (5.7)$$

The effective height h of a half-wave folded dipole [6, p. 4–24] depends on the angle θ between the axis of the dipole and the point of observation, and is given by

$$h = \frac{2\lambda}{\pi} \frac{\cos\left(\frac{\pi}{2} \cos\theta\right)}{\sin\theta} \quad (5.8)$$

The equivalent circuit of the folded dipole is shown in Figure 5.5(d).

5.6 Triangular Dipoles

A dipole can be made more broadband by using triangular sheets of metal instead of straight wires, as shown in Figure 5.6(a). This type of antenna is sometimes called a bowtie antenna. The bowtie has similar radiation patterns and input impedance to the biconical antenna, but it is much lighter in weight and simpler to construct. The antenna is characterized by the flare angle α of the apices and the height A (from the apex to the opposite side) of the triangles. Simplifying the construction to a wire outline results in the significant degradation of broadband performance. But at low frequencies, mesh can be used instead of solid sheets, as long as the mesh spacing is smaller than one tenth of a wavelength at the highest operating frequency.

The larger the values of A and α , the more the radiation pattern in the elevation (z - y) plane varies from the azimuth (x - y) plane, and also, the sidelobes are higher [6, p. 29–5]. Optimum design (a compromise between pattern and impedance characteristics) is obtained by selecting values of α between 60 and 80 degrees and values of A up to 0.58λ . When a bowtie antenna of typical dimensions $38\text{ cm} \times 27$

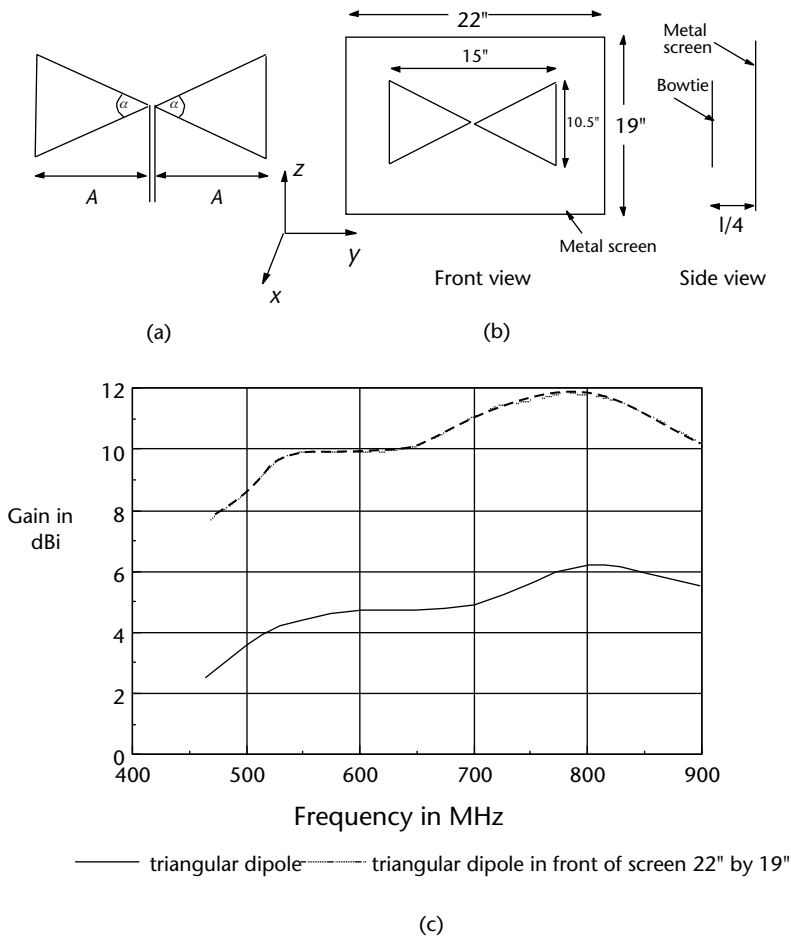


Figure 5.6 The triangular dipole (bowtie) antenna: (a) Physical characteristics, (b) the bowtie in front of a metal screen, and (c) variation of gain with frequency for a bowtie placed in front of a screen.

cm is mounted $\lambda/4$ in front of a flat reflecting screen, as shown in Figure 5.6(b), its gain is increased and its back radiation is reduced. Placing the antenna in front of a screen of size $56 \text{ cm} \times 48 \text{ cm}$ results in a 5-dB improvement in gain over the 470 to 900 MHz frequency range, as shown in Figure 5.6(c).

5.7 Biconical Antennas

The biconical antenna was first used by Oliver Lodge in 1892 [3, p. 340]. Although broadband, this antenna is not frequency-independent when the cones are truncated, as would be the case for a practical antenna. The infinite biconical antenna, shown in Figure 5.7(a), acts as a guide for spherical waves in the same way as an infinite transmission line acts as a guide for plane wave. The feed at the terminals produces a voltage V between the cones, and a total current I flows on the surface of the cones at a distance r from the terminals. The characteristic impedance is defined as the ratio of V to I in the same way as it is defined for transmission lines.

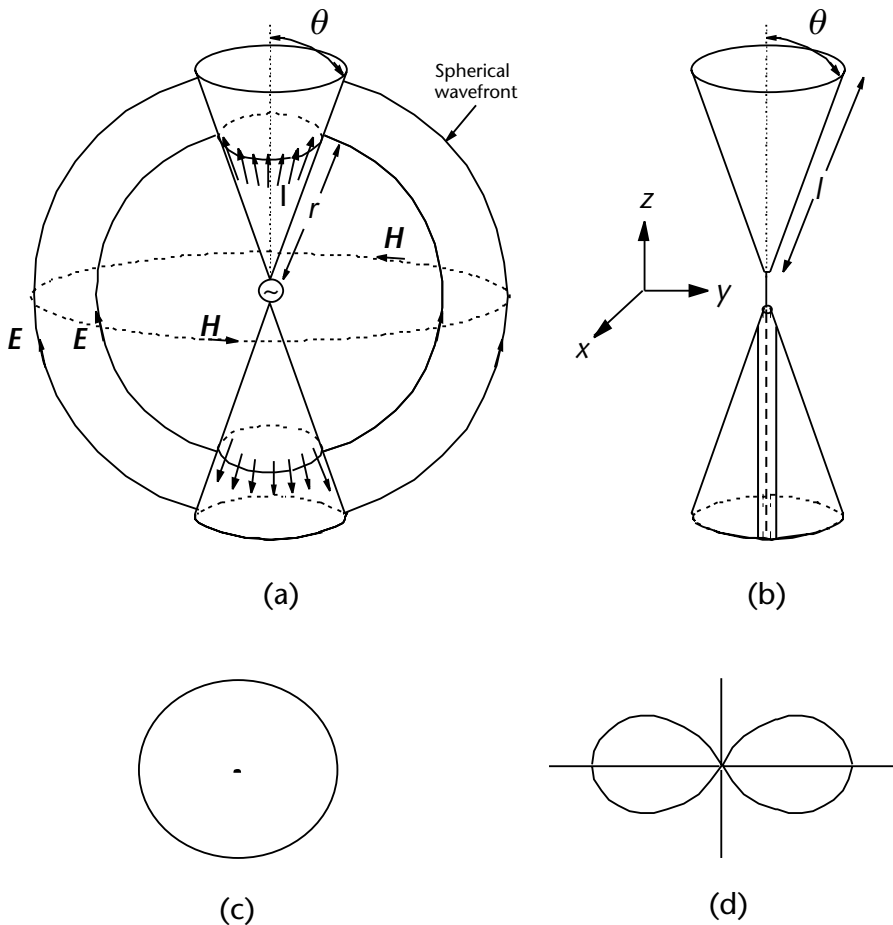


Figure 5.7 The biconical antenna: (a) TEM mode of the biconical antenna, (b) feeding details of the biconical antenna, (c) radiation pattern in x - y (azimuth) plane, and (d) radiation pattern in y - z (elevation) plane.

If we consider only the first or fundamental mode, that is, the transverse electromagnetic (TEM) mode, the electric and magnetic fields are both transverse to the direction of propagation of the wave and perpendicular to each other. The electric field lines are great circles through the polar axis, and the magnetic lines are circles perpendicular to the axis.

Using Maxwell's second equation, we have in this case

$$\nabla \times \mathbf{E} = -j\omega\mu\mathbf{H} \quad (5.9)$$

Expanding the LHS of (5.9) in spherical coordinates, we get

$$\begin{aligned} \nabla \times \mathbf{E} = & \frac{\mathbf{a}_r}{r^2 \sin\theta} \left[\frac{\partial(r \sin\theta E_\phi)}{\partial\theta} - \frac{\partial(r E_\theta)}{\partial\phi} \right] + \frac{\mathbf{a}_\theta}{r \sin\theta} \left[\frac{\partial E_r}{\partial\phi} - \frac{\partial(r \sin\theta E_\phi)}{\partial r} \right] \\ & + \frac{\mathbf{a}_\phi}{r} \left[\frac{\partial(r E_\theta)}{\partial r} - \frac{\partial E_r}{\partial\theta} \right] \end{aligned} \quad (5.10)$$

The electric field does not have a component in the ϕ or radial (r) directions and the E_θ component is independent of ϕ . Thus, the right-hand side of (5.10) reduces to

$$\nabla \times \mathbf{E} = \frac{\mathbf{a}_\phi}{r} \frac{\partial(r E_\theta)}{\partial r} \quad (5.11)$$

In the case of the right-hand side of (5.9), we only have to consider the \mathbf{H}_ϕ component, and this gives

$$-j\omega\mu\mathbf{H} = -\mathbf{a}_\phi j\omega\mu\mathbf{H}_\phi \quad (5.12)$$

Combining (5.11) and (5.12) gives us

$$\frac{1}{r} \frac{\partial(r E_\theta)}{\partial r} = -j\omega\mu\mathbf{H}_\phi \quad (5.13)$$

If we consider Maxwell's first equation for a nonconducting medium $\sigma = 0$, we have

$$\nabla \times \mathbf{H} = j\omega\mu\mathbf{E} \quad (5.14)$$

For the TEM mode, we again only have the \mathbf{H}_ϕ and \mathbf{E}_θ components, and thus Maxwell's first equation is reduced to

$$\frac{\partial(r H_\phi)}{\partial r} = -j\omega\epsilon(r E_\theta) \quad (5.15)$$

It can be shown that the \mathbf{H}_ϕ component [3, p. 345] is given by

$$\mathbf{H}_\phi = \frac{1}{r \sin \theta} H_0 e^{-j\beta r} \quad (5.16)$$

where H_0 is the amplitude of the magnetic field

The intrinsic impedance Z_0 is defined as the ratio of \mathbf{E}_θ to \mathbf{H}_ϕ and is given by

$$Z_0 = \frac{E_\theta r \sin \theta}{H_0} e^{j\beta r} \quad (5.17)$$

From which we can write \mathbf{E}_θ as

$$\mathbf{E}_\theta = \frac{Z_0 H_0}{r \sin \theta} e^{-j\beta r} \quad (5.18)$$

We can calculate the voltage between the points at the radial distance r by taking the line integral of the electrical field \mathbf{E}_θ (with respect to θ) along a great circle between the two points. The angle θ varies between $-\theta_1$ and $+\theta_1$ over this path, where θ_1 is the cone semi-angle. Thus, the voltage is given by

$$V(r) = Z_0 H_0 e^{-j\beta r} \int_{\theta_2}^{\pi-\theta_1} \frac{d\theta}{\sin \theta} \quad (5.19)$$

The biconical antenna that is usually fed from a coaxial line via a balun is shown schematically in Figure 5.7(b). The radiation pattern of the biconical antenna is similar to that of a dipole. In the azimuth (x - y) plane it is omnidirectional, and in the elevation (y - z) plane is a figure of eight as shown in Figure 5.7(c, d). Typical gains of biconical vary between 0 and 4 dBi, and beamwidths in the elevation plane are between 20° and 100° .

The broadband impedance characteristics of the biconical antenna occur when the cone half-angle θ_{bc} lies between 30° and 60° [6, p 4–12]. This angle is not critical and is usually selected to match the characteristic impedance of the transmission line feeding the antenna as closely as possible.

The characteristic impedance of a biconical antenna is given by

$$Z = 120 \log_e \left[\cot \left(\frac{\theta_{bc}}{2} \right) \right] \quad (5.20)$$

where θ_{bc} is the cone half-angle.

Using (5.20) for a biconical antenna of half angle 60° , the characteristic impedance is calculated as 66Ω . The variation of the impedance with cone half angle is shown in Figure 5.8. Measured values of the characteristic impedance for a 6:1 bandwidth biconical antenna of half-angle 60° and cone diameter of one wavelength (at the lowest frequency) has been found to be a constant 50Ω over the bandwidth with a VSWR of < 1.2 [3, p. 64].

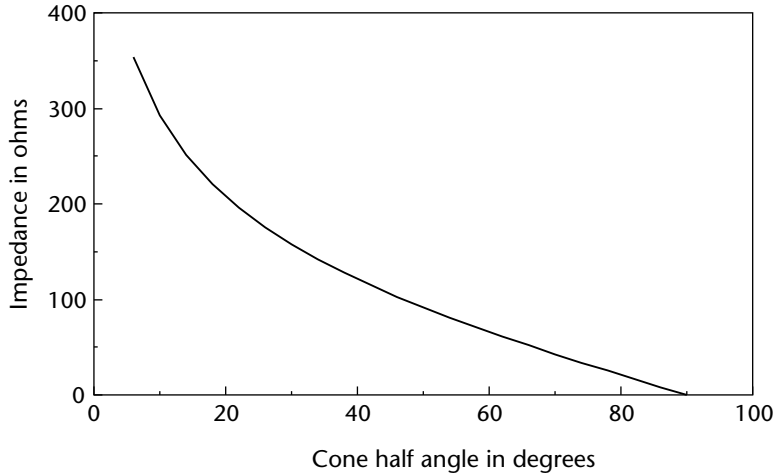


Figure 5.8 Variation of impedance with cone half angle.

For small cone angles $\cot(\theta_{bc}/2)$ is approximately equal to $2/\theta_{bc}$, and thus the characteristic impedance of a small-angled biconical antenna is given by

$$Z = 120 \log_e \left[\frac{2}{\theta_{bc}} \right] \quad (5.21)$$

5.8 Yagi-Uda Antenna

This antenna is often called a Yagi, after the student of Professor Uda (Japan) who first presented the relevant paper in English and performed many of the measurements. However, it was designed by Uda, and should therefore be called a Uda-Yagi. It consists of a single driven dipole and a number of slightly shorter parasitic dipoles in front of it, as shown in Figure 5.9(a). The driven element is a resonant or tuned dipole, or it could be a folded dipole. Parasitic dipoles are ones that are not directly fed but have currents induced in them, in the same way as currents from the primary of a transformer induces a current in the secondary. The parasitic dipole can then reradiate like directly-fed radiating dipoles. These parasitic elements are called directors. A reflector which is slightly longer than the driven element is placed behind the driven element. All elements are parallel to each other and in the same plane. The antenna radiates in the end-fire direction from the reflector towards the shorter directors. Increasing the number of directors increases the gain, but with diminishing returns, so that in practice there is not a large increase in gain when the number of parasitic elements is above about 12 [8, Vol. 2, p. 765]. The radiation pattern in the x - y plane is shown in Figure 5.9(b), and the radiation pattern in the y - z plane is shown in Figure 5.9(c). In the case of uniform Yagi arrays, all the elements have the same circular cross section, the spacings between the elements are the same, and all directors have the same physical length, as shown in Figure 5.9(b). The directors are made the same length for ease of construction, but they do not carry the equal currents.

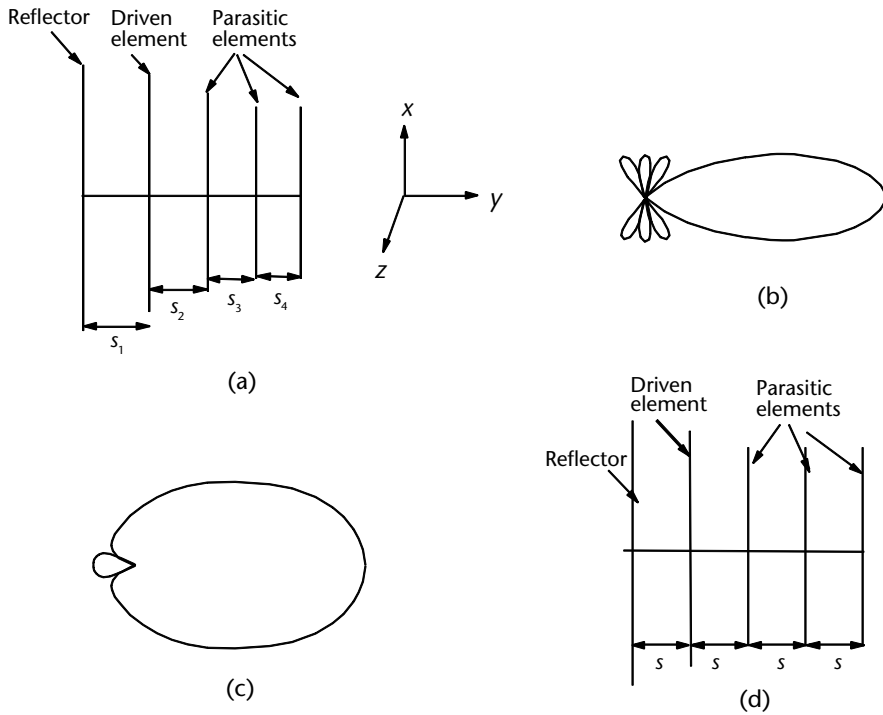


Figure 5.9 The Yagi-Uda dipole array. (a) Yagi-Uda array of dipoles, (b) radiation pattern in the x-y plane, (c) radiation pattern in the z-y plane, and (d) uniform Yagi-Uda array.

The gains obtainable for different number of elements have been computed for uniform Yagis made of wires having diameters from 0.0025λ to 0.02λ and spacings between 0.15λ and 0.3λ [9]. The curve of gain versus the number of elements for a conductor diameter of 0.0025λ shows an average gain of 0.9 dB for each additional element above three, but the gain flattens off after about 5 elements, as shown in Figure 5.10.

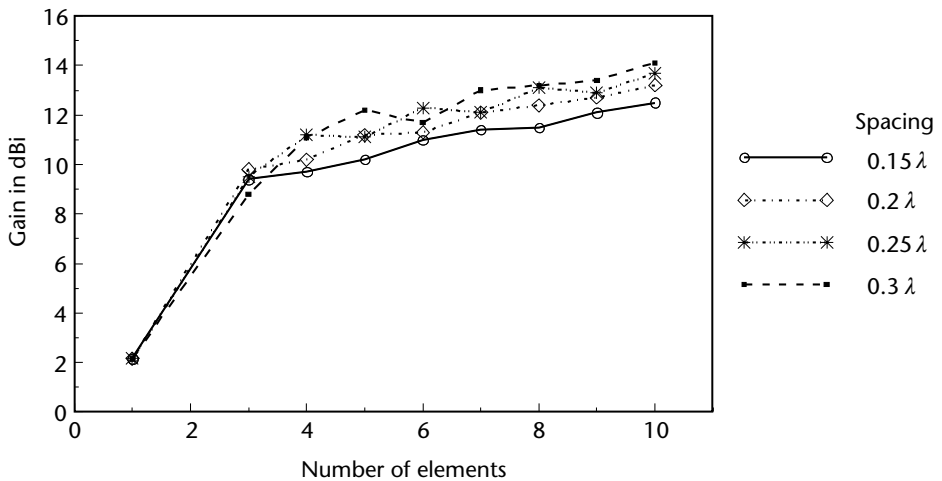


Figure 5.10 Variation of gain with number of elements for uniform Yagis.

Comparison between measured results and computed values suggest that the elements behave as though they are slightly longer than their physical lengths. This is thought to be due to an end effect, and when the elements are slightly shortened, empirically, optimum performance can be obtained at a particular design frequency.

Increasing the number of parasitic elements reduces the radiation resistance of the antenna, so that it does not match the transmission line feeding it. A folded dipole is required to match the resistance of the antenna to the transmission line in these cases. When four elements are used and spaced 0.2λ apart, the input resistance is 45Ω . The antenna can be made more broadband by designing the directors for the upper end of the frequency band and the reflector for the lower end. An antenna with five elements (one reflector and three directors) can have a bandwidth of 60%, but its gain is reduced to around 6 dBi [8, p. 765]. If the antenna is optimized, its gain can be increased to 10 dBi, but its bandwidth is reduced to about 9%.

5.9 Frequency-Independent Antennas

In general, it can be said that the impedance and radiation pattern characteristics of an antenna is determined by its shape and dimensions in terms of wavelength. In 1954, Rumsey suggested that if an antenna could be defined entirely in terms of angles, for instance, instead of any characteristic length dimensions, then it would be possible for such an antenna to have properties which are independent of the frequency of operation. A change of frequency, however, results in rotation of the radiation pattern. This type of antenna, based on the angle condition, can be implemented by the use of conical surfaces and equiangular spirals.

There are two types of frequency-independent (FI) antennas:-

1. Logarithmic conical spirals, called log spirals;
2. logarithmic periodic, called log periodic.

It can be shown that they are both the same type of structure, except that the log periodic has periodicity at discrete angles, whereas the periodicity of the log conical spiral is continuous. One of the characteristics of FI antennas is that the radiation is in the back-fire direction.

5.10 Log Periodic Antenna

The log periodic antenna consists of an array of dipole elements and displays, fairly stable impedance, and pattern characteristics over the design bandwidth. This antenna has self-similar figures with discrete similarity at discrete angles (ϕ) only. The log periodic dipole array (LPDA) antenna is shown schematically in Figure 5.11(a).

It consists of dipoles of decreasing length and spacing, such that the apex angle formed by the intersection of two imaginary lines drawn through the ends of the dipoles on each side of the array is 2α ; and the tan of the half angle α is given by

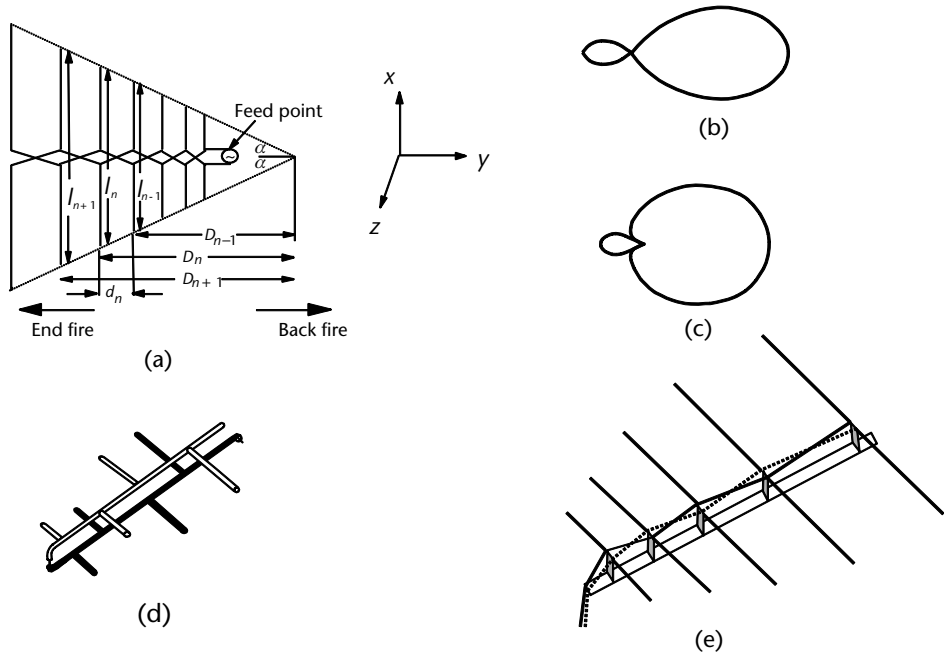


Figure 5.11 The log periodic dipole array (LPDA): (a) Schematic of the log periodic dipole array, (b) radiation pattern in the x - y plane, (c) radiation pattern in the z - y plane, (d) coaxial line 50Ω or 75Ω , (e) 300Ω twin-wire feed for the LPDA.

$$\tan \alpha = \frac{l_n}{2D_n} \quad (5.22)$$

where l_n is the length of the n th element and D_n is the distance of the n th element from the apex. The ratio of the lengths of successive dipoles is equal to the ratio of their distances from the apex and is known as the scaling factor s_f . The scaling factor is given by

$$s_f = \frac{l_n}{l_{n-1}} = \frac{D_n}{D_{n-1}} \quad (5.23)$$

where s_f is a constant of magnitude less than 1, l_n , l_{n-1} are the lengths of the n th and $(n-1)$ th elements (where l_n is larger than l_{n-1}) and D_n , D_{n-1} are the distances of the n th and $(n-1)$ th element from the apex.

A spacing parameter S_p can also be defined, which varies with the element and is given by

$$S_p = \frac{d_n}{2l_n} \quad (5.24)$$

where d_n is the distance between the n th and the $(n+1)$ th element, and l_n is the length of the n th element.

Since l_n is a half wave dipole, it is equal to $\lambda/2$ and thus the spacing parameter S_p is also equal to d_n/λ , that is, it is equal to the spacing in wavelengths at the frequency of the resonant dipole.

Using the relationships of (5.22) and (5.23), the spacing parameter can be rewritten as

$$S_p = \frac{(1 - s_f)}{4} \cot \alpha \quad (5.25)$$

The properties of the antenna at frequencies $f, rf, r^2f \dots r^mf$ are the same. When these frequencies are plotted on a logarithmic scale, these frequencies are equal spaced, and this is the reason for this type of antenna being called a log periodic antenna. If the frequencies are closely spaced, the antenna can provide uniform performance over a wide range of frequencies [8, Vol 2, p. 767]. The center-fed dipoles are connected to a twin transmission line, so that adjacent elements are fed in antiphase, as shown in Figure 5.11 This gives back-fire radiation (in the direction of elements of decreasing length). If the phase reversal is not included, then the radiation occurs in the end-fire direction such that the radiation from the shorter elements is obscured by the longer elements. Scalloped radiation patterns are also produced by end-fire arrays and impedance behavior is erratic [6, p. 14–27]. The array is fed at its high-frequency (shortest element) end and the transmission line is shorted through a stub at its low-frequency end. The upper frequency limit is determined by the length of the shortest dipole and occurs when this length is resonant at approximately half a wavelength. The lower frequency limit is determined by the length of the longest dipole. When the array is fed by a particular frequency, the wave will travel along the array from the shortest element until it encounters the resonant dipole element (i.e., the dipole whose length is approximately half a wavelength). This resonant element will have a lower impedance than any other element, and thus it will extract more energy than any other element. The energy extracted from the wave will progressively increase as the wave travels from the high-frequency end to the resonant element and the energy extracted will decrease beyond this element. The elements that extract energy form the active region, which is restricted to a few elements on either side of the resonant element. As the frequency is increased, the active region moves towards the shorter elements and as the frequency is decreased, it moves towards the longer elements. The width of the active region also reduces with increasing frequency, with the highest frequency having the smallest active region. At the low frequency end up to 50% of the length is used, but at the highest operating frequency only about 15% may be used [3, p. 705]. The effective electrical aperture (the aperture in terms of wavelengths) remains essentially independent of frequency. The antenna can be considered as a cascade of cells, with each cell consisting of a section of transmission line shunt loaded at its center by the dipole element impedance. This dipole impedance also includes the mutual coupling between the elements. This shunt loading results in attenuation in the feeder line [6, p. 14–27]. This attenuation increases as the scaling factor s_f is increased, as long as the spacing parameter S_p does not become too small. In order to ensure that radiation does not occur in the end-fire direction, this attenuation through the active region should be about 20 dB.

The value of the constant s_f varies between 0.76 and 0.98 for values of S_p between 0.06 and 0.2. However, as the value of S_p is reduced the VSWR tends to increase. Typically, VSWR values of around 1.4 are achievable. As s_f approaches its upper limit of 0.98, the elements are more closely spaced and hence the active region contains more elements. The inclusion of more elements in the active region increases the directivity and values of between 8 and 12 dBi are achievable. The apex angle 2α also affects the antenna directivity, and angles vary between 2 and 40 degrees. Small angles result in excessively long antennas, whereas large angles cause disruption of the phasing between elements and result in radiation pattern distortion [7, p. 18]. The antenna resistance has little effect on the directivity [8, p. 769]. For thinner elements the resistance changes more rapidly with frequency, and there is a reduction in the directivity. Thicker elements reduce the Q and hence increase the bandwidth. As the spacing parameter S_p is reduced, the VSWR tends to rise.

At frequencies in the very high-frequency (VHF) range (30–300 MHz), the antennas can be mounted high enough (in terms of wavelengths) to avoid ground effects. However, at frequencies in the high-frequency (HF) range (3–30 MHz), the proximity to the ground results in loss, which reduces gain, and the image of the antenna formed by reflection in the ground plane causes alteration of the radiation pattern. End-loading is also associated with these low frequencies, and makes the elements appear to be electrically longer; this results in the operating frequency being lowered. In the EMC field, log periodics are mainly used at frequencies between 100 and 1,100 MHz.

Half-power beamwidths (HPBW) in the E plane (that is, the plane x - y of the dipoles) are of the order of 50° . The H -plane (y - z plane perpendicular to the plane of the dipoles) HPBW is of the order of 90° . The radiation patterns of the log periodic in the x - y and y - z planes are shown in Figure 5.11(b, c), respectively. Typical feeding arrangements are shown in Figure 5.11(d, e). Phase reversal between adjacent elements is achieved by either connecting alternate monopoles to opposite sides of a transmission line, or by physically crossing the wires of a twin transmission line feed for dipoles supported on insulators [3, p. 708].

Smith [7, p. 18] has developed algorithms for selecting the optimum spacing parameter S_p and scaling factor s_f for LPDAs of specified gains. For a LPDA of linear gain g the spacing parameter is given by

$$S_p = -5.76909996 \times 10^{-4} \times 0.0167208176g + 0.0602945516 \quad (5.26)$$

For gains from 8 to 12 dBi, spacing parameters vary between 0.1428 and 0.1804, as shown in Figure 5.12.

The optimum scaling factor s_f can be calculated from the optimum spacing parameter and is given by

$$s_f = 3.9866009S_p + 0.236230336 \quad (5.27)$$

For the range of spacing parameters from 0.1428 to 0.1804, the scaling factors vary between 0.806 and 0.955 and are shown in Figure 5.12.

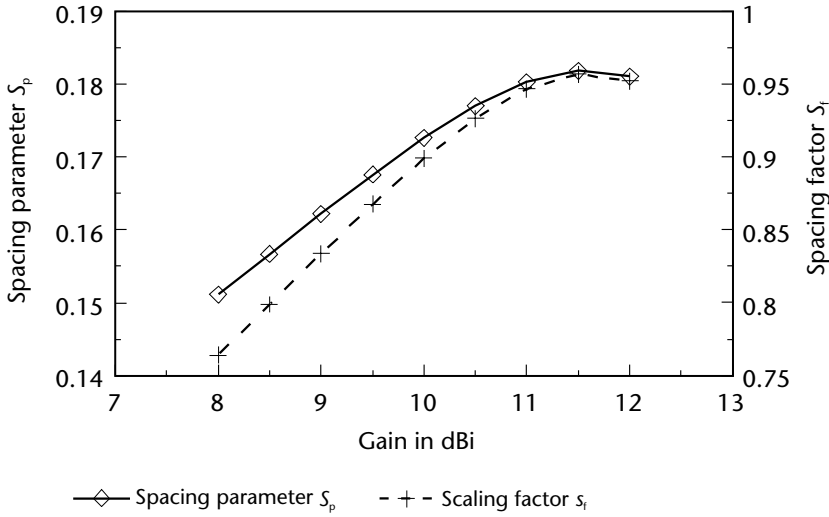


Figure 5.12 Variation of the spacing parameter and scaling factor with gain.

The impedance of the antenna Z can be matched to the transmission line by selecting the correct length-to-diameter ratio (l/d_0) of the element. The impedance Z is given by

$$Z_a = \frac{Z_0^2}{8Z_1} \sqrt{s_f + \left(\frac{8Z_1}{Z_0}\right)} \quad (5.28)$$

where Z_0 is the characteristic impedance of the transmission line and Z_1 is given by

$$Z_1 = 276 \log_{10} \left(\frac{l}{d_0} \right) - 270 \quad (5.29)$$

Using the range of S_p and s_f shown in Figure 5.12, the antenna can be matched to a $75\text{-}\Omega$ line by choosing values of length-to-diameter ratio (l/d_0) between 10.501 and 10.554.

The number of elements depends on the bandwidth and the scaling factor s_f . A design bandwidth (B_s) is calculated which is greater than the desired bandwidth B_w , which is the ratio of the highest to the lowest frequency. This larger design bandwidth is required to accommodate the active region for the high-frequency end. The design bandwidth [6, p. 29–15] is given by

$$B_s = B_w \left[1.1 + 7.7(1 - s_f)^2 \right] \cot \alpha \quad (5.30)$$

The number of elements is given by

$$N = \left[1 - \frac{\log_e B_w}{\log_e (1/S_f)} \right] \quad (5.31)$$

For an LPDA operating from 100 to 1100 MHz (i.e., $B_w = 11$), and an apex angle of 53 degrees (which gives an LPDA of length equal to its width), the design bandwidth is 29 and this gives the number of elements as 21. For an LPDA operating from 200 to 1,000 MHz (i.e., $B_w = 5$) and an apex angle of 53 degrees, the design bandwidth is 5 and this gives the number of elements as 16.

The trapezoidal tooth antenna with curved teeth, introduced by DuHammel in 1957, was the first successful log periodic. It consisted of a self-complementary structure, that is, if the two arrays shown in Figure 5.13(a) were to be folded along the center line of the metal sheet, they would form a single sector with the metal section being of double thickness. It had a bidirectional pattern, that is, it radiated in two directions, into and out of the paper. This was adapted by Isbell to a straight-toothed version, as shown Figure 5.13(b). The teeth act as monopoles. The distance from the back of each tooth to the apex is D_n and r_n is the distance from the front of the teeth. The ratio of r_n/D_n is a measure of the width of the teeth. The scaling factor s_f is defined as above, and the angle subtended by the extreme edges of the teeth (at the apex) is 2α . However, in this case there are two other angles to be considered. The angle 2β defines the angle of the supporting section, and the angle ψ is the angle between the two arrays. When ψ is equal to 180° , it behaves like the one used by DuHammel and gives a bidirectional pattern. If the input impedance is plotted on a Smith's chart over several periods, the points lie on a circle whose center is on the zero-impedance line [6, p. 14–25]. The characteristic impedance of the antenna is the geometric mean of the maximum and minimum values of the resistance (real

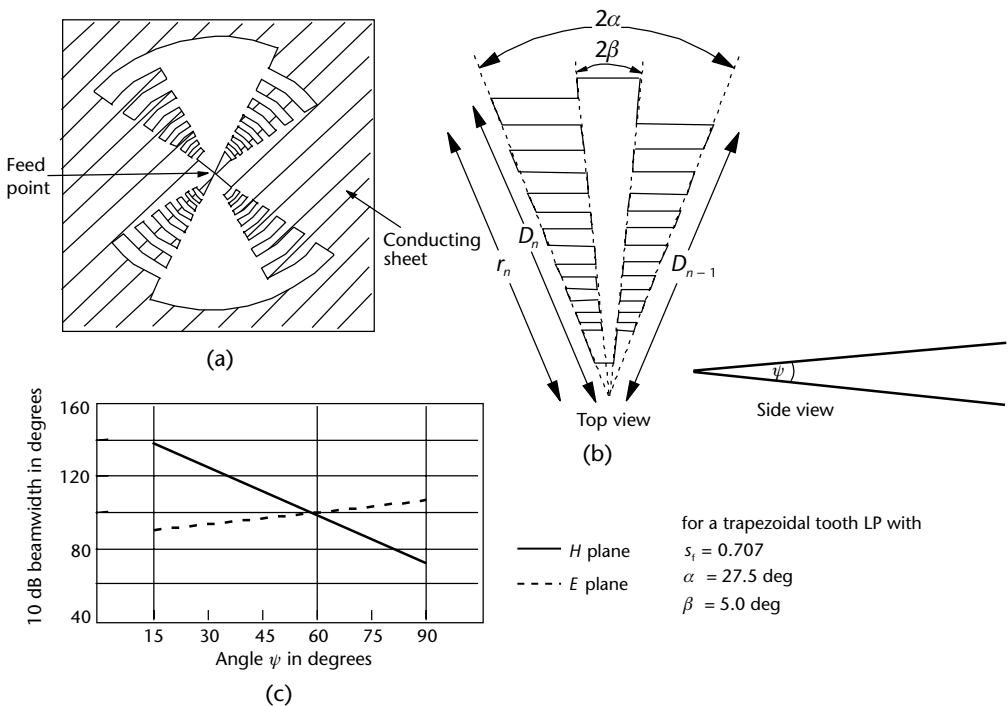


Figure 5.13 The trapezoidal tooth log periodic antenna: (a) DuHammel's trapezoidal tooth LP, (b) straight-toothed trapezoidal tooth LP, (c) beamwidths of the straight-toothed trapezoidal tooth LP.

part of the impedance). The two arrays can be considered as a uniform biconical TEM transmission line. Since the monopoles are attached to the opposite sides of the center supporting strip, the required 180° phase delay is achieved.

This antenna radiates a unidirectional linearly-polarized beam [8, Vol.1, p. 376] with the electric field parallel to the edges of the teeth, as shown in Figure 5.13(b). The variation of the -10 dB beamwidth in the E and H planes with the angle ψ (between the arrays) is shown in Figure 5.13(c) for a scaling factor of 0.707, $\alpha = 22.5^\circ$ and $\beta = 5^\circ$. It can be seen that around $\psi = 60^\circ$ the E and H plane beamwidths are equal. This feature is particularly useful when the log periodic is used as a feed for a reflector that requires circular symmetry.

5.11 BiLog[®]

The BiLog antenna [10] is a hybrid antenna comprised of an LPDA in front of a bowtie antenna. The advantage of using this antenna is that it can be used over a wider range of frequencies, thus obviating the need to use two antennas. Apart from the time saving, the testing results in increased accuracy, since the repositioning of antennas is not required. The BiLog can be used over the frequency range of 30 MHz to 1 GHz. At 30 MHz, the wavelength is 10m, and if an LPDA is used, the longest element would be about 5m.

At the higher frequencies, the antenna acts as a LPDA and does not require a balun when fed by a two-wire transmission line. At the lower frequencies, the antenna acts as a broadband balanced dipole and a balun is required.

The radiation patterns for horizontal polarization of the BiLog at 30 and 150 MHz demonstrate the familiar figure of eight dipole patterns, as shown in Figure 5.14(a). As the frequency is increased, the pattern tends towards the unidirectional pattern of the LPDA, as shown in Figure 5.14(b).

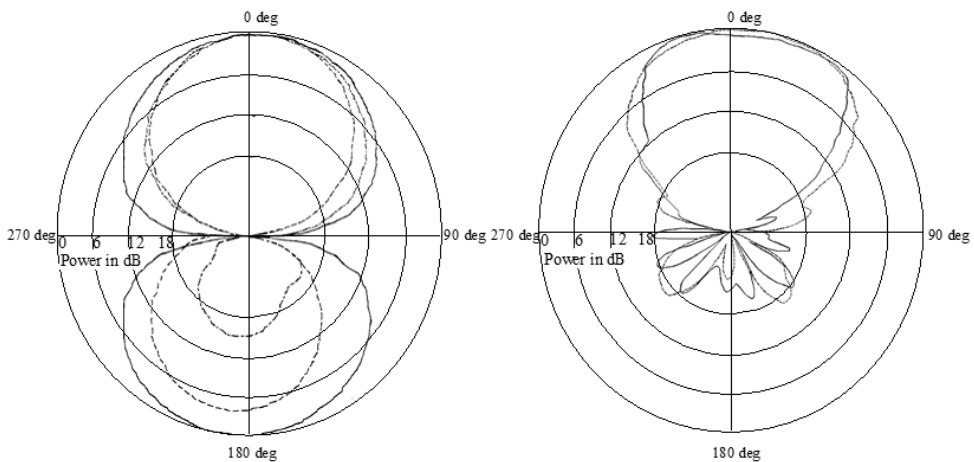


Figure 5.14 Radiation patterns of the BiLog antenna for horizontal polarization. At (a) 30, 150, and 300 MHz, and (b) 650 and 1,000 MHz. (After [10].)

For immunity and susceptibility testing, the input power in watts required to give electric field strengths of 1, 3, and 10 V/m at a distance of 3m from the antenna is shown in Figure 5.15. It can be seen that at the lower end of the frequency range, the input power required is higher, but above 250 MHz the power is almost constant.

The antenna correction factor (ACF) of the BiLog is shown in Figure 5.16 and is compared to those for the LPDA and the biconical antenna. The magnitudes of the antenna factors are similar to the LPDA above 300 MHz, and between 100 and 300 MHz it appears to be better than the biconical antenna.

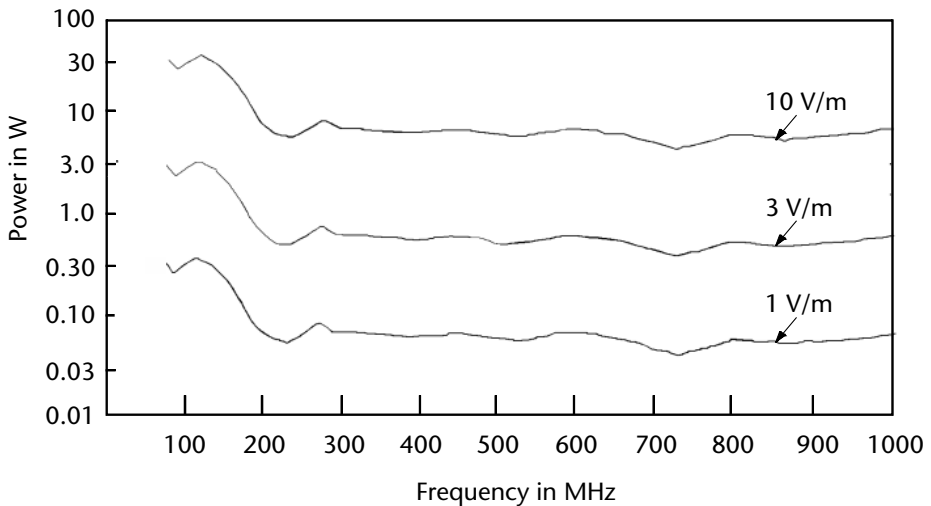


Figure 5.15 Power required for BiLog antenna to produce a given electric field at 3m. (After [10].)

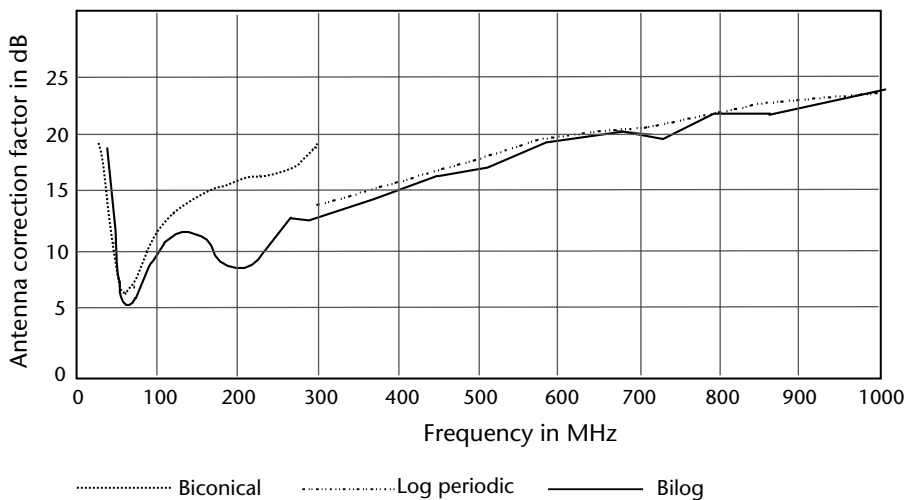


Figure 5.16 Antenna correction factors for the biconical, log periodic, and BiLog antennas. (After [10].)

5.12 Helical Antennas

The helix antenna, as shown in Figure 5.17(a), has a diameter D , and the circumference of the helix is $C = \pi D$. The spacing between turns is S and the length of each turn is L . The pitch angle ψ is related to the spacing and diameter, as shown in Figure 5.17(b), and is given by

$$\tan \psi = \frac{S}{\pi D} \quad (5.32)$$

where

- ψ is the pitch angle in degrees,
- S is the spacing in meters, and
- D is the diameter of the helix in meters.

A helical antenna could consist of a single conductor or multiple conductors. It can radiate in several modes depending on the electrical diameter (the diameter in terms of wavelength). The most common mode is the axial mode of radiation, when the boresight is along the axis, as shown in Figure 5.17(c), and the minor lobes are relatively small. This mode occurs when the circumference C (of one turn) is of the order of one wavelength. When the diameter is much smaller than a wavelength, the helix antenna acts like a dipole and has an omnidirectional radiation pattern perpendicular to its axis, as shown in Figure 5.17(e). This is known as the normal mode. Higher order modes occur when the helix diameter is greater than $\lambda/8$. The single lobe of the axial mode splits up into two lobes known as the conical mode of radiation, as shown in Figure 5.17(d).

The axial-mode helix has wideband impedance characteristics and the radiated electric field is circularly polarized [6, Chapter 13]. Helices wound like a left-hand screw receive left-hand circularly polarized (LHCP) waves, whereas those wound like a right-hand screw receive right-hand circularly polarized (RHCP) waves. Most axial-mode helices are of uniform diameter, but helices of nonuniform diameter are used to give wider bandwidth and improved radiation characteristics. The axial-mode helix can have a 1.7:1 bandwidth and its directivity is close to the maximum attainable of an antenna of that size, over the whole of the bandwidth. This is because the phase velocity is automatically adjusted to the correct value to produce the maximum directivity for each frequency [11, p. 7–1].

The helix usually has a ground plane or is cavity-backed. Cavity-backed helices are preferred, since they reduce back radiation and the forward gain is enhanced, resulting in an improved front-to-back (F/B) ratio. In a typical arrangement for a uniform helix, as shown in Figure 5.18(a), the coaxial feed is connected to the helix via a microstripline-matching transformer. For the frequency range of 650 to 1,100 MHz, the transformer is about 12 cm long, and the cavity has a diameter of 26 cm and a depth of 12.5 cm. The conductor from which the helix is wound could be tubing of a circular cross section or a flat strip, and a lightweight cylindrical foam dielectric is used as the former.

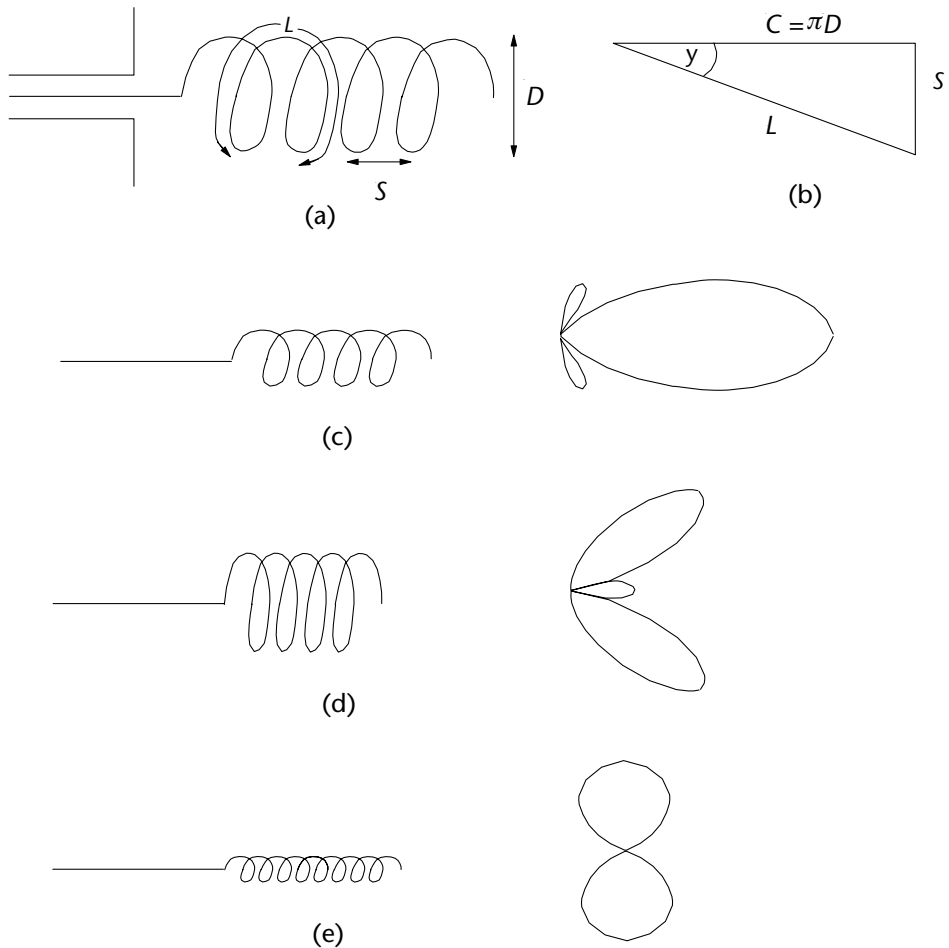


Figure 5.17 The helical antenna: (a) Characteristics of the helical antenna (b) relationship between diameter and length of one turn, (c) axial mode pattern for circumferences of around one wavelength, (d) conical mode pattern for circumferences greater than one wavelength, (e) normal mode pattern for circumferences much less than one wavelength.

The VSWR measured at the input of the matching transformer can be significantly reduced by adding two additional tapered turns at the free end of the helix. These tapered turns reduce the VSWR by suppressing the reflected currents. The cut-off frequency occurs when the circumference of the helix is 0.75λ . The HPBW for pitch angles between 12 degrees and 15 degrees, and helices of circumference C of values $0.67\lambda < C < 1.3\lambda$, can be given by

$$\theta = \frac{52}{\frac{C}{\lambda} \sqrt{\frac{NS}{\lambda}}} \quad (5.33)$$

where

θ is the HPBW in degrees,

C is the circumference of the helix in meters,

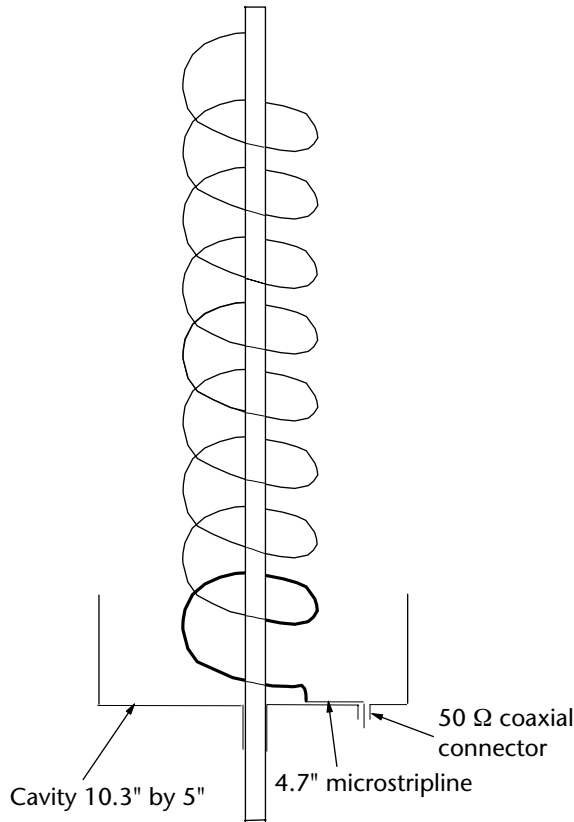


Figure 5.18 Mechanical arrangement of a cavity-backed helix for the frequency range of 650 to 1,100 MHz.

S is the spacing between adjacent turns in meters, and
 N is the number of turns.

The HPBW given by (5.33) is an empirical approximation derived from measured data and applies to helices of at least 3 turns, and to beamwidths between 30 degrees and 60 degrees. The optimum dimensions for a wideband helix in the frequency range 200 to 500 MHz has a pitch angle of 14 degrees, a conductor diameter of 0.017λ , and axial length of 1.65 wavelengths at the center frequency [11, p. 7–3]. These dimensions give a value of approximately 6 turns for the helix. The ground plane diameter must be greater than 0.8λ and the distance between the ground plane and the first turn is half the spacing S , that is, 0.12λ .

When the circumference is of the order of a wavelength ($0.67\lambda < C < 1.3\lambda$), the terminal impedance of the helix is nearly resistive [11, p. 7–6] and the resistance R_b (within 20%) is given by the following empirical relation

$$R_b = \frac{140C}{\lambda} \quad (5.34)$$

where C is the circumference of the helix. This terminal impedance of the helix varies with frequency, but the variation will be less pronounced for helices with a larger number of turns than it is for helices with fewer turns.

The radiation pattern can be obtained to a first approximation, by considering the helix to be an array of N isotropic elements spaced a distance apart. The pattern of the array is the product of the pattern of each isotropic element and the array pattern. The isotropic element has a pattern of approximately $\cos \theta$, and the array has a radiation pattern which is the same as that of a uniformly-illuminated aperture, and thus the resultant electric field radiation pattern is given by

$$E = A \frac{\sin(N\psi/2)}{\sin(\psi/2)} \cos \theta \quad (5.35)$$

where E is the electric field in volts per meter, N is the number of turns, $\psi = kS \cos \theta - \delta$, $k = \pi/\lambda$, δ is the progressive phase between turns and equals kLc/v , L the length of one turn, v is the phase velocity along the helical conductor, c is the velocity of light, and A is the normalization factor equal to $\sin(\pi/2N)$.

When we increase the number of turns we get a narrower beam, which is expected since this is tantamount to increasing the number of elements in an array or increasing the aperture of an antenna.

Helical antennas can also be wound with more than one winding, such as bifilar, quadrifilar, and multifilar helices. The bifilar winding results in backfire radiation and does not generally require a ground plane.

5.13 Large and Resonant Loops

When the circumference of a loop is greater than 0.1λ , the current distribution is significantly different from the uniform distribution assumed in the case of a small loop (see Chapter 4). Assuming uniform current distribution gives predicted radiation resistances that are much less than the measured values, and as the size of the loop increases the calculated radiation resistance (using uniform current distribution) departs even further from the measured values. For instance, if we assume uniform current distribution for a loop of circumference 0.1λ , the calculated radiation resistance is 86% of the actual value, whereas if we have a loop of circumference 0.3λ , the calculated radiation resistance is 26% of the actual value [6, p. 5–9], as shown in Figure 5.19(b). The loop is usually fed by a twin-wire transmission line. The resistance and reactance of the circular loop has been calculated as a function of the electrical circumference (the circumference in terms of wavelength) and are shown in Figure 5.19(b). When the circumference is approximately a whole number of wavelengths, the resistance has minimum values, and these points are known as resonance points, at which the loop radiates the maximum power; whereas when the circumference is an odd number of half wavelengths ($0.5\lambda, 1.5\lambda, 2.5\lambda \dots (2n - 1)\lambda/2$), the resistance has maximum values, and these points are known as anti-resonance points. The actual values of the resistance at these resonance and anti-resonance points are determined by the thickness parameter T_p of the wire forming

the loop. The thickness parameter T_p is a function of the relative radii of the wire and the loop, and is given by

$$T_p = 2 \log_e \left(\frac{2\pi b}{a} \right) \tag{5.36}$$

where b is the radius of the loop and a is the radius of the wire forming the loop.

The resistance is relatively independent of the thickness parameter at the resonance points, but at antiresonance points it can be seen that the greater the thickness parameter, the higher the resistance is. This is to be expected, since for a fixed-loop

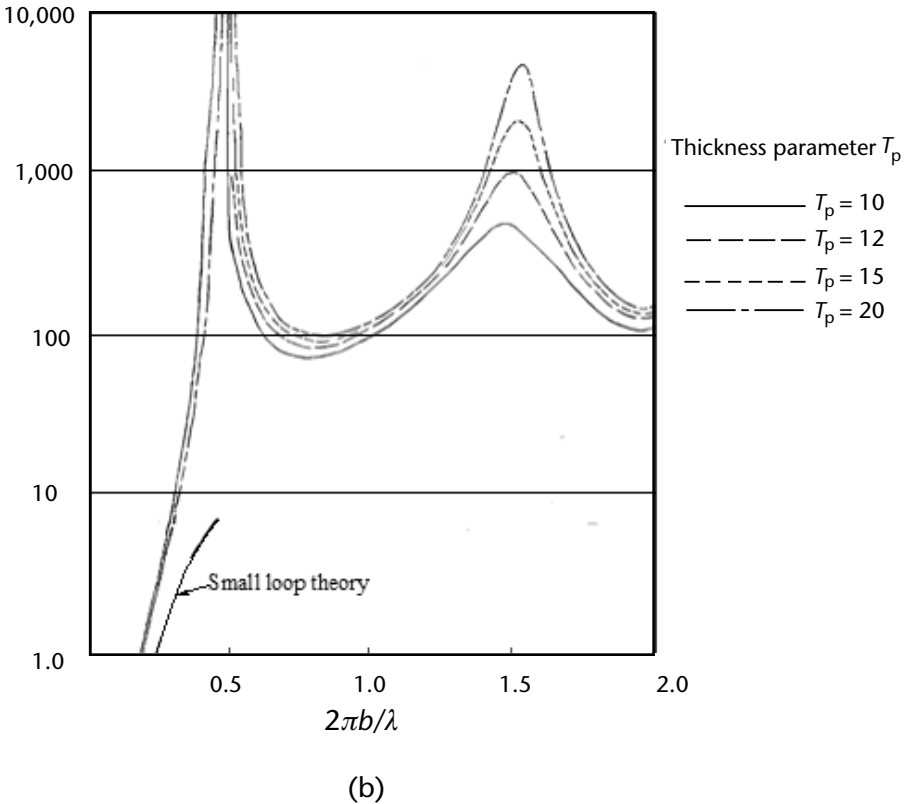
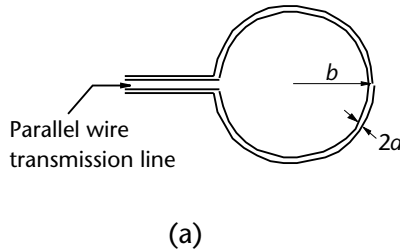


Figure 5.19 Characteristics of the single-turn loop antenna: (a) Physical characteristics of a single-turn loop, and (b) variation of input resistance with electrical circumference.

radius, the larger the thickness parameter, the smaller the radius of the conductor wire is, and hence the increase in resistance. A single-turn loop can be optimized so that it can have a high gain over a frequency range where its length varies between 1λ and 1.7λ . For instance, a loop of diameter 20.3 cm has a directivity of more than 3.5 dB over the frequency range 470 to 806 MHz where the loop circumference varies between 1λ and 1.7λ [6, p. 29–13].

5.14 Double-Ridged Horn

Double-ridged horns are used at frequencies above 100 MHz. The ETS-Lindgren (formerly EMCO) 3106 double-ridged waveguide horn is often used in EMC labs and covers a frequency range of 200 MHz to 1 GHz. However, double-ridged waveguide horns are more commonly used at frequencies above 1 GHz and are described in Chapter 6.

References

- [1] Ramo, S., J. R. Whinnery, and T. Van Duzer, *Fields and Waves in Communication Electronics Second Edition*, John Wiley & Sons, 1984.
- [2] Weiner, M. M., “Monopole Element at the Center of a Circular Ground Plane Whose Radius Is Small or Comparable to a Wavelength,” *IEEE Trans. Antennas and Propagation*, Vol. 35, No. 5, May 1987, pp. 488–495.
- [3] Kraus, J. D., *Antennas*, McGraw-Hill Book Company, 1988.
- [4] Nail, J. J., “Designing Discone Antennas,” *Electronics*, August 1953, pp. 167–169.
- [5] Ramo, S., and J. R. Whinnery, *Fields and Waves in Modern Radio Second Edition*, John Wiley & Sons, 1953.
- [6] Johnson, R. C., and H. Jasik, *Antenna Engineering Handbook*, McGraw-Hill Book Company, 1984.
- [7] Li, S. T., J. W. Rockway, J. C. Logan, and D. W. S. Tam, *Microcomputer Tools for Communications Engineering*, Norwood, MA: Artech House, 1968.
- [8] Rudge, A. W., K. Milne, A. D. Olver, and P. Knight, *Handbook of Antenna Design*, Vols. 1 and 2, Peter Peregrinus Ltd., 1982.
- [9] Green, H. E., *Antenna Designer’s Notebook*, IEEE Antennas and Propagation Society Newsletter, June 1985, pp. 11–13.
- [10] Marvin, A., S. J. Porter, and D. Riley, “30 MHz to 1 GHz in one sweep—the Bilog,” *EMC Test and Design*, No. 4, 1993, p. 28.
- [11] Jasik, H., *Antenna Engineering Handbook*, McGraw-Hill Book Company, 1961.

Selected Bibliography

- Aerospace Recommended Practice ARP 958, “Broadband Electromagnetic Interference Antennas Standard Calibration Requirements and Methods,” Society of Automotive Engineers Inc., 3-1-68.
- Balanis, C. A., *Antenna Theory—Analysis and Design*, Harper and Row, 1982.
- Connor, F. R., *Introductory Topics in Electronics and Telecommunications—Antennas, Second Edition*, Edward Arnold, 1992.

- Fewkes, J. H., and J. Yarwood, *Electricity, Magnetism, and Atomic Physics, Volume 1, Second Edition*, University Tutorial Press Ltd., 1962.
- Jay, F. (ed.), *IEEE Standard Dictionary of Electrical and Electronics Terms, Fourth Edition*, 1988.
- Jordan, E. C., *Electromagnetic Waves and Radiating Systems*, Constable and Co. Ltd., 1953.
- Lucas, J. G., "Antenna Systems," *Student Quarterly Journal*, June 1967, pp. 186–195.
- Mayes, P. E., "Frequency-Independent Antennas: Birth and Growth of an Idea," *IEEE Antennas and Propagation Newsletter*, August 1982, pp. 5–8.
- MIL-STD 461A "Electromagnetic Emission Interference Characteristics Requirements for Equipment," Washington DC. U.S. Government Printing Office, August 1968.
- Rappaport, E., "Antenna Designer's Notebook" *IEEE Antennas and Propagation Newsletter*, February 1988, pp. 12–14.
- Shepherd, D., "A Five-Decade System for Testing RFI Susceptibility" *RF Design*, September 1988, pp. 20–23.

Antennas for Frequencies Above 1 GHz

Above 1 GHz, wire antennas of resonant length are too small to be practicable. Frequency-independent antennas such as the log conical and planar spirals are popular, and aperture antennas such as the double-ridged horns are used. Smooth-walled horns are used where a wide frequency range is not required, and also for calibration purposes.

6.1 Frequency-Independent Antennas

In 1954, Rumsey suggested that if an antenna could be defined in terms of angles instead of any characteristic length dimensions, then it would be possible for such an antenna to have properties which are independent of the frequency of operation. However, such a structure would be infinite in length, and when truncated would not necessarily retain its frequency-independent characteristics because of the reflected fields from the truncation point.

The logarithmic spiral antenna is a true frequency-independent antenna [1, p. 698]. The first practical FI was constructed in 1958 by John D. Dyson at the University of Illinois [1, p. 697]. It was a bidirectional planar spiral. The unidirectional planar spiral was achieved by placing a cavity behind the spiral. The cavity forms an image of the spiral which retransmits through the original spiral, and thus modifies the radiation pattern. Radar-absorbing material (RAM) is placed in the cavity to prevent this reradiation, but this absorbs about 50% of the power input to the antenna.

6.2 Band Theory

The band theory is used to explain the radiation from log spiral antennas, as well as Archimedean spiral antennas. Although there is no mathematical basis for this theory, it is in good agreement with experimental results, and is easily understood and compatible with intuitive reasoning [2].

The spiral antenna behaves like a two-wire transmission line that is gradually transformed into a radiating structure. Allowable radiation bands exist for all circles that have a circumference equal to an integral number of wavelengths. For a more

detailed explanation of the modes of radiation of a spiral, see Section 6.3.1. In the case of the fundamental mode, or mode 1, which has a main lobe along the axis, the radiation can be explained in a way detailed next.

Consider a two-arm spiral, as shown in Figure 6.1(a), fed by currents that are in antiphase (i.e., 180° out of phase), but of equal amplitude. Consider two diametrically opposite points, A and A', on the same arm of the spiral. If the current at A is in an upward direction, the direction of the current at A' will depend on the phase delay caused by the length of the arc AA'. When the arc length is $\lambda/2$, the phase delay is 180° , so that instead of the current at A' being in the opposite direction to the current at A, (as would be the case for DC), it is in the same direction, because of this additional 180° phase delay. A similar situation occurs for the currents at B and B' for the other arm of the antenna. Thus, all the currents are in the same direction at points A, A', B, and B'. These points can all be considered to be at an average diameter of λ/π . The points C, C', D, and D' will similarly have currents in phase with each other but at right angles to the currents at A, A', B, and B'. Since these currents are in time as well as spatial quadrature, the antenna radiates circularly polarized waves. This band of the spiral that has a mean diameter of λ/π is called the first radiation band. This gives the fundamental mode, or mode 1, of radiation.

At other frequencies where the circumference of the spiral is not equal to a wavelength (i.e., the diameter = λ/π), the phase relationship between the currents in adjacent conductors becomes random, so that the net radiated energy is very small.

For mode 2, four arms are required, and the phase between the feed currents to opposite arms is zero or a multiple of 360° . As shown in Figure 6.1(b), the distance along the arc between points F and F' that have in-phase currents will be λ , and thus the radiation band will have a circumference of 2λ , or a diameter of $2\lambda/\pi$. The direction of the current vectors at F and F' are in opposite directions, so that the radiation on axis will be zero, and split beams are obtained on either side of the boresight for this mode (see Figure 6.4).

Band theory can also be used to explain the deterioration in the axial ratio with decreasing spiral diameter for spirals that have their outer periphery left open-circuited or short-circuited. This occurs because the energy traveling outwards towards the periphery is reflected back with an opposite sense. This reflected energy is at a lower level than the energy from the feed point, and thus the result is elliptical polarization. This can be seen in Figure 6.2, where the incident electric field E_i from the feed traveling towards the periphery is RHCP, and the reflected electric field E_r is LHCP. Assuming that the two fields E_i and E_r are in phase at time $t = 0$, we can see that if $E_i > E_r$, the resultant electric field is right-hand elliptically polarized. The ellipticity (the ratio of the minor to major axis) of the resultant electric field depends on the relative magnitudes of E_i and E_r . As E_r becomes of similar magnitude to E_i , the resultant field tends to linear polarization. This occurs when the spiral diameter is very small ($< \lambda/\pi$) and the reflected energy (from the edges) is of a similar magnitude to the initial energy from the feed [2]. Similarly, when the spiral diameter is very large, $E_i \gg E_r$, and the resultant electric field would be nearly circularly polarized, and of the same sense as the incident electric field radiating from the center of the spiral towards the edges.

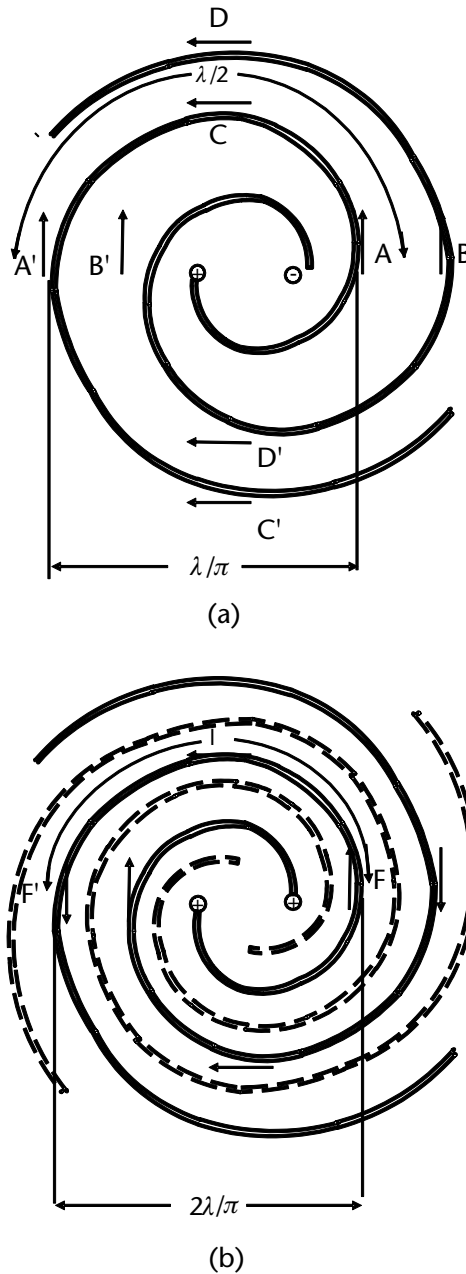


Figure 6.1 Band theory for spiral antennas. (a) Mode 1 radiation with two arms, and (b) mode 2 radiation with four arms.

6.3 Log Spiral

The logarithmic spiral is really an equiangular spiral, but is commonly called a log spiral. The two main types of log spiral are those on flat surfaces and those conformed onto cones (conical log spirals). The planar log spirals may be circular or square; but the circular ones are more commonly used. In order to have radiation of an electric field, we must have a change in the current with time. This can be

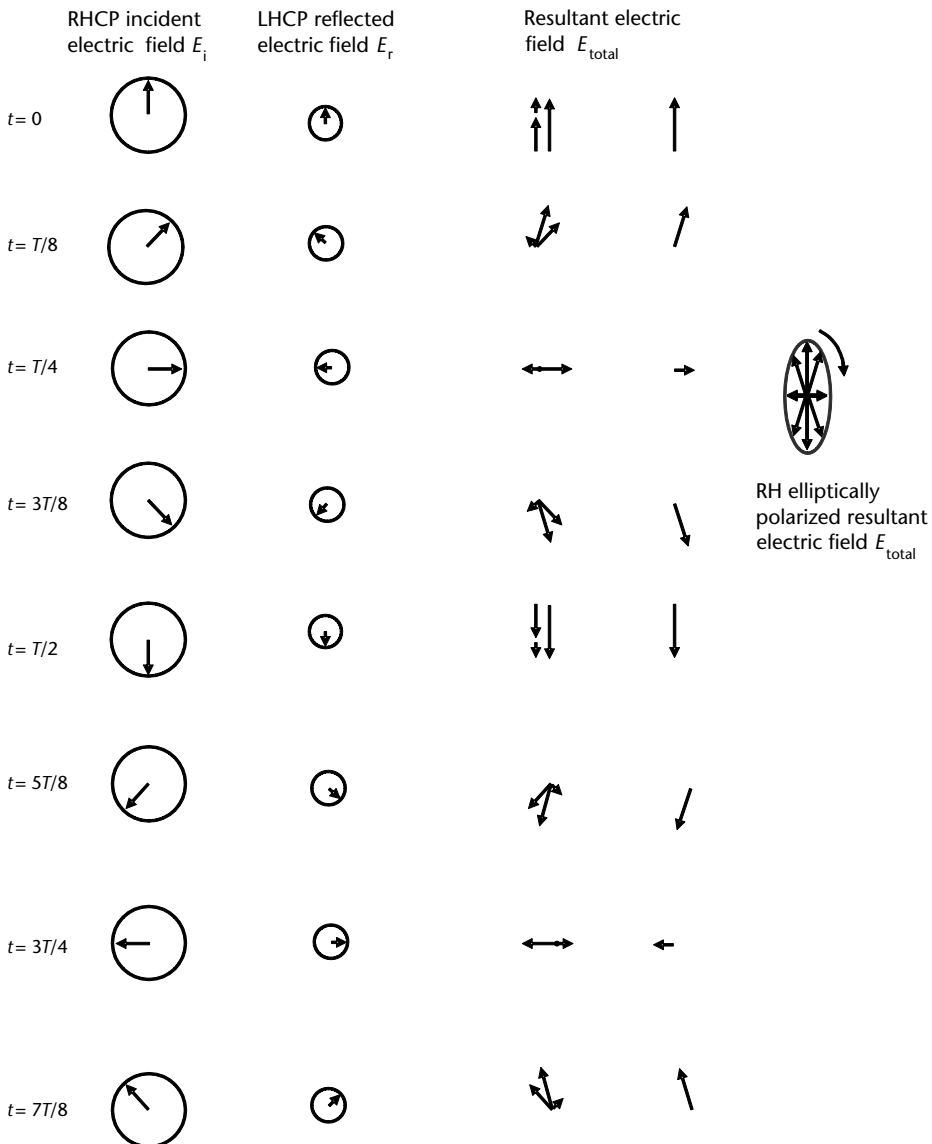


Figure 6.2 The resultant electric field from spiral antennas.

achieved by moving a current element or by changing the rate of current flow with time. Since current is the rate of change of charge with time, the rate of change of current is the same as the acceleration (or deceleration) of a charge. In the spiral antenna, the acceleration of a charge is achieved by the change of direction rather than the change of magnitude of the current. When the conductor (in which the charge is traveling) is bent into an arc normal to the direction in which the charge is traveling, the velocity vector \mathbf{v} of the charge is changed to \mathbf{v}' , as shown in Figure 6.3(a). Using the triangle of forces, as shown in Figure 6.3(b), we can see that $\mathbf{v}' - \mathbf{v}$ is $\delta\mathbf{v}$. The rate of change of $\delta\mathbf{v}$ with time gives us acceleration. The current is also attenuated in the case of a finite structure, as much as 20 dB in the first wavelength

for planar log spirals [3, p. 185] so that the current is negligibly small at the point of truncation. The decay is an approximately constant function of the electrical arm length (i.e., the arm in terms of wavelengths). This has the effect of constantly shortening the active arm length as the frequency is increased. However, since the electrical arm length remains relatively constant, the HPBW is also constant. Even the truncated spiral with just one or two arms can provide FI operation over a wide bandwidth.

The decrease of currents is less rapid for narrow arms or narrow slot structures [4, p. 14–9]. The equations that determine the inner and outer edges of a planar log spiral are given in polar coordinate form by the radius vectors r_1 and r_2 from the center. Both edges of the spiral have the same value of k and a , but one of them is rotated through an angle of δ with respect to the other. Thus, the angle δ defines the angular width of the arms.

$$r_1 = ke^{a(\alpha-\delta)} \quad (6.1)$$

$$r_2 = ke^{a\alpha} \quad (6.2)$$

where r_1 and r_2 are the radial distances to the point P_1 and P_2 on the inner and outer edges of the spiral, as shown in Figure 6.3(a), $\alpha - \delta$ is the angle with respect to the x -axis for the inner spiral, α is the angle with respect to the x -axis for the outer

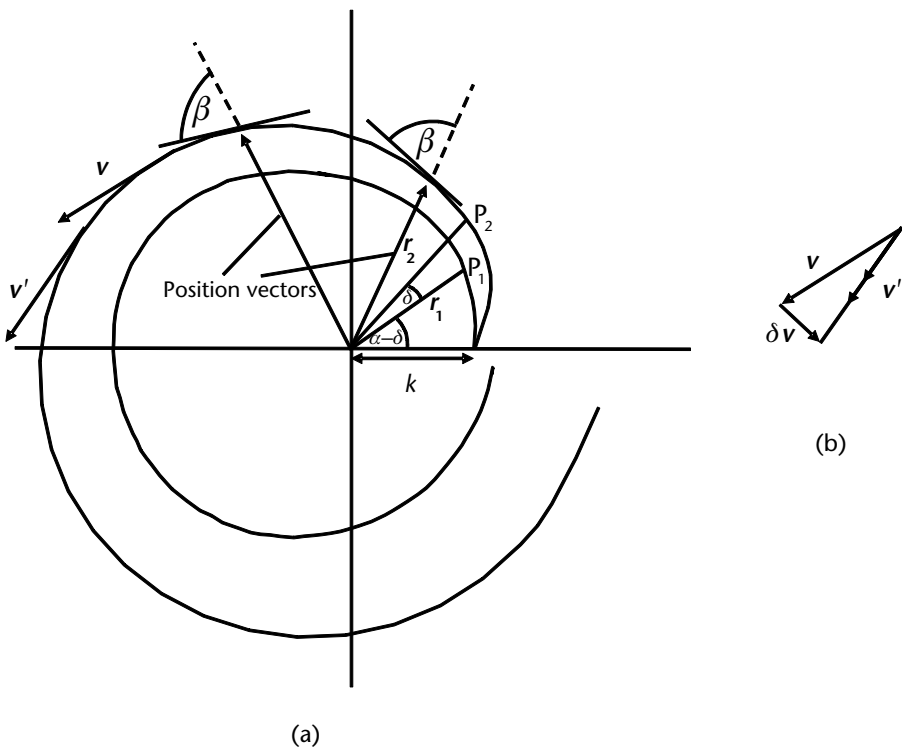


Figure 6.3 The equiangular or log spiral antenna: (a) Velocity vectors for a charge moving in an arc; (b) addition of velocities using the triangle of vectors.

spiral, k is a constant that determines the start of the spiral, and a is a constant known as the expansion coefficient.

Both k and a are positive constants, and a determines the rate of spiral, and usually takes values between 0.2 and 1.2 [3, p. 182]. Dividing (6.1) by (6.2), we get the ratio of r_1 to r_2 , which is given by

$$K_2 = \frac{r_1}{r_2} = e^{-\alpha\delta} \quad (6.3)$$

where K_2 is the ratio of r_1 to r_2

When the angle δ is zero, the inner and outer edges are coincident, and when $\delta = \pi$, the outer edge of the first turn would touch the inner edge of the second turn of the spiral, so that the spiral would become a disk. Thus, in order to maintain a separation between the arms, the angle δ must lie between 0 and π ; which means that K_2 must lie between 1 and $e^{-\pi a}$. When $\delta = \pi/2$, or 90° , we have a self-complementary antenna. A self-complementary antenna has the metal area congruent to the nonmetallic area, so that when the two are superimposed a solid metallic sheet would be obtained. Alternatively, a rotation of the metallic area causes it to be superimposed on the nonmetallic area. The width of the conductors is equal to the space between the conductors.

Taking natural logs, that is, logs to the base e for the general case of r , (6.2) can be rewritten as

$$\log_e r = \log_e k + a\alpha \log_e e \quad (6.4)$$

Since $\log_e e = 1$, (6.4) reduces to $\log_e r = \log_e k + a\alpha$. The rate of change of the radius with angle α is found by differentiating with respect to r , and is given by

$$\frac{dr}{d\alpha} \frac{1}{r} = a \quad (6.5)$$

This gives the rate of change of the radius vector r with angle α as

$$\frac{dr}{d\alpha} = ra \quad (6.6)$$

Thus, the rate of change of r is proportional to the expansion coefficient a . The expansion coefficient a defines the tightness of the spiral. If a is large, then r increases rapidly with angle α and we have a loosely wound spiral; whereas when a is small, r increases slowly and we have a tightly wound spiral.

The angle β , which the spiral (or, strictly speaking, the tangent to the spiral) makes with the position vector at a point on the spiral, is constant and this gives the equiangular spiral its name. The angle β is sometimes called the wrap or winding angle of the arms, and is given by

$$\tan \beta = \frac{1}{a} \quad (6.7)$$

$$\beta = \tan^{-1}\left(\frac{1}{a}\right) \quad (6.8)$$

For loosely wound spirals a is large and angle β is small, and for tightly wound spirals a is small and angle β is large.

An equiangular or log spiral can also be recognized by the fact that the width of the spiral, as well as the distance between the turns, increases as the radial distance from the center increases.

The spirals can have two or more arms. A rotation of $360/N$ (where N is the number of arms) leaves the structure unchanged. Thus if the spiral has 2 arms, a rotation of 180° will superimpose the spiral onto itself where N is the number of arms, whereas if the spiral has 4 arms a rotation of 90° achieves the same result [4].

6.3.1 Modes of Radiation

There are a number of independent modes of radiation available which depend on the number of arms. For N arms there are $(N - 1)$ modes available. The first, or fundamental, mode (which is also known as the sum pattern mode) has a single main lobe coincident with the boresight or main (z -) axis of the spiral. All the other modes have a null on the main axis and two lobes either side of the axis, with the angle of the lobe increasing in proportion to the mode number, as shown in Figure 6.4. These higher-order modes are known as difference pattern modes.

For dual polarization, more than two arms are required. Most of the radiation takes place in the first active region. For good spiral design, this active region has a circumference of approximately M wavelengths, where M is the mode number. Thus, mode 1 has an active region confined to a radius of $\lambda/2\pi$ or 0.16λ , or a diameter d_1 of 0.32λ , as described in Section 6.2. For loosely wound spirals, the attenuation in the first active region may not be large enough, and the waves travel to the second active region.

In addition to these higher-order positive modes, there are negative modes associated with cavity-backed spirals. These are due to the energy being reflected from

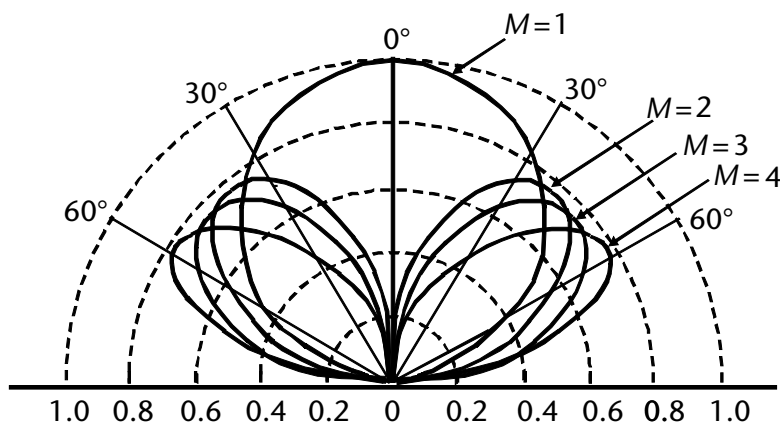


Figure 6.4 The radiation patterns for the different modes of the planar log spiral antenna.

the periphery of the spiral. In general, only the first order negative mode ($M - 1$) is of significance.

In order to obtain radiation on boresight, the opposite arms of the spiral have to be in antiphase; that is, 180° out of phase. The difference pattern modes occur when the opposite arms are fed in-phase.

The phase ϕ_p associated with a particular arm of the spiral [4, p. 14–4] is given by

$$\phi_p = \frac{2\pi Mn}{N} \quad (6.9)$$

where

ϕ_p is the phase in radians;

M is the mode number;

n is the arm number;

N is the total number of arms.

Thus, for mode 1 propagation, the total number of arms is 2, and it can be seen that arm 1 has a phase of π and arm 2 has a phase of 2π . For mode 2, the total number of arms is 4, and the phases obtained for arms 1, 2, 3, and 4 using (6.9), are π , 2π , 3π , and 4π , respectively. Thus, it can be seen that the phase of opposite arms (e.g., 1 and 3) differ by 2π , that is, they are in phase.

6.3.2 Rotation of Radiation Pattern with Frequency

The radiation pattern of the spiral is rotated as the frequency is changed. When the frequency is changed from a frequency of, say, f to f/k_3 (where k_3 is a constant), the pattern is rotated through an angle of $\log_e k_3/a$. This rotation is not observable for tightly wound spirals (large angle β), since the radiation pattern has circular symmetry. However, for loosely wound spirals (small angle β), the beam is elliptical and the rotation of the beam can be observed [5]. Tightly wound spirals and those with wider arms tend to have smoother and more uniform radiation patterns, which exhibit smaller variations in HPBW.

Although the width of a log spiral should increase with its distance from the feed point, in practice, if a metallic strip of constant width (or a wire of constant diameter) is used for each arm, a moderately wide bandwidth of between 5:1 and 10:1 can be obtained for bidirectional spirals [4, p. 14–9].

6.3.3 Planar Log Spiral

The first planar log spiral was constructed by J. D. Dyson in 1958. It was a bidirectional antenna. The planar log spiral can be implemented by either cutting a metal spiral (usually on a dielectric substrate) or by cutting a spiral slot in a metallic ground plate, as shown in Figures 6.5 and 6.6.

The spiral is shown with less than two turns for clarity. The planar log spiral exhibits a decrease of current with distance that is faster than $1/r$ and thus the

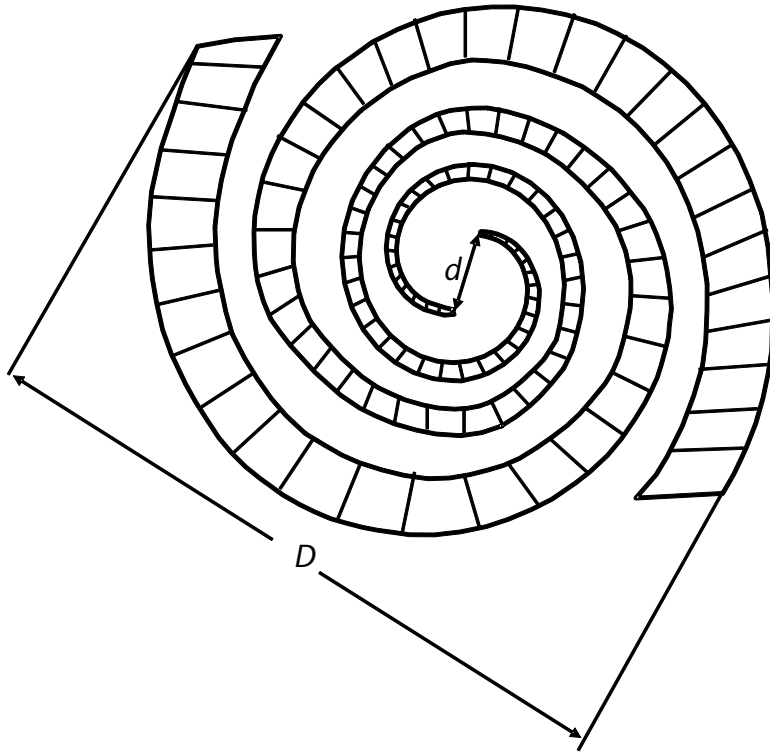


Figure 6.5 The metallic planar log spiral.

end effect becomes negligible at a distance that depends on the exact shape of the structure [4, p. 14–3].

6.3.4 Slot Planar Log Spiral

The planar spiral in slot form, as shown in Figure 6.6(a), is implemented by removing the metallic spiral from an infinite ground plane. This is based on Babinet's principle, which states that a radiating flat strip element can be replaced by the equivalent shape slot in an infinite metallic sheet, since they both have the same radiation characteristics. The slot spiral of Figure 6.6 is shown with less than two turns for clarity.

6.3.4.1 Input Impedance

The log spiral antenna has a theoretical impedance at all frequencies, equal to the intrinsic impedance ξ_0 of free space (120π or 377Ω) divided by the number of arms, [6, p. 520]. This applies to self-complementary spirals with opposite arms interconnected. Thus, for the two-armed spiral antenna the theoretical input impedance is $120\pi/2$ (i.e., 188Ω). However, the measured input impedance is typically between 50 and 100Ω [1, p. 700]. The experimental values are lower because the presence of the cable feeding the structure. Narrow arm structures have higher impedances [4, p. 14–9].

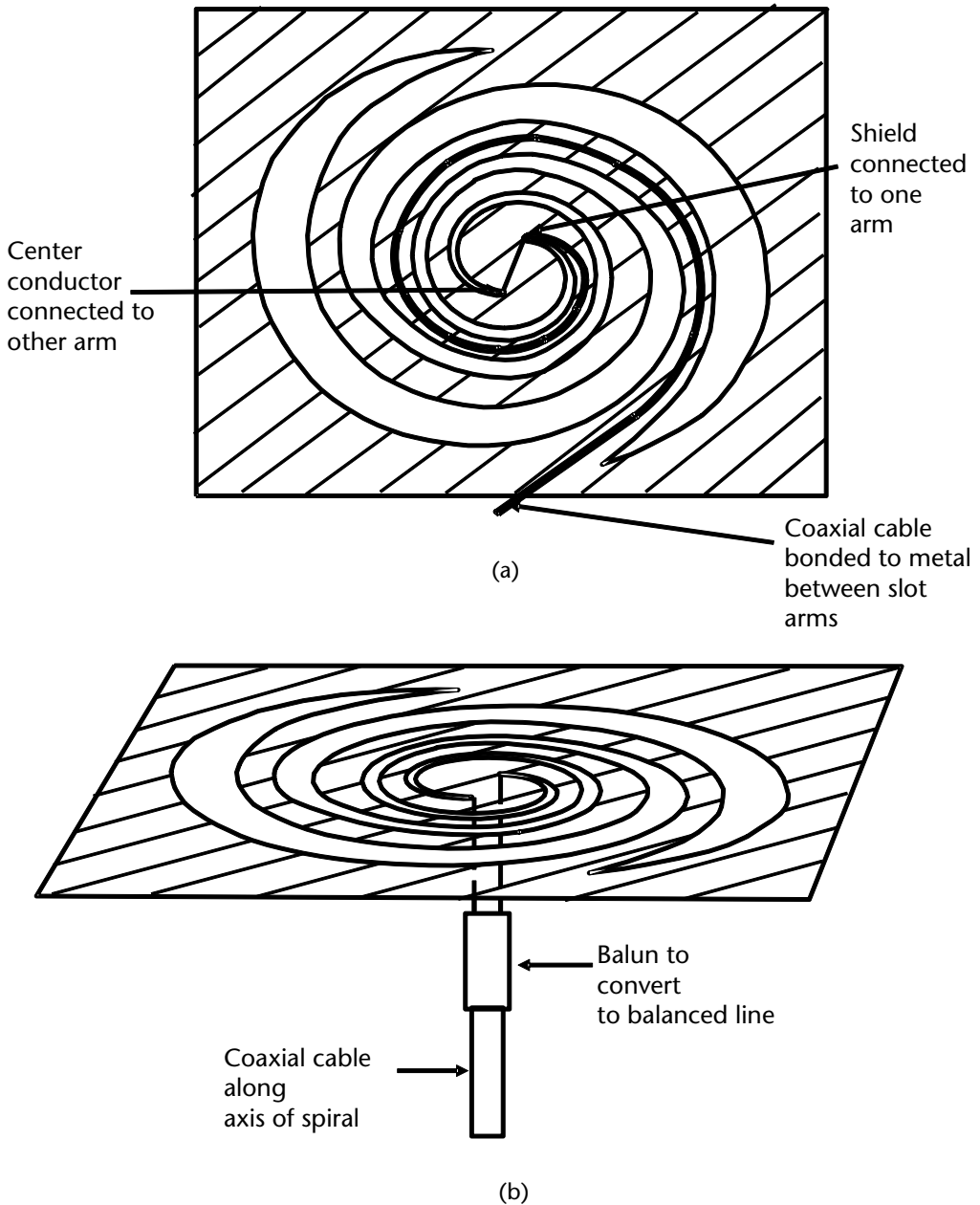


Figure 6.6 Feeding arrangements for the slot form of the planar log spiral. (a) Infinite balun coaxial line feed, and (b) axially-fed coaxial line.

6.3.4.2 The Arm Length of the Spiral

The length of the arm of a spiral is specified as the length along the center line of the arm. In order to calculate the length of an arm, consider the elementary length δl as shown in Figure 6.7.

Using Pythagoras' theorem, we have

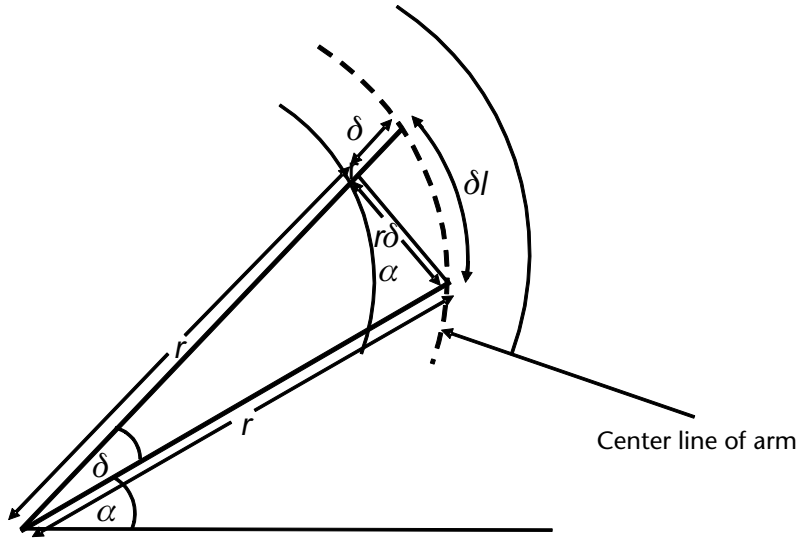


Figure 6.7 Calculation of the arm length of a log spiral.

$$\begin{aligned}\delta l^2 &= (r\delta\alpha)^2 + \delta r^2 = \delta r^2 \left[\left(r \frac{\delta\alpha}{\delta r} \right)^2 + 1 \right] \\ \delta l &= \delta r \left[\left(r \frac{\delta\alpha}{\delta r} \right)^2 + 1 \right]^{\frac{1}{2}} r\end{aligned}\quad (6.10)$$

and thus we can say the following approximation holds

$$dl = \left[\left(r \frac{d\alpha}{dr} \right)^2 + 1 \right]^{\frac{1}{2}} dr \quad (6.11)$$

The total length L is found by evaluating the integral between the limits of r_1 and r_2

$$L = \int_{r_2}^{r_1} \left[\left(r \frac{d\alpha}{dr} \right)^2 + 1 \right]^{\frac{1}{2}} dr \quad (6.12)$$

From (6.6) we can see that $(rd\alpha/dr)$ is equal to $1/a$, and thus (6.12) can be rewritten as

$$L = \int_{r_2}^{r_1} \left[\left(\frac{1}{a} \right)^2 + 1 \right]^{\frac{1}{2}} dr = \left[\left(\frac{1}{a} \right)^2 + 1 \right]^{\frac{1}{2}} (r_2 - r_1) \quad (6.13)$$

6.3.4.3 Figure of Merit

The diameter d (see Figure 6.5) of the start of the spiral governs the high-frequency end of the antenna. This, in turn, is governed by the feed used. The low-frequency limit is determined by the overall diameter D of the spiral. If the diameter d of the feed region is, say, $\lambda_H/10$ (where λ_H is the wavelength at the high-frequency end) and the overall diameter D is $\lambda_L/2$ (where λ_L is the wavelength at the low-frequency end), and the ratio D/d is 25, we have

$$\frac{D}{d} = \frac{25}{1} = \frac{\lambda_L/2}{\lambda_H/10} \quad (6.14)$$

Thus, the ratio of the wavelengths is 1:5, and hence the frequency bandwidth is 5:1. The ratio of D/d is called the dimension ratio and λ_H/λ_L is called the wavelength ratio. The product of the dimension ratio and the wavelength ratio is taken as the figure of merit for a particular structure, and is a measure of how compact an antenna can be made for a given bandwidth. This figure of merit is usually one or greater. In the above case, the dimension ratio is 25 and the wavelength ratio is 1/5, which gives a figure of merit of 5 [4, p. 14–10].

6.3.4.4 Feeding Arrangements

The feed for the spiral can be located axially, and may consist of a coaxial cable with the inner conductor connected to one arm, and the outer conductor connected to the other arm (using a tapered balun for instance), as shown in Figure 6.6(b). Alternatively, a balanced feed can be used by bonding a cable to the underside of the metal between the arms [1, p. 700], as shown in Figure 6.6(a). Because of the rapid attenuation of the field with distance along the spiral, the current flow in the cable is negligible with this arrangement [4, p. 14–9]. The cable may be embedded in the ground plane, or soldered to it, and this arrangement is known as an infinite balun. This is the only type of balun that will allow the fullest use of the infinite impedance and pattern bandwidths of this type of antenna. [3, p. 183]. The main disadvantage of this type of feed is that it requires the use of a sufficient ground plane to carry the feed cable, and as a consequence, the feed region in the center is fairly large. This, in turn, restricts the upper frequency limit of the antenna. When the diameter of the cable approaches the width of the metal to which it is attached, it is necessary to attach a dummy cable to the opposite arm to maintain symmetry of construction and to prevent a tilt in the radiation pattern. Consistently, good radiation patterns can be obtained with spirals between $1\frac{1}{4}$ and $1\frac{1}{2}$ turns.

The electric field components E_θ and E_ϕ , in the θ and ϕ directions (as shown in Figure 6.8(a)), can be measured separately by antennas oriented at right angles to each other. A practical bidirectional planar log spiral has an unsymmetrical radiation pattern that also varies with frequency, as shown in Figure 6.8 (b–i). These are radiation patterns measured by Dyson [3, Figures 8 and 9], at frequencies between 595 MHz and 12 GHz (i.e., a bandwidth of 20:1). These have been obtained for a slot spiral cut into a 1/32-inch-thick copper sheet of a 14-inch square. This sheet is then bolted onto a larger ground plane, but the size of this ground plane has not

been stated. The spiral had $a = 0.30$, $k = 0.2$, $K_2 = 0.62$, the arm length was 38.7 cm, and the maximum diameter was 28.4 cm.

The variation of the HPBW with azimuth angle is quite marked. For instance, at 3.979 GHz the HPBW varies between 60° and 105° , as shown in Figure 6.9(a). If the frequency is varied and the HPBW is viewed in the azimuth plane ϕ , the variation at spot frequencies in the range 2.472 to 7.505 GHz is shown in Figure 6.9(b). A spiral antenna can have any number of arms. However, the variation of the radiation pattern with the expansion coefficient a can only be calculated theoretically for an antenna having an infinite number of arms [6, p. 520]. This is known as a sheath spiral. The variation of the radiation pattern for such a spiral, with the expansion coefficient a , is shown in Figure 6.10. It can be seen that when a is greater than one, the HPBW is proportional to a , and the gain is inversely proportional to a . However, when the expansion coefficient a is less than one, there is no monotonic

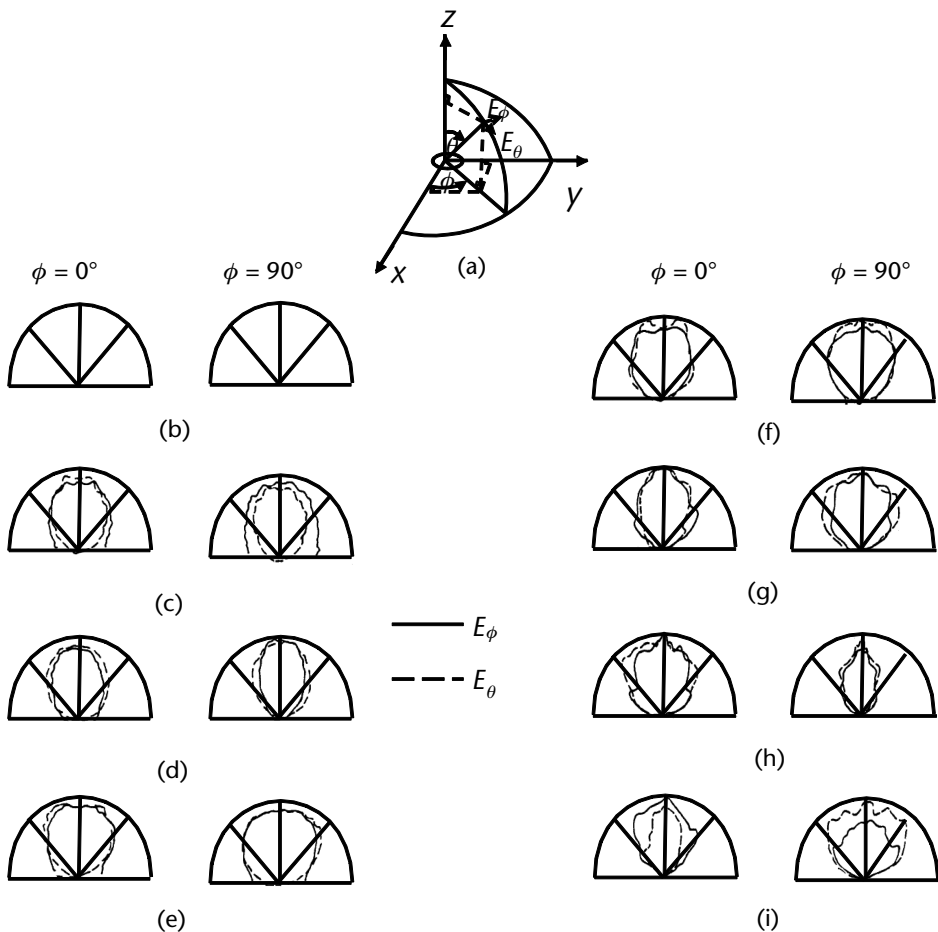


Figure 6.8 Radiation patterns for a planar log spiral in the $\phi = 0$ deg and $\phi = 90$ deg planes for E_ϕ and E_θ . (a) E_ϕ and E_θ vectors; (b) Frequency 595 MHz, axial ratio 1.94; (c) Frequency 1 GHz, axial ratio 1.19; (d) Frequency 1.4 GHz, axial ratio 1.04; (e) Frequency 2 GHz, axial ratio 1.04; (f) Frequency 3.95 GHz, axial ratio 1.07; (g) Frequency 5.6 GHz, axial ratio 1.07; (h) Frequency 9.027 GHz, axial ratio 1.07; (i) Frequency 12 GHz, axial ratio 1.24. (After [3].)

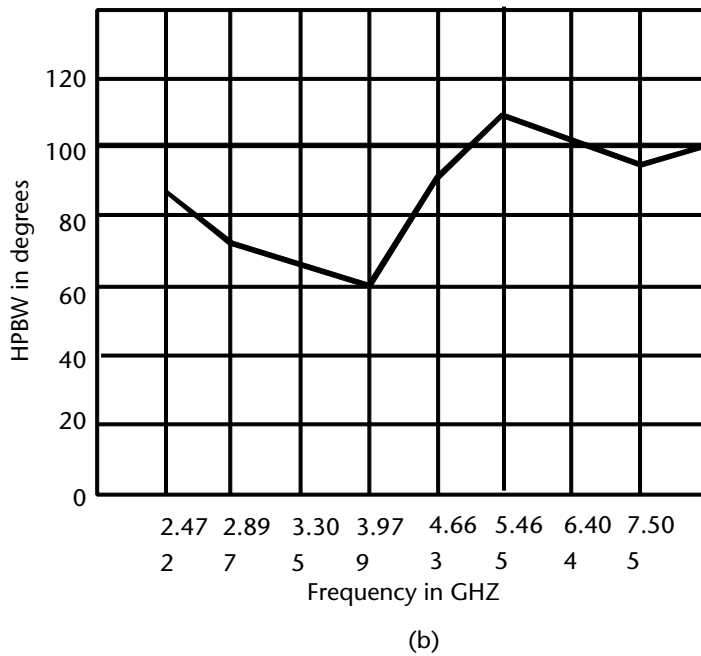
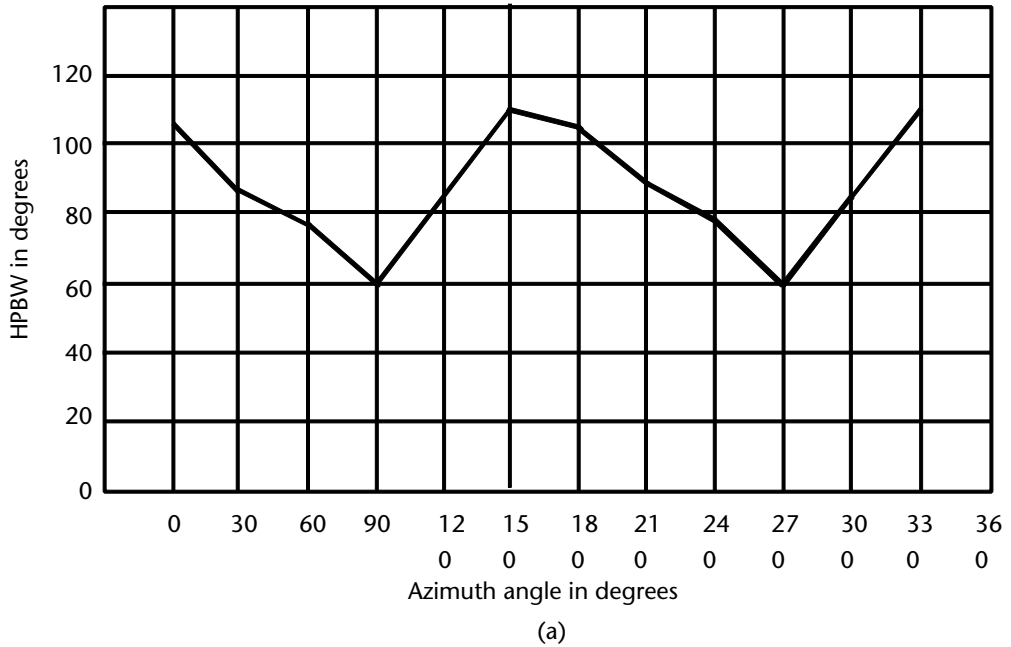


Figure 6.9 Variation of HPBWs of the radiated electric field with azimuth angle and frequency for a planar slot log spiral. (a) Variation of HPBWs in different planes at 3.979 GHz. (b) Variation with frequency of the HPBWs at $\phi = 90$ deg.

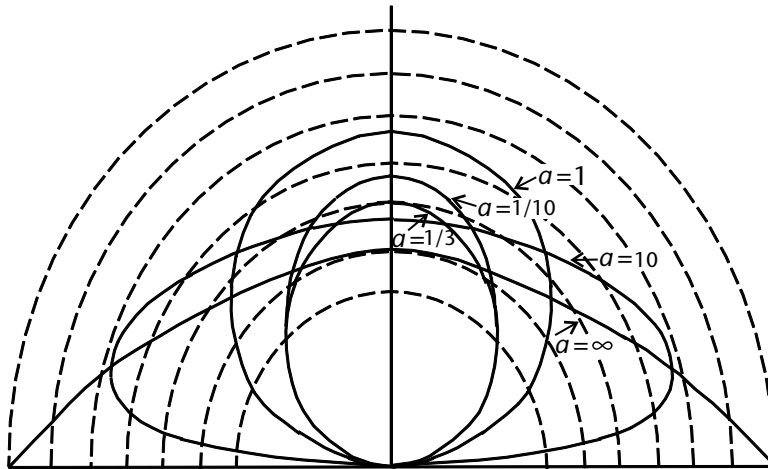


Figure 6.10 Variation of the radiation pattern of a planar log spiral, with the expansion coefficient a , for an infinite number of arms. (After [6, p. 520].)

dependence on a [6, p. 520]. In practice, an antenna with only a few arms (even as few as two) is a reasonably good approximation for a sheath spiral.

6.3.5 Cavity-Backed Spiral

The planar log spiral when placed in front of a cavity ($\lambda/4$ deep), can be used to give an unidirectional radiation pattern. An image of the original spiral is formed, and since it is in antiphase with the original spiral, and appears to be $\lambda/2$ behind the original, it constructively reinforces the field radiated by the original spiral. However, the image of the spiral radiates through the original spiral and distorts the pattern. In addition, since the cavity depth is around $\lambda/4$ for only a limited range of frequencies, the bandwidth is reduced to around 2:1 (i.e., an octave). If the cavity-backed spiral is loaded with radar-absorbing material (RAM) to absorb the radiation, the bandwidth can be increased to 10:1 [4, p. 14–9]. However the absorbing material used in the cavity dissipates about 50% of the total input power to the antenna; thus, the efficiency of the antenna is reduced to less than 50% in the case of a transmitting antenna. In the case of a receive antenna, this dissipative loss raises the antenna noise temperature and thus reduces the system detection threshold [7].

The cavity diameter must be greater than or equal to the spiral diameter. If the cavity diameter is made too large, higher-order coaxial or waveguide modes may be excited in the cavity. This would result in pattern deterioration at these cavity resonant frequencies. If the cavity diameter is made too small, the gain of the antenna is reduced, while the VSWR and ellipticity ratio is increased [2, p. 86]. The planar-backed spiral is also used as a feed for a parabolic reflector.

6.3.6 Conical Log Spiral

The conical log spiral antenna is an equiangular spiral projected onto a conical surface, as shown in Figure 6.11. It can also be considered as a tapered form of the

helical antenna, and for small cone half-angles ($\theta_{hc} \leq 10$ deg) the conical log spiral behaves like a helical antenna. It does not require a cavity in order to produce a unidirectional radiation pattern. The conical log spiral can be used at frequencies below 1 GHz, and commercially available antennas, when made to conform to MIL-STD drawings, cover the frequency ranges from 100 MHz to 1 GHz, 200 MHz to 1 GHz, and 1 to 10 GHz. However, they can be used from about 50 MHz to 18 GHz. Typical HPBW's are of the order of 60° in elevation and azimuth, and gains are of the order of 5 to 8 dBi. They are used for radiated emissions as well as susceptibility measurements.

For conical log spirals that are excited at the apex, the field is transverse to the radial direction and the current decreases inversely as the radial distance r from the center. This decrease is not large enough to make the end effects negligible when the cone is truncated [4, p. 14–3]. Calculated magnitudes of the attenuation are in the range of 7 to 10 dB per wavelength along the spiral arm. End effects produce variations in the radiation pattern.

The constants that govern the shape of the conical log spiral are similar to those of the planar log spiral, but they are dependent on the cone half-angle θ_{hc} . The expansion coefficient a is equal to $a'/\sin\theta_{hc}$, where a' is the expansion coefficient for a planar log spiral. Thus, the conical log spiral equations equivalent to (6.7) and (6.8) for the planar log spiral are given by

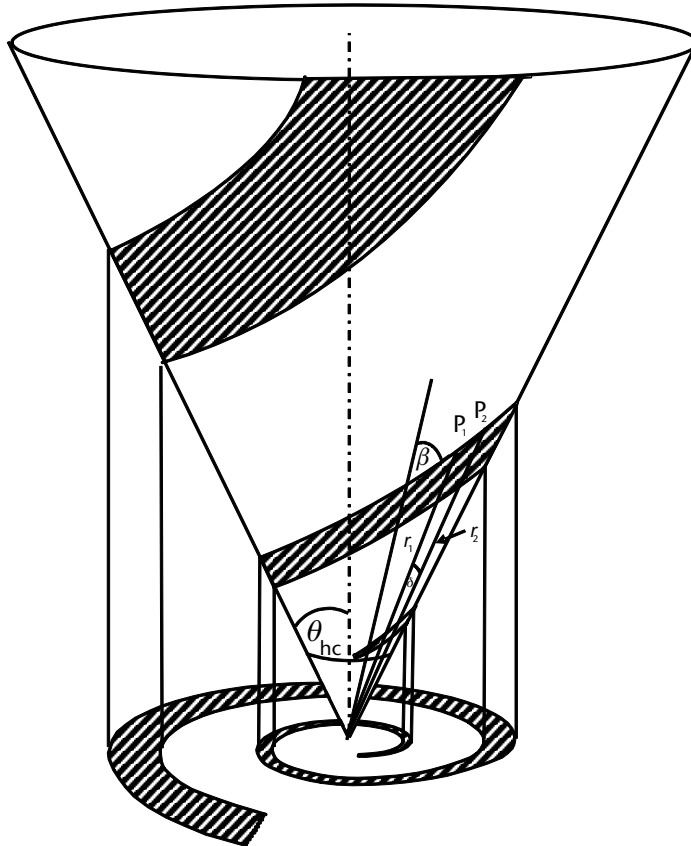


Figure 6.11 The conical log spiral.

$$\begin{aligned}\tan \beta &= \frac{1}{a} = \frac{\sin \theta_{bc}}{a'} \\ \beta &= \tan^{-1} \frac{\sin \theta_{bc}}{a'}\end{aligned}\quad (6.15)$$

where θ_{bc} is the cone half-angle and a' is the expansion coefficient on the equivalent planar spiral. The equations that determine the inner and outer edges of a conical log spiral are given in polar coordinates formed by the radius vectors r_1 and r_2 from the center. Both edges of the spiral have the same value of k and a , but one of them is rotated through an angle of δ with respect to the other. The angle δ thus defines the angular width of the arms.

$$r_1 = ke^{a(\alpha-\delta)} \quad (6.16)$$

$$r_2 = ke^{a\alpha} \quad (6.17)$$

where r_1 and r_2 are the radial distances to the point P_1 and P_2 on the inner and outer edges of the spiral, $\alpha - \delta$ is the angle with respect to the x -axis for the inner spiral, α is the angle with respect to the x -axis for the outer spiral, k is a constant that determines the start of the spiral, and a is a constant known as the expansion coefficient.

Both k and a are positive constants, and a determines the rate of spiral. The ratio of r_1 to r_2 , is given by

$$K_2 = \frac{r_1}{r_2} = e^{-a\delta} \quad (6.18)$$

As the cone half-angle decreases from $\pi/2$ (planar spiral), the spiral becomes more tightly wound. For small values of a' (of the order of 0.02), the main lobe is rotationally symmetrical [8, p. 331]. The pattern rotates with frequency, as in the case of a planar log spiral, but this effect is not observable in the case of rotationally symmetrical beams. Like the planar log spiral, the conical log spiral can be constructed in either conductor or slot form.

The two-arm conical spiral is a symmetrical structure and can be fed by a balanced two-wire transmission line, brought along its axis and a wire connected to each arm. Preferably, this should be a shielded line. A metallic shield or cylinder on the axis appears to have very little effect on the antenna characteristics, as long as its diameter is less than one third of the antenna diameter at any point on the axis [8, p. 495]. The balun to convert from an unbalanced to a balanced line may also be placed inside the antenna, if it is nonradiating and not affected by the fields inside the cone. The tapered line balun, which is extremely wideband, can be used, although there appears to be some interaction between the fields around the balun and those due to the antenna [9, p. 495]. If the pattern degradation can be tolerated, then this balun is ideally suited to the conical log spiral. Alternatively, the feed may be a coaxial cable bonded to the spiral arm (or to the ground plane, in the case of the slot form) as an infinite balun, in the similar manner to the planar case. However, the use of an infinite balun results in an effective increase in the width

of the arms, and the impedance and other parameters will therefore be equivalent to those obtained for larger values of angular width δ .

If the arms are decreased to a narrow constant width, they can be formed from cable alone. In this wire version, the feed cable becomes one arm, and at the apex the center conductor is connected to the outer braid of the dummy cable, which forms the opposite arm of the antenna. The apex diameter of approximately 4 cm is a practical limit of a feed cable of type RG8/U, and an upper-frequency limit of around 1700 MHz [8, p. 333]. If RG141/U cable is used, the apex can be reduced to 2 cm, and thus the upper frequency can be extended. However, this type of antenna constructed from cables results in an effective increase in the width of the arms, and the impedance and other parameters will therefore be equivalent to those obtained for arms of larger widths.

The conical spiral is fed at its apex, and in common with other frequency-independent antennas, provides backfire radiation. However, this backfire radiation occurs only for cone half-angles of 15° or less. As the cone angle is increased, there is a marked deterioration in the front-to-back ratio, until the value 90° is reached, when the antenna becomes a planar spiral and the pattern becomes bidirectional.

6.3.6.1 The Active Region

At the feed region of a two-arm spiral, out-of-phase traveling-wave currents are excited. These currents do not radiate until they reach the active region. The active region is defined as that region which controls the primary characteristics of the radiated field [9]. As the smaller turns are eliminated, there is very little observable change in the near-field distribution until the antenna is truncated at a radius, such that the near field is approximately 3 dB below the maximum recorded near field. This sets the upper edge of the active region. Similarly, as successive turns are removed from the base end, there is a negligible change until the antenna is truncated at a radius, such that the near field is approximately 15 dB below the maximum recorded near field [9, p. 491]. This sets the lower edge of the active region. The active region is therefore defined as that region between the electrical radius r_3^- (at the highest frequency of operation) at which the electric field magnitude is 3 dB below the maximum on the apex side, and the electrical radius r_{15}^+ (at the lowest frequency of operation) at which the magnitude is 15 dB below the maximum on the base side. The axial ratio of the electric field polarization ellipse on the boresight axis, for this active region, is 3 dB or less at the lowest frequencies. The magnitude of the electric field is measured by using a near field small shielded loop probe at a distance of 0.03λ from the surface of the antenna [9, p. 490]. The bounds of the active region vary for different cone half-angles θ_{bc} and wrap-angles β . These bounds are based on the near-field measurements, and they predict the far-field pattern most accurately for cone half-angles θ_{bc} of approximately 20° . For smaller cone angles, the bounds are larger, and for larger cone angles, the bounds are smaller.

6.3.6.2 Bandwidth

The bandwidth of the structure B_s is defined as the ratio of the radius of the base $D/2$, to the radius of the apex $d/2$. The operating bandwidth B_{op} of the antenna is

defined as the ratio of the structure bandwidth B_s to the bandwidth of the active region [9, p. 490]. The bandwidth of the active region B_{ar} is given by

$$B_{ar} = \frac{r_{15}^+}{r_3^-} \quad (6.19)$$

where r_3^- is the electrical radius on the apex side at which the magnitude of the near field is 3 dB below the maximum at the highest frequency of operation and r_{15}^+ is the electrical radius on the base side at which the magnitude of the near field is 15 dB below the maximum at the lowest frequency of operation.

6.3.6.3 Radiation Characteristics

The narrow on-axis beam occurs for small cone angles and wrap angle $\beta = 80^\circ$ approximately, with all turns of the active region being phased for backfire radiation. As the active region increases, the beam broadens and tends towards a multiple beam. In general, as the aperture of an antenna increases, the beam gets narrower. However, in the case of log conical spirals, the phase distribution across the spiral results in radiation occurring in progressively different directions. Larger turns or more widely spaced elements are phased to radiate at an angle to the axis. At a half cone angle of 15° , the radiation is mainly on axis for angles of wrap $\beta = 80^\circ$. However as the angle of wrap is decreased to 45° , a major portion of the active region is phased for broadside radiation.

The directivity of the antenna can be calculated from the HPBWs in the orthogonal planes and is given by [9, p. 493]

$$D_{dB} = 10 \log_{10} \frac{32,000}{\theta_1 \phi_1} \quad (6.20)$$

where D_{dB} is the directivity in dBi (with respect to a circularly polarized isotropic source), and θ_1 and ϕ_1 are the HPBWs in degrees in the orthogonal planes.

The electric field components E_θ and E_ϕ , in the θ and ϕ directions, can be measured separately by antennas oriented at right angles to each other. This variation is due to radiation due to higher-order modes which do not have rotationally symmetrical beams. The difference in HPBWs varies between 3° and 20° , depending on the spiral wrap angle β and the cone half-angle θ_{bc} . The difference in the HPBWs for the E_θ and E_ϕ components [9, Figure 12] is shown in Figure 6.12. In general, it can be said that the difference increases with a decreasing wrap angle and increasing cone half-angle. It can be seen that for very small cone angles of 2° ($\theta_{bc} = 1^\circ$) the difference in the HPBWs is around 3° for a wrap angle of 80° and increases to 9° , for a wrap angle of 45° . For large cone half-angles of 15° , and a wrap angle of 45° , the difference is as high as 20° .

For cone half-angles of 10° , and $\beta = 73^\circ$, the measured HPBWs for E_θ and E_ϕ polarization are 70° and 90° , respectively [8, p. 331]. The HPBW of the order of 40° to 50° can be obtained with small cone antennas. However, the coverage of very wide bandwidths would entail the use of very long antennas for these small cone angles. The length of the antenna, in terms of the longest wavelength λ_L , is given by

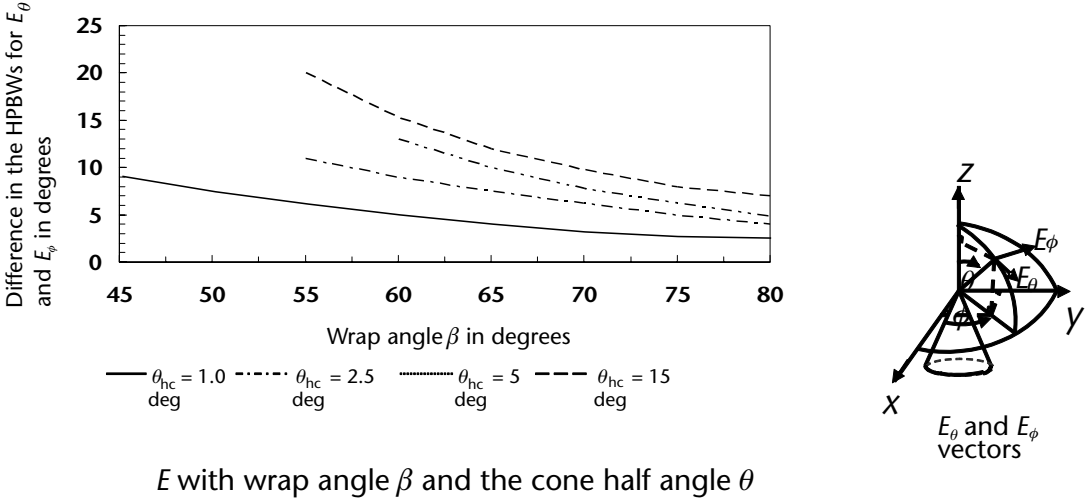


Figure 6.12 Variation of the difference in the HPBWs for the E_θ and E_ϕ components with spiral wrap angle β , with cone half-angles as a parameter.

$$\frac{L}{\lambda_L} = \frac{1}{2 \tan \theta_{hc}} \left[\frac{D}{\lambda_L} - \frac{d}{B\lambda_L} \right] \tag{6.21}$$

where D is the diameter of the base, d is the diameter of the apex, λ_L is the wavelength of the lowest operating frequency, θ_{hc} is the cone half-angle, and B is the operating bandwidth. As the active region moves towards the truncated tip of the cone, the HPBW may at first become narrower and then the pattern may become rough. Any lack of precision in the structure of the antenna will cause the pattern to tilt or become distorted. As the frequency is increased further, the beam broadens and tends to break up into a number of lobes [9, p. 493]. Cone half-angles of 15° or less have higher front-to-back ratios. For K_2 between 0.85 and 0.9, and $\beta = 73^\circ$, an apex diameter of $\lambda_H/4$, and a base diameter of $3\lambda_L/8$ provides a front-to-back (F/B) ratio of 15 dB or more.

The axial ratio of the polarization ellipse for angles off boresight (from 0° to 90°) varies between 2 and 4 dB for a wrap angle $\beta = 45^\circ$ and $\theta_{hc} = 10^\circ$ [4, p. 14–12]. The axial ratio is 2:1 (3 dB) up to about 60° off axis.

In the case of wrap angles $\beta \leq 45^\circ$ and $\theta_{hc} \leq 7.5^\circ$, as the antenna deviates from the self complementary structure of $\delta = 90^\circ$, the front-to-back (F/B) ratio also may deteriorate and the pattern breaks up into many lobes. A large portion of the energy is also radiated in the direction of the base, that is, end-fire instead of backfire radiation. For $\beta = 80^\circ$, the F/B ratio increases from 6 to 25 dB as θ_{hc} decreases from 22.5° to 7.5° [8, p. 14–12].

For self-complementary antennas, $\delta = 90^\circ$, the variation of the average HPBW (for E_ϕ and E_θ polarization) with wrap angle β is shown in Figure 6.13 with the cone angles as a parameter. The HPBWs are much larger for self-complementary antennas.

The approximate directivity can be calculated from these HPBWs by using the formula of (6.20). These directivities have been calculated and are plotted in Figure 6.14 for the HPBWs of Figure 6.13.

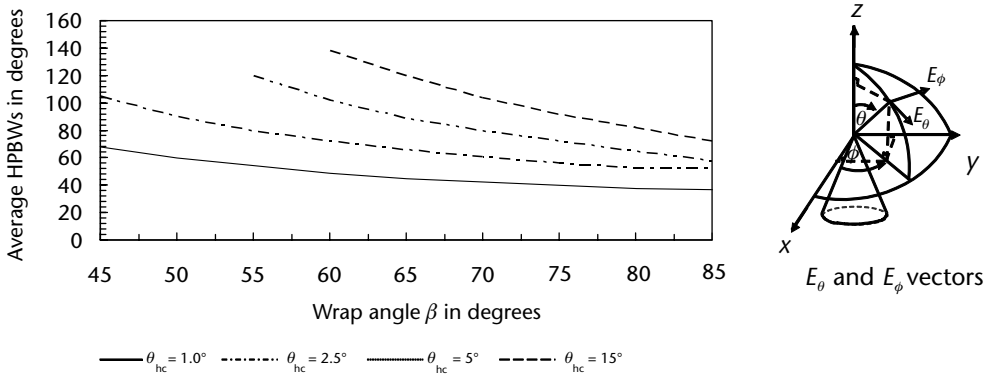


Figure 6.13 Variation of the average HPBWs with spiral wrap angle β , with the cone half-angle as a parameter.

The typical variation of gain and antenna correction factor with frequency for a commercially available conical log spiral is shown in Figure 6.15, for the frequency range of 200 MHz to 1 GHz (ETS-Lindgren 3101). It can be seen that the gain increases rapidly from approximately -6 dBi at 200 MHz, to a value of 3.6 dBi at 350 MHz, and then oscillates between 3.5 and 4.5 dBi. The antenna correction factor varies between 17 and 27 dB, with the minimum value occurring around 350 MHz.

For the frequency range of 1 to 10 GHz (ETS-Lindgren 3102), the typical variation of gain and antenna correction factor with frequency for a commercially available conical log spiral is shown in Figure 6.16. It can be seen that the gain does not increase monotonically, but varies between approximately 0.3 dBi and 4 dBi, reaching its lowest value of 0.3 dBi at 10 GHz. The antenna correction factor, on

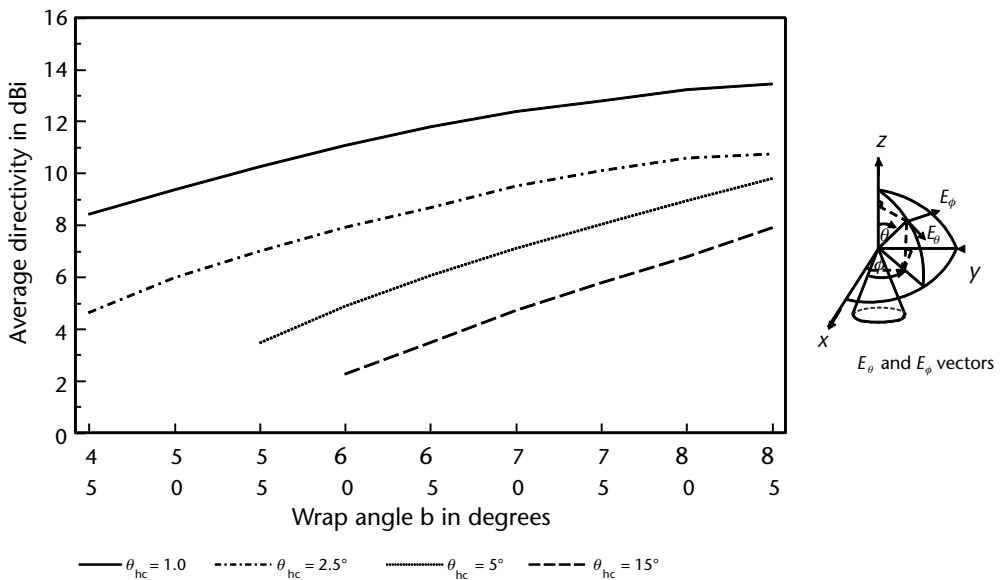


Figure 6.14 Variation of the average directivity for E_θ and E_ϕ with spiral wrap angle β , with the cone half-angle as a parameter.

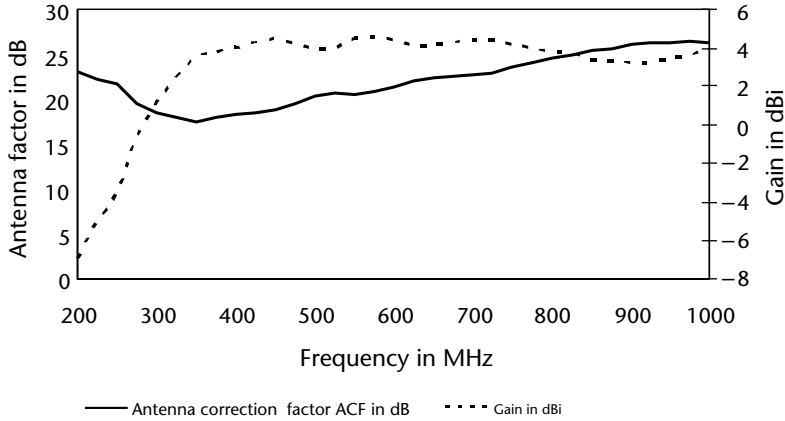


Figure 6.15 Variation of the gain and ACF for a conical log spiral in the frequency range of 200 MHz to 1 GHz.

the other hand, shows a steady increase from its minimum value of about 27 dB at 1 GHz, to its maximum value of 50 dB at 10 GHz.

6.3.6.4 Input Impedance

The mean impedance level appears to slowly decrease with decreasing cone half-angle θ_{bc} [8, p. 333]. The approximate measured input impedance varies between 129Ω and 153Ω for pitch angles of 17° and half cone angles between 10° and 30° . These values were obtained for $K_2 = 0.925$, arm length $L = 1.5\text{m}$, $a = 0.303 \sin \theta_{bc}$, and wrap angle $\beta = 73^\circ$.

The diameter of the base of the spiral determines the lowest frequency, and the diameter is approximately $\lambda/2$ at this frequency. The truncated apex diameter is approximately $\lambda/4$ at the highest frequency [1, p. 703].

The impedance is inversely proportional to the width of the arms. The impedance can be varied between 80Ω and 320Ω by reducing the angular width δ of the arms from 160° to 20° (narrow width). This variation with the angular width is shown

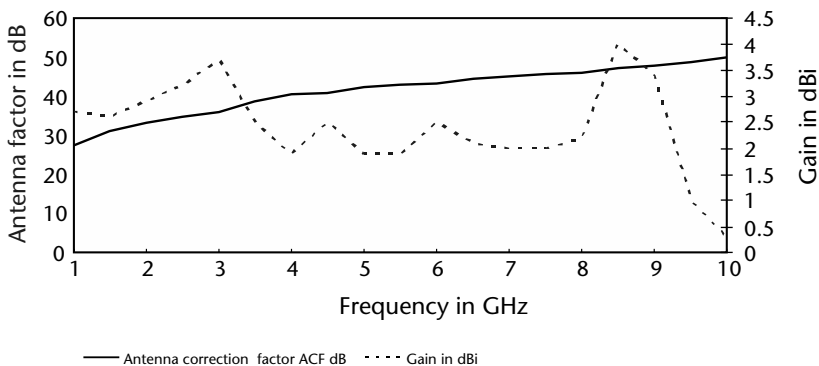


Figure 6.16 Variation of the gain and ACF for a conical log spiral in the frequency range 1 to 10 GHz.

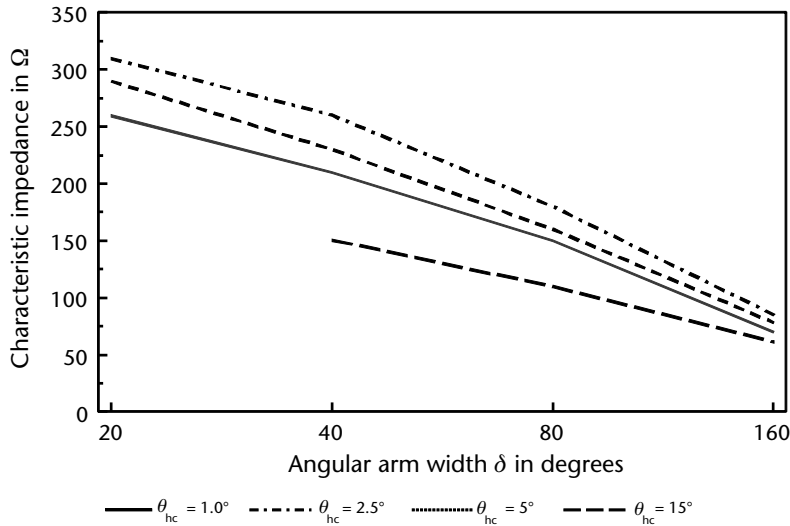


Figure 6.17 Variation of the characteristic impedance of a conical log spiral with the angular arm width δ , with cone half-angle θ_{hc} as a parameter.

in Figure 6.17, with the cone half-angles θ_{hc} of 7.5° , 10° , and 15° as parameters. The impedances obtained for a cone half-angle θ_{hc} of 10° and an infinite balun feed are appreciably lower, and vary between 150Ω and 60Ω .

If the arm width is kept constant at 90° , and the cone angle is increased, the impedance increases, until the cone becomes a plane at $\theta_{hc} = 90^\circ$ and the impedance approaches the theoretical value of 60π or 188Ω [9, p. 496]. As the angle of wrap β increases, the impedance also increases, although the change is very small.

When the antenna is operated at a frequency such that there is no distortion due to the truncated tip or base, the variation of the E_θ and E_ϕ radiation patterns with cone half-angles θ_{hc} , spiral wrap angle β , and angular arm width δ , is shown in Figure 6.18. It can be seen that as the wrap angle is increased, the patterns become more even and tend towards the single-lobe pattern. There is also a smaller difference between the E_θ and E_ϕ electric field patterns. At the small cone half-angle $\theta_{hc} = 7.5^\circ$, the patterns are smoother for the smaller wrap angles ($\beta = 70^\circ$) than they are when θ_{hc} is larger (15°). For $\theta_{hc} < 10^\circ$ and wrap angles $> 75^\circ$ it is possible to use thin arms or even constant width arms [9, p. 498]. The constant width arms can be constructed of coaxial cable, and this is used in many commercially available conical log spirals.

In the plane perpendicular to the axis of the cone, the pattern is almost omnidirectional. As in the case of other FI antennas, the radiation is in the backfire direction.

Dual polarization can be obtained by having another set of spirals wound in the opposite sense on the inside of the cone.

6.3.6.5 Phase Center

The phase center of an antenna is the point from which the EM waves appear to be emanating. The conical log spiral does not have a unique phase center, although an

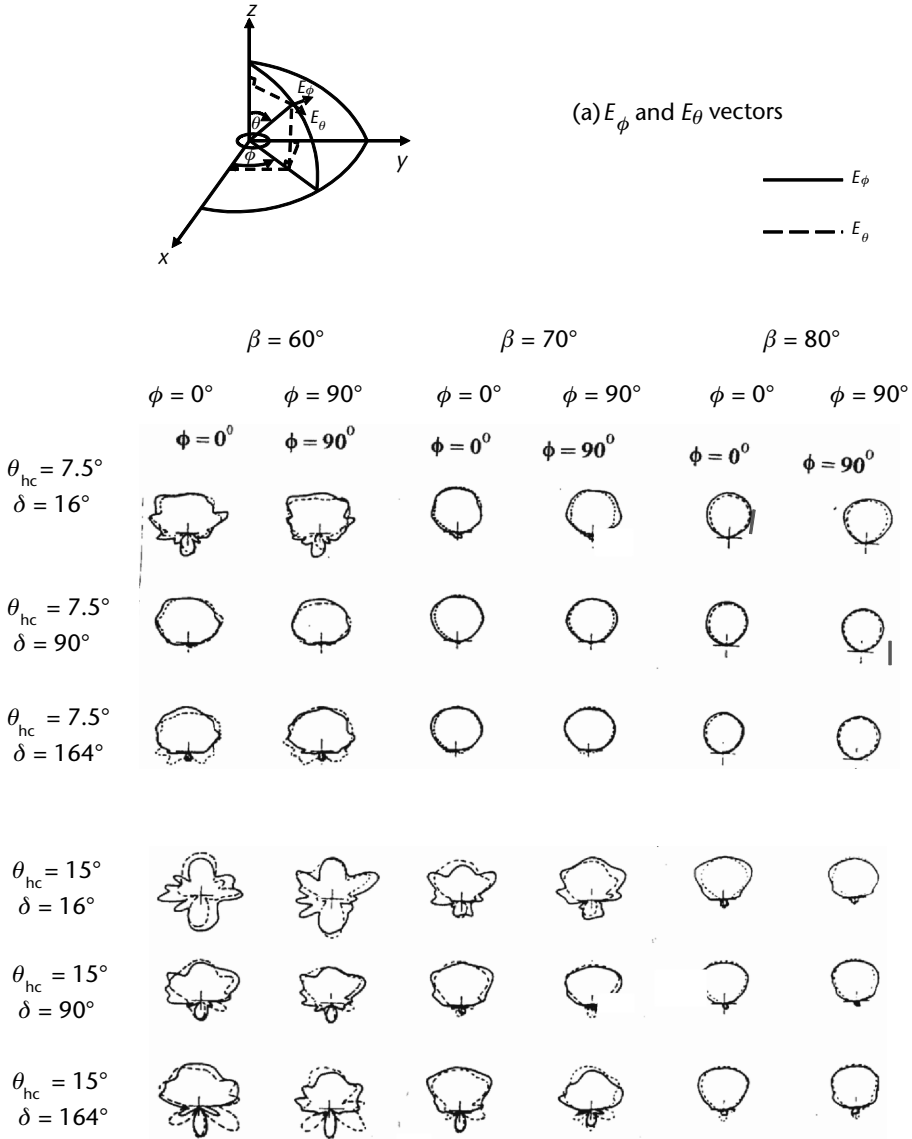


Figure 6.18 The variation of the E_θ and E_ϕ radiation pattern with cone half-angles θ_{hc} , spiral wrap angle β , and angular arm width δ for a conical log spiral. (After [9].)

apparent phase center can be defined over most of the main beam [9, p. 493]. The apparent phase center in terms of the cone radius R_c/λ is given by

$$\frac{R_c}{\lambda} = \frac{1.2 \sin \beta}{2\pi(1.4 + \cos \beta)} \tag{6.22}$$

Because the fields have higher amplitude nearer the apex, the phase center tends to remain in this region, although the radiation region moves further away from the apex at lower frequencies [9, p. 494].

6.4 Archimedes Spiral

The Archimedean spiral, as shown in Figure 6.19(a), is sometimes called an arithmetic spiral. Although the Archimedean spiral is a broadband antenna, it is not a true FI antenna.

The equations that determine the inner and outer edges of the Archimedean spiral are given by $r_1 = a\alpha - \delta$ and $r_2 = a\alpha$. The width of the arm is given by $r_2 - r_1 = a\delta$. Thus, the width of the arm is constant for a fixed value of the expansion coefficient a and angular arm width δ . The adjacent turns of a single spiral are separated by a distance of $2a\pi$.

The angle β , which the radius position vector makes with the tangent to the spiral, is not constant with the angle α , as in the case of log spirals. The angle β is given by

$$\tan \alpha = \beta \quad (6.23)$$

Archimedean spirals must have many turns and be tightly wound to operate over wide bandwidths, whereas equiangular spirals can be constructed with just 1 or 2 turns that are loosely wound. For a tightly wound spiral at distances remote from the origin, the angle β varies slowly with the angle α and the Archimedean spiral closely approximates a tightly wound log spiral [1, p. 698].

6.4.1 Cavity-Backed Archimedean Spiral

An empirical estimate of the gain and axial-ratio variation with the cavity diameter in terms of wavelengths is shown in Figure 6.20 [1, p. 14–16]. The results were obtained for a large number of spirals in the 0.2 to 4 GHz frequency band. The gain curve was normalized to the average axial ratio. The gain relative to an isotropic

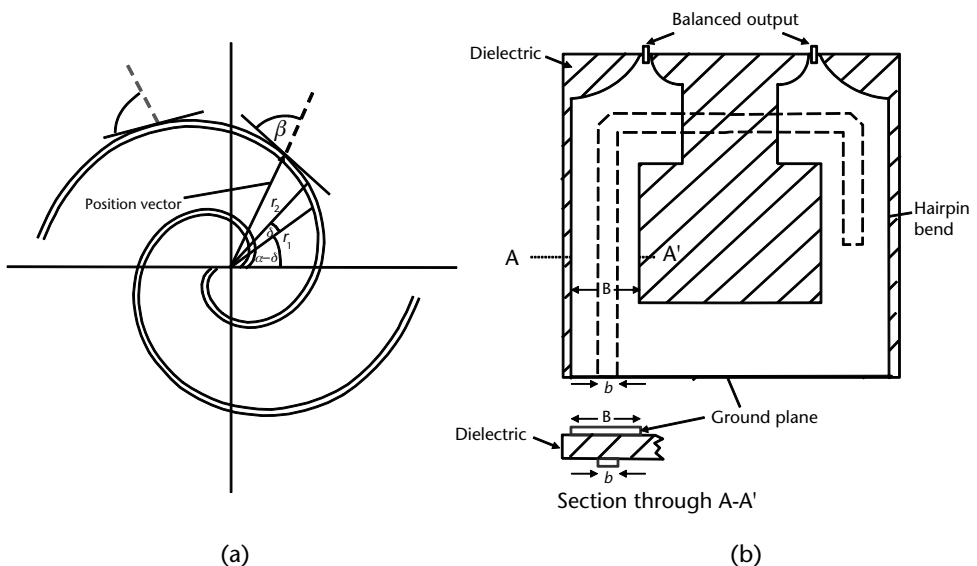


Figure 6.19 (a) The Archimedean spiral, and (b) printed circuit balun.

antenna, that is, the gain in decibels referenced to an isotropic antenna, increases almost linearly until a knee is reached at around $\lambda/3$, and then the gain curve starts to asymptotically approach the maximum gain at 0.5λ .

The boresight axial ratio variation with the cavity diameter is shown in Figure 6.20(b). The deterioration in the axial ratio obtained with the smaller cavity diameters is to be expected, since the energy reflected from the edges of the spiral has the opposite sense of polarization to the energy radiated at the center of the antenna.

The variation of gain (normalized to the maximum gain attainable) with the cavity depth is shown in Figure 6.21. It can be seen that the maximum gain is obtained when the cavity depth c_d is $\lambda/4$. Increasing the number of turns increases the energy radiated, since the effective aperture is now increased.

6.4.1.1 Feeding Arrangements

The feed and/or balun should be symmetrical and nonradiating. The most common feeding method used for the Archimedean spiral is a rigid coaxial line which

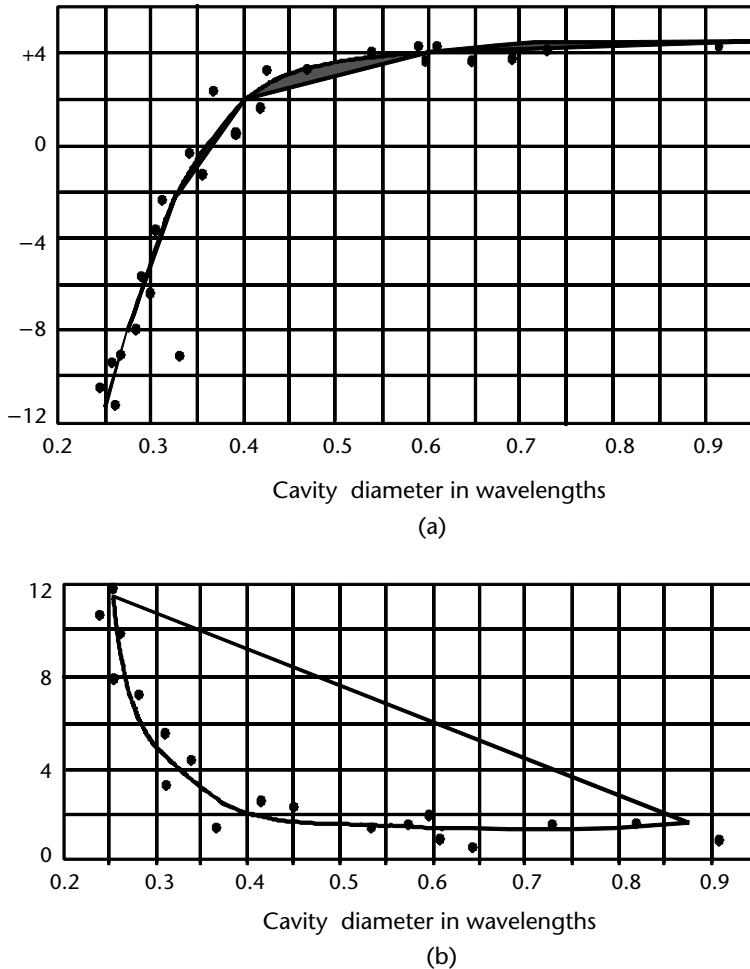


Figure 6.20 Variation of the (a) boresight gain and (b) axial ratio of a cavity-backed Archimedean planar spiral with cavity diameter.

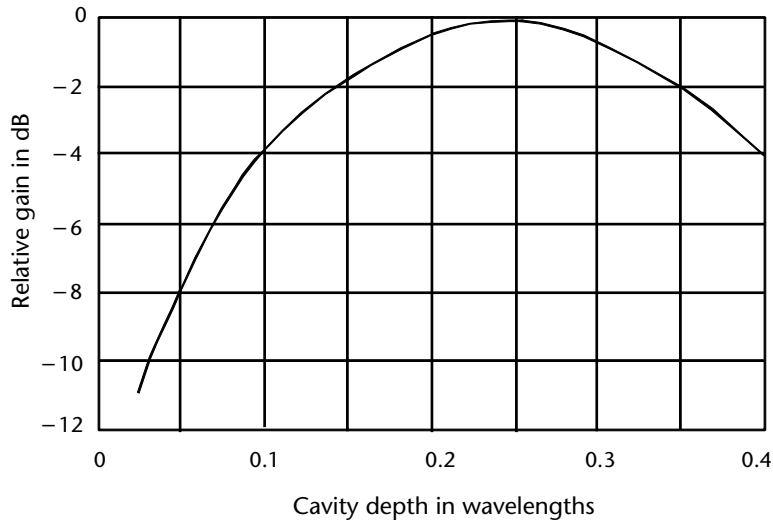


Figure 6.21 Variation of gain with cavity depth for an Archimedean planar spiral.

is placed axially within the cavity. The center conductor is connected to one arm and the outer conductor is connected to the other arm. The coaxial line is tapered to obtain a good match over the frequency range of an octave or more [2, p. 89]. However, the feed itself radiates, giving rise to an unsymmetrical beam, and affecting the ellipticity of the electric field polarization. The beam may also be squinted by a feed that radiates or is not well balanced, and thus gives rise to boresight error.

A printed circuit balun (see Figure 6.19) is another popular balun that may be used. This consists of a hairpin bend used on one side of the board, and a balanced line on the other side. The spiral arms are soldered directly to the balanced line. This type of balun has been used with antennas of octave bandwidth in the 200 MHz to 4 GHz frequency range, and ellipticity ratios of less than 3 dB have been obtained up to 60 degrees off boresight. Boresight errors have also been virtually eliminated, and VSWRs of less than 2:1 have been obtained [2, p. 89].

6.5 Microstrip Planar Spiral

Microstrip antennas are usually fairly narrowband. However, a spiral-mode microstrip (SMM) has been designed by Wang and Tripp [10] that has similar bandwidth to the cavity-backed spiral, and at the same time has the smaller volume and conformability associated with a microstrip antenna. The SMM was constructed with a half-inch wide ring of RAM that was just thick enough to fit between the spiral and the ground plane, and such that it is half underneath and half outside the truncated spiral. The RAM prevents the generation of higher-order phase modes, as well as the generation of the negative first order mode ($M = -1$), which is the first order mode being reflected from the outer periphery of the spiral. The gap widths (between the printed spiral and the ground plane) of 1.5 and 7.6 mm were used for Archimedean and equiangular spirals, and bandwidths of 6:1 were achieved in the frequency range of 2 to 12 GHz. The spiral diameters were 3 inches, and the

diameter of the ground plane was 18 inches (46 cm). The smaller gap widths give lower gains and efficiencies at the lower operating frequencies. The axial ratios of the SMM antennas are larger than those obtained for the cavity spiral. They also suffer from pattern ripples and beam asymmetries, which are thought to be due to the imbalance of the balun feed and the edges of the finite ground plane. When compared with a 2.5-inch diameter cavity-loaded spiral, the gains of 3-inch diameter SMMs (with gap widths of 7.6 mm) were between 1 and 3 dB better over the frequency range 2 to 12 GHz. SMM offers several advantages over the cavity-backed spiral. The cavity-backed spiral has a cavity whose depth has a comparable dimension to the diameter of the spiral. For an antenna with a bandwidth of 2 to 18 GHz, the SMM antenna has a thickness of 0.38 cm (0.15 in) compared with 5.08 cm (2 in) of a cavity-backed spiral.

6.6 Discone Antenna

The principle of the discone antenna has been described in Chapter 5 and its characteristic parameters are shown in Figure 6.22. The discone antenna is often supplied

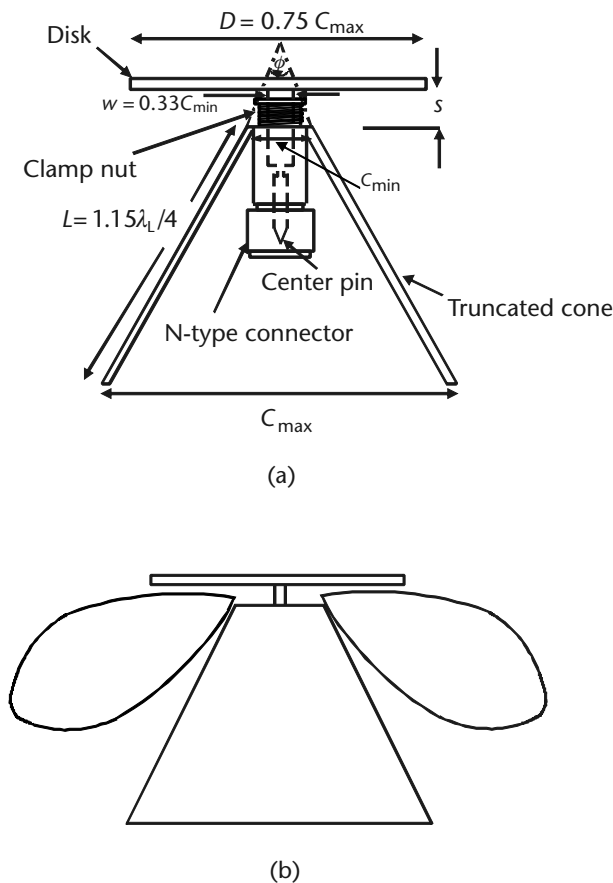


Figure 6.22 The discone or Kandoian antenna in the 1 to 2 GHz frequency range. (a) Physical characteristics of a discone antenna, and (b) radiation pattern of a discone antenna in the elevation plane.

with a snap-on N -type connector, which provides the RF feed as well as the mechanical support for the disk. At frequencies above 1 GHz, the minimum diameter of the cone C_{\min} must of necessity be of the order of $\lambda_H/12$, where λ_H is the wavelength of the highest operating frequency, in order to accommodate the connector. At frequencies between 1 and 2 GHz, Rappaport [11, p. 37] has found that for disccone antennas mounted on the end of N -type connectors, (and thus having values of $C_{\min} = \lambda_H/12$, approximately) the diameter w of the feed pin must be taken into account. The dimension s (disk-to-cone spacing) also has a significant impact on antenna loading for large electrical dimensions of C_{\min} , and must be taken into account. The optimum separation s for a cone flare angle of 45 deg was found to be $0.41 C_{\min}$, but for larger flare angles, $s = 0.5 C_{\min}$ was the optimum spacing. At lower frequencies (below 1 GHz) $s = 0.3 C_{\min}$ was used, as stated in Chapter 5.

The best flare angles (to provide a low VSWR) range between 45 deg and 75 deg, and the diameter of the feed conductor w should be a third of the diameter of the top of the cone ($w = 0.33 C_{\min}$), at frequencies for which C_{\min} is of the order of $\lambda_H/12$ or greater. At lower frequencies ($C_{\min} \leq \lambda_H/75$), the optimum value of w is $0.3 C_{\min}$, as stated in Chapter 5. The impedance of the connector is a function of w/C_{\min} , and for a ratio equal to 0.3, the characteristic impedance of 66.5Ω is obtained, which presents a good match to a 50Ω transmission line. These values achieve a VSWR of 1.3:1 over an octave bandwidth. The disk diameter should also be $0.75 C_{\max}$ and the slant height L should be $1.15\lambda_L/4$ (where λ_L is the wavelength at the lowest operating frequency), instead of values of $0.7 C_{\max}$ and $\lambda_L/4$ respectively for lower frequencies.

Four cones were constructed with $C_{\min} = 19$ mm (0.75 in), and flare angles ϕ of 45 deg, 60 deg, 75 deg, and 90 deg. The body of each cone was soldered to a UG-21D/U N -type connector, and the rear end of the connector was made flush with the top of the cone. Disks of varying diameters were soldered to the rods that were in turn soldered to the center pins of the connectors.

The dimensions for the four antennas are shown in Table 6.1.

The antenna can also be optimized by adjusting the position of the clamp nut. This clamp nut tuning changes the dimension s (disk-to-cone spacing), and also reduces the impedance mismatch created within the connector. An improvement of around 5 dB was obtained in the antennas with larger cone angles (65 to 90 deg) but for the cone flare angle of 45 deg, the disk diameter had to be increased to $1.1 C_{\max}$ and the feed pin diameter had to be reduced to $0.25 C_{\min}$ to obtain an improvement in the VSWR.

Table 6.1 The Parameters of Four Antennas with Different Flare Angles

Flare Angle	Antenna 1	Antenna 2	Antenna 3	Antenna 4
ϕ	45 deg	60 deg	75 deg	90 deg
C_{\max}	74.2 mm	95.2 mm	108 mm	120.5 mm
C_{\min}	19.1 mm	19.1 mm	19.1 mm	19.1 mm
L	73 mm	73 mm	73 mm	73 mm
D	55.65 mm	71.4 mm	81 mm	90.4 mm

6.7 Double-Ridged Horns

Double-ridged horns can be used from around 50 MHz to above 40 GHz, but commercially available horns are usually found in the frequency range of 200 MHz to 2 GHz, and 1 to 18 GHz

The gains of double-ridged horns vary between 2.5 to 8 dBi for the frequency range of 200 MHz to 1 GHz, and 4 to 42 dBi for the frequency range of 1 to 18 GHz. HPBWs vary between 40 deg and 70 deg, in the H and E planes, respectively. Double-ridged horns are particularly useful for immunity and susceptibility testing, since they can handle powers of up to 800W in the lower frequency range and up to 500W in the higher frequency range.

In order to understand the behavior of double-ridged horns, we must consider doubled-ridged waveguides, which are smooth-walled rectangular waveguides with ridges. The basics of waveguide theory are explained in Section 6.7.1.

6.7.1 Waveguide Theory

Waveguides may be of a rectangular, circular, or elliptical cross section. The rectangular waveguides could have smooth inner walls or may have one, two, or four ridges, in which case they are known as ridged waveguides. Waveguides are used at frequencies above about 1 GHz, since coaxial lines are subject to attenuation (which increases with frequency) and they also cannot withstand high power. At lower frequencies, the size of the waveguide becomes too large to be practical, although waveguides are sometimes used for specialized applications at frequencies down to 300 MHz in the case of smooth-walled waveguides, and down to 100 MHz in the case of ridged waveguides. Waveguides cannot support a TEM wave, since one of the requirements for its propagation is two separate conductors.

The EM wave propagates in the waveguide in a similar manner to the way light waves travel in an optic fiber. We can imagine the waves reflected off the metal walls as they travel down the guide. When we draw rays of light in optics, the wavefront moves perpendicular to these rays. Consider a rectangular waveguide of cross section dimensions a and b , as in Figure 6.23(a). The guide is excited at a point between the two side walls, and waves reflect off the side walls. In Figure 6.23(b), the rays are shown reflecting off the walls, whereas in Figure 6.23(c), the wavefronts are shown. The dotted lines indicate troughs and the full lines represent the crests. The waves reflected off the side walls cross and where two troughs cross at point Q , for instance, the resultant is a trough of twice the magnitude of the trough of each individual wave. Similarly, where crests cross (at P for instance) the resultant crest is twice the magnitude of the individual crests. Thus, the resultant wave traveling down the guide is of twice the amplitude of the individual waves. This is the guided wave, and the distance between crests or between troughs is the guide wavelength λ_0 . The distance between P and Q is half this value, and PS is a quarter of this value. The relationship between the guide wavelength and the wavelength of the individual incident waves can be derived using geometry and trigonometry. The wavelength of the individual waves is the same as the wavelength of the waves in free space, and thus this is known as the free-space wavelength λ_0 . In Figure 6.23(c), the distance

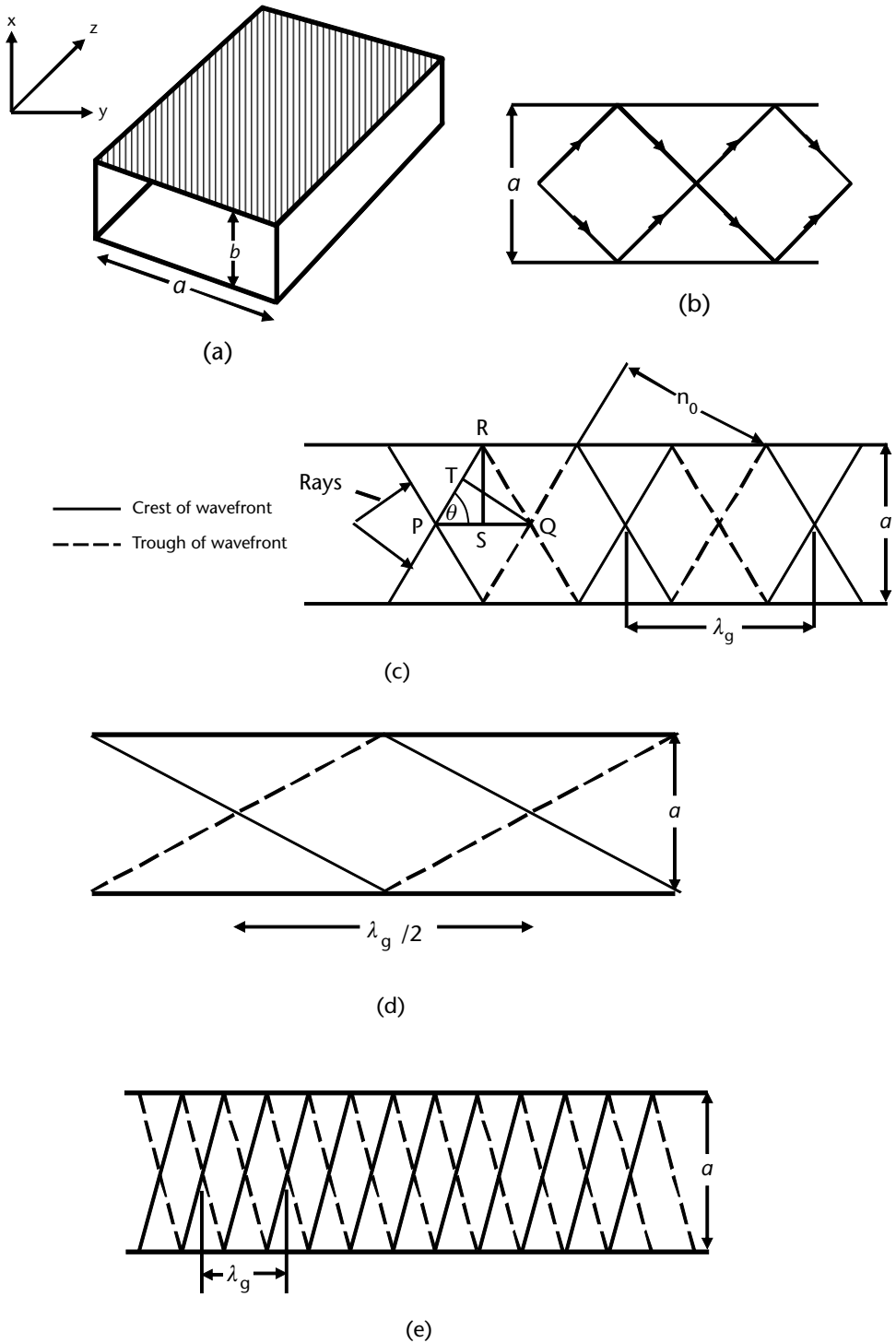


Figure 6.23 Propagation of a TE_{10} wave in a rectangular waveguide: (a) Rectangular waveguide, (b) plan view of rays, (c) plan view of the wavefronts, (d) free-space wavelength slightly greater than $2a$ (λ_g tends to infinity), and (e) free-space wavelength much greater than $2a$ (λ_g tends to λ_0).

denoted by TQ is that between a crest and a trough, and is therefore half this free-space wavelength. The width of the guide is a , and the distance RS is $a/2$.

In triangle PTQ , the sine of angle TPQ is given by

$$\sin \theta = \frac{\lambda_0/2}{\lambda_g/2} \quad (6.24)$$

In triangle PRS using Pythagoras' theorem

$$\begin{aligned} PR^2 &= RS^2 + PS^2 \\ PR &= \sqrt{\left(\frac{a}{2}\right)^2 + \left(\frac{\lambda_g}{4}\right)^2} \\ \sin \theta &= \frac{RS}{PR} = \frac{a/2}{\sqrt{\left(\frac{a}{2}\right)^2 + \left(\frac{\lambda_g}{4}\right)^2}} \end{aligned} \quad (6.25)$$

Equating (6.24) and (6.25), we get

$$\frac{\lambda_0}{\lambda_g} = \frac{a/2}{\sqrt{\left(\frac{a}{2}\right)^2 + \left(\frac{\lambda_g}{4}\right)^2}}$$

Squaring and cross multiplying gives

$$\lambda_0^2 \left[\left(\frac{a}{2}\right)^2 + \left(\frac{\lambda_g}{4}\right)^2 \right] = \frac{\lambda_g^2 a^2}{4}$$

Dividing throughout by $\lambda_0^2 \lambda_g^2 a^2 / 4$ gives

$$\left(\frac{1}{\lambda_g}\right)^2 = \left(\frac{1}{\lambda_0}\right)^2 - \left(\frac{1}{2a}\right)^2 \quad (6.26)$$

Let us now consider what happens as we vary λ_0 . We will consider four cases; when it is equal to $2a$, slightly less than $2a$, much less than $2a$, and greater than $2a$.

1. If $\lambda_0 = 2a$, then the right-hand side of (6.26) becomes zero, and thus the guide wavelength $\lambda_g \rightarrow \infty$. In this case, the frequency tends to zero, that is, the wave does not propagate. The free-space wavelength at which this occurs is known as the cut-off wavelength $\lambda_c (= 2a)$, and the corresponding frequency is known as the cut-off frequency f_c . The waveguide acts as a high-pass filter, and propagation only takes place at frequencies above this cut-off frequency.
2. When λ_0 is slightly less than $2a$, it can be seen that the difference between the two terms on the right-hand side of (6.26) is very small, so that the

reciprocal of the square of the guide wavelength is also very small. This makes the guide wavelength very long, as depicted in Figure 6.23(d).

3. When λ_0 is much smaller than $2a$, it can be seen from (6.26) that the first term on the right-hand side of the equation is the only significant term, which means that the guide wavelength tends to the free-space wavelength, as depicted in Figure 6.23(e).
4. When λ_0 is greater than $2a$, that is, the free-space wavelength is greater than the cut-off wavelength, an interesting situation occurs. The right-hand side of (6.26) is negative, and this makes its square root an imaginary value. This is analogous to the imaginary part of an impedance, and a similar condition applies in this case. The guided wave has a purely reactive impedance, and the guide supports what are known as evanescent modes. These modes store energy in a similar manner to the way capacitors store energy; they do not propagate or dissipate energy. Use is made of this property (of waveguides below cut-off) in the design of ventilation panels for shielded rooms.

6.7.2 Modes in Square and Rectangular Waveguides

Let us now consider what happens at the metal side walls of the waveguide. We apply what are known as boundary conditions. One of these boundary conditions states that at a perfect conductor, the tangential electric field is zero. This is in effect a generalized form of Ohm's law which states that the voltage is equal to the product of the current and resistance. If we have a perfect conductor, the resistance is zero, and thus the voltage is also zero. Since the electric field is the voltage per unit length, the electric field along or tangential to a perfect conductor is also zero. It can be shown that the normal (perpendicular) electric field varies across the broadside dimension a of the waveguide in a sinusoidal manner, from zero at the ends to a maximum at the center.

Other variations of electric field are also possible across this dimension, but one half-sinusoidal variation is the lowest configuration that can be supported by the waveguide. This is known as the dominant or fundamental mode of propagation. For rectangular waveguides, this is the TE_{10} mode where TE stands for transverse electric, and the subscripts 1 and 0 stand for the number of half-wave variations along the y - and x -axes, respectively. In this mode, the electric field only has a component in the x - y plane, transverse to the direction of propagation of the wave. As shown in Figure 6.24(a), the electric field only varies in the y -direction, that is, across the broadside or a dimension of the waveguide; there is no electric field perpendicular to the b dimension of the waveguide, and hence no variation in the x -direction. Since there is one half-wave variation in the y -direction, the first subscript is one, and there is no variation in the x -direction, so the second subscript is zero. If the electric field had been perpendicular to the b dimension of the waveguide, the mode would be called the TE_{01} mode. The magnetic field has a component in the transverse plane as well as in the direction of propagation of the wave, and for this reason, in some older textbooks and papers, the TE modes are called H modes. The magnetic field lines are shown in Figure 6.24(a), with the top surface of the guide detached, for clarity. If there are two half wave variations of the electric field across the broadside dimension then the mode is known as the TE_{20} and the electric field variation for

this mode is shown in Figure 6.24(b). The magnetic field lines are not shown on the top and bottom surfaces, and the top surface of the guide is shown detached, for clarity. Rectangular waveguides are normally chosen for use at certain frequencies so that they only propagate the fundamental TE₁₀ mode (which also presents the lowest attenuation) and the free space wavelength of the center frequency for propagating this mode is around $4a/3$.

These waveguides are usually chosen so that their dimensions lie between the following limits:

$$a = 0.6\lambda_0 \text{ to } 0.9\lambda_0 \quad (6.27)$$

and

$$b = 0.3\lambda_0 \text{ to } 0.45\lambda_0 \quad (6.28)$$

This ensures that only the dominant mode is propagated. Figure 6.25(a) shows the a and b dimensions of a waveguide in terms of the free-space wavelength for the dominant, as well as some of the higher-order modes of propagation [12, Fig.7.8]. The curves and lines in Figure 6.25(a) represent the limiting values of the dimensions for the higher-order modes. Figure 6.25(b) shows the cut-off frequencies normalized to (as a multiple of) the cut-off frequency of the TE₁₀ mode for square waveguides ($b/a = 1$), as well as for rectangular waveguides which usually have an b/a ratio of around 1/2. The modes in oversize waveguides with $b/a = 2$ are also shown for completeness. These oversize waveguides are used for high power applications.

For TE waves, the wave impedance Z_w is given by

$$Z_w = 120\pi \left(\frac{\lambda_g}{\lambda_0} \right) \quad (6.29)$$

Since the guide wavelength λ_g is always greater than the free-space wavelength, Z_w for TE modes is greater than the wave impedance of 120π (377) ohms in free space.

Another set of modes exist where the magnetic field only has components in the plane transverse to the direction of propagation, whereas the electric field has components in the transverse plane as well as in direction of propagation. These are known as the TM or E modes. For TM waves, the wave impedance Z_w is given by

$$Z_w = 120\pi \left(\frac{\lambda_0}{\lambda_g} \right) \quad (6.30)$$

Since the guide wavelength λ_g is always greater than the free space wavelength, Z_w for TM modes is less than the wave impedance of 120π (377) ohms in a free space. Attenuation as a function of frequency for some of the lower-order modes in a rectangular waveguide are shown in Figure 6.26, together with the attenuation in a coaxial cable for comparison [12, Figure 8.2].

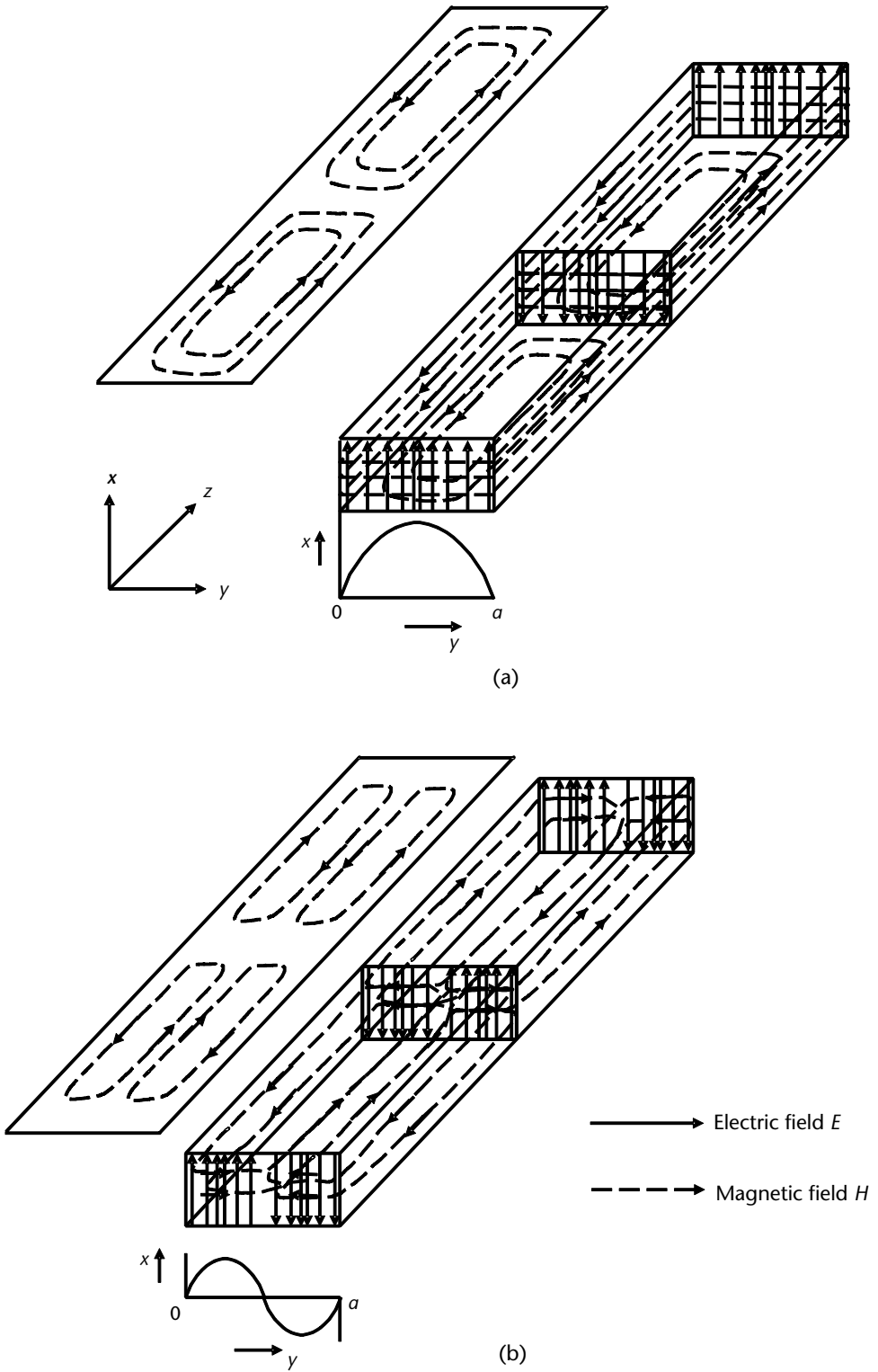


Figure 6.24 Propagation of (a) TE_{10} , and (b) TE_{20} modes, showing the fields in rectangular waveguides.

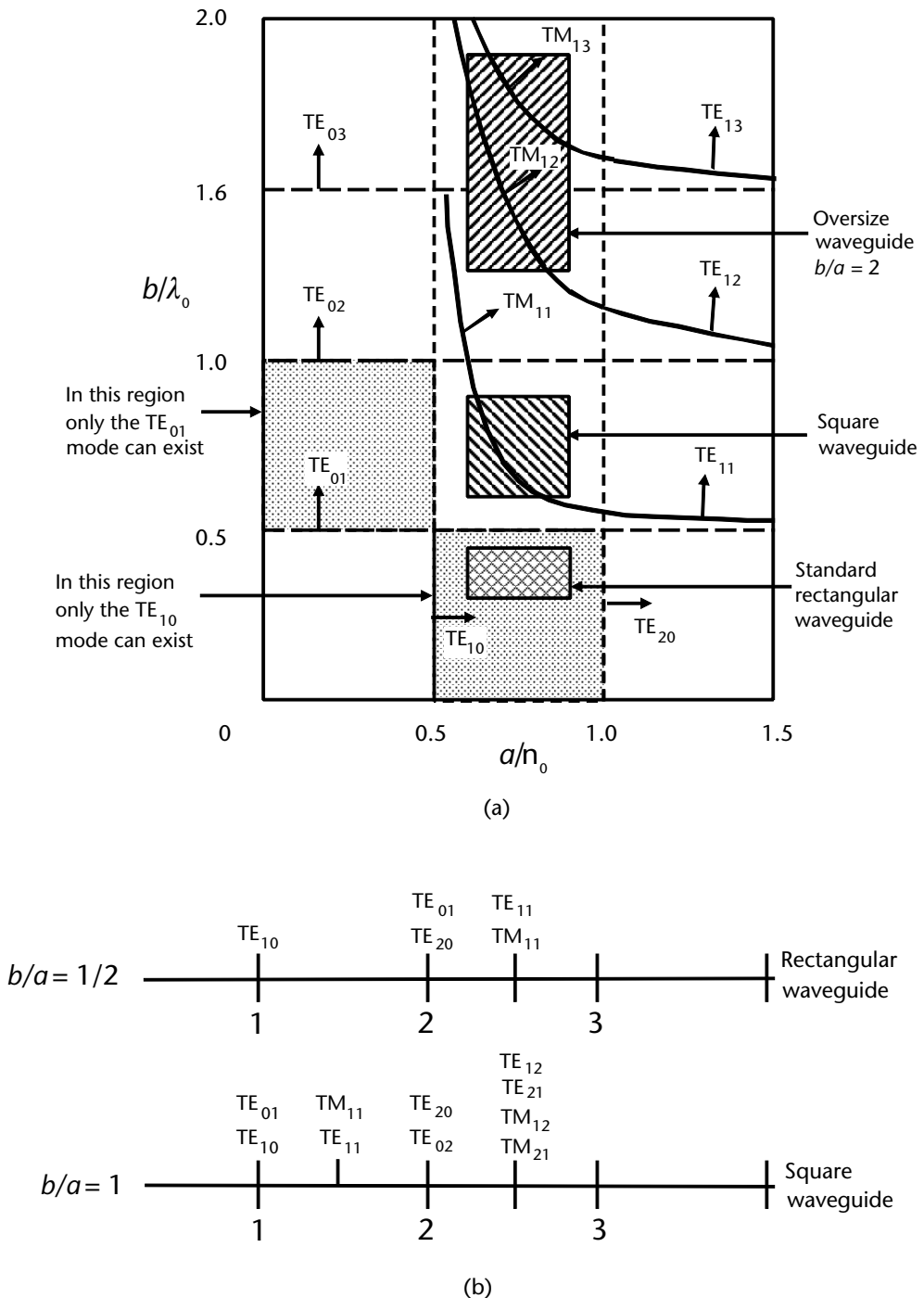


Figure 6.25 Dimensions and cut-off frequencies for some modes in rectangular waveguides: (a) Dimensions of square and rectangular waveguides for various modes, and (b) cut-off frequencies normalized to the cut-off frequency of TE_{10} mode. (After: [12, Figure 7.8].)

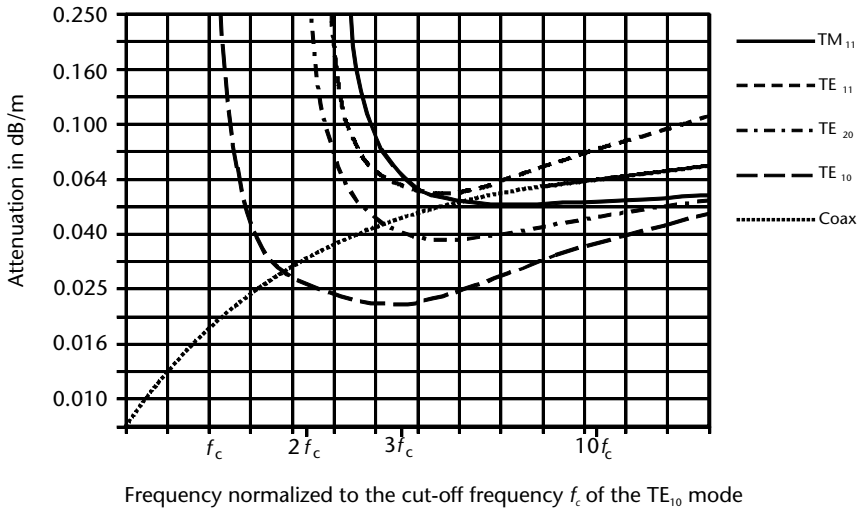


Figure 6.26 Attenuation for some of the modes in a rectangular waveguide as a function of the cut-off frequency of the dominant TE_{10} mode. (After: [12, Figure 8.2].)

6.7.2.1 Rectangular Waveguide Designations

Standard rigid waveguides are chosen so that they only propagate the dominant or TE_{10} mode. There are two main types of designations used for rectangular waveguides. The DEF 5351 designation uses the letters WG, and the EIA RS 216A designation uses the letters WR. In the first case, the letters WG are followed by a number which decreases with frequency, that is, increases with decreasing dimensions of the waveguide. For example, WG10, which is used in the NATO E and F bands (2.3 to 4.2 GHz), has inside dimensions of 7.214 cm (2.84 in) \times 3.404 cm (1.34 in), whereas WG16 which is used in the NATO bands I and J (formerly X-band, 8 to 12.4 GHz) is 2.29 cm (0.9 in) \times 1 cm (0.4 in).

In the case of the other commonly used designation, the letters WR are followed by numbers which decrease with increasing frequency; i.e. the numbers increase with the size of the waveguide. For example WR284 is equivalent to WG10, whereas WR90 is equivalent to WG16. We should note that with the WR designation the number following the WR number is approximately 100 times the larger dimension of the waveguide in inches; that is, it is the value of the broadside dimension in decimal inches. Table 6.2 shows both designations over the 400 MHz to 135 GHz frequency range. By measuring the inside dimensions of a waveguide, we can look up its operating frequency range.

6.7.3 Double-Ridged Waveguides

We have seen that the cut-off wavelength λ_c for the TE_{10} of a particular smooth-walled rectangular waveguide is twice its broad dimension a (i.e., $\lambda_c = 2a$). However when a single or double ridge or septum is used, the cut-off wavelength of the dominant or TE_{10} can be increased to more than 2.5 times this value (i.e., $\lambda_c > 5a$). This means that the lower cut-off frequency of the ridged waveguide is less than two-fifths of that of the smooth-walled guide.

Table 6.2 Rectangular Waveguide Designations and Dimensions

<i>DEF</i> 5351 No.	<i>EIA</i> RS216A No.	<i>Dimensions (in)</i>		<i>Dimensions (mm)</i>		<i>Operating Freq.</i> <i>Range in GHz</i>
		<i>Width</i>	<i>Height</i>	<i>Width</i>	<i>Height</i>	
WG 1	WR 1800	18	9	457.2	228.6	0.41–0.61
WG 2	WR 1500	15	7.5	381	190.5	0.50–0.75
WG 3	WR 1150	11.5	5.75	292.1	146.05	0.61–0.96
WG 4	WR 975	9.75	4.875	247.65	123.82	0.75–1.12
WG 5	WR 770	7.7	3.85	195.58	97.79	0.96–1.45
WG 6	WR 650	6.5	3.25	165.1	82.55	1.12–1.70
WG 7	WR 510	5.1	2.55	129.54	64.77	1.45–2.20
WG 8	WR 430	4.3	2.15	109.22	54.61	1.70–2.60
WG 9	WR 340	3.4	1.7	86.36	43.18	2.20–3.30
WG 10	WR 284	2.84	1.34	72.13	34.036	2.60–3.95
WG 11A	WR 229	2.29	1.145	58.166	29.083	3.30–4.90
WG 12	WR 187	1.87	0.872	47.498	22.148	3.95–5.85
WG 13	WR 159	1.59	0.795	40.386	20.193	4.90–7.05
WG 14	WR 137	1.37	0.622	34.798	15.798	5.85–8.20
WG 15	WR 112	1.12	0.497	28.448	12.624	7.05–10.05
WG 16	WR 90	0.9	0.4	22.86	10.168	8.20–12.4
WG 17	WR 75	0.75	0.375	19.05	9.525	10.0–15.0
WG 18	WR 62	0.62	0.31	15.748	7.874	12.4–18.0
WG 19	WR 51	0.51	.255	12.954	6.476	15.0–22.0
WG 20	WR 42	0.42	0.17	10.668	4.318	18.0–26.5
WG 21	WR 34	0.34	0.17	8.6360	4.318	22.0–33.0
WG 22	WR 28	0.28	0.14	7.112	3.556	26.5–40.0
WG 23	WR 22	0.22	0.11	5.588	2.794	33.0–50.0
WG 24	WR 19	0.188	0.094	4.775	2.387	40.0–60.0
WG 25	WR 15	0.148	0.074	3.759	1.8796	50.0–75.0
WG 26	WR 12	0.122	0.061	3.098	1.5494	60.0–90.0
WG 27	WR 10	0.10	0.05	2.54	1.27	75.0–10.0
WG 28	WR 8	0.08	0.04	2.032	1.016	90.0–135

The bandwidth for single mode transmission can be 4:1 [4, p. 42–34]. The maximum usable bandwidth (MUB) is given by the ratio of the cut-off wavelength of the TE_{10} mode to that of the TE_{20} mode. It should be noted that this is not the useful bandwidth, since the guide is normally operated about 15 to 25% above the cut-off frequency. The ridges can also raise the cut-off frequency of the TE_{30} mode slightly [4, p. 40–5].

The bandwidth of the double-ridged waveguide can be extended further by suppressing the TE_{20} so that the MUB is given by the ratio of the cut-off wavelength of the TE_{10} mode to that of the TE_{30} mode. The ratio of the cut-off wavelength of

the TE₃₀ mode to that of the TE₁₀ mode can be greater than 12:1 for double-ridged waveguides. Dielectric loading is often used for horns of bandwidths greater than 5:1 to reduce the phase error, as in the case of smooth-walled horns. It should be noted that the cut-off frequency can be reduced by the use of these dielectric materials, but this does not increase the bandwidth and usually results in greater loss. The change in the cut-off frequency depends both on the width of the ridge and its height relative to the dimensions of the waveguide. The addition of the double septum or ridge also alters the amplitude distribution across the mouth of the horn, with a corresponding reduction in the sidelobe level down to -30 dB [1, p. 655]. The electric field lines are shown in Figure 6.27(a).

6.7.4 Double-Ridged Waveguide Horns

In the smooth-walled pyramid waveguide horn, the electric field in the H plane (parallel to the broadside) tends to zero at the edges. This gives reduced sidelobes of around 23 dB. In the E plane however, the amplitude is nearly uniform, resulting in a sidelobe level of 13 dB. The introduction of septum plates with heights equal to a quarter of the broadside dimension (so that the gap $b' = 0.5$) gives a stepped amplitude distribution, which is almost a binomial series distribution of 1:2:1. This can reduce the sidelobe level to 30 dB below boresight by accurate positioning of the ridges at the throat of the horn [1, p. 655].

The taper of the ridge height and width must be such that a smooth impedance transition is provided from the characteristic ridge impedance of $Z_0 = 50\Omega$ to the intrinsic impedance of free space, $\xi_0 = 377\Omega$. It has been found experimentally that an exponentially impedance taper of the following form is quite satisfactory [13].

$$Z = Z_0 e^{kx} \text{ for } 0 \leq x \leq \frac{l}{2}$$

$$Z = 377 + Z_0 [1 - e^{k(l-x)}] \text{ for } \frac{l}{2} \leq x \leq l$$

where l is the length of the flare section and k is a constant, such that the impedance of the midpoint of the flared section is the average of the end point impedances.

The simplest type of ridge to fabricate is one of constant width. The length of the flared section should be fairly long so that the impedance transformation is accomplished over a length of the order of half a wavelength at the lowest operating frequency. However if the ridge width is too large near the open mouth of the horn aperture, the H plane distribution may have a large peak in the center and a large phase error occurs in the E plane [13]. Both of these factors result in a reduced gain for the horn. This can be alleviated by allowing the width of the ridges to increase in the flared section.

Consider the double-ridged waveguide shown in Figure 6.27(a). The width of each ridge is a' and the gap is b' , so that the height of each ridge is $(b - b')/2$. The transverse section of the waveguide can be considered to be a junction capacitance (at the central reduced height waveguide section) in parallel with two TE mode transmission lines on either side with open and short-circuit terminations, respectively [14, p. 399]. This equivalent circuit model holds as long as the gap b' is smaller

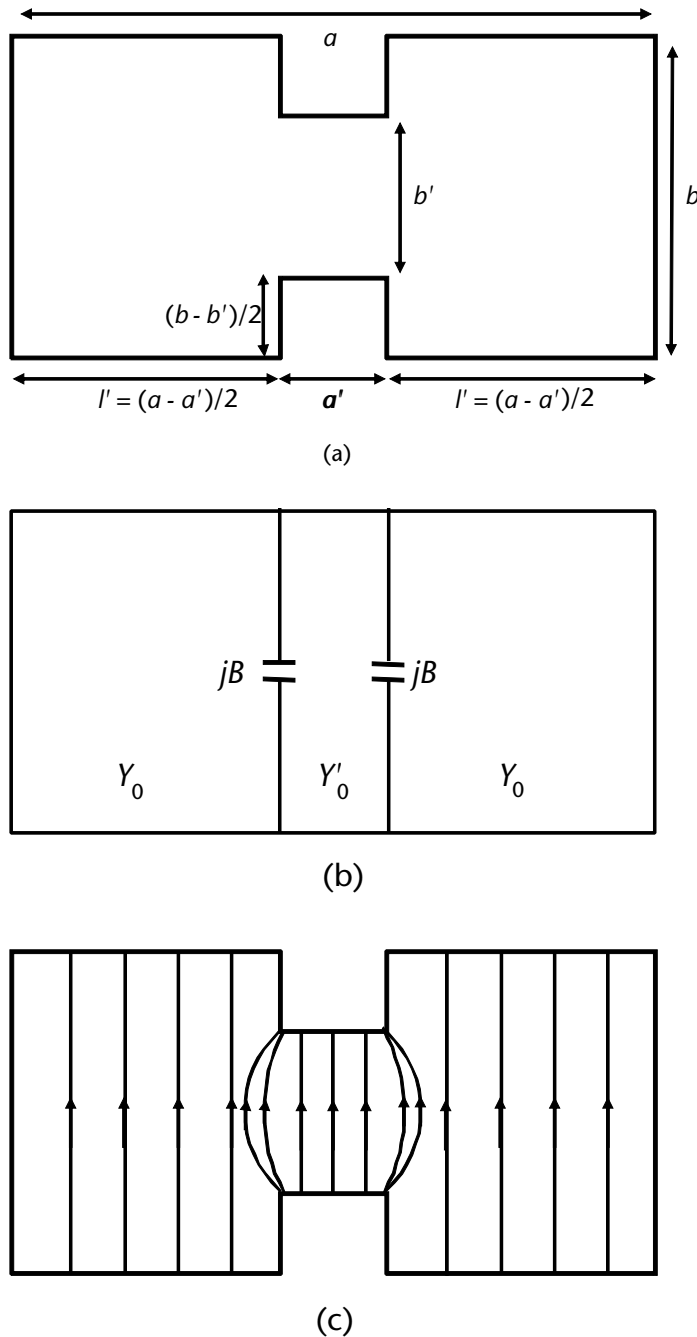


Figure 6.27 Double-ridged waveguide: (a) Ridge dimensions in a double-ridged waveguide, (b) equivalent circuit for cut-off wavelength computation, and (c) electric field for the TE_{10} mode in a double-ridged waveguide.

than the cut-off wavelength λ_c and much smaller than half the width of the normal height guide $(a - a')/2$. At cut-off, the susceptance looking into the shorted parallel plate guide to the right of the ridge is equal in magnitude but opposite in phase to the susceptance of the guide looking to the left [14, p. 399]. The susceptance at

the center is zero at cut-off. The equivalent circuit is valid for $b/\lambda_c < 1$ in the case of the double ridge waveguide.

It is also assumed that no higher-mode interaction exists between the ridge and the narrow side of the guide. This would be the case when the width of unreduced guide $(a - a')$ is much larger than twice the guide height, that is, $(a - a') \gg 2b$.

The guide wavelength λ_g is given by the following resonance condition at the reference plane T

$$\frac{Y'_0}{Y_0} \tan \frac{\pi}{\lambda_0} a' + \frac{B}{Y_0} - \cot \frac{\pi}{\lambda_0} (a - a') = 0 \quad (6.31)$$

where $Y'_0/Y_0 = b/b'$ and λ_c is the cut-off wavelength of the guide. The numerical solution to (6.29) yields the cut-off wavelength for the TE₁₀ normalized to the broadside a of the waveguide, that is, λ_c/a [14, p. 399]. These are plotted in Figure 6.28 for different values of a'/a and for values of b'/b between 0.1 and 0.5.

The cut-off wavelengths for the TE₁₀, TE₂₀, and TE₃₀ are shown in Figure 6.29, for $b'/b = 0.1$ and $a/b = 2$. The maximum usable bandwidths are the ratios of the cut-off wavelengths of the TE₂₀ or TE₃₀ modes to those of the TE₁₀. The MUBs are shown in Figure 6.30. The MUB increases rapidly as the gap between the ridges becomes small. When the gap b' is increased to $0.25b$, the cut-off wavelengths (normalized to the height b) are reduced as shown in Figure 6.31. The bandwidths obtainable with the larger gap between the ridges (shorter ridges) are lower than those obtainable with smaller gaps, and are shown in Figure 6.32 which is to be expected.

The ridged waveguide is much smaller than the smooth-walled guide with the same bandwidth, however, the losses are higher.

The ACF, gain, and HPBW's for a commercially available (the ETS-Lindgren 3106B) double-ridged waveguide horn in the frequency range of 200 MHz to 3 GHz

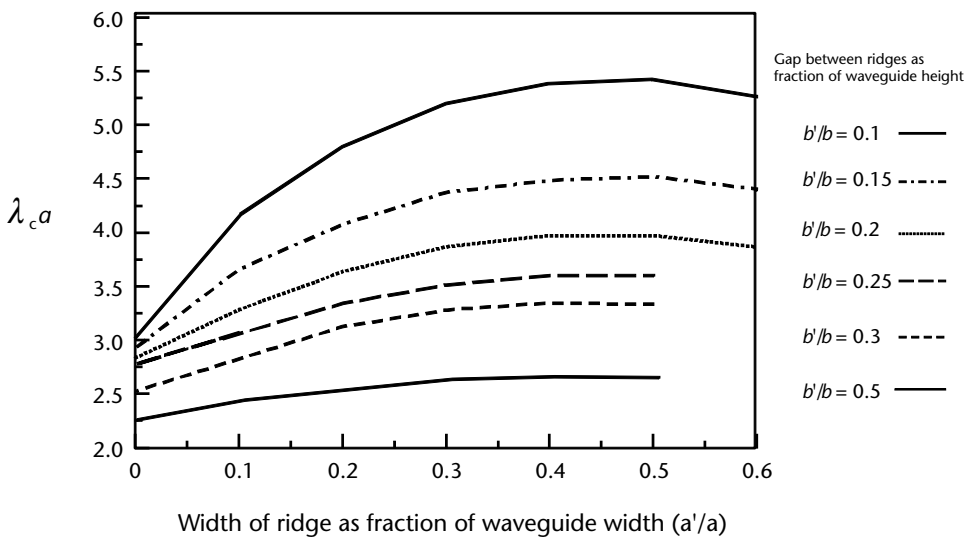


Figure 6.28 Variation of the TE₁₀ mode cut-off wavelength with ridge width a'/a , and for values of b'/b between 0.1 and 0.5, and $a/b = 2$.

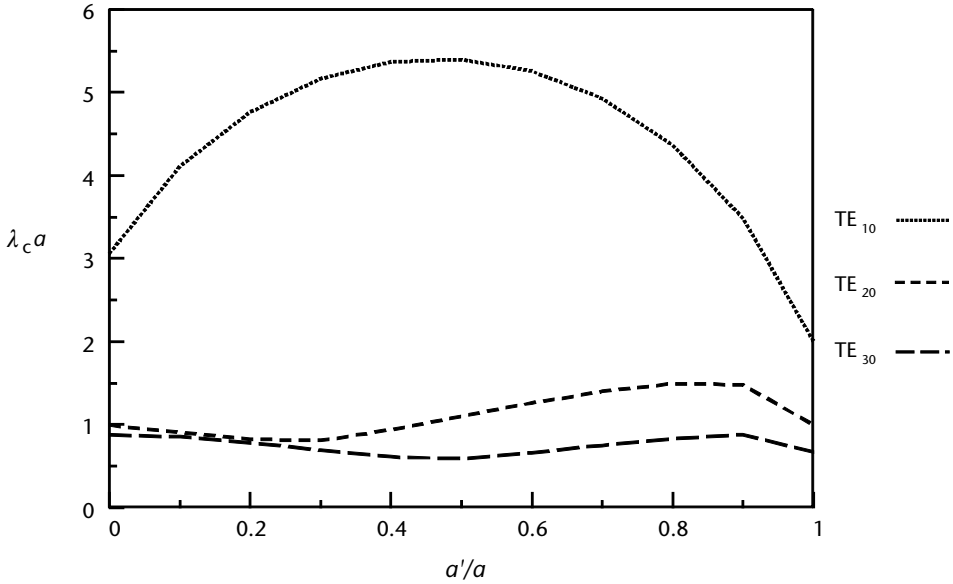


Figure 6.29 The cut-off wavelengths for the TE₁₀, TE₂₀, and TE₃₀ for $b'/b = 0.1$ and $a/b = 2$.

are shown in Figure 6.33. The HPBW's shown are the average of those in the E and H planes. The typical data is based on horizontal polarization.

Double-ridged horns can handle high powers and are therefore used as transmit antennas in, for example, susceptibility/immunity and SE measurements. The far-field distance is normally taken as $2D^2/\lambda$ where D is the diagonal in this case. However, the broadbanding of the horn results in a loss of gain and this reduces the effective aperture D_e . This effective aperture is the diameter of a reflector antenna with the equivalent gain. The HPBW's of a 1- to 10-GHz double-ridged horn, for

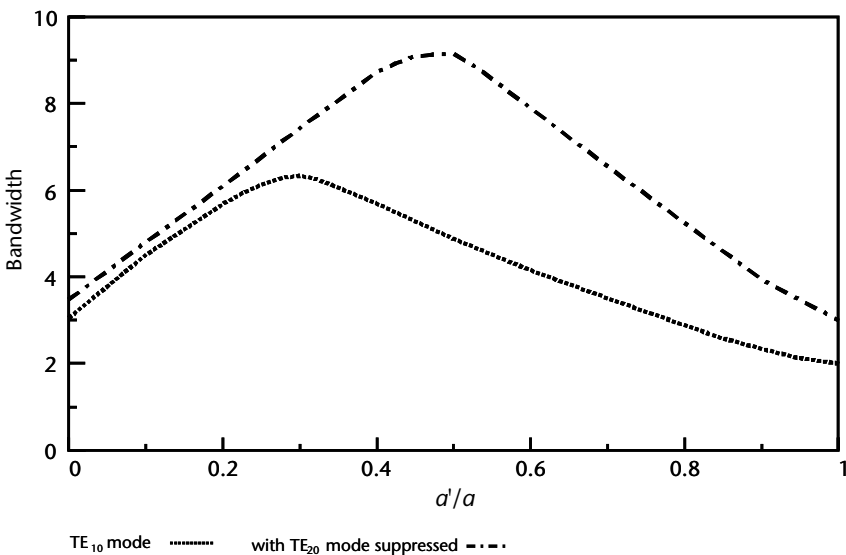


Figure 6.30 The maximum usable bandwidths of double-ridged waveguides with $b'/b = 0.1$ and $a/b = 2$.

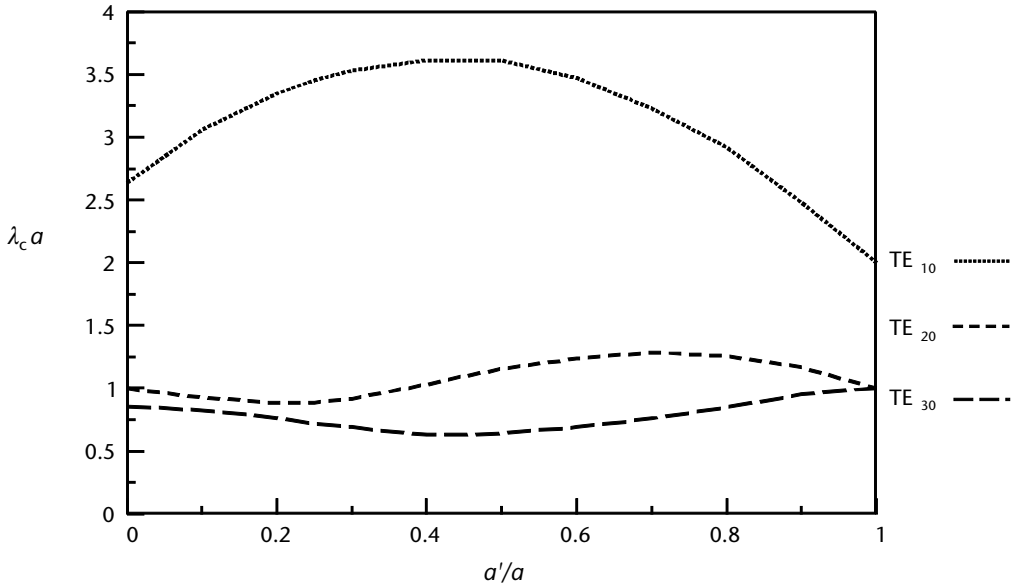


Figure 6.31 The cut-off wavelengths for the TE₁₀, TE₂₀, and TE₃₀ for $b'/b = 0.25$ and $a/b = 2$.

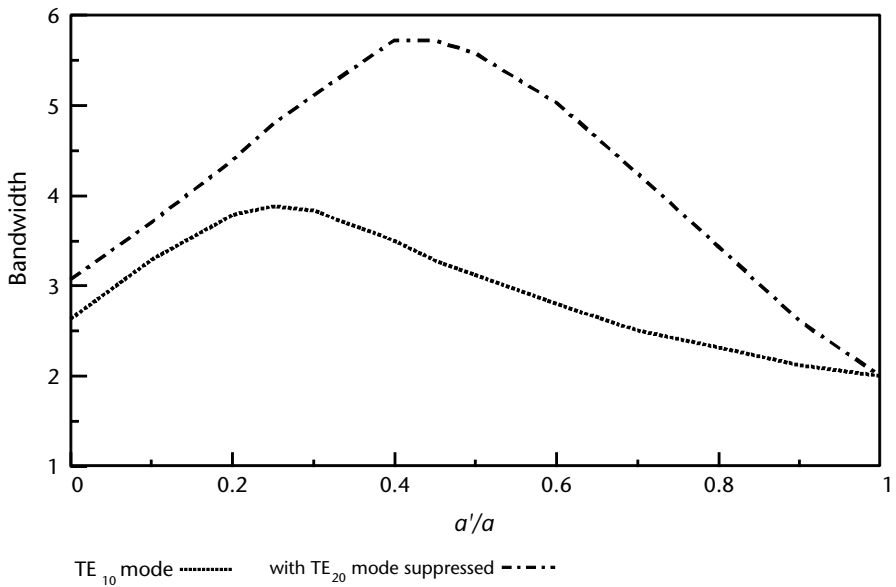


Figure 6.32 The maximum usable bandwidths of double-ridged waveguides with $b'/b = 0.25$ and $a/b = 2$.

example vary between about 72° and 30° . The HPBW θ_H of a hypothetical circular reflector of diameter D_e is given by

$$D_e = \frac{58\lambda}{\theta_H} \tag{6.32}$$

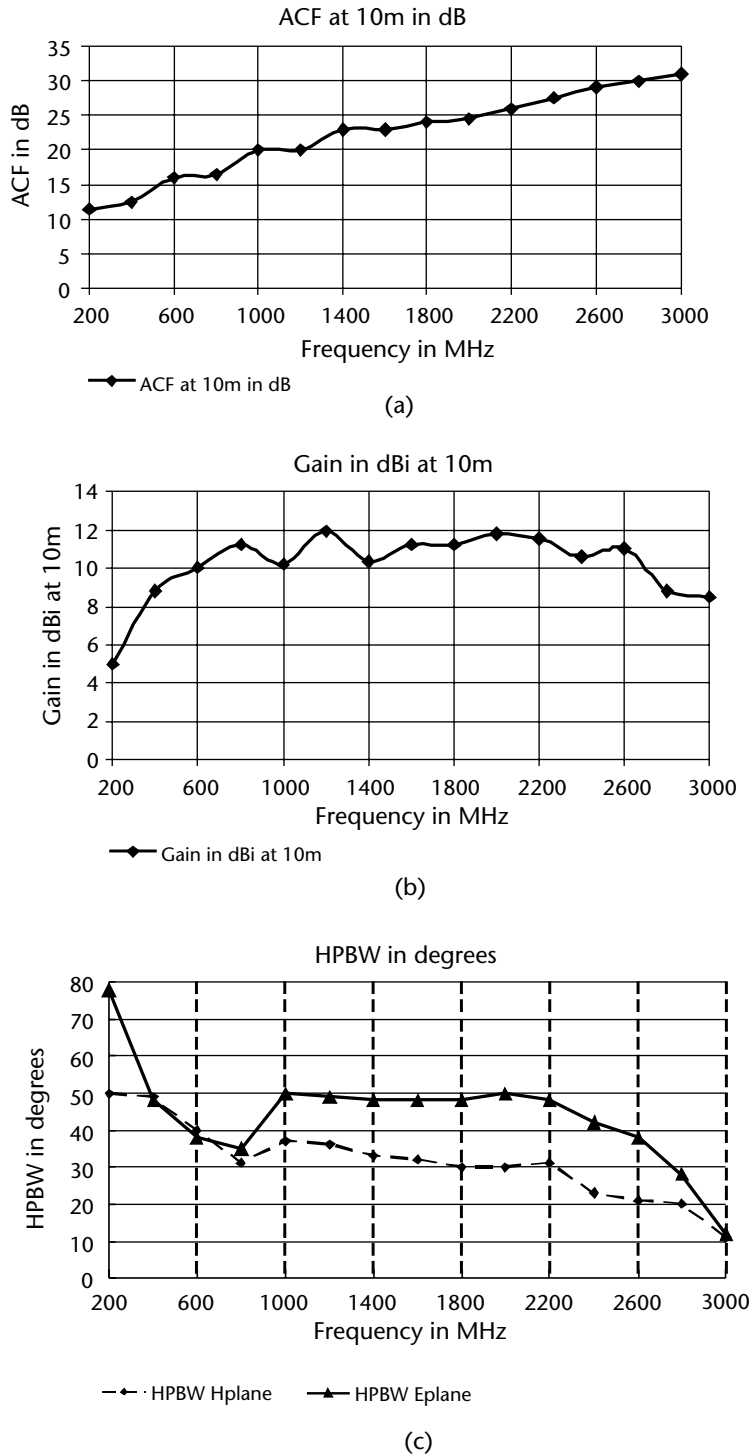


Figure 6.33 The (a) ACF, (b) gain, and (c) HPBWs for a commercially available double-ridged waveguide horn in the frequency range 200 MHz to 3 GHz.

Table 6.3 Comparison between the Far-Field Distances Using the Equivalent Reflector Diameters and Physical Apertures of a Horn

Frequency in GHz	HPBW in H Plane	Equivalent Diameter D_e	Far-Field Distance in (m) Using $2D_e^2/\lambda$	Far-Field Distance in (m) Using $2D^2/\lambda$
1	72	0.242	0.389	0.523
2	62	0.141	0.262	1.045
3	65	0.089	0.159	1.568
5	43	0.081	0.218	2.613
10	38	0.046	0.139	5.226

where

θ_H is the HPBW of the equivalent reflector in degrees;

λ is the wavelength in meters;

D_e is the diameter in meters.

The effective diameter D_e can be calculated at each frequency if we know the HPBWs. The far-field distance is then calculated at each frequency, and these values are listed in column 4 of Table 6.3. The far-field distance using the physical diagonal of the horn of 28 cm, is shown in column 5 of Table 6.3. It can be seen that using these distances the horn would have to be placed much further away (especially at the higher frequencies), with a subsequent reduction in the dynamic range of the whole measurement system. For instance, at 10 GHz the distance would be 5.2m instead of 13.9 cm.

References

- [1] Kraus, J. D., *Antennas*, McGraw-Hill Book Co., International Edition, 1988.
- [2] Bawer, R., and J. J. Wolfe, "The Spiral Antenna," *IRE Int. Conv. Rec.*, No 8, 1960, pp. 84–95.
- [3] Dyson, J. D., "The Equiangular Spiral Antenna," *IRE Trans. on Antennas and Propagation*, April 1959, pp. 181–187.
- [4] Johnson, R. C., and H. Jasik, *Antenna Engineering Handbook*, McGraw-Hill Book Company, 1984.
- [5] Mayes, P. E., and J. D. Dyson, "A Note on the Difference Between Equiangular and Archimedes Spiral Antennas," *IRE Trans. on Microwaves Theory and Techniques*, Vol. 9, March 1961, pp. 203–204.
- [6] Rudge, A. W., K. Milne, A. D. Olver, and P. Knight, *The Handbook of Antenna Design, Volume 1*, Peter Peregrinus Ltd., 1982.
- [7] Wang, J. J. H., and V. K. Tripp, "Spiral Microstrip Antenna Suits EW/ECM Systems," *Microwaves and RF*, December 1993, pp. 147–150.
- [8] Dyson, J. D., "The Unidirectional Equiangular Spiral Antenna," *IRE Trans. on Antennas and Propagation*, October 1959, pp. 329–334.
- [9] Dyson, J. D., "The Characteristics and Design of the Conical Log-Spiral Antenna," *IEEE Trans. Antennas and Propagation*, July 1965, pp. 488–499.

- [10] Wang, J. J. H., and V. K. Tripp, "Design of Multioctave Spiral-Mode Microstrip Antennas," *IEEE Trans. on Antennas and Propagation*, Vol. 39, No. 3, March 1991, pp. 332–335.
- [11] Rappaport, T. S., "Wideband Test Antenna," *RF Design*, April 1988, pp. 37–41.
- [12] Moreno, T., *Microwave Transmission Design Data*, New York Dover Publications Inc., 1948.
- [13] Walton, K. L., and V. C. Sundberg, "Broadband-Ridged Horn Design," *Microwave Journal*, March 1964, pp. 96–101.
- [14] Marcuvitz, N., "Waveguide Handbook," *MIT Rad Lab Series, Volume 10*, McGraw-Hill, 1957, pp. 66–72.

Selected Bibliography

- Bawer, R., and J. J. Wolfe, "Rebuttal," *IRE Trans. on Microwaves Theory and Techniques*, Vol. 9, March 1961, pp. 204–205.
- Nail, J. J., "Designing a Discone Antenna," *Electronics*, August 1953, pp. 167–169.

Calibration of Antennas

This chapter details the calibration of antennas by describing the measurement and calculation of gain, and the calculation of antenna correction factors.

In the measurement of radiated emissions from a device under test (DUT) or in site surveys, antennas provide the interface between the free-space radiated wave and the guided waves (in the transmission line), whose characteristics are measured by the receiver. In susceptibility testing, the antenna is the source of the radiated field and the antenna converts the guided wave from the transmission cable to the free-space wave used to test the DUT.

The field detected by the antenna depends on the spatial orientation (e.g., the direction in which it is pointing), as well as the polarization orientation of the antenna. An antenna (apart from an ideal isotropic one) can receive different proportions of the electric field, depending on the direction in which it is pointing. Along its boresight (the direction of maximum radiation when it is transmitting) it will receive the maximum signal. If a power density of 1 W/m^2 is present at a particular location, and we put an antenna with a linear power gain of 12 at this position, then we will actually measure 12 W/m^2 . Thus, we must know that the linear power gain is 12, in order to deduce that the true power density present is only 1 W/m^2 .

We can either measure or calculate the gain of antennas. Manufacturers usually quote the gains at spot frequencies. The measurement may entail the comparison of the antenna's gain with that of a standard reference antenna. These reference antennas are usually standard gain horns at frequencies above about 1 GHz. At lower frequencies, the reference antennas are usually resonant dipoles.

The antenna detects the electric or magnetic field, but the receiver or analyzer measures the voltage across its input terminals. The signal from the antenna suffers losses between the antenna and the receiver, and thus the conversion between electric field, for example, and the voltage is not a simple matter of relating them by the well known formula of $E = V/h_e$ (where h_e is the effective height of the antenna). A correction factor has to be applied, which is known as the antenna correction factor (or commonly just called the antenna factor), in order to relate the voltage measured by the receiver to the electric field at the antenna location.

7.1 Gain

Let us first consider the difference between directivity and gain. The directivity, or directive gain, is the comparison between a lossless antenna and a fictitious isotropic antenna; whereas the gain (sometimes called the effective gain) is the comparison

between an actual antenna and a particular reference antenna [1, p. 34–21]. The directivity in the case of a transmitting antenna is defined as

$$\text{directivity} = \frac{\text{maximum radiation intensity from a lossless antenna}}{\text{average radiation intensity from an isotropic antenna}} \quad (7.1)$$

The maximum radiation intensity is the maximum power per unit solid angle, and the average radiation intensity from an isotropic antenna is the same as would be obtained if the radiation from an antenna is averaged over a sphere. A similar definition applies to a receiving antenna, since an antenna is a reciprocal device and has the same properties for transmitting as it has for receiving. The directivity does not take into account the heating losses in the antenna, and reflection losses due to the impedance mismatch between the antenna and the generator (or receiver). The gain is defined as the product of the directivity and the efficiency and is given by

$$G = \eta D \quad (7.2)$$

where G is the gain in linear terms (or numeric gain), η is the efficiency as a percentage or fraction, and D is the directivity in linear terms.

The gain and directivity are usually quoted in decibels, in which case the following relation applies

$$G_{\text{dB}} = D_{\text{dB}} + \eta_{\text{dB}} \quad (7.3)$$

where the subscript dB is used to denote the quantities in decibels. Note that since the efficiency is always less than one, η_{dB} is negative.

The efficiency depends on the ohmic (heating) losses in the antenna and the losses due to impedance mismatch between the antenna and the transmission line feeding it. Efficiencies of antennas vary between about 50% and 90%.

Although, strictly speaking, the gain and directivity could apply to any angular position, in practice these terms are only used for boresight or maximum values, unless otherwise specified.

7.1.1 Measurement of Gain

The gain of an antenna can be measured using one, two, or three antennas. The single antenna method requires a smooth, perfectly reflecting metal sheet, and the two antenna method requires two identical antennas. The gain of antennas used as standards are measured, and these standard gain antennas are then compared with the antennas used for testing. These standard gain antennas are not used in test measurements, thus ensuring that they are not damaged. Standard gain antennas are usually smooth-walled pyramidal rectangular horns fed by standard rectangular waveguides. The gain of a pyramidal horn depends mainly on the flare angle, the length of the flare, and the frequency. At lower frequencies, where the horns are too large, resonant dipoles are used, and the gains of unknown antennas are measured by substitution methods.

7.1.1.1 The Friis Transmission Formula

Let us consider the two antennas depicted in Figure 7.1 at a distance R apart. The antenna A is transmitting and the antenna B is the receive antenna.

It can be shown that the effective area A_r , presented by a receiving antenna to a plane wave [2, Chapter 6] is given by

$$A_r = \frac{G_r \lambda^2}{4\pi} \quad (7.4)$$

where A_r is the area of the antenna in squared meters, G_r is the linear (or numeric) gain of the antenna, and λ is the wavelength of the radiation in meters. If the transmitting antenna has a gain of G_t and is radiating a power of P_t watts, then the power density P_d (the power per unit area) at a distance R from the receiving antenna is given by

$$P_d = \frac{P_t G_t}{4\pi R^2} \quad (7.5)$$

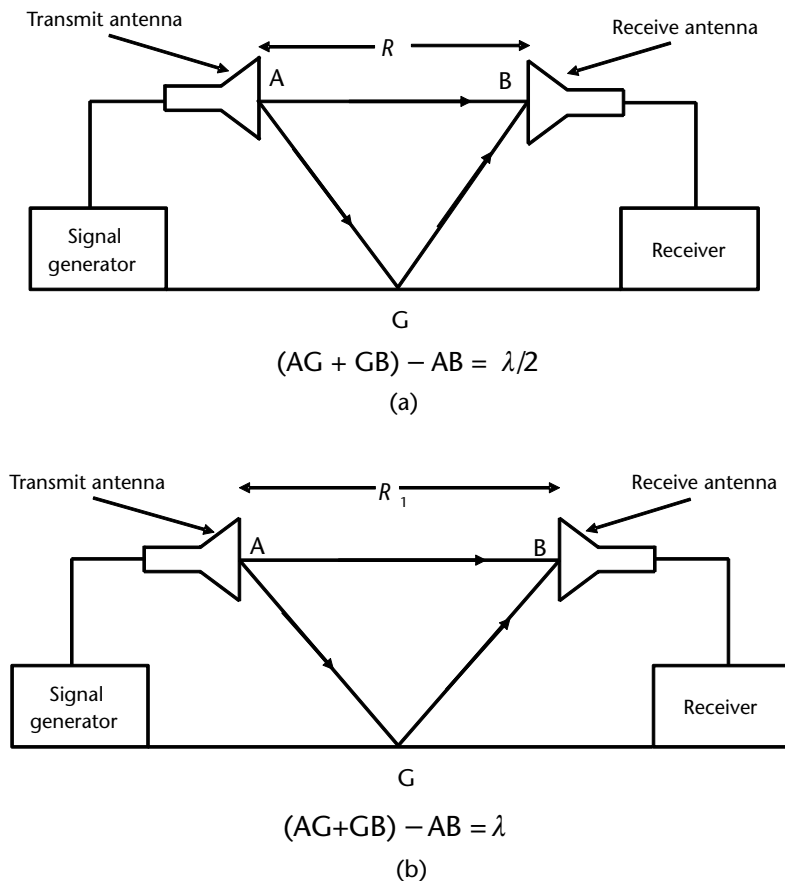


Figure 7.1 Measurement of gain using two antennas: (a) Condition for destructive interference, and (b) condition for constructive interference.

The power P_r received by the antenna B is the power density times the area A_r that it presents to the incident wave, and is given by

$$P_r = P_d A_r = \frac{P_t G_t}{4\pi R^2} \frac{G_r \lambda^2}{4\pi} \quad (7.6)$$

This equation can be rewritten as

$$P_r = P_t G_t G_r \left(\frac{\lambda}{4\pi R} \right)^2 \quad (7.7)$$

It can also be written in decibels as

$$10 \log_{10} P_r = 10 \log_{10} P_t + 10 \log_{10} G_t + 10 \log_{10} G_r + 20 \log_{10} \left(\frac{\lambda}{4\pi R} \right) \quad (7.8)$$

Equation (7.7) is known as the Friis transmission formula. The last term in (7.8) is dependent on the wavelength of the propagating frequency, and on the distance between the antennas. It is known as the space attenuation, or loss factor, L_e . It is always negative in the far field ($R > \lambda/\pi$ for wire antennas, or $> 2D^2/\lambda$ for aperture antennas, where D is the largest dimension of the antenna), but is usually written as a positive quantity since it taken to represent a positive loss rather than a negative gain. Figure 7.2 shows the variation of this space loss or attenuation in decibels L_s versus distance, with frequency as a parameter. The space loss between antennas placed 1λ apart is approximately 22 dB.

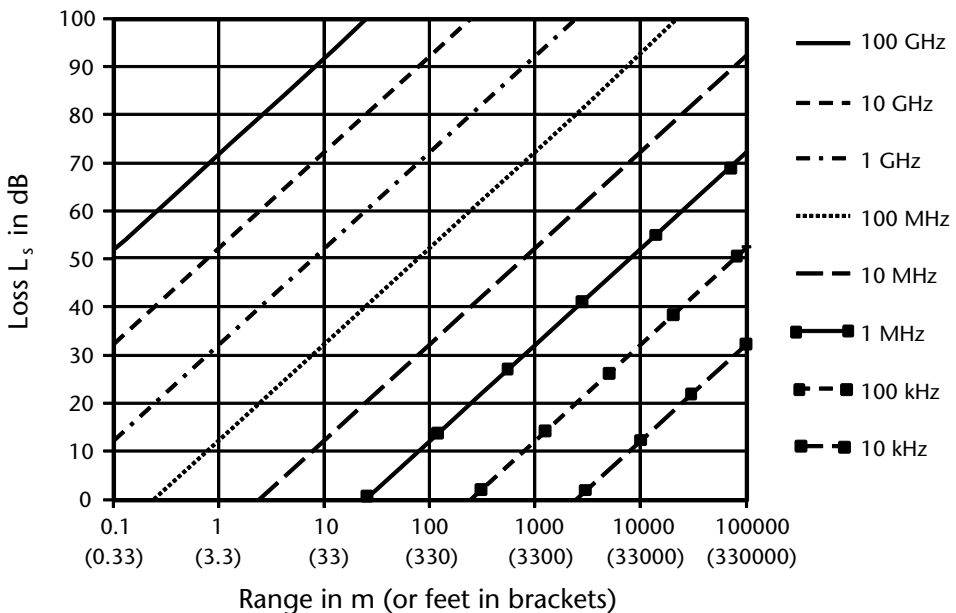


Figure 7.2 Space attenuation versus distance, with frequency as a parameter.

The power P_t transmitted by the transmit antenna is not the same as the power provided by the generator P_g feeding the antenna. There is a loss of power between the antenna and the generator, which depends on the impedance mismatch between the two. This loss of power can be quantified by measuring the complex reflection coefficient of each individually. The complex reflection coefficient of each should be measured to the same reference plane, and a correction term M_t applied to the power output of the generator. The complex reflection coefficient gives the phase as well as the magnitude of the wave reflected by an impedance that is not matched to the characteristic impedance of the system. It can be measured over the whole frequency band of interest by a vector network analyzer, such as a Hewlett-Packard 8510 or a Wiltron 360. The magnitude of the correction term [3, p. 649] is given by

$$M_t = \frac{(1 - |\tau_g|^2)(1 - |\tau_t|^2)}{|1 - \tau_g \tau_t|^2} \quad (7.9)$$

where τ_g and τ_t are the complex reflection coefficients of the generator and transmit antenna, respectively, to the same reference plane. The magnitude (modulus value) of the reflection coefficient is related to the magnitude of the VSWR (voltage standing wave ratio) S , by the following formula

$$|\tau| = \frac{|S - 1|}{|S + 1|} \quad (7.10)$$

The power transmitted by the antenna P_t , and that supplied by the generator P_g , is given by the following relation

$$P_g = P_t M_t \quad (7.11)$$

where M_t is defined by (7.9). If a power meter is used to measure the power from the generator, a correction term has to be applied to the power P_m measured by it. The power P_m is related to the true transmitted power P_g by the following relation

$$P_g = P_m M_m \quad (7.12)$$

The correction term M_m is calculated from the following relation

$$M_m = \frac{(1 - |\tau_m|^2)(1 - |\tau_t|^2)}{|1 - \tau_m \tau_t|^2} \quad (7.13)$$

The received power also requires a similar correction term M_s to be applied to the power measured by the receiver, to allow for the impedance mismatch between the receive antenna and the receiver. The correction term is given by

$$M_s = \frac{(1 - |\tau_t|^2)(1 - |\tau_s|^2)}{|1 - \tau_t \tau_s|^2} \quad (7.14)$$

where τ_r and τ_s are the complex reflection coefficients of the receive antenna and the receiver, respectively, at the same reference plane.

The correction terms M_t and M_s can be replaced by a combined correction term C , which is in decibels and is given by

$$C = 10\log_{10} M_t + 10\log_{10} M_s \quad (7.15)$$

If the transmit and receive antennas do not have the same polarization, then a correction for the polarization mismatch must be used in addition to the correction term of (7.15). If the polarization mismatch is P_{tr} in linear terms, then the correction term C_p in decibels is given by

$$C_p = 10\log_{10} P_{tr} \quad (7.16)$$

Other factors to be taken into consideration are the errors due to near-field effects and multipath effects. The near-field effects are due to: (1) the fact that the near-field components may not have decreased to negligible values at the far-field distance of $2D^2/\lambda$ or λ/π (the magnitude of this correction term is of the order of 0.05 dB); and (2) there is a variation of the electric field across the aperture of the receive antenna. This is known as an amplitude taper and a variation of 0.25 dB can give rise to an error of about 0.1 dB in the magnitude of the gain measurement. Thus, the total errors due to these near-field or proximity effects are of the order of 0.15 dB [3, p. 650].

The multipath effects are caused by interference between the direct wave (from the transmitter to receiver antennas) and the waves that arrive at the receive antenna after reflection. Depending on the relative phases of the waves, constructive or destructive interference can result. When the antennas are separated by less than $2D^2/\lambda$ or λ/π then the multipath interference is primarily due to multiple reflections between the two antennas, whereas at greater distances the multipath interference is mainly the result of reflections from the ground and other objects. The presence of multipath interference can be investigated by varying the distance between the antennas. If multipath effects are present, then the receiver connected to the receive antenna will show an output that resembles a sine wave as the distance between the antennas is increased (or decreased). This is due to the phase differences between the path lengths of the direct and reflected waves; when this path difference is an odd multiple of half-wavelengths, the receiver's output has its minimum value, and when this path difference is a whole number of wavelengths, the output has its maximum value. The direct wave (AB) and a single wave that has undergone one reflection (AG + GB) is depicted in Figure 7.1. When the distance is R , this difference is $\lambda/2$, as shown in Figure 7.1(a), and destructive interference occurs. When this distance is increased to R_1 the difference is λ , as shown in Figure 7.1(b), and constructive interference occurs. In practice there will be more than one reflected wave and some reflected waves will undergo more than one reflection. The measurement also requires that both the transmit and receive antennas are maintained at boresight (i.e., the positions of maximum radiation of the two antennas are collinear).

7.1.2 Purcell's Method

This method is sometimes called the mirror method and involves the use of just one antenna to perform the calibration. The set-up consists of a transmitting antenna such as a pyramidal horn (as shown in Figure 7.3) placed in front of a square

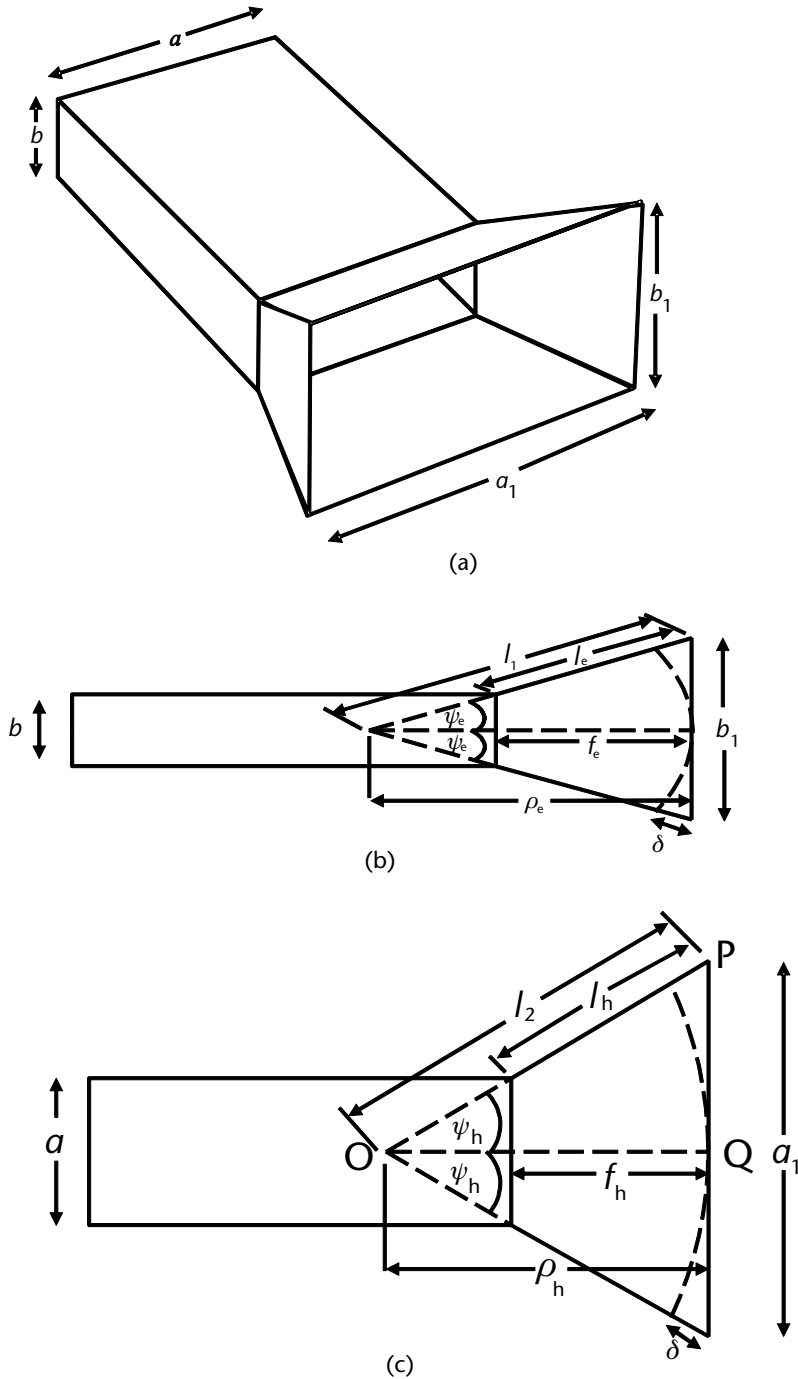


Figure 7.3 Pyramidal horn: (a) Perspective view, (b) side elevation—E plane, and (c) plan view—H plane.

metal reflecting sheet, as shown in Figure 7.4, and the power is received by the same antenna.

The sheet reflects power P_m which can be assumed to come from an image antenna placed as far behind the sheet as the real antenna is in front of it. The normal far-field distance criterion of $R = 2D^2/\lambda$ should be maintained between the antenna and its image, so that the distance between the antenna and the sheet is $R/2 = D^2/\lambda$, where D is the largest dimension of the horn. The sheet should be flat to at least one-sixteenth of a wavelength (see Figure 7.4(c)), and it must be planar to avoid errors in the position and dimensions of the image antenna. The sheet should be large so that diffraction effects at its edges are negligible, and its side h should also be large enough to intercept the main beam [4, p. 585] of width θ ($= 2\lambda/D$) radians between nulls. This results in the following condition, which is shown in Figure 7.4(b).

$$\frac{h/2}{R/2} \geq \frac{\lambda}{D} \quad (7.17)$$

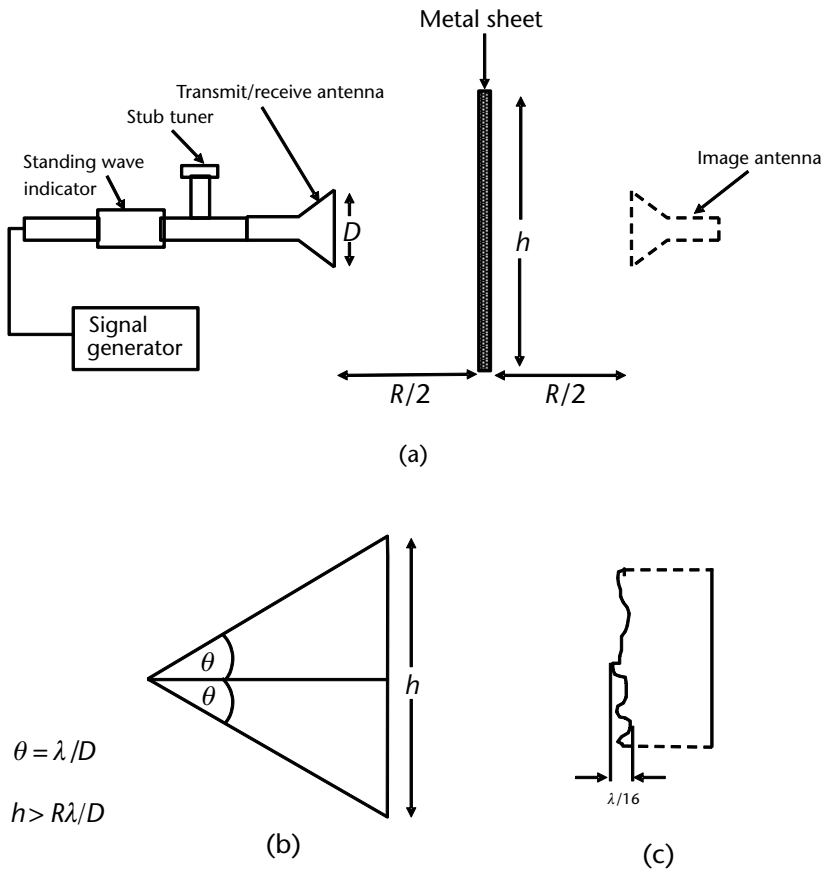


Figure 7.4 Purcell's method for measurement of gain: (a) Measurement set-up for Purcell's method, (b) minimum size for side of sheet, and (c) enlarged view showing smoothness of sheet.

where h is the length of one side of the sheet, R is the distance between the horn and its image, and D is the largest dimension of the horn. This gives the lower limit for h of

$$h \geq \frac{R\lambda}{D} \quad (7.18)$$

For single-frequency measurements using a pyramidal horn, the set-up of Figure 7.4(a) applies. The horn is connected to the signal generator via a standing wave detector (SWD) and a stub tuner. When the transmitted and reflected waves interfere, a standing wave results. The ratio of the maximum to minimum voltage of the standing wave is the VSWR (voltage standing wave ratio). The SWD consists of a probe that is inserted through a longitudinal slot along the center of the broad wall of the rectangular waveguide. The probe can be moved along the longitudinal axis of the waveguide, and its depth into the waveguide can be varied. The probe is connected to a detector (usually a diode), and the detector output is measured on a meter. The probe carriage is moved longitudinally along the axis of the waveguide to record the maximum and minimum values of the standing wave in the waveguide. If there is a very small standing wave, then the ratio of maximum to minimum voltage will be small, and this ratio is one when there is no reflected wave. This condition exists when the waveguide is perfectly matched. When there is a large reflected wave, the VSWR is also large and approaches infinity when the reflected wave is equal to the transmitted wave. The procedural steps for measuring the gain of a pyramidal horn, as shown in Figure 7.3, are now given:

1. The horn is connected to the stub tuner, SWD, and signal generator, and allowed to radiate into free space.
2. The horn is matched to the waveguide run by adjusting the stub tuner (usually a three stub tuner) so that the SWD indicates that the VSWR is very small.
3. The metal sheet is then placed at a distance d ($= R/2$) in front of the horn, such that d is greater than or equal to D^2/λ .
4. The VSWR is measured using the SWD. In the Friis transmission formula, the distance R between the transmitting and receiving horns is now the distance between the horn and its image. The distance between the horn and the metal sheet in Figure 7.4 is d , and thus the distance between the transmit horn and its image is $2d$. Thus $R = 2d$ and (7.7) can be rewritten as

$$P_r = P_t G_t G_r \left(\frac{\lambda}{8\pi d} \right)^2 \quad (7.19)$$

Since the same horn is used for transmitting and receiving, the gains of G_r and G_t can both be replaced by the common value of G . Equation (7.19) thus becomes

$$P_r = P_t G^2 \left(\frac{\lambda}{8\pi d} \right)^2 \quad (7.20)$$

The square root of the ratio of P_r to P_t is the magnitude of the reflection coefficient $|\tau|$, and is given by

$$\sqrt{\frac{P_r}{P_t}} = |\tau| = \frac{G\lambda}{8\pi d} \quad (7.21a)$$

which can be rewritten in the following form

$$\frac{1}{|\tau|} = \frac{8\pi d}{G\lambda} \quad (7.21b)$$

The magnitude of the reflection coefficient τ is related to the VSWR S by the following equation

$$|\tau| = \frac{S-1}{S+1} \quad (7.22)$$

The distance d is varied, the VSWR is measured in each case and the magnitude of the reflection coefficient is calculated. A plot of $|\tau|$ against $1/d$ is shown in Figure 7.5. The plot should give us a straight line, and the slope yields the value of the constant ($8\pi/G\lambda$) on the right hand side of (7.21b), from which G can be calculated at each value of λ . In practice, a straight line is not obtained, because of the edge effects, measurement errors, and the fact that the transmitting horn reradiates some of the power reflected from the sheet. With the measured results shown in Figure 7.5, the best straight line gives a slope of approximately 18. In this case, the frequency at which the measurements were performed was 10 GHz, so that $\lambda = 0.03\text{m}$. The value of linear gain G calculated is thus 45.6, equating to a gain of 16.7 dB.

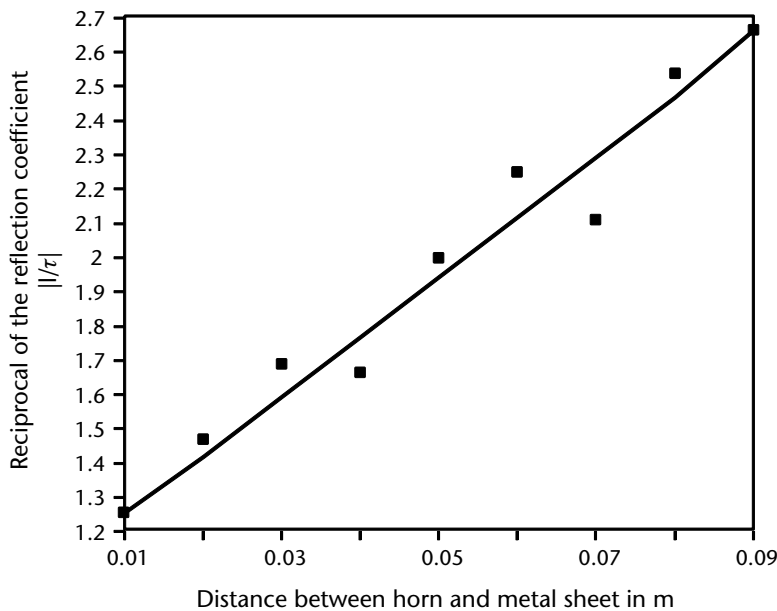


Figure 7.5 Purcell's method measured results.

In the case of swept frequency measurements, the SWD and meter are replaced by a dual directional coupler and connected to a network analyzer. The return loss (from which the VSWR can be calculated) is measured over the whole frequency range of interest, but the principle of the measurement is the same as in the single-frequency measurements described above.

7.1.3 Two-Antenna Method

The Friis formula of (7.7) is used to determine the gain of antennas by employing two identical antennas. The Friis formula can be rewritten for the two antennas as

$$G = \sqrt{\left[\frac{P_r}{P_t}\right] \left(\frac{4\pi R}{\lambda}\right)^2} \quad (7.23)$$

where G is the linear (or numeric) gain of either antenna, P_r is power transmitted by one antenna, and P_t is the power received by the other antenna. Since the gain is usually required in decibels, and the transmitted and received powers are also usually measured in decibels, (7.23) is more conveniently given in decibels in the following form

$$g_{\text{dB}} = \frac{1}{2} \left[20 \log_{10} \left(\frac{4\pi R}{\lambda} \right) - 10 \log_{10} \left(\frac{P_t}{P_r} \right) \right] \quad (7.24)$$

Alternatively, (7.24) can be rewritten in the following form

$$g_{\text{dB}} = \frac{1}{2} \left[20 \log_{10} \left(\frac{4\pi R}{\lambda} \right) + 10 \log_{10} \left(\frac{P_r}{P_t} \right) \right]$$

Note that the ratio of P_t to P_r is inverted, and the sign of its log is changed since

$$-\log_{10} \left(\frac{P_t}{P_r} \right) = +\log_{10} \left(\frac{P_r}{P_t} \right)$$

The received and transmitted powers P_r and P_t are measured, and the correction terms of (7.15) are applied to obtain the corrected values. The principle of the measurement set-up is shown in Figure 7.1, and the checks to ensure that multipath effects are minimised should be undertaken. The distance R between the two antennas is varied to give several values for the received and transmitted powers at each frequency. The average value for the gain can then be calculated from (7.24).

7.1.4 Three-Antenna Method

If two identical antennas are not available, then the gain measurements can be performed by using three antennas. The same measurements as described in Section 7.1.3 are performed with two of the antennas each time. Three sets of measurements

will be required altogether to cover all the combinations. This will result in three simultaneous equations, given by

$$g_1 + g_2 = 20\log_{10}\left(\frac{4\pi R}{\lambda}\right) + 10\log_{10}\left(\frac{P_r}{P_t}\right)_{1,2} \quad (7.25)$$

with antenna 1 used for transmitting and antenna 2 used for receiving

$$g_1 + g_3 = 20\log_{10}\left(\frac{4\pi R}{\lambda}\right) + 10\log_{10}\left(\frac{P_r}{P_t}\right)_{1,3} \quad (7.26)$$

with antenna 1 used for transmitting and antenna 3 used for receiving

$$g_2 + g_3 = 20\log_{10}\left(\frac{4\pi R}{\lambda}\right) + 10\log_{10}\left(\frac{P_r}{P_t}\right)_{2,3} \quad (7.27)$$

with antenna 2 used for transmitting and antenna 3 used for receiving. In (7.25) to (7.27), g_1 , g_2 , and g_3 are the gains in decibels of the first, second, and third antennas, respectively. The measurement involving each pair of antennas is the same as in the case of the two-antenna method of Section 7.1.3. The precautions and correction terms described in Section 7.1.1 also apply in this case. The MIL-STD-461 generally requires 1m antenna separation, whereas commercial specs require a 10m separation.

7.2 Calculation of Gain

The rectangular pyramidal horn is the most commonly used standard horn, and thus the method of calculation of its gain alone is included here. A pyramidal horn, such as the one shown in Figure 7.3, is fed by a standard rectangular waveguide, and the walls of the guide flare in both the E and H planes. The angle of flares and length of the flared section determines the final dimensions of the open mouth of the horn, which in turn determines the gain of the horn.

The gain of a horn depends on:

The dimensions a and b of the rectangular waveguide feeding the horn;

The dimensions a_1 and b_1 of the open end of the horn;

The slant lengths l_e and l_h in E and H planes of the flared section;

The flare angles $2\psi_e$ and $2\psi_h$ in the E and H planes, respectively.

The formulas are given for calculating the total gain of the pyramidal horn. This gain is dependent on the individual gains G_e and G_h that would be obtained by having E - and H -plane sectoral horns with the same flare angles. As long as the aperture of the pyramidal horn in each plane is at least one wavelength, the pattern in one plane is substantially independent of the aperture in the other plane

[5, p. 648]. In order to compute the gain of a pyramidal horn, we may therefore calculate the gains of individual E - and H -plane sectoral horns, and the product of these linear (or numeric) gains together with the efficiency will give us the gain of the pyramidal horn.

7.2.1 E -Plane Sectoral Horn

In the E -plane sectoral horn depicted in Figure 7.6, we can see that the broad walls of the waveguide are flared in the direction parallel to the electric field vector, and the flare angle is $2\psi_e$. The narrow dimension of the guide is increased from b to b_1 at the open mouth of the horn, whereas the broad dimension a remains at the same value. The flared walls have a virtual apex, and the virtual lengths l_1 to the open end are longer than the length ρ_e (the virtual perpendicular distance) by δ . This difference causes the spherical waves emanating from the virtual apex to have a phase difference at the edges of the horn (compared with the wavefronts at the center of the horn). This phase difference (Fermat's principle) is given by

$$\phi = \frac{2\pi\delta}{\lambda} \quad (7.28)$$

where ϕ is the phase difference in radians and λ is the wavelength. Both δ and λ are required to be in the same units. When the phase difference is π , the waves from the edges are in antiphase with those from the center, so that they destructively interfere resulting in a decrease in the gain and an increase in the sidelobe level.

In order to obtain universal relationships between the phase deviation δ and the loss in gain associated with it, it is convenient to express δ in terms of wavelengths. Consider triangle OPQ in Figure 7.6(b). Using Pythagoras' theorem, we can see that

$$\rho_e^2 = l_1^2 - \left(\frac{b_1}{2}\right)^2 \quad (7.29)$$

But since ρ_e is equal to $l_1 - \delta$

$$(l_1 - \delta)^2 = l_1^2 - \frac{b_1^2}{4} \quad (7.30)$$

$$l_1^2 - 2l_1\delta + \delta^2 = l_1^2 - \frac{b_1^2}{4}$$

$$2l_1\delta + \delta^2 = \frac{b_1^2}{4} \quad (7.31)$$

However, since δ is much smaller than the length l_1 , δ^2 is negligible compared with $2l_1\delta$ and can therefore be ignored. Equation (7.31) thus reduces to

$$\delta = \frac{b_1^2}{8l_1} \quad (7.32)$$

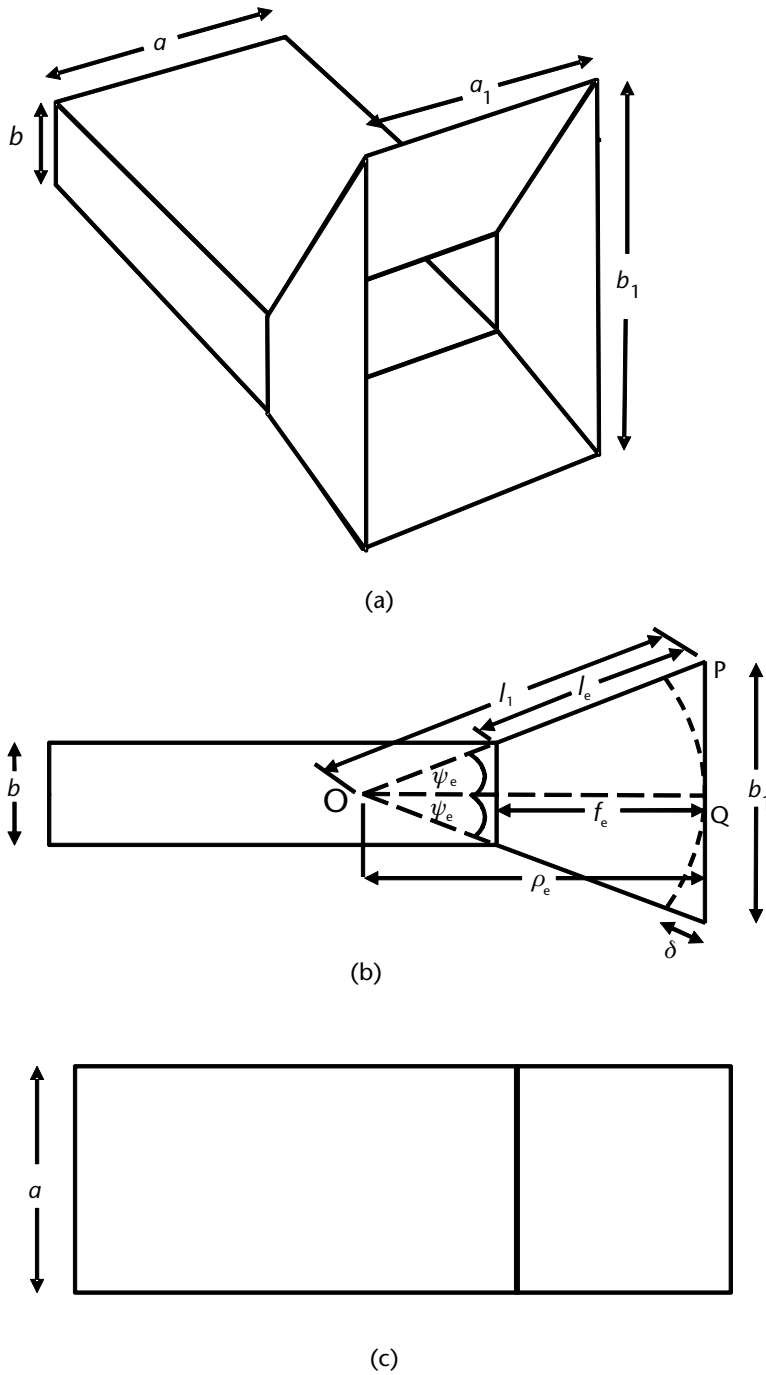


Figure 7.6 E-plane sectoral horn: (a) Perspective view, (b) side elevation, and (c) plan view.

where b_1 is the height of the open mouth of the horn and l_1 is the virtual length of the flared section. The phase deviation, or error T_e in terms of wavelength, is given by

$$T_e = \frac{\delta}{\lambda} = \frac{b_1^2}{8l_1\lambda} \tag{7.33}$$

7.2.1.1 Loss Due to Phase Error

The efficiency of the horn is reduced by the phase error at the open mouth, so that the effective aperture is only about 50% of the actual aperture. This means that efficiencies as low as 50% are to be expected. Thus, the gain could be only half the magnitude of the directivity, or 3 dB less when they are both expressed in decibels.

Dielectric loading of the horn can be used to correct the phase error, so that a uniform phase is obtained across the aperture. Efficiencies as high as 90% are achievable with zero phase taper and uniform amplitude illumination of the mouth of the horn.

The loss in gain due to the phase error is plotted in Figure 7.7 for an *E*-plane sectoral horn. The loss L_e (in decibels) is shown as a function of T_e and T_{es} , and has been given in terms of the virtual slant length l_1 of the flare [1, p. 10–8] as

$$T_e = \frac{\delta}{\lambda} = \frac{(b_1)^2}{8l_1\lambda} \tag{7.34}$$

However, it is more useful to have T_e in terms of the physical slant length l_e of the flared section, which can be easily measured.

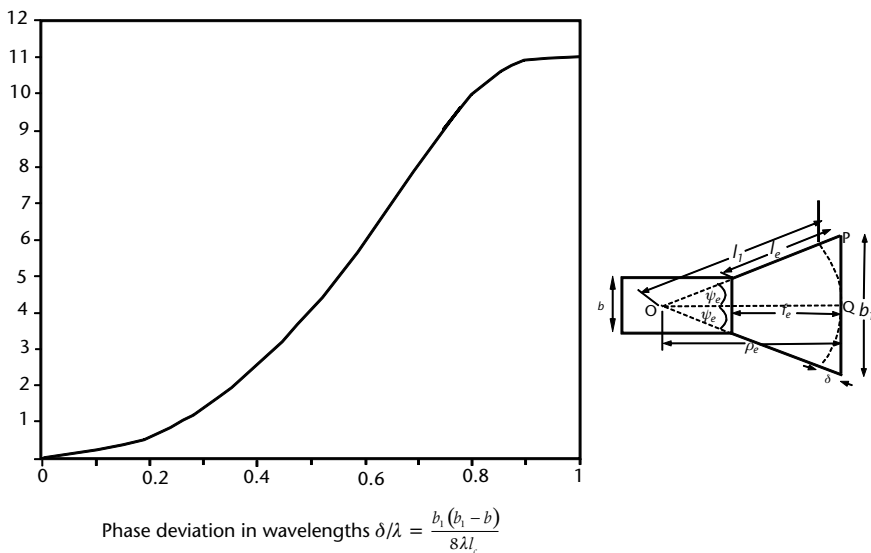


Figure 7.7 Variation of loss with phase deviation—*E*-plane sectoral horn.

Referring to Figure 7.6(b), we can see that the flare semi-angle ψ_e is given by

$$\begin{aligned}\sin \psi_e &= \frac{b_1/2}{l_1} = \frac{(b_1 - b)/2}{l_e} \\ \frac{b_1}{l_1} &= \frac{b_1 - b}{l_e}\end{aligned}\quad (7.35)$$

Thus, T_e can be rewritten in terms of l_e as

$$T_e = \frac{b_1(b_1 - b)}{8\lambda l_e} \quad (7.36)$$

The maximum gain of a horn is directly proportional to the size of its aperture. We can increase the aperture by having a large flare angle, and/or by having a long flare length. However, in order to restrict the phase variation at the open end, we must have a long horn with a small flare angle. While this can be attained at high (millimeter wave) frequencies with relatively small horns, the horns become impractically large at lower frequencies. Thus, some compromise must be sought between the flare angle and the length f_e of the flared section for a particular value of δ . We can see from Figure 7.6(b) that the relationship between the flare semi-angle ψ_e and the virtual length l_1 is given by

$$\begin{aligned}\cos \psi_e &= \frac{\rho_e}{l_1} \text{ or } \cos \psi_e = \frac{\rho_e}{\rho_e + \delta} \\ \rho_e &= (\rho_e + \delta) \cos \psi_e \\ \rho_e(1 - \cos \psi_e) &= \delta \cos \psi_e \\ \rho_e &= \frac{\delta \cos \psi_e}{(1 - \cos \psi_e)}\end{aligned}\quad (7.37)$$

Thus, for a specific value of δ , we can relate the flare angle to the flare length ρ_e . The value of δ that can be tolerated depends on the type of sectoral horn. In the case of the E -plane horn, the maximum value of δ is a quarter of a wavelength at the highest frequency of operation. This gives a phase difference of 90 degrees, or $\pi/2$ radians.

Figure 7.8 shows the variation of the virtual flare length ρ_e with flare semi-angle for a phase error of 90 degrees at 100 MHz, 1 GHz, and 10 GHz. Note that for a given flare semi-angle, the permissible maximum flare length is much smaller at high frequencies than it is at lower frequencies. For instance, for a flare semi-angle of 30 degrees, the maximum permissible flare length at 10 GHz is only about 5 cm, whereas it is 4.8m at 100 MHz.

Since the virtual length ρ_e is not easy to measure, it is more convenient to show the variation of the flare semi-angle ψ_e in terms of the physical lengths l_e of the flared section and the heights b and b_1 (of the waveguide and horn, respectively). Referring to Figure 7.6(b), we can see that

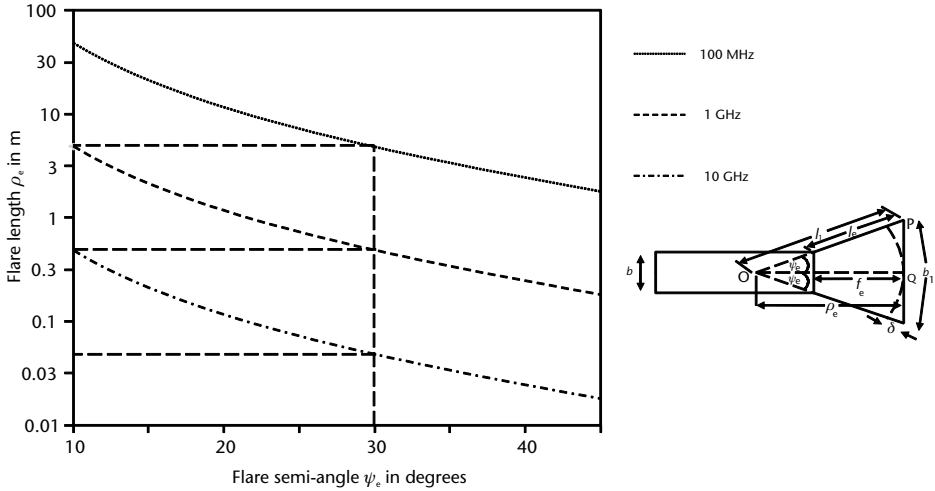


Figure 7.8 Variation of flare length with flare semi-angle for an *E*-plane horn.

$$\tan \psi_e = \frac{b_1}{2\rho_e} = \frac{b_1 - b}{2f_e}$$

$$\rho_e = \left(\frac{b_1}{b_1 - b} \right) f_e$$

and

$$f_e = \sqrt{\rho_e - \left(\frac{b_1 - b}{2} \right)^2}$$

Thus,

$$\rho_e = \left(\frac{b_1}{b_1 - b} \right) \sqrt{l_e^2 - \left(\frac{b_1 - b}{2} \right)^2} \tag{7.38}$$

7.2.1.2 Gain of an *E*-Plane Horn

The numeric or linear gain G_e of an *E*-plane horn is given by the following formula [6, p. 546]:

$$G_e = \frac{64a\rho_e}{\pi\lambda b_1} \left[C^2 \left(\frac{b_1}{\sqrt{2\pi\rho_e}} \right) + S^2 \left(\frac{b_1}{\sqrt{2\pi\rho_e}} \right) \right] \tag{7.39}$$

where a is the width of the waveguide feeding the horn, ρ_e is the virtual length of the horn, b_1 is the height of the open mouth of the horn, C is the Fresnel cosine integral, and S is the Fresnel sine integral.

The Fresnel cosine and sine integrals are defined by the following relationships

$$C(x) = \int_0^x \cos\left(\frac{\pi}{2}x^2\right)dx$$

$$S(x) = \int_0^x \sin\left(\frac{\pi}{2}x^2\right)dx$$

The values of the Fresnel cosine and sine integrals are shown in Figure 7.9.

The gain of an E -plane horn has been calculated using (7.39) for different values of ρ_e , to give the normalized curves of Figure 7.10, which show the gains divided by the width a (in terms of the wavelength). It should be noted that the gains increase to a maximum in each case as b_1/λ is varied, and then start to decrease again. Closer examination of these curves show that the value of the phase deviation at these maxima is 0.25λ . For instance in the case of a horn of length 8λ , the maximum occurs at $b_1/\lambda = 4$, resulting in a value of T_e equal to 0.25, and thus $\delta = 0.25\lambda$. This corresponds to a phase error of 90 degrees or $\pi/2$ radians which is the maximum phase error that can be tolerated for an E plane horn.

7.2.2 H -Plane Sectoral Horn

In the H -plane sectoral horn depicted in Figure 7.11, we can see that the narrow walls of the waveguide are flared in the plane parallel to the magnetic field vector, and the flare angle is $2\psi_b$. The broad dimension of the guide is increased from a to a_1 at the open mouth of the horn, whereas the narrow dimension, or height b , remains at the same value. The flared walls have a virtual apex, and the virtual lengths l_2

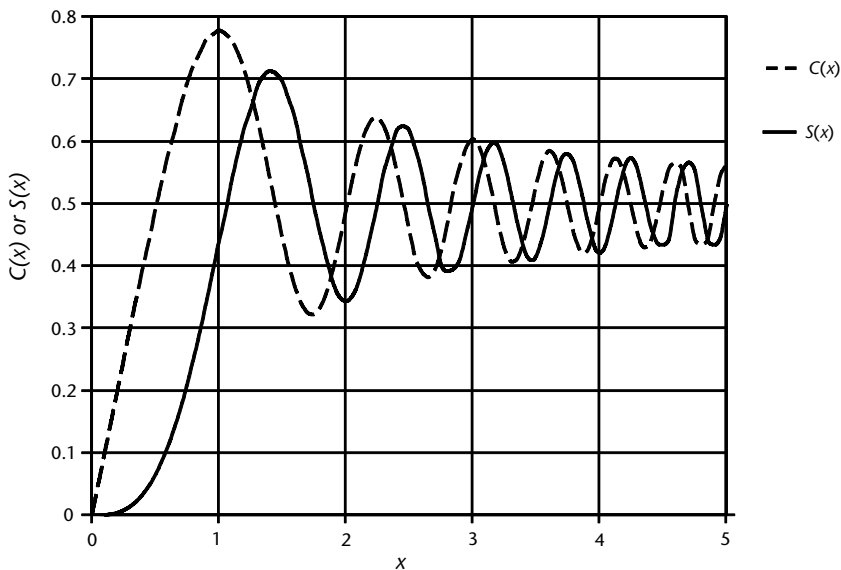


Figure 7.9 Fresnel cosine and sine integrals.

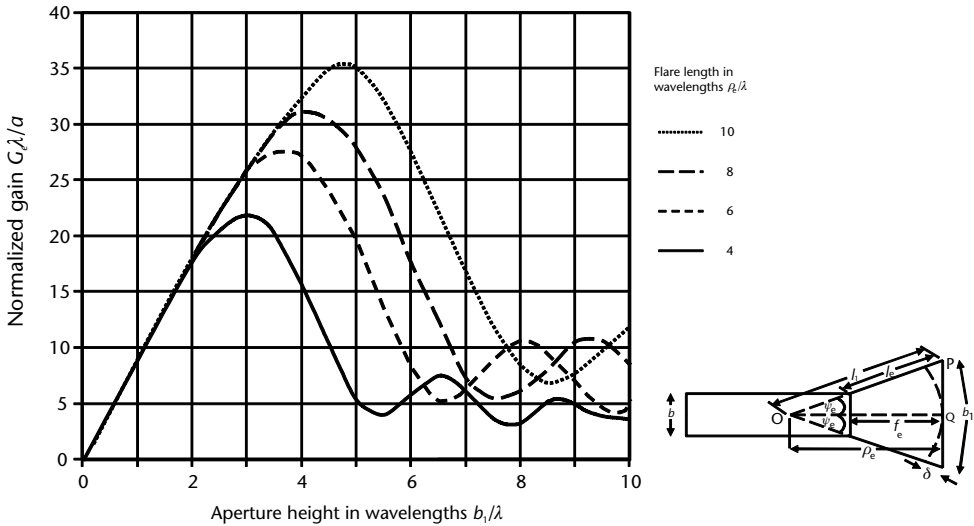


Figure 7.10 Normalized gain for an E-plane sectoral horn.

to the open end are longer than the length ρ_b (the virtual perpendicular distance) by δ . This difference causes the spherical waves emanating from the virtual apex to have a phase difference at the edges of the horn (compared with the waves from the center of the horn). This phase difference results in a loss in gain, as in the case of the E-plane horn described in Section 7.2.1, however, in this case, a larger phase difference can be tolerated. Instead of 90 degrees, a maximum phase difference of 135 degrees can be tolerated for the H-plane sectoral horn when the electric field vector is perpendicular to the H-plane. This phase difference corresponds to a value of δ equal to $3\lambda/8$.

The phase deviation or error in terms of wavelengths T_b can be derived in a similar manner to the case of the E-plane horn, and is given by

$$T_b = \frac{\delta}{\lambda} = \frac{a_1^2}{8l_2\lambda} \tag{7.40}$$

where a_1 is the width of the aperture of the horn and l_2 is the virtual slant length of the flared section.

7.2.2.1 Loss Due to Phase Error

The efficiency of the horn is reduced by the phase error at the open mouth, and the effective aperture is only about 50% of the physical aperture. Thus, the gain could only be half the magnitude of the directivity.

Dielectric loading of the horn can be used to correct the phase error, so that a uniform phase is obtained across the aperture. Efficiencies as high as 90% are achievable with zero phase taper and uniform amplitude illumination of the mouth of the horn.

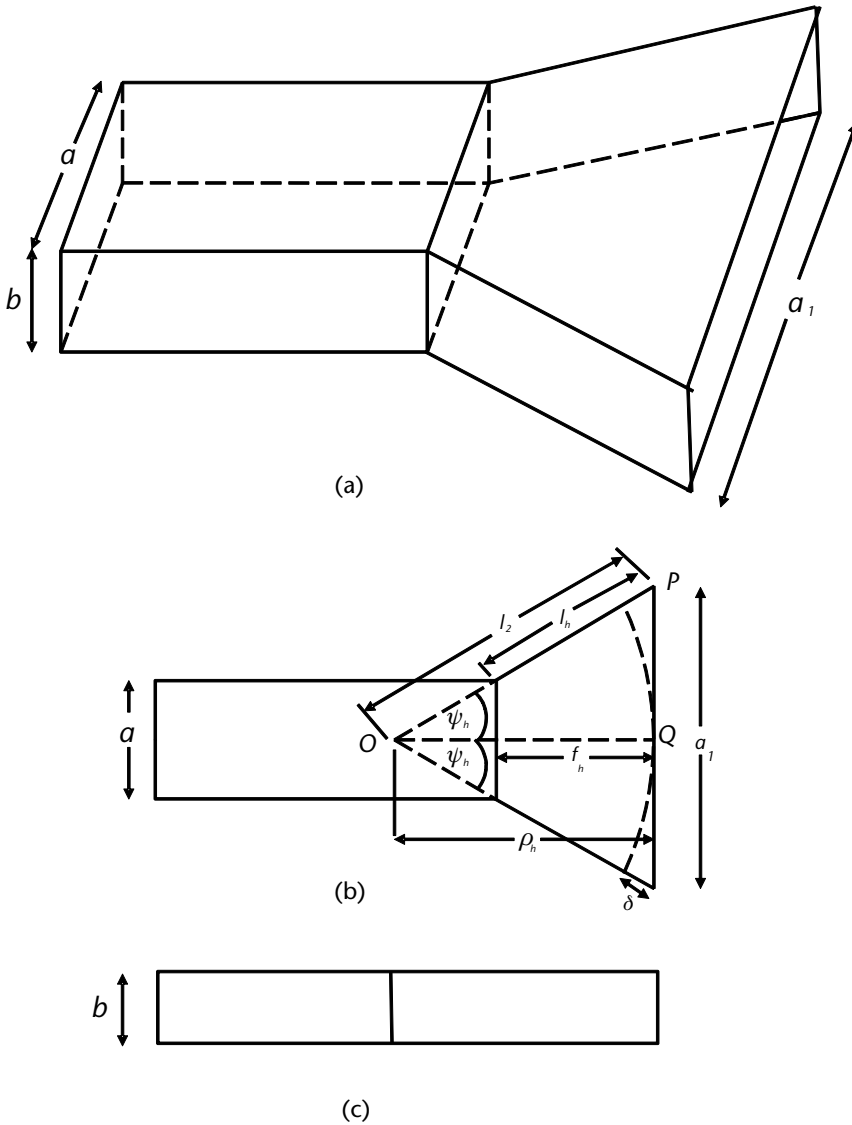


Figure 7.11 H-plane sectoral horn: (a) Perspective view, (b) plan view, and (c) side view.

The loss in gain due to the phase error is plotted in Figure 7.12 for an H-plane sectoral horn. The loss L_b is in decibels, against T_b , has been given in terms of the virtual slant length l_2 [1, p. 10–8] which is the virtual length of the flared section. However, it is more useful to have T_b in terms of the physical slant length l_b of the flared section, which can be easily measured.

Referring to Figure 7.11(b), we can see that the flare semi-angle ψ_b is given by

$$\sin \psi_b = \frac{a_1/2}{l_2} = \frac{(a_1 - a)/2}{l_b} \tag{7.41}$$

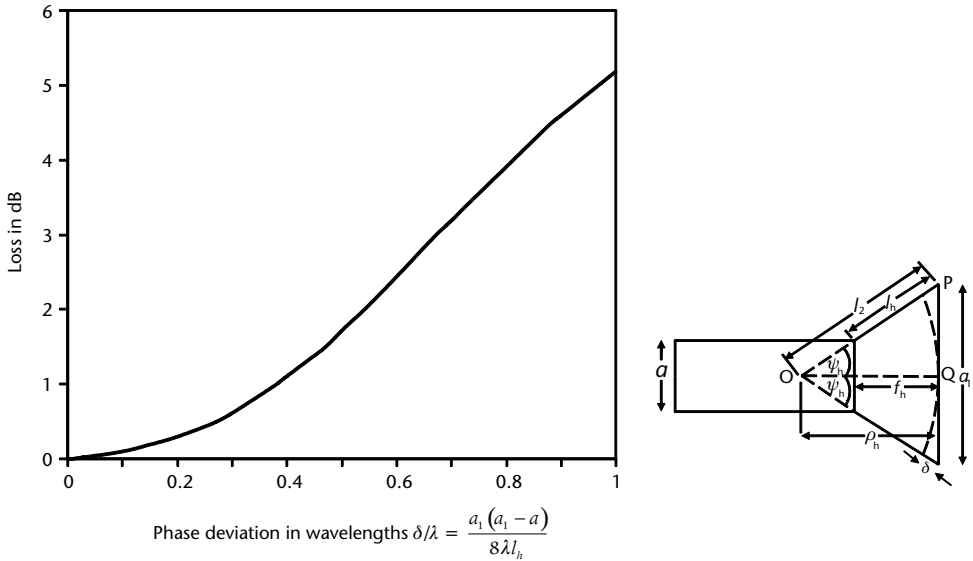


Figure 7.12 Variation of loss with phase deviation for an *H*-plane sectoral horn.

Thus, T_b can be rewritten in terms of l_b as

$$T_b = \frac{a_1(a_1 - a)/2}{8\lambda l_h} \tag{7.42}$$

The maximum gain of a horn is directly proportional to the size of its aperture. We can increase the aperture by having a large flare angle, and/or by having a long flare length. However, in order to restrict the phase variation at the open end, we must have a long horn with a small flare angle. While this can be attained at high (millimeter wave) frequencies with relatively small horns, the horns become impracticably large at lower frequencies. Thus, some compromise must be sought between the flare angle and the length l_b of the flared section for a particular value of δ . We can see from Figure 7.11(b) that the relationship between the flare semi-angle ψ_h and the virtual length l_2 is given by

$$\begin{aligned} \rho_h &= (\rho_h + \delta)\cos\psi_h \\ \rho_h(1 - \cos\psi_h) &= \delta\cos\psi_h; \quad \rho_h = \frac{\delta\cos\psi_e}{(1 - \cos\psi_e)} \end{aligned} \tag{7.43}$$

where ψ_b is the flare semi-angle in degrees, and ρ_b is the virtual length of the flare. Thus, for a specific value of δ we can relate the flare angle to the flare length l_2 . The value of δ that can be tolerated depends on the type of sectoral horn. In the case of the *H*-plane horn, the maximum value of δ is three-eighths of a wavelength at the highest frequency of operation. This gives a phase difference of 135 degrees, or $3\pi/4$ radians.

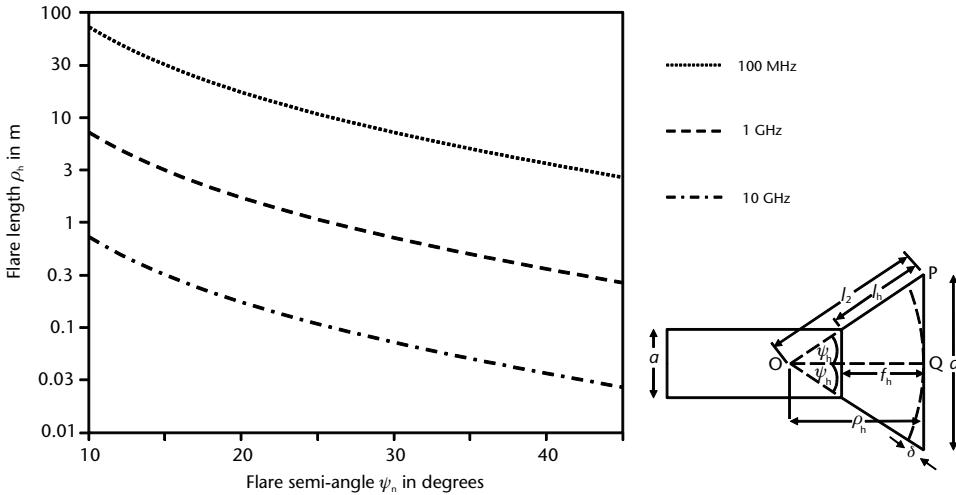


Figure 7.13 Variation of flare length with flare semi-angle for an *H*-plane horn.

Figure 7.13 shows the variation of the virtual flare length ρ_b with flare semi-angle for a phase error of 135 degrees at 100 MHz, 1 GHz, and 10 GHz. Note that for a given flare semi-angle, the maximum permissible flare length is much smaller at high frequencies than it is at lower frequencies. For instance, for a flare semi-angle of 30 degrees, the maximum permissible flare length at 10 GHz is only about 7.3 cm, whereas it is 7.3m at 100 MHz. However, these lengths are about 67% larger than those for an *E*-plane sectoral horn with the same flare angles. Thus, a longer flare length can be tolerated in the *H*-plane sectoral horn than in the *E*-plane sectoral horn.

The virtual flare length ρ_b is related to the physical flare length l_b and the widths a and a_1 of the waveguide and the horn, respectively, by the following expression

$$\rho_b = \left(\frac{a_1}{a_1 - a} \right)_e \sqrt{(l_b)^2 - \left(\frac{a_1 - a}{2} \right)^2} \tag{7.44}$$

7.2.2.2 Gain of an *H*-Plane Sectoral Horn

The linear or numeric gain G_b of an *H*-plane sectoral horn [6, p. 561] is given by

$$G_b = \frac{4\pi b \rho_b}{a_1 \lambda} \left\{ [C(u) - C(v)]^2 - [S(u) - S(v)]^2 \right\} \tag{7.45}$$

where b is the height of the waveguide feeding the horn, ρ_b is the virtual length of the horn, a_1 is the width of the horn aperture, $C(u)$ is the Fresnel cosine integral of u , $C(v)$ is the Fresnel cosine integral of v , $S(u)$ is the Fresnel sine integral of u , and $S(v)$ is the Fresnel sine integral of v , where the Fresnel cosine and sine integrals are given by

$$C(x) = \int_0^x \cos\left(\frac{\pi}{2} x^2\right) dx$$

$$S(x) = \int_0^x \sin\left(\frac{\pi}{2} x^2\right) dx$$

and u and v are given by

$$u = \frac{1}{\sqrt{2}} \left(\frac{\sqrt{\lambda \rho_b}}{a_1} + \frac{a_1}{\sqrt{\lambda \rho_b}} \right)$$

$$v = \frac{1}{\sqrt{2}} \left(\frac{\sqrt{\lambda \rho_b}}{a_1} - \frac{a_1}{\sqrt{\lambda \rho_b}} \right)$$

The Fresnel cosine and sine integrals can be obtained from Figure 7.9.

The gain of an H -plane horn has been calculated using (7.45) for different values of ρ_b , to give the normalized curves of Figure 7.14, which show the gains divided by the width a_1 (in terms of the wavelength). It should be noted that the gains increase to a maximum in each case as a_1/λ is varied, and then start to decrease again. Closer examination of these curves show that the value of the phase deviation at these maxima is $3\lambda/8$. For instance, in the case of a horn of length 8λ , the maximum occurs at $a_1/\lambda = 4.9$, resulting in a value of T of 0.375, and thus $\delta = 0.375\lambda$. This corresponds to a phase error of 135 degrees, or $3\pi/4$ radians, which is the maximum phase error that can be tolerated for an H -plane horn.

7.2.3 Gain of a Pyramidal Horn

The gain of a pyramidal horn can be calculated in three different ways, depending on the degree of accuracy required.

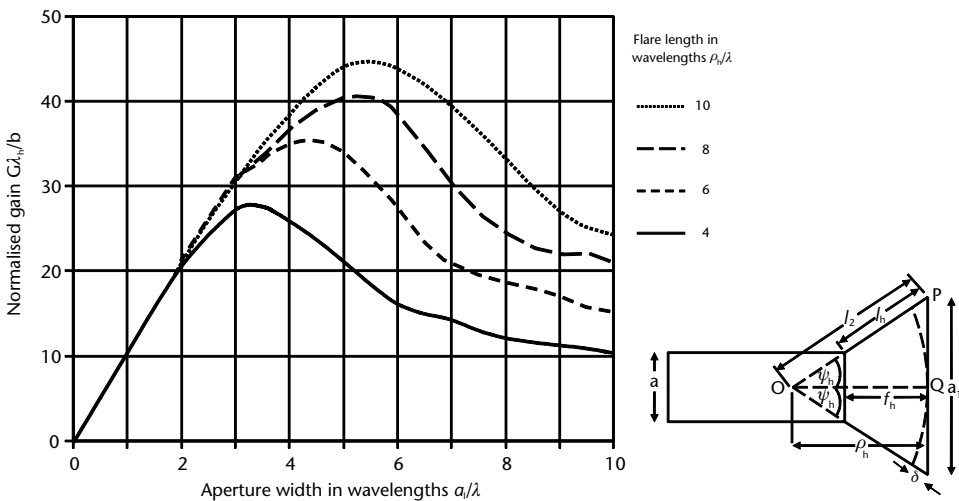


Figure 7.14 Normalized gain for an H -plane sectoral horn.

7.2.3.1 Accurate Calculation

This method involves the calculation of the gains in the E and H plane by assuming that their gains are the same as E - and H -plane sectoral horns with the equivalent dimensions. As long as the aperture of the pyramidal horn in each plane is at least one wavelength, the pattern in one plane is substantially independent of the aperture in the other plane [5, p. 648].

The E -plane gain is given by (7.39), and the Fresnel cosine and sine integrals are shown in Figure 7.9.

The gain in the H plane is calculated from (7.45), where all terms are as previously defined.

The gain of the pyramidal horn is the product of the individual gains of the E - and H -plane horns, divided by a factor that allows for the effect the dimensions of the feeding waveguide have on the resultant gain.

The linear gain G_p of a pyramidal horn [7, p. 16.8] is given by

$$G_p = \frac{\pi\lambda^2}{32ab} G_e G_h \quad (7.46)$$

where a and b are the dimensions of the waveguide feeding the horn, and G_e and G_h are the linear gains in the E and H planes

The dimensions in wavelengths for the midband frequency, in the case of most standard waveguides, are approximately 0.75 and 0.375 for a/λ and b/λ , respectively (see Figure 6.25). The value of $\pi/32$ is approximately 0.098, so that the value of the expression multiplying the E - and H -plane gains is given by

$$\frac{\pi\lambda^2}{32ab} = 0.349 \quad (7.47)$$

Thus, we must multiply the linear gains of the E - and H -plane sectoral horns by 0.349 to obtain the gain for a pyramidal horn at the midband frequency.

In decibels, the expression given by (7.47) is equal to -4.57 . Thus, after adding the gains in decibels for the E - and H -plane sectoral horns, we must subtract 4.57 dB from the result.

The gain in decibels (g_p) for a pyramidal horn is given by

$$g_p = g_e + g_h - 4.57 \quad (7.48)$$

where g_e and g_h are the gains in decibels for the E - and H -plane sectoral horns.

7.2.3.2 Semi-Accurate Method

In this case, the E - and H -plane gains (divided by a and b in wavelengths, respectively) are obtained from Figures 7.10 and 7.14 for the values of ρ_e and ρ_h given. For intermediate values of ρ_e and ρ_h , the values of the gains can be interpolated. The linear gain of the pyramidal horn G_p can be calculated from the following formula

$$G_p = \frac{\pi}{32} \left(G_e \frac{\lambda}{a} \right) \left(G_b \frac{\lambda}{b} \right) \quad (7.49)$$

where a is the width of the waveguide feeding the horn and b is the height of the waveguide feeding the horn. The values for the expressions in brackets are obtained directly from the curves of Figures 7.10 and 7.14, and multiplying the product by the $\pi/32$ gives the gain of the pyramidal horn.

Note that (7.49) is exactly the same as (7.46). If we want to express the gains in dB then the gain of a pyramidal horn g_p is given by

$$g_p = 10 \log_{10} \left(G_e \frac{\lambda}{a} \right) + 10 \log_{10} \left(G_b \frac{\lambda}{b} \right) - 10.08 \quad (7.50)$$

since $10 \log_{10}(\pi/32)$ is equal to -10.08 .

7.2.3.3 Approximate Method

The gain g_p of a pyramidal horn in decibels can be calculated [6, p. 570] from the following approximate formula

$$g_p = 10 \log \left(\frac{32ab}{\pi\lambda^2} \right) - L_e L_b \quad (7.51)$$

where a_1 is the width of the horn aperture, b_1 is the height of the horn aperture, L_e is the loss in decibels for an E -plane horn, and L_b is the loss in dB for an H -plane horn

The values of L_e and L_b can be obtained from Figures 7.7 and 7.12, respectively.

7.3 Example

A standard gain horn has aperture dimensions of 16.5 cm and 8.25 cm, and the lengths of the flare in the E and H planes are 17.75 cm and 17 cm, respectively. The dimensions of the waveguide feeding the horn are 2.29 cm and 1 cm. Calculate the gain at 10 GHz by the three methods described above.

Solution

The lengths in the E and H planes are the ones denoted by l_e and l_b in Figures 7.6 and 7.11. In order to use the formulas in Section 7.2.3, we have to first calculate the values of ρ_e and ρ_b .

We can calculate ρ_e using (7.38)

$$\rho_e = \left(\frac{b_1}{b_1 - b} \right) \sqrt{l_e^2 - \left(\frac{b_1 - b}{2} \right)^2}$$

Using (7.38) and inserting the above values for b_1 , b , and l_e , we get $\rho_e = 18.9$ cm, as shown in Table 7.1.

Table 7.1 Values of b , b_1 , and l_e Used to Derive ρ_e

b	b_1	l_e	b_1-b	$b_1/(b_1-b)$	$l_e^2 - \left(\frac{b_1-b}{2}\right)^2$	$\sqrt{l_e^2 - \left(\frac{b_1-b}{2}\right)^2}$	$\rho_e = \left(\frac{b_1}{b_1-b}\right)\sqrt{l_e^2 - \left(\frac{b_1-b}{2}\right)^2}$
8.25	1	17	7.25	1.138	275.86	16.61	18.90

Table 7.2 Values of a , a_1 , and l_h Used to Derive ρ_h

a	a_1	L_b	a_1-a	$a_1/(a_1-a)$	$l_h^2 - \left(\frac{a_1-a}{2}\right)^2$	$\sqrt{l_h^2 - \left(\frac{a_1-a}{2}\right)^2}$	$\rho_h = \left(\frac{a_1}{a_1-a}\right)\sqrt{l_h^2 - \left(\frac{a_1-a}{2}\right)^2}$
16.5	2.29	17.75	14.21	1.16	264.58	16.27	18.90

Similarly, using (7.44) we get a value for ρ_b of 18.9 cm, as detailed in Table 7.2.

We should expect ρ_e and ρ_b to have the same values, since the two lengths are coincident and represent the perpendicular distance from the virtual apex of the horn to its open end.

We shall now apply the three methods of calculation described above. We will need to calculate the dimensions in terms of wavelengths (see Table 7.3).

At 10 GHz, $\lambda = 3$ cm, $b_1 = 8.25$ cm, giving $b_1/\lambda = 2.75$; $a_1 = 16.5$ cm, giving $a_1/\lambda = 5.5$; $l_e = 17.75$ cm, giving $l_e/\lambda = 5.92$; $l_b = 17$ cm, giving $l_b/\lambda = 5.67$.

7.3.1 Accurate Method

7.3.1.1 E-Plane Gain

The value of $b_1/\sqrt{(2\pi\rho_e)}$ is calculated as 0.7994. The Fresnel cosine and sine integrals for 0.8 can be read from Figure 7.9 as 0.72 and 0.25, respectively. After squaring these we should insert them into the formula of (7.39) to yield a calculated value of the E-plane gain G_e of 19.56.

7.3.1.2 H-Plane Gain

The values of u and v must first be calculated using the following formulas

$$u = \frac{1}{\sqrt{2}} \left(\frac{\sqrt{\lambda\rho_b}}{a_1} + \frac{a_1}{\sqrt{\lambda\rho_b}} \right)$$

$$v = \frac{1}{\sqrt{2}} \left(\frac{\sqrt{\lambda\rho_b}}{a_1} - \frac{a_1}{\sqrt{\lambda\rho_b}} \right)$$

Table 7.3 Values of Variables b_1 , a_1 , and l_h , and l_e in Terms of Wavelength

b_1	b_1/λ	a_1	a_1/λ	l_b	l_b/λ	l_h	l_e/λ
8.25	2.75	16.5	5.5	17	5.67	17.75	5.92

These formulas yield values of $u = 1.87$ and $v = 1.23$. The cosine and sine integrals for u can be read from Figure 7.9 as 0.36 and 0.41, respectively; and those for v are 0.72 and 0.63. Inserting these values into (7.45) yields a calculated value of the H -plane gain G_b of 10.6. The linear gain G_p of the pyramidal horn can now be calculated from (7.46).

The value of the fraction in (7.46) is 0.385, and multiplying it by the values for G_e and G_b (19.56 and 10.6) gives a result of 79.83. Therefore, we have (in decibels) $g_p = 19.02$ dB.

7.3.2 Semi-Accurate Method

The magnitude of ρ_e/λ (and ρ_b/λ) is 6.3λ , but the nearest value to this are the 6λ curves of Figures 7.10 and 7.14. From Figure 7.10 at $b_1/\lambda = 2.75$, we have a value of $G_e a/\lambda = 25$. In decibels, this equates to 13.98. From Figure 7.14, at $a_1/\lambda = 5.5$, we have a value of $G_b b/\lambda = 31$. In decibels, this equates to 14.91. The linear gain G_p of the pyramidal horn is given by (7.49). Inserting the values for G_e and G_b in (7.49) gives a value for $G_p = 76.1$. This gives a value of $g_p = 18.8$ dB.

7.3.3 Approximate Method

The approximate gain g_p in decibels can be calculated from (7.51). In order to find the values of L_e and L_b from Figures 7.7 and 7.12, we have to calculate the values of T_e and T_b from (7.36) and (7.42), respectively. Inserting the values for b , b_1 , λ , and l_e in (7.36) gives a value of $T_e = 0.147$. From Figure 7.7, we get a value of 0.03 dB for L_e . Inserting the values for a , a_1 , λ , and l_b in (7.42) gives a value of $T_b = 0.589$. From Figure 7.12, we get a value of 2.2 dB for L_b .

The value of the first term in (7.51) is 21.87 dB. Inserting this value and the values for L_e and L_b into (7.51) gives a resultant value of $g_p = 19.37$ dB. Thus, we can see that the values for g_p (19.02, 18.8, and 19.37 dB) obtained by the three methods only differ by about 0.6 dB.

7.4 Antenna Correction Factor

This is commonly known as the antenna factor. It is a factor that is used to convert the magnitude of the voltage (in V, mV, μ V, dBV, dBmV, or dB μ V) obtained at the terminals of the receiver, to the electric field intensity present at the position of the antenna. Thus the electric field E at the antenna is given by

$$E = V \times (AF) \quad (7.52)$$

where E is in volts per meter, V is in volts, and AF is the antenna factor. If we examine (7.52) dimensionally, we can see that since E is in volts per meter and V is in volts, the antenna factor AF must be in meters. In a 50- Ω system, AF can be taken as approximately given by the following relation [8]

$$AF = \frac{9.73}{\lambda\sqrt{G}} \quad (7.53)$$

where G is the linear or numeric gain and λ is the wavelength at the frequency of operation.

The Society of Automotive Engineers (SAE) also defines an antenna factor (AF_2) which is called the apparent gain. This is the difference obtained in the receiver reading when: (1) the transmit and receive antennas are placed at least one meter apart, and (2) the antennas are disconnected and the cables from the signal generator and receiver are connected directly together. Thus, the losses in the balun and tuning or matching networks are measured.

In order to calculate the antenna factor [9], we should take into account (1) the losses in the balun and matching network, and (2) the losses due to mismatch between the antenna and receiver.

The power density is defined as the vector cross product (see Chapter 3) of the electric and magnetic field vectors (\mathbf{E} and \mathbf{H}). The magnitude of the power density \mathbf{P}_d is the vector cross product of the modulus values of the \mathbf{E} and \mathbf{H} fields (see Section 3.6) and is given by

$$P_d = |\mathbf{E}| \times |\mathbf{H}| \quad (7.54)$$

where \mathbf{P}_d is in watts per meter squared, \mathbf{E} is the electric field intensity in volts per meter, and \mathbf{H} is the magnetic field intensity in amperes per meter. The ratio of \mathbf{E} to \mathbf{H} is known as the intrinsic impedance of the wave Z_w , and in the case of a plane wave in free space, this has a value of 120π . Thus (7.54) can be written as

$$\mathbf{P}_d = \frac{|\mathbf{E}|^2}{Z_w} \quad (7.55)$$

If the effective area of the antenna is A , then the power P in watts available at the antenna is given by

$$P = \frac{E^2 A}{\xi} \quad (7.56)$$

If a receiver of impedance Z_r is connected to the antenna, then by Thevenin's theorem, the antenna is represented by an EMF V and the current I is given by

$$I = \frac{V}{(Z_a + Z_r)} \quad (7.57)$$

When the antenna and receiver are purely resistive (of resistances R_a and R_r), the power transferred is given by

$$P = I^2 R_r = \frac{V^2 R_r}{(R_a + R_r)^2} \quad (7.58)$$

Figure 7.15 shows that if the receiver resistance R_r is varied between values of $0.25 R_a$ to $2.5 R_a$, the power transferred for an input voltage of 1V varies between

0.002 and 0.0035 W for an antenna resistance of 73Ω . (This is the approximate resistance of a resonant dipole—see Section 5.4). The maximum power of 0.0035 W is transferred when the receiver resistance R_r is the same as that of the antenna R_a . The receiver is considered to be matched when this condition exists. Note that when the receiver resistance is half or double that of the antenna resistance, the power transferred has the same magnitude of 91% of the maximum power. The magnitude of the maximum power P_{\max} given by (7.58) can be rewritten as

$$P_{\max} = \frac{V^2}{4R_r} \quad (7.59)$$

since $R_r = R_a$.

If the effective height of the antenna is h_e , then (since voltage V is equal to the product of the electric field E and the effective height) the maximum power available at the antenna is given by

$$P_{\max} = \frac{E^2 h_e^2}{4R_a} \quad (7.60)$$

This assumes that the antenna is directly connected to the receiver and that they both have the same resistance. However, this is not the case in practice, since the antenna has a higher resistance than the connecting cable and receiver. A dipole has a resistance between 72 and 73Ω , whereas the receiver and connecting cable normally have resistances of 50Ω . A balun is also required to convert the balanced output of the dipole to the unbalanced coaxial cable. In order to transfer the maximum power, a balun-and-matching (B/M) network is used to provide a conjugate match to the antenna. There are conjugate mismatch losses associated with this type

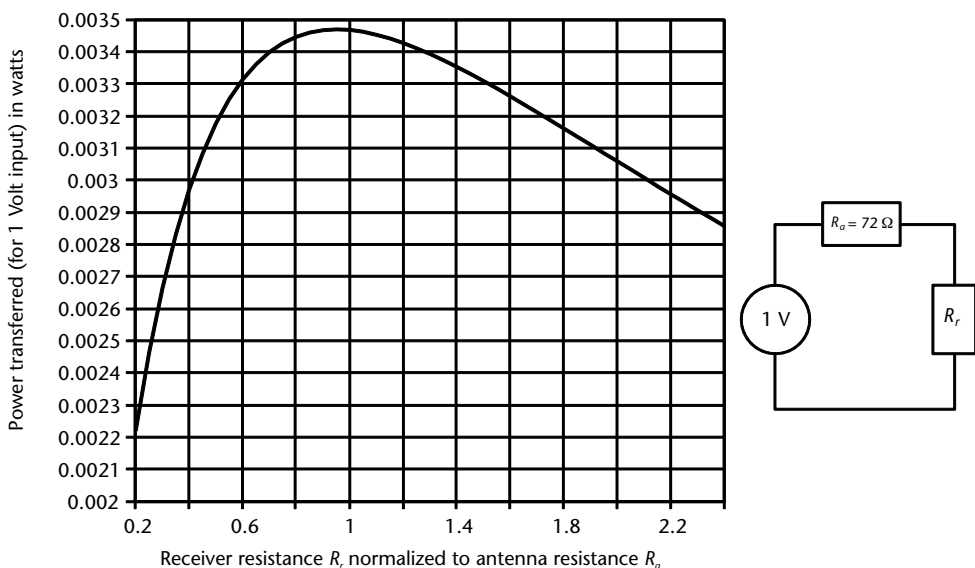


Figure 7.15 Power transfer between an antenna and a receiver.

of matching, as well as dissipative or ohmic losses in the B/M network and connecting cables. The correct antenna factor should take into account all these power losses. The total of these losses [9] can be shown by the following ratio

$$\frac{\text{Power available from the antenna}}{\text{Power delivered to the receiver}} = M_{ab}^2 K_{bu}^2 M_{ar}^2 e^{2\alpha l} \tag{7.61}$$

where

$$M_{ab}^2 = \frac{\text{power available from the antenna}}{\text{power delivered to the B/M network}}$$

$$K_{bu}^2 = \frac{\text{power delivered to the B/M network}}{\text{power available from the B/M network}}$$

$$M_{ar}^2 = \frac{\text{power available from the B/M network}}{\text{power delivered to the receiver cable}}$$

$$e^{2\alpha l} = \frac{\text{power delivered to the receiver cable}}{\text{power delivered to the receiver input}}$$

α is the attenuation factor of the cable, and l is the length of cable from the unbalanced output of the B/M network to the input of the receiver. Note that the M_{ab}^2 and M_{ur}^2 are not the same as the correction terms of Section 7.1.1.

Referring to Figure 7.16, which shows the simplified equivalent circuit of the measuring system, the maximum power available from the antenna to the B/M network (assuming the B/M network is matched to the antenna) is given by

$$P_{\text{max}} = \frac{V^2}{4R_a} \tag{7.62}$$

where V is the voltage due the electric field E and h_e (the effective height of the antenna) and R_a is the resistance of the antenna.

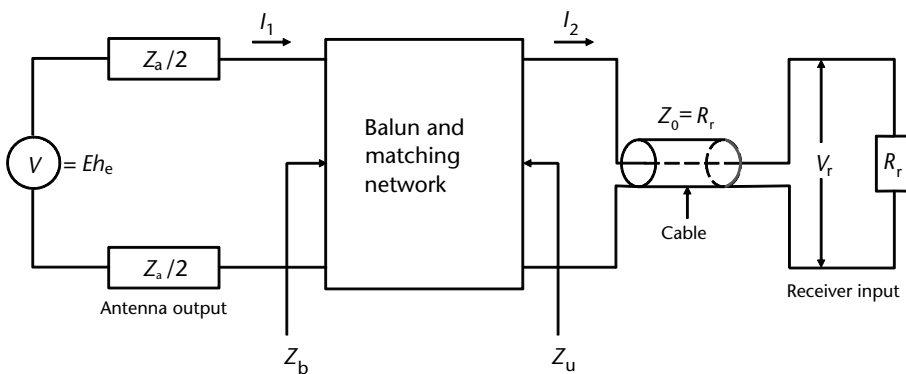


Figure 7.16 Simplified equivalent circuit of the measurement system.

The power transferred to the B/M network is given by

$$P_{\max} = \frac{V^2 R_a}{|Z + Z_b|^2} \quad (7.63)$$

where Z_0 is the impedance presented to the balun-and-matching network, and R_a is the resistance.

Combining (7.62) and (7.63) gives the expression for M_{ab}^2 as

$$M_{ab}^2 = \frac{V^2}{4R_a} \frac{|Z_a + Z_b|^2}{V^2 R_b} \quad (7.64)$$

which reduces to

$$M_{ab}^2 = \frac{|Z_a + Z_b|^2}{4R_a R_b} \quad (7.65)$$

Similarly, the expression for M_{ur}^2 can be given by

$$M_{ur}^2 = \frac{|Z_u + R_r|^2}{4R_a R_r} \quad (7.66)$$

The expressions for M_{ab}^2 and M_{ur}^2 represent the conjugate mismatch losses at the input and output of the B/M network [9].

The equivalent circuit of the B/M network is shown in Figure 7.17. It can be shown that

$$Z_b = Z_{11} - \frac{Z_{12}^2}{Z_{11} + R_r} \quad (7.67)$$

and

$$Z_u = Z_{22} - \frac{Z_{12}^2}{Z_{11} + Z_a} \quad (7.68)$$

The expression for K_{bu}^2 is given by

$$K_{bu}^2 = \frac{4R_b R_u}{|Z_{12}|^2} \frac{|(Z_{11} + Z_a)(Z_{12} + R_r)|^2}{|(Z_{11} + Z_a)(Z_{22} + R_r) - Z_{12}^2|^2} \quad (7.69)$$

The maximum power available at the antenna is given by (7.60), and the maximum power delivered to the receiver is given by

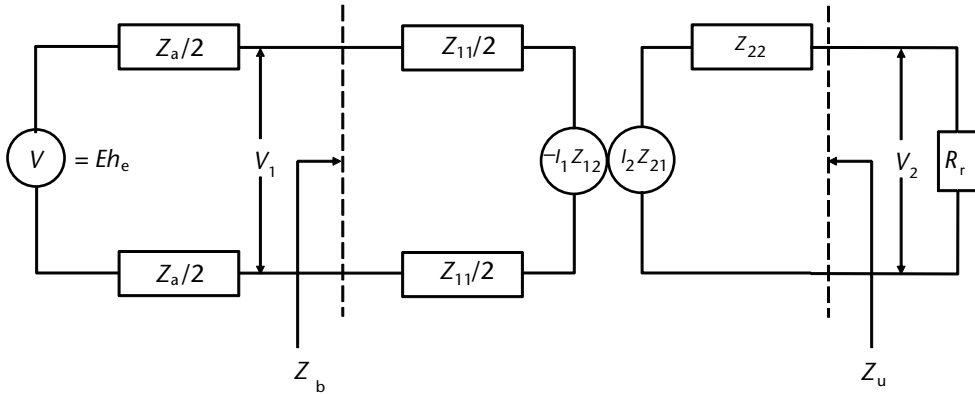


Figure 7.17 Open-circuit two-port network equivalent of the balun-and-matching network, with source and load connected.

$$P_{\max} = \frac{V_r^2}{R_r}$$

where V_r is the voltage at the receiver input and R_r is the resistance of the receiver. Thus, the ratio of the power available at the antenna to the power delivered to the receiver is given by

$$\frac{\text{Power available at antenna}}{\text{Power delivered to the receiver}} = \frac{\mathbf{E}^2 h_e^2 R_r}{4R_a^2 V_r^2} \tag{7.70}$$

Equating (7.61) and (7.70) gives

$$\frac{\mathbf{E}^2 h_e^2 R_r}{4R_a^2 V_r^2} = M_{ab}^2 K_{bu}^2 M_{ar}^2 e^{2\alpha l}$$

from which we get the ratio of \mathbf{E} to V_r i.e., the antenna factor, as

$$\frac{\mathbf{E}}{V_r} = \frac{2}{h_e} \sqrt{\frac{R_r}{R_a}} M_{ab} M_{ur} K_{bb} e^{\alpha l} \tag{7.71}$$

The values for the antenna factor at four different frequencies was calculated [9] using equation (7.71) in the case of the Schwarzbeck dipole [10]. It was assumed that the length of the cable connecting the balun to the output connector, was 0.5m; and the cable type was RG 214/U. The loss associated with this type of cable is given by

$$e^{2\alpha l} = (0.0015F + 1.11)^{0.03}$$

where F is the frequency in MHz.

Table 7.4 Comparison Between Calculated and Published Antenna Factors for the Schwarzbeck Dipole

Frequency (MHz)	$2/h_e$ (dB)	$(R_a/R_{ar})^{1/2}$ (dB)	M_{ab} (dB)	K_{bu} (dB)	M_{aur} (dB)	e^{al}	e^{al} (dB)	E/V_r Calculated	E/V_r Published
30	-4.04	1.65	0.35	9.62	0	1.0040	0.017	7.60	7.45
100	6.42	1.65	0.35	9.62	0	1.0069	0.026	18.07	17.94
300	15.9	1.65	0.35	9.62	0	1.0134	0.058	27.64	27.35
1000	26.42	1.65	0.35	9.62	0	1.029	0.124	38.46	38.03

The calculated individual components as well as the resultant antenna factors are listed in Table 7.4 and compared with the manufacturer's published data [10]. It can be seen that there is very good agreement between the calculated and measured values published by the manufacturer.

References

- [1] Jasik, H., *Antenna Engineering Handbook*, McGraw-Hill Book Company, Inc., 1961.
- [2] Slater, J. C., *Microwave Transmission*, New York: McGraw-Hill, 1942, Chapter 6.
- [3] Rudge, A.W., K. Milne, A. D. Olver, and P. Knight, *Handbook of Antenna Design*, Vol. 1, Chapter 8, pp. 647–651.
- [4] Silver, S., *Microwave Antenna Theory and Design*, McGraw-Hill Book Company, Inc., 1947.
- [5] Krauss, J. D., *Antennas*, McGraw-Hill Book Company, Inc., 1988.
- [6] Balanis, C. A., *Antenna Theory Analysis and Design*, New York: Harper and Row, 1982.
- [7] Schelkunoff, S. A., and H. T. Friis, *Antennas Theory and Practice*, New York: John Wiley & Sons, Inc., 1952.
- [8] SAE Aerospace Recommended Practice ARP 958, *Electromagnetic Interference Measurement Antennas; Standard Calibration Method*, March 1, 1968.
- [9] Bennett, W. S., "Properly Applied Antenna Factors," *IEEE Trans. on EMC*, Vol. 28, No. 1, February 1986, pp. 2–6.
- [10] Schwarzbeck, C., „Antennenfaktoren u Korrekturen Praz-Dipole VHAP-10dB,“ *Dipl-Ing Mess-Elektronik*, D-6901 Schonau-Alteneudorf, W. Germany, 1981.

Introduction to Electromagnetic Compatibility Measurements

This chapter covers the main EMC measurements necessary to ensure that equipment is compliant with legal regulations and military standards. It gives an overview of specified limits, test philosophy, measurement set-ups, and instrumentation in the EMC field. Other disciplines covered by the field of EMC are shielding effectiveness, radio monitoring, and electrostatic discharge (ESD).

The IEEE dictionary [1] defines EMC as a measure of equipment tolerance to external EM fields, as well as the ability of a device to function satisfactorily in its EM environment without introducing intolerable disturbance to that environment or to other devices. It is accepted that some unwanted EM signals (or noise) will be generated, but it is the level or amplitude of these signals that is important. Standards define the maximum level of these signals at each frequency. When these signals are of sufficient amplitude to affect the performance of other devices, then electromagnetic interference (EMI) is said to exist. The term RFI (radio frequency interference) is used interchangeably with EMI, although EMI is a later definition that includes the whole of the EM spectrum, whereas RFI is generally considered to be between 10 kHz and 10 GHz. However, EMI is the more commonly used expression to denote RFI, and is used throughout this book. EMI manifests itself in performance degradation, malfunction, or failure of electrical or electronic equipment. Degradation is defined by the International Electrotechnical Commission (IEC) as an unwanted change in the operational performance of a device due to EMI. The source of these spurious signals can be natural, as well as man-made.

In order to establish the EMC compliance of a device, certain measurements have to be performed. The unwanted signals can be received from or transmitted to other devices through conduction or radiation. Conducted signals require metal or dielectric materials, and tend to occur at frequencies below 30 MHz, whereas radiated signals, which can be transmitted through a vacuum or free space, take place mainly above 30 MHz. There is a very fine dividing line between conducted signals that couple capacitively (or inductively) between unconnected circuits, and radiated signals in the near field of an antenna. However, if the distances involved are very small in terms of wavelengths (order of 1/100th of a wavelength or so), then the mechanism of energy transfer can be considered to be conduction, whereas for larger distances the mechanism of transfer is through radiation, and the energy is characterised in terms of electric and magnetic fields rather than in terms of currents and voltages. The emissions can be:

- Intentional, as in the case of a radio broadcast or air traffic signal, or
- Unintentional, as in the case of computers and other equipment.

We can quantify the EMI caused by a device by measuring its radiated and conducted emissions and its EMC by measuring its immunity or susceptibility to specified levels of radiated and conducted fields.

Shielding effectiveness is the ability of a material to exclude or confine EM waves. This is becoming a very important part of EMC measurements, and is not covered to any great extent by many textbooks. Its increasing importance is in part due to the practice of many manufacturers not to consult EMC specialists at the design stage, and then attempt to shield equipment at the production stage to comply with the relevant standards. Radio monitoring is defined by the IEEE as the observation of the characteristics of transmitted signals. This is important, since it is necessary to ensure that the electromagnetic environment is maintained at a low enough level so that equipment placed in this environment will function satisfactorily. Radio monitoring is covered in a separate chapter in this book, dealing with the radiation from transmitters. ESD is becoming more important as human-generated ESD voltage increases. This increase is mainly due to the use of man-made materials, and low humidity levels in the house and work environment.

There are various national and international standards that specify the levels to which equipment must comply. In 1933, the Comité International Spécial des Perturbation Radioélectronique (CISPR) committee of the IEC was the first organization to propose EMC standards. The European Community (EC) has adopted a number of common standards called Europäische Norm (EN) which apply to emissions and immunity for a number of different nonmilitary equipment. The ENs in Europe are controlled by the members of CENELEC, which comprises 34 national standards bodies such as in BSI (British Standards Institution) in the UK, and DKE (Deutsche Kommission Elektrotechnik) in Germany. As the European standardization bodies have agreements in place with the international bodies, most of these EN specifications are based on IEC standards. These ENs will apply to all equipment to be sold within the European Union (EU) and European Free Trade Area (EFTA) countries. In addition, other regions have adopted ENs, including Australia, New Zealand, and the Middle East. In the USA, the Federal Communications Commission (FCC), and in Japan, the Voluntary Control Council for Interference (VCCI) are the regulatory bodies that specify the emissions standards to which equipment has to demonstrate compliance.

8.1 Radiated Emissions

The EM waves emitted by a device into space are termed radiated emissions. Radiated emissions do not require a medium for transmission of energy. These emissions can affect the performance of other equipment, as well as the device that is itself the source of the emission. When the emissions affect other equipment it is termed intersystem interference, and when the source of the emissions is within the equipment itself it is called intrasystem interference. The FCC regards the EMI test process as the framework of the source-transfer function-measurement relationship

[2]. The equipment under test (EUT) is the source, the test site in conjunction with the receiving antenna is the transfer function, and the measurement is undertaken by a tuneable receiver or a spectrum analyzer. The EMF or potential measured by the receiver is usually in microvolts or decibels per microvolt ($\text{dB}\mu\text{V}$), and this level is related to the electric field present at the antenna location by the antenna factor. The antenna factor thus converts the voltage measured by the receiver to the electric field in microvolts per meter ($\mu\text{V}/\text{m}$) or decibel-microvolts per meter ($\text{dB}\mu\text{V}/\text{m}$), making allowances for the gain of the antenna, and the losses in the balun and cables between the antenna and receiver.

8.1.1 Differential and Common Mode Radiation

The radiated emissions can be classified as differential-mode or common-mode radiation [3, p. 185]. Differential-mode radiation is produced by currents flowing in opposite directions in the go and return cables or lines, so that they behave like a loop antenna.

Common-mode radiation is caused by currents flowing in the same direction along adjacent cables. These are usually the greatest source of radiated emissions. The reason for this can be seen by referring to Figure 8.1(a). Consider the currents I_A and I_B flowing in the wires A and B, respectively, that are separated by a distance b . These cause magnetic fields \mathbf{H}_A and \mathbf{H}_B , at distances r_1 and r_2 (where $r_1 + b = r_2$), which are of different magnitudes, to add together on the side nearer to wire A, since they are in the same direction. A similar situation occurs all along the length of the pair of wires at different radii and on the other side of the wires nearer wire B. As the distance b between the wires is decreased, the distances r_1 and r_2 are nearly equal, and the magnitudes of \mathbf{H}_A and \mathbf{H}_B are also nearly equal, so that their resultant is almost double that of their individual magnitudes. These magnetic fields represent a loss of energy which is radiated as EMI.

In the case of the corresponding differential mode currents shown in Figure 8.1(b), the magnetic fields \mathbf{H}_A and \mathbf{H}_B at distances r_1 and r_2 are in opposite directions so their resultant is their difference. When the separation between the wires (b) is small, r_1 and r_2 are nearly equal and thus \mathbf{H}_A and \mathbf{H}_B will be nearly equal, so that their difference is nearly zero. This means that very little energy will be radiated by differential-modes currents.

8.1.2 Measurement of Radiated Emissions

To comply with standards, the emissions from the device have to be below a specified level. This level is different for each frequency. The EMC engineer would normally perform measurements over the whole frequency range of interest, either on an Open Area Test Site (OATS) or (increasingly) in a semi-anechoic chamber, by using a spectrum analyzer or measuring receiver. Anechoic chambers are becoming more commonplace as they allow automated measurements and do not experience interference from background sources. If the radiated emissions are below the specified levels (but preferably at least 6 dB below the specified limits), the EUT is considered to be in compliance. However, instead of using a peak-reading spectrum analyzer for outdoor measurements, the most commonly used detectors

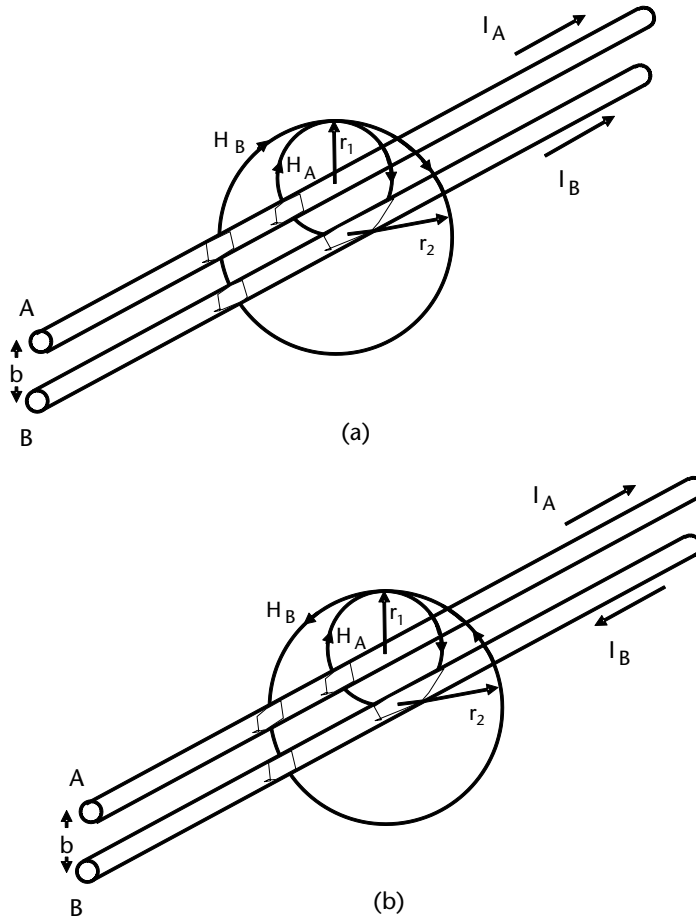


Figure 8.1 (a) Common-mode and (b) differential-mode radiated emissions for parallel wires.

are quasi-peak and peak receivers. Peak detectors are used in measurements for compliance with military standards such as MIL-STD 462, whereas quasi-peak detectors are recommended by bodies such as CISPR for compliance with national standards and legal regulations. Many receivers can also measure average electric field intensity. As the quasi-peak detector was designed to protect AM modulated signals, there is a trend to adopt a new detector called the RMS Average which is designed to protect digitally modulated signals.

Since most electronic equipment nowadays is microprocessor-controlled, we shall consider the regulations for this type of equipment. The FCC defines a computer device as any electronic system that uses digital techniques, and generates or uses timing signals at a clock rate greater than 10 kHz [4, p.44]. Most regulatory bodies classify computer equipment according to its user environment. The FCC and the European Standards use classes A and B, whereas the VCCI uses classes 1 and 2.

8.1.3 Classes of Computer Equipment

Class A refers to equipment used in commercial, industrial, or business environments, and class B includes digital devices such as personal computers and similar

electronics devices that are marketed for use by the general public. The fact that a desktop computer is often used in a business or industrial environment does not affect its classification. If the same computer can be used in the residential environment, it will be classified as class B device. Peripheral devices (such as modems, printers, etc.) acquire the classification of the computer to which they are connected. However, if the peripherals can be shown (because of price or performance) to be not suitable for use in the domestic environment, then these peripherals can be classified as class A.

Class B equipment is subject to more stringent requirements than class A, that is, the permitted levels of radiated emissions for class B equipment are lower than those for class A. Class A equipment only requires verification, whereas class B requires certification. The verification process is relatively simple and easy. Manufacturers test their equipment, and as soon as compliance is attained, the equipment can be labelled and marketed. To place equipment on a particular market, the manufacturer is required to hold a technical file consisting of:

- A general description of the radio equipment;
- Photographs or illustrations;
- Versions of software or firmware affecting compliance;
- User information and installation instructions;
- Conceptual design and manufacturing drawings;
- Descriptions and explanations necessary for the understanding of the operation of the equipment;
- A list of the harmonized standards, applied in full or in part, of which the references have been published in the Official Journal of the European Union;
- Copy of the EU declaration of conformity;
- Results of design calculations made, examinations carried out, and other relevant similar elements;
- Test reports.

For computer equipment, the EU and FCC operate a self-certification process.

Radiated emissions from class A are specified at a measurement distance of 10m, whereas the emissions from class B equipment can be undertaken at a distance of 3m. The 30-m limit has been discontinued in this frequency band, as the measurement of these levels is difficult on many sites because of ambient noise sources, and in addition, the difficulties of scanning the antenna height to 6m. Figure 8.2 shows the maximum level of radiated emissions specified by the FCC for the two classes of equipment. The limits above 1 GHz are shown in Table 8.1.

The radiated limits specified by the European Standards for the radiated electric field for 3m test distance are shown in Figures 8.4 and 8.5 [5].

8.1.4 Measuring Radiated EMI

The different regulatory bodies stipulate limits as well as different measurement set-ups for compliance. The measurement details for the IEC compliance are given here as an example. The IEC standards cover a frequency range from 9 kHz to 6 GHz. A loop antenna is used to cover the frequency range from 9 kHz to 30 MHz.

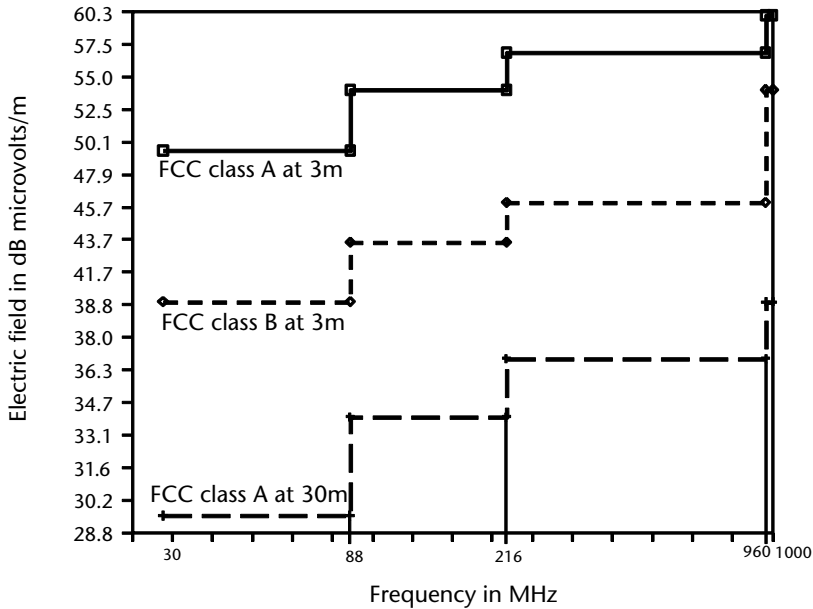


Figure 8.2 FCC radiated electric field limits for computers up to 1 GHz.

A biconical antenna is used to cover the frequency range from 30 to 200 MHz. A log periodic antenna is used to cover the frequency range from 200 to 1,000 MHz. A horn antenna is used from 1 to 6 GHz. The antennas are each placed 3m away from the EUT (equipment under test) and the frequency range is swept.

Details of the FCC indoor measurement for radiated emissions are now given. The EUT is placed on a 0.8-m high rotatable wooden table (must be expanded polystyrene for testing above 1 GHz). The area of the table depends on the size of the EUT. The antenna is mounted on a mast adjustable over at a height of 1 to 4m and 3m away from the EUT. The measuring receiver is set to a scan of an appropriate frequency range, and the IF bandwidth is set to the relevant resolution bandwidth for the frequency range being observed. The I/O (input-output) cables are moved to defined positions as shown in the standard, and the sub assemblies are arranged 10 cm apart. The I/O cables are also draped over the sides of the EUT to pick up emissions from the EUT's internal logic. Several layouts are tried out to establish the worst-case readings on the spectrum analyzer. The spectrum analyzer is then tuned to another frequency span and the same procedure is repeated. The measurements

Table 8.1 FCC Radiated Electric Field Limits Above 1 GHz

Frequency Range (MHz)	Class	Distance (m)	Detector	Limits (dB μ V/m)
1,000 to 40,000	A	10	Peak	69.5
1,000 to 40,000	A	10	Average	49.5
1,000 to 40,000	B	3	Peak	74
1,000 to 40,000	B	3	Average	54

are then performed at frequency intervals up to the highest required frequency. A schematic of the measurement set-up is shown in Figure 8.3. For both the 3m and 10m distance measurements, the antenna has to be moved between heights of 1 to 4m to record the maximum level of the radiated emissions. The EUT is then rotated in the horizontal plane to investigate the position that gives the highest level of emission for both horizontal and vertical polarization of the antenna.

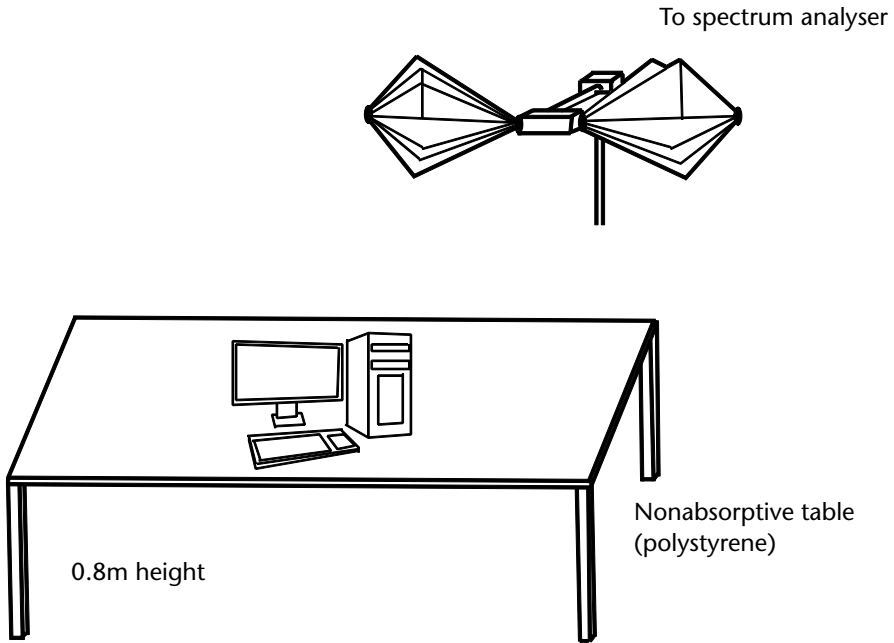


Figure 8.3 The measurement set-up for radiated emissions testing.

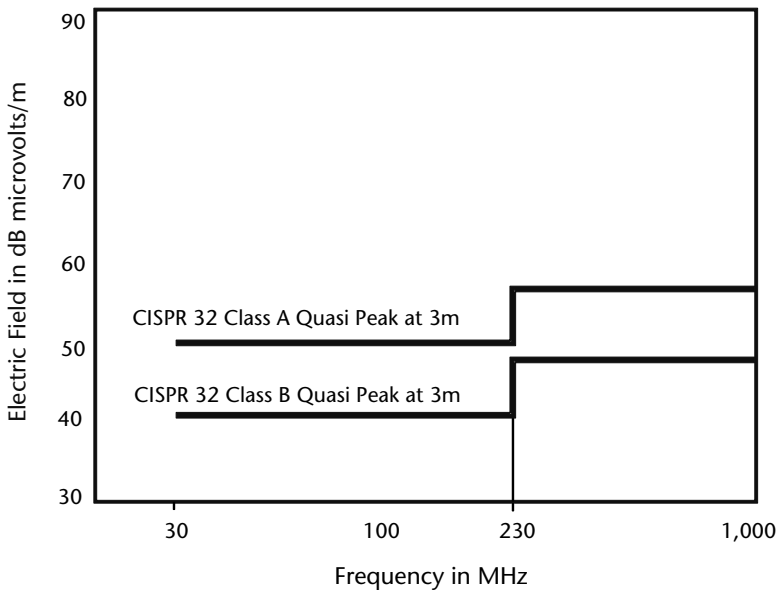


Figure 8.4 CISPR 32/EN 55022 radiated electric field limits below 1 GHz.

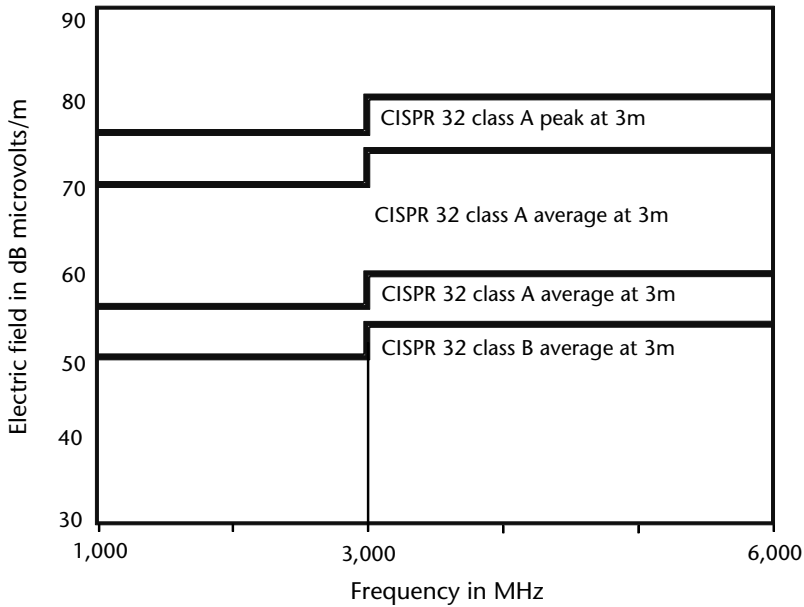


Figure 8.5 CISPR 32/EN 55022 radiated electric field limits above 1 GHz.

Both FCC and EN standards have an upper frequency limit depending on the highest internal frequency. The FCC requirement for unintentional radiators is to measure to the fifth harmonic of the highest internal frequency, up to a maximum of 40 GHz. The limit is the same from 1 GHz to 40 GHz. The European requirements are shown in Table 8.2.

The CISPR 32/EN 55032 limits between 30 MHz and 1 GHz as shown in Figure 8.4 are the same as in the predecessor standard EN 55022, and are based on the quasi-peak detector. CISPR 22/EN 55022 was updated to include limits above 1 GHz, and these have been adopted in CISPR 32/EN 55032. The limits above 1 GHz are stated in terms of peak and average limits to reflect the protection of digital modulation techniques used by radios in this frequency range, shown in Tables 8.3 and 8.4. To reflect the non-OATS facilities, CISPR 32/EN 55032 includes the use of fully anechoic rooms (FAR) and free-space OATS (FSOATS). A FSOATS is usually a semi-anechoic chamber or OATS with an absorber placed on the ground plane between the EUT and measurement antenna. It is used at frequencies above 1 GHz and has the same limits applied as the FAR.

Table 8.2 CISPR 32/EN 55032 Required Highest Frequency for Radiated Measurement

<i>Highest Internal Frequency (F_x)</i>	<i>Highest Measured Frequency</i>
$F_x < 108$ MHz	1 GHz
108 MHz $< F_x < 500$ MHz	2 GHz
500 MHz $< F_x < 1$ GHz	5 GHz
$F_x > 1$ GHz	$5 \times F_x$ up to a maximum of 6 GHz

The free-space facilities are based on having absorber material on the floor, which ensures the absence of a ground reflected component. The traditional OATS was designed to ensure a consistent reflected signal from the ground plane. The disadvantage of the reflected signal from the ground plane is that there could be destructive interference between the direct wave and reflected wave which caused a null. As such, it is necessary to scan the antenna height to avoid this null. With the free-space technique, it is not necessary to scan the antenna height to avoid the null, however, it is necessary to scan to ensure that directional signals are detected.

A difference of 6 dB is expected for measured field strengths above a ground plane (for example, using an OATS), as compared with free space (for example using a FAR). A simple OATS geometrical optic model is shown in Figure 8.6: two rays impinge on the receive antenna above a ground plane; namely the one transmitted directly between the transmit and receive antennas and the one reflected by the ground plane.

The difference in phase relation of the two rays results in an interference pattern which corresponds to the function of the height of the receive antenna above the ground. The resulting effect ranges from cancellation to doubling of the direct

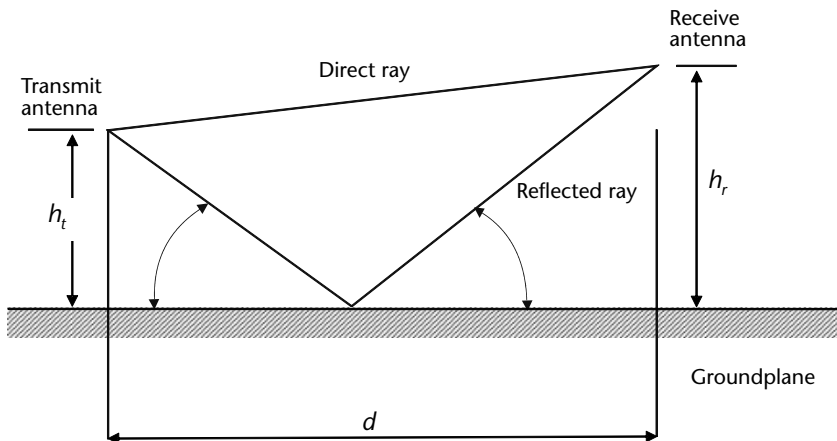


Figure 8.6 Ray diagram for radiated emissions measurement.

Table 8.3 CISPR 32/EN 55032 Class A Radiated Limits

Frequency Range (MHz)	Test Site	Distance (m)	Detector	Class A Limits (dB μ V/m)
30 to 230	OATS/SAC	10	Quasi peak	40
230 to 1,000	OATS/SAC	10	Quasi peak	47
30 to 230	FAR	10	Quasi peak	42 to 35
230 to 1,000	FAR	10	Quasi peak	42
1,000 to 3,000	FSOATS	3	Average	56
3,000 to 6,000	FSOATS	3	Average	60
1,000 to 3,000	FSOATS	3	Peak	76
3,000 to 6,000	FSOATS	3	Peak	80

Table 8.4 CISPR 32/EN 55032 Class B Radiated Limits

<i>Frequency range (MHz)</i>	<i>Test Site</i>	<i>Distance (m)</i>	<i>Detector</i>	<i>Class A limits (dBμV/m)</i>
30 to 230	OATS/SAC	10	Quasi-peak	30
230 to 1,000	OATS/SAC	10	Quasi-peak	37
30 to 230	FAR	10	Quasi-peak	32 to 25
230 to 1,000	FAR	10	Quasi-peak	32
1,000 to 3,000	FSOATS	3	Average	50
3,000 to 6,000	FSOATS	3	Average	54
1,000 to 3,000	FSOATS	3	Peak	70
3,000 to 6,000	FSOATS	3	Peak	74

ray. As such, during OATS measurements, h_r is varied until constructive interference (or doubling) is obtained.

8.2 Radiated Susceptibility and Immunity

IEC/EN 61000-4-3 is a basic standard which requires that equipment is tested to a level of severity that depends on the EM radiation to which it is exposed when it is used. Product standards refer to the basic standard and assign appropriate test levels. There are four test levels, defined as follows:

- Level 1: low-level EM radiation environments, such as those typical of radio or television broadcasting stations that are located at a distance of more than 1 km, and radiated levels of low-power transceivers.
- Level 2: Moderate EM radiation environments such as portable transceivers that are at least 1m away from the equipment.
- Level 3: Severe EM radiation environments such as high power transceivers that are close to the equipment.
- Level 4: Open test level for very severe EM radiation environments. This level is subject to negotiation between the user and the manufacturer, or it can be defined by the product standard.

The IEC defines susceptibility of equipment as the characteristic of the equipment that results in undesirable responses when subjected to EM energy. The term susceptibility is usually used for military equipment, whereas the term immunity is used for nonmilitary equipment. In the case of military equipment, the standards are typically more stringent, that is, the equipment has to be capable of withstanding higher levels than nonmilitary equipment. When military equipment produces or processes classified data, it is also required to be produced to what are known as TEMPEST standards, so that unauthorized access to the data is not possible.

In general, military equipment requires between 30 and 60 dB more shielding than comparable commercial equipment, to meet the more stringent standards [6].

Automotive manufacturers also specify very stringent test levels that are similar to military test levels.

The susceptibility of a device is measured by placing the device in an EM environment of specified electric field or power density. The measurements can be performed in an enclosure such as a screened room, an anechoic chamber, or a TEM cell (see Section 9.5.2).

Military standards, such as MIL-STD 461, address equipment and systems levels and cover susceptibility as well as emissions.

Equipment has to be immune to various EM signals. These include radiated electric and magnetic field strengths, and conducted common- and differential-mode voltages. Details of these measurements and the various levels specified by the different standards are adequately covered in textbooks. These standards are adopted in most regions world-wide including Europe [7].

8.2.1 Immunity to Radiated Electric Field Strength

IEC stipulates immunity to radiated electric field strength over the frequency range of 80 MHz to 6 GHz for commercial environments. The test level depends on the frequency and the product type. Residential, commercial, and light industrial equipment including information technology equipment has a level set at 3 V/m, whereas medical equipment has levels set at between 10 V/m and 28 V/m at some frequencies [7, p. 18]. Below 80 MHz, the test standards are based on conducted test methods as the wavelengths are too long for common products to act as efficient receptors. The following frequency limits typically apply:

- Ports for power cables to be tested over the frequency range of 150 kHz to 80 MHz;
- Ports which are not intended to have data cables attached to them of lengths greater than 3m need not be tested below 80 MHz.

Radiated immunity field uniformity requirements are such that the transmit antenna is typically located between 1 and 3m. These higher fields and longer distances increase the power requirements of the test facility.

8.2.2 Immunity to Conducted Radiated Interference

At frequencies below 80 MHz, commercial standards specify conducted radiofrequency testing. This is because at longer wavelengths (over 3.75m) the dimensions of most equipment are not large enough to act as an efficient receptor. Most of the interference enters the system via cables, which can be long enough to act as efficient antennas for a radiated signal, or can act as efficient transmission lines to conduct remotely generated interference into the equipment. This test typically only applies to cables that can be longer than 3m, usually utility cables, Ethernet, and telephone lines. The frequency range of 150 kHz to 80 MHz is to be covered with test levels of 3 Ve.m.f. (electromotive force) and 10 Ve.m.f.

The preferred test method is to use a coupling/decoupling network (CDN), as this presents a controlled $150\text{-}\Omega$ impedance to the cable, which represents the common-mode impedance seen by a long cable above a ground plane. Other methods include the electromagnetic clamp and current injection probe which is favored in military standards. The electromagnetic clamp is a combined electric field and current injection probe which attempts to couple efficiently at both high and low frequencies between 150 kHz and 80 MHz . The current injection probe has no impedance control and the injected current can vary widely compared to the original calibration level which is measured using a $50\text{-}\Omega$ -defined impedance, whereas the EUT can have a higher or lower input impedance depending on the type of circuit. For example, if the input impedance is high, a high voltage occurs on the cable as the current probe drives a constant current. If the input impedance is less than $50\text{ }\Omega$, then a high current and low voltage will result. Typical setups are shown in Figures 8.7–8.9.

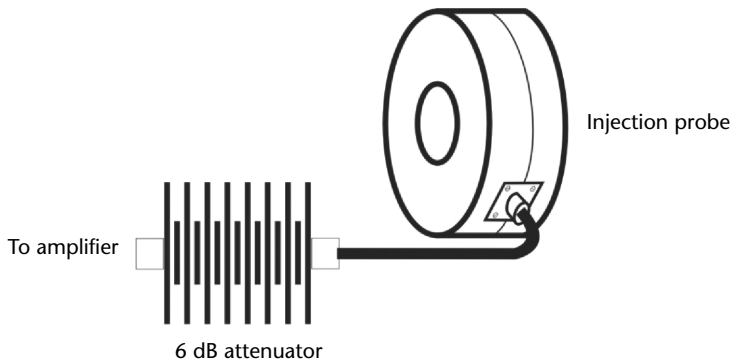


Figure 8.7 Conducted immunity arrangement using bulk current injection.

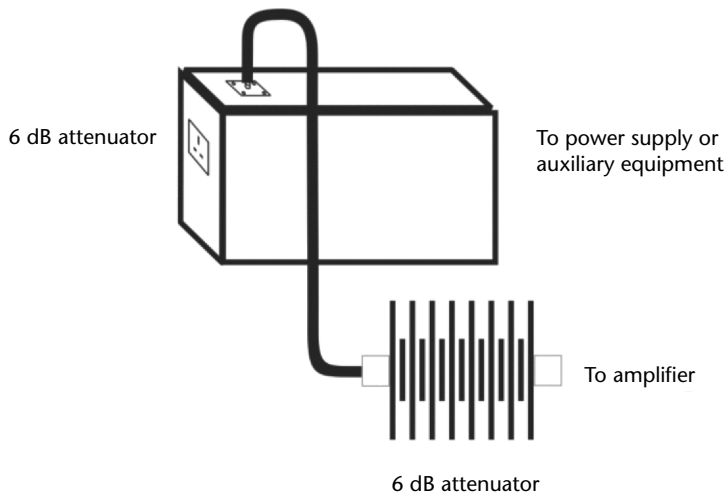


Figure 8.8 Conducted immunity arrangement using CDN.

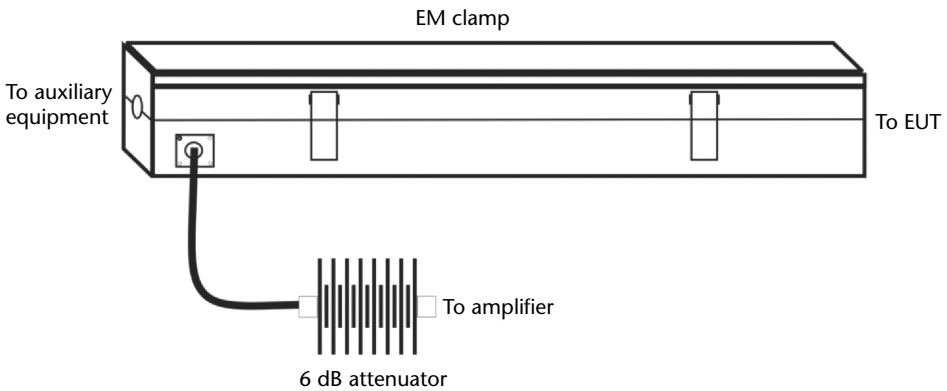


Figure 8.9 Conducted immunity arrangement using electromagnetic clamp.

8.2.3 Magnetic Field Immunity

The magnetic field immunity levels stipulated by the IEC/EN [7] are as follows:

- For uniform magnetic fields such as those provided by a Helmholtz coil or a simple loop, the level is between 1 A/m and 30 A/m over the frequency range 50 to 60 Hz.
- For point source magnetic fields, the level is 160 dBpT over the frequency range 30 Hz to 30 kHz.
- For power frequencies, the magnetic field induction level is 20A in the test circuit.

8.2.4 Immunity to Electrical Fast Transients

The immunity to electrical fast transients (EFT) (mains spikes) stipulated by the IEC/EN standards [7] are to levels of between 1 and 2 kV on mains ports and 500V to 1 kV on signal ports. (1 kV/500V is for residential, light industrial, and commercial, and 2 kV/1 kV for industrial.) The transient has a bandwidth of around 400 MHz.

There are two coupling methods specified. For power cables, a CDN is used, which uses 33 nF coupling capacitors. For signal cables, a capacitive coupling clamp is used, which comprises a metal enclosure through which the cable is passed. The clamp represents a capacitance of 100 pF [8].

The EFT is caused by arcing across switches that supply inductive loads. As the conventional electromechanical switch is opened, the back EMF from the inductive load causes the voltage across the switch to rise to a point that arcing occurs. At this point, current flows and the back EMF collapses. When the voltage drops to a certain level, the arc across the switch extinguishes. The voltage across the switch re-establishes and the process repeats itself until the energy from the inductive load is dissipated or the switch has opened sufficiently for the arc not to be sustained. The frequency of the arcing varies between 5 and 100 kHz, and the standards allow the use of either a 5-kHz repetition rate or a 100-kHz repetition rate. Figure 8.10 shows the voltage transients generated by a switch opening, and Figure 8.11 shows details of the fast transient test waveform.

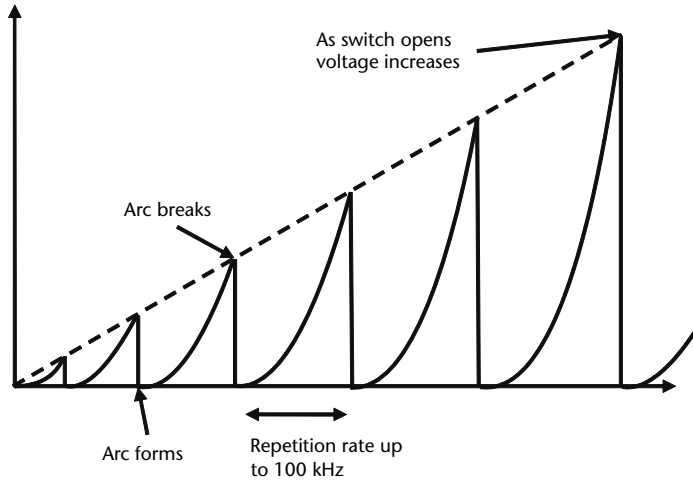


Figure 8.10 Voltage transients generated by a switch opening.

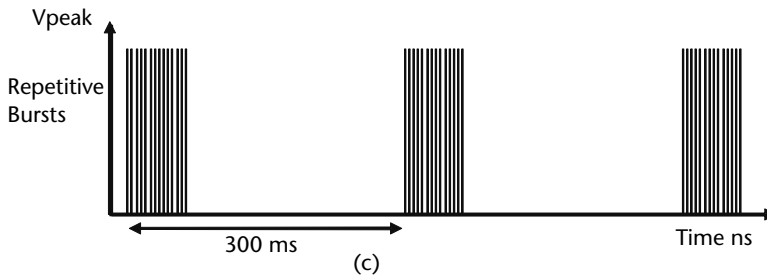
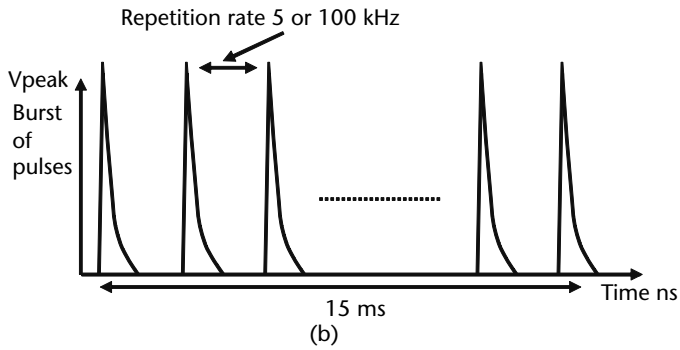
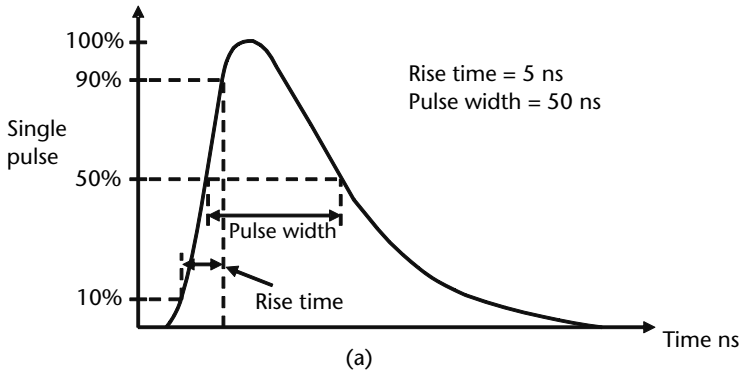


Figure 8.11 Details of fast transient test waveform.

8.2.5 Immunity to Electrostatic Discharges

The electrostatic discharge levels stipulated by IEC/EN are typically 8 kV for air discharge and 4 kV for contact discharge. Some standards require immunity to be demonstrated up to higher levels. For example, medical device standards (IEC/EN 60601-1-2) stipulate test levels up to 15 kV for life support apparatuses. The transient has a bandwidth of over 1 GHz [9].

There are two forms of electrostatic discharges required, contact and air. Air discharges are applied to surfaces declared by the manufacturer to be nonconductive. Contact discharges are applied to conductive surfaces. The contact discharge method was developed to improve test repeatability, as the air discharge is highly dependent on temperature, humidity, and speed of approach of the ESD simulator to the EUT. The contact discharge is favored as the electrostatic discharge is applied via a high voltage relay, which ensures good repeatability. Air discharges are dependent on the ambient temperature, humidity, atmospheric pressure, and the speed at which the gun approaches the EUT. Care needs to be taken to ensure that the ground lead of the ESD simulator is held away from the EUT, as it can affect coupling.

ESD discharges are also applied to the vertical coupling plane (VCP) and the horizontal coupling plane (HCP) to simulate induction. If a product does not have a ground path, such as battery powered devices, then they must be discharged after each ESD application.

Some standards require the ESD to be carried out starting at lower levels and increasing the voltage up to the specified level. This is because lower discharge voltages can have a higher bandwidth due to a faster rise time of the pulse [10].

The ESD simulator has a capacitor and resistor network to replicate the human body model (see Figure 8.12). The most common network is the 150-pF/330- Ω network, as is used for medical devices, and residential and commercial equipment. Automotive standards specify a variety of capacitor/resistor combinations, including 150 pF/330 Ω , 330 pF/330 Ω , 150 pF/2,000 Ω , and 330 pF/2,000 Ω [11].

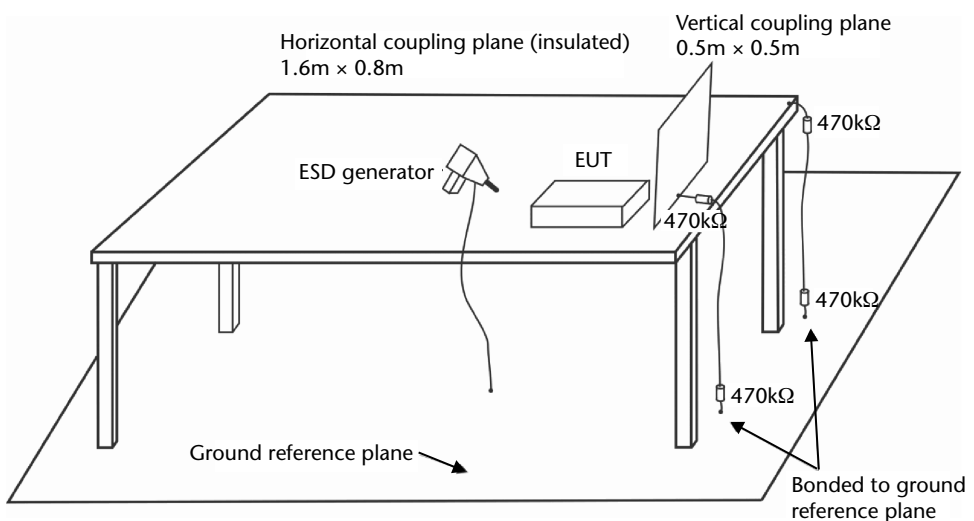


Figure 8.12 Electrostatic discharge test arrangement.

8.3 Conducted Emissions and Immunity

Conductive coupling can take place via resistive, capacitive, or inductive paths. A line impedance stabilization network (LISN) is connected between the mains power supply and the mains cable of the EUT as shown in Figure 8.13.

Line-conducted emissions refer to the voltage fed back to the mains from the EUT. There are two main sources for these signals. They travel from the EUT's logic

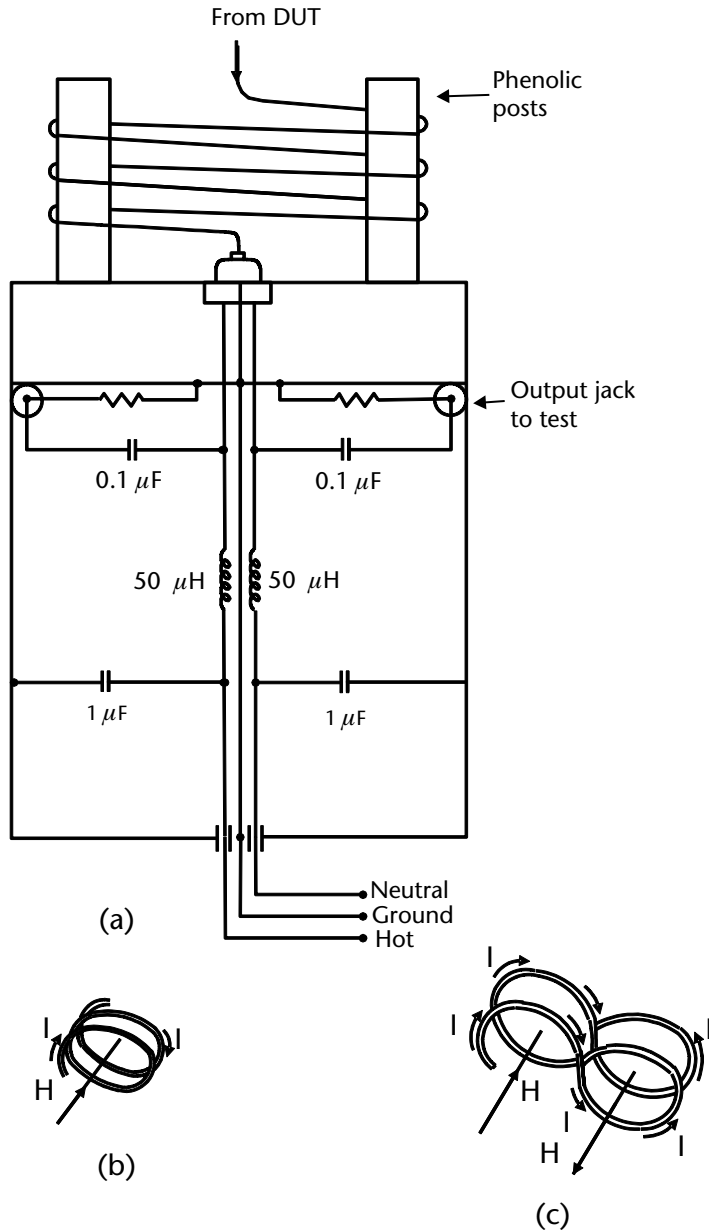


Figure 8.13 Line conducted emissions using an LISN: (a) Typical LISN set-up, (b) power cable wound in same direction, and (c) power cable wound into figure eight.

circuits through the power supply and back through the LISN. The second source for signals above 15 MHz is from digital circuits, such as the computer and its cables, which are picked up by the AC power cable acting as a receiving antenna. This latter source of emission can vary because it is dependent on cable placement [2]. The regulations stipulate that the level of these emissions in the frequency range 0.15 to 30 MHz must be less than $65 \text{ dB}\mu\text{V}$ (varies with frequency) for class B equipment. For class A equipment, the limits are $79 \text{ dB}\mu\text{V}$ and lower.

Line conducted emissions vary less with cable placement than radiated emissions, so these measurements lend themselves to automation. The FCC performs conducted emissions in an indoor test set-up. The EUT is placed on a 0.8-m-high wooden table which has a surface area of nominally $1\text{m} \times 1.5\text{m}$, but it may be larger or smaller to accommodate various sized EUTs. The AC cable is connected to an LISN. The AC cable is wound in a figure eight, if necessary, to reduce inductive effects. Figure 8.13(a) shows the LISN with typical internal circuitry. If the cable is wound in the same direction, there is a resultant magnetic field, as in Figure 8.13(b). However, if a figure eight configuration is used as in Figure 8.13(c), then the magnetic field in each section of the figure eight is in the opposite direction to that in the other, so that the fields cancel each other out and their resultant is zero. The EUT's I/O cables are arranged on the rest of the table. The engineer moves the I/O cables about to find the position that gives the maximum level of emissions. The AC power cable is kept rigid while these I/O cables are moved about. If a spectrum analyzer is used, an attenuator or a limiter is added to protect the analyzer from the low-frequency transients that would otherwise damage it. A measuring receiver with a quasi-peak detector may also be used [2]. Although a screened room is desirable for conducted emission testing, it is not necessary,

8.3.1 Immunity to Conducted Common- and Differential-Mode Voltages

The conducted immunity levels proposed by the IEC/CISPR [7] are as follows for residential, commercial, and light industrial environments:

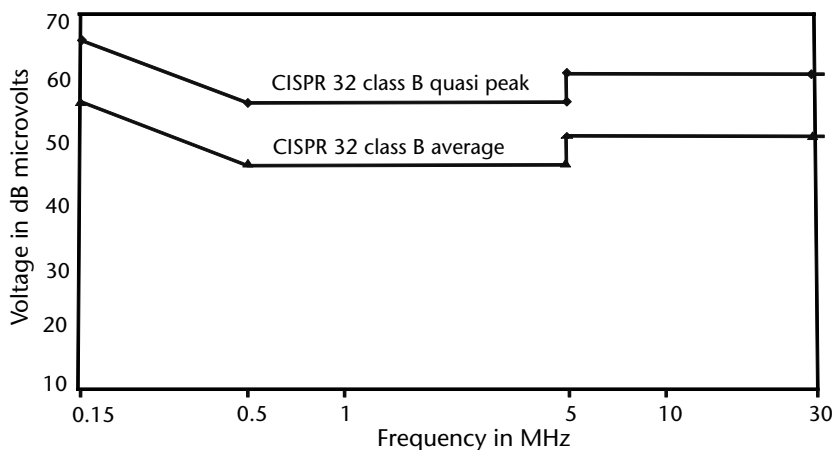


Figure 8.14 EN 55032 conducted limits for class B equipment.

3V rms for common-mode conduction over the frequency range of 50 kHz to 400 MHz;

For industrial environments the levels are at 10 V/m.

The preferred method of conducting this test is to use CDNs. This network is designed to present a common-mode impedance of 150Ω for the cable. Therefore, for a single conductor, a $100\text{-}\Omega$ resistance is used which, in series with the $50\text{-}\Omega$ output of the generator, yields a $150\text{-}\Omega$ impedance. For a two-wire conductor, a $200\text{-}\Omega$ resistance per line is used. This can be used up to at least four or eight wires, however, as the number of lines increases the balance becomes more difficult. The CDN provides the best control of the line impedance and protection of the auxiliary equipment which should not be subjected to the injected interference.

Alternative methods include the current injection probe which is favored by military standards. However, this method is not favored for the commercial standards, as the impedances are not controlled. In addition, the injection current probe is rather inefficient, requiring more expensive power amplifiers to attain the test levels. An improvement is the electromagnetic clamp which uses a long ferrite load to improve the isolation of the auxiliary equipment, and also allows a combined current injection and capacitive coupling technique to be used which reduces the required amplifier power.

8.4 Shielding Effectiveness of Solid Materials

The radiated emissions can be prevented from entering or leaving a device by adequate shielding. The shielding effectiveness depends on:

- The conductivity of the shield;
- The permeability of the shield;
- The permittivity of the shield;
- The thickness of the shield;
- The frequency of the incident radiation;
- The distance between the source and shield;
- The shape of the shield.

The shield should be grounded, and if made of aluminum it should not be anodized. Anodizing makes the aluminum nonconducting, so that it cannot be used as a ground. Electrolytic tin-plated steel, on the other hand, is a low-cost material that lends itself to the formation of multiple shields that can be soldered together [12]. Shielding materials can also be painted or sprayed onto surfaces. Nickel is often used as paint coating, but copper is almost four times more conductive for the same thickness, and the water-based copper is also more environmentally friendly [13]. It is also cheaper and easier to apply. A nickel coating increases resistance to corrosion, which is useful in outdoor locations.

Steel has a relative magnetic permeability of around 1,000, and is a good shield at low frequencies [14]. Copper has good conductivity and is relatively light. It is

used in solid and mesh form. Bronze is usually used in mesh form and in cases where magnetic and high frequency performance is not severe.

The SE of a material is the attenuation it presents to an electromagnetic wave, and is defined as the insertion loss in decibels obtained in the presence of the material. At low frequencies (i.e., far below 1 GHz), and when the source is in the near field of antennas, the electric and magnetic fields are considered separately and the shielding effectiveness can be defined for E-mode and H-mode, respectively.

Thus, the SE for the electric field is given by

$$SE = 20 \log_{10} \left(\frac{E_1}{E_2} \right) \quad (8.1)$$

where

E_1 is the electric field intensity in the absence of the material;

E_2 is the electric field intensity in the presence of the material.

SE for the magnetic field is given by

$$SE = 20 \log_{10} \left(\frac{H_1}{H_2} \right) \quad (8.2)$$

where

H_1 is the magnetic field intensity in the absence of the material;

H_2 is the magnetic field intensity in the presence of the material.

Solid materials prevent the penetration of electric and magnetic fields by three mechanisms:

1. Reflection (R) at the air–material interfaces;
2. Absorption (A) as the fields travel through the material;
3. Multiple internal reflections (MR) at the material–air interface.

Figure 8.15 shows the path traced by a wave incident at the surface of a shield. If the incident fields are E_1^i and H_1^i , then we can see that at the first air–material interface, parts of the fields are reflected (E_1^r and H_1^r) and parts are transmitted (E_1^t and H_1^t). These transmitted fields travel to the second material–air interface and suffer some absorption, so that when they reach this second interface the waves have lower levels (E_2^i and H_2^i). These incident waves at the back surface of the material are also partly transmitted as E_2^t and H_2^t , and partly reflected as E_2^r and H_2^r . The reflected waves are transmitted back to the first material–air interface, suffering some absorption, and the incident fields at this first material–air interface are E_3^i and H_3^i . At this interface they will again be partly reflected (E_3^r and H_3^r) and partly transmitted (E_3^t and H_3^t). The transmitted waves (E_3^t and H_3^t) due to multiple

internal reflections are not in phase with the first reflected waves (E_1^i and H_1^i) and thus reduce the resultant reflection loss of the material. Thus the contribution (MR) to the total shielding effectiveness is also called a correction term. It will only be significant under certain conditions. If the absorption of the shield is greater than 15 dB, or if thickness of the material is greater than the skin depth, then the fields will be greatly attenuated, so that the value of MR will be negligible.

8.4.1 Reflection Loss

The reflection loss depends on the type of wave incident on the shield. At frequencies where the source to shield distance is less than $< \lambda/2\pi$, there are three types of waves to be considered: magnetic mode reflection loss R_b , electric mode reflection loss R_e , and the reflection loss experienced by a plane wave R_p . Although the theoretical magnetic and electric reflection losses can be calculated, in practice, these fields cannot exist independently; thus, a predominantly magnetic field will always have an accompanying electric field, and a predominantly electric field will have an accompanying magnetic field. The magnitudes of the three types of reflection losses are shown in Figure 8.16. For a source-to-shield distance of 1m, this is equal to 2π at a frequency of 47.7 MHz. It can be seen that the theoretical reflection loss of a magnetic field alone is much less than that of a plane wave, but in practice, because there is also a small electric field present, the measured magnetic reflection loss is greater than the theoretical one. Similarly, the theoretical electric field reflection loss is higher than that for a plane wave, but in practice, because of the presence of a magnetic field, the measured values are lower than the theoretical ones.

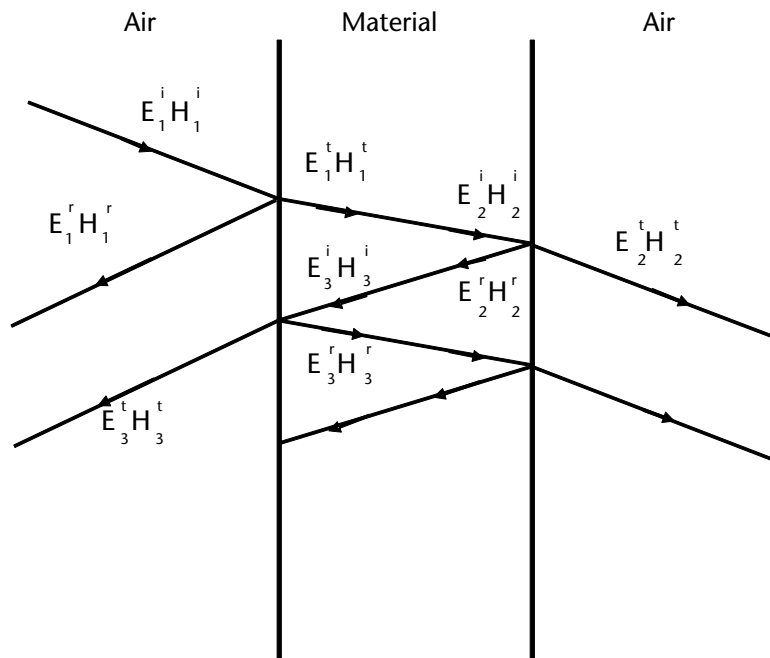


Figure 8.15 Path traced by a wave incident at the surface of a shield.

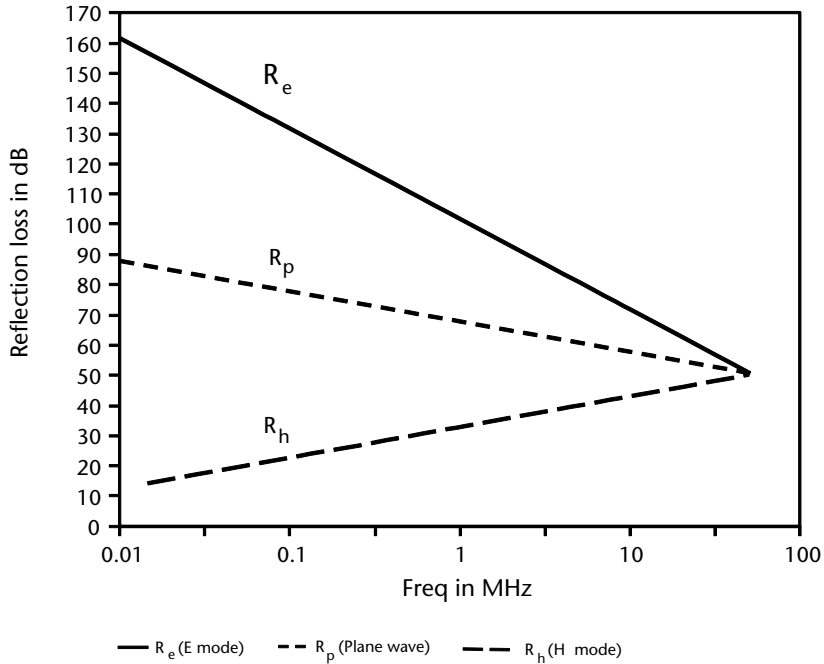


Figure 8.16 Reflection loss for electric, magnetic, and plane waves.

8.4.1.1 Magnetic Mode Reflection Loss

In the near field ($< \lambda/2\pi$) of magnetic field generators such as loops, and at low frequencies ($<< 2$ GHz) the magnetic field is more dominant and the wave impedance is lower than it would be under plane wave conditions. The reflection loss in this case is called the magnetic mode reflection loss and is given by:

$$R_b = 20 \log_{10} \left[0.452 \sqrt{\frac{\mu_r}{fr^2\sigma_r}} \right] + 0.136 \left[\sqrt{\frac{fr^2\sigma_r}{\mu_r}} \right] + 0.356 \quad (8.3)$$

where

R_b is the magnetic mode reflection loss in decibels;

r is the source-to-shield distance in inches;

f is the frequency in hertz;

μ_r is the magnetic permeability relative to a vacuum/air;

σ_r is the conductivity relative to copper.

If the source-to-shield distance is in meters, the following formula should be used:

$$R_b = 20 \log_{10} \left[0.01173 \sqrt{\frac{\mu_r}{fD^2\sigma_r}} \right] + 5.35 \left[\sqrt{\frac{fD^2\sigma_r}{\mu_r}} \right] + 0.356 \quad (8.4)$$

where D is in meters.

Another simpler formula that gives very slightly different values at frequencies above 10 kHz is given by:

$$R_b = 14.6 + 10 \log_{10} \left(\frac{fr^2 \sigma_r}{39.37^2 \mu_r} \right) \quad (8.5)$$

where

- R_b is the magnetic mode reflection loss in decibels;
- r is the source-to-shield distance in inches;
- f is the frequency in hertz;
- μ_r is the magnetic permeability relative to a vacuum/air;
- σ_r is the conductivity relative to copper.

If the source-to-shield distance is in meters, then the following formula applies:

$$R_b = 14.5 + 10 \log_{10} \left(\frac{fD^2 \sigma_r}{\mu_r} \right) \quad (8.6)$$

where

- R_b is the magnetic mode reflection loss in decibels;
- D is the source-to-shield distance in meters;
- f is the frequency in hertz;
- μ_r is the magnetic permeability relative to a vacuum/air;
- σ_r is the conductivity relative to copper.

The comparison between the values obtained for the two above formulas is demonstrated by Table 8.5 for a source-to-shield distance of 1m in the case of SAE 1045 steel, which has a relative magnetic permeability of 1,000 and a conductivity of 0.10 relative to copper. It can be seen that the detailed formula gives values for R_b that are about 0.5 (3.6%) higher at 10 kHz, and 0.03 lower (-0.05%) at 50 MHz.

Table 8.6 shows the magnitudes of R_b for different materials at three different frequencies. The values of relative magnetic permeability of the materials have been taken at 150 kHz and are lower at the frequencies above 150 kHz.

Since these formulas are rather complex, the variation of the magnetic reflection loss with the independent variables is not easy to see. However, if we vary just one of the variables while keeping the other variables constant, then we can see the effect of each of the variables on the magnetic reflection loss R_b .

8.4.1.1.1 Variation of Magnetic Reflection Loss with Permeability

Let us first of all consider the variation of the R_b as the relative magnetic permeability is increased from 1,000 to 80,000, while the conductivity relative to copper is kept at a constant value of 0.3, and the source shield distance is 1m. Figure 8.17

Table 8.5 Theoretical Magnetic Reflection Loss Using Equations (8.3) and (8.4)

Frequency (MHz)	R_b Approx Formula Equation 8.5	R_b Detailed Formula Equation 8.4	Percentage Difference between 8.4 and 8.5 Formulas
0.01	14.6	15.14	3.58
0.05	21.59	21.81	1.03
0.1	24.6	24.75	0.6
0.5	31.59	31.64	0.15
1	34.6	34.62	0.07
5	41.59	41.58	-0.02
10	44.6	44.59	-0.03
50	51.59	51.56	-0.05

$D = 1\text{m}$; μ_r is the magnetic permeability relative to a vacuum/air, and equals 1,000; and σ_r is the conductivity relative to copper, and equals 0.1.

shows the variation of R_b at three different frequencies, namely 10 kHz, 1 MHz, and 50 MHz. Examination of the curves reveals that as the permeability increases, the H -mode reflection loss R_b decreases. As the relative permeability increases from 1,000 to 10,000 by a factor of 10 (10 dB), the magnitude of R_b decreases by 10 dB,

Table 8.6 Theoretical Magnetic Reflection Loss for Different Materials

Material	Conductivity Relative to Copper	Magnetic Permeability μ_r Relative to a Vacuum	R_b Approximate Formula (150 kHz)	R_b Approximate Formula (1 MHz)	R_b Approximate Formula (50 MHz)
Aluminum	0.61	1	64.21	72.45	89.44
Beryllium	0.1	1	56.36	64.6	81.59
Brass	0.26	1	60.51	68.75	85.74
Cadmium	0.23	1	59.98	68.22	85.21
Copper	1	1	66.36	74.6	91.59
Gold	0.7	1	64.81	73.05	90.04
Hypernick	0.06	80,000	5.11	13.35	30.34
Iron	0.17	1,000	28.67	36.9	53.89
Lead	0.08	1	55.39	63.63	80.62
Magnesium	0.38	1	62.16	70.4	87.39
Mu-metal	0.03	80,000	2.1	10.34	27.33
Nickel	0.2	1	59.37	67.61	84.6
Permalloy	0.03	80,000	2.1	10.34	27.33
Phosphor bronze	0.18	1	58.91	67.15	84.14
Silver	1.05	1	66.57	74.81	91.8
Stainless steel	0.02	1,000	19.37	27.61	44.6
Tin	0.15	1	58.12	66.36	83.35
Zinc	0.29	1	60.98	69.22	86.21

from 49 to 39 dB at 1 MHz. Thus, R_b is inversely proportional to the relative permeability. We can also see that as the frequency is increased by a factor of 100 (20 dB) the magnitude of R_b also increases by 20 dB, from 9 dB at 10 kHz (and relative permeability of 10,000) to 29 dB at 100 MHz. Thus, R_b is directly proportional to the frequency. However, we must also be aware of the fact that although the distance between the source and shield has remained at a constant value of 1m, the electrical distance (i.e., the distance in terms of wavelength) has effectively decreased as the frequency is increased. If the shield-source distance is maintained at the same electrical distance, then the magnitude of R_b would decrease with increasing frequency. For instance, if the source-shield distance is maintained at 1/20th of the wavelength, then Figure 8.18 shows the variation of R_b with the magnetic permeability, using frequency as a parameter. The magnitude of R_b for a material with relative permeability of, say, 20,000 is 70 dB at 10 kHz, but reduces to 30 dB at 100 MHz. However, we must also be aware of the fact that the relative permeability of a material tends to decrease with frequency. For instance, the relative permeability of steel decreases from around 1,000 at DC to 300 at 400 MHz, and a mere 1 at about 1 GHz [15, Table A1]. Summarizing, we can say that the magnitude of R_b is inversely proportional to the relative permeability of the shield and proportional to the frequency if the physical source-shield distance is kept constant.

8.4.1.1.2 Variation of Magnetic Reflection Loss with Source-Shield Distance

Figure 8.19 shows the effect of varying the distance between the source and shield from 0.01 to 1m for a material with relative permeability of 1,000 and conductivity 0.3 relative to copper for three different frequencies. As the source-shield distance is increased by a factor of 10 (10 dB) from 0.01 to 0.1 (at 1 MHz, for instance), the

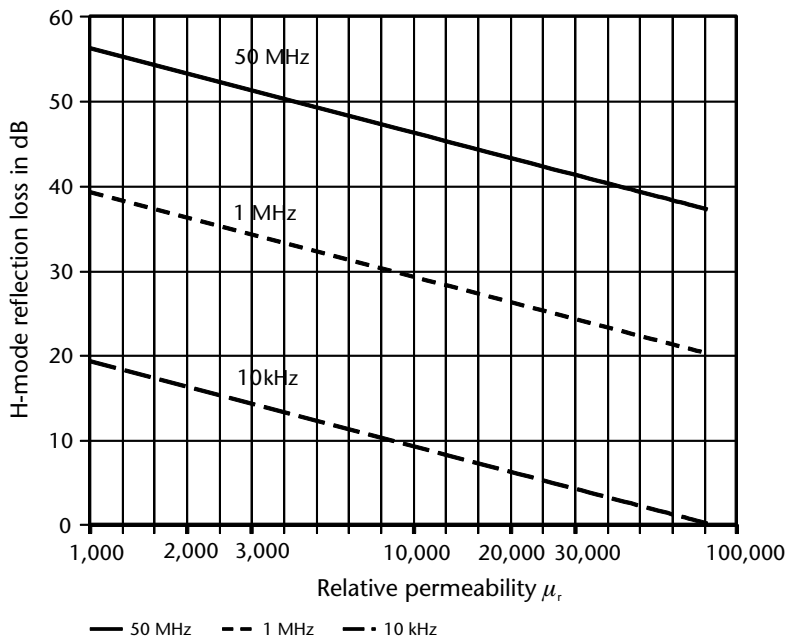


Figure 8.17 Variation of H -mode reflection loss with relative permeability for a source-shield distance of 1m and relative conductivity of 0.3.

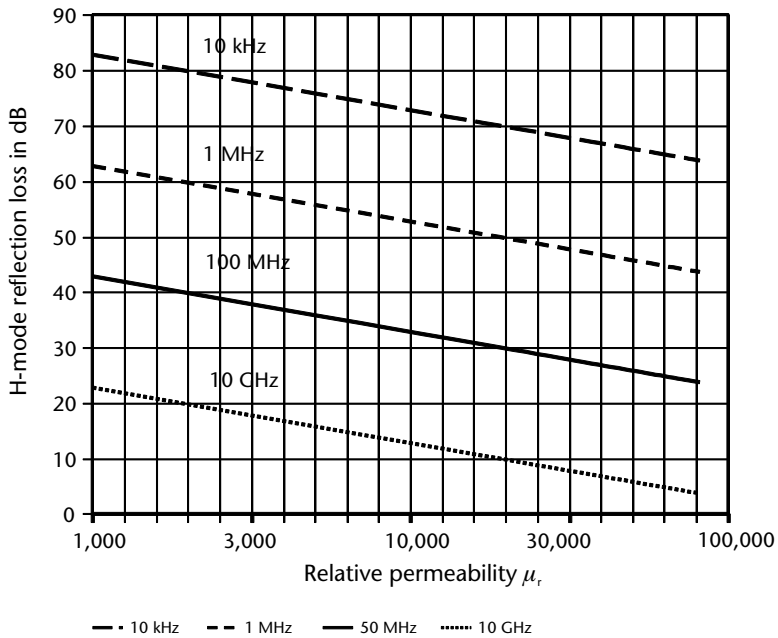


Figure 8.18 Variation of *H*-mode reflection loss with relative permeability for a source-shield distance of 0.05λ and relative conductivity of 0.3.

magnitude of R_b increases by 20 dB (or a factor of 100) from 19 to 39 dB. Thus, R_b is proportional to the square of the frequency.

If we vary the electrical distance (i.e., the distance in terms of the wavelength) then Figure 8.20 shows the variation of R_b with electrical distance from 0.01 to 0.16

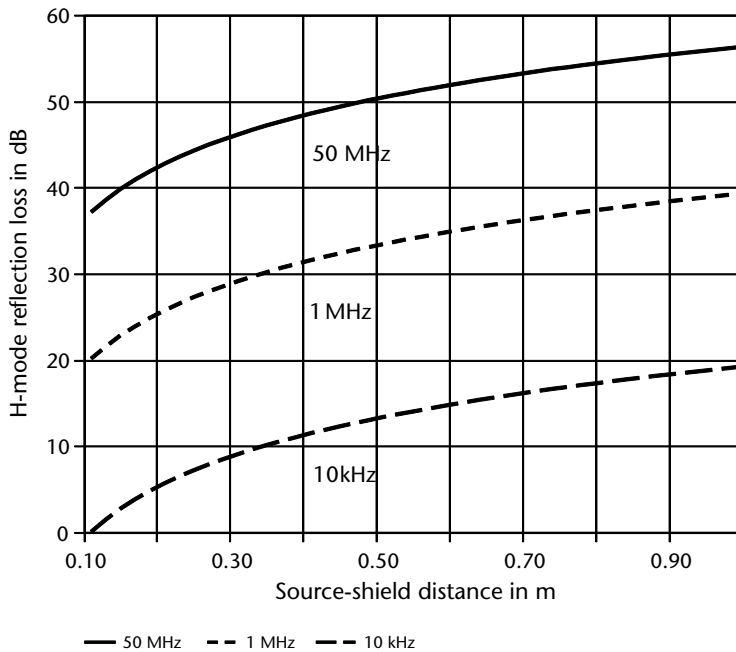


Figure 8.19 Variation of *H*-mode reflection loss with source-shield distance in meters for a relative permeability of 1,000 and relative conductivity of 0.3.

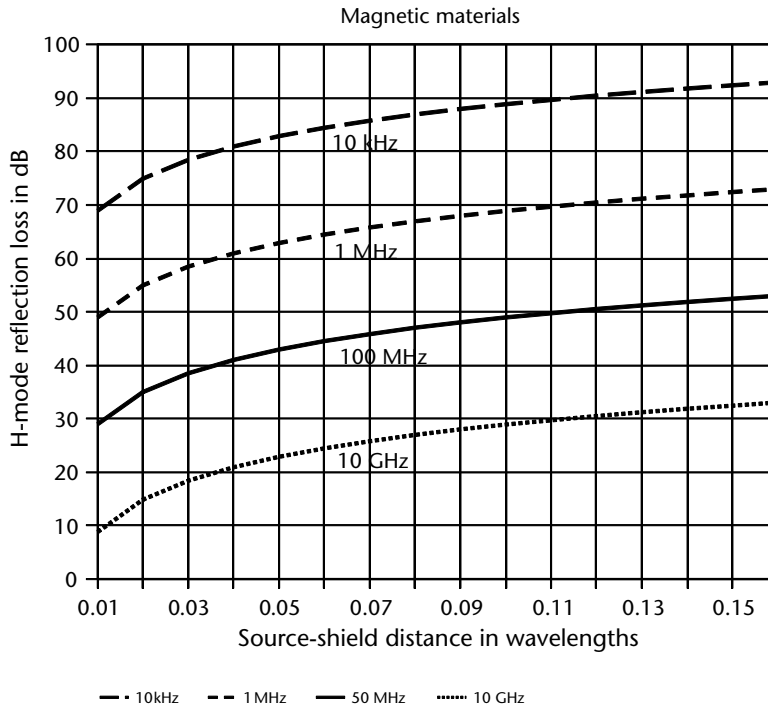


Figure 8.20 Variation of H -mode reflection loss with source-shield distance in wavelengths for a relative permeability of 1,000 and relative conductivity of 0.3.

wavelengths. We can see that the magnitude of R_b increases with increasing source-shield electrical distance, but R_b decreases with increasing frequency. At a source-shield distance of 0.09 wavelengths, for instance, the value of R_b decreases from 87 dB at 10 kHz, to 27 dB at 10 GHz. Summarizing, we can say that as we physically move the shield away from the source, the magnetic reflection loss increases as the square of the distance, and as the frequency is increased for a fixed separation of the source and shield, the magnitude of R_b also increases in linear proportionality.

8.4.1.1.3 Variation of Magnetic Reflection Loss with Relative Conductivity

We shall look at the variation of R_b with conductivity for magnetic as well as non-magnetic materials. If we have a nonmagnetic material with a relative permeability of 1, and the source-to-shield distance is maintained at a constant distance of 1m, we can see from Figure 8.21 that as the conductivity is increased the magnitude of the magnetic reflection loss R_b increases. For instance, at 10 kHz, if the relative conductivity is increased by a factor of 10 (10 dB) from 0.1 to 1.0, the magnitude of R_b also increases by 10 dB from 45 to 55 dB. We should also note that at a constant value of the conductivity, as the frequency is increased, the magnitude of R_b also increases in direct proportion.

However, if the electrical distance is kept constant at 1/20th of a wavelength (0.05λ), then we can see from Figure 8.22 that as the frequency is increased, and at a particular value of conductivity, the magnitude of R_b decreases. For instance, at a relative conductivity of 0.4, R_b has a magnitude of 114 dB at 10 kHz, but a factor of 100 higher at 1 MHz, R_b falls by 20 dB to 94 dB (a factor of 100 less).

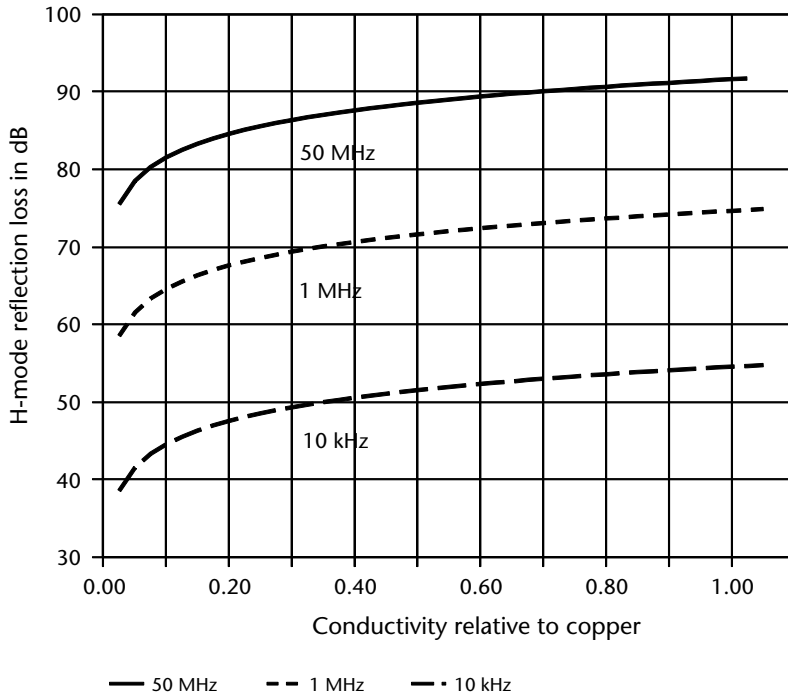


Figure 8.21 Variation of *H*-mode reflection loss with relative conductivity for a source-shield distance of 1m and relative permeability of 1.

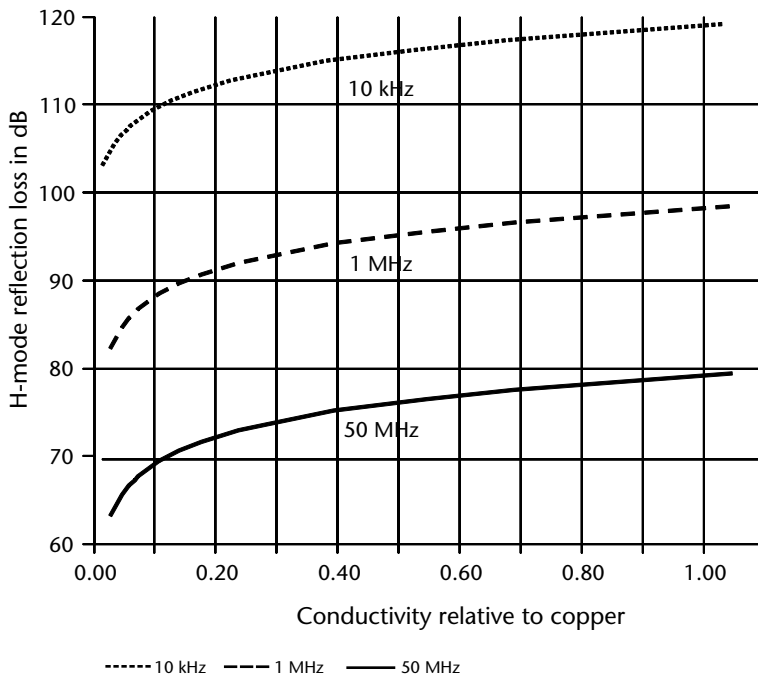


Figure 8.22 Variation of *H*-mode reflection loss with relative conductivity for a source-shield distance of 0.05λ and relative permeability of 1.

Summarizing, we can say that at a fixed physical distance R_b is directly proportional to the conductivity as well as the frequency.

A similar set of graphs are shown in Figures 8.23 and 8.24 for nonmagnetic materials which have a relative permeability of 1. Note that since R_b is inversely proportional to the relative permeability, the nonmagnetic materials have a higher magnetic reflection loss R_b than magnetic materials at a given value of conductivity. This is not an intuitive deduction. The magnetic reflection loss is quite low on the whole, compared with the reflection loss obtained to electric fields.

8.4.1.1.4 Dependence of R_b

Summarizing the dependence of R_b on the permeability, conductivity, and frequency, we can say that at a fixed physical distance between the shield and source

- R_b is inversely proportional to relative permeability (see Figure 8.17);
- R_b is proportional to conductivity for magnetic as well as nonmagnetic materials (see Figures 8.21 and 8.23);
- R_b is proportional to frequency (see Figures 8.17, 8.19, 8.21, and 8.23);
- R_b is also proportional to the square of source-shield physical distance (see Figure 8.19).

The dependence of R_b on the magnetic permeability, frequency, conductivity, and source-to-shield distance can be deduced from the simplified equations of (8.5) and (8.6), but is not obvious from (8.3) and (8.4). Table 8.6 lists the magnitudes

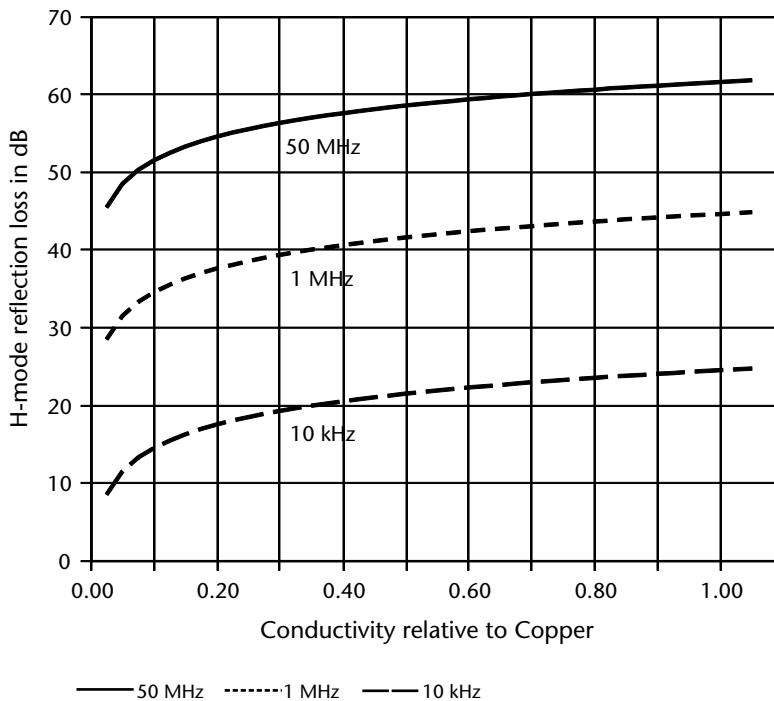


Figure 8.23 Variation of H -mode reflection loss with relative conductivity for a source-shield distance of 1m and relative permeability of 1,000.

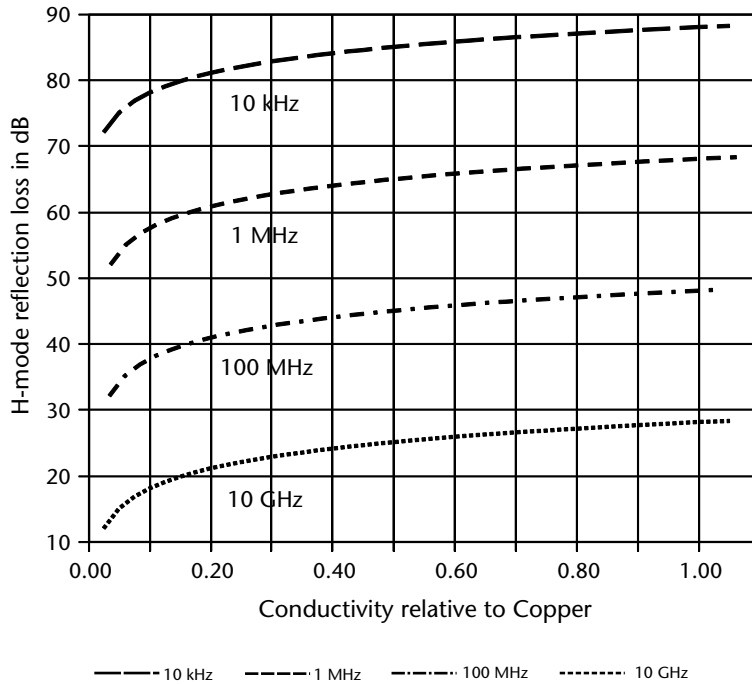


Figure 8.24 Variation of H -mode reflection loss with relative conductivity for a source-shield distance of 0.5λ and relative permeability of 1,000.

of R_b for some of the more common magnetic and nonmagnetic materials for a source-shield distance of 1m at three different frequencies. It is assumed that the magnetic materials are not saturated, and that the magnetic permeabilities are constant with frequency. The H -mode shielding effectiveness for iron is very low at low frequencies. For example, at 60 Hz, to obtain a SE of 100 dB, a 0.3-in (7.6 mm) thick shield is required [16].

8.4.1.2 Electric Mode Reflection Loss

In the near field of monopoles, dipoles, and so forth, the electric field is more dominant and the wave impedance is higher than that of a plane wave. The reflection loss, in this case, is called the electric mode reflection loss and is given by

$$R_e = 353.8 - 10 \log_{10} \left(\frac{r^2 f^3 \mu_r}{\sigma_r} \right) \quad (8.7)$$

where

r is the distance between the source and shield in inches;

f is the frequency in hertz;

$\mu_r = \mu/\mu_0$ is the magnetic permeability relative to a vacuum/air;

σ_r is the conductivity relative to that of copper.

If the source-to-shield distance is in meters, then the electric mode reflection loss is given by

$$R_e = 321.8 - 10 \log_{10} \left(\frac{D^2 f^3 \mu_r}{\sigma_r} \right) \quad (8.8)$$

where

D is the distance between the source and shield in meters;

f is the frequency in hertz;

$\mu_r = \mu/\mu_0$ is the magnetic permeability relative to a vacuum/air;

σ_r is the conductivity relative to that of copper.

Note that in some instances, the formula for the electric field reflection loss is quoted as

$$R_e = 321.8 + 10 \log_{10} \left(\frac{\sigma_r}{D^2 f^3 \mu_r} \right) \quad (8.9)$$

This formula is also correct, since the change of sign results in inversion of the quotient, due to the following identity

$$-10 \log_{10}(A) = +10 \log_{10} \left(\frac{1}{A} \right) \quad (8.10)$$

where A is a constant.

We can see from (8.9) that

- R_e is inversely proportional to the relative permeability (see Figure 8.25). At 1 MHz, as the relative permeability is increased by a factor of 10 (10 dB) from 1,000 to 10,000, R_e is decreased by 10 dB from 111 dB to 101 dB.
- R_e is inversely proportional to the square of the source-shield distance. Referring to Figure 8.26, at 1 MHz, as the distance is increased from 0.1 to 1.0 by a factor of 10 (10 dB), the magnitude of R_e decreases 20 dB from 161 to 141 dB. If we vary the electrical distance (i.e., the distance in terms of the wavelength) then Figure 8.27 shows the variation of R_e with electrical distance from 0.01 to 0.16 wavelengths. We can see that the magnitude of R_e decreases with increasing source-shield electrical distance, and R_e also decreases with increasing frequency.
- R_e is proportional to the relative conductivity (see Figure 8.28). For instance, at 1 MHz, when the relative conductivity is increased from 0.1 to 1.0 by a factor of 10 (10 dB), R_e also increases by 10 dB from 131 dB to 141 dB.
- R_e is inversely proportional to the cube of the frequency (for example, see Figure 8.28). At a conductivity of 0.7 for instance, R_e has a value of 200 dB at 10 kHz, which reduces by 60 dB to 140 dB when the frequency is increased by a factor of 100 (20 dB).

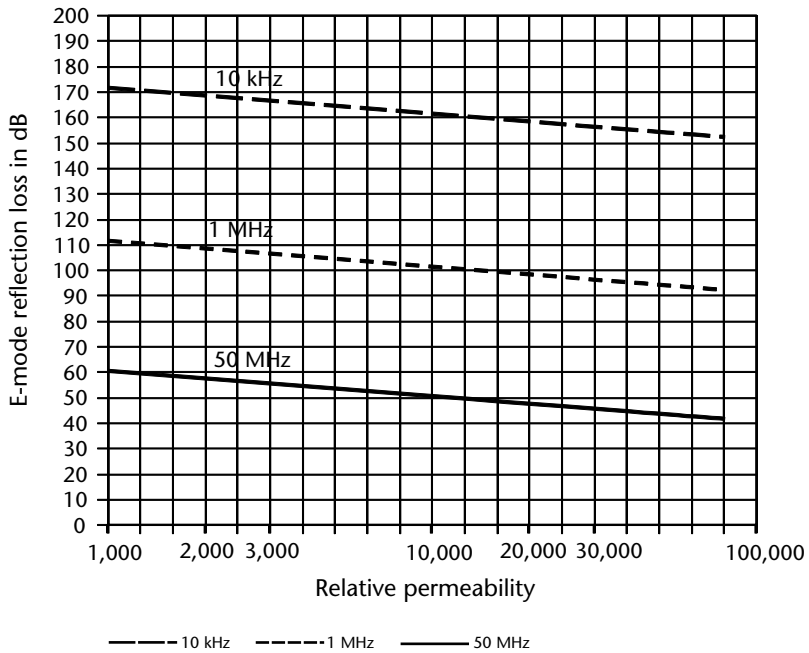


Figure 8.25 Variation of *E*-mode reflection loss with relative permeability for a source-shield distance of 1m and relative conductivity of 0.3.

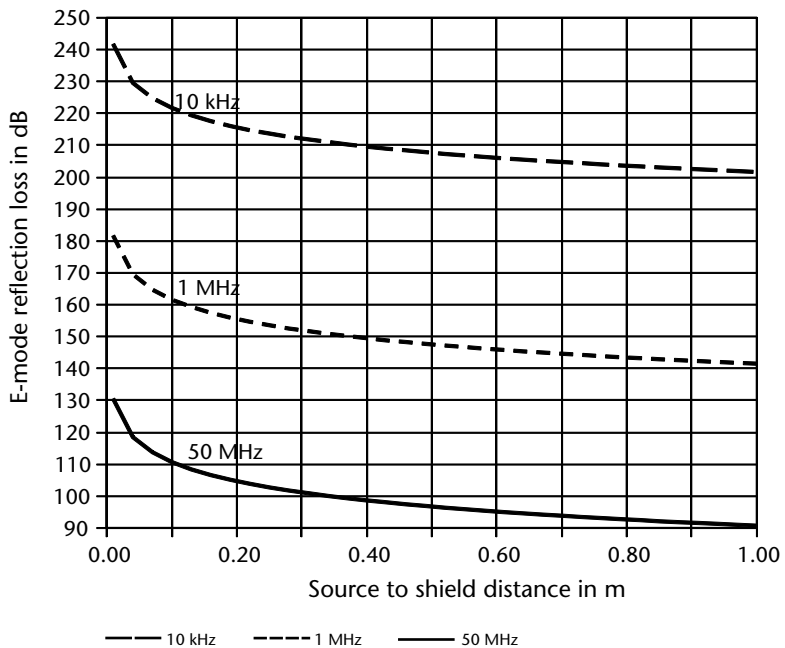


Figure 8.26 Variation of *E*-mode reflection loss with source-shield distance in meters for copper (relative permeability of 1 and relative conductivity of 1).

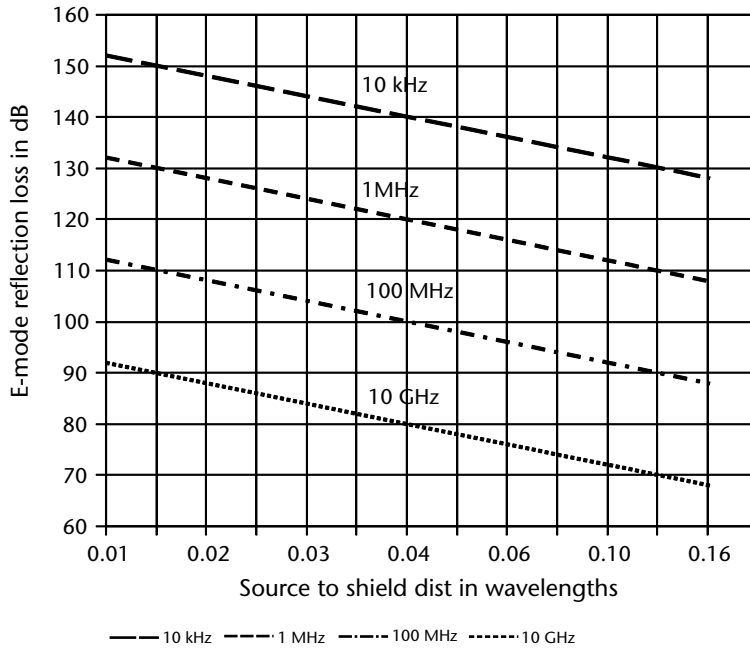


Figure 8.27 Variation of E-mode reflection loss with source-shield distance in wavelengths for copper (relative permeability of 1 and relative conductivity of 1).

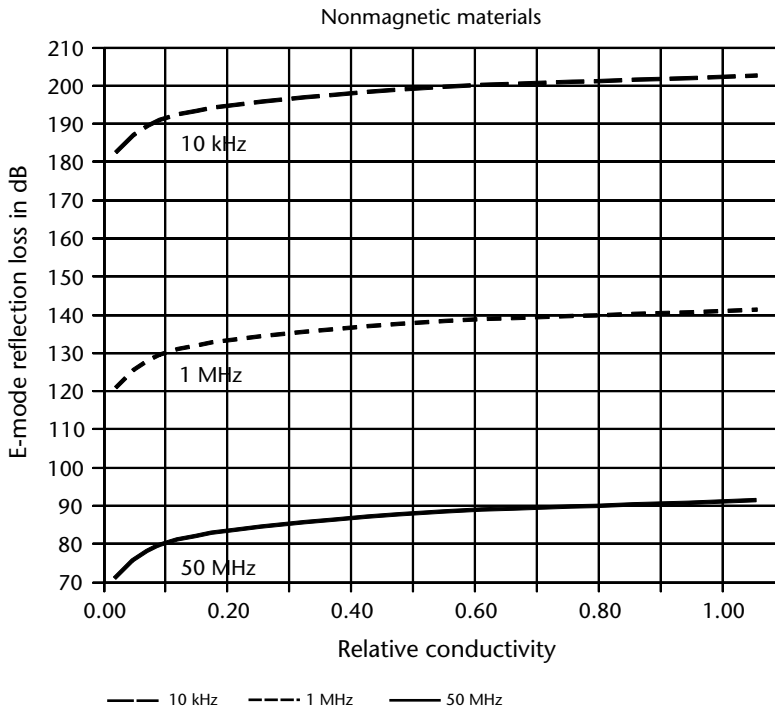


Figure 8.28 Variation of E-mode reflection loss with relative conductivity for a source-shield distance of 1m and relative permeability of 1.

Reflection loss for the electric field is greatest at low frequencies and for high conductivity materials [12]. It decreases with frequency and tends to infinity at DC. The reflection at the surface of the material depends on its surface resistivity.

The resistivity of the material is the resistance of unit thickness, unit width, and unit length. Thus, the resistivity has units of ohms multiplied by area (length squared) divided by length; that is, ohms per meter. In the case of surface resistance, there is no thickness, so the surface resistivity is the resistance of unit width and unit length. Thus, the units of surface resistivity are ohms multiplied by a unit of length and divided by a unit of width, which results in units of ohms. Since the surface resistivity has the same units as the resistance, it is expressed in ohms per square (Ω/sq) to distinguish it from resistance. The term per square means that it is the resistance of a square of a surface. Any unit may be used for the width and length of the surface area, as long as the units are used for both dimensions.

This is most important between frequencies from 1 MHz to 1 GHz. High conductivity or low resistivity is required for good screening. The magnitudes of R_e at three different frequencies for some common materials are shown in Table 8.7. It is assumed that the magnetic materials are not saturated, and that the magnetic permeabilities are constant with frequency.

Table 8.7 Theoretical Magnetic Reflection Loss for Different Materials with a Source-to-Shield Distance of 1m

<i>Material</i>	<i>Conductivity Relative to Copper</i>	<i>Magnetic Permeability Relative to a Vacuum</i>	R_e (10 kHz)	R_e (1 MHz)	R_e 100 MHz
Aluminum	0.61	1.00	199.45	139.45	79.45
Brass	0.26	1.00	195.75	135.75	75.75
Cadmium	0.23	1.00	195.22	135.22	75.22
Copper	1.00	1.00	201.60	141.60	81.60
Gold	0.70	1.00	200.05	140.05	80.05
Hypernick	0.06	80000	189.38	129.38	69.38
Iron	0.17	1000.	193.90	133.90	73.90
Lead	0.08	1.00	190.63	130.63	70.63
Magnesium	0.38	1.00	197.40	137.40	77.40
Mumetal	0.03	80000	186.37	126.37	66.37
Nickel	0.20	1.00	194.61	134.61	74.61
Permalloy	0.03	80000	186.37	126.37	66.37
Phosphor bronze	0.18	1.00	194.15	134.15	74.15
Silver	1.05	1.00	201.81	141.81	81.81
Stainless steel	0.02	1000	184.61	124.61	64.61
Tin	0.15	1.00	193.36	133.36	73.36
Zinc	0.29	1.00	196.22	136.22	76.22

8.4.1.3 Plane Wave Reflection Loss

In the far field of antennas, the wavefront is plane and the wave impedance is 377Ω . In this case, the source-to-shield distance does not affect the shielding effectiveness of the shield. The plane wave reflection loss R_p is given by

$$R_e = 168 - 10\log_{10}\left(\frac{f\mu_r}{\sigma_r}\right) \quad (8.11)$$

where

f is the frequency in hertz;

μ_r is the relative permeability;

σ_r is the conductivity relative to that of copper.

Equation (8.11) can be rewritten, using the identity of (8.10), as

$$R_e = 168 + 10\log_{10}\left(\frac{\sigma_r}{f\mu_r}\right) \quad (8.12)$$

Figures 8.29 through 8.31 show the variation of the plane wave reflection loss with relative permeability and relative conductivity (for magnetic and nonmagnetic materials). From these figures and (8.11) we can see that the plane wave reflection loss is

- Inversely proportional to the relative permeability (see Figure 8.29). As the relative permeability increases from 2,000 to 20,000 (by a factor of 10 or 10 dB) at 100 MHz, the magnitude of R_p decreases 10 dB from 50 to 40 dB.
- Inversely proportional to the frequency. In Figure 8.29, as the frequency is increased by a factor of 100 (20 dB) from 1 to 100 MHz, the magnitude of R_p decreases from 70 to 50 dB at a relative permeability of 2,000.
- Directly proportional to the relative conductivity. In Figure 8.30, as the conductivity is increased from 0.1 to 1 at 100 MHz, the magnitude of R_p increases from 78 to 88 dB.

The variation of plane wave reflection loss with relative conductivity for a relative permeability of 1,000 is shown in Figure 8.31.

The theoretical values of the plane wave reflection loss at three different frequencies for some common materials are given in Table 8.8. It is assumed that the magnetic materials are not saturated, and that the magnetic permeabilities are constant with frequency.

8.4.2 Absorption Loss

The absorption loss A of planar materials is given by

$$A = 3.34t\sqrt{\sigma_r\mu_r f} \quad (8.13)$$

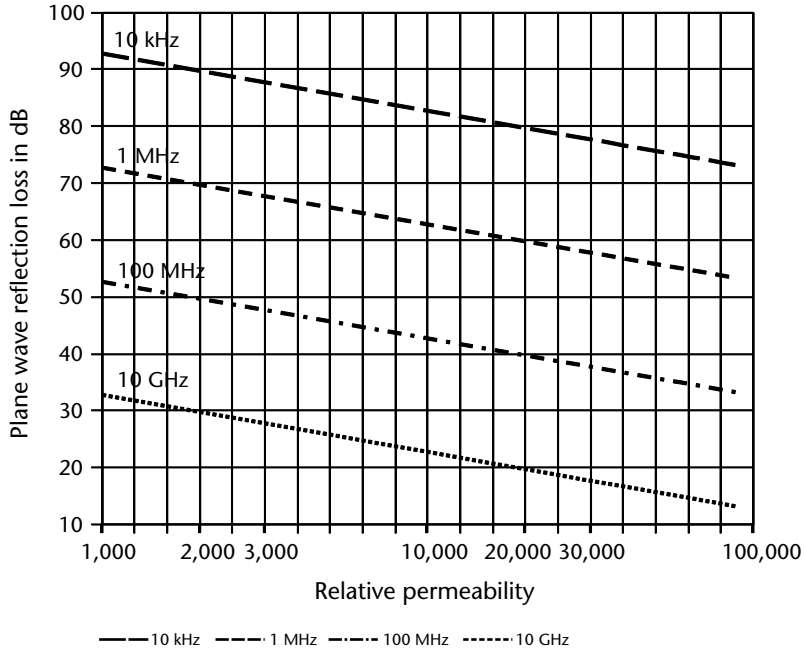


Figure 8.29 Variation of plane wave reflection loss with relative permeability for a relative conductivity of 0.3.

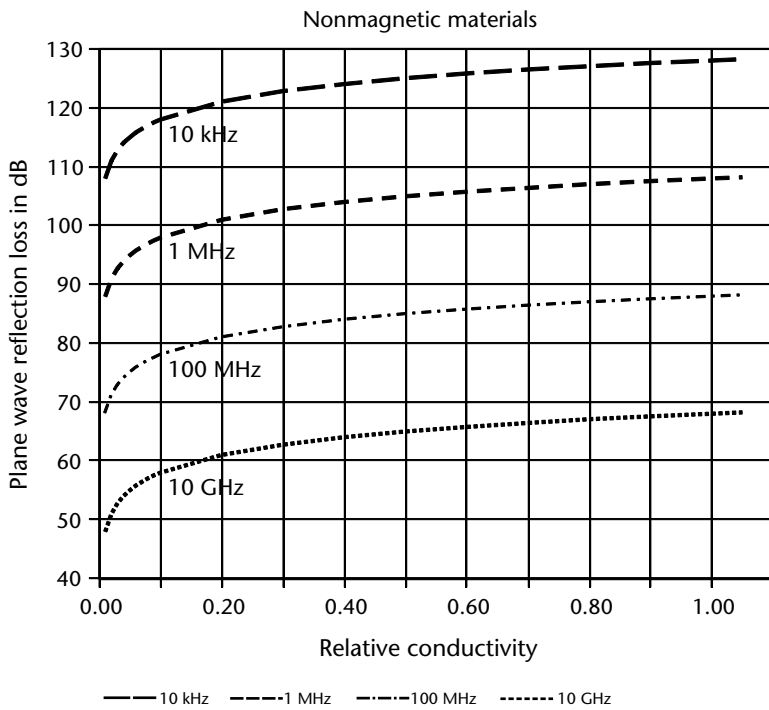


Figure 8.30 Variation of plane wave reflection loss with relative conductivity for a relative permeability μ_r of 1.

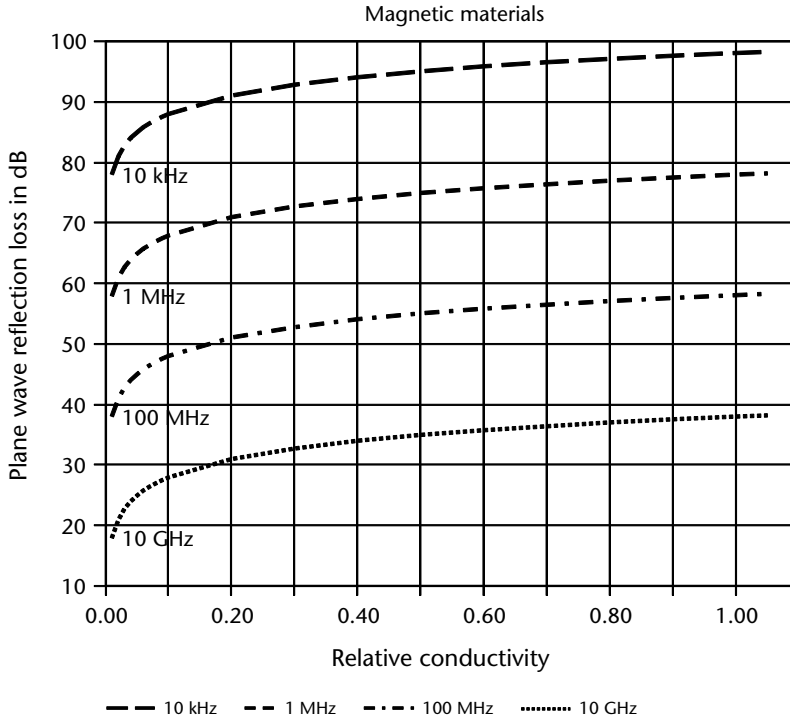


Figure 8.31 Variation of plane waves reflection loss with relative conductivity for a relative permeability μ_r of 1,000.

Table 8.8 Theoretical Plane Wave Reflection Loss for Different Materials

Material	Conductivity Relative to Copper	Magnetic Permeability Relative to a Vacuum	R_p (100 kHz)	R_p (1 MHz)	R_p (50 MHz)
Brass	0.26	1.00	110.39	102.15	85.16
Cadmium	0.23	1.00	109.86	101.62	84.63
Copper	1.00	1.00	116.24	108.00	91.01
Gold	0.70	1.00	114.69	106.45	89.46
Hypernick	0.06	80000	54.99	46.75	29.76
Iron	0.17	1000	78.54	70.30	53.31
Lead	0.08	1.00	105.27	97.03	80.04
Magnesium	0.38	1.00	112.04	103.80	86.81
Mu-metal	0.03	80000	51.98	43.74	26.75
Nickel	0.20	1.00	109.25	101.01	84.02
Permalloy	0.03	80000	51.98	43.74	26.75
Phosphor bronze	0.18	1.00	108.79	100.55	83.56
Silver	1.05	1.00	116.45	108.21	91.22
Stainless steel	0.02	1000	69.25	61.01	44.02
Tin	0.15	1.00	108.00	99.76	82.77
Zinc	0.29	1.00	110.86	102.62	85.63

where

A is in decibels;

t is the thickness in inches;

μ_r is the magnetic permeability relative to vacuum/air;

f is the frequency in hertz;

σ_r is the conductivity relative to copper.

If the thickness of the shield is in meters, then the absorption loss A is given by

$$A = 131T\sqrt{\sigma_r\mu_rf} \quad (8.14)$$

where T is the thickness in meters.

Figures 8.32 and 8.33 show the absorption loss obtained by thin shields of thicknesses 1 and 10 μm , respectively. Since the relative permeabilities of magnetic materials vary between 1,000 and 80,000, the absorption losses of magnetic materials are much higher than those obtained with nonmagnetic materials. Thus, in the case of nonmagnetic materials, there is little point in increasing the thickness beyond the skin depth (see (8.14) for a definition of skin depth). Figure 8.34 shows the variation of the absorption with relative conductivity for nonmagnetic materials with relative permeabilities of 1. From these figures and (8.13), it can be seen that the following applies:

- The absorption is proportional to the thickness of the material. Referring to Figures 8.32 and 8.33, we can see that for a particular frequency and relative permeability, the absorption loss for the 10- μm -thick shield of Figure 8.33 is ten times higher than the absorption loss for the 1- μm -thick shield of Figure 8.32.
- The absorption is proportional to the square root of the relative magnetic permeability. In Figure 8.32, as the relative permeability increases by a factor of 10 from 2,000 to 20,000, the magnitude of A increases at 1 MHz by a factor of 3.16, from 3.16 to 10. Since 3.16 is the square root of 10, it follows that A is proportional to the square root of the relative permeability.
- The absorption is proportional to the square root of the relative conductivity. In Figure 8.34, as the conductivity is increased by a factor of 10, from 0.1 to 1 at a frequency of 1 MHz, the magnitude of A increases by a factor of 3.16, from 40 to 126.
- The absorption is proportional to the square root of the frequency. Referring again to Figure 8.34, as the frequency is increased by a factor of 100 from 10 kHz to 1 MHz, the magnitude of A increases by a factor of 10, from 10 dB to 100 dB at a relative conductivity of 0.6.

The absorption is independent of the distance between the source and the shield, and is also independent of the type of wave. It is the same for a magnetic, electric, or plane wave. If the absorption is less than 15 dB, the shield is designated as electrically thin. As the frequency is increased, the skin depth decreases. The skin depth

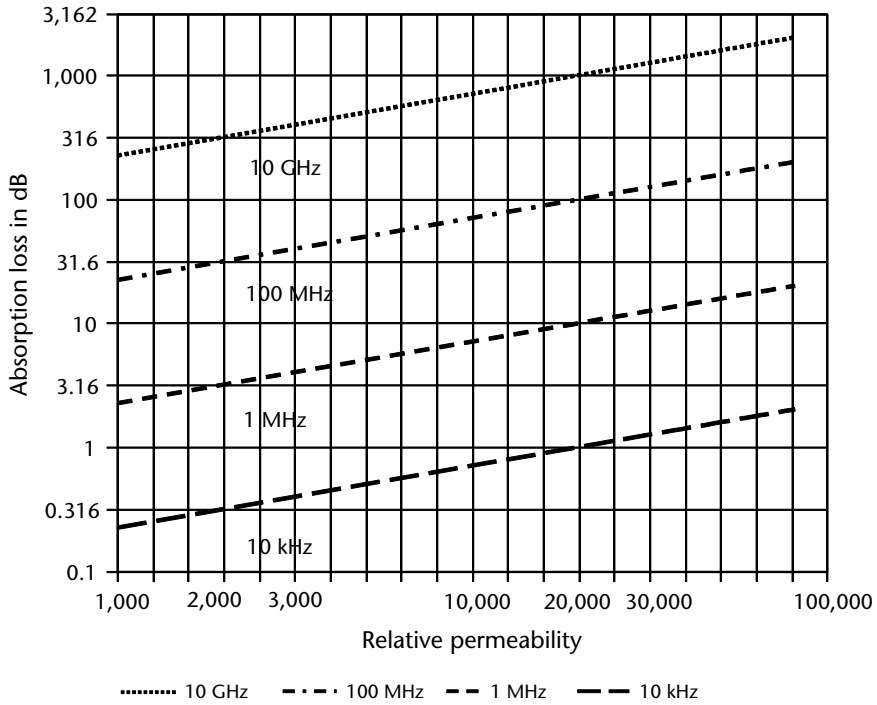


Figure 8.32 Variation of absorption loss with relative permeability for a 1- μm shield of relative conductivity 0.3.

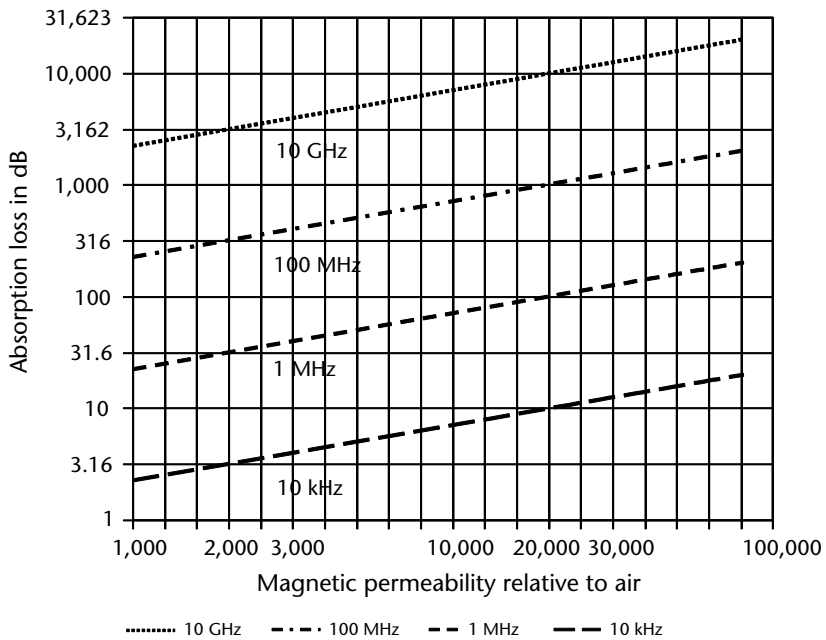


Figure 8.33 Variation of the absorption loss with relative permeability for a 10- μm shield of relative conductivity of 0.3.

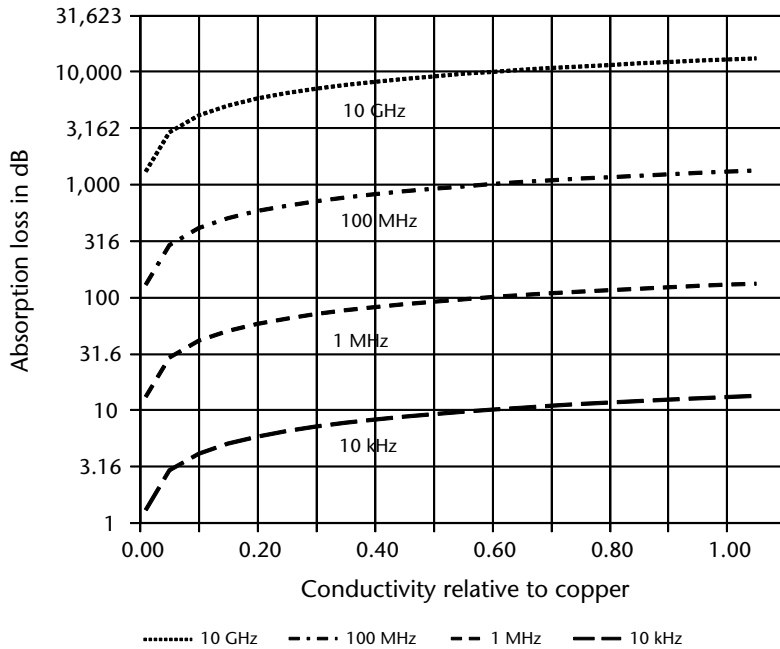


Figure 8.34 Variation of absorption loss with relative conductivity for a 10- μm shield of relative permeability μ_r of 1.

δ in meters is defined as the depth of penetration in a conductor when the electric field falls to $1/e$ (where e is 2.718) of its magnitude at the surface of the conductor. The skin depth is given by

$$\delta = \frac{1}{\sqrt{\pi\sigma\mu f}} \tag{8.15}$$

where

- δ is the skin depth in meters;
- σ is the conductivity in siemens per meter (S/m);
- μ is the permeability in henries per meter (H/m); and
- f is the frequency in hertz.

Table 8.9 lists the absorption loss at three different frequencies for some common materials. We can see that the absorption loss for magnetic materials is much higher than that for nonmagnetic materials. It is assumed that the magnetic materials are not saturated, and that the magnetic permeabilities are constant with frequency.

8.4.3 Multiple Reflection Loss

The multiple reflection loss in decibels is given by

$$MR = 20\log_{10}[1 - e^{-(2T/\delta)}] \tag{8.16}$$

where T is the thickness in meters, and δ is the skin depth in meters.

Table 8.9 Theoretical Absorption Loss for Different Materials with a Material Thickness of 0.1 mm

<i>Material</i>	<i>Conductivity Relative to Copper</i>	<i>Magnetic Permeability Relative to a Vacuum</i>	<i>A (100 kHz)</i>	<i>A (1 MHz)</i>	<i>A (50 MHz)</i>
Aluminum	0.61	1.00	3.96	10.23	72.35
Beryllium	0.10	1.00	1.60	4.14	29.29
Brass	0.26	1.00	2.59	6.68	47.23
Cadmium	0.23	1.00	2.43	6.28	44.42
Copper	1.00	1.00	5.07	13.10	92.63
Gold	0.70	1.00	4.24	10.96	77.50
Hypernick	0.06	80000	351.51	907.59	6417.66
Iron	0.17	1000	66.15	170.80	1207.76
Lead	0.08	1.00	1.44	3.71	26.20
Magnesium	0.38	1.00	3.13	8.08	57.10
Mu-metal	0.03	80000	248.56	641.77	4537.97
Nickel	0.20	1.00	2.27	5.86	41.43
Permalloy	0.03	80000	248.56	641.77	4537.97
Phosphor Bronze	0.18	1.00	2.15	5.56	39.30
Silver	1.05	1.00	5.20	13.42	94.92
Stainless steel	0.02	1000	22.69	58.58	414.26
Tin	0.15	1.00	1.97	5.07	35.88
Zinc	0.29	1.00	2.73	7.05	49.88

This is a correction term that is nearly always negative so that it reduces the reflection loss of the shield. It has to be considered only in cases where the material is much thinner than the skin depth, or when the absorption is less than about 10 dB. Since the correction term is only dependent on the thickness of the shield and the absorption loss, it is also independent of the source-shield distance and the type of incident wave.

8.4.4 Total Shielding Effectiveness

The total shielding effectiveness of a planar material depends on the type of incident field. The only difference is in the reflection loss presented to the incident fields. The absorption and multiple reflection losses are the same for all types of incident fields. Figures 8.35 to 8.37 show the insertion loss for the individual components, as well as the total SE obtained for magnetic, electric, and plane waves. These are for a 1- μ m-thick SAE 1045 steel shield at a source-shield distance of 1m.

In the case of copper, the SE is mainly due to the high reflection loss to the electric mode, so there is little to be gained from increasing the thickness. Tables 8.10 to 8.14 list the theoretical individual components for a 0.1-mm-thick shield of copper, aluminum, SAE 1045 steel, tin, and μ -metal at four different frequencies. It is assumed that the magnetic materials are not saturated, and that the magnetic permeabilities are constant with frequency.

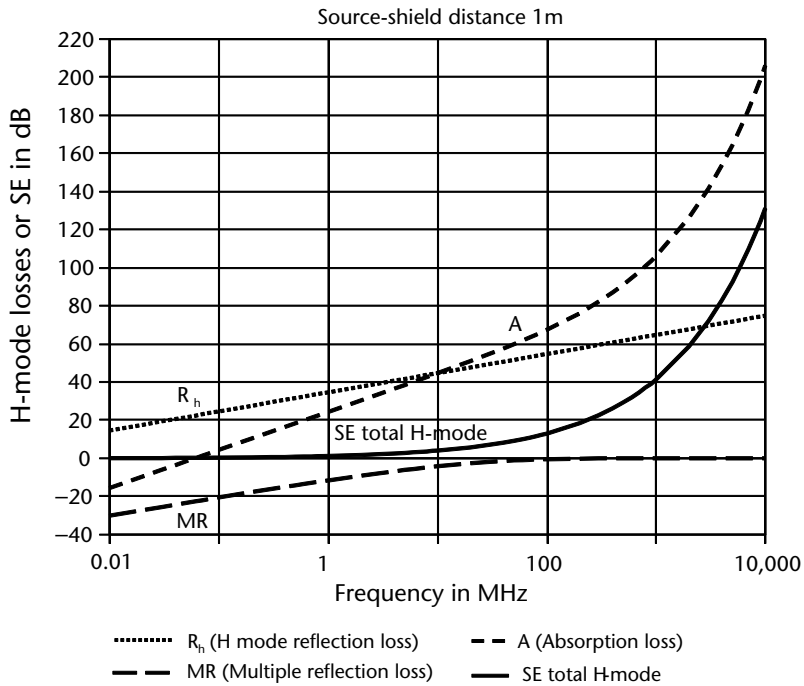


Figure 8.35 Variation of H-mode shielding effectiveness with frequency for 1 μm of SAE 1045 steel with relative permeability of 1,000 and relative conductivity of 0.1.

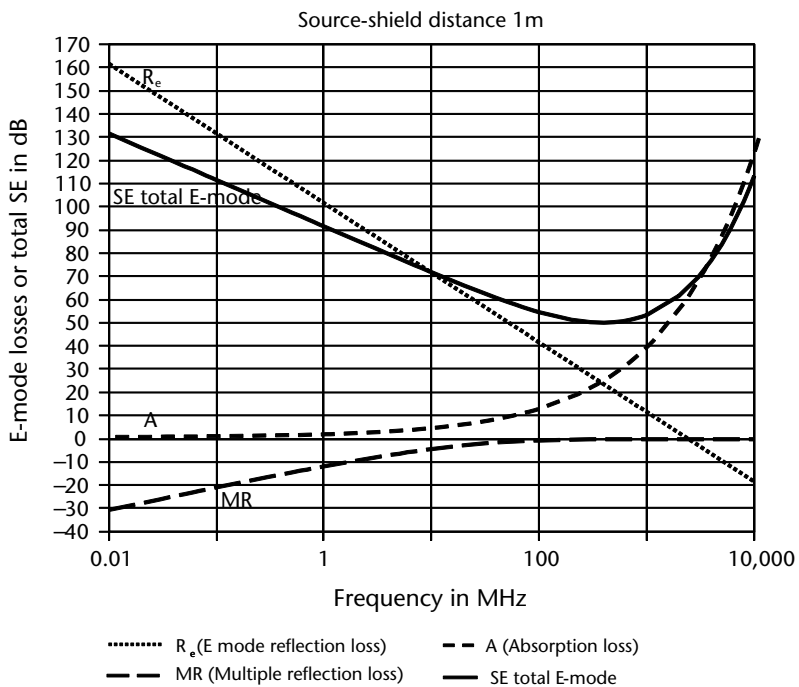


Figure 8.36 Variation of E-mode shielding effectiveness with frequency for 1 μm of SAE 1045 steel with relative permeability of 1,000 and relative conductivity of 0.1.

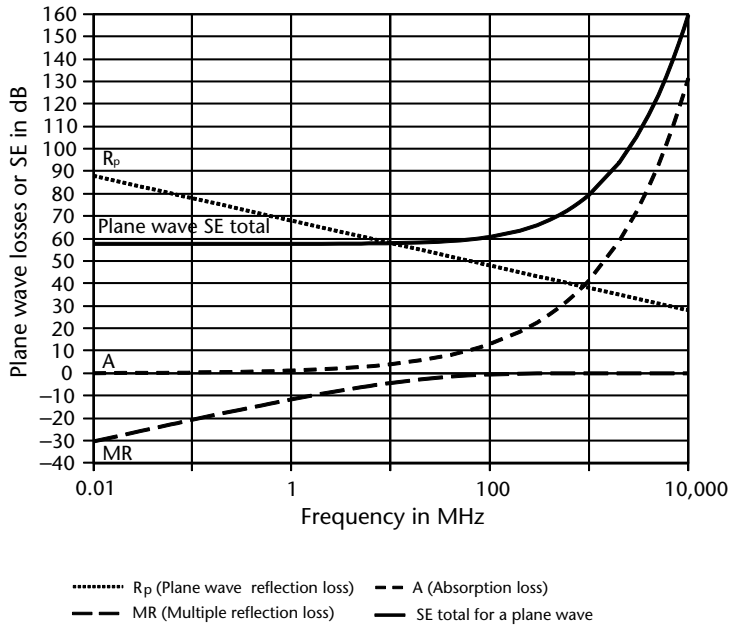


Figure 8.37 Variation of plane wave shielding effectiveness with frequency for 1 μm of SAE 1045 steel with relative permeability of 1,000 and relative conductivity of 0.1.

Table 8.10 Theoretical Shielding Effectiveness of Copper with a Source-to-Shield Distance of 1m, Relative Magnetic Permeability of 1, and Thickness of 0.1 mm

Frequency	50 Hz	1 kHz	10 kHz	1 MHz	100 MHz
R_e	270.83	231.80	201.80	141.80	81.80
R_b	31.59	44.60	54.60	74.60	94.60
R_p	151.01	138.00	128.00	108.00	88.00
A	0.09	0.42	1.31	13.14	131.40
MR	-39.42	-26.57	-17.02	-2.14	0.00
SE E-mode	231.50	205.64	186.10	152.80	213.20
SE H-mode	-7.74	18.44	38.90	85.60	226.00
SE plane wave	111.68	111.84	112.30	119.00	219.40

Table 8.11 Theoretical Shielding Effectiveness of Aluminum with a Source-to-Shield Distance of 1m, Relative Magnetic Permeability of 1, Conductivity Relative to Copper of 0.61, and Thickness of 0.1 mm

Frequency	50 Hz	1 kHz	10 kHz	1 MHz	100 MHz
R_e	268.68	229.65	199.65	139.65	79.65
R_b	29.44	42.45	52.45	72.45	92.45
R_p	148.86	135.85	125.85	105.85	85.85
A	0.07	0.32	1.03	10.26	102.63
MR	-41.56	-28.67	-19.02	-3.16	0.00
SE E-mode	227.20	201.30	181.66	146.75	182.28
SE H-mode	-12.04	14.10	34.46	79.55	195.08
SE plane wave	107.38	107.50	107.86	112.95	188.48

Table 8.12 Theoretical Shielding Effectiveness of SAE 1045 steel with a Source-to-Shield Distance of 1m, Relative Magnetic Permeability of 1,000, Conductivity Relative to Copper of 0.1, and Thickness of 0.1 mm

<i>Frequency</i>	<i>50 Hz</i>	<i>1 kHz</i>	<i>10 kHz</i>	<i>1 MHz</i>	<i>100 MHz</i>
R_e	230.83	191.80	161.80	101.80	41.80
R_b	-8.41	4.60	14.60	34.60	54.60
R_p	111.01	98.00	88.00	68.00	48.00
A	0.93	4.16	13.14	131.40	1314.00
MR	-19.84	-8.37	-2.14	0.00	0.00
SE <i>E</i> -mode	211.92	187.59	172.80	233.20	1355.80
SE <i>H</i> -mode	-27.32	0.39	25.60	166.00	1368.60
SE plane wave	92.10	93.79	99.00	199.40	1362.00

Table 8.13 Theoretical Shielding Effectiveness of Tin with a Source-to-Shield Distance of 1m, Relative Magnetic Permeability of 1, Conductivity Relative to Copper of 0.15, and Thickness of 0.1 mm

<i>Frequency</i>	<i>50 Hz</i>	<i>1 kHz</i>	<i>10 kHz</i>	<i>1 MHz</i>	<i>100 MHz</i>
R_e	262.59	223.56	193.56	133.56	73.56
R_b	23.35	36.36	46.36	66.36	86.36
R_p	142.77	129.76	119.76	99.76	79.76
A	0.04	0.16	0.51	5.09	50.89
MR	-47.63	-34.68	-24.86	-7.04	-0.02
SE <i>E</i> -mode	215.00	189.04	169.21	131.61	124.43
SE <i>H</i> -mode	-24.25	1.84	22.01	64.41	137.23
SE plane wave	95.17	95.24	95.41	97.81	130.63

Table 8.14 Theoretical Shielding Effectiveness of μ -Metal with a Source-to-Shield Distance of 1m, Relative Magnetic Permeability of 80,000, Conductivity Relative to Copper of 0.03, and Thickness of 0.1 mm

<i>Frequency</i>	<i>50 Hz</i>	<i>1 kHz</i>	<i>10 kHz</i>	<i>1 MHz</i>	<i>100 MHz</i>
R_e	206.57	167.54	137.54	77.54	17.54
R_b	-32.67	-19.66	-9.66	10.34	30.34
R_p	86.75	73.74	63.74	43.74	23.74
A	4.55	20.36	64.37	643.73	6437.26
MR	-7.76	-0.87	-0.01	0.00	0.00
SE <i>E</i> -mode	203.36	187.03	201.91	721.27	6454.80
SE <i>H</i> -mode	-35.88	-0.17	54.71	654.07	6467.60
SE plane wave	83.54	93.23	128.11	687.47	6461.00

8.5 Measuring Shielding Effectiveness

The shielding effectiveness can be measured under *H*-mode, *E*-mode, or plane wave conditions. In the *E*- or *H*-mode SE measurement, the position of the source, MUT (material under test), and receive antenna are critical, and small differences in positioning can result in large differences in measured values of SE. The measurement can be performed in free space or in a guided wave system. The free-space measurement is usually undertaken in an OATS or shielded enclosures, whereas the guided wave systems include TEM and stripline cells. These are described in Chapter 9. The choice of measurement depends on the frequency range as well as on the expected magnitude of the SE of the material.

8.5.1 Magnetic or *H*-Mode SE Measurements

One type of magnetic loop cavity, described by Hariya and Masahiro[17], consists of two 3-mm-thick flanged copper boxes of square cross section (see Figure 8.38). Each box has a 90° corner reflector through which a quarter of a loop antenna protrudes, the remainder of the loop being contained within each of the boxes. The MUT is clamped between the flanges. The insertion loss obtained with the MUT is compared with the insertion loss obtained without the sample. When the sample is inserted, it loads the instrument, and in order to establish the degree of loading, the return loss of the instrument is measured with and without the sample in place. The maximum difference between the magnitudes of the return loss in these two cases is about 2.5 dB, indicating that although some loading and impedance mismatch does occur, it is not appreciable. The transmission characteristics of the device demonstrated some resonance above 900 MHz, but below 400 MHz the measured values agree quite well with predicted values. This device can be used to measure SE magnitudes up to about 120 dB. Materials with poor surface conductivity have to be treated to ensure that good contact is obtained with the flanges.

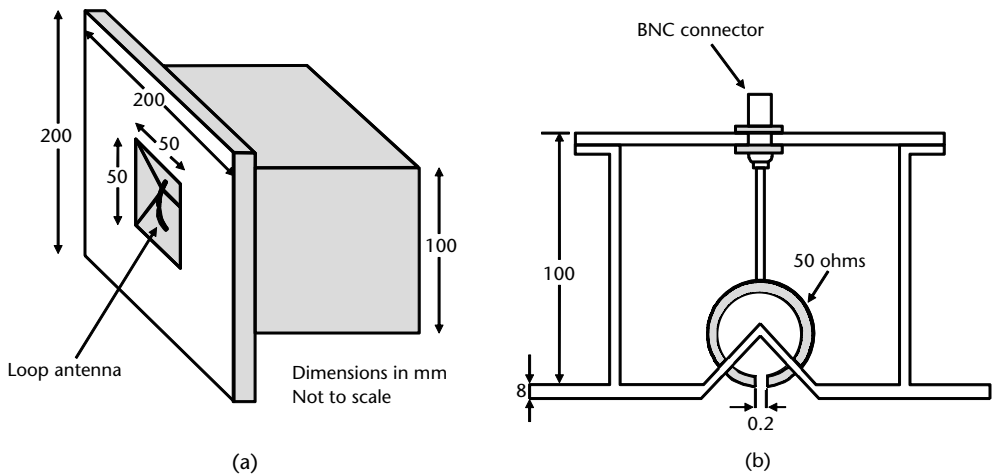


Figure 8.38 Magnetic mode SE measurement instrument: (a) external, (b) internal.

8.5.2 Electric or E-Mode SE Measurements

The device specified by the American Society for Testing and Materials (ASTM) [18] consists of 2 boxes, each 18 cm × 12 cm × 16 cm high (see Figure 8.39). There is an aperture in the abutting surface of each box to accept a specimen of 15 cm × 7.5 cm. The MUT is held in place by spring fingers, and silver paint is used to improve contact. The device can be used to measure the SE of materials up to about 50 dB over the frequency range 100 kHz to 1 GHz. However, measurement of a gold calibration standard (consisting of a gold film on a polymeric substrate) showed a marked variation with frequency which did not occur on the same calibration standard in an ASTM coaxial TEM cell. The main advantages of this device are that the positions of the antennas are fixed and that the boxes are small enough to be below the cut-off of the dominant TE_{10} up to 833 MHz. Thus, the resonances experienced in shielded rooms are avoided. However, the field distribution of the incident energy is not known, and the results obtained with this device do not compare favorably with other devices such as TEM cells.

8.5.3 Plane Wave SE Measurements

In free space, the plane wave is obtained by having the MUT in the far field of an antenna. In principle, this measurement involves producing a field by use of a transmitting antenna and measuring the field at a receiving antenna in the absence and presence of the MUT. If this measurement were to be performed in an OATS, it would require an infinitely large sheet of the MUT in order to prevent the energy from multipath rays affecting the result. Depending on the path length of these multipath rays, their phases would differ from the direct rays and thus there could be constructive or destructive interference with the direct rays. Thus, free-space

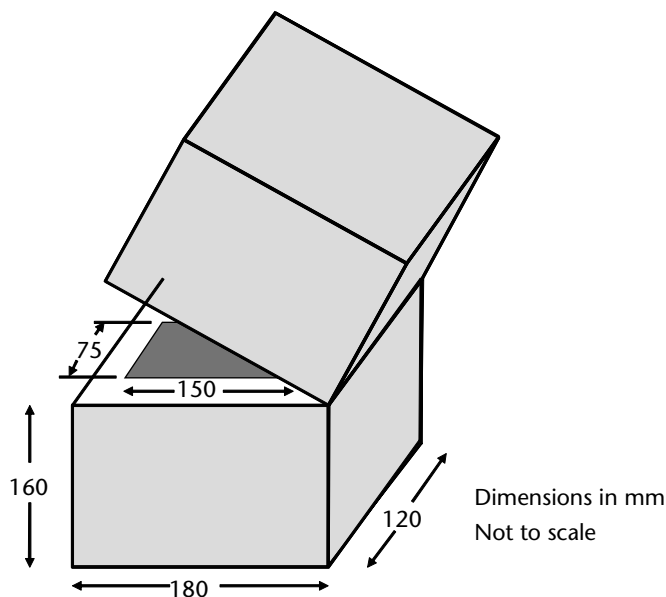


Figure 8.39 Electric field SE measurements using a dual-shielded box.

measurements could give spurious results. The multipath signals can be gated-out [19] by using a time domain set-up, as shown in Figure 8.40. The pulse contains a frequency spectrum, so instead of sweeping the source and receiver over a band of frequencies, a single pulse is used. The impulse generator produces a pulse and triggers the oscilloscope so that the latter only receives the direct signal and not any of the multipath signals. The time between the direct path pulse and the first multipath pulse is called the clean time. The shorter the pulse, the higher the upper-frequency limit of the test is. The low-frequency limit is dictated by the power available, the size of the sample, and the clean time. Higher power is required at low frequencies, since the MUT has to be placed further away from the antennas to meet the far-field condition. The size of the sample has to be larger, since if the pulse contains lower frequencies, it will be broader and thus, if the material size is the same the clean time will be reduced. A fast Fourier transform (FFT) is performed on the received pulse to obtain the frequency information. This set-up is very efficient in regards to measurement time, but the dynamic range is only about 50 to 60 dB. The frequency range is about 160 MHz to 1.5 GHz, but the upper-frequency limit can be extended to 3.5 GHz by the use of shorter pulses. The use of large sheets of the MUT can be avoided by using a large metal sheet with an aperture to take smaller sheets of the MUT. However, in this case, care must be taken to ensure that the effects of aperture coupling do not affect the field incident on the MUT.

Another set-up is to perform the measurements in two adjacent shielded rooms with an interconnecting aperture, over which the MUT is mounted for measurement. The shielded rooms should be at least partly lined, and the MUT should be placed in the far field of both antennas. While the far-field condition can be fairly easily achieved at the higher frequencies (above about 1 GHz), at the lower frequencies this condition is far more difficult to attain, since the longer distances to obtain

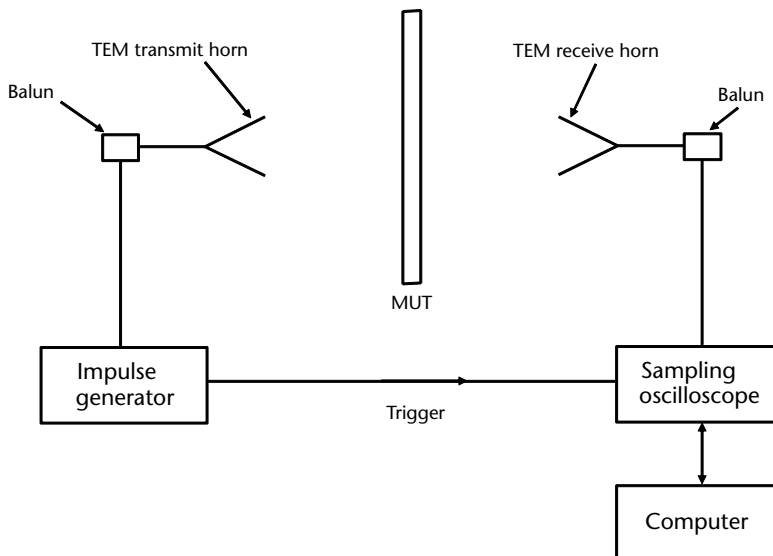


Figure 8.40 Time domain free-space SE measurements.

far-field conditions necessitate a larger size of rooms. To cover the same dynamic range, a higher power will be required from the transmitting antenna to allow for the increased loss between the MUT and each of the antennas.

8.5.3.1 Guided Wave SE Measurements

Plane waves can also be produced in any guided system that can support a TEM wave. This necessitates a two-conductor transmission line. The MUT is compared to the insertion loss of a reference sample or air. The circular coaxial TEM cells from ASTM and NBS are shown in Figure 9.8 and described in Chapter 9. In the case of the ASTM cell, the center conductor is continuous, and the MUT is an annular (ring-like) shape that fits between the inner and outer conductor. The reference sample is also the same shape. Materials with SE values of up to 90 dB can be measured with this cell, but contact resistance is a major problem, especially for materials with high SE. These materials also have good conductivity and thus their impedances are low (lower than the characteristic impedance of the cell), so that they load the cell.

The shielding effectiveness of the MUT is given by

$$SE = 20 \log_{10} \left(1 - \frac{Z_0}{2(Z_l + Z_c)} \right) \quad (8.17)$$

where

Z_0 is the characteristic impedance of the unloaded cell;

Z_l is the impedance presented by the loaded cell; and

Z_c is the contact impedance of the MUT.

For good conductors, the value of Z_l is small, and it can be seen from (8.16) that as Z_l gets smaller, the contact impedance Z_c becomes more significant. Large values of contact impedance reduce the magnitude of SE in (8.16), and as Z_l gets smaller, it also becomes increasingly difficult to match the loaded fixture to the characteristic impedance of the line.

The flanged TEM cell developed by NBS (see Chapter 9) does not have the same problems with contact resistance as the ASTM cell. The sample MUT has the shape of a solid disk, whereas the reference sample consists of two parts. One part is in the form of a disk (to fit the inner conductor of the cell), and the other is a ring to fit between the flanges of the outer conductor. Thus, there is no material between the inner and outer conductor of the cell for the reference measurement. The flanged NBS cell gives more consistent results than the ASTM cell.

Another cell that overcomes the disadvantages of the ASTM cell is the square coaxial cell proposed by Hariya and Masahiro [17]. The cell has a flat inner conductor that is shorter than the outer one, so the inner conductor does not make contact the sample when it is placed between the two halves of the fixture. One half of the cell is shown in Figure 8.41.

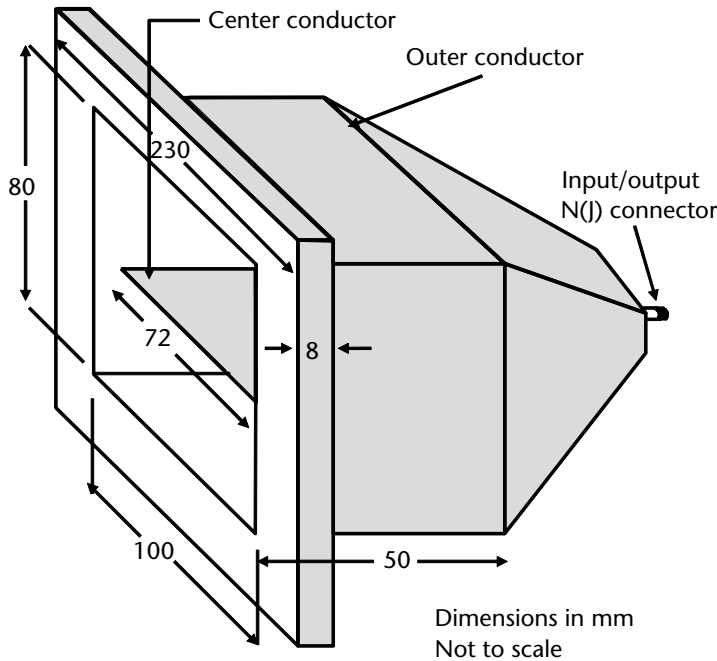


Figure 8.41 Rectangular TEM cell for SE plane wave measurement.

8.5.4 Ventilation Holes

Ventilation holes are required for cooling purposes, and seams are used to join sheets of materials used to improve the SE of equipment. A common rule of thumb for seams and holes is that no hole diameter or seam should be greater than 1/100th of a wavelength [12]. Holes used for ventilation should be carefully chosen with regard to diameter and spacing. The shielding effectiveness is proportional to the spacing s , and inversely proportional to the cube of the diameter d . Thus, the greater the hole spacing, the less is the EM leakage, and the larger the hole diameter, the greater is the EM leakage [12].

8.6 Electrostatic Discharge

Electrostatic charge was one of the first forms of electricity to be discovered. The word electricity comes from the Greek word for amber, which is *elektron*. The discovery of electrostatics is attributed to Thales (640–538 BC), who noticed that the amber spindle (used to spin silk) attracted the silk. However, it was not until 2,000 years later that the sixteenth century Royal Physician Gilbert (1540–1603) discovered that other materials such as glass could also retain charge in the same way as amber. We must all be familiar with rubbing balloons to enable them to stick to walls. The charge is built up by friction on the balloon and then it is attracted to any neutral insulating surface. A similar charge can be built up by walking across a nylon carpet, for instance, and if we were to then touch a metal object such as a radiator, then we might be subjected to a shock and in the dark we may see a spark

or small arc. If the radiator is touched tentatively with a finger, the shock is much greater than it would be if the radiator had been grabbed with the whole hand. This is because the pointed finger has a higher charge density (charge per unit area) than a rounded blunt surface. In other words, the surface charge density increases with curvature. The charge also builds up more in dry conditions than in humid ones. This is because with increased humidity, the water vapor causes the charges to leak away. The variation of the electrostatic voltage with humidity for various human activities [20] is listed in Table 8.15.

The use of man-made materials also results in a increase in charge. An electrostatic voltage of up to 15 kV can be generated by walking across a nylon carpet [15, p. 13]. Peak human voltages can reach up to 35 kV, and peak currents can reach 5 to 10A. The energy stored by human beings can vary between 20 to 30 mJ, whereas the energy stored in furniture is 5 to 6 mJ [21]. When these voltages are discharged upon electronic devices, they can cause considerable damage. In manufacturing, the main parameters of concern are the peak voltage and energy in the pulse. This is because the failures in electronic devices are caused by voltage breakdown of dielectrics, or by thermal heating due to the energy contained in the pulse, which results in thermal failure. In the field however, the main parameters of concern are usually peak currents and rise times. This is because failure modes are impedance and frequency related. It is difficult to determine whether voltage or current causes the damage. Practically speaking, once the dielectric breakdown voltage has been reached, it is the current that does the damage through I^2R heating.

8.6.1 ESD Spectrum

The frequency spectrum of an ESD pulse depends on the shape of the pulse in the time domain, that is, the amplitude variation with time. The frequency spectrum of the pulse is the Fourier transform of the time domain function. An approximate spectrum for one type of human generated ESD pulse is discussed here. These pulses have typical rise times of 1 to 3 ns [22]. A rise time of 1 ns corresponds to a bandwidth of π times the rise time This represents a frequency bandwidth of 318 MHz, which means that 1 GHz design rules must be applied to ESD shielding and grounding. The ESD pulse has been found to contain components above 1 GHz.

Table 8.15 Variation of the Magnitude of Electrostatic Voltage at Two Different Ranges of Relative Humidities

	<i>ES Voltage in Volts</i>	
	<i>Relative Humidity Range 10–20%</i>	<i>Relative Humidity Range 65–90%</i>
Walking on carpet	35,000	1,500
Walking on vinyl floor	12,000	250
Working at bench	6,000	100
Handling vinyl envelopes	7,000	600
Packing polyethylene bag	20,000	1,200
Sliding on foam padded chair	18,000	1,500

The waveform from a typical human ESD event is shown in Figure 8.42(a), and its frequency spectrum is shown in Figure 8.42(b) [22, Figure 1]. The envelope of the spectrum is also shown with slopes of zero, 20 dB/decade, and 40 dB/decade, respectively.

Components sensitive to ES voltages of less than 15,000V are considered to be ESD-sensitive. The hazard from human-generated ESD depends on the capacitance and resistance of the human body, as well as the impedance of the EUT. Earth straps should be worn when working with electronic components. Resistors of 1 M Ω should be used, so that the discharge to earth occurs slowly [9, p. E-7-75].

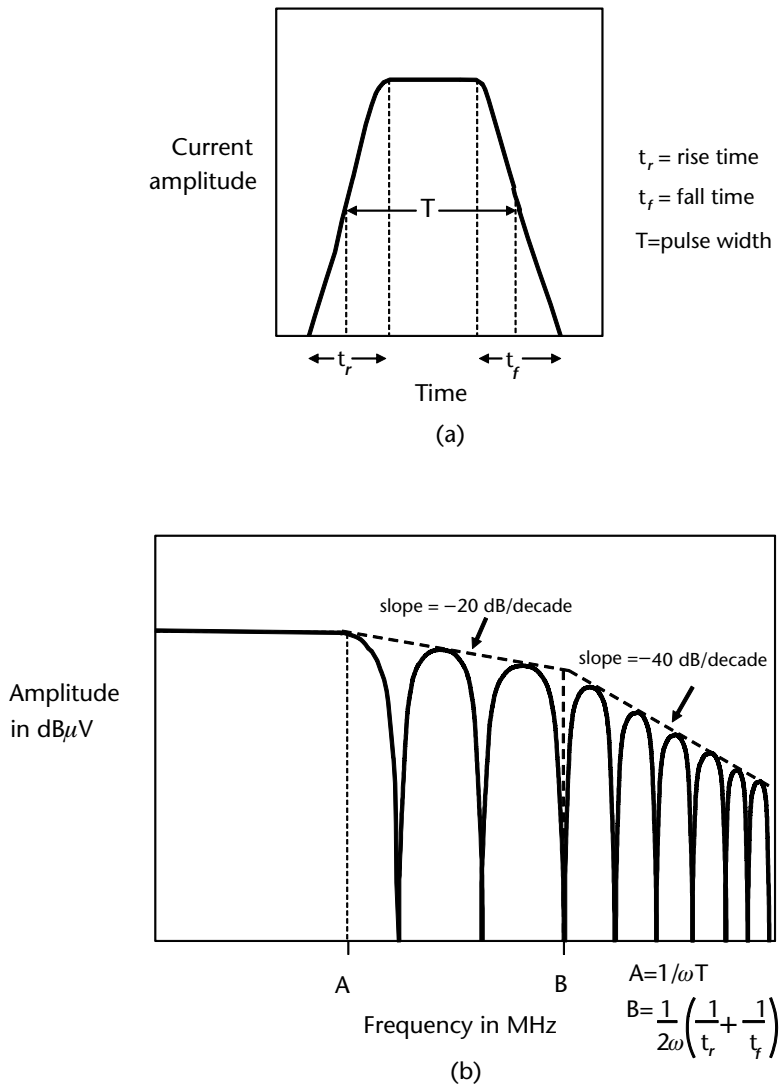


Figure 8.42 Waveform and spectrum for a human ESD: (a) Typical human-generated ESD current waveform, and (b) positive frequency spectrum of typical human ESD.

8.6.2 Direct and Indirect ESD

The direct discharge is discharge directly through a device, whereas the indirect discharge is coupling through the electromagnetic field that is radiated by the ESD pulse [22].

8.6.2.1 Direct ESD

Electronic devices are particularly vulnerable to direct ESD during manufacture and repair or servicing. During normal operation of a device, the vulnerable circuits should also be protected from ESD. The I/O cables are often decoupled by connecting capacitors between these cables and the power return path. This results in the ESD currents flowing in the circuit return paths, which could cause an upset. However, if the capacitors are connected directly to the chassis, then the ESD currents will be steered away from the power return path [22]. One way of increasing the immunity of a device is to use solid-state clamping devices between critical points and ground. When the ESD voltage increases above a specified value, the clamping device is turned on and provides a low impedance shunt path to ground [21]. In some cases, the clamping device may not respond fast enough to prevent damage. In these cases, a faster-acting current-carrying protection shunt is used to handle the initial current until the more robust clamping device can take over.

8.6.2.2 Indirect ESD

If a discharge occurs through the air, between the source and a metal plate, an EM field is radiated. This type of discharge is called an indirect ESD. This is often the cause of lock-up of computers and mysterious ESD failures. Modern logic has leading edge rates approaching 1 ns, which are of the same order as the rise time of human-generated ESD. This can result in an upset, since the ESD pulse is accepted as valid data [22].

8.6.3 ESD Models

In order to standardize ESD testing, several models have been developed. The human body model, for instance, is like a 100 to 300 pF capacitor discharging through 1 to 3 k Ω of resistance. There is a fast discharge from the hand and arm, followed by a slower discharge from the whole body [22]. The human threshold for feeling of ESD is 2,000V, and thus it is possible to damage equipment without any indication. This may not cause destruction of the equipment, but only weaken it so that it is likely to fail at a later date. Levels for ESD testing are:

Commercial ESD testing 150pF 330 ohms

Automotive ESD testing 330pF 2000 ohms

8.6.4 Testing for ESD Susceptibility

Testing for ESD susceptibility is a relatively simple and inexpensive matter with an ESD gun. The gun simulates the voltages and currents from the human body. In the direct ESD test, the gun is discharged into all exposed metal surfaces, including

the keyboard, external ports, indicators, and so forth. These should be capable of withstanding 8 to 25 kV. In the case of plastic cases, the indirect ESD test is performed. The gun is discharged into a nearby metal plate. This results in a radiated EM field to which the circuit inside the plastic case is subjected. However, it is difficult to repeat test results with different guns, since no two commercially available guns are alike [23].

The susceptibilities of various electronic devices to ESD [9, p. E-7-76] from 3M Static Control Systems are listed in Table 8.16

8.7 Instrumentation

The main test instruments used for EMC work involve the measurement of electric field strength or voltage. Modern measuring receivers are based on spectrum analyzers and fast Fourier transform (FFT) processing implemented after the detector stage. Many receivers also have audible tuning circuits. For swept frequency measurements, spectrum analyzers are used, which have CRT displays with digital markers and storage facilities. Automated measurements have computer control, with raw data processed almost instantaneous or stored on floppy disks for processing later. The instrumentation is only discussed in very general terms.

8.7.1 Measuring Receivers

Measuring receivers measure the electric field intensity at the terminals of the antenna, and allowance is made for the losses in the cables, baluns, and so forth. However, measuring receivers are expensive as they are required to meet the CISPR

Table 8.16 Range of ESD Susceptibility

<i>Device Type</i>	<i>Susceptibility in Volts</i>
VMOS	30 to 1,000
MOSFET	100 to 200
GaAsFET	100 to 300
EPROM	100
JFET	140 to 7,000
SAW	150 to 500
Op Amp	190 to 2,500
CMOS	250 to 3,000
Schottky diode	300 to 2,500
Thick- and thin-film resistors	300 to 3,000
Bipolar transistor	380 to 7,000
ECL (PCB board level)	500 to 1,500
SCR	680 to 1,000
Modern VLSI (with built-in protection)	1,000 to 3,000

pulse detector requirements [24, p. 17]. In addition, they have a better sensitivity than spectrum analyzers as they use tracking preselectors in the input stage.

8.7.2 Spectrum Analyzers

Basic spectrum analyzers do not meet the CISPR requirement for quasi-peak and RMS Average detectors. They measure the amplitude of each frequency over a band of frequencies that is scanned at a selected rate. The characteristics of the signal affect the test procedures. The instrumentation may include a low noise preamplifier to improve sensitivity and the spectrum analyzer must be calibrated. Preamplifiers are also prone to overload, which means that care must be taken in their use. Allowance must also be made for the loss in the cables. A cable with the same loss versus frequency characteristics as the cable used in the measurement must be inserted between a signal generator and the spectrum analyzer to determine the insertion loss of the cable used over the whole frequency band. In order to ascertain whether the EUT is the source of the emission, the spectrum analyzer is scanned with and without the EUT turned on. The spectrum analyzer is scanned in peak hold in each case, and the response stored for comparison. The problem frequencies can then be definitely attributed to the EUT and further investigated in greater detail.

The peak value of the input signal is measured independent of its repetition rate. The bandwidth of the receiver must be wide enough to accommodate peak signals with short rise and fall times. The shorter the rise time of a signal, the larger its bandwidth is. The Fourier transform of a signal effectively converts a pulse in the time domain, that is, the electric field variation with time to the frequency domain. The frequency domain shows the frequency characteristics of a pulse, that is, the amplitude of each frequency that when combined gives the pulse its particular shape. A more detailed explanation of the Fourier transform is given in Chapter 3.

CISPR quasi-peak measurements require that the receivers have half-power bandwidths of 200 Hz, 9 kHz, and 120 kHz in the frequency ranges of 10–150 kHz, 150 kHz–30 MHz, and 30–1,000 MHz, respectively [9, p. 9–21].

References

- [1] IEEE, *Standard Dictionary of Electrical and Electronics Terms, Fourth Edition*, 1988.
- [2] Dash, G., "Understanding EMI Test Methods Eases Product Acceptance," *Electronic Design News*, May 28, 1983, pp 183–191.
- [3] Chatterton, P. A., M. A. Houlden, *EMC Electromagnetic Theory to Practical Design*, John Wiley & Sons, 1991.
- [4] Tsantes, T., "Independent EMI Test Labs Provide Aid as FCC's Compliance Deadline Nears," *EDN*, August 4, 1983, pp. 41–47.
- [5] Mertel, H. R., "Design and Test for RFI Regulations of United States and CISPR, Part 1: Introduction, the CISPR, FCC, and VDE Limits," Fifth Symposium on EMC, Zurich, March 1983.
- [6] Gerke, D., "A Fundamental Review of EMI Regulations," *RF Design*, April 1987, pp. 57–62.
- [7] Heirman, D. N., "International Activity in Product Immunity Standards and Testing," *EMC Test and Design*, May/June 1992, pp. 16–19.

- [8] EN 610004-4, *Electromagnetic Compatibility (EMC) Testing and Measurement Techniques*, “Electrical Fast Transient/Burst Immunity Test,” 2015.
- [9] Kaiser, B. E., “Electromagnetic Interference and Control,” *Frost and Sullivan Course*, October 1990, London.
- [10] EN 610004-2, “Electrostatic Discharge Immunity Test,” *Electromagnetic Compatibility (EMC) Testing and Measurement Techniques*, 2008.
- [11] ISO 10605:2008, *Road Vehicles—Test Methods for Electrical Disturbances from Electrostatic Discharge*, 2008.
- [12] Duncan, D., “A Low Cost Method of RFI/EMI Shielding,” *EMC Technology*, October/November 1984, pp. 75–76.
- [13] Spraylat Catalogue—Series 599 Copper Conductive Coatings.
- [14] Hardy, S. M., “A Less Expensive Tempest Alternative,” Vol. 15, No. 6, June 1992, pp. 54–61.
- [15] Jackson, G. A., “The Achievement of Electromagnetic Compatibility,” *ERA Technology Report* 90-0106, February 1990.
- [16] Schulz, R. B., V. C. Plantz, and D. R. Brush, “Shielding Theory and Practice,” *IEEE Trans on EMC*, Vol. 30, No. 3, August 1988, pp. 187–201.
- [17] Hariya, E., and U. Masahiro, “Instruments for Measuring the EM Shielding Effectiveness,” *International Symposium on Electromagnetic Compatibility*, October 16–18, 1984.
- [18] Simon, R. M., “ASTM Testing for EMI/RFI Shielding,” *Wescon ‘84 Conference Record*, IEEE, Anaheim CA, October 30—November 1, 1984.
- [19] Wilson, P. F., and M. T. Ma, “A Study of Techniques for Measurement of Electromagnetic Shielding Effectiveness of Materials,” *National Bureau of Standards*, NBS/TN1095, May 1986.
- [20] Rzepecki, R. H., *Machine Design*, March 26, 1981.
- [21] Boxleitner, W., “How to Defeat Electrostatic Discharge,” *IEEE Spectrum*, August 1989, pp. 36–40.
- [22] Gerke, D., “Electrostatic Discharge as an EMI Issue,” *RF Design*, November 1988, pp. 65–71.
- [23] Keenan, R. K., and L. D. Ros, “Some Fundamental Aspects of ESD Testing,” *IEEE International Symposium on EMC*, 1991, pp. 236–241.
- [24] Johnson, R. W., “FCC Rules and Digital Equipment Testing for Compliance,” *Test and Measurement World*, April 1982, pp. 16–20.

Selected Bibliography

- EN 60601-1-2, *Medical Electrical Equipment*, “General Requirements for Basic Safety and Essential Performance.”
- IEC Standards Publication—IEC 61000-4 Series*, “Electromagnetic Compatibility for Industrial Process Measurement and Control Equipment,” Bureau Central de la Commission Electronique Internationale, Geneve, Suisse, 1984.

Theory and Applications of Measurement Sites and Enclosures

This chapter describes test enclosures, from TEM cells to shielded rooms and OATS (open area test sites), that are used for many EMC applications. Other topics also covered are RAM (radar absorbing material) and ventilation panels that are used in shielded rooms.

In order to understand the principles of TEM cells, we must understand the propagation of EM waves in parallel plates and coaxial lines. Shielded rooms are like large rectangular waveguides that are shortened and closed at both ends to form a cavity. Unlined shielded rooms are prone to problems at certain frequencies. In order to appreciate these problems, we must understand how EM waves behave in rectangular cross section closed cavities. This chapter relates the shielded room to a rectangular waveguide, and qualitatively deals with the limitations and precautions necessary when using a shielded room at some frequencies. Shielded rooms have ventilation panels that comprise waveguides beyond cut-off. These are explained in a qualitative manner, but formulas for calculating the attenuation of these waveguides are also given.

9.1 TEM Waves

EM waves are guided along transmission lines so that EM energy is carried by them from one part of the transmission line to the other. These waves, composed of electric and magnetic fields, change periodically in time and have clearly defined configurations that satisfy the boundary conditions of Maxwell's equations. In free space, the electric and magnetic fields are at right angles to each other and to the direction of propagation of the wave. This type of wave is known as a TEM (transverse electromagnetic) wave, and it can also be propagated as a guided wave in any two-conductor transmission line, such as parallel wires, coaxial lines, and striplines. The guided TEM wave can be propagated down to a frequency of zero hertz (i.e., dc). All other modes have a higher cut-off frequency, below which propagation cannot occur. Modes are more fully explained in Section 9.3.1. The TEM mode in a transmission line is known as the principal mode, and the variation of the electric field with distance is shown in Figure 9.1(a), where the electric fields are shown as solid lines and the magnetic field lines are shown dotted.

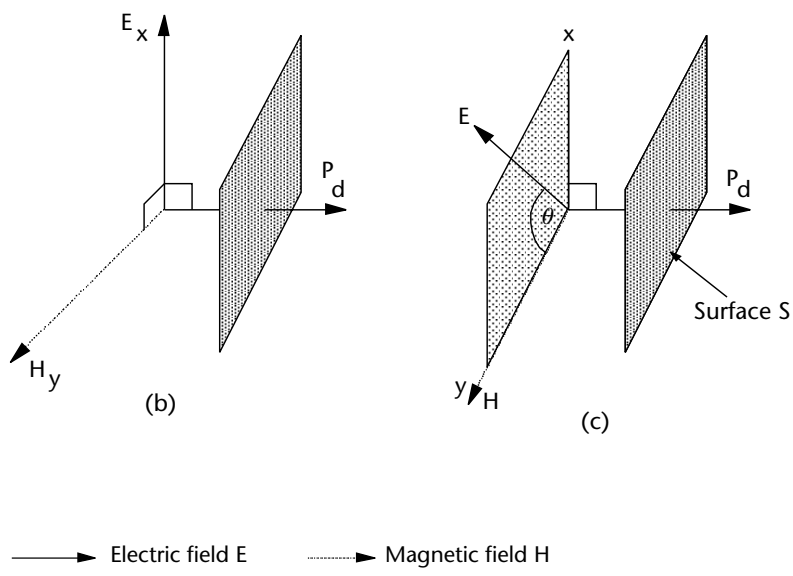
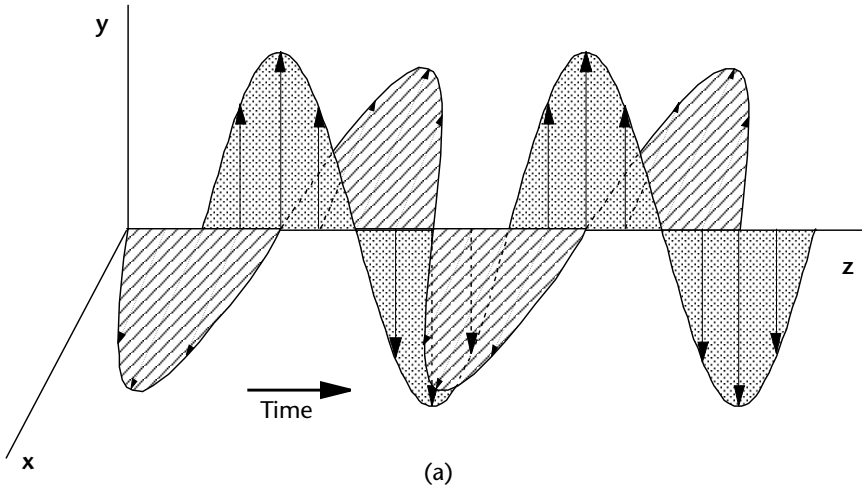


Figure 9.1 Plane wave propagation and Poynting's power flux density vector: (a) A plane, or TEM, wave in free space, (b) E and H vectors for a TEM wave, and (c) Poynting's power flux vector P_d .

9.1.1 Power Flux Density

In the case of the TEM wave, the electric and magnetic fields are perpendicular to each other, and the plane containing them is perpendicular to the direction of propagation of the EM energy.

The vector cross product of the electric and magnetic fields is also a vector which is equal to the power flux density (power per square area), known as Poynting's vector P_d . We can see that if we multiply volts per meter by amperes per meter, we would get volt-amperes per square meter (VA/m^2), which is watts per square meter

(W/m²). The relationship between the three vectors shown in Figure 9.1(b) is defined by the following equation

$$\mathbf{P}_d = \mathbf{E} \times \mathbf{H} \quad (9.1)$$

where

- \mathbf{P}_d is in watts per square meter;
- \mathbf{E} is the electric field vector in volts per meter;
- \mathbf{H} is the magnetic field vector in amperes per meter.

The magnitude of \mathbf{P}_d is given by

$$|\mathbf{P}_d| = |\mathbf{E}||\mathbf{H}|\sin\theta \quad (9.2)$$

where

- $|\mathbf{E}|$ is the magnitude of \mathbf{E} ;
- $|\mathbf{H}|$ is the magnitude of \mathbf{H} ;
- θ is the angle between the electric and magnetic field vectors. In the case of a TEM wave, the angle between these vectors is 90°.

Note that the magnitude of the electric and magnetic fields are those in the plane perpendicular (i.e., the transverse plane) to the direction of propagation or power flow. The maximum values of these fields occur when the \mathbf{E} and \mathbf{H} vectors are in this transverse plane; any component parallel to the direction of propagation will not contribute to the power flux density. We can see that algebraically the maximum value of \mathbf{P}_d occurs when the sine of the angle between the electric and magnetic fields is 1, that is, angle θ is 90°, or the fields are perpendicular to each other in the plane transverse to the direction of the propagation of the wave. Thus, the TEM wave has the maximum value of Poynting's vector. The power density through a surface S , as shown in Figure 9.1(c), has a maximum value when Poynting's vector is perpendicular to it.

9.1.2 Wave Impedance

The EM wave can be considered to have an impedance, depending on its configuration. If the wave is incident on a surface with the same impedance, the surface can be said to be matched, in the same way as a load is matched to a transmission line. When this occurs, no energy will be reflected and the wave is totally absorbed. This impedance is known as the intrinsic or characteristic impedance Z_w of the wave, and in the case of a TEM wave in a medium, it is given by

$$Z_w = \frac{E_x}{H_y} = \sqrt{\left(\frac{\mu}{\varepsilon}\right)\left(\frac{1}{1 + \frac{\sigma}{j\omega\varepsilon}}\right)} \quad (9.3)$$

where

Z_w is in ohms;

E_x is the electric field along the x -axis in volts per meter;

H_y is the magnetic field along the y -axis in amperes per meter;

μ is the permeability of the medium in henries per meter;

ϵ is the permittivity of the medium in farads per meter;

σ is the conductivity of the medium in siemens per meter.

If the TEM wave is in free space, the conductivity is zero. Thus, the characteristic impedance Z_0 of TEM wave in free space is given by

$$Z_0 = \left(\frac{\mu_0}{\epsilon_0} \right) = 120\pi \quad (9.4)$$

Since $\mu_0 = 4\pi \times 10^{-7}$ H/m, and $\epsilon_0 = 1/36\pi \times 10^7$ F/m.

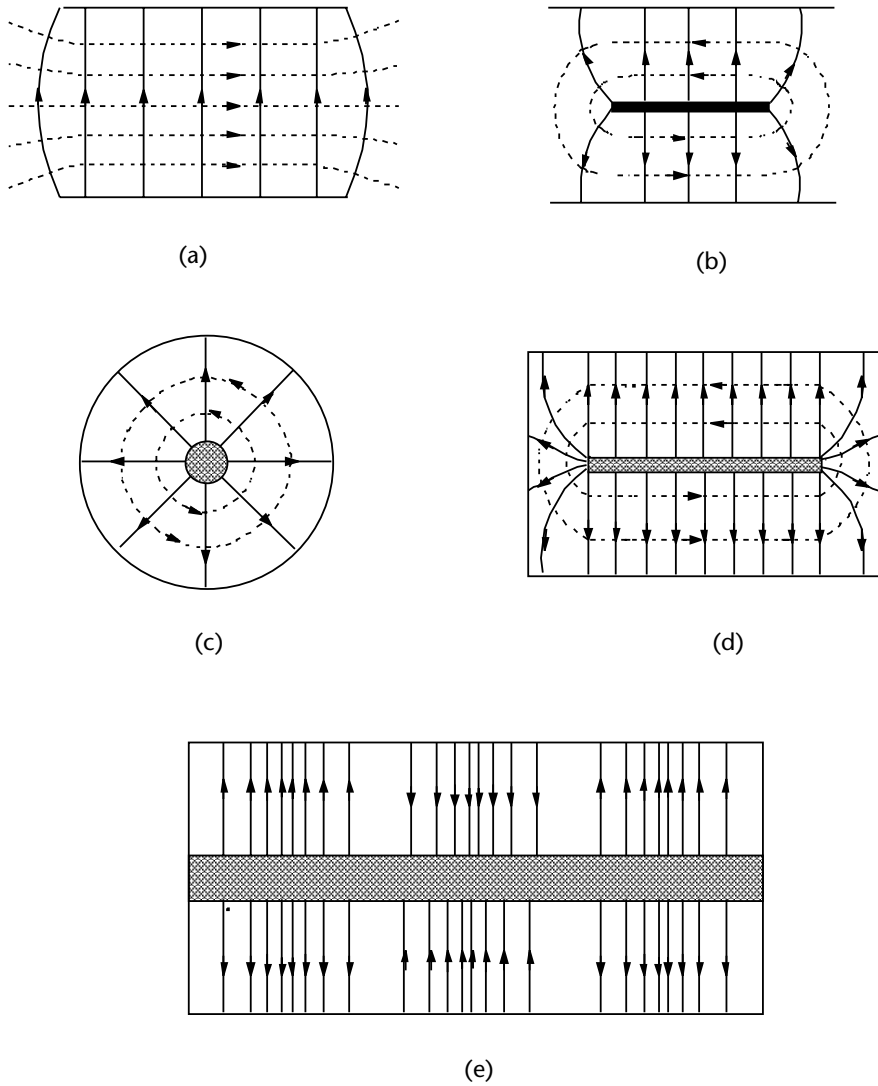
The characteristic wave impedance is often quoted at its approximate value of 377Ω .

9.1.3 TEM Transmission Lines

Transmission lines which can support the TEM waves require two separate conductors. The electric (solid lines) and magnetic (dotted lines) fields for some of these common transmission lines are shown in Figures 9.2(a–e). Note that when the magnetic lines are evenly spaced, they will also represent the lines of equipotentials (with the electric field lines perpendicular to them). In Figure 9.2(e), which shows the longitudinal cross section of a circular coaxial line, the closer the spacing of the electric field lines, the greater the magnitude of the electric field is. The electric field variation with distance in the direction of propagation is sinusoidal. We should also note that there is a sinusoidal variation with time, which effectively moves this electric field pattern forward by half a sine variation every half-period in time. The coaxial line is one of the most efficient ways of containing the EM energy. However, the spacing between the inner and outer conductors in a coaxial line is maintained by dielectric (in the form of beads or a continuous hollow cylinder). As the frequency increases, the losses in the dielectric also increase and the energy is increasingly attenuated. Another source of energy loss is the outer conductor, which is often of braided form. Energy can leak through holes in the braid, and the amount of the leakage is proportional to the electrical size of the hole, that is, the size of the hole as a fraction of the wavelength. Energy can escape through gaps that are as small as 1/100th of a wavelength. As the frequency increases, the wavelength decreases, and the gaps in the outer conductor become a larger fraction of this wavelength causing the EM energy loss to increase.

9.1.3.1 Characteristic Impedance of Transmission Lines

When a line is longer than 0.1 of a wavelength at its highest operating frequency, we cannot ignore the properties of the line. The current distribution in it (due to the



—————> Electric field - - - - -> Magnetic field

Figure 9.2 TEM wave propagation in some transmission lines: (a) Parallel plate, (b) stripline, (c) circular coaxial line, (d) rectangular coax, and (e) cross sectional view of a circular coax showing electric field lines.

EMF at the input end) is not uniform. The line behaves as though it has resistive and reactive components distributed along its length. Each section of the go and return cables forms a unit loop, which can be represented by a shunt capacitance C and conductance G between the two cables, and a series resistance R and inductance L [1, p. 669]. If the line is a pair of parallel identical conductors, it is balanced and the resistance R and inductance L are equally divided between each cable, as shown in Figure 9.3. Normally an incident wave traveling from left to right towards the

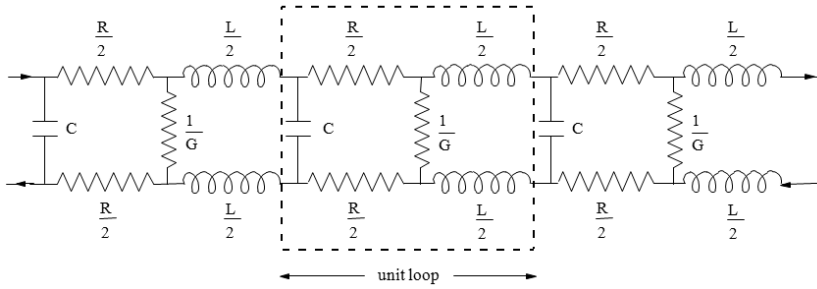


Figure 9.3 Equivalent circuit of a balanced transmission line.

termination is partly reflected. The reflected and incident waves combine to form a standing wave. If the termination is matched (made equal) to the impedance of the unit loop of the line, there is no reflected wave, and hence no standing wave.

The impedance of this unit loop is known as the characteristic impedance Z_0 and is given by

$$Z_0 = \sqrt{\frac{R + j\omega L}{G + j\omega C}} \quad (9.5)$$

where

- R is the series resistance in ohms;
- G is the shunt resistance in siemens;
- L is the series inductance in henries;
- C is the shunt capacitance in farads.

If the line is lossless, the resistive parts are zero, so that $R = 0$ and $G = 0$. Equation (9.5) for the characteristic impedance reduces to

$$Z_0 = \sqrt{\frac{L}{C}} \quad (9.6)$$

This is the general formula for a lossless transmission line, and the magnitudes of L and C will depend on the shape and size of the particular transmission line and the dielectric material.

9.1.3.2 Parallel Plate Transmission Lines

In the case of a parallel plate transmission line, the idealized electric and magnetic field variation are shown in Figure 9.4. Both the electric and magnetic fields are spaced uniformly across the cross section of the line, except at the edges, where fringing of the electric field occurs in practice.

The characteristic impedance Z_0 of the parallel plate line of width b and spacing a , supporting the TEM wave (when the medium in the space between the parallel plates has a permittivity ϵ and permeability μ), is given by

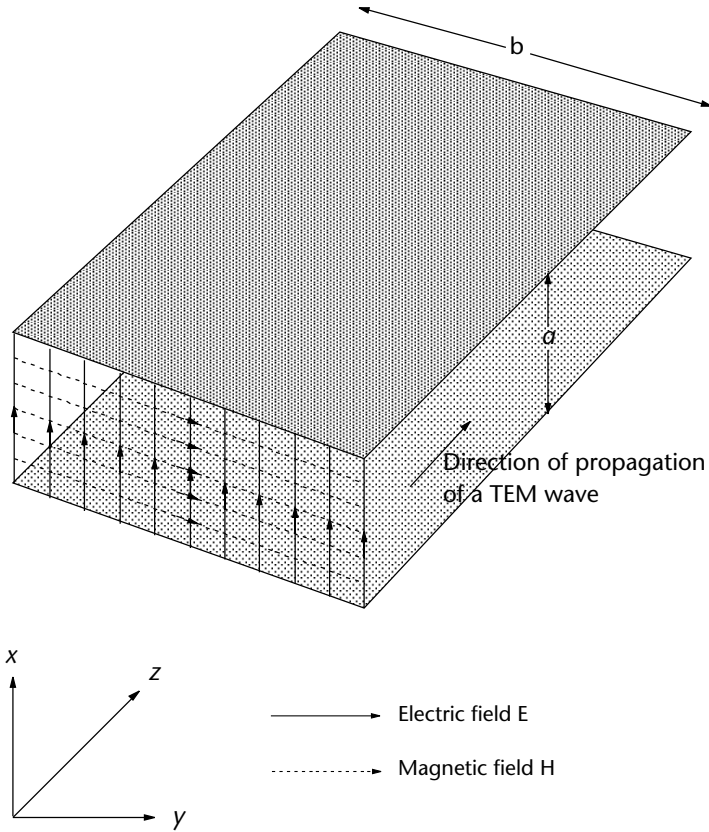


Figure 9.4 Propagation of a TEM wave in an ideal parallel plate transmission line.

$$Z_0 = \frac{a}{b} \sqrt{\left(\frac{\mu}{\epsilon}\right) \left(\frac{1}{1 + \frac{1}{\sigma + j\omega\epsilon}}\right)} \tag{9.7}$$

where

Z_0 is in ohms;

μ is the permeability of the medium in henries per meter;

ϵ is the permittivity of the medium in farads per meter;

σ is the conductivity of the medium in seimens per meter.

If the medium between the parallel plates is air, the conductivity is zero and the permittivity and permeability are the same as that for free space, so the formula for the characteristic impedance Z_0 reduces to

$$Z_0 = \frac{a}{b} \sqrt{\left(\frac{\mu_0}{\epsilon_0}\right)} \tag{9.8}$$

9.1.3.3 Coaxial Lines

Coaxial lines can have circular, rectangular, or square cross sections. The circular coaxial lines have cylindrical inner conductors and hollow cylindrical outer conductors, whereas the rectangular and square coaxial lines have hollow outer conductors and thin plate-like inner conductors that are sometimes called septums.

9.1.3.3.1 Circular Coaxial Lines

For a circular coaxial line with inner and outer conductors with diameters of radii a and b , the formulas for calculating the series and shunt resistances and reactances per unit length are given by [2, p. 4]

$$R_{ac} = \frac{1}{2\pi} \left[\frac{1}{a} + \frac{1}{b} \right] \sqrt{\frac{\omega\mu\rho}{2}} \quad (9.9)$$

$$G = \omega C \tan \delta \quad (9.10)$$

$$C = \frac{2\pi}{\log_e \left(\frac{b}{a} \right)} \quad (9.11)$$

$$L = \frac{\mu}{2\pi} \log_e \left(\frac{b}{a} \right) \quad (9.12)$$

The characteristic impedance Z_0 for a lossless coaxial line is given by

$$Z_0 = 60 \sqrt{\frac{\mu_r}{\epsilon_r}} \log_e \left(\frac{b}{a} \right) \quad (9.13)$$

If it is preferred to use logarithms to a base 10, then the following formula should be used

$$Z_0 = 138 \sqrt{\frac{\mu_r}{\epsilon_r}} \log_{10} \left(\frac{b}{a} \right) \quad (9.14)$$

For (9.9) to (9.14):

- R_{ac} is the ac resistance in ohms per meter;
- ω is the angular frequency in radians per second;
- μ is the permeability of the dielectric material in henries per meter;
- μ_r is the relative permeability of the dielectric material;
- ρ is the resistivity of the conductor in ohms per meter;
- $\tan \delta$ is the loss tangent of the dielectric material;
- ϵ is the permittivity of the dielectric material in farads per meter;
- $\epsilon_r = \epsilon/\epsilon_0$ is the relative permittivity of the dielectric material;
- G is the shunt conductance in siemens per meter;

- C is the capacitance in farads per meter;
- L is the inductance in henries per meter.

The dimensions of standard coaxial lines are usually chosen to give characteristic impedances of 50 or 75Ω . For an air dielectric coaxial line however, a ratio of $b/a = 3.6$ gives the lowest attenuation [3, p. 64]. This ratio gives a characteristic impedance of 77Ω . Coaxial lines are operated over a frequency range, such that only the TEM mode is propagated. Nevertheless, higher order modes are sometimes excited by discontinuities in the line, or a sudden change in geometry. Some of the higher order modes are shown in Figure 9.5.

The higher-order modes are not excited if the upper-frequency limit is restricted to a wavelength equal to the circumference at the arithmetic mean of the inner and outer diameters. This wavelength of the critical frequency [3, p. 69] is given by

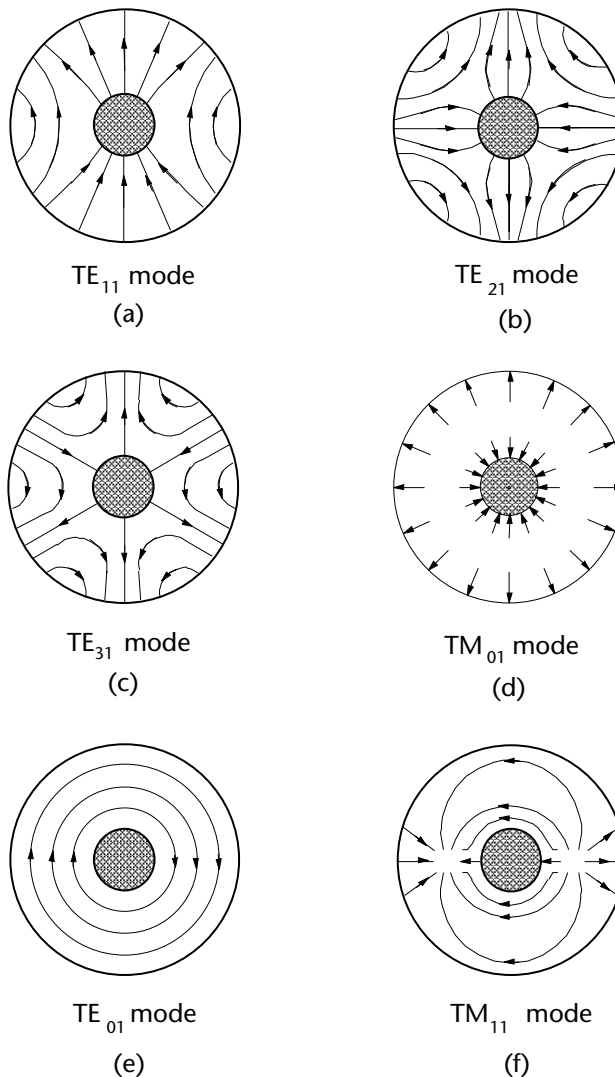


Figure 9.5 Higher-order modes in coaxial lines showing the electric field lines: (a) TE_{11} mode, (b) TE_{21} mode, (c) TE_{31} mode, (d) TM_{01} mode, (e) TE_{01} mode, and (f) TM_{11} mode.

$$\lambda_c = \pi(a + b) \quad (9.15)$$

The critical frequency f_c is given by

$$f_c = \frac{c}{\pi\sqrt{\epsilon_r}(a + b)} \quad (9.16)$$

where

c is the speed of light through free space in meters per second;

a is the radius of the inner conductor in meters;

ϵ_r is the relative permittivity of the dielectric material;

b is the radius of the outer conductor in meters.

9.1.3.3.2 Rectangular and Square Coaxial Lines

In the case of rectangular and square cross sections shown in Figure 9.6, the outer conductor is a hollow rectangle or square, and the center conductor is a solid rectangle of thickness or height t .

In the case of the square cross section coaxial line, the characteristic impedance is given by [4, p. 345]

$$Z_0 = \frac{94.15}{\sqrt{\epsilon_r} \left(\frac{w}{b \left(1 + \frac{t}{2b} \right) + \frac{C}{0.885\epsilon_r}} \right)} \quad (9.17)$$

where

b is half the width of the outer conductor in centimeters;

w is half the width of the inner conductor or septum in centimeters;

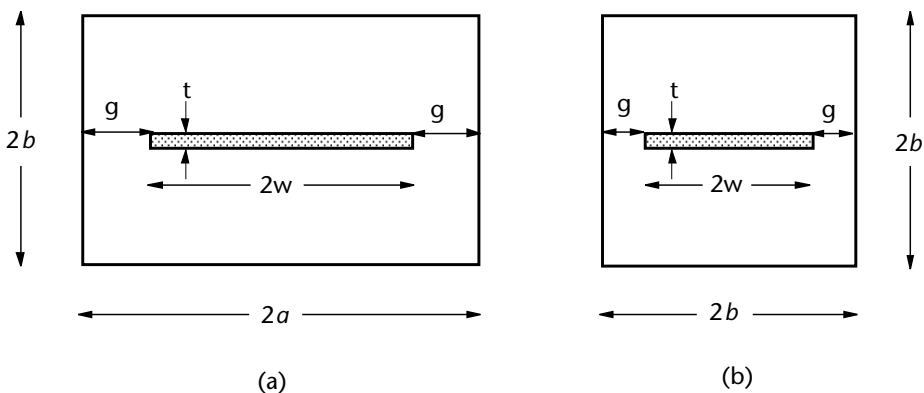


Figure 9.6 Coaxial line with (a) rectangular and (b) square cross sections.

t is the thickness of the inner conductor in centimeters;
 C is the capacitance per unit length in picofarads per centimeters;
 ϵ_r is the relative permittivity or dielectric constant of the material inside the coaxial line.

The characteristic impedance of a rectangular cross section coaxial line is a complex expression containing Jacobian elliptical functions, but a simpler expression, given below, is usually adequate for most practical purposes, where the center conductor is a thin plate or septum [5, p. 394].

$$Z = \frac{Z_0}{4 \left\{ \left(\frac{w}{b} \right) + \frac{2}{\pi} \right\} \left[1 + \coth \left(\frac{\pi g}{2b} \right) \right]} \quad (9.18)$$

where

Z_0 is the impedance of free space;
 a is half the width of the outer conductor;
 b is half the height of the outer conductor;
 w is half the width of the inner conductor or septum in centimeters;
 g is the gap between the inner conductor and the vertical wall of the outer conductor (see Figure 9.6).

9.2 TEM Cells

As explained in Section 9.1, a transverse electromagnetic (TEM) wave exists when the electric and magnetic fields are perpendicular to each other, and they are both transverse to the direction of propagation of the wave. This is the type of wave that is known as a plane wave, and it exists in free space (in the far field of antennas) and in some transmission lines. In order to propagate in transmission lines, there must be two separate conductors. In other words, a TEM wave cannot propagate in a waveguide, but it can be supported by a coaxial line or a parallel plate. The parallel plate lines used for measurement are sometimes called stripline cells, and the rectangular and square coaxial line cells are known as TEM or Crawford cells. These cells are used to provide uniform fields for susceptibility and immunity measurements, as well as for the measurement of shielding effectiveness of sheet materials.

9.2.1 Parallel Stripline Cells

The parallel plate cell is commonly referred to as a stripline cell and was described in MIL-STD 462 [6, p. 90] as consisting of two horizontal aluminum plates held 45 cm (18 in) apart by wooden posts at each end. The top plate of width 60 cm (24 in) and length 3m (120 in), is supported by three wooden strips along its length, and the lower plate of the same length but 30 cm wider (as shown in Figures 9.7(a–d) and

9.8) is backed by plywood. At one end, there was a transition to a standard N-type coaxial connector for the signal input, and the other end is connected to a load that is matched to the impedance of the line. The size of the EUT is restricted to a maximum height of 25 cm, and the maximum frequency of operation is 35 MHz. The limitation in frequency was caused by the abrupt impedance discontinuities at the feed point and load end of the parallel plate. Later designs used a tapered design at each end, which ensured better impedance matching. The size of the EUT can be increased by increasing the dimensions of the cell, but this results in a reduction in the maximum usable frequency. The electric field between the plates will take the approximate form shown in Figure 9.7(e), where some fringing occurs at the edges with asymmetric distortion on the side where the lower plate projects beyond the upper one. Electric field strengths of 10 V/m are obtainable with this type of cell.

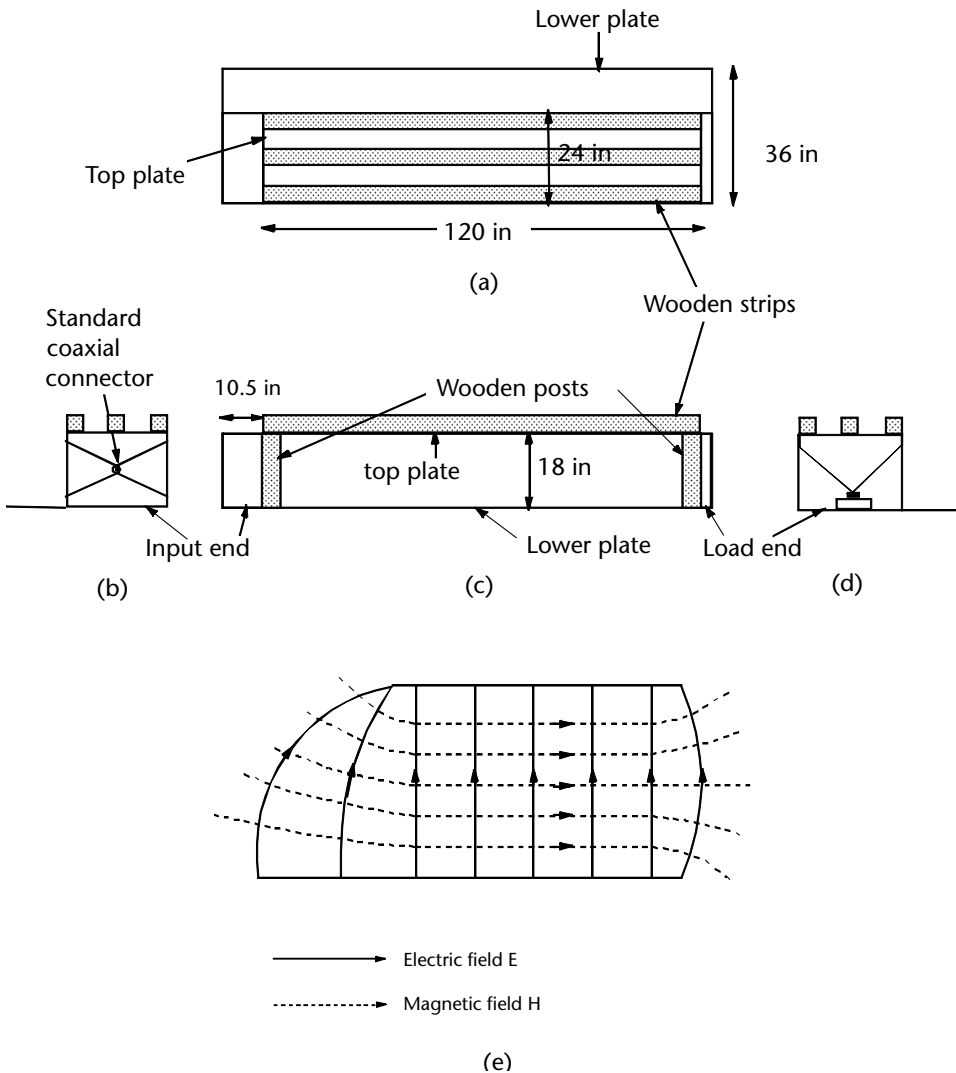


Figure 9.7 Parallel plate stripline cell: (a) Plan view, (b) end view, (c) side elevation, (d) end view, and (e) approximate pattern of the electric and magnetic field lines.

The parallel plate cell is also described in MIL-STD 461G [7, p. 156] for applying transient electromagnetic fields. UNECE (United Nations Economic Commission for Europe) Regulation 10 [8, p. 93] for automotive sub assembly testing also describes a square TEM cell. The cell described consists of two horizontal aluminum plates held 80 cm (31.5 in) apart by wooden posts at each end. Both plates are of width 80 cm and length 80 cm. At the feed end there is a resistive matching circuit, and at the other end there is a nominal 150Ω resistive termination. The size of the EUT is restricted to one third of the volume of the cell, and the maximum frequency of operation is 200 MHz. The size of the EUT can be increased by increasing the dimensions of the cell, but this will result in a reduction in the maximum usable frequency, since the field uniformity over the useable volume deteriorates. The electric field between the plates will take the approximate form shown in Figure 9.9(e), where some fringing occurs at the edges. The parallel plate and matching networks are shown in Figures 9.10 and 9.11.

MIL STD 461G specifies the use of a large parallel plate cell for transient radiated susceptibility testing with a 50 kV pulse with a rise time of approximately 2 ns, indicating a bandwidth of over 160 MHz. The dimensions are not specified, but the high voltages involved necessitate adequate clearances. One third of the height and one half of the width is allowed as the working volume.

9.2.2 Circular Coaxial TEM Cells

These cells are like enlarged coaxial air-filled lines which are tapered at both ends to be connected to standard 50Ω connectors. They are mainly used to measure the shielding effectiveness of sheet materials. The cells are used in the frequency range of 1 MHz to around 1.8 GHz. The upper-frequency limit is restricted to prevent the excitation of higher-order modes, and the lower-frequency limit is determined by the measuring equipment. There are two types of commonly used circular coaxial TEM cells, the continuous-conductor (CC) and the flanged version. The formulas for the different parameters of a coaxial line are given in (9.9) to (9.14).

9.2.2.1 Continuous-Conductor TEM Cell

This cell, shown in Figure 9.12(a), was developed by the ASTM [9] consists of tapered sections from standard $50\text{-}\Omega$ connectors to a central cylindrical section.

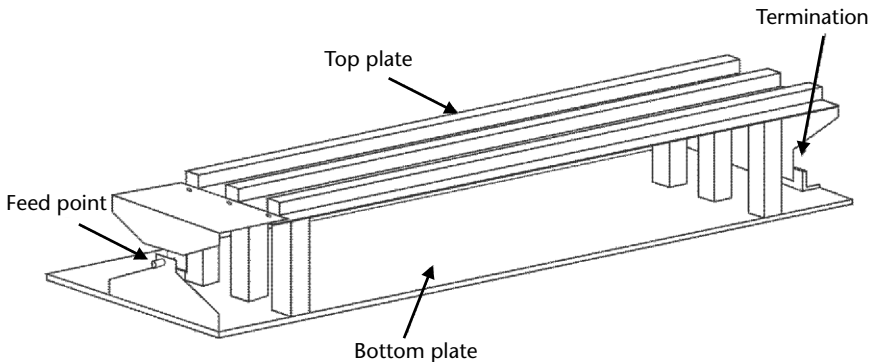


Figure 9.8 Parallel plate stripline cell with trellis.

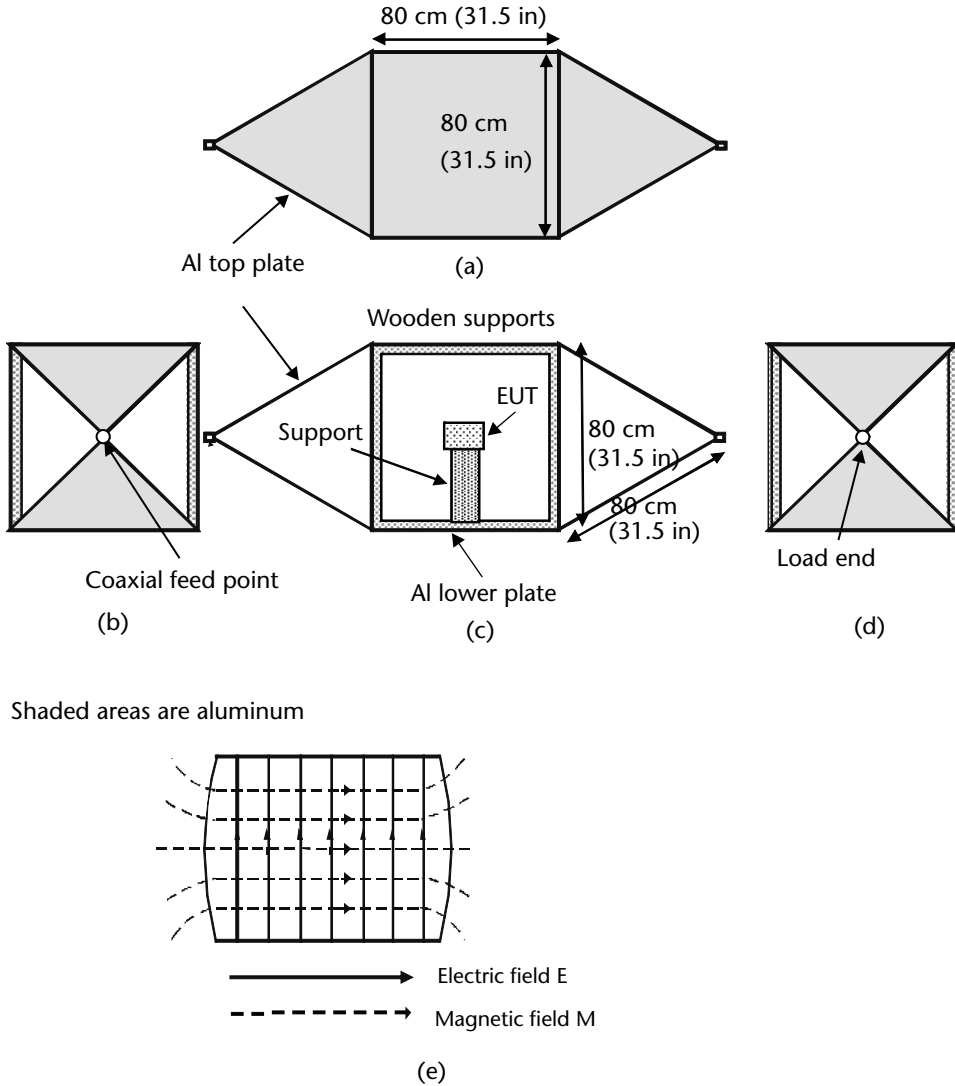


Figure 9.9 TEM cell. (a) Plan view, (b) end view, (c) side elevation, (d) end view.

The central section has inner and outer conductors of diameters of 4.35 cm and 9.90 cm, giving a theoretical impedance of 49.3Ω . The cell can be disassembled for insertion of a washer-like annular sample of the MUT. The quoted frequency range of the cell is from 1 MHz to 1.4 GHz. However, if the criterion by Moreno is used, that is, (9.16), then the maximum frequency without the excitation of higher-order modes is 1.34 GHz.

A reference attenuation test is carried out using a sample comprising an annulus and a small disk which completes the inner and outer coaxial circuits. A test sample is then inserted that comprises a solid disk, which means the air space is replaced by the MUT. The difference between the two results yields the shielding effectiveness. The material should be electrically thin to ensure adequate capacitive coupling across the sample joint, as described in ASTM D 4935-99 [10, p. 1].

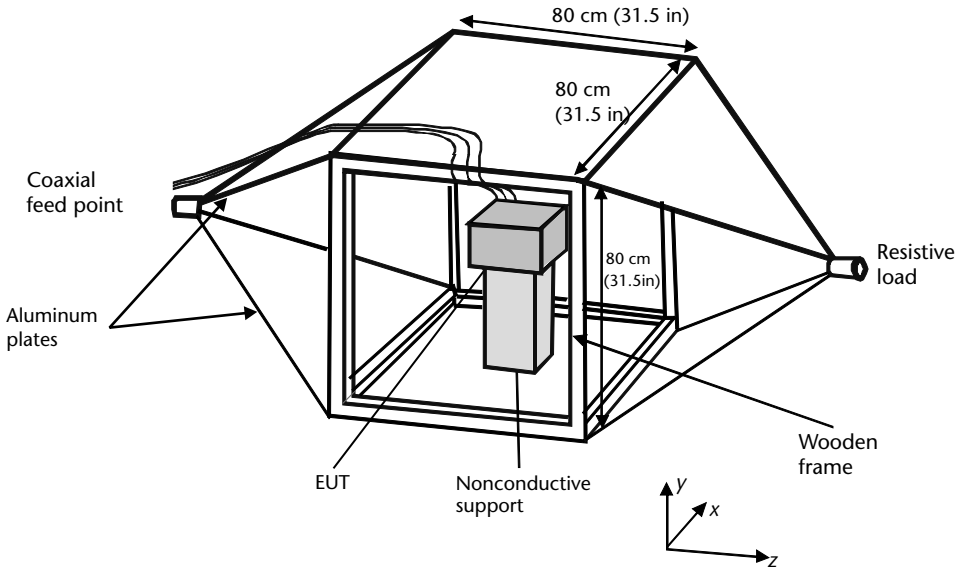


Figure 9.10 Parallel plate cell.

9.2.2.2 Flanged Coaxial TEM Cell

Figure 9.12(b) is similar to the ASTM cell described in Section 9.2.2.1, but it can be disassembled into two flanged sections, between which the circular disk-shaped sample is inserted, as shown in Figure 9.12(c). The reference sample, on the other hand, consists of two parts; a circular disk of the same diameter as the inner conductor, and a circular annulus with inner and outer dimensions to match the flanges of the cell, as shown in Figure 9.12(d). Thus, in the case of the reference sample, there is no material in the space between the inner and outer conductors of the cell. The inner conductor of the cell is 3.2 cm and the inside diameter of the outer conductor is 7.6 cm. Using (9.14) gives a characteristic impedance of 51.8Ω . The outside dimension of the flange is 13.3 cm. The quoted frequency range of the

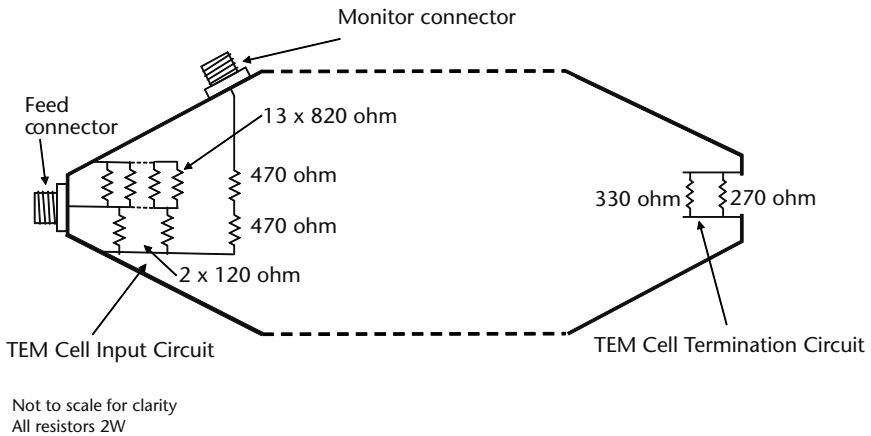


Figure 9.11 Parallel plate cell matching circuits.

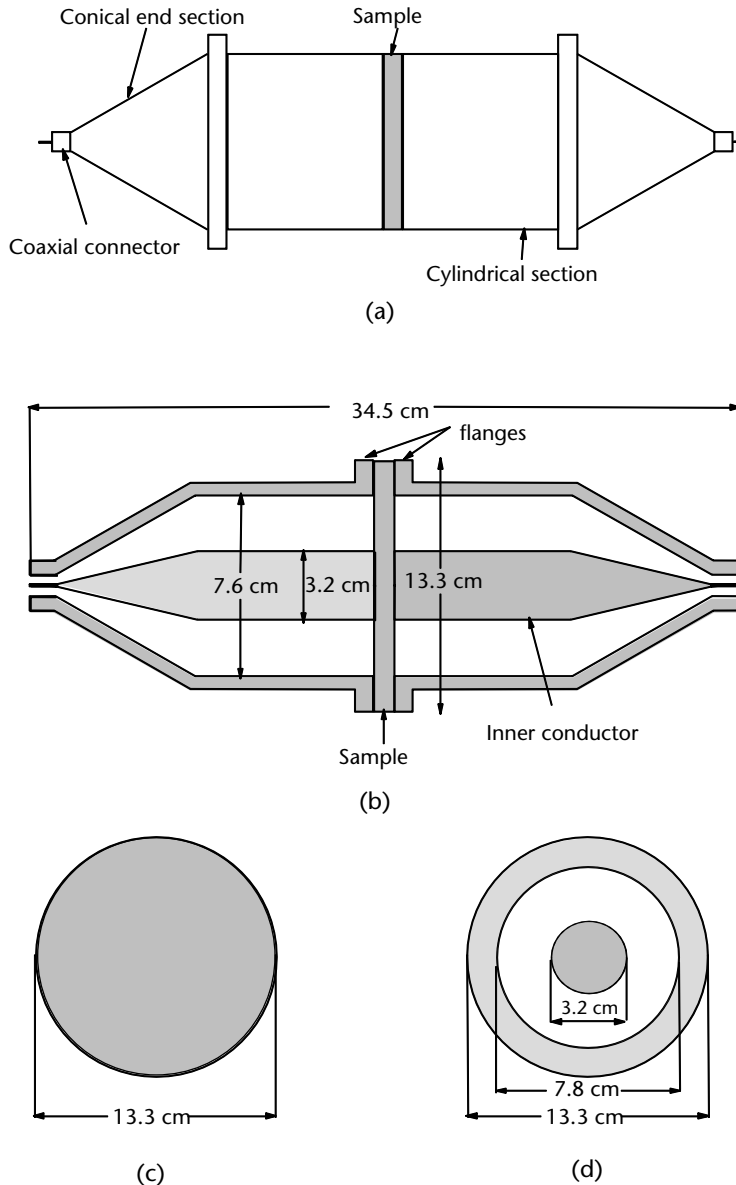


Figure 9.12 Circular coaxial TEM cells (not to scale): (a) ASTM circular coaxial TEM cell, (b) longitudinal cross section of the NBS flanged circular coaxial TEM cell, (c) disk-shaped sample, and (d) reference sample consisting of an annulus and a small disk.

cell is from 1 MHz and 1.8 GHz, but using Moreno's criterion given in (9.16), the upper-frequency limit is 1.77 GHz.

9.2.3 Rectangular and Square TEM Cells

These cells are used to produce uniform fields, mainly for susceptibility measurements and for calibration, but the dual TEM cell is also used for testing the shielding effectiveness of planar materials.

9.2.3.1 The Crawford Cell

The Crawford cell is sometimes called a TEM cell, although the latter is a generic term covering all cells supporting a TEM wave mode. It consists of a rectangular or square cross section outer conductor, and the center conductor is a thin tapered plate (sometimes called a septum) supported by dielectric posts. Rectangular cross section cells are slightly shorter than square cross section cells for a given cut-off frequency [4, p. 345]. It can produce a higher E -field intensity than the parallel or stripline cell, and it can be used at higher frequencies for fundamental or dominant mode propagation without the propagation of higher-order modes. It should be noted, however, that some higher-order modes are excited as the cross section of the cell changes abruptly from the tapered to the uniform rectangular or square cross section. However, if the dimensions of the uniform cross section portion are carefully chosen, these modes are attenuated before they reach the EUT.

9.2.3.1.1 Square Crawford Cell

The impedance of a 3-m long TEM cell of square cross section varies between 48.5 and 52.5 Ω [4, p. 345]. The formula for the characteristic impedance of this type of coaxial line is given by (9.17). The ratio of the width of the inner conductor to that of the outer conductor varies between 0.82 and 0.83. For a capacitance per unit length of $C=0.087$ pF/cm and a septum plate thickness of 0.157 cm, the cut-off frequencies are given in Table 9.1

Reference should be made to Section 9.2.3.2 about the upper-frequency limits of rectangular and square TEM cells.

The TEM cell, described in IEC 61000-4-20 [11], is used for objects that are limited in size. It is recommended that the EUT size is less than 0.33 times the height (y -axis), 0.6 times the width (x -axis) and 0.6 times the length (z -axis) of the cell dimensions [11, p. 14]. The EUT shall be at least 0.05 times the septum height above the bottom plate. MIL STD 461G recommends that the EUT size is less 0.5 times the width and 0.5 times the length [7, p. 157]. The frequency range of the TEM cell is given by Crawford [12, p. 3]

$$f = \frac{c}{2w} \quad (9.19)$$

where c is the speed of light in meters per second and w is the width the cell in meters.

For an 800-mm-wide cell, this equates to an upper-frequency limit of 187 MHz, although the Automotive EMC Directive allows their use up to 400 MHz.

Table 9.1 Cut-Off Frequencies for TEM Cells

$2b$ in Centimeters	$2w$ in Centimeters	Cut-Off Frequency (MHz)
150	124	100
50	41	300
30	25	500

The cell is a square cross section coaxial line with a transition to a standard circular cross section coaxial line of 50Ω . The cell has two tapered sloping sections joined by a square section, as shown in Figure 9.16. The center conductor, which is sometimes referred to as a septum, is also tapered and supported by dielectric posts. The cell must be placed at least 2m away from walls, metallic objects and the associated measuring equipment. The EUT must be placed in the center of the cell and on a nonconducting table, as recommended in IEC/EN 61000-4-3 [13].

TEM cells can be used for emissions testing, immunity testing, and calibration of field probes. For emissions and immunity testing, the field is calibrated at a minimum of five positions in the xy -plane which represents the front face of the EUT (four at the corners and one at the center). If the distance between any two adjacent points is more than 0.5m, more calibration points must be added, as specified in IEC 61000-4-20. The field uniformity must be within 6 dB overall at 75% of the electric field component measurements. The frequencies are measured at 1% steps. The upper frequency of a TEM cell is typically up to 1GHz and is verified by a TEM mode verification test where the x and z secondary components must be within 6 dB of the electric field along the y -axis (predominant component) for 75% of the frequencies. Exceptions to these rules of up to 10 dB are accepted for up to 5% of the test frequencies. For immunity applications, the calibration procedure ensures that the applied field across the reference plane is always greater than the specified test level. A field probe is used that has a maximum dimension of less than 10% of the septum height and also has to be smaller than one quarter of a wavelength of the highest calibration frequency. The probes shown in Figures 9.13 and 9.14 have an antenna length of less than 1.75 in (18mm).

The calibration of the cell is carried out using either the constant forward power method or constant field strength method. In the constant forward power method, the variation in field strength across all of the points is measured with a defined forward power. In the constant field strength method, the forward power is adjusted at each frequency and point to maintain a fixed field strength. As power meters are subjected to a more rigorous calibration procedure than field probes (which only may be calibrated at a single level) then the method that adjusts the forward power is more accurate. In

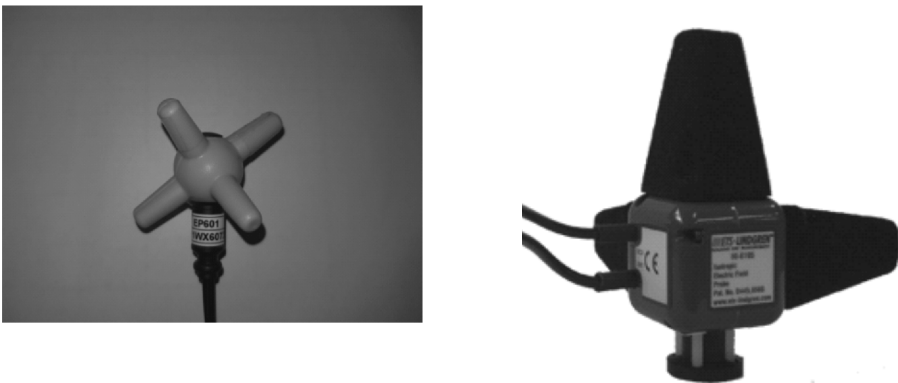


Figure 9.13 Electric field probes.

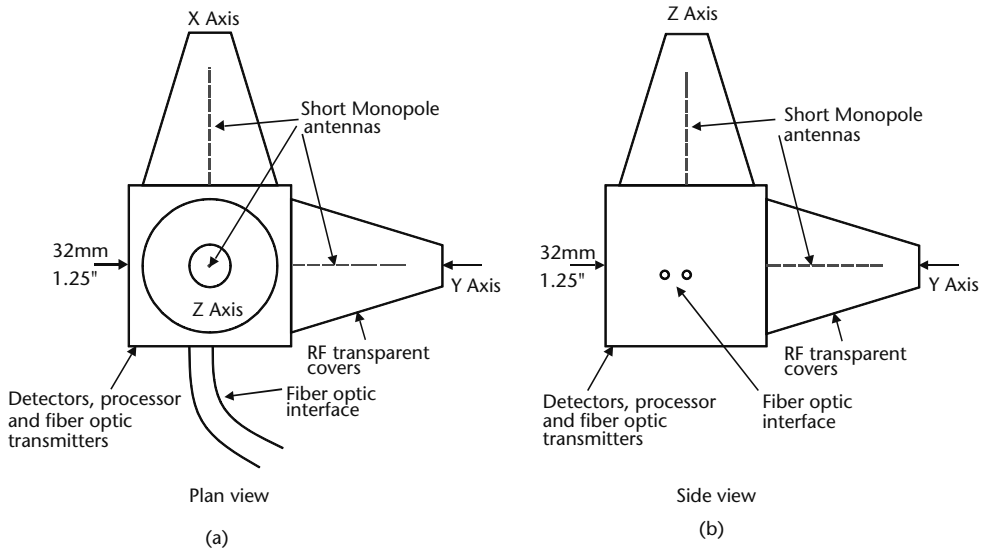


Figure 9.14 Electric field probe design.

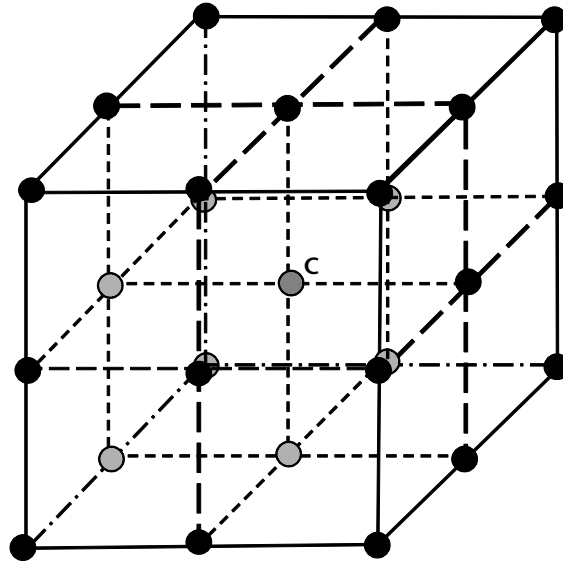
commercial testing to EN 61000-4-3 [13], the unmodulated field is established at one point, usually at a level of 1.8 times the highest test level to reflect 80% AM modulation that will be used during the actual testing stage. In the constant field method, the other points are then measured and the power level adjusted to achieve the same field strength. When the calibration procedure is complete, the forward power at each frequency is calculated to ensure that the field uniformity is achieved across all of the points, bearing in mind the criteria stated above. At the end of this process, a calibration file is generated which is used to perform the test on the EUT.

The TEM cell specified by IEC 61000-4-3 [13] is used to establish standard fields for field probe calibrations. When used as a calibration tool, the usable volume and frequency of a TEM cell has to be established by performing measurements at 27 points on a virtual cube, including one at the center (as shown in Figure 9.15) with the distance between the points being 10% of the septum height [11, p. 64]. The calibration volume is much smaller than that allowed for emissions or immunity testing and is specified at a maximum of 20% of the septum height. The standard deviation of calibration data shall be less than 1 dB for a GTEM and 0.6 dB for the dual TEM cells.

A TEM cell with dimensions of $0.8\text{m} \times 0.8\text{m} \times 0.8\text{m}$ is limited to an upper-frequency limit of 200 MHz by UNECE [8].

9.2.3.1.2 Rectangular Crawford Cell

For a Crawford cell [5, p. 394] of rectangular cross section, the working area is about one third of the separation between the center and outer conductors, where the electric field intensity is uniform to within a few percent. The cell, which is shown Figure 9.16, has an impedance given by the approximate formula of (9.18).



27 measuring points including center point

- Edges are solid lines -.- or long dash dot if hidden
- — — — Long dashed lines join the visible measuring points
- - - - - Dashed lines join the hidden measuring points
- Black circles are measuring points visible on the surface of the cube
- Grey circles are hidden measuring points
- C is the center of the cube

Figure 9.15 Validation points for TEM cell.

9.2.3.2 Cut-Off Frequency of Rectangular and Square TEM Cells

The highest usable frequency of a rectangular TEM cell with propagation of the TEM mode alone depends on the first higher-order mode to be propagated and its cut-off frequency.

For a rectangular coaxial line with an aspect ratio of $a/b = 2$ and a very thin septum, the first higher-order mode to be propagated is the TE_{10} mode, which is the fundamental mode in a rectangular waveguide (see Section 9.3.1). The cut-off frequency of the TE_{10} mode is also the same as that for a hollow rectangular waveguide with the same broadside dimension. In this case, since the larger cross section dimension of the rectangular TEM cell is $2a$, the cut-off wavelength is $4a$. In order to ensure that only the TEM mode will propagate, the cell must not be used above this cut-off frequency. Additionally, in order to ensure that any evanescent modes (see Section 9.3.3) are strongly attenuated, the cell should be used at a frequency far below this cut-off frequency. Another higher-order mode is the TE_{01} mode, which propagates when the electric field vector is turned through 90° relative to the cell.

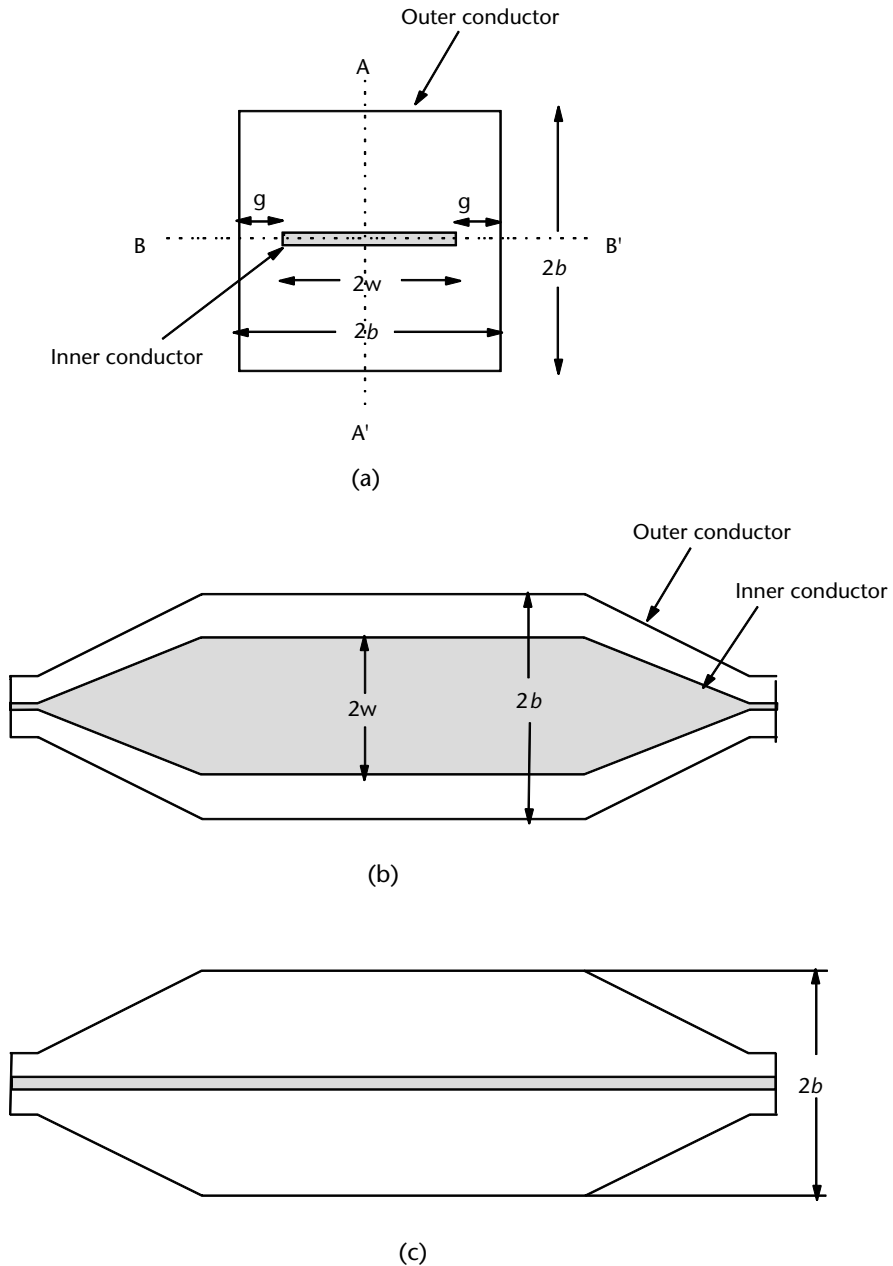


Figure 9.16 Crawford TEM cell with square cross section: (a) Transverse cross section, (b) longitudinal section through BB' , and (c) longitudinal section through AA' .

Thus, the dimension perpendicular to the electric field is now $2b$ instead of $2a$ (see Section 9.3.1). This mode can be propagated when the width of the septum $2w$ is large compared with the broadside dimension $2a$ of the cell, as shown in Figure 9.6(a). This is due to the fact that the capacitive effects between the septum and the side walls of the cell result in the electrical dimensions of the height $2b$ appearing greater than the width a [12].

The cut-off frequencies of both the TE_{10} and TE_{01} modes in a rectangular (or circular) TEM cell depend on:

- The aspect ratio of ab [14];
- the ratio of the width of the septum to the width of the outer conductor parallel to the septum (w/a) [14];
- the characteristic impedance of the cell Z_0 [14].

Let us first consider which the lowest-order mode to propagate is. Gruner [14] has shown that under certain conditions, the first higher mode to propagate is not the TE_{10} mode (as in a hollow rectangular waveguide), but the TE_{01} mode. As we vary the aspect (ab) of the cell and the width of the septum with respect to the dimension a (i.e., as we vary the ratio w/a), either the TE_{10} mode or TE_{01} mode will propagate, depending on the values of these ratios. Referring to Figure 9.17(a), the curve is the dividing line between the TE_{01} mode and the TE_{10} mode. For values of w/a and ab below this line, the TE_{10} mode is dominant, whereas for values above the line, the TE_{01} mode is dominant. For instance, if we have a rectangular cell with an ab ratio of 2, and a w/a ratio less than 0.71, we can see from the graph of Figure 9.17(a) that the TE_{10} mode will be first mode to propagate. However, if the width of the inner conductor is increased so that w/a is greater than 0.71, while keeping the aspect ratio constant, then we can see from the graph that the TE_{01} mode will be the first mode to propagate. For example, if ab is 2 and the ratio of w/a is 0.8, the TE_{01} mode will be the first higher-order mode to propagate. This mode has a cut-off wavelength that is twice as large as that of the TE_{10} mode (since a is twice as large as b).

Thus, TEM cells that have dimensions with these ratios will have cut-off frequencies which are only half those of cells where the TE_{10} mode is the first higher-order mode to propagate. When the value of the ratio w/a is 0.71, and ab is 2, the TE_{01} and TE_{10} modes have the same cut-off frequencies.

Weil [15] has eliminated the effect of the ratio w/a by plotting the cut-off wavelength normalized to the cut-off wavelength of the TE_{10} mode for different impedances. Figure 9.17(b) shows how the cut-off wavelength varies with the aspect ratio for lines of characteristic impedances from 50 to 150 Ω . If we look at the 50- Ω line, we can see that it crosses the TE_{10} mode cut-off wavelength line at $ab=1.93$. If this ratio exceeds 1.93, the cut-off wavelength is greater than for the TE_{10} mode, giving a cut-off frequency less than that for the TE_{10} mode, which is normally assumed to be the first higher-order mode to propagate. For instance, if we have a square cross section cell ($ab=1$) then we can see that for a given impedance, the ratio of $4a/\lambda_c$ is always less than that for a rectangular cell, where $ab>1$. A 50- Ω square cell has $4a/\lambda_c = 0.51$, giving a cut-off wavelength of $7.8a$, whereas for a rectangular cell with $ab=1.5$, the value on the y -axis is 0.78 which gives a cut-off wavelength of $5.12a$. If the normal criterion is used, that is, the cut-off frequency of the TE_{10} , the square cell would have a cut-off wavelength ($4a$) roughly half that of the $7.8a$, obtained from the graph of Figure 9.17(b). This gives an upper-frequency limit almost 95% higher than the correct value.

Table 9.2 lists the cut-off frequencies using the TE_{10} , TE_{01} , and corrected cut-off frequencies for some commercially available TEM cells.

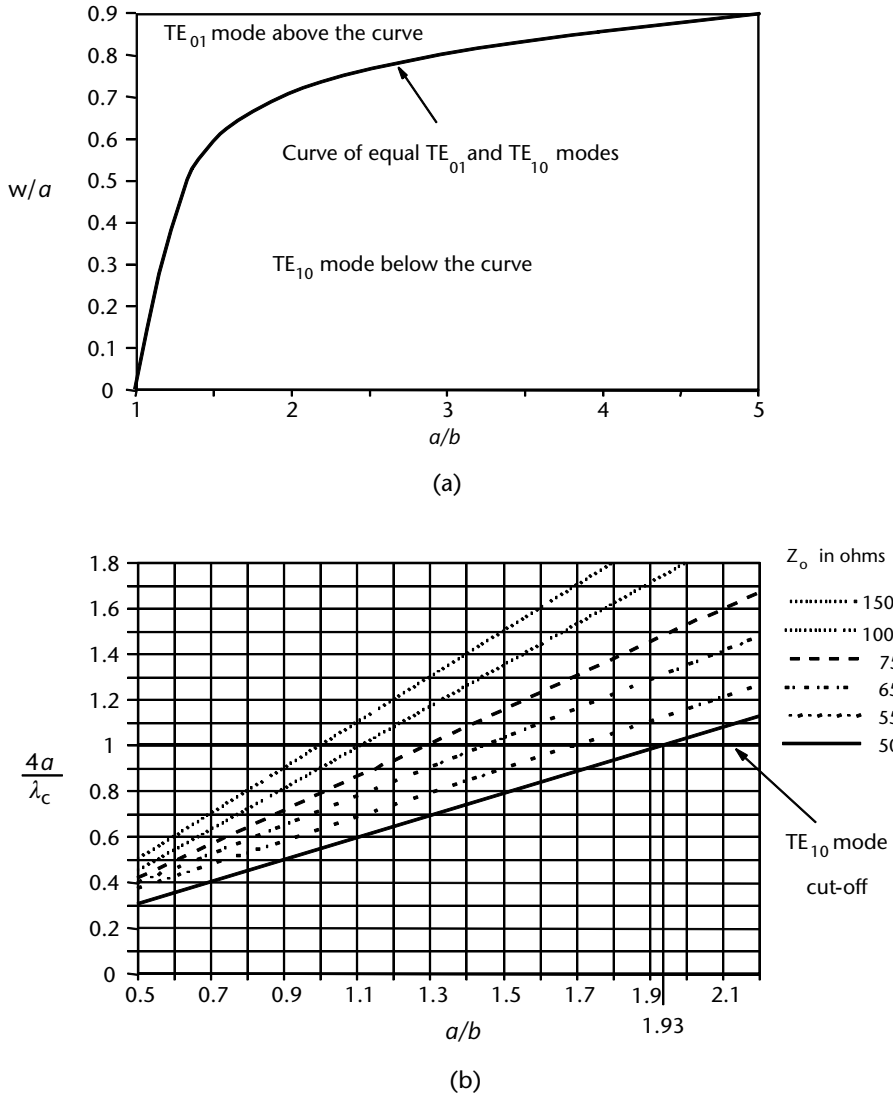


Figure 9.17 The cut-off frequencies for rectangular and square TEM cells: (a) Excitation of the TE₀₁ and TE₁₀ modes for different aspect ratios and widths of center conductor, and (b) cut-off frequencies for the TE₀₁ and TE₁₀ modes for different aspect ratios, with characteristic impedance as a parameter.

Table 9.3 shows the cut-off frequencies for NBS Crawford cells. For a more detailed explanation of these corrected cut-off frequencies, reference should be made to the papers by Gruner [14] and Weil [15].

9.2.3.3 Dual TEM Cell

The dual TEM cell (DTC) shown in Figure 9.18(a) consists of two TEM cells mounted one on top of the other with aligned apertures between the two. Each cell has outer conductors measuring 18 cm × 12 cm, and a septum or inner conductor with width of 13.6 cm. One cell is used as the transmitting cell, and the input signal is applied

Table 9.2 Predicted Cut-Off Frequencies for Commercially Available TEM Cells

<i>Manufacturer and Model Number</i>	<i>Manufacturer's Upper Frequency Limit (MHz)</i>	<i>Normal TE₁₀ Mode Cut-Off Frequency (MHz)</i>	<i>Normal TE₀₁ Mode Cut-Off Frequency (MHz)</i>	<i>Corrected TE₁₀ Mode Cut-Off Frequency (MHz)</i>
IFI CC 101	100	125.4	182.9	66.3
IFI CC 101-5	150	182.1	125.1	100.2
IFI CC 102	200	250	166.8	133.3
IFI CC 103	300	388.5	249.6	204.4
IFI CC 105	500	513.3	333.5	292.4
IFI CC 110	1,000	1,010.6	663.5	530.5
Narda 8802	250	250	150	128.2
Narda 8801	500	500	300	256.4

to one of its ports while its other port is terminated in a matched load [14, p. 19]. This type of configuration is used for testing the shielding effectiveness of materials which are usually in planar/sheet form. A sample of the MUT is inserted across the aperture between the two cells. We can see from Figure 9.18(b) that the electric field is perpendicular to the sample for the wave propagating from port 1 to port 2, so that the wavefront is not perpendicular to the sample but almost parallel to it, that is, striking it at grazing incidence. The wave impedance is not that of a plane wave (377Ω). The aperture couples energy to the two output ports (3 and 4) asymmetrically, and both low-impedance (magnetic mode) and high-impedance (electric mode) shielding effectiveness can be measured simultaneously. The NBS DTC uses TEM cells with cross-sectional dimensions of width $2a = 9$ cm, height $2b = 6$ cm, and the gap g between the septum and adjacent side wall of 1.1 cm. The apertures in the intercommunicating cell walls are 5.08 cm square, and the frequency ranges from 1 MHz to 1 GHz.

9.2.3.4 GTEM Cell

The gigahertz TEM (GTEM) cell minimizes the generation of higher-order modes by not having any abrupt changes in geometry (that could result in the excitation of higher-order modes) that are present in the Crawford TEM cell. The cell shown in Figures 9.19 and 9.20 is like a giant pyramid laid on its side with a standard circular

Table 9.3 Predicted Cut-Off Frequencies for the NBS Crawford Cells

<i>TE₀₁ Mode Cut-Off Frequencies for $\lambda = 2a$ (MHz)</i>	<i>Corrected TE₀₁ Mode Cut-Off Frequencies</i>	
	<i>Square Cell ($a/b = 1$) (MHz)</i>	<i>Rectangular Cell ($a/b = 1.669$) (MHz)</i>
100	58	86
300	174	258
500	430	430

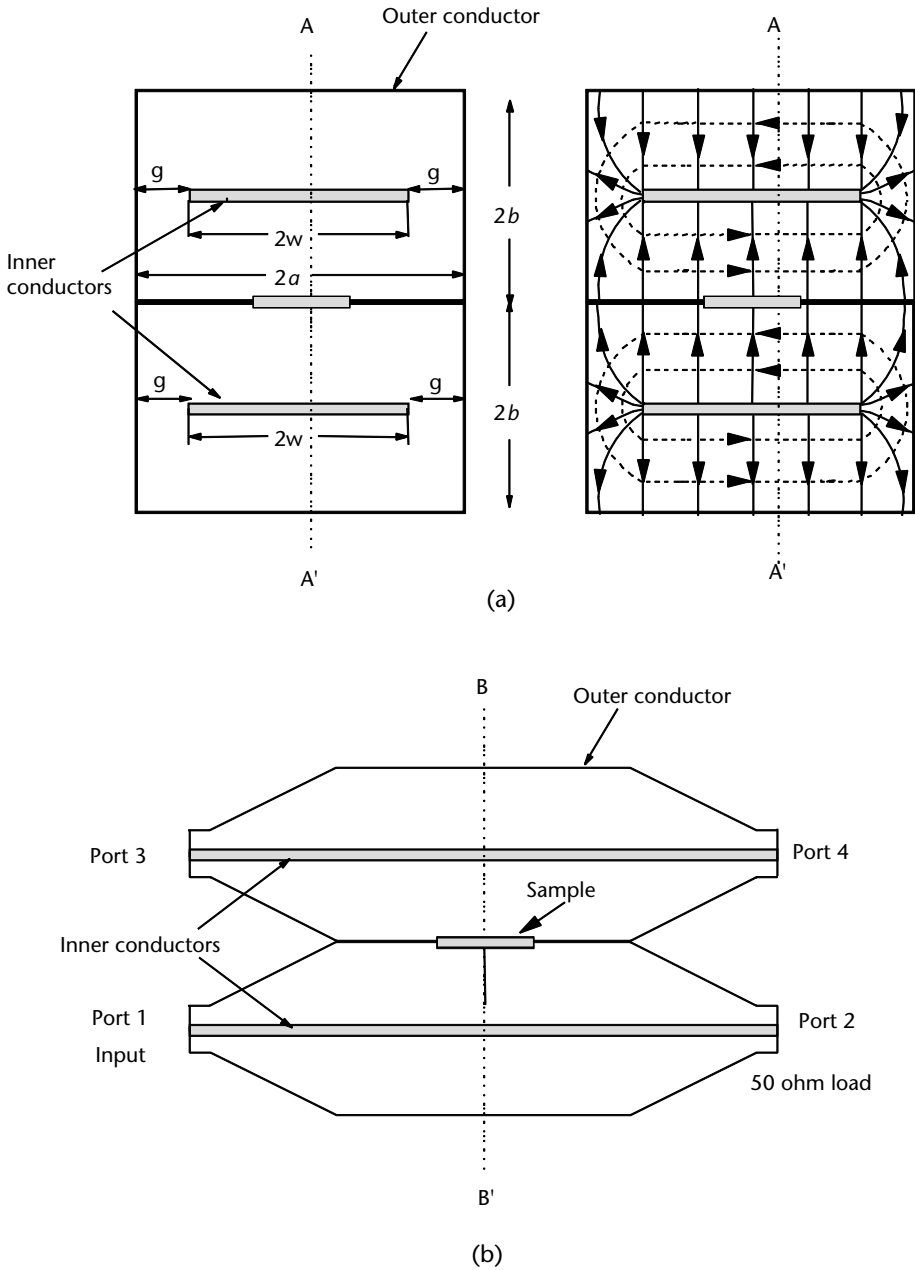


Figure 9.18 DTC set-up: (a) Transverse cross section through BB', and (b) longitudinal cross section through AA'.

coaxial connector at its apex and a constant impedance resistive termination at its base (or load) end. This end also has pyramid shaped absorbers to attenuate any undesirable higher order that may be generated by irregularities. The shape of the cross section is rectangular, the same as that of the Crawford TEM cell, with outer and (plate or septum) inner conductors of increasing dimensions from the apex to the load end. The characteristic impedance of the GTEM cell is typically 50Ω and

the frequency range is 30 to 1,000 MHz. The size depends on the dimensions of the equipment to be tested. No dimension of the EUT should be greater than 90% of the distance from the floor to the septum or center conductor. The EUT tends to capacitively load the cell, but if the volume of the EUT is kept small, the effects are negligible. Desktop computers tested in the GTEM cell have exhibited negligible loading effects when the maximum floor to septum separation is 1.75m [16].

The septum of the GTEM is terminated in a 50- Ω resistor. The width of the center conductor, though, does not allow a connection to just one resistor, because the capacitive and inductive effects would cause reflections at the connection to rear wall for higher frequencies. An array of resistors will also minimize the effects of a parasitic inductance that would occur with a single resistor. By using parallel paths, the impedance caused by the parasitic inductance is reduced, because the reciprocal of total inductance of the parallel connection is the sum of reciprocals of individual inductances of all inductors. At frequencies where the cross sectional

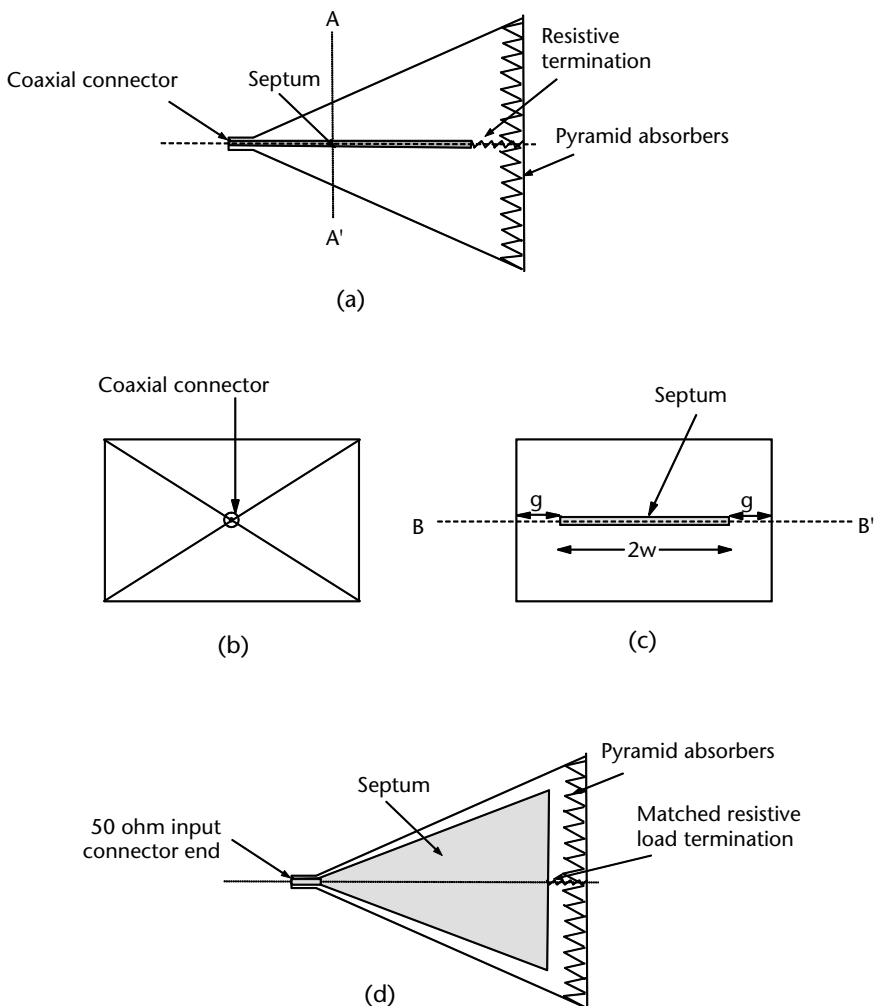


Figure 9.19 GTEM contigual cell: (a) Schematic vertical cross sectional view, (b) end view, (c) transverse cross section through AA', and (d) longitudinal cross section through BB'.

dimensions of the cell exceed half a wavelength, the waves start propagating in higher-order modes rather than in TEM mode, as described in Section 9.2.3.2. The cut-off wavelength is twice the larger cross section dimension of the rectangular cell. At higher frequencies, propagation in higher-order modes occurs [17]. These higher-order modes cannot be terminated by the resistors, as they are waveguide modes. Thus, radiated fields are terminated using suitable pyramidal absorbers.

The RF absorbers should have a sufficient return loss at frequencies down to 500 MHz or even down to 200 MHz. This means there is a certain frequency band in which a crossover from TEM to waveguide propagation takes place, and therefore a crossover from resistive termination to wave termination is necessary. In that intermediate frequency band, both parts are not completely effective and only the combination leads to an acceptable reflection coefficient [17].

9.3 Modes in Circular Waveguides

In the case of circular waveguides, the boundary conditions also apply, but the derivation of the cut-off frequency for the fundamental and the higher-order modes are more complex since they involve the roots of the Bessel functions, and are given by

$$\lambda_c = \frac{2\pi r}{u'_{mn}} \quad (9.20)$$

where

λ_c is the cut-off wavelength;

r is the radius of the guide;

u'_{mn} is the n th root of the Bessel equation $J'_m(u) = 0$ for a TM wave, and the n th root of the Bessel equation $J_m(u) = 0$ for a TE wave.

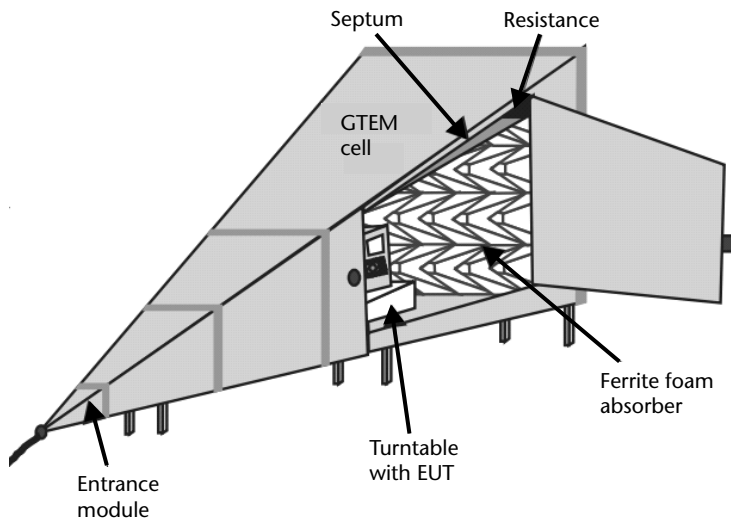


Figure 9.20 GTEM cell.

For a more rigorous treatment, the reader is referred to [18, pp. 66–72].

The fundamental mode of propagation is the TE_{11} mode. The first subscript stands for one half-wave variation along half a circumference concentric with the guide wall, and the second subscript is one more than the number of field reversals along a radial path in the plane, transverse to the direction of propagation [3, p. 116]. The cut-off wavelength for this mode is given by

$$\lambda_c = 3.412r \tag{9.21}$$

where r is the radius of the waveguide in the same units as the wavelength.

Although this is the fundamental mode, it does not provide the lowest attenuation, as is the case for rectangular waveguides. The mode that provides the least attenuation is the TE_{01} mode, which is the fifth-order mode of propagation. Figure 9.21(a) shows the field variations for three of the lower-order modes for a circular waveguide. The TE_{01} mode is used for long lengths of waveguide runs. The attenuation per unit length as a function of the cut-off frequency f_c is shown in Figure 9.21(b). It can be seen that the attenuation of the TE_{01} mode decreases with increasing frequency (above a minimum value at around $4.5 f_c$), whereas that of the dominant TE_{11} mode increases with frequency.

9.3.1 Cut-Off Waveguide Ventilation Panels

Ventilation is required for screened rooms, but these would also normally result in EM leakage. In order to avoid the leakage, use is made of the property of waveguides beyond cut-off (see Section 6.7.1). Ventilation panels consist of a matrix of

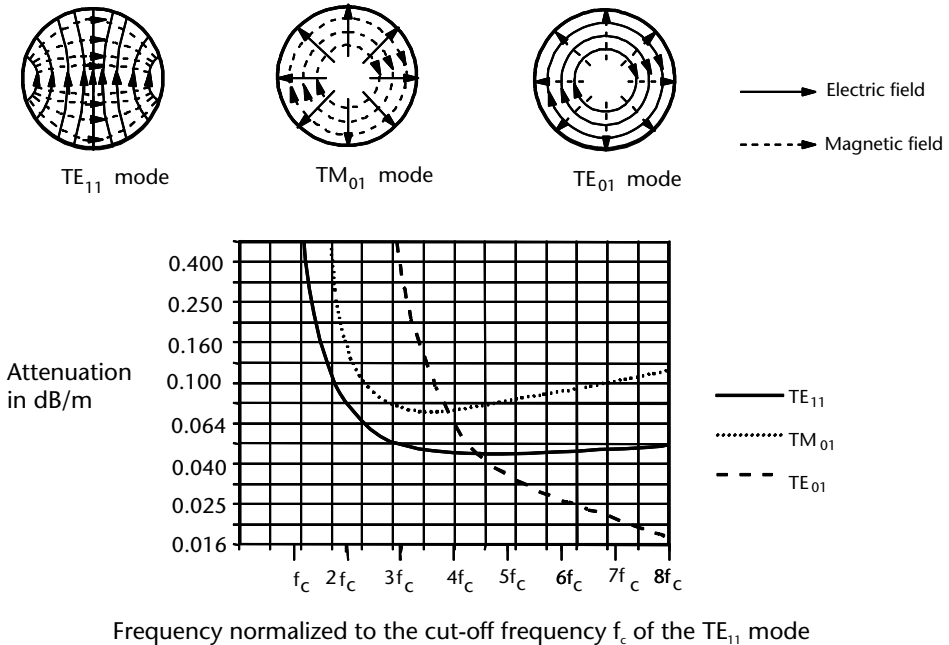
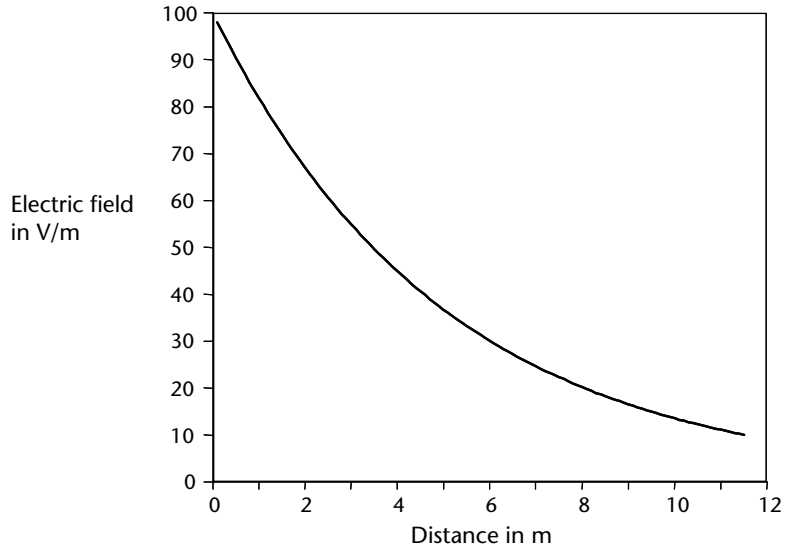
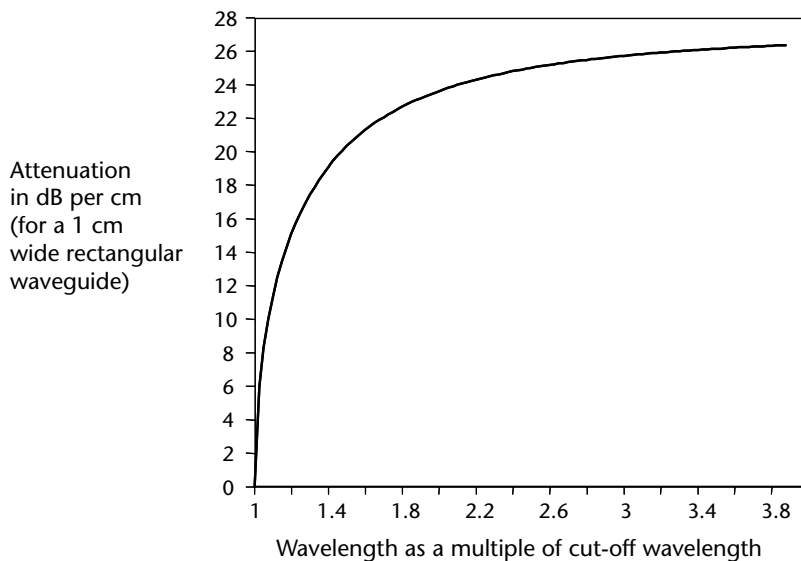


Figure 9.21 Attenuation for some of the modes in a circular waveguide as a function of the cut-off frequency of the dominant TE_{11} mode.

interlocking waveguides (beyond cut-off) in a flanged box which can be installed into the wall of a shielded room. Typical materials used are steel waveguides brazed together and tin dipped for good conductivity [19, p. 35]. The ventilation panels may be used in conjunction with fans. The cut-off waveguide does not support the normal propagating modes, but supports modes known as evanescent modes (see Section 6.7.1). These modes decay exponentially from the point of excitation, as shown in Figure 9.22(a), so that the electric field variation with distance is given by the following formula



(a)



(b)

Figure 9.22 Attenuation of evanescent modes: (a) Decay of the electric field with distance for evanescent modes, and (b) attenuation of evanescent modes with wavelength.

$$E = E_o e^{\alpha z} \quad (9.22)$$

where

E is the electric field at a distance z from the point of excitation;

E_o is the electric field at the point of excitation;

α is the attenuation in decibels per unit length of the waveguide.

If the wavelength is in meters, then the attenuation will be in decibels per meter.

These evanescent modes store energy, but do not propagate or dissipate energy. The input impedance of a waveguide below cut-off is purely reactive, that is, it does not have a resistive or real part of impedance. This technique is useful in reducing the leakage from apertures by replacing the hole with a tube of rectangular or circular cross section. The dimensions of the cross section are chosen to suit the highest operating frequency of the room. The critical dimension is the one perpendicular to the electric field, but for general use, if the room is to be suitable for any type of polarization, the smallest dimension should be chosen to be much less than the highest operating frequency. The length of the tube will determine the magnitude of the attenuation, since the field decays to a lower value the longer the length of the tube. The following sections give the formulas for calculating the attenuation of cut-off waveguides.

9.3.1.1 Rectangular, Square, and Polygonal Cross Section Cut-Off Waveguides

If a square or rectangular waveguide has a dimension of a perpendicular to the incident electric field vector, then it will not propagate a wave whose free-space wavelength is equal to or greater than $2a$. The dimensions of the cut-off waveguide are chosen so that neither of its cross section dimensions are greater than half the free-space wavelength of the highest operating frequency of the shielded room. This ensures that the waveguide is beyond cut-off, regardless of the electric field orientation. Thus, if the highest operating frequency of the room is 15 GHz, its free-space wavelength is 2 cm, and so the smallest dimension of the cut-off waveguide must be less than 1 cm. In practice, the cut-off waveguide dimensions are chosen to be much less than 1 cm, and the smaller these dimensions are relative to the wavelength of the highest operating frequency of the room, the greater the attenuation it provides is. The attenuation is also dependent on the length of the cut-off waveguide, since the electric field decays with distance (see Section 9.3.3). The attenuation in decibels per unit length of waveguide is given by

$$\alpha = 8.69 \sqrt{\left(\frac{2\pi}{\lambda_c}\right)^2 - \epsilon_r \left(\frac{2\pi}{\lambda}\right)^2} \quad (9.23)$$

where

α is the attenuation in decibels per unit length of the waveguide;

λ_c is the cut-off wavelength of the waveguide;

ϵ_r is the dielectric constant or relative permittivity of the material filling the guide (this value is equal to one for air);
 λ_0 is the free wavelength of the incident wave.

This equation reduces to

$$\alpha = \frac{54.6}{\lambda_c} \sqrt{1 - \epsilon_r \left(\frac{\lambda_c}{\lambda_0} \right)^2} \quad (9.24)$$

When the free-space wavelength is much larger than the cut-off frequency, that is, when the incident frequency is far below the cut-off frequency, the second term under the square root sign λ_c/λ_0 tends to zero and (9.23) reduces to the following:

$$\alpha = \frac{54.6}{\lambda_c} \quad (9.25)$$

For a rectangular waveguide, the cut-off wavelength λ_c is $2a$ (where a is the dimension perpendicular to the electric field vector).

$$\alpha = \frac{27.3}{a} \quad (9.26)$$

If we have a waveguide whose largest cross section dimension a is 1 cm, the cut-off wavelength is 2 cm ($2a$). This corresponds to a frequency of 15 GHz. In order to calculate the attenuation per unit length, we have to consider the frequency of the incident wave; in the case of a shielded room, this frequency is its highest operating frequency. If the highest operating frequency is 10 GHz, its wavelength is 3 cm. Since this is not much larger than the cut-off wavelength of 2 cm, we must use (9.24). This gives us a value of 20.35 dB/cm, or 2035 dB/m. However, if the highest operating frequency of the room is only 100 MHz, its wavelength is 3m, and since this is much longer than the cut-off wavelength, we can use (9.24) which will give us an attenuation of 27.3 dB/cm. It is useful to see that if we had used (9.24), we would have obtained a value of 27.16 dB/cm. For a waveguide of length 5 cm, the attenuation would be more than 135 dB up to 100 MHz, and 100 dB at 10 GHz. The attenuation per centimeter of evanescent modes in a 1-cm-wide rectangular waveguide as a function of wavelength is shown in Figure 9.22(b). The wavelength is normalized to (expressed as a multiple of) the cut-off wavelength.

9.3.1.2 Circular Cut-Off Waveguides

In the case of circular waveguides, propagation will not occur for a wave whose wavelength is equal to or greater than 1.706 times the diameter of the waveguide. The same equation (as for rectangular cut-off waveguides) applies when the wavelength of the highest operating frequency is not much lower than the cut-off wavelength. The attenuation per unit length given by (9.27) is

$$\alpha = \frac{54.6}{\lambda_c} \sqrt{1 - \left(\frac{\lambda_c}{\lambda_0}\right)^2} \quad (9.27)$$

where

α is the attenuation in decibels per unit length of the waveguide;

λ_c is the cut-off wavelength of the waveguide;

λ_0 is the free wavelength of the incident wave.

When the wavelength of the highest operating frequency is much larger than the cut-off wavelength of the dominant TE_{11} mode, (9.30) reduces to the following (using (9.21) for the cut-off wavelength) for a circular waveguide of radius r

$$\alpha = \frac{16}{r} \quad (9.28)$$

If the radius is in centimeters, then the attenuation will be in decibels per centimeter.

9.3.1.2.1 Honeycomb Air Vents

The air vents for shielded rooms commonly use commercially available extruded aluminum honeycomb material as shown in Figures 9.23 and 9.24, that is used in aircraft structures. There must be good bonding between cell walls. This material is extruded in large quantities and has a high strength-to-weight ratio for structural applications, and since the hexagon cross section approximates a circular cross section waveguide, this can be used as a cost-effective substitute for circular waveguides. The material commonly used for air vents has a 3-mm (0.125-in) nominal width and an 18-mm (0.75-in) depth/length.

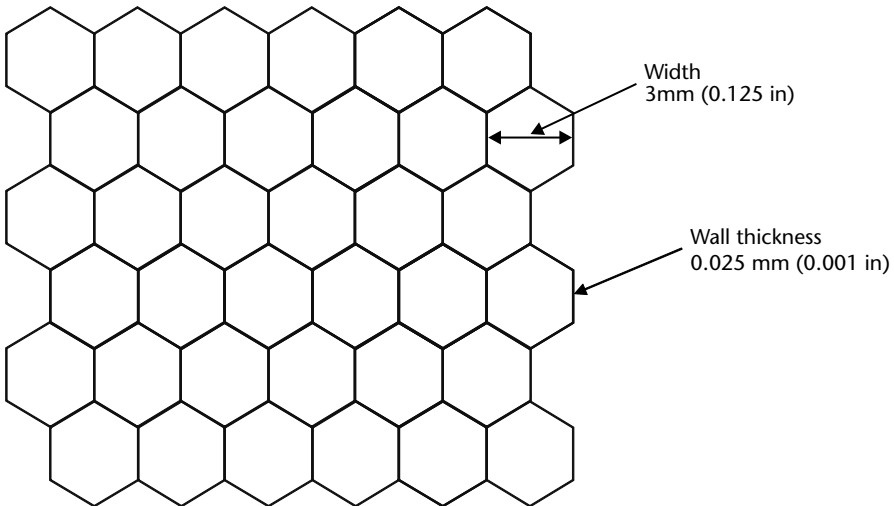


Figure 9.23 Typical dimensions of a honeycomb air vent.

For a 1.5-mm (0.0625-in) nominal radius of a circular waveguide, the cut-off wavelength according to (9.21) is 58.6 GHz. Since most shielded rooms operate at frequencies below 18 GHz, it can be seen from (9.33) that the attenuation is 192 dB for frequencies well below cut-off and for a length/depth of 18 mm (0.75 in).

Aluminum extrusion is an automated cost-effective process, and is used to produce honeycomb-shaped formats, as these have a high strength-to-weight ratio for applications in aircraft, trains, and fast ships [20].

9.4 Resonant Cavities

Under certain conditions, the electric and magnetic fields in a shielded room may follow the same pattern as the fields in a rectangular waveguide cavity. At particular frequencies, the waves are not traveling but are resonant. The resonance is similar to the resonance that occurs with sound waves in organ pipes, where longer pipes resonate at the lower frequencies, and shorter pipes are resonant at the higher frequencies. In a shielded room, this condition occurs when any dimension of the room is an integral multiple of half a wavelength at any frequency. At the lowest resonant frequency, one dimension of the shielded room is equal to one half of a wavelength. For higher harmonics, where the frequency is an integral multiple of the lowest resonant frequency, the shielded room also resonates and the dimension is an integral multiple of half a wavelength at these higher frequencies. The effect of these resonances is to cause spurious results at these frequencies in measurements performed in shielded rooms.

The resonant frequencies are given by the following formula:

$$f = \frac{c}{2} \sqrt{\left(\frac{l}{a}\right)^2 + \left(\frac{m}{b}\right)^2 + \left(\frac{n}{z_0}\right)^2} \quad (9.29)$$

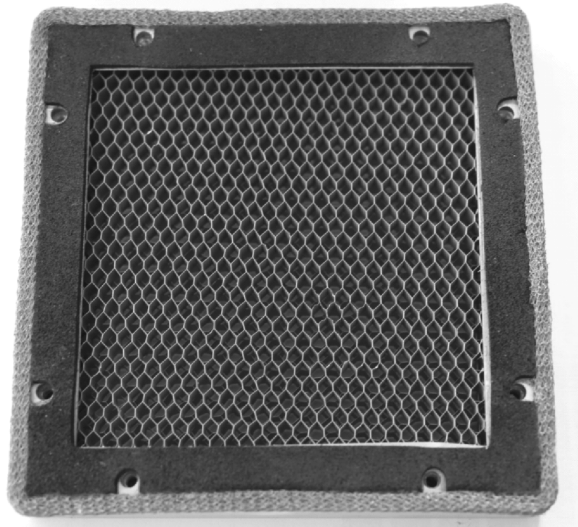


Figure 9.24 Honeycomb air vent.

where

c is the speed of light in meters per second;

l , m , and n are positive integers, of which only one may be zero for each mode of resonance; and,

a , b , and Z_o are the dimensions of the chamber in meters.

However, it should be noted that these resonant frequencies are when the room is empty. When there is any equipment or other metal objects in the room, the cavity is loaded and the resonant frequency is lower than that of the unloaded cavity.

In a large cavity, the total number of modes [3, p. 218]) for a wavelength range of $d\lambda$ is given by

$$N = \frac{8\pi V d\lambda}{\lambda_m^4} \quad (9.30)$$

where

$d\lambda$ is the difference between the minimum and maximum wavelengths;

V is the volume of the cavity;

λ_m is the center wavelength.

Any units of lengths may be used for the wavelengths and the dimensions of the cavity, as long as the same units are used for both.

9.4.1 Degeneracy

If we have modes with subscripts l , m , and n , these three can be arranged in 3! ways (i.e., 6 ways). Since both TE and TM modes can exist with these subscripts, altogether there are 12 different modes that can be supported by a rectangular cavity for each set of values of l , m , and n . If the sides of the cavity are equal, then it can be seen that by substitution into (9.29), all of the 12 modes will have the same resonant frequency. This is known as twelve-fold degeneracy. If two of the sides of a cavity are the same, there will be 2! modes for TE modes and the same number for TM modes. Since in this case 4 modes will have the same resonant frequency, this is known as four-fold degeneracy. Similarly, if all sides of the cavity are different, there will only be two-fold degeneracy.

9.4.2 Mode Stirrers

Mode stirrers are used in shielded rooms to even out the fields due to the geometry of the room. In order to understand the manner in which mode stirrers work, we must consider overmoded rectangular waveguides. In these guides, as opposed to the standard waveguides, the higher-order modes are allowed to propagate. We have seen how the electric field has a maximum at the center of the waveguide when the dominant mode is supported. Standard waveguides are restricted in their frequency

range so that they do not support either evanescent modes or higher-order modes. In Figure 9.25(a), we can see how the higher-order modes are propagated as the magnitude of b/λ_0 is increased. This magnitude can be increased by increasing b while keeping the wavelength constant, or by decreasing the wavelength (i.e., by increasing the frequency), and keeping the value of b constant. Shielded rooms are like large rectangular waveguides with fixed dimensions, but the wide operating frequency range is equivalent to decreasing the wavelength as the frequency increases, so that higher-order modes are propagated. There may be TE and TM modes up to several orders. For the sake of clarity, we shall just consider the TE_{n0} modes up to the sixth order. The electric fields are shown at one instant in time in Figure 9.25(a–f) for the individual modes from TE_{10} to TE_{60} , and in Figure 9.25(g) the modes are shown superimposed. We can see in the latter figure that there are several positions along the a dimension where the electric field is at a maximum. At another point in time half a period later, the electric field is shown in Figure 9.25(h). Ideally, in a shielded room, we would like the electric field to be uniform over the whole room. Although we cannot have a finite magnitude for the tangential electric field at the walls of the room because of boundary conditions, we would like the variation in the electric field everywhere else to be as small as possible so that when we measure the field from an EUT, we can attribute the field to that device and not to the geometry of the room. At high frequencies, there are many higher-order modes, and the room is said to be overmoded or multimoded. However, at the lower frequencies where the room is of the order of a wavelength, only one or two modes may be present, and thus the electric field may have only one or two maxima. In an attempt to randomize and even out the fields in an overmoded cavity, a mode stirrer is used in the same way as it is used in microwave ovens, where we would like the food to be heated uniformly. The mode stirrer consists of a set of metal plate reflectors called paddles, and the fields are reflected by them, so that they are time averaged and appear uniform. When we are performing swept frequency measurements, we must ensure that the frequency is swept at a much slower rate than the rotation rate of the mode stirrer. Each frequency traditionally required 200 paddle positions, so this was a very time consuming method at low frequencies (less than 200 MHz) where the average room is not heavily moded, but at higher frequencies (1 GHz and above) where many more modes exist, less time is required [21, p. 21].

9.5 Shielded Rooms

A shielded room could be an unlined rectangular cuboid or an absorber-lined chamber (ALC). A shielded room is useful for measuring the radiated emissions, as well as susceptibility (or immunity) and the shielding effectiveness of materials.

9.5.1 Unlined Shielded or Screened Rooms

Although the terms shielded room and screened room are used synonymously, the term shielded room is often used as a generic term to include both lined and unlined rooms, whereas the term screened room is usually used to indicate an unlined shielded room. It should be noted however that the term screen is also used

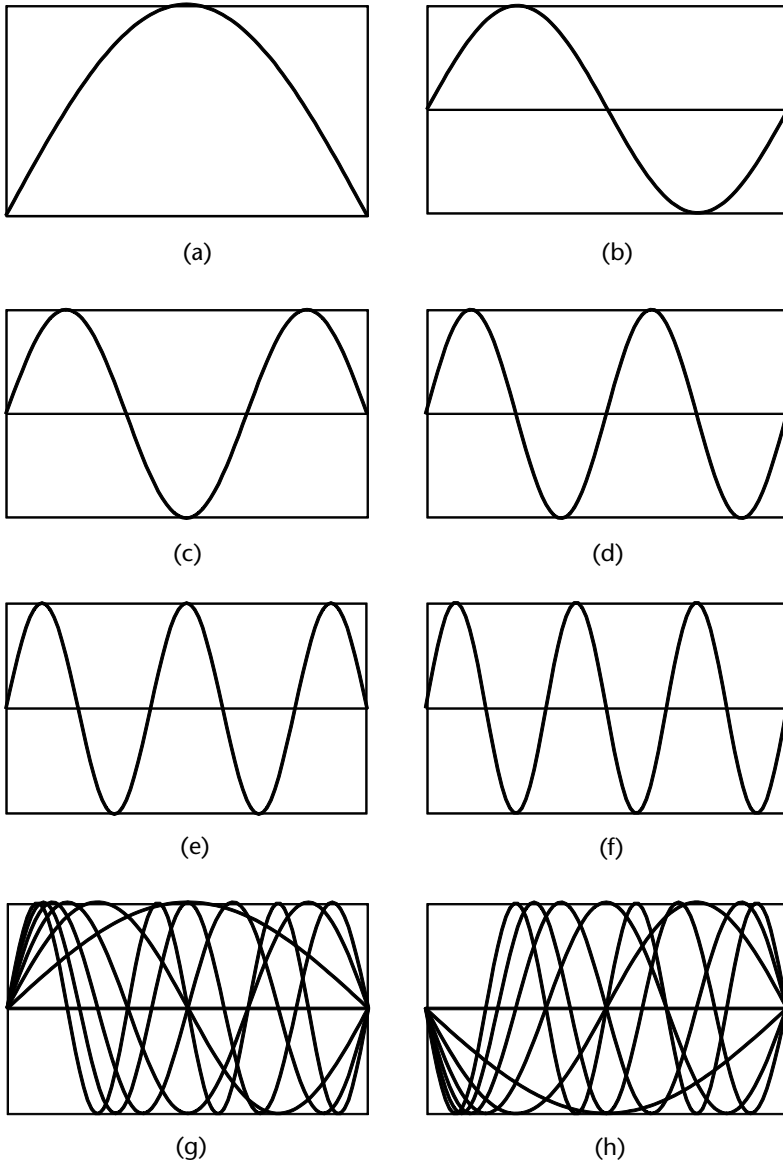


Figure 9.25 Six TE modes in an overmoded rectangular cavity: (a) TE_{10} mode, (b) TE_{20} mode, (c) TE_{30} mode, (d) TE_{40} mode, (e) TE_{50} mode, (f) TE_{60} mode, (g) six TE modes superimposed, and (h) half a period later.

to denote nonsolid or woven material in cables, and doubled-walled wire cages are also called screened rooms. A screened room prevents EM waves outside the room from entering and those inside the chamber from leaking outside, but this is only over the operating frequency range of the room. We may generally assume that the lower the frequency of operation, the thicker the walls; but at higher frequencies the leakage occurs through small apertures, and thus the seams between adjoining walls and doors have to fit tighter. Leakage can occur through apertures that are

as small as 1/100th of a wavelength. At 10 GHz, where the wavelength is 3 cm, apertures as small as 0.3 mm can cause problems. On the other hand, at 30 MHz the wavelength is 10m, and thus apertures of the order of 10 mm can be tolerated. The metal walls of the shielded rooms reflect the EM waves, in much the same way as sound waves are reflected in the room. Because of the nature of waves, constructive and destructive interference can take place, resulting in resonances (see Section 9.4) that can give spurious results in measurements.

The walls of screened rooms are usually made of solid steel plates, or a sandwich of two steel plates separated by a thicker sheet of wood (typically particle board). Steel is chosen since it has good absorption properties at frequencies above about 10 kHz, and provides a good compromise between EM attenuation and economic cost. At low frequencies, the absorption of steel is directly proportional to its thickness. The steel plates are welded together to ensure that there are no gaps. At lower frequencies where the wavelength is large, wire cages may be used instead of solid walled chambers.

9.5.2 Absorber-Lined Chambers

Absorber-lined chambers could be partly or fully lined with RAM (radar absorbing material). If the chamber is completely lined with RAM, then it is usually called an anechoic (no echo) chamber. Partly lined chambers are used as a compromise solution for economic reasons, since absorbers are relatively expensive. In addition, lining a room with absorbers reduces the effective volume of the room.

9.5.2.1 Absorbers

Absorbers are commonly known as RAM (radar absorbing material). The most commonly used RAM consists of polyurethane foam, which is loaded with a material such as carbon. The electric field is attenuated by dielectric losses in the loaded foam, and the reflected wave at the air-absorber interface is also low. The absorber is usually designed to be backed by a metal plate or foil, and the reflectivity of the absorber is compared to a perfect metal conductor. The reflectivity is quoted in decibels, and values between -20 and -45 dB can be expected at the specified frequencies. We should note that the negative sign here indicates that the reflected wave is 20 to 45 dB lower than the incident wave. The reflectivity in decibels, R_{dB} , is related to the percentage of reflected power, R_p , by the following formula:

$$R_p = [10^{(R_{\text{dB}}/10)}] \times 100 \quad (9.31)$$

Thus, a -45 -dB reflectivity means that only 0.0032% of the power is reflected.

These reflectivities are only obtainable at low angles of incidence, and incidence angles greater than about 45 degrees should be avoided. The absorber may also change the polarization of the incident electric field, but this is a second order effect and will not be discussed here. The reflectivity of the absorber may also be a function of the incident wave polarization, depending on the composition of the absorbing material.

Some other types of absorbers are available, including ferrite and Jaumann type of absorbers. Lossy resins are also available for molding into custom-built shapes or for spraying onto metal surfaces, but these types will not be discussed here.

9.5.2.1.1 Carbon-Loaded Foam RAM

This type of RAM is available in flat sheet form and in pyramid, convoluted (egg-box), or conical shapes. They are based on loading the foam with conductive particles such as carbon to absorb the electric field. The flat sheet RAM is made up of layers of different conductivities, so that the resistance of successive layers changes in discrete steps. The pyramid RAM, on the other hand, consists of continuous variations of the conductivity, so there is a gradual change in the resistivity of the material.

9.5.2.1.2 Flat Sheet RAM

This absorber tends to have a broader frequency range than the shaped variety, but its reflectivity is not as good. It consists of a number of layers of polyurethane carbon-loaded foam, as shown in Figure 9.26(a), of varying resistivities that are bonded together. The absorber is not reversible, in other words, it can only be used facing one way. It has a front surface (which is often a lighter color) for the incident radiation, and a back surface which should be backed by, or preferably bonded to, a metal surface for optimum performance. The lower the operating frequency of the absorber, the greater its thickness is; at 600 MHz, the thickness of the absorber is about 10 cm, but at 20 GHz the thickness is only about 0.5 cm. Absorbers can be used successfully at frequencies higher than those specified; the limit is only applicable to the low-frequency end of the operating range. Reflectivities of the order of -25 dB are the best that can be expected with much poorer performance (-10 dB) at the lower end of the operating frequency range. The front layer of the absorber, which receives the incident wave from free space, has less resistive loading than the other layers, and thus has the highest impedance. Ideally, the impedance of this layer should be equal to the characteristic impedance of the wave that is incident on it, that is, in the case of a plane wave, it should have a real impedance or resistance of 377Ω . The impedance of successive layers is gradually decreased, with the last layer having a very low impedance, approaching that of a good metal conductor. The resistance is thus decreased in discrete steps; the number of these steps is equal to the number of layers.

Carbon-loaded fiber matting is also available, which has similar performance to the foam-loaded type, but it cannot be used at low frequencies; its low-frequency limit being higher than that of the foam type, at around 1 GHz.

The other types of sheet absorbers are thin flexible sheets of lossy foams, which used for special purposes and not as absorbers per se, and will therefore not be discussed here.

9.5.2.1.3 Pyramid, Conical, and Convoluted (Egg-Box) Absorbers

In the case of these absorbers, the variation in impedance is implemented by geometrically shaping the carbon-loaded foam. This type of absorber has the best performance with reflectivities of up to -50 dB, when the thickness of the absorber is at least twice the wavelength of the incident radiation. This represents a reflection of only about 0.001% of the incident power. The pyramid absorber, shown in Figure

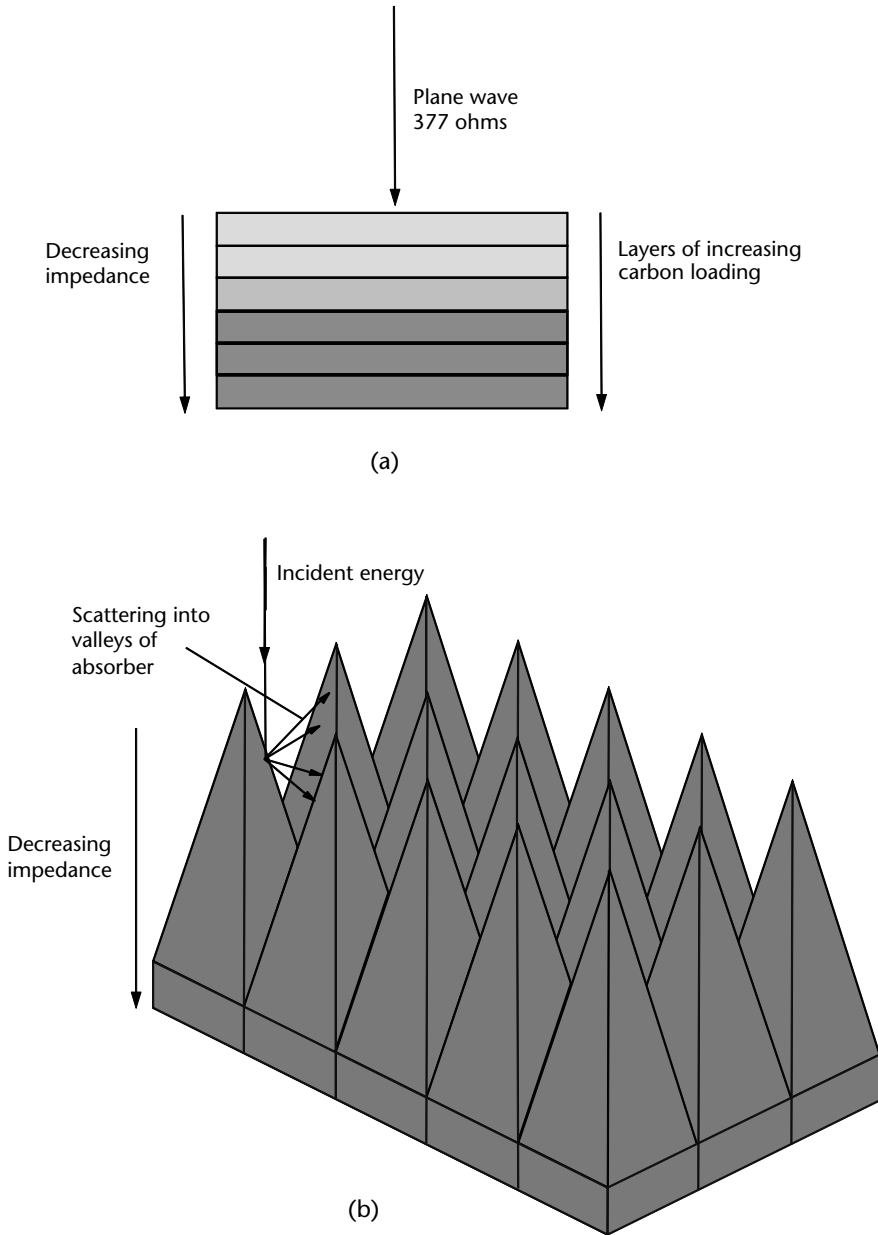


Figure 9.26 Carbon-loaded RAM: (a) Flat sheet RAM, and (b) pyramid RAM.

9.26(b), comprises four triangular, inclined sides on a square base. The height of the pyramid (including the base) varies from around 10 cm to 4.6m for frequencies down to 30 MHz [19, p. 26]. At 100 MHz, for instance, the length of the pyramid absorber is around 1.8m. Several pyramids are joined together to form square or rectangular modular units. The pyramid taper provides a continuous impedance taper (to the incident wave) which varies from a high impedance at the tip of the taper to a very low impedance at the back, where it is usually in contact with a good metal conductor. The incident wave is attenuated increasingly as it travels through

the material. The absorber also scatters or diffuses the incident energy in different directions (at the air-absorber interface) so that it is absorbed into the other surfaces of the absorber within the valleys of the material, as shown in Figure 9.26(b). Note that in this case, the variation of impedance is gradually varied, whereas in the case of the flat sheet RAM, the impedance variation is implemented in discrete steps. When used as floor material, the valleys between the pyramids can be filled with rigid foam, such as expanded polystyrene, and then covered with a vinyl coating. Alternatively, the RAM may also be covered by rigid glass foam laminate to allow it to be used for the floor [4, p. 356].

9.5.2.1.4 Combined Ferrite and Pyramidal Absorber

Ferrite tile-lined rooms are effective in the lower frequency range and are relatively ineffective at high frequencies, above 600 MHz. Because pyramidal absorbers become very long at low frequencies, chambers can become very large with a relatively poor usage of floor space. As a result, a combination of pyramidal and ferrite absorbers was developed as shown in Figure 9.27. The ferrite is installed first, and then pyramidal absorbers on top. The longer wavelength passes through the pyramidal absorber and is absorbed by the ferrite. As a result, much shorter pyramidal absorbers can be used, resulting in a more efficient use of laboratory floor space.

It is important that the pyramidal absorber and ferrite impedances are matched. The ferrite tile is designed to present an impedance of 377Ω to the incident wave, and is most effective at frequencies between 30 and 600 MHz [22]. This is achieved by keeping the ratio of the permeability and permittivity equal to unity as the characteristic impedance in the equation equates to 377Ω which is the impedance of free space. A pyramidal absorber that operates from about 200 to 1,000 MHz is

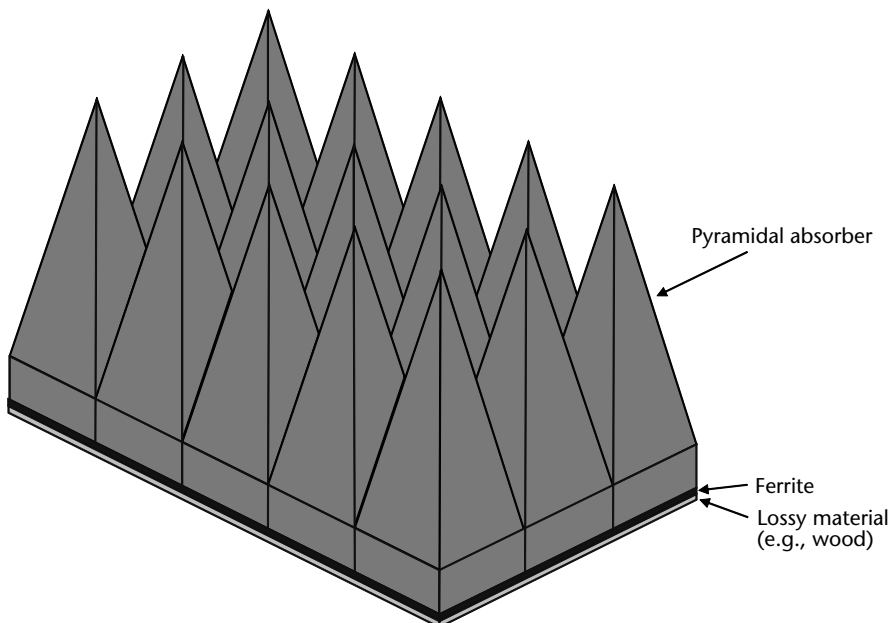


Figure 9.27 Combined pyramid RAM and ferrite with dielectric spacer.

used with the ferrite base. The wave at lower frequencies, below 600 MHz, passes through the absorber and is absorbed by the ferrite tile.

$$Z_0 = 377\sqrt{\frac{\mu}{\epsilon}} \quad (9.32)$$

Where

- Z_0 is the characteristic impedance of free space in ohms;
- μ is the permeability of the material in henries per meter;
- ϵ is permittivity of the material in farads per meter.

If the impedance of the wave passing through the pyramidal absorber is too low, then a mismatch occurs at the ferrite absorber incident surface, compromising performance. The pyramidal absorber for use with ferrite tiles has a lower carbon content (7%), which ensures that at lower frequencies the wave impedance is not affected and allows the wave to reach the ferrite. At frequencies above 600 MHz, the 7%-loaded pyramidal absorber presents a 377- Ω impedance to the incident wave, which is reduced to zero ohms at the base (see Figure 9.28). The pyramidal absorber would normally have a carbon loading of 26% when used without a ferrite backing [23, p. 40]. The absorbers would normally be at least 2 ft (0.61m) in height to be effective at frequencies above 200 MHz [23, p. 40]. The ferrite tile may also require a lossy dielectric layer between the tile and the metal surface of the shielded room to minimize the deterioration in performance that can occur between 600 and 1,000 MHz. Tiles are typically 6 mm thick with 12.7 mm plywood backing as a dielectric [23, p. 42].

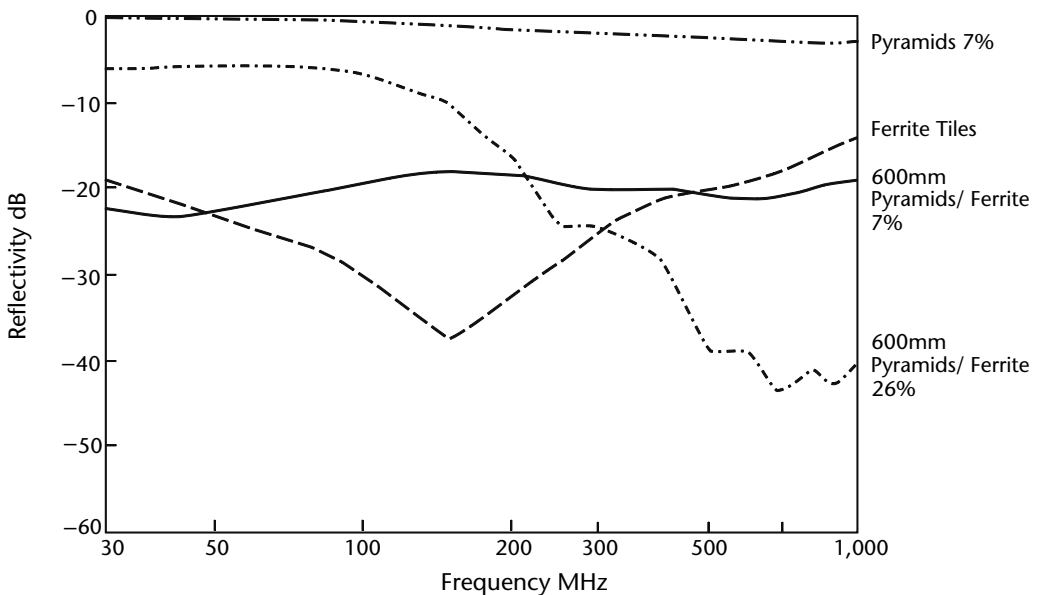


Figure 9.28 Comparison between the attenuation of different absorbers.

The attenuation/reflectivity is measured by propagating a wave from a transmit antenna to be incident at an angle of 45 degrees towards the absorber, and measuring the reflected signal in volts per meter using a receive antenna as shown in Figure 9.29. The level of the reflected signal is compared to the reference level obtained using a flat metal surface at the same distance and angle of incidence, and the difference between the two signals is known as the reflectivity of the absorber in decibels.

Figure 9.28 compares the reflectivity of pyramid RAM (of 7% carbon loading) over the frequency range 30 to 1,000 MHz with ferrite tiles, as well as a combination of pyramid RAM backed by ferrite tiles for waves at normal incidence. It can be seen that the pyramid RAM with 7% carbon loading on its own is poor at low frequencies, and the performance only increases slightly at the higher frequencies as the length of the pyramids become significant with respect to the wavelength. Using a 600-mm-long pyramid RAM (with 7% carbon loading) and backed by ferrite tiles with 26% ferrite loading, the reflectivity is worse than -8 dB, and although it increases to -40 dB around 1,000 MHz, the increase is not monotonic and this wide variation of performance with frequency makes this unsuitable except for very narrow band applications. The plot using solely ferrite tiles shows an average reflectivity of around -20 dB, but from 30 to 150 MHz it increases with a peak at 150 MHz, at which it then deteriorates at the high frequencies. This nonmonotonic variation of performance with frequency makes this unsuitable for broadband applications.

Using pyramid RAM of length 600 mm (with 7% carbon loading) backed by the ferrite tiles results in a more constant, albeit reduced, reflectivity of better than -18 dB over the full frequency range. Hence, this combination of 600 mm pyramid RAM backed by ferrite tiles with 26% ferrite loading is most suitable for chambers operating over the frequency range of 30 to 1,000 MHz.

9.5.3 Anechoic Chambers

When a screened room is lined with RAM, it is known as an anechoic (no echo) chamber. The level of the reflections from the walls, floor, and ceiling of the room

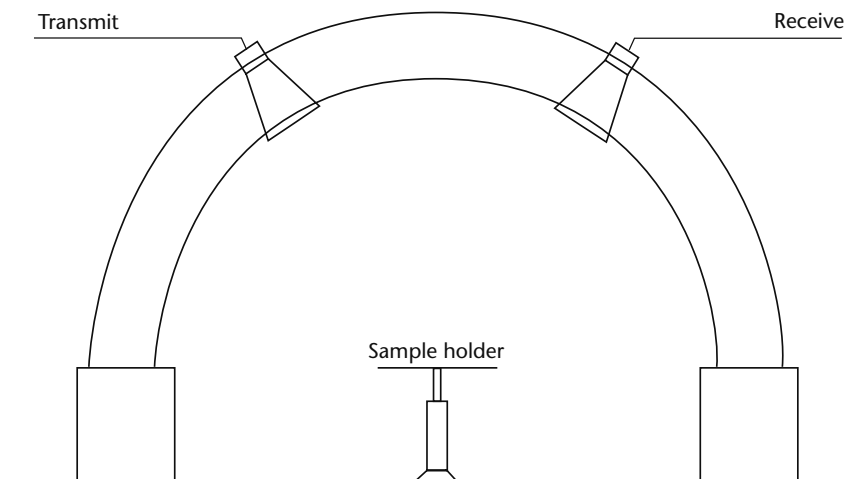


Figure 9.29 Measurement of reflectivity.

are reduced by lining the room with RAM. The level of these secondary or multipath reflections is not uniform throughout the volume of the room, and there is a relatively small volume within the room (called the quiet zone) where the level of these reflections are at a minimum.

9.5.3.1 Quiet Zone

There is more than one definition of the quiet zone. Sometimes it is defined as the volume where rays enter after at least two reflections [24, p. 679], and sometimes as the volume in which the reflections from the internal surfaces of the chamber are at a specified level below that of the direct ray from the transmitting antenna [5, p. 381]. The latter definition is the more common and also the more meaningful definition. This level can be as high as -60 dB for high performance anechoic chambers, but is a function of frequency, the type of absorber and the position within the quiet zone.

9.5.3.1.1 Rectangular Chambers

The early anechoic chambers were of uniform cross section. The width of the chamber is chosen so that the angle of incidence of a ray (from the transmitting antenna) on the side walls is kept to below a certain value. The maximum value of the angle of incidence depends on the RAM used to line the chamber, and values between 45 and 60 degrees are quite common. The chamber should be long enough to ensure that far-field conditions prevail at the lowest frequency of operation. A length-to-width ratio of 3 is recommended to ensure that far-field (i.e., plane wave) conditions prevail. However, if this ratio is reduced to 2 , the side wall reflections are minimized. This is because fewer of the reflections from the side walls reach the quiet zone, and those that do enter the quiet zone are reflections as a result of small angles of incidence where the absorber has a better reflection performance. Chambers are often lined with the same type of absorbers on all the walls, but it is better to line the end wall with higher performance RAM, since the main lobe of the transmitting antenna illuminates one of these walls. Higher-performance RAM is also used for areas along the side walls where the first reflections from the transmitting antenna occur, as shown in Figure 9.30(a).

An anechoic chamber is also known as a fully anechoic room (FAR) or a free space open area test site (FSOATS), and is required for measurements above 1 GHz. A FAR has absorbers on all six room surfaces including, sometimes, below a non-conductive turntable which is raised above the absorber. The difference between a FSOATS and a FAR is that the FAR has all of the surface covered, whereas the FSOATS only has an area of absorber placed between the turntable and the transmit antenna. The absorber must have a maximum height of 30 cm (12 in) and a minimum rated attenuation of 20 dB. The performance requirements for a FAR are based on a technique called site voltage standing wave ratio S (S_{VSWR}) as specified in CISPR 16-1-4 [25]. The S_{VSWR} test measures the standing wave in the chamber by moving a transmit antenna along six points on a straight line in the chamber, as shown in Figure 9.31. A signal generator is connected to the transmit antenna and the received signal is measured at the receive antenna. The signal level as measured at one point is taken as the reference level, and the variation between the results at

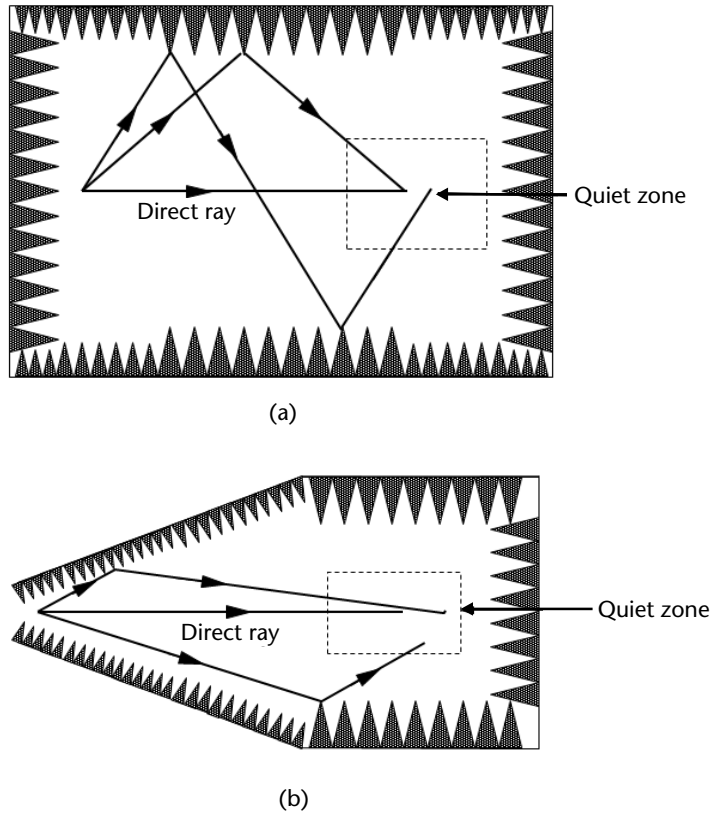


Figure 9.30 (a) Rectangular and (b) Tapered anechoic chambers.

each of the six measurements must be less than 6 dB, which is a VSWR of less than 2:1. The process is carried out for both vertical and horizontal polarizations. The site validation is carried out in a volume in the shape of a cylinder, which encloses the EUT, and is located at a height of 30 cm to account for the absorber located on the floor. The receive antenna, which is typically a broadband horn (or may be a log periodic), is directed at the center of the turntable and is not moved right or left during the measurement process. The free-space loss between the front location, for example F6, is measured first and stored as the reference. The next five locations are 2 cm, 10 cm, 18 cm, 30 cm, and 40m away from the receive antenna. This process is repeated for the front, right, and left positions. If the test volume diameter will be greater than 1.5m, it is also necessary to measure the center position. If the test volume is more than 0.5m between top and bottom positions, it is also necessary to verify the S_{VSWR} at the front position at the top of the test volume. Similar to a VSWR test on a transmission line, the measurement device moving along the line measures the maxima and minima of the standing wave. Each line is treated as a standalone measurement. By setting limits on the S_{VSWR} , the effectiveness of the test site can be verified. Two alternative measurement methods are allowed. At least one of either the transmit or receive devices must have an isotropic or dipole characteristic. In other words, it is not permitted to use a directional antenna at both ends. Typically, a miniature biconical is used for the transit antenna to ensure low antenna directivity. It is normal to use two miniature biconicals to cover the

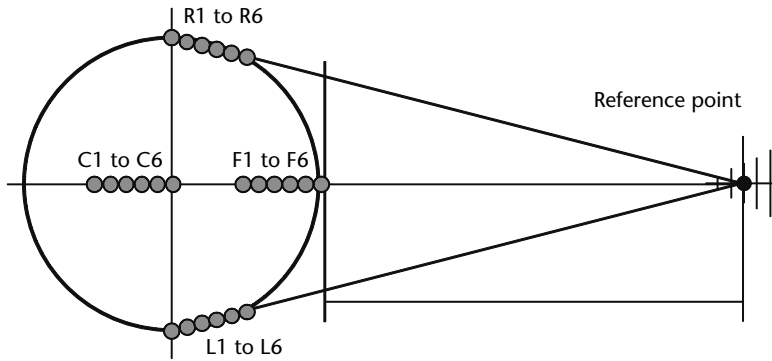


Figure 9.31 Location of antenna positions for S_{VSWR} test.

frequency ranges of 1 to 6 GHz and 6 to 18 GHz. The test is performed in 50-MHz steps from 1 to 18 GHz using a network analyzer or similar equipment. Unlike NSA measurements, there is no absolute free-space attenuation relationship that has to be established. The technique simply verifies the absence of unacceptable resonances in the room. The verification is performed at the front, middle, left, and right extremities of the turntable.

The h_a is the portion of the test volume that is obstructed by absorber placed on the floor (30 cm maximum) as shown in Figure 9.32. The h_1 height is located at the middle of the test volume, or 1.0m above the bottom of the test volume, whichever is lower—shown as h_2 . The h_2 height is located at the top of the test volume and is required to be tested when h_2 is separated by at least 0.5m from h_1 .

The FAR may also be used at frequencies below 1 GHz, as outlined in CISPR 16-1-4 [25]. The qualification test is based on the theoretical free-space attenuation. The equation for this is shown below

$$AS = 20\log_{10} \left[\frac{5Z_0}{2\pi} \times \frac{d}{\sqrt{1 - \frac{1}{(\beta d)^2} + \frac{1}{(\beta d)^4}}} \right] - 20\log_{10}(f_M) + F_{aR} + F_{aT} \quad (9.33)$$

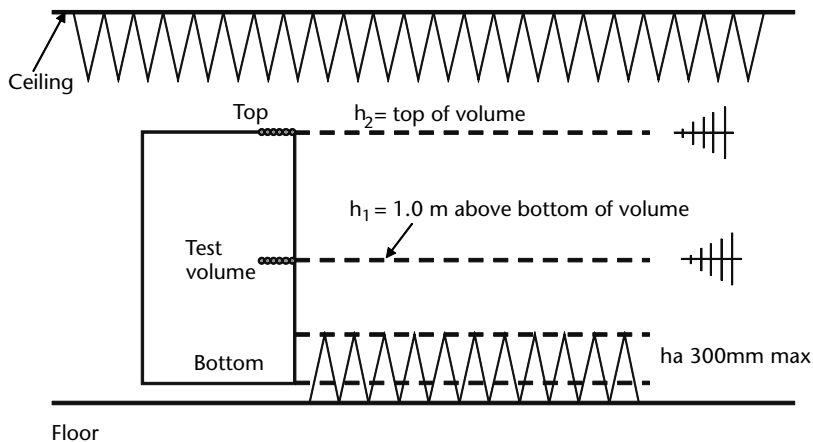


Figure 9.32 Test volume in a FAR.

where

F_{aR} and F_{aT} are the antenna factors of the receive and transmit antennas (dB/m);

D is the distance between the phase centers of both antennas (m);

Z_0 is the reference impedance (i.e., 50Ω);

β is defined as $2\pi/\lambda$;

f_M is the frequency (MHz).

9.5.3.1.2 Tapered Anechoic Chambers

The tapered chamber was first introduced in 1967. It can be used at a lower frequency (less than 1,000 MHz) than a rectangular chamber of the same size. It also has a wider quiet zone than a rectangular chamber of the same width. It consists of a pyramidal or conical tapered section joined to a section of rectangular cross section, as shown in Figure 9.30(b). The tapered section can be considered as a horn which is radiating into a rectangular section. The tapered section is usually about twice as long as the rectangular section. In the tapered region, the angle of incidence with the side walls is nearly 90° (grazing incidence) and thus RAM that has high absorption for large angles of incidence is required for these areas.

9.6 Open Area Test Sites

OATS were developed to measure the radiated emissions from equipment. The EUT is placed on a turntable typically at a height of 0.8m and is rotated in the horizontal plane through 360 degrees to ensure that directional emissions are detected. The receive antenna, which is located at 3m, 5m, or 10m away from the EUT, is scanned in height from 1 to 4m to avoid the null caused by the wave in the direct path being 180 degrees out of phase with the reflected path from the ground plane. This ensures that the level is measured at the point where the maximum in-phase contribution from the reflected path occurs. Measurements are carried out using horizontal and vertical polarizations of the electric field antennas. The emissions from the EUT are highly dependent on cable orientation and its antenna. It is necessary to ensure that the maxima are measured because of the high variability of the test and the effect of the EUT configuration on emissions. This includes scanning the antenna height, rotating the EUT, and adjusting the cables connected to the EUT to ensure that the maximum emissions configuration is measured.

Open area test sites may be completely uncovered, or a site covered by a material of low dielectric constant. The FCC specifies an optional ground plane, whereas CISPR specifies a minimum size for a ground plane. A ground plane is considered a necessity, especially for vertical polarization. Materials commonly used for ground planes are solid metal sheets, metal foil, perforated metal, expanded metal, wire cloth, wire screen, and metal grating (CISPR 16-1-4) [25].

The mesh is not as good as a solid ground plane, but it provides better drainage. The ground plane should lie on the surface, so that it can be inspected for signs of corrosion and noncontinuity.

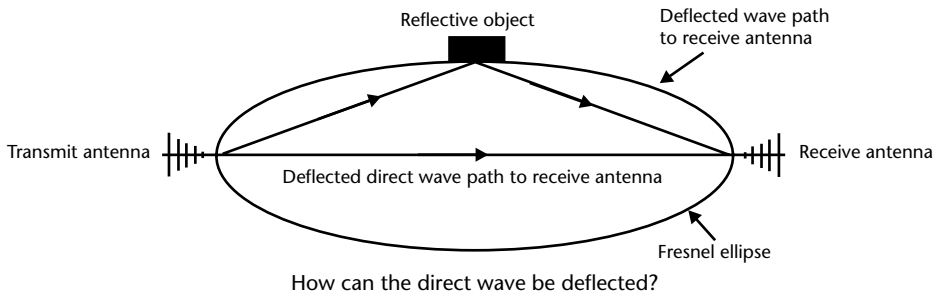


Figure 9.33 Effect of a reflective object.

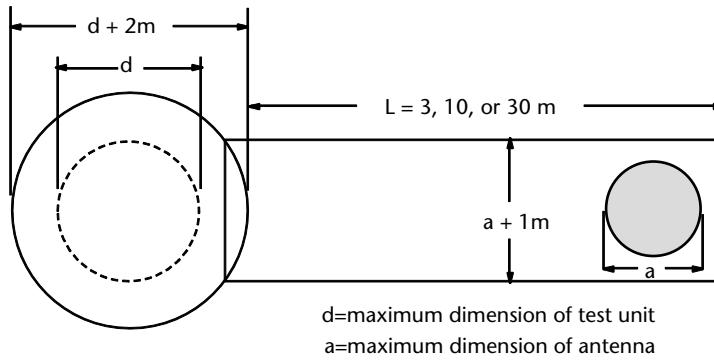
The size of the ground plane recommended by CISPR 16-1-4 is shown in Figure 9.34(a), whereas the Fresnel ellipse shown in Figure 9.35 defines the approximate size of the ground plane recommended by FCC/OST MP-4 [4, p. 357, 371]. FCC/OST MP-4 has been replaced by ANSI 63.7 [26]. The Fresnel ellipse defines a zone in which a reflective surface may cause a reflected signal, which could be out of phase with the direct signal at the receive antenna, thereby causing a null, as shown in Figure 9.33.

Note that the size of the ellipse is a function of the antenna separation D . The effect of the Fresnel ellipse is discussed in ANSI 63.7:2015. The Fresnel ellipse is defined in the following manner: The distance D between the transmit and receive antennas must be chosen such that the path lengths between the reflected ray ($AS + SB$) and the direct ray (AB) is half a wavelength. Since we know that an ellipse is defined as the locus of a point that is a fixed distance from two other points (known as the foci, A and B in this case), all the reflected rays such as ($AS + SB$) and ($AT + TB$) must be equal. If the transmit and receive antennas are each placed $D/2$ away from the nearest edge of the ellipse, then the reflected rays such as ($AS + SB$) will be equal to $2D$. It can be shown that if $AB = SB$ (each will be equal to D), then by drawing a perpendicular from S to AB and using Pythagoras' theorem, this perpendicular is equal to $D\sqrt{3}/2$. Since this is the semi-minor axis of the ellipse, then the minor axis is $D\sqrt{3}$.

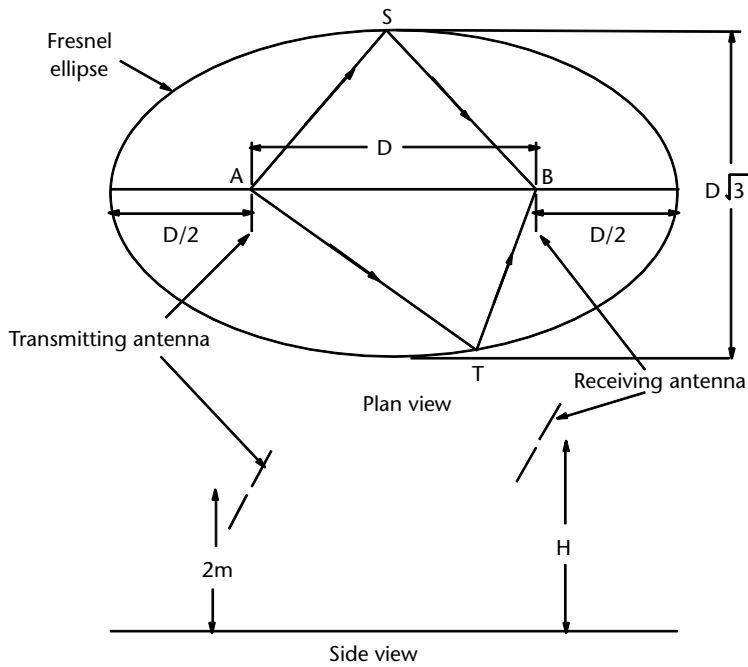
For biconical antennas, the reference or calibration point is the center of the balun. For log periodic antennas, the calibration is marked on the antenna as chosen by the manufacturer, and is normally 50% between the shortest and longest elements.

The size and shape of the obstruction-free areas vary depending on the measurement distance and whether or not the EUT will be rotated. For sites with a turntable, the recommended obstruction-free area is an ellipse, which encompasses the receiving antenna and EUT, and has a length of twice the measurement distance and a width equal to the product of the measurement distance and the square root of three. These dimensions are designed to ensure that the path of the undesired reflection from any reflective object on the perimeter is twice the length of the direct ray path. For a 3-m site, the first Fresnel ellipse is larger than the obstruction free-area ellipse. The ANSI standard recommends that if the site fails to meet the normalized site attenuation criteria, the area that is outside of the obstruction-free ellipse but enclosed within the first Fresnel ellipse should be investigated for reflective objects.

The first Fresnel ellipse is normally when the difference between the direct and reflected ray differs by a path length of $D + \lambda/2$; this gives D between the foci and



(a)



(b)

Figure 9.34 OATS: (a) Minimum size of ground plane per CISPR 22, and (b) FCC set-up for site attenuation.

major axis of $2D$ and minor axis of $D\sqrt{3}$. The second Fresnel ellipse is when the difference is $D + 3\lambda/2$.

The ANSI Standard C63.7:2015 acknowledges that the original rationale for using twice the direct ray path length was to ensure that the scattered electric field would be at least 6 dB, that is, half-power down from the direct signal between the EUT and receiving antenna, and hence would have minimal impact on the direct path measurement. However, it has been found that that a spurious reflected signal 6 dB down from the direct path signal can cause 2 to 3 dB errors in the measurements. As such, it is necessary to investigate the reflective obstructions to ensure that adequate

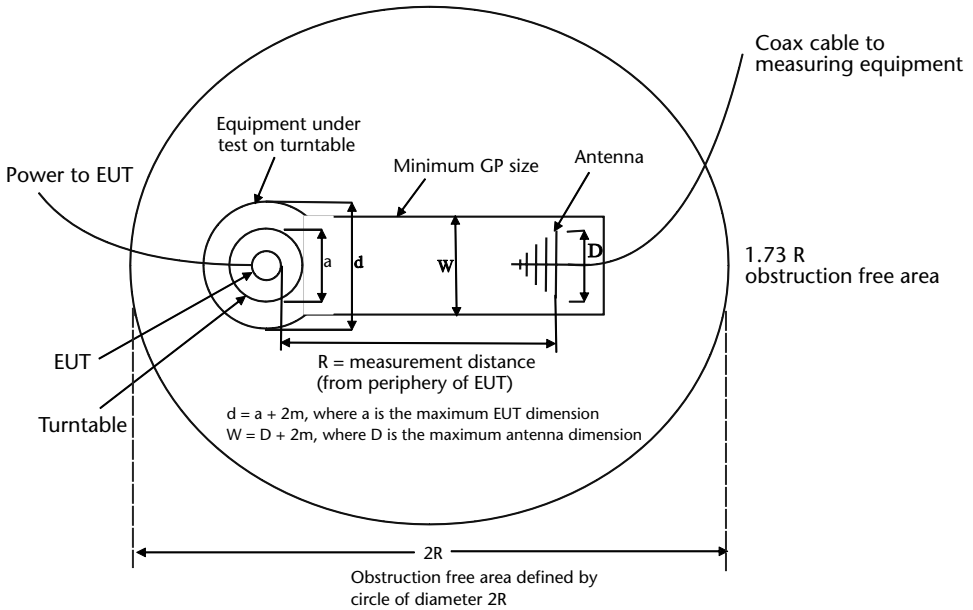


Figure 9.35 ANSI OATS as used by the FCC. R equals the measurement distance from the calibration point on the antenna (from the periphery of the EUT).

performance is achieved. A further area of concern is the magnitude of a ground plane edge reflection which is affected by the electrical termination to the surrounding ground material. In addition, the reflection-free area recommended for 3-m sites is smaller than the Fresnel ellipse. As such, the obstruction-free area is a minimum requirement, and for optimum site performance, a larger obstruction-free area and ground plane is advisable. Table 9.4 shows the recommended dimensions in ANSI 63.

The ellipse should be free of all obstructions, such as trees and bushes, and not have any above or below ground EM reflecting objects. It should be in an area of low RF ambients, and the terrain should be level to within about 4.5 cm [25]. Bonding between the panels of the ground plane is of paramount importance, and spacing intervals equal to 1/10th of the wavelength at the highest operating frequency are recommended. For a site that has an upper-frequency limit of 1,000 MHz, the wavelength is 30 cm, and thus the bonding interval should be 3 cm. However, bonding intervals of 12 cm (which represents 0.4 of the wavelength at 1,000 MHz) have been used successfully [27].

The site itself produces attenuation, and this attenuation factor must be measured. This factor is dependent on the transmit and receive antenna gains, their heights, the frequency of operation, and the ground reflected waves. There is also some reflection of other metal objects, but this is more difficult to quantify. The attenuation is measured using dipoles or broadband antennas [25] at 1, 5, and 10

Table 9.4 ANSI 63.4 Recommendations for OATS dimensions.

$R = 3m$	$R = 10m$	$R = 30m$
$6m \times 5.2m$	$20m \times 17.3m$	$60m \times 52m$

Table 9.5 OATS NSA Measurement [25]

<i>Method</i>	<i>Polarization</i>	<i>Transmit Antenna Height</i>
Tuned half-wave dipoles	Horizontal	2m
Tuned half-wave dipoles	Vertical	2.75m
Broadband	Horizontal and vertical	1m

MHz intervals in the frequency ranges of 30 to 100 MHz, 100 to 500 MHz, and 500 to 1,000 MHz, respectively.

The transmitting antenna is positioned at fixed heights, as shown in Table 9.5, whereas the receiving antenna height is adjusted for maximum reception. This height should be varied between 1 and 4m for antenna separations of 3 and 10m. The antennas are calibrated and the antenna factors are known. The reading S_1 in decibels of the receiver should be recorded at each frequency, and the NSA calculated based on either the antenna calibration data or the calculated free-space antenna factors for dipoles. The NSA data provided in the standard makes allowance for the losses in the path length between the EUT and the receive antenna (which is a function of frequency, as well as the physical distance). Allowance is also made for the factors due to the gains of the antennas and the constructive interference due to reflection from the ground plane.

If tuned half-wave dipoles are used, their free-space antenna factors can be calculated using this equation:

$$AF = 20\log_{10}\left(\frac{2\pi}{\lambda}\right) + 10\log_{10}\left(\frac{73}{50}\right) \quad (\text{dB}) \quad (9.34)$$

If the OATS has an all-weather cover, or if the test is being carried out in a semi-anechoic chamber, then a volumetric NSA must be measured using broadband antennas at five positions on the turntable: front, back, left, right, and middle. The NSA is carried out without an EUT present. In addition, two transmit antenna heights are required, for two polarizations (horizontal and vertical), and for two heights (1 and 2m horizontal, 1 and 1.5m vertical).

9.6.1 Free-Space OATS

A free-space open area test site (FSOATS) is an OATS with absorber placed on the ground plane between the EUT and the antenna. CISPR 32/EN 55032 [28] only allows its use at frequencies above 1 GHz. The qualification of a FSOATS is the same as a fully anechoic room. For FCC, ANSI 63.4 [29] allows a similar practice for frequencies above 1 GHz, providing the absorber is less than 30 cm high as the test volume may be obstructed [25, p. 45].

9.6.1.1 Theoretical Site Attenuation Factors

The site attenuation (A_S in decibels) may be calculated theoretically by taking into account the path losses, the gains of the antennas, and the reflection from the ground plane [25]. The theoretical site attenuation is given by:

$$A_s = 20 \log_{10} \left[\frac{5Z_0}{2\pi} \times \frac{d}{\sqrt{1 - \frac{1}{(\beta d)^2} + \frac{1}{(\beta d)^4}}} \right] - 20 \log_{10}(f_M) + F_{aR} + F_{aT} \quad (9.35)$$

where

F_{aR} and F_{aT} are the antenna factors of the receive and transmit antennas (dB/m);

D is the distance between the phase centers of both antennas (m);

Z_0 is the reference impedance (i.e., 50Ω);

β is defined as $2\pi/\lambda$;

f_M is the frequency (MHz).

This theoretical site attenuation does not take into account antenna near-field correction factors. These are significant at distances of 5m (frequencies less than 60 MHz) and 3m (frequencies less than 110 MHz). CISPR 16-1-4 recommends that numerical modeling code such as NEC is used to calculate the site attenuation based on the antennas used, test distance, and test volume. In practice, site attenuation measurements are carried out using antennas calibrated on a reference site at a calibration laboratory. For best results, a pair of antennas (transmit and receive) should be used.

For a half-wave dipole, the magnitudes of G_t and G_r are each equal to 2.15 dBi. Note that the negative signs indicate that the site attenuation factor is reduced because of these gains. The magnitudes of A_s are plotted in Figure 9.36 for values of D equal to 3, 5, 10, and 30m [25].

9.7 Reverberation Chamber

Chambers are unlined shielded rooms that use a mode stirrer to enable either emissions or immunity tests to be carried out. As the room is unlined, multimodes occur within the room volume. The number of modes is dependent on the dimensions of the room and the wavelength. Therefore, as the frequency is swept, the number of modes changes and the field uniformity varies. To ensure that the EUT is adequately characterized, mode stirrers in the form of rotation paddles or vanes are used to ensure that at each frequency there is adequate illumination of, in the case of immunity, the EUT, or in the case of emissions, the receive antenna. The mode stirring is carried out in all three planes and two or three stirrers are mounted on the walls of the chamber. These chambers are normally used at frequencies above 100 MHz, as the dimensions of the mode stirrers at lower frequencies become very large. Good reverberant properties at a specified frequency of operation require a minimum chamber size. Room-sized reverberation chambers (e.g., volumes between 75 m^3 and 100 m^3) are typically operated from 200 MHz to 18 GHz [30]. In this case, the longest room dimension is 6m, which is one quarter of a wavelength at 200 MHz.

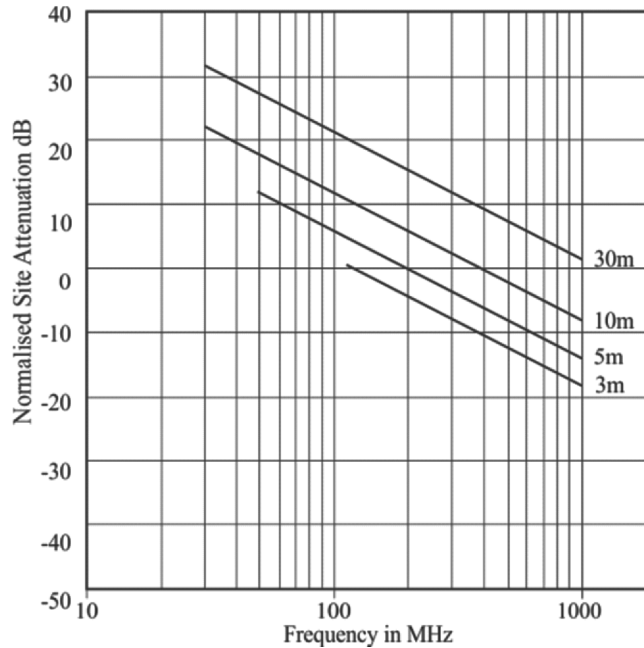


Figure 9.36 Theoretical site attenuation for distances of 3, 5, 10, and 30m.

The stirrers should have one dimension that is at least one-quarter wavelength at the lowest frequency, and a separate stirrer can be used for horizontal and vertical polarizations. EN 61000-4-21 recommends that the stirrers should be as large as possible and should extend to three quarters of the room smallest dimension. The location of the stirrers is not critical. The use of a turntable is optional. Figures 9.37–9.39 show different designs of stirrers.

Two methods of rotating the stirrer are used: mode stirred is where the stirrer is rotated continuously, and mode tuned is when the stirrer is stepped in discrete steps. Mode stirring allows faster measurements and has the advantage that the stirrer is moving continuously and prevents transient effects that can occur when the stirrer is stepped, however, it can pose problems in ensuring that a sufficient dwell time occurs at each frequency. Mode tuning has the advantage that the stirrer can be held at each position to ensure that defined dwell time is achieved, however, transient effects caused by the stirrer stopping and starting are a disadvantage [31, p. 106].

For calibration, EN 61000-4-21 [30] and RTCA DO 160G [32] only allow mode tuning to be used, with a minimum of 12 stirrer steps required. Mode stirring can be used during the EUT test.

The advantages of the reverberation chamber include the lower cost of the chamber as it is unlined, and the ability to test all angles of incidence for complex scenarios.

The chamber should be free of absorbing materials such as wood. Polystyrene foam is a suitable material for the support table. The reverberation chamber depends on reflective surfaces and there are no absorber materials used in the chamber.

The suitability of a reverberation chamber is determined by performing a coupling attenuation between a fixed transmit antenna and receive antenna. The antennas used are typically log periodic and horn antennas to determine the maxima

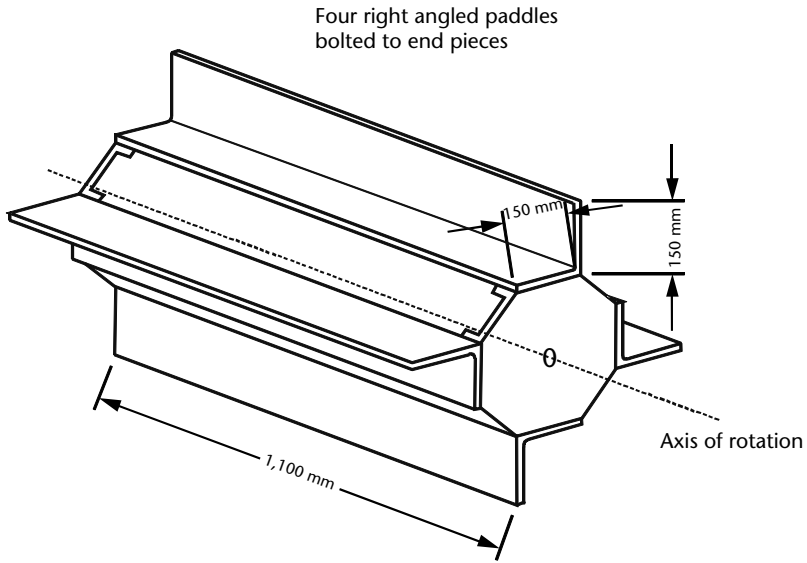
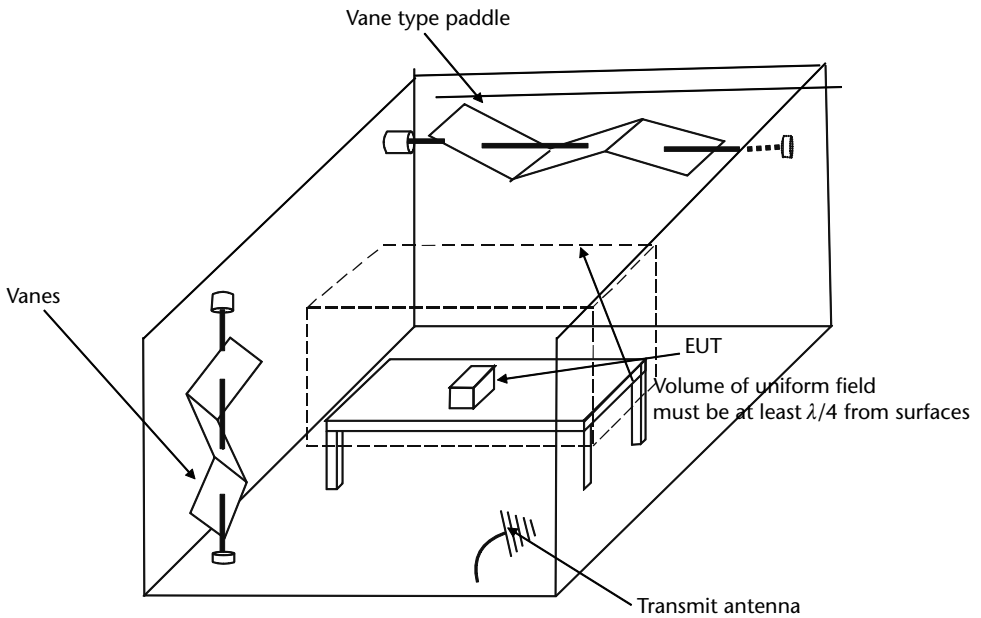


Figure 9.37 Example of a typical paddle stirrer. It is good for frequencies down to 68 MHz.

and minima. Peak hold is typically used, and the stirrer/paddles are rotated at least five times in each integrating period. The transmit antenna is then set to the other polarization and the process repeated. Compliance with these criteria ensures that the chamber adequately illuminates the EUT in a uniform manner. Figure 9.40 shows the compliance criteria called up in CISPR 16-1.



Top and front surface removed for clarity

Figure 9.38 Layout of reverberation chamber.

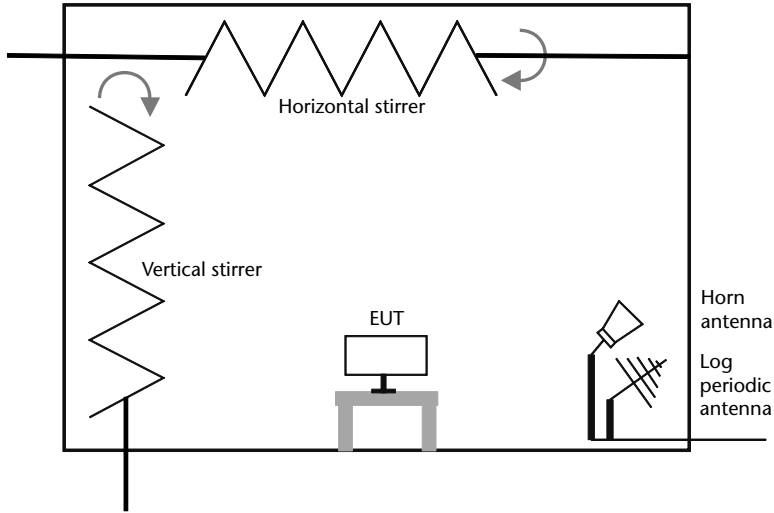


Figure 9.39 Side elevation view of reverberation chamber.

9.7.1 Reverberation Chamber Requirements of EN 61000-4-21

IEC/EN 61000-4-21, which uses the same method as RTCA DO-160G [32, Section 20.6, p. 20–16], has a more detailed description of the design and calibration of reverberation chambers. The standard assumes that the chambers will be used above at least 100 MHz. The purpose of the validation is to ensure that all points in the working volume meet the field uniformity criteria. The field uniformity must be verified at eight locations for EN 61000-4-21, at the eight corners of the test volume. RTCA DO-60G additionally requires that the ninth center point of the EUT volume is verified.

The field is measured at all of the validation points using a three-axis probe. The field uniformity is considered uniform if the standard deviation is less than

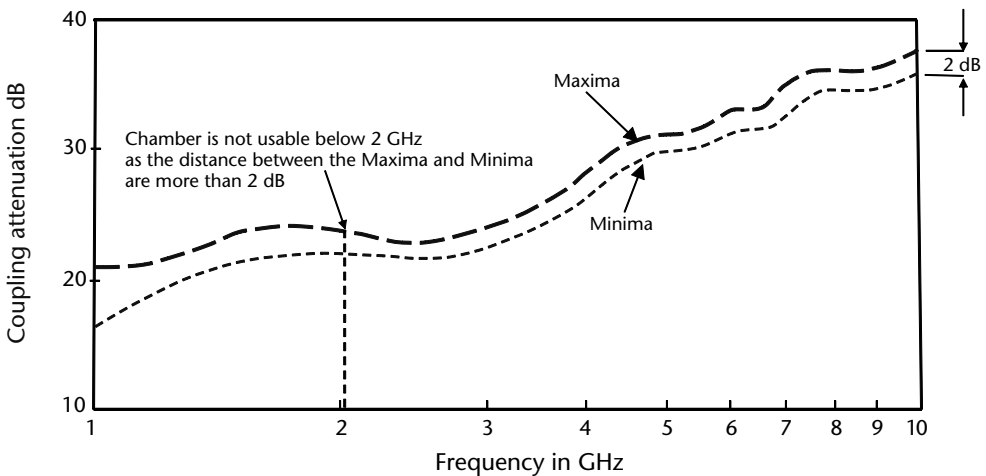


Figure 9.40 CISPR 16-1-4 [25] defines the performance and allows for a 2-dB range of coupling attenuation.

3 dB at frequencies above 400 MHz. Between 100 and 400 MHz, the standard deviation slopes linearly on a semi-log plot from 3 to 6 dB, as shown in Figure 9.41.

A receive antenna is located at various locations inside the working volume during the validation procedure, as the power received on this antenna will be needed later to verify the chamber performance before testing an EUT. The use of reverberation chambers does not rely on antenna factors. The procedure assumes that the power delivered to the transmit antenna is radiated into the chamber with a certain antenna efficiency, which is typically 0.75 for a log periodic and 0.9 for a horn antenna [30, p. 47].

9.7.2 Validation Procedure

The procedure uses a transmit antenna, a receive antenna, and field probe. The receive antenna is for monitoring and does not form part of the validation process.

The field uniformity is verified in an empty chamber. For field uniformity, a field probe is used. It is only necessary to verify the uniformity up to one decade above the lowest frequency of use. The field uniformity is verified at 8 points, the eight corners of the volume of the uniform field. This process is carried out using the mode tuned mode, which means that discrete rotational stirrer steps are used. The number of steps depends on the result of the test; more steps may be used to obtain field uniformity and a minimum of twelve must be used. The transmit antenna must be linearly polarized, usually a log periodic or horn. The same antenna should be used for the EUT testing.

The field probe is located at one of the eight validation points, and the input power adjusted to produce the desired validation level on the field probe. The stirrer is then rotated in discrete steps and the three field components from the field are

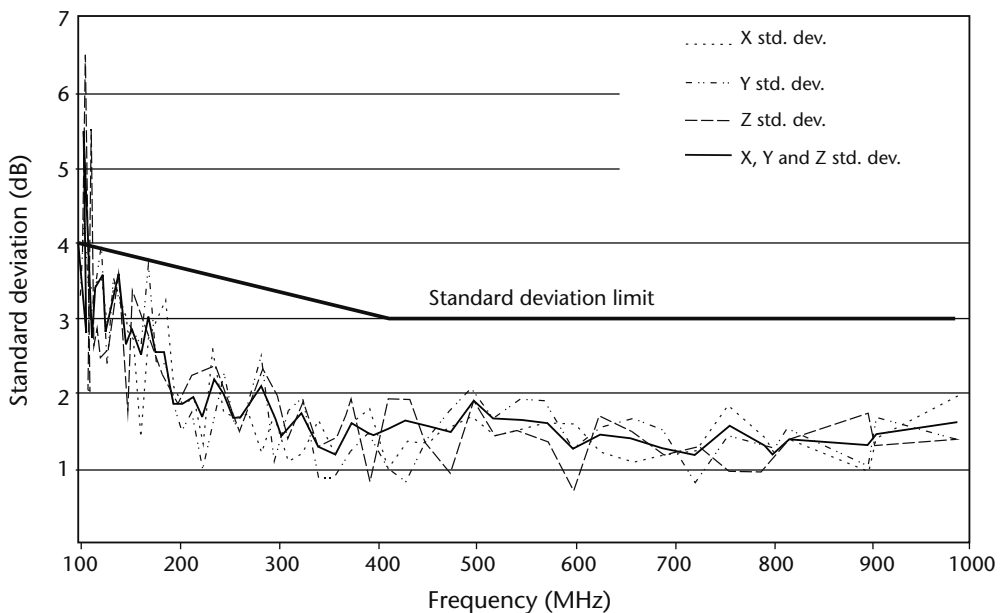


Figure 9.41 Standard deviation of E field in empty chamber.

recorded at each step. Three criteria are recorded for the stirrer's 360 degree rotation, the maximum field in each of the x -, y -, and z -axes, the vectorial field (root sum square of the three axes), and the average input power over the antenna rotation. This process is repeated for all frequency steps up to ten times the start frequency.

From the 24 measurements at the 8 points and three axes, the values for individual axes are normalized as follows.

For the x -axis:

$$\vec{E}_{x\text{norm}} = \frac{E_{x\text{max}}}{\sqrt{P_{\text{input}}}} \quad (9.36)$$

$E_{x\text{norm}}$ = normalized maximum measurement from each probe axis;

$E_{x\text{max}}$ = maximum measurement from the x -axis over the nine measurement points;

P_{input} = average input power to the chamber during the tuner rotation.

This is repeated for the y - and z -axes.

For the 8 normalized E-field maximums in each axis, the average is calculated as follows.

For the x -axis:

$$\langle \vec{E}_x \rangle_8 = \frac{(\sum \vec{E}_x)}{8} \quad (9.37)$$

where

$\langle \vec{E}_x \rangle_8$ = average of the normalized maximum measurements from each probe axis

\vec{E}_x = result from 10.36

Note: $\langle \quad \rangle$ denotes arithmetic mean

This is repeated for the y - and z -axes.

For the 24 normalized E-field maximums, the average is calculated as

$$\begin{aligned} \langle \vec{E}_x \rangle &= \vec{E}_{x\text{norm}} \text{ from equation above} \\ \langle \vec{E}_x \rangle_{24} &= \frac{(\sum \vec{E}_{x,y,z})}{24} \end{aligned} \quad (9.38)$$

For each validation frequency, the standard deviation is calculated for one stirrer rotation:

$$\sigma_x = \sqrt{\frac{\sum (\vec{E}_{ix} - \langle \vec{E}_x \rangle_8)^2}{8 - 1}} \quad (9.39)$$

This is repeated for the y - and z -axes.

For all the vectors at each frequency over one tuner rotation, the standard deviation is calculated as

$$\sigma_{24} = \sqrt{\frac{\sum_{m=1}^8 \sum_{n=1}^3 (\vec{E}_{mn} - \langle \vec{E} \rangle_{24})^2}{24 - 1}} \quad (9.40)$$

where E_{mn} equals the individual measurements of all vectors (m = probe locations, and n = isotropic probe axes x , y , and z).

The standard deviation relative to the mean is

$$\sigma \text{ (dB)} = 20 * \log_{10} \left(\frac{\sigma + \langle \vec{E}_{x,y,z} \rangle}{\langle \vec{E}_{x,y,z} \rangle} \right) \quad (9.41)$$

If the standard deviation for the individual components σ_x , σ_y , and σ_z and the 24 total data set do not exceed the levels shown in Figure 9.41, the chamber is compliant.

Figure 9.41 shows the example shown in EN 61000-4-21. As can be seen, the standard deviation exceeds the limit at frequencies below 120 MHz. This sets the lowest usable frequency. The system performance can be improved by increasing the number of stirrer steps, or improving the accuracy of the input power by taking account of reflected power from the transmit antenna. It is also possible to reduce the size of the working volume.

A chamber requires a minimum of one stirrer. Improved field uniformity can be achieved by using additional stirrers. If a chamber has a very high Q , then it may be difficult to achieve the field uniformity and it is recommended to reduce the Q by adding absorber. The standard also states that chambers with no more than 6 to 100 modes at the lowest frequency are unlikely to meet the field uniformity required.

9.7.3 Testing an EUT

Before testing an EUT, it is necessary to verify that the EUT is not adversely loading the chamber. This is performed by injecting a transmit signal into the chamber via the transmit antenna and recording the received power from a receive antenna which is located inside the working volume but at least one quarter of a wavelength away from the EUT. One stirrer rotation is completed at each frequency. The mean received power must be similar to the mean receive level measured during the eight measurements to form the validation. During validation, the receive antenna is moved to different positions within the test volume.

The chamber loading factor (CLF) is calculated using the chamber validation factor (CVF)

$$CVF = \left(\frac{\text{Average received power from receive antenna}}{\text{Average input power to transmit antenna}_t} \right) \quad (9.42)$$

The antenna validation factor (AVF) is calculated by

$$AVF = \left(\frac{\text{Average received power}}{\text{Average received power measured during chamber calibration}} \right) \quad (9.43)$$

The chamber loading factor is

$$CLF = \left(\frac{CVF}{AVF} \right) \quad (9.44)$$

This process is necessary to ensure that the EUT is not loading the chamber to the point where the EUT will not be measured properly. The CLF should be less than the measurement uncertainty allows.

Further calculations are required to determine the chamber time constant. This is to ensure that an adequate dwell time is achieved at each frequency during immunity testing.

$$Q \text{ (dB)} = \left(\frac{16 * \pi^2 * V}{\eta_{Tx} * \eta_{Rx} * \lambda^3} \right) * (CVF) \quad (9.45)$$

where

η_{Tx} and η_{Rx} equal the antenna efficiency factors, typically 0.75 for a log periodic and 0.9 for a horn antenna;

V is the chamber volume (m^3);

λ is the free-space wavelength (m).

The quality factor is used to calculate the chamber time constant

$$\tau = \frac{Q}{2 * \pi * f} \quad (9.46)$$

where

τ is the time constant (s);

f is the frequency (all frequencies above 400 MHz must be calculated).

If τ is more than 40% of the pulse width at 10% of the frequencies, then the pulse width must be increased or loading must be added to the chamber to reduce the Q factor.

9.7.4 Immunity Testing

For immunity testing, the transmit antenna should be located in the same position as the validation was performed. The desired electric field test level is used to calculate the required input power to the transmit antenna at each frequency. The input power is based on the average of the 24 measurements taken during validation.

$$P_{\text{input}} = \left[\frac{E_{\text{test}}}{\langle \vec{E} \rangle_{24 \text{ or } 8} * \sqrt{CLF(f)}} \right]^2 \quad (9.47)$$

where

E_{test} is the radiated immunity test level (V/m);

$\langle \vec{E} \rangle_{24 \text{ or } 8}$ is the average normalized E field of the measurements taken during validation; and,

$CLF(f)$ is the chamber loading factor at each frequency.

The dwell time at each frequency must take into consideration EUT response time, modulation frequency, and the time for the stirrer to move to a new position. The time shall always be greater than 0.5 seconds at each of the minimum of twelve stirrer positions.

The immunity test method is different from the test carried out in an anechoic chamber which simulates plane wave conditions. As a result, the reverberation chamber test is based on a power level metric with the maximum or average power level being the critical factor. For this reason, it is necessary to record the maximum and average power level with the receive antenna, with a requirement that the levels shall be within 3 dB of the levels measured during chamber validation.

9.8 Radiated Emissions

Emissions measurements using reverberation chambers raise issues. The apparent amplitude variation of the emitted signal can cause issues for traditional EMC detectors. For example, the quasi-peak detector has a long time constant and the effect of stirrer rotation could give false readings. When considering such detectors, it is advisable to observe the emission for a number of time constants at each stirrer position. The quasi-peak detector has a discharge time constant of 550 ms for frequencies between 300 and 1,000 MHz. In addition, the chamber quality factor (Q) can distort short duration pulses of less than 10 μ s. For peak measurements, the minimum measurement time at each frequency is given by CISPR 16-2-3:2016 [33]. The minimum sweep time is T_{smin}

$$T_{\text{smin}} = T_{\text{min}} * \frac{\text{Frequency Span}}{0.5 * B_{\text{res}}} \quad (9.48)$$

where

B_{res} is the resolution bandwidth of the measuring receiver;

T_{min} is the minimum measurement (dwell) time at each frequency.

The minimum dwell time at each frequency is dependent on features of the product, such as pulses caused by intermittent signals and time for the stirrer to stop moving. Each step has to be at least one-half of the resolution bandwidth to ensure that all emissions are encompassed by the frequency scan.

The equipment should be arranged in the validated test volume. It is not necessary to manipulate the interface cables, as would be required on an open area test site. The transmit antenna should be kept in the chamber as it was used during validation. The receive antenna should not be directed at the EUT or the transmit antenna, and is preferably directed into a corner. It is necessary to perform the loading test as described in the radiated immunity section.

The radiated emissions can be measured using mode stirring or mode tuning modes. However, the standard recommends that mode stirring, where the stirrer is rotating continuously, is used only for peak measurements and not when using other detectors that using averaging.

The radiated emissions measurement is based on the received power which can be converted to field strength.

The conducted power is measured from the receive antenna and corrected for antenna and chamber losses to obtain the radiated power level that the EUT is emitting.

Therefore, the radiated power is

$$\text{Radiated Power} = \frac{\text{Received Antenna Power} * \text{Antenna efficiency}}{\text{Chamber Validation Factor}} \quad (9.49)$$

9.8.1 Free-Space Field

The far-field electric field can be calculated using the common relationship for power transmitted from an antenna:

$$E \left(\frac{\text{V}}{\text{m}} \right) = \sqrt{\frac{D * P_{\text{radiated}} * 377}{4 * \pi * r^2}} \quad (9.50)$$

where

P_{radiated} is the radiated power from (9.49);

r is the distance in far-field conditions;

D is the directivity of the EUT. This is assumed to be 1.7 to represent a dipole of length of between one-half and one full wavelength.

It should be noted that the level calculated is not always the same as that measured on an open area test site. The level measured in a reverberation chamber is

the total power emanating from the EUT simultaneously in all directions, whereas the OATS measures in specific directions only.

References

- [1] Fewkes, J. H., and J. Yarwood, *Electricity, Magnetism, and Atomic Physics*, Vol. I, University Tutorial Press, 1962, p. 669.
- [2] Connor, F. R., *Introductory Topics in Electronics and Telecommunication: Wave Transmission*, Edward Arnold.
- [3] Moreno, T., *Microwave Transmission Design Data*, Dover Publications, 1948.
- [4] Kaiser, B., *Principles of EMC, Third Edition*, Norwood MA: Artech House, 1987.
- [5] Bailey, A. E., *Microwave Measurements*, Peter Peregrinus, 1985.
- [6] MIL-STD 462 1967.
- [7] MIL-STD 461G, *Department of Defense Interface Standard Requirements for the Control of Electromagnetic Interference Characteristics of Subsystems and Equipment*.
- [8] United Nations Economic Commission for Europe (UNECE) Regulation 10 Rev 5.
- [9] ASTM (American Society for Testing and Materials).
- [10] ASTM D 4935-99 *Standard Test Method for Measuring the Electromagnetic Shielding Effectiveness of Planar Materials*, pp. 1–3.
- [11] IEC 61000-4-20:2010 *Testing and Measurement Techniques—Emission and Immunity Testing in Transverse Electromagnetic (TEM) Waveguides*.
- [12] Crawford, M. L., “Generation of Standard EM Fields Using TEM Transmission Cells,” *IEEE Transactions on Electromagnetic Compatibility*, Vol. EMC-16, No. 4, November 1974.
- [13] IEC-61000-4-3:2010, *Radiated, Radio-Frequency, Electromagnetic Field Immunity Test*.
- [14] Gruner, L., “Estimating Rectangular Coaxial Cut-Off,” *Microwave Journal*, Vol. 22, April 1979, pp. 88–92.
- [15] Weil, C. M, W. T. Jones, and J. B. Kinn, “Frequency Range of Large-Scale TEM Mode Rectangular Striplines,” *Microwave Journal*, Vol. 24, November 1981, pp. 93–100.
- [16] Wiess, D., “A User’s Insight into Radiated Emission Testing with GTEM Cells,” *IEEE International Symposium on EMC*, 1991, pp. 137–162.
- [17] De Leo, R., T. Rozzi, C. Svara, and L. Zappelli “Rigorous Analysis of the GTEM Cell,” *IEEE Transactions on Microwave Theory and Techniques*, Vol. 39, No. 3, March 1991, pp. 488–499.
- [18] Marcuvitz, N., “Waveguide Handbook,” *MIT Rad Lab Series*, Vol. X, McGraw-Hill, 1957, pp. 66–72.
- [19] Belling & Lee Intac, Ltd, “Electromagnetic Shielded Enclosures,” 1986, p. 26.
- [20] Paik, J. K., A. K. Thayamballi, and G. S. Kim, “The Strength Characteristics of Aluminum Honeycomb Sandwich Panels,” *Thin-Walled Structures*, No. 35 (1999), Elsevier Press, pp. 205–231.
- [21] Wilson, P. F., and M. T. Ma, “A Study of Techniques for Measuring the Electromagnetic Shielding Effectiveness of Materials,” *National Bureau of Standards, Technical Note 1095*, May 1986.
- [22] G. Dash, “How RF Anechoic Chambers Work,” Ampyx LLC, 1999.
- [23] Holloway, C. L., R. R. DeLyser, and R. F. German, “Comparison of Electromagnetic Absorber Used in Anechoic and Semi-Anechoic Chambers for Emissions and Immunity Testing of Digital Devices,” *IEEE Transactions on Electromagnetic Compatibility*, Vol. 39, No. 1, February 1997, pp. 33–47.
- [24] Rudge, A. W., *Handbook of Antenna Design, Volume I*, Peter Peregrinus Ltd., p. 670.

- [25] CISPR 16-1-4/EN 55016-1-4:2010, *Specification for Radio Disturbance and Immunity Measuring Apparatus and Methods—Part 1-4*, “Antennas and Test Sites for Radiated Disturbance Measurements.”
- [26] ANSI C63.7-2015 *American National Standard Guide for Construction of Test Sites for Performing Radiated Emission Measurements*.
- [27] Tarico, F., “Experiences in Building an Open Area Test Site,” *IEEE National Symposium on EMC*, Denver, CO, 1989, pp. 157–162.
- [28] CISPR 32/EN 55032:2015 *Electromagnetic Compatibility of Multimedia Equipment—Emission Requirements*.
- [29] IEEE C63.4:2014, *American National Standard for Methods of Measurement of Radio-Noise Emissions from Low-Voltage Electrical and Electronic Equipment in the Range of 9 kHz to 40 GHz*.
- [30] IEC 61000-4-21:2011, *Electromagnetic Compatibility Part 4-21*, “Testing and Measurement Techniques—Reverberation Chamber Test Methods.”
- [31] Boyes, S. J., and Y. Huang, *Reverberation Chambers: Theory and Applications to EMC and Antenna Measurements*.
- [32] RTCA DO-160G, *Environmental Conditions and Test Procedures for Airborne Equipment*, Section 20.6.
- [33] CISPR 16-2-3:2016, *Specification for Radio Disturbance and Immunity Measuring Apparatus and Methods—Part 2-3*, “Methods of Measurement of Disturbances and Immunity—Radiated Disturbance Measurements.”

List of Acronyms and Abbreviations

OTLP	zero transmission level point
AAS	advanced antenna system
ABET	Accreditation Board for Engineering and Technology
AC	alternating current
ACA	American Communications Association
ACARS	ARINC Communications Addressing Reporting System
ACCESS	automatic computer-controlled electronic scanning system
ACE	Association for Cooperation in Engineering
ACET	Advisory Committee for Electronics and Telecommunications
ACF	antenna correction factor
ACGIH	American Conference of Governmental Industrial Hygienists
ACI	automatic card identification
ACIL	American Council of Independent Laboratories
ACIS	Association for Computing and Information Sciences
ACM/GAMM	Association for Computing Machinery/German Association for Applied Mathematics and Mechanics
ACOS	Advisory Committee on Safety
ACPDS	Advisory on Personal Dosimetry Services
AEA	American Electronics Association
AEA	American Engineering Association
AEA	Association of Engineers and Associates
AEC	American Engineering Council
AEI	Associazione Elettrotecnica Italiana
AEM	Association of Electronic Manufacturers
AEPSC	Atomic Energy Plant Safety Committee
AERE	Atomic Energy Research Establishment (UK)
AF	antenna factor
AF	audio frequency

AFCCE	Association of Federal Communication Consulting Engineers
AFNOR	Association Francaise des Normes (France)
AGARD	Advisory Group for Aerospace Research and Development (NATO)
AGED	Advisory Group on Electron Devices
AGEP	Advisory Group on Electronic Parts
AGET	Advisory Group on Electronic Tubes
AHAM	Association of Home Appliance Manufacturers
ALC	absorber lined chamber
A/m	ampere per meter
AM	amplitude modulation
ANSI	American National Standards Institute
ANZAAS	Australian and New Zealand Association for the Advancement of Science
aps	assumed perfect site
AR	axial ratio
ARCG	American Research Committee on Grounding
ARINC	Aeronautical Radio Incorporated
ARMMS	Automated RF and Microwave Measurement Society
ARMS	Aerial Radiological Measurements and survey
ARMS	Amateur Radio Mobile Society
ARP	aerospace recommended practice
ARTE	Admiralty Research Test Establishment (UK)
ASA	American Standards Association (now ANSI)
ASAC	Asian Standards Advisory Committee
ASCH	American standard code of information interchange
ASEE	Association of Supervisory Electrical Engineers
ASET	American Society for Engineering Technology
ASI	American Standards Institute
ASM	American Society for Materials
ASTM	American Society for Testing and Materials
AT	ampere-turn
BABT	British Approvals Board for Telecommunications
BALUN	balanced to unbalanced
BAPT	German postal service (for EMC laws)
BBC	broadband conducted
BC	back-conducted

BCI	bulk current injection
BCI	broadcast interference
BEAME	British Electrical and Allied Manufacturers
BECTO	British Electric Cable Testing Organization
BEMS	Bioelectromagnetics Society
B/M	balun and matching (network)
BS	British Standard
BW	bandwidth
BW	beamwidth
CAA	Civil Aviation Authority (UK)
CAMESA	Canadian Military Electronics Standards Agency
CARS	community antenna relay service
CATV	community antenna television
CB	citizen's band (radio)
CBEMA	Computer and Business Equipment Manufacturer's Association
CCA	CENELEC Certification Agreement
CCB	Common Carrier Bureau (FCC)
CCI	combined form of CCIR and CCIT
CCIR	International Radio Consultative Committee
CCITT	Comite Consultatif International des Telegraphique etTelephonique
CCITT	International Telegraph and Telephone Consultative Committee
CDM	charged device model (ESD)
CE	Commite European
CE	conducted emissions
CE	compromising emanation (TEMPEST)
CECC	CENELEC Electronics Components Committee
CEI	Council of Engineering Institutions
CEM	computational electromagnetics
CEN	Commite European de Normalisation
CEN	European Standard Coordinating Committee
CENELEC	Comite European de Normalisation Electrotechnique (European Committee for Electrotechnical Standardisation)
CERL	Central Electricity Research Laboratory
CGA	colour graphics adapter (640 × 200 pixels)

CGM	computer graphics metafile
CGS	centimetre gramme second (system of units)
CI	conducted interference
CIA	Computer Industry Association
CIP	current injection probe
CISPR	Center for International Systems Research (Department of State)
CISPR	Comite International Special des Perturbation Radio Electronique
CMR	common-mode rejection
CMRR	common-mode rejection ratio
CMV	common-mode voltage
CNET	Centre National d'Etudes des Telecommunication (France)
COMAR	Committee on Man and Radiation (IEEE)
COMSEC	communications security
CONELRAD	control of electromagnetic radiation
COSHH	control of substances hazardous to health
CP	circularly polarised
CPEM	Conference on Precision Electromagnetic Measurement
CPSE	counterpoise
CRT	cathode ray tube
CS	conducted susceptibility
CSA	Canadian Standards Association
CT2	cordless telephone (second generation)
CUI	called unit identify
CW	carrier wave
CW	continuous wave
CYMB	cyan yellow magenta black
CYMK	cyan yellow magenta black
dB	decibel
dBa	decibel referenced to 1 amp
dB(A/m ²)	decibel referenced to 1 amp per square metre
dBa	decibel adjusted
DBAO	digital bloc k AND-OR
dBa0	noise power on dBa referred to or measured at 0TLP
dBc	decibels relative to the carrier
dB _i	decibel referenced to an isotropic (antenna)
dB _j	relative RF signal levels (j = Jerrold Electronics)

dBk	decibels referred to one kilowatt
dBm	decibels referred to one milliwatt
dBm/m ²	dB referred to one milliwatt per square meter
dBm/m ² /MHz	dB referred to one milliwatt per square meter per megahertz
dBm(PSOPH)	noise power in dBm referred measured by a set with psophometric weighting
dB μ A	dB referred to one microamp
dB μ A/m	dB referred to one microamp per metre
dB μ V	dB referred to one microvolt
dB μ V/m	dB referred to one microvolt per metre
dBRN	decibels above reference noise
DBS	direct broadcast by satellite
dBV	decibels referred to 1 Volt
dBW	decibels referred to 1 Watt
dBx	decibels above the reference coupling
DC	direct current
DCI	direct current injection
DFT	discrete Fourier transform
DIN	Deutsches Institut fur Normung (German Standards Organisation)
Div	divergence
DOC	Department of Communications (Canada)
DoD	Department of Defense (USA)
DOT	Department of Transportation
DRA	Defence Research Agency (UK)
DSB	double sideband
DSSC	double sideband suppressed carrier (modulation)
DTC	dual TEM cell
DTSC	digital termination shielded chamber
DUT	device under test
EBU	European Broadcasting Union
EC	Engineering Council
EC	European Communities
ECAC	Electromagnetic Analysis Center
ECC	Electronic Calibration Center (NBS)
ECE	Economic Commission for Europe (CEE Geneve)
ECMA	Electronic Computer Manufacturers Association

ECMA	European Computer Manufacturers Association
ECMWF	European Centre for Medium-Range Weather Forecasting
ECP	electromagnetic compatibility program
EED	electroexplosive device
EED	electromagnetic energy density
E ³	electromagnetic environmental effects
EEM	electric equipment monitoring
EEPA	Electromagnetic Energy Policy Alliance
EFT	electrical fast transients
EGA	enhanced graphics array (640 × 350 pixels)
EIA	Electronic Industries Association
EIAJ	Electronic Industries Association of Japan
EIRP	equivalent isotropically radiated power
EITB	Engineering Industry Training Board
EM	electromagnetic
EMC	electromagnetic compatibility
EMC	electromagnetically coupled
EMC	electromagnetic coupling
EMCAB	Electromagnetic Compatibility Advisory Board
EMCOM	emission control
EMCP	electromagnetic compatibility program
EMCS	electromagnetic compatibility standardisation (program)
EMCTP	electromagnetic compatibility test plan
EME	electromagnetic energy
EMEE	electromagnetic environmental effects
EMETF	electromagnetic environmental test facility
e.m.f.	electromotive force
EMF	electromotive force
EMH	electromagnetic health
EMI	electromagnetic interference
EMICP	electromagnetic interference control plan
EMINT	electromagnetic intelligence
EMP	electro-magnetic pulse (radiation)
EMR	electromagnetic radiation
EMS	electromagnetic susceptibility
EMSEC	emanation security (TEMPEST)
EMU	electromagnetic unit
EMV	Gesetz (German EMC law)

EN	Europäische Norm (European standard)
EOTC	European Organisation for Testing and Certification
EPA	Environment Protection Agency
ERP	effective radiated power
ERP	equivalent radiated power
ERTZ	equipment radiation TEMPEST zone
ESA	electrostatic attraction
ESD	electrostatic discharge
ESDS	electrostatic discharge sensitive
ESTLA	electrically short tuned loop antenna
ETL	Electrotechnical Laboratory (Japan)
ETSI	European Telecommunications Standards Institute
EUT	equipment under test
FAA	Federal Aviation Administration (USA)
F/B	front-to-back ratio
FC	ferrite core
FCC	Federal Communications Commission (USA)
FEA	Federal Energy Administration
FEANI	Federation Europeane d'Associations Nationales d'Ingenieurs (France)
FERROD	ferrite-rod antenna
FFT	fast Fourier transform
FG	function generator
FI	frequency independent
FM	frequency modulation
FMCW	frequency modulated continuous wave
FMCW	frequency modulated carrier wave
FOB	Field Operations Bureau (FCC)
FOL	fibre optic link
FS	field strength
FSM	field strength meter
FT	Fourier transform
FTC	Federal Trade Commission
FTZ	Fernmelde Technischer Zentralamt (Germany)
GSM	group special mobile
G/T	antenna gain-to-noise temperature
GTD	geometrical theory of diffraction

HBM	human body model (ESD)
HCP	horizontal coupling plane (for ESD testing)
HEMP	high altitude electromagnetic pulse
HERF	hazards of electromagnetic radiation to flight
HERF	hazards of electromagnetic radiation to fuel
HERO	hazards of electromagnetic radiation to ordnance
HERP	hazards of electromagnetic radiation to personnel
HIRF	high intensity radiated fields
HP	horizontal polarisation
HPBW	half power beamwidth
HPM	high power microwaves
HSI	hardness surveillance illuminator
IAC	Industry Advisory Committee
IBS	Institute for Basic Standards
ICAO	International Civil Aviation Organization
ICP	inherently conductive polymers
IDP	inherently dissipative polymers
IEC	International Electrotechnical Commission
IEE	Institution of Electrical Engineers (UK)
IEEE	Institute of Electrical and Electronics Engineers (USA)
IEEJ	Institute of Electrical and Engineers (Japan)
IEPS	International Electronics Packaging Society
IES	Institute of Environmental Sciences
IICIT	International Institute of Connector and Interconnection Technology
INIRC	International Non-Ionizing Radiation Committee
IPC	Institute for Interconnecting and Packaging Electronics Circuits
IRPA	International Radiation Protection Association
IRR	International Radio Regulations
IRT	Institute für Rundfunktechnik GmHB (Germany)
ISDN	integrated services digital network
ISHM	International Society for Hybrid Microelectronics
ISM	industrial scientific and medical
ISO	International Standards Organization
ITE	information technology equipment
ITE	Institute of Telecommunications Engineers
ITEM	Interference Technology Engineers' Master

ITU	International Telecommunication Union (UNO)
JEDEC	Joint Electron Device Engineering Council
kWh	kilowatt-hour
LA	lighting arrestor
LASSY	Licence Administration Support System
LCR	inductance-capacitance-resistance (network)
LE	antenna effective length (for electric field antennas)
LEM	antenna effective length (for magnetic field antennas)
LEMP	electromagnetic pulse generated by a nearby lightning strike
LHCP	left hand circular polarisation or circularly polarised
LISN	line impedance stabilisation network
LLD	low level detector
LLSC	low level sweep coupling
ln	Naperian or natural logarithm (to the base e)
log	logarithm (usually to the base 10)
LORAN	long range navigation
LORAP	long range aerial photography
LPDA	log-periodic dipole antennas or array
LSB	lower sideband
LSN	line stabilisation network
LUF	lowest usable frequency
MAGGI	Million Ampere Generator (Aldermaston, UK)
Maser	microwave amplification by stimulated emission of radiation
MCS	Mobile Communications Systems (IEEE vehicular Technology Technical Committee)
MCW	modulated continuous wave
MDS	minimum detectable (or discernible) signal
MIC	minimum ignition current
MIC	mutual interference chart
MIL	Defense Logistics Agency (USA)
MIL-I	military specification on interference
MIL-STD	military standard (book)
mil	one-thousandth of an inch
MKS	meter-kilogram-second
MM	machine model (ESD)

MMB	Mass Media Bureau (FCC)
MMF	magnetomotive force
MoD	Ministry of Defence (UK)
MOF	maximum operating frequency
MP-4	an FCC measurement procedure
MPE	maximum permissible exposure
MPL	maximum permissible level
MPW	modified plane wave
MS	military standard sheet, prefix to numbered series issued by DoD (USA)
MSC	mode stirred cavity
MTF	modulation transfer function
MUB	maximum usable bandwidth
MUF	maximum usable frequency
MUT	material under test
NAB	National Association of Broadcasters
NACSEM	National COMSEC/EMSEC Information Memorandum (TEMPEST)
NACSI	National COMSEC Instruction (TEMPEST)
NACSIM	National COMSEC Instruction Memorandum (TEMPEST)
NAMAS	National Measurement Accreditation Service (UK)
NARTE	National Association of Radio and Telecommunications Engineers
NASA	National Aeronautics Space Administration
NATA	North American Telecommunications Association
NATLAS	National Testing Laboratory Accreditation Scheme (UK)
NBC	narrowband conducted
NBC	nuclear biological and chemical
NBS	National Bureau of Standards (USA) now NIST
NBSFS	NBS frequency standard
NEC	numerical electromagnetics code
NEMA	National Electrical Manufacturer's Association
NEMP	nuclear electromagnetic pulse
NEPA	National Environment Policy Act
NFP	near field probe
NFPA	National Fire Protection Association
NIH	National Institute of Health

NIST	National Institute of Standards and Technology (USA)
NMR	normal-mode rejection
NPL	National Physical Laboratory (UK)
NRC	National Research Council
NRC	Nuclear Regulatory Commission
NRL	National Research Laboratory (USA)
NRPB	National Radiological Protection Board (UK)
NRTL	nationally recognized testing laboratory
NSA	normalised site attenuation
NSA	National Security Agency
NTG	Nachrichtentechnische Gesellschaft (German Communications Society)
NTIA	National Telecommunications and Information Administration (US Department of Commerce)
NTISSI	National Telecommunications and Information Systems Security Instruction
NTP	normal temperature and pressure
NTZ	Nachrichtentechnische Zeitschrift (Germany)
NTSC	National Television System Committee (US)
NVLAP	National Voluntary Laboratory Accreditation Program
OATS	open area test site
OBR	optical bar code
oe	oersted (ampere per metre)
OEM	original equipment manufacturer
OET	Office of Engineering and Technology (FCC)
OSHA	Occupational Health and Safety Administration
OST	Office of Science and Technology
P-P	peak to peak
PBS	Public Broadcasting Service
PCZ	physical control zone (TEMPEST)
pd	potential difference
PDS	power density spectra
PF	power factor
PLC	power-line carrier
PM	phase modulation
PM	pulse modulation
PadB	perceived noise level expressed in decibels
POE	point of entry (TEMPEST)

PRB	Private Radio Bureau (FCC)
PRF	pulse repetition frequency
PRI	pulse repetition interval
PRR	pulse repetition rate
PSD	power spectral density
PSOPH	psophometric weighting
PTFE	polytetrafluoroethylene
PTM	pulse time modulation
PW	plane wave
PWS	plane wave spectrum
QP	quasi peak
QPA	quasi-peak adapter
QRM	man-made interference
RAC	Representative Advisory Committee
radar	radio assisted detection and ranging
RADFAC	radiation facility
RADHAZ	radiation hazards
RADIMT	radiation intelligence
radome	radar dome
RAE	Royal Aeronautical Establishment (now DRA)
RAM	radar absorbing material
RBE	radiation biological effectiveness
RD	radiation detector
RE	radiated emission
REC	radiant energy conversion
REG	radar environment generator
RF	radio frequency
RFA	reticulated radio absorber
RFC	radio-frequency compatibility program
RFEG	radio frequency environment generator
RFI	radio-frequency interference
RFPG	radio frequency protection guidelines
RH	radiological health
RHE	radiation hazard effects
RI	radio interference
RM	radio monitoring
RMS	radiation monitoring system

RMS	root mean square
RRSWG	random repetitive square wave pulse generator
RS	radiated susceptibility
RSS	root sum square
RTMA	Radio Television Manufacturers' Association
SA	spectrum analyser
SAE	Society of Automotive Engineers
SAMPE	Society for the Advancement of Material and Process Engineering
SAR	specific absorption rate
SB	sideband
s/c	signal-to-clutter ratio
SCSI	small computer system interface
SE	shielding or screening effectiveness
SELDS	shielded enclosure leak detection system
SEV	Schweizerische Elektrotechnischer Verein (Swiss Electrotechnical Association)
SI	Systeme Internationale d'Unites (International system of units)
SIR	signal-to-interference ratio
SMC	stirred mode cavity
SNI	signal-to-noise improvement
SNR	signal-to-noise ratio
SPEHS	single point excitation for hardness surveillance
SPG	single point ground
SS	Swedish Standard
SSB	single sideband
SSBSC	single-sideband suppressed carrier
SSSC	single-switched suppressed carrier
SSPM	single-sideband pulse modulation
stat	electrostatic units in CGS system (prefix)
SUT	site under test
SWR	standing wave ratio
TE	transverse electric (field)
TEM	transverse electromagnetic
TEMPEST	US government radiated emissions security program
TM	transverse magnetic (field)
TSB	twin sideband

TSI	threshold signal-to-interference ratio
TVAR	TEMPEST Vulnerability Assessment Request
TVS	transient voltage suppressor
TWSB	twin sideband
TWT	travelling-wave tube
TWTA	travelling-wave tube amplifier
UL	Underwriter's Laboratory
UNO	United Nations Organisation
UPS	uninterruptible power supply
USB	upper sideband
UUT	unit under test
UWB	ultra wideband
VCCI	Voluntary Control Commission for Interference (Japan)
VCP	vertical coupling plane (for ESD testing)
VDE	Verband Deutsche Elektrotechniker—Society of German Electrical Engineers
Vfg	Verfugung (FTZ regulations that affect EDP equipment)
VGA	video graphics array (640 × 480 pixels)
V/Hz	volts per hertz
VP	vertical polarisation
VSWR	voltage standing wave ratio
WARC	World Administrative Radio Conference
WG	waveguide
WG	Working Group (CISPR)
XPD	cross polar discrimination
XT	cross talk

Preferred Scientific Prefixes

<i>Prefix</i>	<i>Abbreviation</i>	<i>Decimal Equivalent</i>
Exa	E	10^{18}
Peta	P	10^{15}
Tera	T	10^{12}
Giga	G	10^9
Mega	M	10^6
Kilo	k	10^3
Centi	C	10^{-2}
Milli	m	10^{-3}
Micro	μ	10^{-6}
Nano	n	10^{-9}
Pico	p	10^{-12}
Femto	f	10^{-15}
Atto	a	10^{-18}

Notes: Uppercase K is common usage to denote memory as kilobytes in computing technology. However, a kilobyte is not strictly 1,000 bytes, but 1,024 or 2^{10} bytes. Thus, lowercase k stands for 1,000, whereas uppercase K stands for 1,024.

Optical wavelengths are often quoted in angstrom units.

Angstrom (\AA) is 10^{-10}m .

List of Scientific Constants

Avogadro's constant $N_a = 6.02 \times 10^{23} \text{ mol}^{-1}$

Boltzmann's constant $k = 1.38 \times 10^{-23} \text{ J K}^{-1}$

Base of the Napierian or natural system of logarithms, $e = 2.718$

Intrinsic impedance of a plane wave in free space $Z_0 = 120$ or 377Ω

Electronic charge $e = 1.602 \times 10^{-19} \text{ C}$

Faraday's constant $F = 9.65 \times 10^4 \text{ C mol}^{-1}$

Gravitational acceleration $g = 9.81 \text{ ms}^{-2}$

Gravitational constant $G = 6.67 \times 10^{-11} \text{ m}^3\text{s}^{-2} \text{ kg}^{-1}$

Molar gas constant $R = 8.3 \text{ J mol}^{-1} \text{ K}^{-1}$

Neper is equal to 8.68 dB, $\{20 \log(e)\}$.

Permeability of free space $= 4 \times 10^{-7} \text{ Hm}^{-1}$

Permittivity of free space $= 1/(36\pi \times 10^8)$ or $8.85 \times 10^{-12} \text{ Fm}^{-1}$

Pi $= \pi = 3.142$

Speed of electromagnetic waves in a vacuum, $c = 2.99773 \times 10^8 \text{ ms}^{-1}$ (usually taken as $3 \times 10^8 \text{ ms}^{-1}$)

Speed of sound in free space in dry air at STP is 331.5 m/s

APPENDIX D

Conductivities of Common Metals

<i>Metal</i>	<i>Conductivity in Siemen/m</i>	<i>Conductivity Relative to Cu</i>	<i>Multiplier for Skin Depth</i>
Aluminum	3.538×10^7	0.61	1.28
Beryllium	5.8×10^6	0.10	3.16
Brass (70% Cu)	1.450×10^7	0.25	2.00
Brass (90% Cu)	2.41×10^7	0.42	1.54
Cadmium	1.334×10^7	0.23	2.09
Copper	5.8×10^7	1.00	1.00
Gold	4.06×10^7	0.70	1.20
Iron	9.86×10^7	0.17	2.43
Lead	4.64×10^6	0.08	3.54
Magnesium	2.204×10^7	0.38	1.62
Mu-metal	1.74×10^6	0.03	5.77
Nickel	1.16×10^6	0.20	2.24
Permalloy	1.74×10^6	0.03	5.77
Phosphor-bronze	5.8×10^6	0.18	2.36
Silver	6.09×10^7	1.05	0.98
Stainless steel	1.16×10^6	0.02	7.87
Tin	8.7×10^6	0.15	2.58
Zinc	1.68×10^7	0.29	1.86

Dielectric Constants and Loss Tangents of Common Materials

This is the same as the permittivity of the material relative to the permittivity of a vacuum. The dielectric constant of a material is made up of a real ϵ'_r and an imaginary ϵ''_r part, and is given by $\epsilon_r = \epsilon'_r + j\epsilon''_r$. The ratio of the imaginary to real parts of the relative permittivity is the loss tangent, $\tan\delta$. The dielectric constant changes with frequency so the magnitude is quoted at two frequencies.

<i>Material</i>	<i>Dielectric Constant</i>		<i>Tan δ</i>	
	<i>3 GHz</i>	<i>10 GHz</i>	<i>3 GHz</i>	<i>10 GHz</i>
Alumina (99%) ceramic	8.7	9.7–10.3		0.0004
Corning glass 1990	7.99	7.94	0.00199	0.0032
Teflon (PTFE) glass woven fibre	2.1	2.17–2.55		0.0009–0.0022
Fibreglass BK-164	3.88	3.99	0.01	0.0131
Ice (–12°C)	3.20	3.17	0.0009	0.0007
Mica—glass bonded		7.5		0.0020
Plexiglass	2.60	2.59	0.0057	0.0067
Polyethylene	2.32	2.31	0.0050	0.0044
Polystyrene hydrogenated	2.25	2.25	0.00016	0.00041
Teflon (PTFE) unreinforced	2.1	2.08	0.00015	0.00037
Quartz fused		3.78		0.001
Water (at 25°C)	77	55	0.15	0.54

Conversion Table for dBμV to μV, dBV, dBW, dBm, and Watts

To convert decibels relative to microvolts (dBμV) to μV, the following formula should be used:

$$\mu\text{V} = 10^{(\text{dB}\mu\text{V}/10)}$$

To convert the power in milliwatts to power in dBm, the following formula is used:

$$\text{dBm} = 10\log_{10}(\text{mW})$$

To convert volts to watts using a characteristic impedance of R , $V = \sqrt{PR}$ where V is the voltage expressed in volts, P is the power expressed in watts, and R is the resistance expressed in ohms.

The relation between dBV and dBW is given by:

$$20 \log_{10} V = 10\log_{10} P + 10\log_{10} R$$

The voltage ratio in dBV is given by $V = 20\log_{10} (V_1/V_2)$ where V_1 and V_2 are measured in volts.

The following table assumes an impedance of 50 ohms.

<i>dBμV</i>	<i>Voltage</i>		<i>dBV</i>	<i>dBW</i>	<i>dBm</i>	<i>Power</i>	
0	1	μV	-120	-137	-107	20	fW
1	1.12	μV	-119	-136	-106	25.2	fW
2	1.26	μV	-118	-135	-105	31.7	fW
3	1.41	μV	-117	-134	-104	39.9	fW
4	1.58	μV	-116	-133	-103	50.2	fW
5	1.78	μV	-115	-132	-102	63.2	fW
6	2	μV	-114	-131	-101	79.6	fW
7	2.24	μV	-113	-130	-100	100.2	fW
8	2.51	μV	-112	-129	-99	126.2	fW
9	2.82	μV	-111	-128	-98	0	fW
10	3.16	μV	-110	-127	-97	200	fW

<i>dBμV</i>	<i>Voltage</i>		<i>dBV</i>	<i>dBW</i>	<i>dBm</i>	<i>Power</i>	
11	3.55	μ V	-109	-126	-96	251.8	fW
12	3.98	μ V	-108	-125	-95	317	fW
13	4.47	μ V	-107	-124	-94	399.1	fW
14	5.01	μ V	-106	-123	-93	502.4	fW
15	5.62	μ V	-105	-122	-92	632.5	fW
16	6.31	μ V	-104	-121	-91	796.2	fW
17	7.08	μ V	-103	-120	-90	1	pW
18	7.94	μ V	-102	-119	-89	1.26	pW
19	8.91	μ V	-101	-118	-88	1.59	pW
20	10	μ V	-100	-117	-87	2	pW
21	11.22	μ V	-99	-116	-86	2.52	pW
22	12.59	μ V	-98	-115	-85	3.17	pW
23	14.13	μ V	-97	-114	-84	3.99	pW
24	15.85	μ V	-96	-113	-83	5.02	pW
25	17.78	μ V	-95	-112	-82	6.32	pW
26	20	μ V	-94	-111	-81	7.96	pW
27	22.4	μ V	-93	-110	-80	10.02	pW
28	25.1	μ V	-92	-109	-79	12.62	pW
29	28.2	μ V	-91	-108	-78	15.89	pW
30	31.6	μ V	-90	-107	-77	20	pW
31	35.5	μ V	-89	-106	-76	25.18	pW
32	39.8	μ V	-88	-105	-75	31.7	pW
33	44.7	μ V	-87	-104	-74	39.91	pW
34	50.1	μ V	-86	-103	-73	50.24	pW
35	56.2	μ V	-85	-102	-72	63.25	pW
36	63.1	μ V	-84	-101	-71	79.62	pW
37	70.8	μ V	-83	-100	-70	100.2	pW
38	79.4	μ V	-82	-99	-69	126.2	pW
39	89.1	μ V	-81	-98	-68	158.9	pW
40	100	μ V	-80	-97	-67	200	pW
41	112.2	μ V	-79	-96	-66	251.8	pW
42	125.9	μ V	-78	-95	-65	317	pW
43	141.3	μ V	-77	-94	-64	399.1	pW
44	158.5	μ V	-76	-93	-63	502.4	pW
45	177.8	μ V	-75	-92	-62	632.5	pW
46	199.5	μ V	-74	-91	-61	796.2	pW
47	223.9	μ V	-73	-90	-60	1	nW
48	251.2	μ V	-72	-89	-59	1.26	nW
49	281.8	μ V	-71	-88	-58	1.59	nW
50	316.2	μ V	-70	-87	-57	2	nW

<i>dBμV</i>	<i>Voltage</i>		<i>dBV</i>	<i>dBW</i>	<i>dBm</i>	<i>Power</i>	
51	354.8	μ V	-69	-86	-56	2.52	nW
52	398.1	μ V	-68	-85	-55	3.17	nW
53	446.7	μ V	-67	-84	-54	3.99	nW
54	501.2	μ V	-66	-83	-53	5.02	nW
55	562.3	μ V	-65	-82	-52	6.32	nW
56	631	μ V	-64	-81	-51	7.96	nW
57	707.9	μ V	-63	-80	-50	10.02	nW
58	794.3	μ V	-62	-79	-49	12.62	nW
59	891.3	μ V	-61	-78	-48	15.89	nW
60	1	mV	-60	-77	-47	20	nW
61	1.12	mV	-59	-76	-46	25.18	nW
62	1.26	mV	-58	-75	-45	31.7	nW
63	1.41	mV	-57	-74	-44	39.91	nW
64	1.58	mV	-56	-73	-43	50.24	nW
65	1.78	mV	-55	-72	-42	63.25	nW
66	2	mV	-54	-71	-41	79.62	nW
67	2.24	mV	-53	-70	-40	100.24	nW
68	2.51	mV	-52	-69	0	126.19	nW
69	2.82	mV	-51	-68	-38	158.87	nW
70	3.16	mV	-50	-67	-37	200	nW
71	3.55	mV	-49	-66	-36	251.79	nW
72	3.98	mV	-48	-65	-35	316.98	nW
73	4.47	mV	-47	-64	-34	399.05	nW
74	5.01	mV	-46	-63	-33	502.38	nW
75	5.62	mV	-45	-62	-32	632.46	nW
76	6.31	mV	-44	-61	-31	796.21	nW
77	7.08	mV	-43	-60	-30	1	μ W
78	7.94	mV	-42	-59	-29	1.26	μ W
79	8.91	mV	-41	-58	-28	1.59	μ W
80	10	mV	-40	-57	-27	2	μ W
81	11.22	mV	-39	-56	-26	2.52	μ W
82	12.59	mV	-38	-55	-25	3.17	μ W
83	14.13	mV	-37	-54	-24	3.99	μ W
84	15.85	mV	-36	-53	-23	5.02	μ W
85	17.78	mV	-35	-52	-22	6.32	μ W
86	19.95	mV	-34	-51	-21	7.96	μ W
87	22.39	mV	-33	-50	-20	10.02	μ W
88	25.12	mV	-16	-49	-19	12.62	μ W
89	28.18	mV	-31	-48	-18	15.89	μ W
90	31.62	mV	-30	-47	-17	20	μ W

<i>dBμV</i>	<i>Voltage</i>		<i>dBV</i>	<i>dBW</i>	<i>dBm</i>	<i>Power</i>	
91	35.48	mV	-29	-46	-16	25.18	μ W
92	39.81	mV	-28	-45	-15	31.7	μ W
93	44.67	mV	-27	-44	-14	39.91	μ W
94	50.12	mV	-26	-43	-13	50.24	μ W
95	56.23	mV	-25	-42	-12	63.25	μ W
96	63.1	mV	-24	-41	-11	79.62	μ W
97	70.79	mV	-23	-40	-10	100.2	μ W
98	79.43	mV	-22	-39	-9	126.2	μ W
99	89.13	mV	-21	-38	-8	158.9	μ W
100	100	mV	-20	-37	-7	200	μ W
101	112.2	mV	-19	-36	0	251.8	μ W
102	125.9	mV	-18	-35	-5	317	μ W
103	141.3	mV	-17	-34	-4	399.1	μ W
104	158.5	mV	-16	-33	-3	502.4	μ W
105	177.8	mV	-15	-32	-2	632.5	μ W
106	199.5	mV	-14	-31	-1	796.2	μ W
107	223.9	mV	-13	-30	0	1	mW
108	251.2	mV	-12	-29	1	1.26	mW
109	281.8	mV	-11	-28	2	1.59	mW
110	316.2	mV	-10	-27	3	1	mW
111	354.8	mV	-9	-26	4	2.52	mW
112	398.1	mV	-8	-25	5	3.17	mW
113	446.7	mV	-7	-24	6	3.99	mW
114	501.2	mV	-6	-23	7	5.02	mW
115	562.3	mV	-5	-22	8	6.32	mW
116	631	mV	-4	-21	9	7.96	mW
117	707.9	mV	-3	-20	10	10.02	mW
118	794.3	mV	-2	-19	11	12.62	mW
119	891.3	mV	-1	-18	12	15.89	mW
120	1	V	0	-17	13	20	mW
121	1.12	V	1	-16	14	25.18	mW
122	1.26	V	1	-15	15	31.7	mW
123	1.41	V	3	-14	16	39.91	mW
124	1.58	V	4	-13	17	50.24	mW
125	1.78	V	5	-12	18	63.25	mW
126	2	V	6	-11	19	79.62	mW
127	2.24	V	7	-10	20	100.2	mW
128	2.51	V	4	-9	21	126.2	mW
129	2.82	V	9	-8	22	158.9	mW
130	3.16	V	10	-7	23	200	mW

<i>dBμV</i>	<i>Voltage</i>		<i>dBV</i>	<i>dBW</i>	<i>dBm</i>	<i>Power</i>	
131	3.55	V	11	-6	24	251.8	mW
132	3.98	V	12	-5	25	317	mW
133	4.47	V	13	-4	26	399.1	mW
134	5.01	V	14	-3	27	502.4	mW
135	5.62	V	15	-2	28	632.5	mW
136	6.31	V	16	-1	29	796.2	mW
137	7.08	V	17	0	30	1	W
138	7.94	V	18	1	31	1.26	W
139	8.91	V	19	2	32	1.59	W
140	10	V	20	3	33	2	W

APPENDIX G

The Electromagnetic Spectrum

Frequency	DC 0	AC 50/60 Hz	500MHz $5 \cdot 10^8 \text{ Hz}$	30GHz $3 \cdot 10^{10} \text{ Hz}$	300GHz $3 \cdot 10^{11} \text{ Hz}$	430THz $43 \cdot 10^{13} \text{ Hz}$	750THz $75 \cdot 10^{13} \text{ Hz}$	60PHz $6 \cdot 10^{16} \text{ Hz}$	50EHZ $5 \cdot 10^{19} \text{ Hz}$	1000EHZ 10^{21} Hz	10 ⁷ EHZ 10^{25} Hz
		RF	microwaves	mm waves	infrared	Visible light	Ultra violet	X-rays	Gamma rays	Cosmic rays	
Wavelength	5000/6000 km	60cm	1cm	1mm	0.7 μm $7 \cdot 10^{-7} \text{ m}$	0.4 μm $4 \cdot 10^{-7} \text{ m}$	5 nm $5 \cdot 10^{-9} \text{ m}$	6 pm $6 \cdot 10^{-12} \text{ m}$	0.3 pm $3 \cdot 10^{-13} \text{ m}$	30 am $3 \cdot 10^{-17} \text{ m}$	

APPENDIX H

Frequency Band Designations

NATO	A	B	C	D	E	F	G	H	I	J	K	L	M	N	
GHz	0	0.25	0.5	1	2	3	4	6	8	10	20	40	60	100	200
UK IEE	L	S	C	X	J	K	Q	V	O						
GHz	1	2	4	8	12	18	27	40	60	90					
USA	I	G	P	L	S	X	K	Q	V	W					
GHz	0.1	0.15	0.225	0.39	1.55	5.2	10.9	36	46	56	100				
IRR	ELF	VLF	LF	MF	HF	VHF	UHF	SHF	EHF						
	0	3kHz	30kHz	300kHz	3MHz	30MHz	300MHz	3GHz	30GHz	300GHz					
ITU	HF	VHF	UHF	L	S	C	X	Ku	K	Ka	mm				
	3MHz	30MHz	300MHz	1GHz	2GHz	4GHz	8GHz	12GHz	18GHz	27GHz	40GHz	300GHz			
Aircraft bands	225MHz		400MHz		2.5GHz		4GHz		6GHz		12.5GHz		40GHz		
	HF	VHF	UHF	L	S	C	X	K	Q						
	2MHz	30MHz	225MHz	1GHz	3GHz	3.5GHz	7.5GHz	33GHz	50GHz						
Common usage	RF	Microwaves								mm waves					
	300MHz									30GHz	300GHz				

APPENDIX I

Conversion Between Gain in dB and Gain as a Linear Ratio Gain in dBi to Linear Gain

To calculate intermediate values of gain in dBi, multiply linear gains. For example, for 5.6 dBi, multiply the 5 and 0.6 dBi values, that is, $3.162 * 1.148 = 3.26998$.

Gain dBi	-10.0	-9.0	-8.0	-7.0	-6.0	-5.0	-4.0	-3.0	-2.0
Linear gain	0.100	0.126	0.158	0.200	0.251	0.316	0.398	0.501	0.631
Gain dBi	-1.0	-0.9	-0.8	-0.7	-0.6	-0.5	-0.4	-0.3	-0.2
Linear gain	0.794	0.813	0.832	0.851	0.871	0.891	0.912	0.933	0.955
Gain dBi	0.1	0.2	0.3	0.4	0.5	0.6	0.7	0.8	0.9
Linear gain	1.023	1.047	1.072	1.096	1.122	1.148	1.175	1.202	1.230
Gain dBi	1	2	3	4	5	6	7	8	9
Linear gain	1.259	1.585	1.995	2.512	3.162	3.981	5.012	6.310	7.943
Gain dBi	10	20	30	40	50	60	70	80	90
Linear gain	10	100	1000	10 ⁴	10 ⁵	10 ⁶	10 ⁷	10 ⁸	10 ⁹
<i>Linear gain to gain in dBi</i>									
Linear gain	0.1	0.2	0.3	0.4	0.5	0.6	0.7	0.8	0.9
Gain dBi	-10.0	-7.0	-5.2	-4.0	-3.0	-2.2	-1.5	-1.0	-0.5
Linear gain	1	2	3	4	5	6	7	8	9
Gain dBi	0	3.01	4.77	6.02	6.99	7.78	8.45	9.03	9.54
Linear gain	10	20	30	40	50	60	70	80	90
Gain dBi	10.00	13.01	14.77	16.02	16.99	17.78	18.45	19.03	19.54
Linear gain	100	200	300	400	500	600	700	800	900
Gain dBi	20.00	23.01	24.77	26.02	26.99	27.78	28.45	29.03	29.54
Linear gain	1000	2000	3000	4000	5000	6000	7000	8000	9000
Gain dBi	30.00	33.01	34.77	36.02	36.99	37.78	38.45	39.03	39.54
Linear gain	10000	20000	30000	40000	50000	60000	70000	80000	90000
Gain dBi	40.00	43.01	44.77	46.02	46.99	47.78	48.45	49.03	49.54

APPENDIX J

The Periodic Table Listed Alphabetically by Chemical Symbol

<i>Symbol</i>	<i>Element</i>	<i>Group</i>	<i>Atomic Number</i>	<i>Atomic Weight</i>
Ac	Actinium	3A	89	227.0278
Ag	Silver	1B	47	107.868
Al	Aluminum	3B	13	26.981
Am	Americium	3A	95	243
Ar	Argon	Gas	18	39.948
As	Arsenic	5B	33	74.9216
At	Astatine	7B	85	210
Au	Gold	1B	79	196.9665
B	Boron	3B	5	10.81
Ba	Barium	2A	56	137.33
Be	Beryllium	2A	4	9.01218
Bi	Bismuth	5B	83	208.9804
Bk	Berkelium	3A	97	247
Br	Bromine	7B	35	79.904
C	Carbon	4B	6	12.011
Ca	Calcium	2A	20	40.08
Cd	Cadmium	2B	48	112.41
Ce	Cerium	3A	58	130.12
Cf	Californium	3A	98	251
Cl	Chlorine	7B	17	35.453
Cm	Curium	3A	96	247
Co	Cobalt	8	27	58.9332
Cr	Chromium	6A	24	51.996
Cs	Caesium	1A	55	132.9054
Cu	Copper	1B	29	63.54
Dy	Dyprosium	3A	66	162.5
Ee	Einsteinium	3A	99	252
Er	Erbium	3A	68	167.2
Eu	Europium	3A	63	151.96
F	Fluorine	7B	9	18.9984

<i>Symbol</i>	<i>Element</i>	<i>Group</i>	<i>Atomic Number</i>	<i>Atomic Weight</i>
Fe	Iron	8	26	55.84
Fm	Fermium	3A	100	257
Fr	Francium	1A	87	223
Ga	Gallium	3B	31	69.72
Gd	Gadolinium	3A	64	157.25
Ge	Germanium	4B	32	72.5
H	Hydrogen	1	1	1.00794
He	Helium	7	2	4.0026
Hf	Hafnium	4A	72	178.4
Hg	Mercury	2B	80	200.5
Ho	Holmium	3A	67	164.9304
I	Iodine	7B	53	126.9045
In	Indium	3B	49	114.82
Ir	Iridium	8	77	192.2
K	Potassium	1A	19	39.0983
Kr	Krypton	Gas	36	83.80
La	Lanthanum	3A	57	138.905
Li	Lithium	1A	3	6.94
Lr	Lawrencium	3A	103	260
Lu	Lutetium	3A	71	174.967
Md	Mendelevium	3A	101	258
Mg	Magnesium	2A	12	24.305
Mn	Manganese	7A	25	54.938
Mo	Molybdenum	6A	42	95.94
N	Nitrogen	5B	7	14.0067
Na	Sodium	1A	11	22.98977
Nb	Niobium	5A	41	92.9064
Nd	Neodymium	3A	60	144.2
Ne	Neon	Gas	10	20.17
Ni	Nickel	8	28	58.69
No	Nobelium	3A	102	259
Np	Neptunium	3A	93	237.0482
O	Oxygen	6B	8	15.999
Os	Osmium	8	76	190.2
P	Phosphorus	5B	15	30.973
Pa	Protactinium	3A	91	231.0359
Pb	Lead	4B	82	207.2
Pd	Palladium	8	46	106.42
Pm	Promethium	3A	61	145
Po	Polonium	6B	84	209

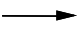







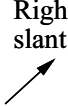



<i>Symbol</i>	<i>Element</i>	<i>Group</i>	<i>Atomic Number</i>	<i>Atomic Weight</i>
Pr	Praseodymium	3A	59	140.9077
Pt	Platinum	8	78	195.0
Pu	Plutonium	3A	94	244
Ra	Radium	2A	88	226.0254
Rb	Rubidium	1A	37	85.467
Rh	Rhodium	8	45	102.99055
Re	Rhenium	7A	75	186.207
Rn	Radon	Gas	86	222
Ru	Ruthenium	8	44	101.0
S	Sulphur	6B	16	32.06
Sb	Antimony	5B	51	121.7
Sc	Scandium	3A	21	44.9559
Se	Selenium	6B	34	78.9
Si	Silicon	4B	14	28.085
Sm	Samarium	3A	62	150.3
Sn	Tin	4B	50	118.6
Sr	Strontium	2A	38	87.62
Ta	Tantalum	5A	73	180.9479
Tb	Terbium	3A	65	158.9254
Tc	Technetium	7A	43	98
Te	Tellurium	6B	52	127.60
Th	Thorium	3A	90	232.0381
Ti	Titanium	4A	22	47.8
Tl	Thallium	3B	81	204.383
Tm	Thulium	3A	69	168.9342
U	Uranium	3A	92	238.0289
V	Vanadium	5A	23	50.9415
W	Tungsten	6A	74	183.8
Xe	Xenon	Gas	54	131.2
Y	Yttrium	3A	39	88.9059
Yb	Ytterbium	3A	70	173
Zn	Zinc	2B	30	65.38
Zr	Zirconium	4A	40	91.22

APPENDIX K

Magnetic Permeabilities of Common Metals

<i>Material</i>	<i>Conductivity Relative to Copper</i>	<i>Relative Magnetic Permeability</i>	<i>Absolute Permeability (H/m)</i>
Aluminum	0.61	1	0.00000126
Beryllium	0.1	1	0.00000126
Brass	0.26	1	0.00000126
Cadmium	0.23	1	0.00000126
Copper	1	1	0.00000126
Gold	0.7	1	0.00000126
Hypernick	0.06	80000	0.10053096
Iron	0.17	1000	0.00125664
Lead	0.08	1	0.00000126
Magnesium	0.38	1	0.00000126
Mu-metal	0.03	80000	0.10053096
Nickel	0.2	1	0.00000126
Permalloy	0.03	80000	0.10053096
Phosphor-bronze	0.18	1	0.00000126
Silver	1.05	1	0.00000126
Stainless steel	0.02	1000	0.00125664
Tin	0.15	1	0.00000126
Zinc	0.29	1	0.00000126

Polarization Matching Matrix

		Transmitter polarization					
		Horizontal 	Vertical 	Right slant 	Left slant 	RHCP 	LHCP 
Receiver polarization	Horizontal 	Yes	No*	Yes but 3 dB loss	Yes but 3 dB loss	Yes but 3 dB loss	Yes but 3 dB loss
	Vertical 	No*	Yes	Yes but 3 dB loss	Yes but 3 dB loss	Yes but 3 dB loss	Yes but 3 dB loss
	Right slant 	Yes but 3 dB loss	Yes but 3 dB loss	Yes	No*	Yes but 3 dB loss	Yes but 3 dB loss
	Left slant 	Yes but 3 dB loss	Yes but 3 dB loss	No*	Yes	Yes but 3 dB loss	Yes but 3 dB loss
	RHCP 	Yes but 3 dB loss	Yes but 3 dB loss	Yes but 3 dB loss	Yes but 3 dB loss	Yes	No*
	LHCP 	Yes but 3 dB loss	Yes but 3 dB loss	Yes but 3 dB loss	Yes but 3 dB loss	No*	Yes

* Although cross-polarization cannot be detected by perfect antennas, practical antennas have levels of cross-polar discrimination of the order of -20 dB. Detection is possible at these levels.

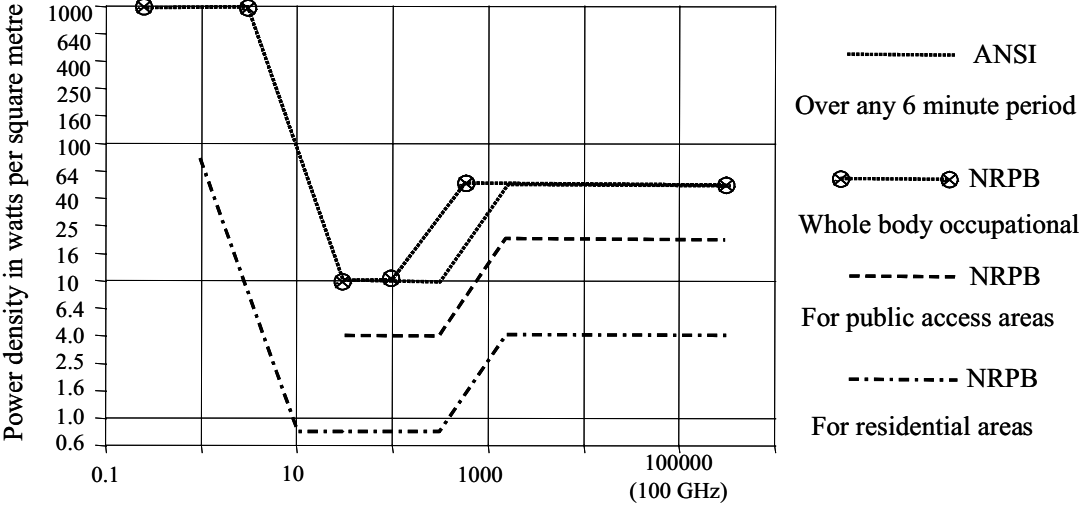
APPENDIX M

Resistivities of Common Materials

<i>Material</i>	<i>Resistivity in Ohm/m</i>	<i>Resistivity Relative to Copper</i>
Aluminum	2.83×10^{-8}	1.64
Beryllium	17.24×10^{-8}	10.00
Brass	6.63×10^{-8}	3.85
Cadmium	7.50×10^{-8}	4.35
Copper	1.72×10^{-8}	1.00
Gold	2.46×10^{-8}	1.43
Iron	10.14×10^{-8}	5.88
Lead	21.55×10^{-8}	12.50
Magnesium	4.54×10^{-8}	2.63
Nu-metal	57.47×10^{-8}	33.33
Nickel	8.62×10^{-8}	5.00
Permalloy	57.47×10^{-8}	33.33
Phosphor-bronze	9.58×10^{-8}	5.56
Silver	1.64×10^{-8}	0.95
Stainless steel	86.21×10^{-8}	50.00
Tin	11.49×10^{-8}	6.67
Zinc	5.95×10^{-8}	3.45

APPENDIX N

Radio Frequency Protection Guides for Nonionizing Radiation



List of Symbols

a	broadside dimension of waveguide side of triangle coefficient of x^2 term of a quadratic radius of a coil expansion coefficient for a planar log spiral antenna
a'	width of the ridge of a ridged waveguide expansion coefficient for an equivalent planar log spiral antenna
a_1	broadside dimension of open end of an H -plane sectoral horn
\mathbf{a}_r	unit vector in polar coordinate system
\mathbf{a}_ϕ	unit vector in polar coordinate system
\mathbf{a}_θ	unit vector in polar coordinate system
A	angle number length of vector area of a loop in m^2 or cm^2 height (from apex to opposite side) of one arm of a bowtie antenna
\mathbf{A}	vector vector field
A_f	antenna correction factor
α	current division factor (folded dipole) angle between the magnetic field vector due to a single coil and the plane containing the coil flare angle of a triangular dipole (bowtie) antenna in deg half-angle of a LPDA angle between the radius vector of a spiral and the x -axis attenuation factor of a cable
b	narrow dimension of waveguide radius of outer conductor of coaxial cable radius of loop

	side of triangle
	coefficient of x term of a quadratic
	effective increase in the height of a top loaded monopole
b_1	height of open end of an E -plane sectoral horn
B	angle
	magnetic flux density scalar in tesla (T)
	number
	length of vector
\mathbf{B}	vector
	magnetic flux density vector in tesla (T) or picotesla (pT)
B_{ar}	bandwidth of the active region of a conical log spiral
B_s	design bandwidth in hertz (Hz)
B_w	bandwidth in hertz (Hz)
β	half-angle of a supporting section of a trapezoidal tooth LPDA
	winding or wrap angle of a spiral antenna
c	side of triangle
c_d	cavity diameter for a planar log spiral
C	angle
	the constant term of a quadratic
	capacitance in farads (F)
	circumference of a helical antenna
	combined correction term of M_t and M_s in dB
C_{\max}	diameter of the base of the cone of a discone antenna
C_{\min}	diameter of the top of the cone of a discone antenna
C_p	correction term to allow for the polarization mismatch, in dB
$C(x)$	Fresnel cosine integral
d	diameter of the feed region of a planar log spiral antenna
	distance between horn and metal sheet in Purcell's method
dA	area of a small loop in m^2
dl	elementary length in meters
d_n	distance between the n th and $(n + 1)$ th element of a LPDA
D	electric flux/displacement density scalar in coulombs per square meter (C m^{-1})
	linear or numeric directivity
	diameter of a circular aperture
	diameter of a helical antenna in meters
	maximum dimension of an aperture antenna
	overall diameter of a planar log spiral antenna

D_{dB}	directivity in dB directivity in dB (dB referred to a circularly polarized isotropic source)
D_{dBi}	directivity in dBi (dB referred to an isotropic source)
D_e	effective aperture diameter of an equivalent reflector antenna
D_m	angle in mathematical degrees
D_n	angle in navigational degrees distance of the n th element from the imaginary apex of a LPDA distance of the back of the n th tooth from the imaginary apex of a trapezoidal tooth LPDA
D_{n1}	normal component of the electric flux density in medium 1, in volts per meter ($V\ m^{-1}$)
D_{n2}	normal component of the electric flux density in medium 2, in volts per meter ($V\ m^{-1}$)
D_{t1}	tangential component of the electric flux density vector in medium 1, in coulombs per square meter ($C\ m^{-2}$)
D_{t2}	tangential component of the electric flux density vector in medium 2, in coulombs per square meter ($C\ m^{-2}$)
D	electric flux/displacement density vector in coulombs per square meter ($C\ m^{-2}$)
δ	skin depth in meters (m) angular width of the arm of a spiral antenna
E	electric field intensity in volts per meter ($V\ m^{-1}$)
E_i	incident electric field intensity in volts per meter ($V\ m^{-1}$)
E_r	reflected electric field intensity from the edges of a spiral antenna in volts per meter ($V\ m^{-1}$) electric field intensity in the radial direction, in volts per meter ($V\ m^{-1}$)
E_ϕ	electric field intensity in the azimuth plane, in volts per meter ($V\ m^{-1}$)
E_{n1}	normal component of the electric field vector in medium 1, in volts per meter ($V\ m^{-1}$)
E_{n2}	normal component of the electric field vector in medium 2, in volts per meter ($V\ m^{-1}$)
E_{t1}	tangential component of the electric field vector in medium 1, in volts per meter ($V\ m^{-1}$)
E_{t2}	tangential component of the electric field vector in medium 2, in volts per meter ($V\ m^{-1}$)
E	electric field vector in volts per meter ($V\ m^{-1}$)
ϵ	permittivity in farads per meter ($F\ m^{-1}$)
ϵ_1	permittivity in medium 1, farads per meter ($F\ m^{-1}$)
ϵ_2	permittivity in medium 2, farads per meter ($F\ m^{-1}$)

η	efficiency
η_{dB}	efficiency in dB
η_{op}	operating efficiency
f	frequency in hertz (Hz)
F	frequency in megahertz (MHz)
ϕ	magnetic flux in webers (Wb) angle in the azimuth plane phase difference in radians (rad)
ϕ_1	half power beamwidth in the azimuth plane, in degrees
ϕ_p	phase associated with the arm of a spiral antenna, in radians (rad)
g_1	gain of horn 1 in dB
g_2	gain of horn 2 in dB
g_3	gain of horn 3 in dB
g_{dB}	gain in dB
g_p	gain of a pyramid horn in dB
G	linear or numeric gain
G_{dBi}	gain in decibels referred to isotropic (dBi)
G_e	linear or numeric gain of an E -plane sectoral horn
G_h	linear or numeric gain of an H -plane sectoral horn
G_p	linear or numeric gain of a pyramid horn
h	height of antenna distance between feed point of a dipole and its center
h	effective length/height of a half-wave dipole in meters
h_{eff}	effective length/height of the monopole in meters
H	magnetic field intensity scalar in amperes per meter (A m^{-1}) half length of a dipole in meters
H_0	amplitude of the magnetic field intensity in amperes per meter (A m^{-1})
H_ϕ	magnetic field intensity in the azimuth plane in amperes per meter (A m^{-1})
H_r	magnetic field intensity in the radial direction in amperes per meter (A m^{-1})
\mathbf{H}_t	total or resultant magnetic field intensity vector for a coil, in amperes per meter (A m^{-1})
H_θ	magnetic field intensity in the elevation plane in amperes per meter (A m^{-1})
H_{n1}	normal component of the electric field vector in medium 1, in amperes per meter (A m^{-1})
H_{n2}	normal component of the electric field vector in medium 2, in amperes per meter (A m^{-1})

H_{t1}	tangential component of the magnetic field vector in medium 1, in amperes per meter ($A\ m^{-1}$)
H_{t2}	tangential component of the magnetic field vector in medium 2, in amperes per meter ($A\ m^{-1}$)
\mathbf{H}	magnetic field intensity vector in amperes per meter ($A\ m^{-1}$)
\mathbf{i}	unit vector along x -axis in rectangular coordinate system
I	current in amperes (A)
I_1	current in the upper arm of a dipole in amperes (A) current along the inner conductor of a coaxial cable in amperes (A)
I_2	current in the lower arm of a dipole in amperes (A) current along the outer conductor of a coaxial cable in amperes (A)
I_3	current along the outside of the outer conductor of a coaxial cable in amperes (A)
$I(z)$	current at a distance z along a monopole in amperes (A)
I_{\max}	maximum current in a monopole
j	square root of -1 , imaginary axis of Argand diagram
\mathbf{j}	unit vector along x -axis in rectangular coordinate system
\mathbf{J}_d	displacement current density vector in amperes per meter ($A\ m^{-1}$)
\mathbf{J}_s	surface current density vector in amperes per meter ($A\ m^{-1}$)
\mathbf{k}	unit vector along x -axis in rectangular coordinate system
k	phase constant ($= 2\pi/\lambda$) constant that determines the start of a spiral antenna
K_2	ratio of the radial distances of the inner and outer edges of the arm of a log spiral antenna
k_3	constant (log spiral antenna)
l	length in m physical length of a monopole in meters length of a transmission line in meters
l_e	slant length of an E -plane sectoral horn
l_b	slant length of an H -plane sectoral horn
l_n	length of the n th element from the imaginary apex of a LPDA
l/d_0	length-to-diameter ratio of the element of a LPDA
L	length of a turn of a helix antenna length of a log spiral antenna slant height of the cone for a discone antenna
L_a	inductance of antenna in ohms (Ω)
L_e	loss in dB due to phase error for an E -plane sectoral horn
L_b	loss in dB due to phase error for an H -plane sectoral horn
L_{ext}	external inductance of a single turn loop in ohms (Ω)

λ	wavelength in meters
λ_g	guide wavelength in meters
λ_c	wavelength at the cut-off frequency in meters
λ_H	wavelength at the highest operating frequency in meters
λ_L	wavelength at the lowest operating frequency in meters
λ_0	free-space wavelength in meters
μ	magnetic permeability in henries per meter (H m^{-2})
μ_1	magnetic permeability in medium 1, in henries per meter (H m^{-2})
μ_2	magnetic permeability in medium 2, in henries per meter (H m^{-2})
M_t	magnitude of the correction term applied to the power output of the generator
M_m	magnitude of the correction term applied to the power measured by the power meter
M_r	magnitude of the correction term applied to the power measured by the receiver, to allow for the mismatch between the receive antenna and the receiver
\mathbf{n}	unit vector normal to a surface
N	number of turns of a coil or helical antenna
ω	angular frequency in radians per second (rad/s)
P	power in watts (W)
P_1	power in watts (W)
P_2	power in watts (W)
P_d	magnitude of power density in watts per meter (W m^{-2})
\mathbf{P}_d	Poynting's power flux density vector in watts per meter (W m^{-2})
P_g	power received by (or supplied to) generator in watts (W)
P_m	power measured by power meter in watts (W)
	linear polarization mismatch
P_{\max}	maximum power in watts (W)
P_r	received power in watts (W)
P_t	transmitted power in watts (W)
P_{rad}	radiated power in watts (W)
PF_{loss}	loss power factor
PF_{rad}	radiation power factor
r	radial distance from a radiating dipole or loop
r_1	radial distance from center of a spiral
r_2	radial distance from center of a spiral
R	length of position vector
	distance between a horn and its image, in Purcell's method
\mathbf{R}	position vector

R_a	radiation resistance of antenna in ohms (Ω)
R_e	effective resistance of antenna in ohms (Ω)
R_b	terminal resistance of a helical antenna in ohms (Ω)
Re	real part of a complex number
R_{ixt}	internal resistance of a single turn loop in ohms (Ω)
$R(kl)$	function shown in Figure 5.4
r_{15}^+	is electrical radius on the base side (of a conical log spiral) at which the magnitude of the near field is 15 dB below the maximum, at the highest frequency of operation
r_3^+	is electrical radius on the apex side (of a conical log spiral) at which the magnitude of the near field is 3 dB below the maximum, at the highest frequency of operation
r_n	distance of the front of the n th tooth from the imaginary apex of a trapezoidal tooth LPDA
R_c	cone radius of a conical log spiral antenna
R_r	radiation resistance of antenna in ohms (Ω)
ρ_e	virtual perpendicular length of an E -plane sectoral horn
ρ_b	virtual perpendicular length of an H -plane sectoral horn
ρ_s	surface charge density in coulombs per square meter ($C\ m^{-2}$)
ψ	angle between arrays of LPDAs pitch angle of a helical antenna
ψ_e	flare angle in the E -plane of a horn
ψ_b	flare angle in the H -plane of a horn
s	disk-to-cone spacing for a discone antenna
s_f	scaling factor for a LPDA
S	surface spacing between turns of a helical antenna in m
	voltage standing wave ratio (VSWR)
S_p	spacing parameter for a LPDA
$S(x)$	Fresnel sine integral
t	time in seconds
T_e	phase error/deviation in terms of wavelengths for an E -plane sectoral horn
T_b	phase error/deviation in terms of wavelengths for an H -plane sectoral horn
T_p	thickness parameter of the wire of a loop
θ	angle in the elevation plane angle between vectors
θ_1	half power beamwidth in degrees

θ_E	half power beamwidth in the E plane, in degrees
θ_H	half power beamwidth in the H plane, in degrees
τ_g	complex reflection coefficient of the generator
τ_r	complex reflection coefficient of the receive antenna
τ_s	complex reflection coefficient of the receiver
τ_t	complex reflection coefficient of the transmit antenna
ν	velocity of a EM wave in m s^{-1}
ν	velocity of a EM wave in medium 1, in m s^{-1}
ν_x	velocity in x direction in m s^{-1}
ν_y	velocity in y direction in m s^{-1}
ν_z	velocity in z direction in m s^{-1}
\mathbf{v}	velocity vector in m s^{-1}
V	voltage in volts (V)
V_l	voltage across a load in volts (V)
V_1	voltage in volts (V)
V_2	voltage in volts (V)
V_{oc}	open-circuit voltage in volts (V)
w	diameter of the feed conductor for a disccone antenna
x	abscissa, coordinate of rectangular Cartesian system variable
X_a	self reactance of antenna in ohms (Ω)
X_e	effective reactance of antenna in ohms (Ω)
$X(kl)$	function shown in Figure 5.4
ξ_0	intrinsic impedance of a free space wave
y	coordinate of rectangular Cartesian system variable
Y_0	susceptance of the waveguide of normal height propagating the TE_{10} mode
Y'_0	susceptance of the waveguide of reduced height
z	coordinate of rectangular Cartesian system
Z	input impedance of a shielded single turn loop in ohms (Ω)
Z_0	characteristic impedance in ohms (Ω)
	intrinsic impedance of a wave in ohms (Ω)
Z_a	self impedance of antenna in ohms (Ω)
	total impedance of antenna in ohms (Ω)
Z_d	impedance of a half-wave resonant dipole antenna in ohms (Ω)
Z_e	radiation impedance of antenna in ohms (Ω)
Z_E	characteristic impedance of a waveguide propagating a TE mode in ohms (Ω)
Z_f	impedance of the differential mode in ohms (Ω)

Z_H	characteristic impedance of a waveguide propagating a TM mode in ohms (Ω)
Z_{in}	input impedance of a folded dipole antenna in ohms (Ω)
Z_{int}	internal impedance of a shielded single turn loop in ohms (Ω)
Z_l	impedance of a load in ohms (Ω)
Z_r	impedance of the common mode in ohms (Ω)
Z_w	characteristic impedance of waveguide in ohms (Ω)
$Z_{\lambda/4}$	impedance of half of a resonant half-wave dipole in ohms (Ω)

About the Authors

Thereza Macnamara has 32 years of industrial experience including EMC radiated emissions, antenna and network design, and antennas on structures, and also worked as a patent examiner and lecturer.

She attained her first degree in applied physics at the University of Surrey and her master's degree in microwaves at London University. After two years of teaching physics up to the advanced level, she worked as a microwave engineer at G&E Bradley. She then worked as a research physicist for Morganite Research and Development, before returning to work as a microwave engineer at Flann Microwave Instruments, working on waveguide components and thermistor detectors. At Wayne-Kerr Laboratories and Bradley Electronics she was in charge of upgrading, maintaining, and calibrating a standard EM field facility from 400 MHz to 33 GHz. After a short break to have a family, she returned to work as an examiner at the British Patent Office and lecturing in mathematics and physics while her children were growing up.

As a senior RF engineer at ERA Technology's R&D division she designed printed circuit antennas and antenna feed networks, and developed a series for deriving the position and number of frequency invariant phase shifters for Butler matrices. She submitted a patent application for novel beamforming networks, was an adviser for patents and trademarks, and conducted computer literacy, graphics training, and technical seminars.

Her EMC experience at ERA includes RF monitoring, explosive atmospheres and EED (electroexplosive devices), expert witness calculations for the CAA, troubleshooting for the petrochemical industry to resolve problems with LOS communications and biological hazards, and is the author of a code of practice for land-based drilling. She has developed measurement techniques for shielding effectiveness (SE) in the magnetic and electric modes, as well as under plane wave conditions, and designed and successfully implemented anechoic hoods for SE measurements in the 1 GHz to 10 GHz frequency range.

Her most recent experience of 17 years with BAE Systems covers installation and integration of antennas on all platforms (land, sea, and air) from entire layouts to single retrofit installations. She was the school's ambassador to promote engineering and technical authority for numerous internal and external projects within BAE Systems, and headed the antenna team in the R&D department.

She has worked on Nimrod, Typhoon, Harrier, JSF, Hercules, and Tornado with varying degrees of involvement in the antenna and RF interoperability disciplines.

She was the technical leader/coordinator of the EU research project IPAS (Installed Performance of Antennas on AeroStructures) involving 10 European

companies, and developed an empirical formula for coupling between non-LOS antennas on aircraft.

She is the author of the first edition of *Handbook of Antennas for EMC* and a reference textbook entitled *Introduction to Antenna Placement and Installation* (Wiley 2010), as well as various papers, and also authored the section entitled “Installed Antenna Performance Design and Verification” in the Aerospace Encyclopedia as part of the Aerospace Series List. The *Handbook of Antennas for EMC* was on the indicative reading list of Glasgow Caledonian University for the antennas and propagation module.

She was the special guest lecturer at the AMTA (Antenna Measurement Techniques Association) 36th Annual Meeting & Symposium in Tucson, Arizona in 2014, and in 2016 she was selected as one of the “Inspirational Women in Engineering,” and an interview with her publisher, John Wiley and Sons, was posted on YouTube.

John McAuley attained his first degree in engineering at Ulster Polytechnic and his master’s degree in electronics at Queen’s University Belfast. After eight years as a senior engineer at Short Brothers PLC Missile Systems Division, he worked as a senior EMC engineer at ERA Technology, contributing to research projects. He then worked as EMC Centre Manager at the Irish state test laboratory, Eolas. In 1997, he was seconded to set up Compliance Engineering Ireland Ltd, and has been managing director since. For twenty years he has been chairman of the Irish National EMC and Electromagnetic Fields and the Human Health committees, and attends the European Electrotechnical (CENELEC) standards committees TC210 and TC106X. For a period of three years, while chairman of the Electrotechnical Council of Ireland, he was the president of the International Electrotechnical Committee (IEC) in Ireland. He is a notified body signatory for the European EMC and Radio Equipment Directives.

Index

A

Absolute gain, 12

Absorber-lined chambers (ALC)

absorbers, 309–14

carbon-loaded foam RAM, 310

combined ferrite and pyramidal absorber,
312–14

defined, 309

egg-box absorbers, 310–12

flat sheet RAM, 310

Absorption loss

characteristics of, 255

defined, 252–55

with relative conductivity, 257

with relative permeability, 256

skin depth and, 257

source-shield distance and, 255

theoretical, 258

See also Shielding effectiveness

Accurate method

defined, 208

E-plane gain, 210

H-plane gain, 210–11

pyramidal horn, 208

See also Gain calculation

Acronyms and abbreviations, 335–48

Ampere's law, 65

Anechoic chambers

as fully anechoic room (FAR), 315

overview, 314–15

quiet zone, 315

rectangular chambers, 315–18

tapered chambers, 316, 318

Angles

as argument, 40

convention for, 27–28, 29

cosine formula, 32, 33

defined, 27

sine formula, 32–33

trigonometric functions of, 30, 31

ANSI OATS, 320–21

Antenna correction factor

antenna factor values and, 216–17

BiLog antenna, 131

calibration and, 211–17

conical log spirals, 159, 160

defined, 15–16, 211

double-ridge horns, 182

effective antenna height and, 213

electric field and, 211

equivalent circuit of B/M network and, 215

equivalent circuit of measurement system
and, 214

intrinsic impedance and, 212

maximum power available and, 215

power density and, 212

power transfer and, 213

power transferred to B/M network and,
215

receiver resistance and, 212–13

Antennas

aperture size, 15

bandwidth, 13–15

calibration, 185–217

characteristics of, 3–26

far field, 79–81

front-to-back ratio, 13

introduction to, 1–26

main lobe, 8–12

planes of measurement, 4

polarization, 16–20

radiation pattern, 5–8

radiation resistance, 4–5

receiving and transmitting differences,
86–88

requirements for EMC, 1–3

sidelobes, 12–13

- Antennas (*Cont.*)
 types of, 2–3
See also specific antennas
- Antennas (above 1 GHz)
 Archimedes spiral, 163–65
 band theory and, 139–41
 discone antenna, 166–67
 double-ridged horns, 168–83
 frequency-independent antennas, 139
 log spiral, 141–62
 microstrip planar spiral, 165–66
 overview, 139
- Antennas (below 1 MHz)
 baluns, 88–89
 effective height, 94–95
 effective length, 93–94
 E-field, 95–101
 far fields, 84–85
 H-field, 102–9
 matching, 92–93
 mechanism of radiation, 83–85
 near fields, 84–85
 operating efficiency, 92
 overview, 83
 radiation power factor, 89–92
 small, 88
 wave impedance, 85–86
- Antennas (between 1MHz and 1 GHz)
 biconical antennas, 119–22
 BiLog antenna, 130–31
 Cavitenna, 114
 discone antenna, 112–14
 double-ridged horns, 137
 folded dipoles, 115–17
 frequency-independent antennas, 124
 helical antennas, 132–35
 large and resonant loops, 135–37
 log-periodic antennas, 124–30
 overview, 111
 resonant and large dipoles, 114–15
 resonant monopoles, 111–12
 triangular dipoles, 118–19
 Yagi-Uda antenna, 122–24
- Antenna theory
 boundary conditions, 70–73
 far field, 79–81
 fields due to radiating dipole, 73–75
 Maxwell's equations, 64–70
 overview, 57
 power flux density for plane wave, 75–78
 radiation resistance, 78–79
 scalar and vector fields, 59–64
 unit vectors, 57–59
 wave impedance for plane wave, 78
- Antenna validation factor (AVF), 330
- Aperture
 circular, 21–22, 24–26
 defined, 15
 rectangular, 20, 24
- Aperture antennas, 79–81
- Aperture size
 beamwidth from, 22–23
 defined, 15
 gain from, 23–26
- Approximate gain calculation, 209, 211
- Archimedes spiral
 cavity-backed, 163–65
 cavity depth and, 165
 defined, 163
 feeding arrangements, 164–65
 gain variation, 164, 165
 illustrated, 163
 printed circuit balun, 163, 165
See also Spiral antennas
- Argand diagram, 39
- Argument, 40
- Azimuth plane, 4
- B**
- Baluns, 88–89
- Band theory
 deterioration in axial ratio and, 140
 illustrated, 141
 use of, 139
- Bandwidth
 defined, 13
 double-ridged waveguides, 176–77
 expression methods, 14
 as fraction or multiple of an octave, 15
 percentage, 14–15
- Beamwidth
 from aperture size and shape, 22–23
 defined, 8–9
 definition of, 9–10
 gain from, 20–22
 half-power (HPBW), 127, 133–34, 151–52
 straight-toothed trapezoidal tooth LP, 129
 10-dB, 9, 10
 3-dB, 9, 10
- Biconical antennas
 broadband impedance characteristics, 121

- from coaxial cable, 121
- cone half angle, 122
- defined, 119
- feeding details, 119
- of half angle, 121
- illustrated, 119
- intrinsic impedance, 121
- Maxwell's equations and, 120
- radiation pattern, 119
- BiLog antenna
 - antenna correction factors, 131
 - defined, 130
 - power requirements, 131
 - radiation pattern, 130
- Boundary conditions
 - circular waveguides, 299
 - at interface of two media, 71
 - normal component of electric field, 72–73
 - normal component of magnetic field, 73
 - tangential component of electric field, 70–71
 - tangential component of magnetic field, 71–72
- Bowtie antennas, 118–19
- C**
- Calibration
 - antenna correction factor and, 211–17
 - calculation of gain and, 196–209
 - example, 209–11
 - gain and, 185–96
 - square Crawford cell, 290
- Carbon-loaded foam RAM, 310, 311
- Cavitenna, 114
- Cavity-backed Archimedes spiral, 163–65
- Cavity-backed spiral, 153
- Chamber loading factor (CLF), 330
- Chamber validation factor (CVF), 329
- Characteristic impedance
 - circular coaxial line, 280
 - gigahertz TEM (GTEM) cells, 296–97
 - rectangular cross section coaxial line, 283
 - TEM transmission lines, 276–77
- Circular aperture
 - with nonuniform illumination, 21–22, 25–26
 - with uniform illumination, 21, 25
- Circular coaxial lines, 280–82
- Circular coaxial TEM cells
 - continuous-conductor, 285–86
 - defined, 285
 - flanged, 287–88
 - illustrated, 288
- Circular polarization, 18, 19
- Circular waveguides
 - attenuation of evanescent modes, 301
 - boundary conditions, 299
 - cut-off, 303–4
 - fundamental mode, 300
 - modes in, 299–305
- Class A equipment, 222–23
- Class B equipment, 222–23
- Clean time, 264
- Coaxial lines
 - characteristic impedance, 280
 - circular, 280–82
 - higher-order modes in, 281
 - overview, 280
 - rectangular, 282–83
 - square, 282–83
 - See also* TEM transmission lines
- Combined balun/transformer, 93
- Combined ferrite and pyramidal absorbers, 312–14
- Common-mode radiated emissions, 221, 222
- Complex numbers
 - addition of, 40–41
 - complex conjugate, 42
 - polar representation of, 41
- Computer equipment, classes of, 222–23
- Conducted immunity
 - with bulk current injection, 230
 - with CDN, 230
 - common and differential-mode voltages, 235–36
 - defined, 229
 - with electromagnetic clamp, 231
 - line, using LISN, 234
 - overview, 229
 - test methods, 230
- Conduction current density, 65
- Conductive coupling, 234
- Conductivities, of common metals, 353
- Conical log spiral, 20–21
- Conical log spirals
 - active region, 156
 - antenna correction factor, 159, 160
 - bandwidth, 156–57
 - defined, 153–54
 - directivity, 157, 159
 - excited at apex, 154

- Conical log spirals (*Cont.*)
 with frequency-independent antennas, 156
 gain variation and, 159, 160
 HPBW, 157–59
 illustrated, 154
 input impedance, 160–61
 phase center, 161–62
 radiation characteristics, 157–60
 radiation pattern variation, 162
 rate of spiral, 155
 self-complementary, 158
 two-armed, 155
- Conjugate matching, 42
- Continuous-conductor TEM cell, 285–86
- Conversion table, 357–61
- Cosine formula, 32, 33
- Coupling/decoupling network (CDN), 230, 236
- Crawford cells
 defined, 289
 rectangular, 291
 square, 289–91, 293
See also TEM cells
- Cross product
 defined, 44
 unit vectors, 58–59
 of vectors, 44–46
- Curl of vector, 62–64
- Cut-off frequencies
 predicted, commercially available TEM cells, 296
 predicted, NBS Crawford cells, 296
 of rectangular and square cells, 292–95
 TE modes, 294
- Cut-off waveguides
 circular, 303–4
 polygonal cross section, 302–3
 rectangular, 302–3
 square, 302–3
 ventilation panels, 300
- D**
- dBm and dBmV relationship, 36
- $\text{dB}\mu\text{V}$ conversion table, 357–61
- Degeneracy, 306
- Degradation, 219
- Dielectric constants, of common materials, 355
- Differential-mode radiated emissions, 221, 222
- Dimensions
 checking formulas for, 55
 of commonly used physical quantities, 54
 defined, 52
- Dipoles
 folded, 115–17
 large, 114–15
 resonant, 114–15
 small, 96–97
 triangular, 118–19
- Direct ESD, 269
- Directional antennas
 defined, 2
 illustrated, 3
- Directivity
 of antenna, 11
 defined, 10, 186
 gain versus, 185–86
 linear, 20
 in physical media, 11
- Discone antenna
 defined, 112
 disk-to-cone spacing, 113
 flare angles, 167
 in one to two GHz frequency range, 166
 physical characteristics, 113
 radiation pattern, 113–14
 with snap-on N-type connector, 167
- Displacement current density, 65–66
- Divergence
 of magnetic flux density, 69
 of vector field, 61–62
- Dot product, 44, 45
- Double-inductive transformer, 93
- Double-ridged horns
 antenna correction factor, 182
 antennas (above 1 GHz), 168–83
 antennas (between 1MHz and 1 GHz), 137
 cut-off wavelengths, 179, 180, 181
 defined, 177
 gain, 182
 high powers and, 180
 HPBW, 180–83
 maximum useable bandwidth, 180, 181
 overview, 168
 ridge fabrication, 177
 waveguide theory and, 168–71
- Double-ridged waveguides
 bandwidth, 176–77
 cut-off frequency, 177
 defined, 175

equivalent circuit, 178
illustrated, 178
Dual TEM cell (DTC)
defined, 295–96
set-up, 297
use of, 296
DuHammel's trapezoidal tooth LP, 129

E

Effective gain. *See* Gain
Effective height
antennas (below 1 MHz), 94–95
defined, 94
use of term, 94–95
Effective length
antennas (below 1 MHz), 93–94
defined, 93–94
top-loaded monopoles, 98–99
E-field antennas
defined, 95
ground plane dependence, 98
parallel element generator, 101
short monopoles, 97–98
small dipole, 96–97
top-loaded monopoles, 98–101
Egg-box absorbers, 310–12
Electrical fast transients (EFT), 231–32
Electric field probe, 291
Electric fields
normal component of, 72–73
shielding effectiveness for, 237
tangential component of, 70–71
Electric flux density, 66
Electric mode reflection loss
characteristics of, 248
defined, 247
at low frequencies, 251
material resistivity and, 251
with relative conductivity, 253, 254
with relative permeability, 253
SE measurements, 263
source-shield distance, 248, 251
theoretical, 252, 254
variation of, 249–50
See also Reflection loss
Electromagnetic interference (EMI)
IEC standards, 223–24
radiated, measuring, 223–28
use of, 219
Electromagnetic spectrum, 363

Electromotive force (EMF), 35, 67
Electrostatic discharge (ESD)
component sensitivity, 268
defined, 219
direct, 269
discovery, 266–67
human, waveform and spectrum for, 268
immunity to, 233
indirect, 269
man-made materials and, 267
models, 269
range of susceptibility, 270
spectrum, 267–68
susceptibility testing, 269–70
variation of voltage magnitude, 267
Elevation plane, 4
Elliptical polarization, 18–19, 20
EMC
antenna requirements for, 1–3
compliance standards, 220
compliance to regulations, 219
engineers, math for, 27–55
EMC measurements
conducted emissions and immunity, 234–36
electrostatic discharge (ESD) and, 266–70
instrumentation, 270–71
introduction to, 219–71
overview, 219–20
radiated emissions, 220–28
radiated susceptibility and immunity,
228–33
shielding effectiveness and, 220
shielding effectiveness measurement and,
262–66
shielding effectiveness of solid materials
and, 236–61
EM field equations. *See* Maxwell's equations
EM fields
due to current element, 74–75
due to radiating dipole, 73–75
at large distances from wire antennas, 75
E-plane sectoral horn
defined, 197
efficiency of, 199
gain calculation and, 197–202
gain of, 201–2
illustrated, 198
loss due to phase error, 199–201
maximum gain, 200
normalized gain for, 203
phase deviation and loss in gain and, 197

E-plane sectoral horn (*Cont.*)
 variation of flare length, 200–201
 variation of loss with phase deviation, 199
 Equipment under test (EUT)
 antenna placement and, 224
 in radiated emissions, 221
 rotation of, 225, 318
 testing, 329–30
 verification, 329
 Equivalent circuits, 89

F

Faraday's law, 67
 Far field
 antennas (below 1 MHz), 84–85
 for aperture antennas, 79–81
 defined, 79
 for wire antennas, 79
 FCC radiated electric field limits, 224
 First equation, Maxwell's, 65–67
 Flanged coaxial TEM cell, 287–88
 Flat sheet RAM, 310, 311
 Folded dipoles
 from coaxial cable, 116
 defined, 115
 equivalent circuit, 116, 117
 excitation of, 116–17
 half-wave, 117
 input impedance, 117
 physical characteristics, 116
 twin wire transmission lines, 116
 Fourier analysis, 48, 49
 Fourier transforms
 defined, 48–50
 illustrated, 51
 uses of, 50
 Fourth equation, Maxwell's, 69–70
 Fraunhofer region, 80
 Free space, plane wave in, 85
 Free-space field, 332–33
 Free space open area test site (FSOATS)
 defined, 315, 322
 qualification of, 322
 theoretical site attenuation factors, 322–23
See also Open area test sites (OATS)
 Frequency band designations, 365
 Frequency-independent antennas, 124, 139
 Fresnel cosine and sine integrals, 201–2, 207
 Fresnel zones, 80

Friis transmission formula
 correction term, 189–90
 defined, 188
 multipath effects and, 190
 near-field effects and, 190
 received power and, 189
 Front-to-back ratio, 13
 Fully anechoic room (FAR)
 absorbers, 315
 defined, 315
 test volume in, 317

G

Gain
 absolute, 12
 from aperture size and shape, 23–26
 Archimedes spiral, 164, 165
 from beamwidth, 20–22
 conical log spiral variation, 159, 160
 conversion table, 367
 defined, 10, 185–86
 directivity versus, 185–86
 double-ridged horns, 165, 182
 of *E*-plane sectoral horn, 201–2
 of *H*-plane sectoral horn, 206–7
 linear, 367
 overview, 186
 relative, 11–12
 Yagi-Uda antenna variation, 159
 Gain calculation
E-plane sectoral horn, 197–202
H-plane sectoral horn, 202–7
 overview, 196–97
 in pyramidal horn, 207–9
 Gain measurement
 Friis transmission formula, 187–90
 Purcell's method, 191
 space attenuation versus distance and,
 188
 three-antenna method, 195–96
 two-antenna method, 187, 195
 Gauss' theorem, 68–69
 Gigahertz TEM (GTEM) cells
 characteristic impedance, 296–97
 defined, 296
 illustrated, 299
 RF absorbers, 299
 schematic, 298
 septum, 298

- Gradients
 - of scalar fields, 59–61
 - writing, 60
- Ground plane dependence, E-field antennas, 98
- Guided wave SE measurements, 265
- H**
- Half-power (HPBW)
 - conical log spirals, 157–59
 - double-ridged horns, 180–83
 - helical antennas, 133–34
 - slot planar log spiral, 151, 152
- Helical antennas
 - cavity-backed helices, 132, 134
 - characteristics of, 133
 - circumference, 134–35
 - conductors, 132
 - defined, 132
 - HPBW, 133–34
 - mode patterns, 133
 - radiation pattern, 135
 - VSWR, 133
- Helmholtz coils, 102–4
- H-field antennas
 - Helmholtz coils, 102–4
 - overview, 102
 - simple multiturn loop probe, 108–9
 - single-turn shielded loops, 106–7
 - small magnetic loops, 104–5
- Honeycomb air vents, 304–5
- H*-plane sectoral horn
 - defined, 202
 - dielectric loading of, 203
 - gain of, 206–7
 - illustrated, 204
 - loss due to phase error, 203–6
 - maximum gain, 205
 - normalized gain for, 207
 - overview, 202–3
 - variation of flare length, 205–6
 - variation of loss with phase deviation, 205
 - virtual flare length, 206
- I**
- IEC/EN 61000-4-3, 228
- Immunity
 - conducted arrangement using bulk current injection, 230
 - conducted arrangement using CDN, 230
 - conducted arrangement using electromagnetic clamp, 231
 - to conducted radiated interference, 229–31
 - to electrical fast transients (EFT), 231–32
 - to electrostatic discharges, 233
 - magnetic field, 231
 - to radiated electric field strength, 229
 - testing, 331
- Indirect ESD, 269
- Inductance-capacitance-resistance (ICR) network, 4
- Input impedance
 - conical log spirals, 160–61
 - folded dipoles, 117
 - slot planar log spiral, 147
- Instrumentation
 - measuring receivers, 270
 - spectrum analyzers, 271
- International Electrotechnical Commission (IEC)
 - degradation definition, 219
 - immunity to radiated electric field strength, 229
 - susceptibility definition, 228
 - test levels, 228
- Inverse trigonometric functions, 32–33
- Isotropic antennas, 2
- J**
- Jacobian elliptical functions, 283
- K**
- Kandoian antenna, 112–14, 166–67
- L**
- Large dipoles, 114–15
- Large loops, 135–37
- Linear gain, 367
- Linear polarization, 17
- Line conductive emissions, 235
- Logarithms
 - in multiplication of numbers, 34
 - natural, 34
 - rule, 34–35

- Log-periodic antennas
 defined, 124
 design bandwidth, 128
 frequencies, 127
 half-power beamwidths (HPBW), 127
 log-periodic dipole array (LPDA), 124, 125, 127, 129
 number of elements, 128
 optimum scaling factor, 127
 properties of, 126
 radiation pattern, 125
 range of spacing parameters, 127–28
 spacing parameter, 125, 126, 128
 trapezoidal tooth, 129–30
- Log-periodic dipole array (LPDA), 124, 125, 127, 129
- Log spirals
 arms, 145
 cavity-backed spiral, 153
 changing current with time and, 141–42
 conical, 153–62
 loosely wound, 145
 modes of radiation, 145–46
 planar, 143
 planar log spirals, 146–47
 radiation pattern, 145
 rate of change of radius vector, 144
 rotation of radiation pattern, 146
 slot planar, 147–53
 types of, 141
 velocity vectors, 143
 width of conductors, 144
See also Spiral antennas
- Loss tangents, of common materials, 355
- M**
- Magnetic field intensity, 66
- Magnetic fields
 immunity, 231
 normal component of, 72–73
 tangential component of, 71–72
- Magnetic flux density, 69–70
- Magnetic mode reflection loss
 defined, 239
 dependence of R_b , 246–47
 overview, 239–40
 with permeability, 240–42
 relative conductivity, 244–46
 with relative permeability and relative conductivity, 242–44, 245–47
 SE measurements, 262
 with source-shield distance, 242–44
 theoretical, 241
See also Reflection loss
- Main lobe
 beamwidth, 8–10
 boresight directivity/gain, 10–12
 defined, 8
 illustrated, 9
- Matching antennas, 92–93
- Math, for EMC engineers
 angles, 27–28
 Fourier analysis and transforms, 48–50, 51
 fundamental units and dimensions, 52–55
 overview, 27
 parameters, 50–52
 powers, indices, and logarithms, 33–36
 real and complex numbers, 36–42
 scalars and vectors, 42–48
 trigonometry, 28–33
- Maxwell, James Clerk, 62, 65
- Maxwell's equations
 defined, 64
 in deriving component fields, 74–75
 as EM field equations, 65
 first equation, 65–67
 fourth equation, 69–70
 overview, 64–65
 second equation, 67–68
 third equation, 68–69
- Measuring receivers, 270
- Metals
 conductivities of, 353
 magnetic permeabilities of, 373
- Microstrip planar spiral, 165–66
- MIL-STD 461, 229
- Minimum sweep time, 331–32
- Mirror method. *See* Purcell's method
- Mode stirrers, 306–7
- Modulus, 39
- Monopoles
 radiation pattern for, 99
 resonant, 111–12
 short, 97–98
 top-loaded, 98–101
- Multipath effects, 190
- Multiple reflection loss, 257–58
- N**
- Natural logarithms, 34
- Navigation, angle convention for, 28
- Near-field effects, 190

- Near fields, 84–85
- Normal component
 - of electric field, 72–73
 - of magnetic field, 72–73
- Numbers
 - complex, 40–42
 - multiplication of, 34–35
 - real, 36–40
- O**
- Omnidirectional antennas
 - defined, 2
 - illustrated, 3
- Open area test sites (OATS)
 - ANSI, 320–21
 - attenuation factor, 321
 - covered, 318
 - defined, 318
 - ellipse size, 319
 - FCC set-up for site attenuation, 320
 - first Fresnel ellipse, 319–20
 - freedom from obstructions, 321
 - free-space (FSOATS), 322–23
 - geometrical optical model, 227
 - in measurement of radiated emissions, 221, 226–28
 - minimum size of ground plane, 320
 - NSA measurement, 322
 - size and shape of, 319
 - uncovered, 318
- Operating efficiency, 92
- P**
- Parallel element E-field generator, 101
- Parallelogram rule, 42, 43
- Parallel plate cells, 287
- Parallel plate transmission lines, 278–79
- Parallel stripline cells
 - defined, 283
 - illustrated, 284
 - in MIL-STD 461G, 285
 - with trellis, 285
 - See also* TEM cells
- Parameters
 - mathematical definition of, 50–52
 - used by engineers, 52, 53
- Percentage bandwidth, 14–15
- Periodic table (alphabetically by symbol), 369–71
- Permeability, 240–42
- Phase center
 - conical log spirals, 161–62
 - defined, 161
- Phasors
 - addition of waveforms with, 47
 - defined, 46
 - use of vectors as, 46–48
- Planar log spirals
 - current attenuation, 143
 - defined, 146
 - illustrated, 147
 - slot, 147
 - variation of radiation pattern, 153
- Plane wave reflection loss
 - characteristics of, 252
 - defined, 252
- Plane waves
 - in free space, 85
 - power flux density for, 75–78
 - wave impedance for, 78
- Plane wave SE measurements
 - clean time, 264
 - guided wave, 265–66
 - rectangular TEM cell for, 266
 - time domain free-space, 264
- Polarization
 - circular, 18, 19
 - defined, 16–20
 - elliptical, 18–19, 20
 - linear, 17
 - sense of, 19
- Polarization matching matrix, 375
- Polar plots, 7–8
- Polygonal cross section cut-off waveguides, 302–3
- Position vectors, 42
- Power density
 - antenna correction factor and, 212
 - average, 77
 - radiation resistance and, 79
- Power flux density
 - defined, 75–78
 - illustrated, 76
 - magnitude, 76
 - for plane wave, 75–78
 - TEM waves, 274–75
- Powers, indices, and logarithms, 33–36
- Poynting's power flux vector, 55
- Purcell's method
 - defined, 191–92

- Purcell's method (*Cont.*)
 illustrated, 192
 measured results, 194
 measurement set-up, 192
 procedural steps, 193
 reflection coefficient magnitude, 194
 sheet, 192–93
 single-frequency measurements, 193
See also Gain measurement
- Pyramid absorber, 310–12
- Pyramidal horn
 accurate gain calculation, 208
 approximate method, 209
 gain in, 207–9
 semi-accurate gain calculation, 208–9
- Q**
- Quadratic functions, 37, 38
- Quiet zone, 315
- R**
- Radiated emissions
 CISPR 32/EN 55022 radiated electric field limits, 225, 226
 CISPR 32/EN 55032 radiated limits, 226, 227, 228
 classes of computer equipment, 222–23
 common-mode, 221, 222
 differential-mode, 221, 222
 FCC electric field limits, 224
 free-space facilities, 227
 free-space field, 332–33
 measurement of, 221–22, 331–33
 measuring radiated EMI and, 223–28
 minimum dwell time, 332
 minimum sweep time, 331–32
 overview, 220–21
 ray diagram for measurement, 227
- Radiation pattern
 backlobe, 14
 biconical antennas, 119
 BiLog antenna, 130
 conical log spirals, 162
 defined, 5
 discone antenna, 113–14
 helical antennas, 135
 large dipoles, 115
 log-periodic dipole array (LPDA), 125
 log spirals, 145, 146
 measurement of, 5–6
 for monopoles, 99
 peculiarity, 5
 plotting, 6
 polar plots, 7–8
 rectangular/Cartesian plots, 6–7
 resonant dipoles, 115
 resonant monopole, 112
 showing sidelobe levels, 12
 slot planar log spiral, 151
 Yagi-Uda antenna, 123
- Radiation power factor
 antennas (below 1 MHz), 89–92
 defined, 89
 operating efficiency, 92
- Radiation resistance
 of current element, 78
 defined, 4, 78
 power density and, 79
 tuning circuits, 5
- Radio frequency protection guides, 379
- RAM (radar absorbing material)
 carbon-loaded foam, 310, 311
 combined ferrite and pyramidal, 312–14
 defined, 309
 flat sheet, 310, 311
 overview, 310
 pyramid, 310–12
 reflectivity of, 314
- Real numbers, 36–40
- Receiving antennas
 current distribution on, 87
 transmitting antenna differences, 86–88
- Reciprocal trigonometric functions, 28
- Rectangular aperture, 20, 24
- Rectangular/Cartesian plots, 6–7
- Rectangular chambers
 defined, 315
 FAR, 315, 317
 FSOATS, 315
 illustrated, 316
 location of antenna position, 317
 site validation, 316
See also Anechoic chambers
- Rectangular coaxial lines, 282–83
- Rectangular Crawford cell
 cut-off frequency of, 292–95
 defined, 291
- Rectangular horn, 21, 23–24

- Rectangular waveguides
 - attenuation of modes, 175
 - cut-off, 302–3
 - cutoff frequencies, 174
 - designations, 175, 176
 - dimensions, 174, 176
 - electric field modes, 171–72
 - frequencies and choosing, 172
 - magnetic field modes, 172
 - modes in, 171–75
 - propagation of modes, 173
 - Reflection loss
 - electric mode, 247–51
 - illustrated, 239
 - magnetic mode, 239–47
 - multiple, 257–58
 - plane wave, 252, 253–54
 - types of, 238
 - wave incident type and, 238
 - See also* Shielding effectiveness
 - Relative conductivity, 244–46
 - Relative gain, 11–12
 - Resistivities, of common materials, 377
 - Resonant cavities
 - defined, 305
 - degeneracy, 306
 - formulation, 305–6
 - mode stirrers, 306–7
 - TE modes, 308
 - Resonant dipoles, 114–15
 - Resonant loops, 135–36
 - Resonant monopoles, 111–12
 - Reverberation chambers
 - advantages of, 324
 - antenna validation factor (AVF), 330
 - chamber loading factor (CLF), 330
 - chamber validation factor (CVF), 329
 - defined, 323
 - frequency of operation, 323
 - immunity testing, 331
 - layout, 325
 - paddle stirrer illustration, 325
 - performance definition, 326
 - requirements, 326–27
 - side elevation view, 326
 - standard deviation of E field, 327
 - stirrer dimension, 324
 - stirrer rotation, 324
 - suitability, 324–25
 - testing and EUT and, 329–30
 - validation frequency, 328–29
 - validation procedure, 327–29
- S**
- Scalar fields
 - gradient of, 59–61
 - spatial rates of change, 59
 - Scalar product, 44, 45
 - Scalars, 42
 - Scientific constants, 351
 - Scientific prefixes, preferred, 349
 - Screened rooms, 307–9
 - Second equation, Maxwell's, 67–68
 - Self-impedance, 4
 - Semi-accurate gain calculation, 208–9, 211
 - Shielded rooms
 - absorber-lined chambers (ALCs), 309–14
 - anechoic chambers, 314–18
 - screened, 307–9
 - types of, 307
 - unlined shielded, 307–9
 - use of, 307
 - Shielded single-turn loops, 106–7
 - Shielding effectiveness
 - absorption loss, 252–57
 - defined, 220
 - dependencies, 236
 - for electric field, 237
 - E*-mode measurements, 263
 - grounding and, 236
 - guided wave SE measurements, 265
 - H*-mode measurements, 262
 - measurement of, 262–66
 - multiple reflection loss, 257–58
 - plane wave measurements, 263–66
 - reflection loss, 238–52
 - of solid materials, 236–61
 - total, 258–61
 - ventilation holes, 266
 - Short monopoles, 97–98
 - Sidelobes
 - defined, 12
 - illustrated, 12
 - levels, 12–13
 - position, 13
 - Simple multiturn loop probe, 108–9
 - Single-turn loop, 136
 - Single-turn shielded loops, 106–7
 - SI units, 52, 53, 55

- Slot planar log spiral
 - arm length of the spiral, 148–49
 - feeding arrangements, 148, 150–53
 - figure of merit, 150
 - HPBW, 151, 152
 - input impedance, 147
 - radiation pattern, 151
 - Small antennas, below 1 Mhz, 88
 - Small dipoles, 96–97
 - Small magnetic loops, 104–5
 - Source-shield distance, 242–44
 - Spectrum analyzers, 271
 - Spiral antennas
 - Archimedes spiral, 163–65
 - band theory and, 139–41
 - behavior, 139–40
 - log spiral, 141–62
 - microstrip planar spiral, 165–66
 - resultant electric field from, 142
 - Square coaxial lines, 282–83
 - Square Crawford cell
 - calibration, 290
 - cut-off frequency of, 292–95
 - defined, 289
 - illustrated, 293
 - use of, 290
 - Square cut-off waveguides, 302–3
 - Square root, 38
 - Stokes' theorem, 66, 68
 - Straight-toothed trapezoidal tooth LP, 129
 - Stripline cells. *See* Parallel stripline cells
 - Susceptance, 40–41
 - Susceptibility
 - defined, 228
 - ESD, 269–70
 - measurement of, 229
 - Symbols, list of, 381–89
- T**
- Tangential component
 - of electric field, 70–71
 - of magnetic field, 71–72
 - Tapered chambers, 316, 318
 - TEM cells
 - circular coaxial, 285–88
 - continuous-conductor, 285–86
 - cut-off frequency of, 292–95
 - defined, 283
 - dual (DTC), 295–96, 297
 - flanged coaxial, 287–88
 - gigahertz (GTEM), 296–99
 - illustrated, 286
 - parallel stripline, 283–85
 - rectangular Crawford, 291
 - square Crawford, 289–91, 293
 - validation points for, 292
 - TE modes, 171–72
 - TEMPEST standards, 228
 - TEM transmission lines
 - balanced, equivalent circuit, 278
 - characteristic impedance, 276–77
 - coaxial, 280–83
 - conductors, 276
 - parallel plate, 278–79
 - wave propagation in, 277
 - TEM waves
 - defined, 273
 - existence of, 283
 - in free space, 276
 - overview, 273
 - power flux density, 274–75
 - propagation, 273, 277, 279
 - transmission lines that support, 276–83
 - wave impedance, 275–76
 - Test levels, 228
 - Third equation, Maxwell's, 68–69
 - Three-antenna method, 195–96
 - TM modes, 172
 - Top-loaded monopoles
 - defined, 98
 - effective length, 98–99
 - types of, 100
 - Total antenna impedance, 91
 - Total shielding effectiveness
 - defined, 258
 - E*-mode, relative permeability and relative conductivity, 259
 - H*-mode, relative permeability and relative conductivity, 259
 - plane wave, relative permeability and relative conductivity, 260
 - theoretical, 260–61
 - Transmitting antennas
 - current distribution on, 87
 - receiving antenna differences, 86–88
 - top-loaded monopoles, 99
 - Trapezoidal tooth log-periodic antenna, 129–30
 - Triangle rule, 42–43

Triangular dipoles, 118–19
Trigonometric functions
 of angle, 30, 31
 defined, 28
 inverse, 32–33
 reciprocal, 28
 variations of, 28, 31
Trigonometric identities, 32
Trigonometry, 31
Tuning circuits, 4, 5
Two-antenna method, 187, 195

U

Units, fundamental, 52, 53
Unit vectors
 cross product, 58–59
 defined, 57
 illustrated, 58
 use of vectors as, 57
Unlined shielded rooms, 307–9

V

Vector fields
 divergence of, 61–62
 spatial rates of change, 59
Vector product, 44, 45
Vectors
 addition, 42–43
 cross product of, 44–46
 curl of, 62–64
 dot product of, 44, 45
 multiplication, 44–45
 parallelogram rule, 42, 43
 phasors, 46–48
 position, 42

 subtraction, 42–43
 triangle rule, 42–43
 unit, 57–59
 velocity, 143
Velocity vectors, 143
Ventilation holes, 266
Ventilation panels, 300–305

W

Waveguides
 circular, 299–305
 double-ridged, 175–77
 rectangular, modes in, 171–75
 square, modes in, 171–75
 types of, 168
 wave propagation in, 168, 169
Waveguide theory, 168–71
Wave impedance
 antennas (below 1 MHz), 85–86
 for plane wave, 78
 TEM waves, 275–76
 variations with distance from source, 86
Wire antennas
 EM fields at large distances from, 75
 far field for, 79

Y

Yagi-Uda antenna
 defined, 122
 gains, 123
 illustrated, 123
 measured and computed results comparison,
 124
 radiation pattern, 123
 uniform array, 123

**Recent Titles in the Artech House
Antennas and Electromagnetics Analysis Library**

Christos Christodoulou, Series Editor

Adaptive Array Measurements in Communications, M. A. Halim

Advanced Computational Electromagnetic Methods and Applications,
Wenhua Yu, Wenxing Li, Atef Elsherbeni, Yahya Rahmat-Samii, editors

*Advances in Computational Electrodynamics: The Finite-Difference Time-Domain
Method*, Allen Taflove, editor

*Advances in FDTD Computational Electrodynamics: Photonics and
Nanotechnology*, Allen Taflove, editor; Ardavan Oskooi and
Steven G. Johnson, coeditors

Analysis Methods for Electromagnetic Wave Problems, Volume 2,
Eikichi Yamashita, editor

Antenna Design for Cognitive Radio, Youssef Tawk, Joseph Costantine, and
Christos Christodoulou

Antenna Design with Fiber Optics, A. Kumar

*Antenna Engineering Using Physical Optics: Practical CAD Techniques and
Software*, Leo Diaz and Thomas Milligan

*Antennas and Propagation for Body-Centric Wireless Communications, Second
Edition*, Peter S. Hall and Yang Hao, editors

Antennas and Site Engineering for Mobile Radio Networks, Bruno Delorme

Antennas for Small Mobile Terminals, Kyohei Fujimoto and Koichi Ito, editors

Analysis of Radome-Enclosed Antennas, Second Edition, Dennis J. Kozakoff

Applications of Neural Networks in Electromagnetics, Christos Christodoulou and
Michael Georgiopoulos

The Art and Science of Ultrawideband Antennas, Second Edition, Hans G. Schantz

AWAS for Windows Version 2.0: Analysis of Wire Antennas and Scatterers,
Antonije R. Djordjević, et al.

Broadband Microstrip Antennas, Girsh Kumar and K. P. Ray

Broadband Patch Antennas, Jean-François Zürcher and Fred E. Gardiol

CAD of Microstrip Antennas for Wireless Applications, Robert A. Sainati

The CG-FFT Method: Application of Signal Processing Techniques to Electromagnetics, Manuel F. Cátedra, et al.

Computational Electrodynamics: The Finite-Difference Time-Domain Method, Third Edition, Allen Taflove and Susan C. Hagness

Design and Applications of Active Integrated Antennas, Mohammad S. Sharawi and Oualid Hammi

Electromagnetics and Antenna Technology, Alan J. Fenn

Electromagnetic Modeling of Composite Metallic and Dielectric Structures, Branko M. Kolundzija and Antonije R. Djordjevic

Electromagnetic Waves in Chiral and Bi-Isotropic Media, I. V. Lindell, et al.

Electromagnetics, Microwave Circuit and Antenna Design for Communications Engineering, Peter Russer

Engineering Applications of the Modulated Scatterer Technique, Jean-Charles Bolomey and Fred E. Gardiol

Fast and Efficient Algorithms in Computational Electromagnetics, Weng Cho Chew, et al., editors

Frequency-Agile Antennas for Wireless Communications, Aldo Petosa

Fresnel Zones in Wireless Links, Zone Plate Lenses and Antennas, Hristo D. Hristov

Handbook of Antennas for EMC, Second Edition, Thereza Macnamara with John McAuley

Handbook of Reflector Antennas and Feed Systems, Volume I: Theory and Design of Reflectors, Satish Sharma, Sudhakar Rao, and Lotfollah Shafai, editors

Handbook of Reflector Antennas and Feed Systems, Volume II: Feed Systems, Lotfollah Shafai, Satish Sharma, and Sudhakar Rao, editors

Handbook of Reflector Antennas and Feed Systems, Volume III: Applications of Reflectors, Sudhakar Rao, Lotfollah Shafai, and Satish Sharma, editors

Introduction to Antenna Analysis Using EM Simulators, Hiroaki Kogure, Yoshie Kogure, and James C. Rautio

Iterative and Self-Adaptive Finite-Elements in Electromagnetic Modeling, Magdalena Salazar-Palma, et al.

LONRS: Low-Noise Receiving Systems Performance and Analysis Toolkit, Charles T. Stelzried, Macgregor S. Reid, and Arthur J. Freiley

Measurement of Mobile Antenna Systems, Second Edition, Hiroyuki Arai

Microstrip Antenna Design Handbook, Ramesh Garg, et al.

Microwave and Millimeter-Wave Remote Sensing for Security Applications, Jeffrey A. Nanzer

Mobile Antenna Systems Handbook, Third Edition, Kyohei Fujimoto, editor

Multiband Integrated Antennas for 4G Terminals, David A. Sánchez-Hernández, editor

New Foundations for Applied Electromagnetics: The Spatial Structure of Fields, Said Mikki and Yahia Antar

Noise Temperature Theory and Applications for Deep Space Communications Antenna Systems, Tom Y. Otoshi

Phased Array Antenna Handbook, Third Edition, Robert J. Mailloux

Phased Array Antennas with Optimized Element Patterns, Sergei P. Skobelev

Plasma Antennas, Theodore Anderson

Polarization in Electromagnetic Systems, Second Edition, Warren Stutzman

Printed MIMO Antenna Engineering, Mohammad S. Sharawi

Quick Finite Elements for Electromagnetic Waves, Giuseppe Pelosi, Roberto Coccioli, and Stefano Selleri

Radiowave Propagation and Antennas for Personal Communications, Third Edition, Kazimierz Siwiak

Reflectarray Antennas: Analysis, Design, Fabrication and Measurement, Jafar Shaker, Mohammad Reza Chaharmir, and Jonathan Ethier

RF Coaxial Slot Radiators: Modeling, Measurements, and Applications, Kok Yeow You

Solid Dielectric Horn Antennas, Carlos Salema, Carlos Fernandes, and Rama Kant Jha

Switched Parasitic Antennas for Cellular Communications, David V. Thiel and Stephanie Smith

Ultrawideband Antennas for Microwave Imaging Systems, Tayeb A. Denidni and Gijo Augustin

Ultrawideband Short-Pulse Radio Systems, V. I. Koshelev, Yu. I. Buyanov, and V. P. Belichenko

Understanding Electromagnetic Scattering Using the Moment Method: A Practical Approach, Randy Bancroft

Wavelet Applications in Engineering Electromagnetics, Tapan Sarkar, Magdalena Salazar Palma, and Michael C. Wicks

For further information on these and other Artech House titles, including previously considered out-of-print books now available through our In-Print-Forever® (IPF®) program, contact:

Artech House
685 Canton Street
Norwood, MA 02062
Phone: 781-769-9750
Fax: 781-769-6334
e-mail: artech@artechhouse.com

Artech House
16 Sussex Street
London SW1V HRW UK
Phone: +44 (0)20 7596-8750
Fax: +44 (0)20 7630 0166
e-mail: artech-uk@artechhouse.com

Find us on the World Wide Web at: www.artechhouse.com
